

Se Won Suh

# AsCA '06/CrSJ

Programme & Abstracts



Joint Conference of  
the Asian Crystallographic Association and  
the Crystallographic Society of Japan

**Joint Conference of  
the Asian Crystallographic Association and  
the Crystallographic Society of Japan**

# **AsCA '06/CrSJ**

---

**Epochal Tsukuba, Japan  
20-23 November, 2006**

**<http://pfwww.kek.jp/AsCA06/>**



# Table of Contents

Committees	(2)
Conferenece Sponsors	(4)
Directory of Epochal Tsukuba	(6)
General Information	(8)
Info for Authors/Presenters	(9)
Program Timetable	(11)
Oral Abstracts	1
Poster Abstracts	119
Author Index	453

# Committees

## Asian Crystallographic Association

President: Prof. Mamannamana VIJAYAN  
*Indian Institute of Science, India*

## Crystallographic Society of Japan

President: Prof. Tomitake TSUKIHARA  
*Osaka University, Japan*

## International Program Committee for AsCA'06/CrSJ

Chair: Prof. Soichi WAKATSUKI	<i>PF/IMSS/KEK (JP)</i>
Prof. Brendan J. KENNEDY	<i>The University of Sydney (AU)</i>
Prof. Jennifer L. MARTIN	<i>University of Queensland (AU)</i>
Dr. Joanne E. ETHERIDGE	<i>Monash University (AU)</i>
Prof. Ashwini NANGIA	<i>University of Hyderabad (IND)</i>
Prof. Mamannamana VIJAYAN	<i>Indian Institute of Science (IND)</i>
Prof. Donglai FENG	<i>Fudan University (CN)</i>
Prof. Zihe RAO	<i>Tsinghua University (CN)</i>
Prof. Moonhor REE	<i>POSTECH (KR)</i>
Prof. Yu WANG	<i>National Taiwan University (TW)</i>
Prof. Yih-Cherng LIOU	<i>National University of Singapore (SP)</i>
Dr. Masaki TAKATA	<i>RIKEN/JASRI (JP)</i>
Prof. Youichi MURAKAMI	<i>Tohoku University (JP)</i>
Prof. Masami TERAUCHI	<i>Tohoku University (JP)</i>
Prof. Keiichiro OGAWA	<i>The University of Tokyo (JP)</i>
Prof. Takashi KAMIYAMA	<i>IMSS/KEK (JP)</i>
Prof. Genji KURISU	<i>The University of Tokyo (JP)</i>
Prof. Osamu NUREKI	<i>Tokyo Inst. of Technology (JP)</i>
Prof. Keiichi NAMBA	<i>Osaka University (JP)</i>
Prof. Yoshiyuki AMEMIYA	<i>The University of Tokyo (JP)</i>
Prof. Mamoru SATO	<i>Yokohama City University (JP)</i>
Prof. Izumi NAKAI	<i>Tokyo Science University (JP)</i>

## Local Organizing Committee for AsCA'06/CrSJ

Chair: Prof. Kazumasa OHSUMI	IMSS/KEK
Prof. Shin-ichi ADACHI	IMSS/KEK
Dr. Noriyuki IGARASHI	IMSS/KEK
Prof. Takashi KAMIYAMA	IMSS/KEK
Prof. Hiroshi SAWA	IMSS/KEK
Dr. Zui FUJIMOTO	NIAS
Dr. Yoshio MATSUI	AML/NIMS
Dr. Yoichi MICHIE	AML/NIMS
Dr. Takashi MOCHIKU	SMC/NIMS
Dr. Chiya NUMAKO	Tokushima University
Prof. Ken-ichi OHSHIMA	Tsukuba University
Prof. Soichi WAKATSUKI	IMSS/KEK
Dr. Hijiri KITO	AIST
Mr. Kazuyuki NIGORIKAWA	IMSS/KEK

### AsCA'06/CrSJ Secretariat:

Ms. Yoshimi TAKAHASHI	IMSS/KEK
Ms. Yasuko MATSUMOTO	RIKEN

## IUCr Scientific Freedom Policy Statement

The Organizing committee of AsCA'06/CrSJ shall observe the basic policy of non-discrimination and affirms the right and freedom of scientists to associate in international scientific activity without regard to such factors as citizenship, religion, creed, political stance, ethnic origin, race, colour, language, age or gender, in accordance with the Statutes of the International Council for Science.

At this Conference no barriers will exist which would prevent the participation of *bona fide* scientists.

# Conference Sponsors

Asian Crystallographic Association  
Crystallographic Society of Japan  
International Union of Crystallography  
High Energy Accelerator Research Organization  
Rigaku Corporation  
Bruker AXS  
Mar USA

## Evening Social Functions:

### Monday November 20

#### Welcome Party

Time: 18:00 – 20:30      Location: Multi-Purpose Hall

### Tuesday November 21

#### Bruker AXS Dinner Buffet

Time: 19:00 - 21:00      Location: Okura Frontier Hotel Tsukuba

### Wednesday November 22

#### Rigaku Banquet

Time: 19:00 - 21:00      Location: Hotel Grand Shinonome

### Thursday November 23

#### Mar USA Farewell Party

Time: 18:30 - 20:30      Location: Multi-Purpose Hall

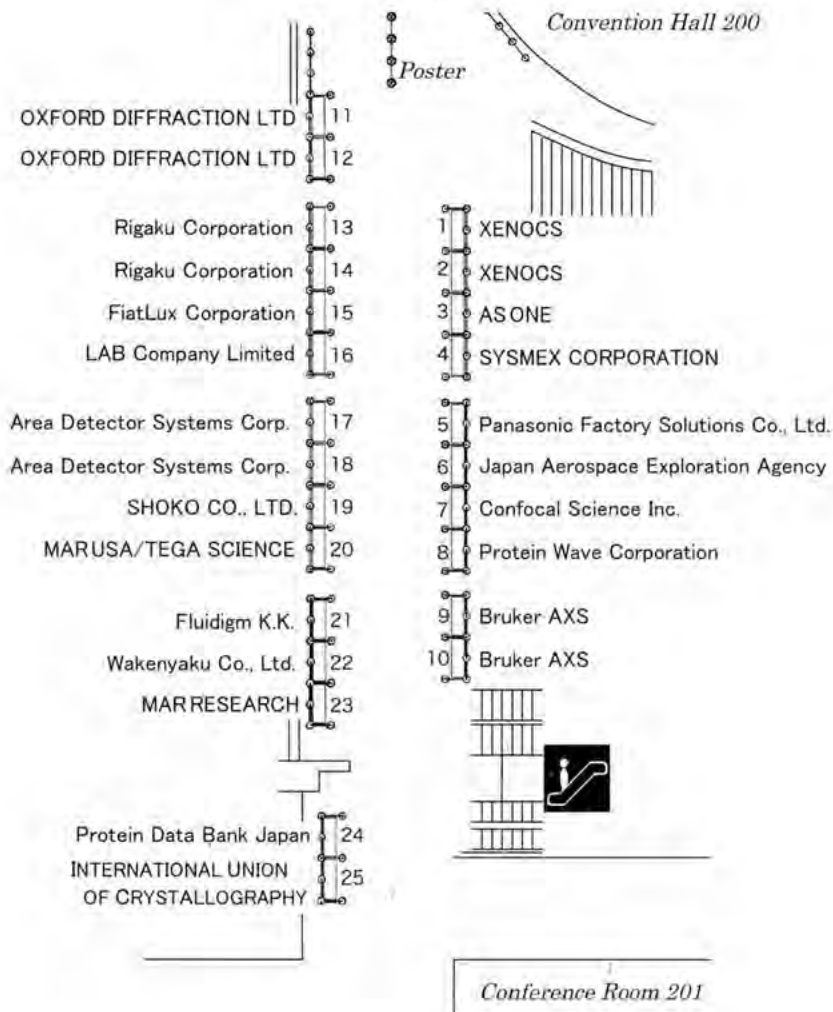
# Exhibition Layout:

Exhibit Hours Nov. 21 (Tue) 11:00 -18:00

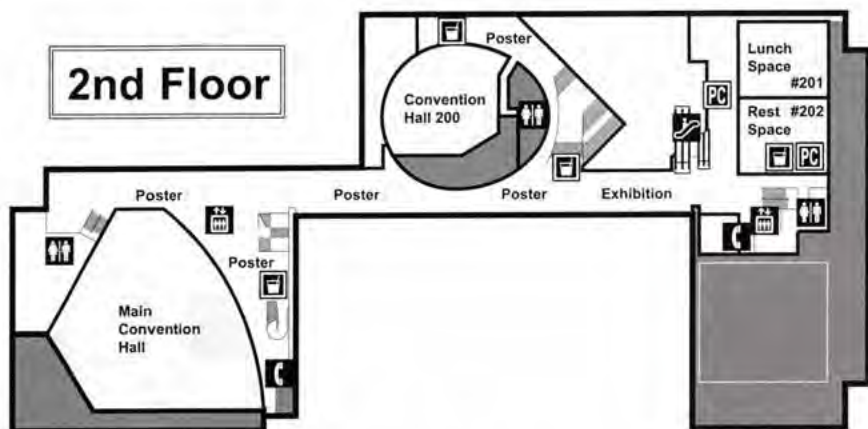
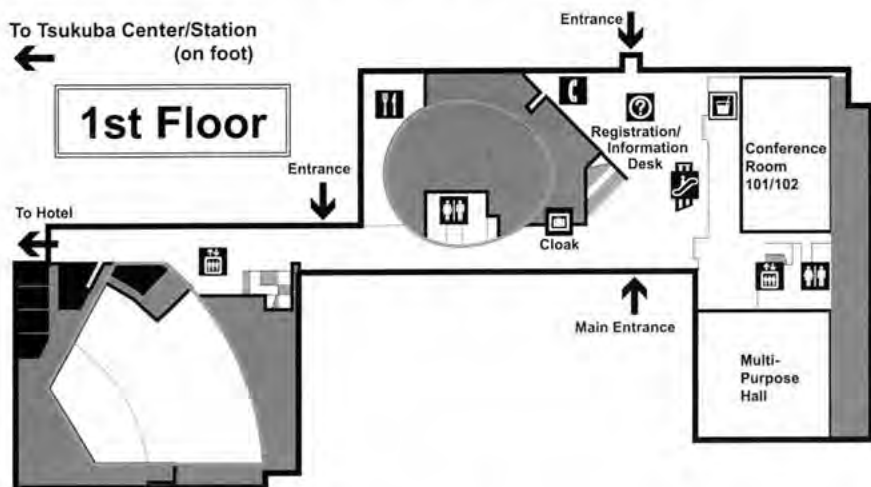
Nov. 22 (Wed) 9:00 -18:00

Nov. 23 (Thu) 9:00 -13:00

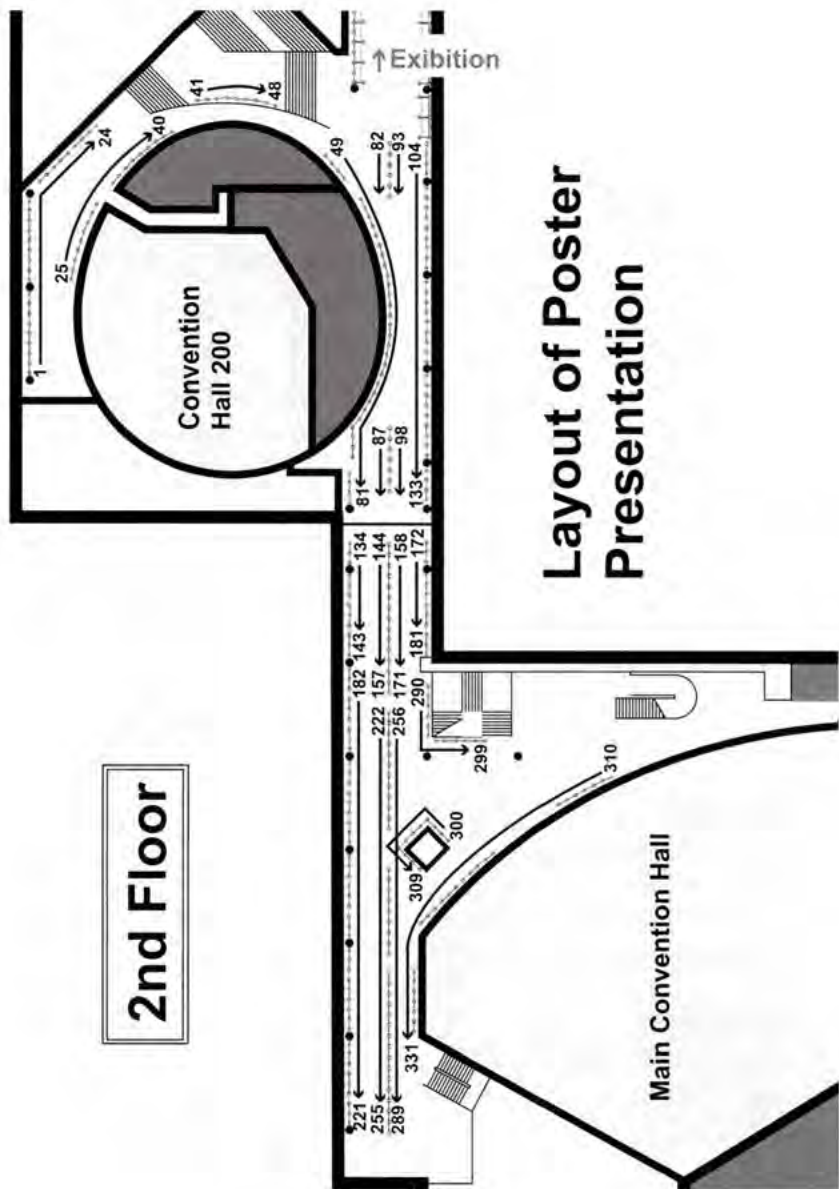
## 2nd Floor Foyer



# Directory of Epochal Tsukuba



## Floor Map



# General Information

## Registration:

The Registration Desk is situated just inside the main entrance. The opening hours are 15:00-18:00, Nov. 20, and 8:30-17:00, Nov. 21-23. The congress material is handed to pre-registered participants upon their arrival.

On-site registration is possible and the fee can be paid in cash (yen) or credit card.

## Name Tags:

Name tags are required for entry to all scientific sessions, lunches and evening functions. The color of the name tag indicates the type of participant:

<b>Full Registrants</b>	<b>Orange</b>
<b>Students</b>	<b>Green</b>
<b>Keynote and Award Lecturers</b>	<b>Red</b>
<b>Exhibitors</b>	<b>Blue</b>
<b>Staff</b>	<b>Black</b>

For inquiries, please visit the information desk or contact the support staff who are wearing navy armbands.

## Internet:

12 multi-language PCs are available for e-mail and internet access in front of Room #201 and network ports inside Room #202 on the second floor. Epochal Tsukuba is equipped with a wireless hot point. It enables the participants to use their own PCs for internet connection.

## Lunches:

Lunch box is served daily to all registered participants in front of Room #201 and #202 on Nov 21-23. Both rooms and lobby are available for your lunch.

# Info for Authors/Presenters

## Oral Presentations:

### Length of Talk

Type	Total	Talk	Discussion
Keynote	50 min	40 min	10 min
Award Lecture	40 min	30 min	10 min
	25 min	20 min	5 min
Contributed Oral	15 min	12 min	3 min
	20 min	15 min	5 min
	25 min	20 min	5 min
	30 min	25 min	5 min

### Available Equipment

PC	IBM compatible, MS-Windows XP and Macintosh OS-X
Soft	Microsoft Office (PowerPoint)2003 for Windows, PowerPoint98 Viewer for Macintosh
Others	Projector, Presentation Mouse, Laser Pointer, Microphone, Acrobat Reader 7.0

Oral presenters can bring CDR, USB memories or their own PCs.

Oral presenters can make sure of the compatibility in the preview desk in advance. The preview desk is situated in front of Conference Room 101/102 (first floor).

**All oral presenters are kindly requested to come to the presentation desk in each hall/room 15 minutes prior to their session. Presenters should hand their data in CDR or USB memories or their own PCs to the staff with navy armband.**

For practical and security reasons, internet facilities are not available to the presenters. Although our best care will be taken in handling the presentation files, the organizers cannot take responsibility for loss or damage.

## Poster Presentations:

Poster presentations are held at foyer on the second floor (see p.7) from 10:00 on Nov. 21 to 15:00 on Nov. 23. All posters must be displayed during the poster presentations. Authors are kindly requested to set up their poster with the supplied pins between 8:30 and 10:00 on Nov. 21 and to remove it between 15:00 and 17:30 on Nov. 23.

The poster number indicates the following information,

PDD-XXX

DD refers to the date of the core time of Poster Session.

XXX refers to the serial number of your poster.

Poster Number	Session Name	Core Time
P21-XXX	Poster Session 1*	10:00-12:00 on Nov. 21 (Tue.)
P22-XXX	Poster Session 2	10:30-12:00 on Nov. 22 (Wed.)
P23-XXX	Poster Session 3	10:30-12:00 on Nov. 23 (Thu.)

**\*All posters assigned to Poster Session 1 are the poster award candidates. At the banquet of 21st, the CrSJ and IUCr poster awards will be announced. All candidate Authors should join the banquet.**

### Poster Board Size

900 mm width x 2100 mm height

A0 size poster (841 mm width x 1189 mm height) is recommended.

# **Program Timetable**



## AsCA'06/CrSJ Overview

	Nov. 20 (Mon.)	Nov. 21(Tue.)	Nov. 22 (Wed.)	Nov. 23 (Thu.)
8:30				
9:00		<b>Keynote Lecture</b> 1	<b>Oral Session</b> 1, 2 & 3	<b>Oral Session</b> 1, 2 & 3
9:50		9:00-9:50		
10:00			8:30-10:30	8:30-10:30
10:30		<b>Poster Session</b> 1		
11:00			<b>Poster Session</b> 2	<b>Poster Session</b> 3
11:00	<b>CrSJ Manager Meeting</b> 11:00-13:00			
12:00		Lunch	<b>AsCA Council</b> 11:40-13:00	<b>IUCr2008</b> 11:40-13:00
13:00				
	<b>Councilor Meeting</b> 13:00-15:00	<b>Oral Session</b> 1, 2 & 3 13:00-15:00	<b>Oral Session</b> 4, 5 & 6 13:00-15:00	<b>Oral Session</b> 4, 5 & 6 13:00-15:00
15:00		Coffee break		
15:20	<b>International Meeting</b> 15:00-17:00	<b>General Meeting of CrSJ</b>	<b>Oral Session</b> 7, 8 & 9	<b>Oral Session</b> 7, 8 & 9
16:00		<b>Award Lectures</b> 1, 2 & 3 16:00-17:30	15:20-17:20	15:20-17:20
17:00	<b>REGISTRATION</b>			
17:30			Coffee break	
17:40		<b>Keynote Lecture</b> 2	<b>Keynote Lecture</b> 3	<b>Keynote Lecture</b> 4
18:00		17:40-18:30	17:40-18:30	17:40-18:30
18:30	<b>Welcome party (Multi-Purpose Hall)</b>			<b>Mar USA</b>
19:00		<b>Braker AXS Dinner Buffet</b> (Okura Frontier Hotel Tsukuba)	<b>Rigaku Banquet</b> (Hotel Grand Shinonome)	<b>Farewell party (Multi-Purpose Hall)</b>
20:30				
21:00				

## AsCA'06/CrSJ Program Timetable

	Nov. 20 (Mon.)	Nov. 21 (Tue.)
8:30		
9:00		<b>Keynote Lecture 1 (A)</b> <b>S. Kitagawa</b>
9:50		
10:00		<b>Poster Session 1</b> (Foyer, 2F) 10:00-12:00
11:00	<b>CrSJ Manager Meeting</b> (301) 11:00-13:00	
12:00		<b>Lunch</b>
13:00	<b>Councilor Meeting</b> (303) 13:00-15:00	<b>Oral Session</b> 1. Structural Genomics and High-Throughput Crystallography (A) 2. Crystal Engineering and Supramolecular Chemistry I (B) 3. Advances in Powder Diffraction (C)
15:00		<b>Coffee break</b>
15:20	<b>International Meeting</b> (303) 15:00-17:00	<b>General Meeting of CrSJ</b> (Main Hall) 15:20-16:00
16:00	<b>REGISTRATION</b>	<b>Award Lectures (A)</b> M. Sugishima (16:00-16:25) T. Nogi (16:25-16:50) S. Wakatsuki (16:50-17:30)
17:00		
17:30		
17:40		<b>Keynote Lecture 2 (A)</b> <b>Z. Rao</b> 17:40-18:30
18:00		
18:30	<b>Welcome party</b> (Multi-Purpose Hall) 18:00 - 20:30	
19:00		<b>Bruker AXS Dinner Buffet</b> (Okura Frontier Hotel Tsukuba) 19:00 - 21:00
20:30		
21:00		

(A): Main Convention Hall, (B): Convention Hall 200, (C): Conference Room 101/102

	<b>Nov. 22 (Wed.)</b>	<b>Nov. 23 (Thu.)</b>
8:30	<b>Oral Session</b> 1.Macromolecular Assemblies: proteins/DNA/RNA (A) 2.Crystal Engineering and Supramolecular Chemistry II (B) 3.Inelastic X-ray Scattering (C)	<b>Oral Session</b> 1.Membrane and Membrane-Associated Proteins (A) 2.Atomic Resolution Structure of Biological Macromolecules I (B) 3.X-ray and Neutron Scattering of Strongly Correlated Electron Systems (C)
10:30	<b>Poster Session 2</b> (Foyer, 2F) 10:30-12:00	<b>Poster Session 3</b> (Foyer, 2F) 10:30-12:00
12:00	<b>Lunch</b>	<b>Lunch</b>
	AsCA Council (304) 11:40-13:00	IUCr2008 (303) 11:40-13:00
13:00	<b>Oral Session</b> 4.Computational Developments (A) 5.Materials Science I (B) 6.Advancements in Small Angle X-ray Scattering (C)	<b>Oral Session</b> 4.Cool Structures (A) 5.Materials Science II (B) 6.Nanotechnology: Surface and Interface (C)
15:00	<b>Coffee break</b>	
15:20	<b>Oral Session</b> 7.Protein Crystallization and Post-Crystal Treatments - New Tricks & Tools (A) 8.Magnetic Structures (B) 9.Electronic Structure and Bonding by X-ray Diffraction, CBED, EELS, EXAFS (C)	<b>Oral Session</b> 7.Disease Related Proteins (A) 8.Atomic Resolution Structure of Biological Macromolecules II (B) 9.Dynamic Aspects of Molecular Crystals (C)
17:20	<b>Coffee break</b>	
17:40	<b>Keynote Lecture 3 (A)</b> <b>S. Iwata</b> 17:40-18:30	<b>Keynote Lecture 4 (A)</b> <b>C. Howard</b> 17:40-18:30
18:30		
19:00	<b>Rigaku Banquet</b> (Hotel Grand Shinonome) 19:00 - 21:00	<b>Mar USA Farewell party</b> (Multi-Purpose Hall) 18:30 - 20:30
20:30		
21:00		

## November 21, Tuesday

**Keynote Lecture 1** (9:00-9:50)

*Main Convention Hall*

*Chair: Masaki Takata*

09:00 K21-001 **Crystal and Functional Engineering for Unique Microporous Materials**  
Susumu Kitagawa

**Oral Session 1** (13:00-15:00)

*Main Convention Hall*

**Structral Genomics and High-Throughput Crystallography**

*Chair: Atsushi Nakagawa / Co-Chair: Se Won Suh*

- 13:00 OA21-101 **Mail-in Data Collection Service at SPring-8 Protein Crystallography Beamline**  
Kazuya Hasegawa, Nobuo Okazaki, Go Ueno, Hironori Murakami, Yuji Fukumoto, Hisanobu Sakai and Masaki Yamamoto
- 13:20 OA21-102 **Transition Metal Derivatives for SAD Method**  
Atsuo Suzuki, Akihito Fukushima and Takashi Yamane
- 13:40 OA21-103 **S-SAD Phasing at RIKEN Structural Genomics Beamline of SPring-8**  
Raita Hirose, Yuki Nakamura, Tomokazu Hasegawa, Akihito Yamano and Kensaku Hamada
- 14:00 OA21-104 **Current Status of Macromolecular Crystallography Beamlines at the Photon Factory**  
Naohiro Matsugaki, Masanori Kobayashi, Yusuke Yamada, Noriyuki Igarashi, Masahiko Hiraki, Yurii A. Gaponov and Soichi Wakatsuki
- 14:20 OA21-105 **Structural Genomics of Mycobacterial Recombination and Repair**  
Mamannamana Vijayan
- 14:40 OA21-106 **Progress in the Whole Cell Project of a Model Organism, *Thermus thermophilus* HB8**  
Akio Ebihara, Mayumi Kanagawa, Chizu Kuroishi, Noriko Nakagawa, Ryoji Masui, Takaho Terada, Mikako Shirouzu, Kunio Miki, Shigeyuki Yokoyama and Seiki Kuramitsu

**Oral Session 2 (13:00-15:00)**

*Convention Hall 200*

**Crystal Engineering and Supramolecular Chemistry I**

*Chair: Yu Wang / Co-Chair: Hidehiro Uekusa*

- 13:00 OB21-101 **Formation of Helical Organic Supramolecular Chains in an Elastic Zincophosphate Lattice**  
Sue-Lein Wang
- 13:20 OB21-102 **Crystal Engineering of Microporous Chiral Coordination Polymers Based on L-tartrate Ligands**  
Ian D. Williams
- 13:40 OB21-103 **Crystal Engineering of Isopropylbenzophenone Derivatives and the Morphology Change by Asymmetric Photoreaction**  
Hideko Koshima, Michitaro Fukano and Yuya Ide
- 14:00 OB21-104 **Host Framework in Inclusion Compound of 1,1,2,2-tetrakis (4-hydroxyphenyl) ethane, (TEP)**  
Hidehiro Uekusa, Naonori Akai, Natsuki Amanokura and Masami Kaneko
- 14:15 OB21-105 **The Chirality Transfer between 1D Helical Chains**  
Tong-Bu Lu, Jin-Zhong Gu, Long Jiang and Wen-Guan Lu
- 14:30 OB21-106 **Incompatible Host-Guest Strategy to Enclathrate Discrete Water Clusters**  
Tomoji Ozeki, Setsuko Nakamura, Takuto Yamawaki and Katsuhiko Kusaka
- 14:45 OB21-107 **Self Assembled Nanomaterials Based on Porogenic Water Soluble Calixarenes**  
Mohamed Makhā, Colin L. Raston, Christopher Smith and Alex Sobolev

**Oral Session 3 (13:00-15:00)**

*Conference Room 101/102*

**Advances in Powder Diffraction**

*Chair: Chris Howard / Co-Chair: Takashi Kamiyama*

- 13:00 OC21-101 **High Resolution Powder Diffraction Studies at ESRF**  
Andy Fitch

- 13:30 OC21-102 **IBARAKI Materials Design Diffractometer for J-PARC**  
Toru Ishigaki, Akinori Hoshikawa, Masao Yonemura, Takashi Kamiyama, Stefans Harjo, Kazuya Aizawa, Takashi Sakuma, Yo Tomota, Yukio Morii, Masatoshi Arai, Kazuhiro Ebata, Yoshiki Takano and Takuro Kasao
- 13:55 OC21-103 **Powder Diffraction Software: Choosing the Right Tool for the Right Job**  
Maxim Avdeev
- 14:20 OC21-104 **Neutron and Synchrotron Diffraction Studies on Structural Phase Transitions in 1:3 Ordered Perovskites  $\text{Sr}_{4-x}\text{Ba}_x\text{NaSb}_3\text{O}_{12}$**   
Qingdi Zhou and Brendan J. Kennedy
- 14:40 OC21-105 **Single Crystal XRD Pattern Obtained from Magnetically Aligned Powder**  
Tsunehisa Kimura, Fumiko Kimura and Masashi Yoshino

**Award Lectures (16:00-17:30)**

*Main Convention Hall*

*Chair: Tomitake Tsukihara*

- 16:00 A21-201 **Structural Basis for Heme Degradation by Heme Oxygenase**  
Masakazu Sugishima
- 16:25 A21-202 **Structure Determination of a Signaling-Competent Reelin Fragment by X-ray Crystallography and Electron Tomography**  
Terukazu Noji, Norihisa Yasui, Tomoe Kitao, Kenji Iwasaki and Junichi Takagi
- 16:50 A21-203 **Synchrotron Protein Crystallography and Structural Proteomics of Protein Transport and Glycosylation**  
Soichi Wakatsuki

**Keynote Lecture 2 (17:40-18:30)**

*Main Convention Hall*

*Chair: Jennifer L. Martin*

- 17:40 K21-301 **Structural Insights into SARS Coronavirus Proteins**  
Zihe Rao

## November 22, Wednesday

Oral Session 1 (8:30-10:30)

Main Convention Hall

### Macromolecular Assemblies: Proteins/DNA/RNA

Chair: Osamu Nureki / Co-Chair: Anders Liljas

- 08:30 OA22-001 **Structural Basis for Rab11-Dependent Membrane Recruitment of FIP3/Arfophilin-1**  
Tomoo Shiba, Hiroshi Koga, Hye-Won Shin, Masato Kawasaki, Ryuichi Kato, Kazuhisa Nakayama and Soichi Wakatsuki
- 09:00 OA22-002 **Crystal Structures and Evolutionary Relationship of Two Different Lipoamide Dehydrogenases (E3s) from *Thermus thermophilus***  
Hiroshi Kondo, Ella Czarina, Magat Juan, M. Tofazzal Hossain, Wataru Adachi, Tadashi Nakai, Nobuo Kamiya, Ryoji Masui, Seiki Kuramitsu, Kaoru Suzuki, Takeshi Sekiguchi and Akio Takenaka
- 09:20 OA22-003 **Crystal Structure of Extracellular Giant Hemoglobin of Pogonophoran *Oligobranchia mashiko***  
Nobutaka Numoto, Taro Nakagawa, Akiko Kita, Yuichi Sasayama, Yoshihiro Fukumori and Kunio Miki
- 09:40 OA22-004 **Multiplex Formation of Repetitive Sequences  $d([G]_nA)_m$  by Non-Watson-Crick Pairings**  
Yoshiteru Sato, Kenta Mitomi, Hiromu Sugiyama, Satoru Shimizu, Ella Czarina Magat Juan, Jiro Kondo and Akio Takénaka
- 10:00 OA22-005 **Functional Interactions of the Translation Elongation Factors**  
Anders Liljas

Oral Session 2 (8:30-10:30)

Convention Hall 200

### Crystal Engineering and Supramolecular Chemistry II

Chair: Roger Bishop / Co-Chair: Sue Lein Wang

- 08:30 OB22-001 **Significance of High Z' Structures in Crystallization Mechanisms**  
Gautam R. Desiraju

- 08:50 OB22-002 **eCrystals: A Route for Open Access to Small Molecule Crystal Structure Data**  
Michael B. Hursthouse, Simon C. Coles, Jeremy G. Frey, Andrew Milsted, Leslie Carr, Monica Duke, Traugott Koch and Elizabeth Lyon
- 09:10 OB22-003 **Control of Molecular Aggregation in Inclusion Crystals by Phase Transition**  
Fumio Toda
- 09:30 OB22-004 **Hydrogen Bonded Ladder Structures**  
Roger Bishop, Vi T. Nguyen, Isa Y. Chan, Donald C. Craig and Marcia L. Scudder
- 09:45 OB22-005 **Ring-Opening Isomerization: Relationship between Discrete Molecular Architectures and Coordination Polymers**  
Cheng-Yong Su, Zhi-Min Liu and Mei Pan
- 10:00 OB22-006 **Structures and Non-Linear Optical Properties of Lanthanide Complexes**  
Wing-Tak Wong
- 10:15 OB22-007 **Chirality Scaffolding Crystallization**  
Reiko Kuroda, Sayoko Hasebe, Yoshitane Imai and Tomohiro Sato

**Oral Session 3 (8:30-10:30)**  
**Inelastic X-ray Scattering**

*Conference Room 101/102*

*Chair: Jun'ichiro Mizuki / Co-Chair: Hiroshi Kawata*

- 08:30 OC22-001 **Element- and Site-Specific Phonon Density of States Measured by Nuclear Resonant Inelastic Scattering of Synchrotron Radiation**  
Makoto Seto
- 09:00 OC22-002 **Inelastic X-ray Scattering for Investigating Exotic Superconductors**  
Alfred Q. R. Baron
- 09:30 OC22-003 **Theory of Resonant Inelastic X-ray Scattering in Cuprates**  
Takami Tohyama, Kenji Tsutsui and Sadamichi Maekawa

- 10:00 OC22-004 **Low-Energy Charge Excitations by Inelastic X-ray Scattering: From Collective Excitations in Simple Materials to d-d Excitations in Mott Insulators**  
Yong Cai

**Oral Session 4 (13:00-15:00)** *Main Convention Hall*  
**Computational Developments - SAD Phasing, Refinement, Model Building, Validation**

*Chair: Isao Tanaka / Co-Chair: Thomas Garret*

- 13:00 OA22-101 **Evaluation of the Experimental Conditions for Lower Energy SAD Phasing at the Photon Factory**  
Yusuke Yamada, Noriyuki Igarashi, Tadashi Satoh, Naohiro Matsugaki and Soichi Wakatsuki
- 13:25 OA22-102 **On the Use of the Loopless Free Crystal Mounting Method for the Longer X-ray S-SAD Phasing**  
Nobuhisa Watanabe
- 13:50 OA22-103 **OASIS Applications - SAD Phasing and Fragment Extension at Different Resolution**  
Deqiang Yao, Yuanxin Gu, Chaode Zheng, Zhengjiong Lin, Haifu Fan and Nobuhisa Watanabe
- 14:10 OA22-104 **Effective Techniques to Prepare Iodine Derivatives for I-SAD Phasing by Vaporizing Iodine Labelling (VIL) and Hydrogen Peroxide VIL (HYPER-VIL)**  
Hideyuki Miyatake, Tomokazu Hasegawa and Akihito Yamano
- 14:35 OA22-105 **Structure Determination of a Novel Fungal Pathogen Protein Using Cobalt SAD Phasing with a Cu-Rotating Anode X-ray Generator**  
Gregor Guncar, Ching-I A. Wang, Jade K. Forwood, Trazel Teh, Ann-Maree Catanzariti, Horst Schirra, Peter A. Anderson, Jeffrey G. Ellis, Peter N. Dodds and Bostjan Kobe

**Oral Session 5 (13:00-15:00)** *Convention Hall 200*  
**Materials Science I**

*Chair: Dhananjai Pandey / Co-Chair: Sunggi Baik*

- 13:00 OB22-101 **Disorder and Diffusion Path of Mobile Ions in Ionic Conductors**  
Masatomo Yashima

- 13:30 OB22-102 **High-Resolution Neutron and X-ray Powder Diffraction Studies on Phase Transitions in  $(1-x)\text{Pb}[(\text{Mg}_{1/3}\text{Nb}_{2/3})\text{O}_3]\text{-xPbTiO}_3$  Ceramics**  
Akhilesh Kumar Singh, Dhananjai Pandey, Oksana Zaharko, Songhak Yoon, Namsoo Shin and Sunggi Baik
- 14:00 OB22-103 **Structural Phase Transition in  $(1-x)\text{Pb}(\text{Fe}_{1/2}\text{Nb}_{1/2})\text{O}_3\text{-xPbTiO}_3$  Ceramics near the Morphotropic Phase Boundary Region**  
Satendra Pal Singh, Akhilesh Kumar Singh and Dhananjai Pandey
- 14:15 OB22-104 **Perovskites: Sorting Out**  
Maxim Avdeev
- 14:30 OB22-105 **Crystal Structure and Microwave Dielectric Properties on the Tngstenbronze-Type Like  $\text{Ba}_{6-3x}\text{R}_{8+2x}\text{Ti}_{18}\text{O}_{54}$  Solid Solutions**  
Hitoshi Ohsato
- 14:45 OB22-106 **The Commensurate Modulated Structure of the Thermal Quenching Meta-Stable State in Spin Crossover Complex  $[\text{Fe}(\text{abpt})_2(\text{Ncs})_2]$**   
Chou-Fu Sheu, Szu-Miao Chen, Shih-Chi Wang, Gene-Hsiang Lee, Liu Yi-Hung and Yu Wang

**Oral Session 6 (13:00-15:00)** **Conference Room 101/102**  
**Advancements in Small Angle X-ray Scattering**  
*Chair: Yoshiyuki Amemiya / Co-Chair: Hideki Seto*

- 13:00 OC22-101 **Recent Advancements in Small Angle X-ray Scattering: Synchrotron Grazing Incidence X-ray Scattering, Specular X-ray Reflectivity and Their Combinations**  
Moonhor Ree, Jinhwan Yoon, Kyuyoung Heo, Kyeong Sik Jin, Sangwoo Jin, Byeongdu Lee, Jehan Kim and Kwang-Woo Kim
- 13:25 OC22-102 **Nanostructure and Transition of Polyelectrolyte Brush at the Air/Water Interface by X-ray and Neutron Reflectometry**  
Hideki Matsuoka

- 13:50 OC22-103 **In-situ Observation of Forming Cell-Sized Liposome from Dry Lipid Films**  
Mafumi Hishida, Hideki Seto, Norifumi L. Yamada and K. Yoshikawa
- 14:15 OC22-104 **SAXS-WAXS Study Of Heterogeneous Nucleation of *n*-Alkane Crystals in O/W Emulsion System**  
S. Ueno, Y Shinohara, Y. Amemiya and K. Sato
- 14:40 OC22-105 **Study of Rubber Filled with Silica by 2D-USAXS and XPCS**  
Yuya Shinohara, Hiroyuki Kishimoto and Yoshiyuki Amemiya

**Oral Session 7 (15:20-17:20)** *Main Convention Hall*  
**Protein Crystallization and Post-Crystal Treatments - New Tricks & Tools**

*Chair: K. Byrappa / Co-Chair: Peter Metcalf*

- 15:20 OA22-201 **Crystallization and Evaluation of HEWL Crystals at Wide Range of pH**  
Wakari Iwai, Daichi Yagi, Takuya Ishikawa, Yuki Ohnishi, Ichiro Tanaka and Nobuo Niimura
- 15:50 OA22-202 **Crystallization of DNA Oligomers by a Simple Temperature-Control Technique**  
Toshiyuki Chatake, Osamu Matsumoto and Tatsuhiko Kikkou
- 16:20 OA22-203 **Crystal Structure and Functional Study of Thalassemic Mouse/Human Transgenic Hemoglobins**  
Chariwat Samanchat, Lukana Ngisara, Jisnuson Svasti, Duangporn Jamsai, Suthat Fucharoen and Palangpon Kongsaree
- 16:40 OA22-204 **Analysis of Crystal Growth of Trigonal Ribonuclease A**  
Hideaki Takusagawa, Masanori Ootaki, Shigefumi Yamamura and Yoko Sugawara
- 17:00 OA22-205 **Purification and Crystallization of HutP Protein that Regulate Hut Operon of *Bacillus cereus***  
Balasundaresan Dhakshnamoorthy, Tomoko S. Misono, Gopinath C.B. Subash, Kumar K.R. Penmetcha and Hiroshi Mizuno

**Oral Session 8 (15:20-17:20)**

*Convention Hall 200*

**Magnetic Structures**

*Chair: Shane Kennedy / Co-Chair: Kazuhisa Kakurai*

- 15:20 OB22-201 **Rare Earth Magnetic Materials: 1-2-2 Intermetallic Compounds**  
Stewart J. Campbell and Michael Hofmann
- 15:50 OB22-202 **Magnetic Structure Study on NpTGa<sub>5</sub> (T: Fe, Co, Ni and Rh)**  
Fuminori Honda
- 16:20 OB22-203 **Magnetism and Unusual Behavior of Multiferroic Hexagonal Manganites RMnO<sub>3</sub>**  
Je-Geun Park
- 16:50 OB22-204 **Field-Induced Magnetic Phase Transitions and the Relevance with Ferroelectricity in Multiferroic Compounds of RMn<sub>2</sub>O<sub>5</sub> (R = Er, Ho)**  
Hiroyuki Kimura, Shuichi Wakimoto, Youichi Kamada, Yukio Noda, Kazuhisa Kakurai, Koji Kaneko, Naoto Metoki and Kay Kohn

**Oral Session 9 (15:20-17:20)**

*Conference Room 101/102*

**Electronic Structure and Bonding by X-ray Diffraction, CBED, EELS, EXAFS**

*Chair: Makoto Sakata / Co-Chair: Siggj Schmid*

- 15:20 OC22-201 **Extraction of Polarisabilities and Hyperpolarisabilities from X-ray Constrained Wavefunctions: Applications to a Series of NLO Compounds**  
Dylan Jayatilaka, Andrew Whitten, Paraprathim Munshi, Mark Spackman, Mike Turner, Dima. Yufit and Judith A. K. Howard
- 16:00 OC22-202 **The MEM Charge Density Studies from Multi High Resolution Synchrotron Powder X-ray Diffraction Data**  
Eiji Nishibori, Shinobu Aoyagi, Kenichi Kato, Masaki Takata and Makoto Sakata
- 16:20 OC22-203 **3d-Orbital Determination of Ni<sup>2+</sup> in NiP<sub>2</sub> Crystals by X-ray AO Analysis**  
Zaw Win, Kiyooki Tanaka and Ichimin Shirotani

16:40 OC22-204 **Combined EXAFS and Neutron Diffraction Study of the Structure of Superionic Conducting Glasses; AgI-AgPO<sub>3</sub> and Ag<sub>2</sub>S-AgPO<sub>3</sub>**  
Abby Scott, Shane J. Kennedy and Evvy Kartini

17:00 OC22-205 **Electrostatic Potential Analysis of the Ferroelectric Phase of BaTiO<sub>3</sub> Using Convergent-Beam Electron Diffraction**  
Kenji Tsuda and Michiyoshi Tanaka

**Keynote Lecture 3 (17:40-18:30)**

*Main Convention Hall*

*Chair: Soichi Wakatsuki*

17:40 K22-301 **Towards Structure Determination of Human Membrane Proteins**  
So Iwata

## November 23, Thursday

**Oral Session 1 (8:30-10:30)**

*Main Convention Hall*

### **Membrane and Membrane-Associated Proteins**

*Chair: Jacqui Gulbis / Co-Chair: Satoshi Murakami*

- 08:35 OA23-001 **Crystal Structure of Mitochondrial Respiratory Membrane Protein Complex II**  
Fei Sun, Xia Huo, Yujia Zhai, Aojin Wang, Jianxing Xu, Dan Su, Mark Bartlam and Zihe Rao
- 09:00 OA23-002 **Reorganisation of the Pore during Gating of Inward Rectifier K<sup>+</sup> Channels**  
Jacqueline M Gulbis, Anling Kuo, Jonathan M. Elkins and Declan A. Doyle
- 09:25 OA23-003 **Structural Basis of GTPase Gate for Protein Import into Chloroplasts**  
Chwan-Deng Hsiao, Yuh-Ju Sun, Farhad Forouhar and Hsou-Min Li
- 09:50 OA23-004 **Crystal Structure of DsbB-DsbA Complex Revealing a Cysteine Relocation Mechanism**  
Kenji Inaba, Satoshi Murakami, Mamoru Suzuki, Atsushi Nakagawa, Eiki Yamashita, Kengo Okada and Koreaki Ito
- 10:10 OA23-005 **Crystal Structures of Archaerhodopsin-1 and -2**  
Tsutomu Kouyama, Keiko Yoshimura and Nobuo Enami

**Oral Session 2 (8:30-10:30)**

*Convention Hall 200*

### **Atomic Resolution Structure of Biological Macromolecules I**

*Chair: Kunio Miki / Co-Chair: Jennifer L. Martin*

- 08:30 OB23-001 **High Resolution X-ray Diffraction Data from 5 Micron Diameter Protein Crystals - Towards the Atomic Structure of Insect Virus Polyhedra**  
Peter Metcalf, Fasseli Coulibaly, Elaine Y. Chiu, Hajime Mori, Peter Haebel, Sascha Guttman and Clemens Schulze-Briese
- 09:00 OB23-002 **Atomic Resolution Crystal Growth in Microgravity**  
Masaru Sato, Hiroaki Tanaka, Koji Inaka, Sachiko Takahashi, Shigeru Sugiyama, Mari Yamanaka, Satoshi Sano, Moritoshi Motohara, Tomoyuki Kobayashi and Tetsuo Tanaka

09:30 OB23-003 **Subatomic Resolution Crystal Structure of Subtilisin ALP I from Alkalophilic *Bacillus* NKS-21**  
Hirofumi Kurokawa and Youhei Yamagata

10:00 OB23-004 **Atomic Resolution Crystal Structure of Iron-Bound Ovotransferrin N-Lobe**  
Bunzo Mikami, Kimihiko Mizutani, Aiko Tanabe and Masaaki Hirose

**Oral Session 3 (8:30-10:15)** *Conference Room 101/102*  
**X-ray and Neutron Scattering of Strongly Correlated Electron Systems**  
*Chair: Rob Robinson/ Co-Chair: Youichi Murakami*

08:30 OC23-001 **On the Nature of the Superconducting Transition in YBCO**  
Mohana Yethiraj, David K. Christen, Masatoshi Arai, Tetsuya Yokoo, Sonya Crowe, Paul Mck. Donald and Lionel Porcar

09:00 OC23-002 **Orbital Order in DyB<sub>2</sub>C<sub>2</sub> and TbB<sub>2</sub>C<sub>2</sub> Observed with Resonant Soft X-ray Diffraction**  
A. M. Mulders, U. Staub, V. Scagnoli, S. W. Lovesey, E. Balcar, G. van der Laan, Y. Tanaka, A. Kikkawa, K. Katsumata and J. M. Tonnerre

09:30 OC23-003 **Simulation of Diffuse Scattering in Neutron Diffraction Pattern of Superconducting Deuterated Sodium Cobaltate**  
Mitsuko Onoda, Kazunori Takada, Dimitri Argyriou, Yong Nam Choi and Takayoshi Sasaki

09:45 OC23-004 **Structure Analysis of Lattice Modulation of Multiferroic Compound YMn<sub>2</sub>O<sub>5</sub> by SR X-ray**  
Yukio Noda, Hiroyuki Kimura, Youichi Kamada, Yoshihisa Ishikawa, Satoru Kobayashi, Yusuke Wakabayashi, Hiroshi Sawa, Naoshi Ikeda and Kay Kohn

10:00 OC23-005 **Surface X-ray Scattering Study of the Orbital Ordering at a Cleaved Surface of the Layered Manganite La<sub>0.5</sub>Sr<sub>1.5</sub>MnO<sub>4</sub>**  
Yusuke Wakabayashi, Mary H. Upton, Stephane Grenier, John P. Hill, Christie S. Nelson, Jong-Woo Kim, Philip J. Ryan, Alan I. Goldman, Hong Zheng and John F. Mitchell

**Oral Session 4 (13:00-15:00)**

**Main Convention Hall**

**Cool Structures**

*Chair: K. Sekar / Co-Chair: Mamoru Sato*

- 13:00 OA23-101 **tRNA-Dependent Amino Acid Transformation by GatCAB**  
Akiyoshi Nakamura, Min Yao, Sarin Chimnaronk, Naoki Sakai and Isao Tanaka
- 13:30 OA23-102 **Complete Crystallographic Analysis of the Dynamics of CCA-Addition**  
Kozo Tomita, Ryuichiro Ishitani, Shuya Fukai and Osamu Nureki
- 14:00 OA23-103 **Structure of the Insulin Receptor Ectodomain Homodimer**  
Michael C. Lawrence, Neil Mckern, Victor Streltsov, Meizhen Lou, Timothy Adams, George Lovrecz, John Bentley, Peter Hoyne, Maurice Frenkel and Colin Ward
- 14:30 OA23-104 **A Functionally Rotating Mechanism Revealed in Crystal Structures of the Multidrug Transporter, AcrB, with Bound Substrates**  
Satoshi Murakami

**Oral Session 5 (13:00-14:45)**

**Convention Hall 200**

**Materials Science II**

*Chair: Yukio Noda / Co-Chair: Hiroshi Sawa*

- 13:00 OB23-101 **Micro-Focus X-ray Diffractometry for Time Resolved Structure Analysis -A Development of X-ray Pinpoint Structural Measurement at the SPring-8 (1)**  
Haruno Murayama, Nobuhiro Yasuda, Jungeun Kim, Yoshimitsu Fukuyama, Shigeru Kimura, Yoshihiro Kuroiwa, Kenichi Kato, Yutaka Moritomo, Yoshihito Tanaka, Koshiro Toriumi and Masaki Takata
- 13:30 OB23-102 **The Bilbao Crystallographic Server**  
Mois I. Aroyo, Juan Manuel Perez-Mato, Cesar Capillas, Danel Orobengoa and Hans Wondratschek
- 13:45 OB23-103 **Photochromic Reaction Mechanism and Structural Change of Trans-Biindenylideneidone Derivatives**  
Akiko Sekine, Kumiko Aruga, Hidehiro Uekusa, Katsuya Souno and Koichi Tanaka

- 14:00 OB23-104 **A Study of Accurate Charge Density and Bonding Nature of  $\text{CoSb}_3$  at  $T = 10 \text{ K}$**   
Atsuko Ohno, Bo B. Iversen, Shinobu Aoyagi, Eiji Nishibori, Makoto Sakata and Satoshi Sasaki
- 14:15 OB23-105 **Structural Analysis of Star-Shape Polystyrenes Using Synchrotron X-ray Scattering**  
Sangwoo Jin, Tomoya Higashihara, Kyeong Sik Jin, Jinhwan Yoon, Kyuyoung Heo, Jehan Kim, Kwang-Woo Kim, Akira Hirao and Moonhor Ree
- 14:30 OB23-106 **Structural Study Of II-VI Core-Shell Quantum Dots by Synchrotron Anomalous Powder Diffraction and Small Angle X-ray Scattering**  
Hwo-Shuenn Sheu, Wei-Ju Shih, Wei-Tsung Chuang, Ying-Huang Lai and U-Ser Jeng

**Oral Session 6 (13:00-15:00)**

**Conference Room 101/102**

**Nanotechnology: Surface and Interface**

*Chair: Shigeru Kimura / Co-Chair: Moonhor Ree*

- 13:00 OC23-101 **Ferroelectric Nanostructures**  
 Songhak Yoon, Hee Han, Yongjun Park, Min Gyu Kim, Namsoo Shin, Ran Ji, Dietrich Hesse, Marin Alexe, Kornelius Nielsch, Ulrich Goessele and Sunggi Baik
- 13:30 OC23-102 **Grazing Incidence X-ray Scattering for Characterizing Advanced Nanomaterials**  
Kazuhiko Omote and Yoshiyasu Ito
- 14:00 OC23-103 **Interaction between Specular Reflection and Back Scattering**  
Daisuke Arai, Shuji Kusano, Yousuke Nodumi, Mitsuhiro Hashimoto, Toshio Takahashi, Yasuhiko Imai, Yoshitaka Yoda, Keiichi Hirano and Xiao-Wei Zhang
- 14:20 OC23-104 **Conductance and Stochastic Switching of Ligand-Supported Linear Metal Atom Chains**  
Shie-Ming Peng, I-Wen Peter Chen, Ming-Dung Fu, Wei-Hsiang Tseng, Jian-Yuan Yu, Sung-Hsun Wu, Chia-Jui Ku and Chun-Hsien Chen

- 14:40 OC23-105 **Observation of 2D Nanostructures Using X-ray Reciprocal-Lattice Space Imaging**  
Osami Sakata, Masashi Nakamura, Takayuki Watanabe and Hiroshi Funakubo

**Oral Session 7 (15:20-17:20)**

*Main Convention Hall*

**Disease Related Proteins**

*Chair: Peter Colman / Co-Chair: Yin-Cherng Liou*

- 15:20 OA23-201 **Structure of the Munc18c Protein Involved in Insulin-Stimulated Glucose Transport**  
Jennifer L. Martin, Shu-Hong Hu, Catherine F. Latham, Christine L. Gee, Michelle Christie, Fred Meunier and David E. James
- 15:45 OA23-202 **The First Structure of Myo-Inositol Oxygenase: An Enzyme Implicated in Diabetes Mellitus**  
Peter M. Brown, Tom T. Caradoc-Davies, James M. Dickson, Kerry L. Loomes, Garth J.S. Cooper and Edward N. Baker
- 16:05 OA23-203 **The Structure of the LIF:LIF Receptor Complex - A Prototype for Receptor Heterodimerisation in the Gp130/IL-6 Family**  
Thomas PL Garrett, Trevor Huyton, Cindy S. Luo, Mei-Zhen Lou, Jian-Guo Zhang, Douglas J. Hilton and Nicos A. Nicola
- 16:35 OA23-204 **Perspectives of New Influenza Virus Targeted Drug Design Based on Human Neu2 Sialidase's Structure**  
Leonard M. G. Chavas, Ryuichi Kato, Maretta C. Mann, Robin J. Thomson, Jeffrey C. Dyason, Marc von Itzstein, Jennifer Mckimm-Breschkin, Peter M. Colman, Paola Fusi, Bruno Venerando, Guido Tettamanti, Eugenio Monti and Soichi Wakatsuki
- 17:00 OA23-205 **Structure of Plasmodium vivax P25 and Its Complex with Transmission-Blocking Antibody**  
Ajay Kumar Saxena, K. Singh, H. P. Su, M. M. Klein, A. W. Stower, A. J. Saul, C. Long and D. N. Garboczi

**Oral Session 8 (15:20-17:20)**

**Convention Hall 200**

**Atomic Resolution Structure of Biological Macromolecules II**

*Chair: Mitchell Guss / Co-Chair: Mamannamana Vijayan*

- 15:20 OB23-201 **Anaerobic and Aerobic Structures of Ferredoxin II from *Desulfovibrio Gigas* at Ultrahigh Resolution**  
Chun-Jung Chen, Yin-Cheng Hsieh, Yi-Hung Lin, Yen-Chieh Huang and Ming-Yih Liu
- 15:50 OB23-202 **X-ray Structure of in-situ HIV-1 Protease-Product Complex: Observation of a LBHB between Catalytic Aspartates**  
Madhusoodan V. Hosur, Amit Das, Vishal Prashar, Smita Mahale, Laurence Serre and Jean-Luc Ferrer
- 16:20 OB23-203 **Structural Basis for Recognition of High Mannose-Type Glycan by Canine Cargo Receptor VIP36**  
Tadashi Satoh, Nathan Cowieson, Wataru Hakamata, Masaaki Kurihara, Hiroko Ideo, Ryuichi Kato, Katsuko Yamashita and Soichi Wakatsuki
- 16:50 OB23-204 **Structural Basis on the Catalytic Reaction Mechanism of Novel 1,2- $\alpha$ -L Fucosidase (AfcA) from *Bifidobacterium bifidum***  
Masamichi Nagae, Atsuko Tsuchiya, Takane Katayama, Kenji Yamamoto, Soichi Wakatsuki and Ryuichi Kato

**Oral Session 9 (15:20-17:20)**

**Conference Room 101/102**

**Dynamic Aspects of Molecular Crystals**

*Chair: Keiichiro Ogawa / Co-Chair: Ian Williams*

- 15:20 OC23-201 **Molecular Dynamics in Crystals on the Basis of X-ray Thermal Parameters and NQR Data in Organic and Inorganic Chlorine Compounds**  
L. Ramu and R. Chandramani
- 15:40 OC23-202 **An Intermediate State in Phase Transition Cycles of  $\text{Na}_2\text{dGMP}$  Hydrate**  
Shigefumi Yamamura, Tadashi Moriguchi, Shigetaka Yoneda and Yoko Sugawara

- 16:00 OC23-203 **X-ray Diffraction Analyses of Cis-Trans Photoisomerization of Olefins**  
Jun Harada, Mayuko Harakawa and Keiichiro Ogawa
- 16:20 OC23-204 **Temperature Dependence of Crystalline State Photoisomerization of an Organo-Dirhodium Dithionite Complex**  
Yoshiki Ozawa, Takae Yonezawa, Tomomi Yokoyama, Minoru Mitsumi, Koshiro Toriumi, Hidetaka Nakai, Yoshihito Hayashi and Kiyoshi Isobe
- 16:40 OC22-205 **Dynamic Structural Change in the Gas Adsorption Process on Microporous Coordination Polymer**  
Yoshiki Kubota, Masaki Takata, Ryotaro Matsuda, Ryo Kitaura, Susumu Kitagawa and Tatsuo C. Kobayashi
- 17:00 OC23-206 **100ps-Resolved X-ray Diffraction at the NW14A, Photon Factory Advanced Ring**  
Shin-ichi Adachi, Shunsuke Nozawa, Ryoko Tazaki, Laurent Guerin, Kohei Ichiyangagi, Matthieu Chollet, Tokushi Sato, Ayana Tomita, Eric Collet, Marylise Buron-Le Cointe, Johan Hebert, Herve Cailleau, Hiroshi Sawa, Hiroshi Kawata and Shin-ya Koshihara

**Keynote Lecture 4 (17:40-18:30)**

*Main Convention Hall*

*Chair: Brendan J. Kennedy*

- 17:40 K23-301 **Structures and Phase Transitions in Perovskites - Sorting out the Subtleties**  
Christopher J. Howard

## Poster Sessions

November 21, Tuesday

- P21-003 **Valence Transitions and Oxygen Vacancies in  $\text{Ba}_2\text{LnSn}_x\text{Sb}_{1-x}\text{O}_{6-\delta}$**   
Paul Saines and Brendan Kennedy
- P21-006 **Crystal structure of the parent misfit-layered cobalt oxide  $[\text{Sr}_2\text{O}_2]_q\text{CoO}_2$**   
Takuro Nagai, Kei Sakai, Maarit Karppinen, Toru Asaka, Koji Kimoto, Atsushi Yamazaki, Hisao Yamauchi and Yoshio Matsui
- P21-009 **X-ray reflectometry and diffraction study of Co(Pt)/AlN annealed multilayer film**  
Takashi Harumoto, Yasuaki Hodumi and Yoshio Nakamura
- P21-012 **Observation of the photoinduced phase transition of the spin-Peierls organic radical crystal TTTA with powder photodiffraction**  
Pance Naumov, Jonathan Hill, Masahiko Tanaka and Kenji Sakurai
- P21-015 **Ab-initio Structure Determination of 1-(2-Hydroxy-5-methoxy-4-methyl-phenyl)-ethanone and 1-(2-Benzyloxy-5-methoxy-4-methyl-phenyl)-ethanone from Laboratory X-ray Powder Data**  
Swastik Mondal and Monika Mukherjee
- P21-018 **Isostructural relationship of  $(\text{Rb}_2\text{H}_2\text{O})\text{C}_2\text{O}_4$  to  $(\text{Ti}_2)\text{C}_2\text{O}_4$ : substitution of one water molecule for two lone electron pairs**  
Takuya Echigo and Mitsuyoshi Kimata
- P21-021 **An analysis of the different behavior displayed by OMCTS and 6CB molecules confined between mica surfaces**  
Fabio Pichierra, Masashi Mizukami, Kenichi Kusakabe and Kazue Kurihara
- P21-024 **Characterization of arsenic accumulating minerals in the iron sediments by SR  $\mu$ -XRF imaging,  $\mu$ -XAFS and XRD**  
Satoshi Endo, Izumi Nakai, Akiko Hokura, Yasuhiro Kato and Yasuko Terada

- P21-027 **Crystal growth and structure refinement of spinel-type  $\text{Li}_4\text{Ti}_5\text{O}_{12}$**   
Kunimitsu Kataoka, Yasuhiko Takahshi, Norihito Kijima, Junji Akimoto and Ken-ichi Ohshima
- P21-030 **Low temperature XRD analysis of  $\text{BaTiO}_3$**   
Koichi Ishibashi, Kazuyosi Arai, Ryuji Matsuo and Katsuhiko Inaba
- P21-033 **Structural Analysis of Chrysocolla by Anomalous X-ray Scattering (AXS) Coupled with Reverse Monte Carlo (RMC) Simulation**  
Yasutaka Takemaru, Kazumasa Sugiyama and Masatoshi Saito
- P21-036 **Vapor induced solid-state phase transition and photoreactivity change investigated by *ab initio* powder crystal structure determination**  
Kotaro Fujii, Yasunari Ashida, Hidehiro Uekusa, Shinya Hirano, Shinji Toyota and Fumio Toda
- P21-039 **Lattice parameter determination by using fitting in Hough space of CBED pattern**  
Yosifumi Yasuda and Koh Saito
- P21-042 **Crystal and molecular structure investigation of *cis*-(+)-3-Acetoxy-2-(4-methoxyphenyl)-4-oxo-2,3,4,5-tetrahydro-1,5-benzothiazepine-1-oxide**  
A. David Stephen, K. A. Nirmala, N. Kalyanam and P. Kumaradhas
- P21-060 **Crystal structure analysis and microwave dielectric properties of  $\text{LaAlO}_3\text{-SrTiO}_3$  solid solutions**  
Yumi Inagaki, Shotaro Suzuki, Isao Kagomiya, Ken-ichi Kakimoto, Hitoshi Ohsato, Katsuhiko Sasaki, Kotaro Kuroda and Takeshi Shimada
- P21-063 **A New Ammonium Borogermanate Made of Infinite Chain Building Blocks Synthesized by Flux Method**  
Jing-Tai Zhao, Ding-Bang Xiong, Hao-Hong Chen, Man-Rong Li and Xin-Xin Yang
- P21-066 **Flux Synthesis of New Bis(Salicylato)borates**  
Alex S-F. Au-Yeung, Mingmei Wu, Gavin Wan, Herman Sung and Ian Williams

- P21-069 **Hydrothermal Crystallization of Salts and Adducts of Tetrahydropalmitine (THP) - A Component From Traditional Chinese Medicine**  
Fanny Shek, Wan-Yee Wong, Herman Sung, Hong Xue and Ian Williams
- P21-072 **Dimensional and Structural Control of Magnesium Tartrate Coordination Polymers**  
Pokka Pang, John Cha, Andy Leung, Herman Sung, Alvin Siu, Yu-fong Yen and Ian Williams
- P21-075 **Group 13 Tartrate and Oxalate Hydroxides**  
Herman Sung, Alex Au-Yeung, Pokka Pang and Ian Williams
- P21-078 **Correlations between interface structures and magnetic properties of Co/Cu multilayers sputter-grown on Ta buffers**  
Kotaro Ishiji and Hiroo Hashizume
- P21-081 **Spin crossover phenomenon of  $\mu$ -bpt dinuclear one-dimensional complexes with different bridge ligands**  
Szu-Miao Chen, Yu Wang, Sheu Chou Fu, Chen Ko Wa and Lee Gene Hsiang
- P21-084 **Fabrication and characterization of Electrodeposited Aluminum Nanocrystalline**  
Delphic Chen, Han-Hong Wang and Jui-Chao Kuo
- P21-087 **Small imperfection causes a very small molecule to pack in a very large cell: Sodium saccharinate 1.875 hydrate with unit cell of 15.6 nm<sup>3</sup>**  
Pance Naumov, Gligor Jovanovski, Orhideja Grupce, Branko Kaitner, David Rae and Seik Weng Ng
- P21-090 **A new 3-D incommensurate structure in the Bi-Re-O system**  
Neeraj Sharma and Chris Ling
- P21-093 **Identical One Dimensional Molecular Assembly in Conformational Polymorphs of Racemic 2,4-di-O-Acetyl 6-O-Tosyl -myo-Inositol 1,3,5-Orthoformate**  
K. Manoj, R. Gonnade, M. Bhadbhade and M. Shashidhar

- P21-096 **Crystal structure and optical properties of  $(\text{Ga}_{1-x}\text{Zn}_x)(\text{N}_{1-x}\text{O}_x)$  oxynitride photocatalyst ( $x = 0.13$ )**  
Yong Phat, Masatomo Yashima, Kazuhiko Maeda, Kentaro Teramura, Tsuyoshi Takada and Kazunari Domen
- P21-099 **Supramolecular Structure of Cocrystallized Catechol and Hexamine**  
Kadsada Sala and Kenneth Haller
- P21-102 **Correlation between  $\text{H}_2$  gas sensitivity and structure of o-, m- and p-dipyridyldiketopyrrolopyrroles as viewed from the electron delocalization within the molecule and the crystal structure**  
Tsuyoshi Hirota, Tomohiko Imoda, Hiroo Takahashi and Jin Mizuguchi
- P21-105 **Structural Systematics of Complexes of Lanthanoid Picrates with Unidentate O-donor Ligands**  
Eric Chan, Allan White, Brian Skelton and Jack Harrowfield
- P21-108 **X-ray structural study of manganese intercalated titanium disulfides**  
Takuro Kawasaki and Ken-ichi Ohshima
- P21-111 **Search for the new Pb-free solder materials**  
Son Van Phung, Akira Fujitsuka and Ken-ichi Ohshima
- P21-114 **New Series of Oxalato-Gallophosphate Structures Containing Transition Metal Centers**  
Wen-Ming Chang and Sue-Lein Wang
- P21-117 **Hydrogen gas sensors based upon perylene-imide derivatives with pyridyl rings**  
Kazuyuki Sato, Kazuyuki Hino, Hiroo Takahashi and Jin Mizuguchi
- P21-120 **Crystal structure and microwave dielectric properties of Ni substituted cordierite ceramics**  
Mio Terada, Keizou Kawamura, Isao Kagomiya, Ken-ichi Kakimoto and Hitoshi Ohsato

- P21-123 **Synchrotron X-ray Single-Crystal Structure Analysis of Partially-Disordered Tb<sub>3</sub>RuO<sub>7</sub>**  
Tsuyoshi Suwa, Nobuo Ishizawa and James Hester
- P21-126 **Atomic Short-Range Order in Disordered Pd<sub>2</sub>Mn Alloy**  
Yin Suo, Rokuro Miida, Toetsu Shishido and Ken-ichi Ohshima
- P21-129 **Connection of Supramolecular Clusters with Triphenylmethylamine Disulfonate**  
Shinji Uehara, Norimitsu Tohnai, Ichiro Hisaki and Mikiji Miyata
- P21-132 **Investigation on structural Phase Transition in Langbeinites**  
Tayur Guru Row and Diptikanta Swain
- P21-135 **Chiral Recognition of Racemic Alcohols in Lattice Inclusion Compounds**  
Kazuaki Aburaya, Ichiro Hisaki, Norimitsu Tohnai and Mikiji Miyata
- P21-138 **Processing and characterization of ferroelectric nanostructures**  
Songhak Yoon, Hee Han, Yongjun Park, Min Gyu Kim, Namsoo Shin, Ran Ji, Dietrich Hesse, Marin Alexe, Kornelius Nielsch, Ulrich Goessele and Sunggi Baik
- P21-141 **Structural and magnetic studies on CuMPt<sub>6</sub> (M= 3d elements) ternary alloys**  
Ejaz Ahmed, Yuji Fuji, Miwako Takahashi, Hiroshi Iwasaki and Ken-ichi Ohshima
- P21-144 **Variability in Halogen Interactions: In-situ cryocrystallization of low melting substituted trifluoroacetophenones**  
Deepak Chopra, Vijay Thiruvankatam and Tayur Narasimha Row
- P21-147 **A Tunable Solid-State Luminescence System Consisting of 4,4''-Terphenyldisulfonic Acid and 1,2,4,5-Tetracyanobenzene with Aliphatic Amines**  
Keisuke Inoue, Norimitsu Tohnai, Ichiro Hisaki and Mikiji Miyata

- P21-150 **Ab-initio structure determination of 4-O-(4-methoxybenzoyl)-2-methyl-N-(2-pyridyl)-2H-1,2-benzothiazine-3-carboxamide-1,1-dioxide from laboratory X-ray powder diffraction data**  
Santu Chakraborty, Soumen Ghosh, Sarbani Pal and Alok Kumar Mukherjee
- P21-153 **Anomalous bonding behavior in Racemic 1,1'-Bi-2,2'-naphtholbiscarbonate**  
Tayur Guru Row, Sosale Chandrasekhar, Susanta Kumar Nayak and Guruprasad Kulkarni
- P21-156 **Structural analyses of two N-[(3'-aryl) prop-2'-ynyl]-N, N'-1, 2-phenylene di-p- tosylamides: Supramolecular structure formed by N-H...O, C-H...O, C-H...pi;(arene) interactions**  
Soumen Ghosh and Alok Mukherjee
- P21-159 **Two methods of preparation of Silver nanoparticles in 3-18 nm scale**  
Asal Kiazadeh and Azadeh Tadjarodi
- P21-162 **Crystal structure of the photo-excited state of three-coordinated gold(I) complex**  
Manabu Hoshino, Hidehiro Uekusa, Yoshiki Ozawa and Koshiro Toriumi
- P21-165 **Synthesis and Structures of Organically Modified Zinc Vanadates**  
Samroeng Krachodnok, Kittipong Chainok, Kenneth Haller, Herman Sung, Fanny Shek and Ian Williams
- P21-168 **Charge density distribution of iron atoms on [Fe(II)(bpy)<sub>3</sub>][Fe(II)<sub>2</sub>(ox)<sub>3</sub>] complex**  
Jey Jau Lee and Yu Wang
- P21-184 **Purification, Crystallization and Preliminary analysis of Hemoglobin from Turkey (Meleagiris gallopova) and Domestic Pigeon (Columba livia)**  
Charles Packianathan, Sundaresan Sigamani, Neelakandan Kamariah, Palani Kandavel and Ponnuswamy Mondikalipudur Nanjapa goundar

- P21-187 **Crystal Structures of the dTDP-4-keto-2,3,6-trideoxy-3-aminohexose Reductase (DnmV) from *Streptomyces peucetius*: Implications for the Inhibition and Catalytic Mechanisms**  
Yi-Wei Chang, Chih-Chien Wu, Yuh-Ju Sun, Hsien-Tai Chiu and Chwan-Deng Hsiao
- P21-190 **Crystal Structure of the Human FOXK1a-DNA Complex and Its Implications on the Diverse Binding Specificity of Winged Helix/Forkhead Proteins**  
Kuang-Lei Tsai, Cheng-Yang Huang, Chia-Hao Chang, Yuh-Ju Sun, Woei-Jer Chuang and Chwan-Deng Hsiao
- P21-193 **Structural and biochemical characterization of circadian clock related protein Pex in *Synechococcus* sp. Strain PCC 7942**  
Kyouhei Arita, Kumiko Igari, Mayuko Akaboshi, Toshiyuki Shimizu, Hiroshi Hashimoto, Shinsuke Kutsuna and Mamoru Sato
- P21-196 **Coupling crystallography with kinetic studies leads to identification of a previously unknown binding pocket**  
Nyssa Drinkwater, Christine Gee, Joel Tyndall, Gary Grunewald, Wu Qian, Michael McLeish and Jennifer Martin
- P21-199 **A new class of oxidoreductases: structure and function of DsbA3 from *Wolbachia pipientis***  
Mareike Kurz, Begona Heras, Inaki Iturbe-Ormaetxe, Scott O'Neill and Jenny Martin
- P21-202 **Crystal structure of archaeal photolyase with two FAD molecules**  
Masahiro Fujihashi, Nobutaka Numoto, Yukiko Kobayashi, Akira Mizushima, Masaya Tsujimura, Akira Nakamura, Yutaka Kawarabayasi and Kunio Miki
- P21-205 **Crystal structures of M11L in the presence and absence of a Bak BH3 domain: structural insight into virus-mediated inhibition of apoptosis**  
Marc Kvangsakul, Mark Van Delft, Walter Fairlie, Jacqui Gulbis, David Huang and Peter Colman

- P21-208 **First Results of Axiom 200, a High-speed, Photon-counting X-Ray Area Detector**  
Martin Adam, Matt Benning, Yacouba Diawara, Roger Durst and Bram Schierbeek
- P21-211 **Developments In High-Throughput Crystallography For the Home Laboratory**  
Martin Adam, Matthew Benning and Sue Byram
- P21-214 **Rab27b structure swaps under GDP binding**  
Leonard Chavas, Seiji Torii, Hironari Kamikubo, Masato Kawasaki, Kentaro Ihara, Ryuichi Kato, Mikio Kataoka, Tetsuro Izumi and Soichi Wakatsuki
- P21-217 **Water-mediated crystal transformation of D-xylose isomerase**  
Masanori Ootaki, Hiroyuki Konosu, Hideaki Tagusagawa, Shigefumi Yamamura and Yoko Sugawara
- P21-220 **Crystal structure of bispecific antibody R310 against modified protein and DNA with oxidized lipids**  
Sohei Ito, Mitsugu Akagawa and Koji Uchida
- P21-223 **Isolation, Purification and Crystallization of Ribosome inactivating protein from Barley (*Hordeum vulgare*)**  
Etti Sundaresan, Karthe Ponnuraj and Shanmugam Guruswamy
- P21-226 **ADP-Ribose Pyrophosphatase from *Thermus thermophilus* HB8, as A Target for Time-Resolved X-Ray Crystallography**  
Kentaro Kai, Ikuko Miyahara, Noriko Nakagawa, Seiki Kuramitsu and Nobuo Kamiya
- P21-229 **Structural analysis of Tollip C2 domain**  
Masato Akutsu, Masato Kawasaki, Yohei Katoh, Ryuichi Kato, Kazuhisa Nakayama and Soichi Wakatsuki
- P21-232 **A 3D visualization system, VESTA, for electronic and structural analysis**  
Koichi Momma and Fujio Izumi

- P21-235 **Crystallization and preliminary X-ray studies of a ferredoxin-NAD(P)<sup>+</sup> reductase from the green sulfur bacterium *Chlorobium tepidum***  
Norifumi Muraki, Daisuke Seo, Tomoo Shiba, Hidehiro Sakurai and Genji Kurisu
- P21-238 **Crystal structure of Formin Homology 2 domain of human DAAM1**  
Shuya Fukai, Masami Yamashita, Tomohito Higashi, Yusuke Sato, Ryutaro Shirakawa, Toru Kita, Hisanori Horiuchi and Osamu Nureki
- P21-241 **The oligomerization state of SKD1 is regulated by ATP**  
Michio Inoue, Masato Kawasaki, Hironari Kamikubo, Mikio Kataoka, Ryuichi Kato, Tamotsu Yoshimori and Soichi Wakatsuki
- P21-244 **The crystal structure of cellulase module Cel44A from *Clostridium thermocellum***  
Yu Kitago, Shuichi Karita, Nobuhisa Watanabe, Kazuo Sakka and Isao Tanaka
- P21-247 **Crystal structures of the CERT START domain in complex with ceramides and specific inhibitors reveal recognition and transport mechanisms of ceramides**  
Norio Kudo, Keigo Kumagai, Soichi Wakatsuki, Masahiro Nishijima, Kentaro Hanada and Ryuichi Kato
- P21-250 **Rational Design of a Novel Molecular Switch for Nano-Biotechnology**  
Mohammad Yousef, Nicole Bischoff, Collin Dyer, Walt Baase and Brian Matthews
- P21-253 **The Development of Nervous System in *Drosophila*; a Structural Approach**  
Mohammad Yousef and Brian Matthews
- P21-256 **New mechanism for broad substrate-specificity of enzymes**  
Teruya Nakamura, Hiroyuki Kamiya, Masaki Mishima, Sachiko Toma, Shinji Ikemizu, Masahiro Shirakawa, Yusaku Nakabeppu and Yuriko Yamagata

- P21-259 **Crystal Structure of Phospholipase A2 Complex with Indomethacin at 1.4 Å Resolution Reveals a Non-Competitive Ligand-Binding Site within the Hydrophobic Channel**  
Nagendra Singh, R. Prem Kumar, Sujata Sharma, Marcus Perbandt, Punit Kaur, Christian Betzel and Tej Singh
- P21-262 **Crystal Structures of the complexes of C-terminal lobe of lactoferrin with NSAIDs : Structural basis of the prevention of NSAID induced gastropathy by lactoferrin revealed**  
Mau Sinha, Sujata Sharma, Nagendra Singh and Tej Singh
- P21-265 **Refinement of high resolution X-ray structure; the case of Taka-amylase A and Lysozyme**  
Akifumi Higashiura, Hiroaki Tanaka, Koji Inaka, Masaru Sato, Shigeru Sugiyama, Sachiko Takahashi, Mari Yamanaka, Moritoshi Motohara, Satoshi Sano, Tomoyuki Kobayashi, Mamoru Suzuki, Tetsuo Tanaka and Atsushi Nakagawa
- P21-268 **Loop and scaffold of serine protease inhibitors: role in religation and specificity**  
Susmita Khamrui, Jhimli Dasgupta, Jiban Dattagupta and Udayaditya Sen
- P21-271 **Crystal structure of goat lactoperoxidase at 3.5 Å resolution**  
Amit Singh, E.S. Ethayathulla, Nagendra Singh, Sujata Sharma and Tej Singh
- P21-274 **Sugar recognition by lactoferrin: Crystal structure of the complex formed between C-lobe of bovine lactoferrin and a pentasaccharide at 2.38 Å resolution**  
Rishi Jain, Nagendra Singh, Talat Jabeen, Sujata Sharma, Asha Bhushan and Tej Singh
- P21-277 **Antifungal activities of lactoferrin peptides: Crystal structural studies of complexes formed between fungal protease proteinase K and lactoferrin/designed peptides**  
R. Prem Kumar, Amit Singh, Nagendra Singh, Sujata Sharma, Asha Bhushan, Punit Kaur and T. Singh

- P21-280 **Crystal structures of the complexes of secretory glycoproteins with designed peptides**  
A.S. Ethayathulla, Devendra Srivastava, Janesh Kumar, Rishi Somvanshi, Nagendra Singh, Sujata Sharma, Sharmistha Dey, Asha Bhushan and T. Singh
- P21-283 **Crystal structure of the Buffalo lactoperoxidase complex with thiocyanate at 2.75 Å resolution**  
Ishfaq Sheikh, A. Ethayathulla, Amit Singh, Nagendra Singh, Sujata Sharma and T. Singh
- P21-286 **Recognition of Sugar Modules by C-Terminal Half (C-Lobe) of Lactoferrin: Crystal Structure of C-Lobe Complexes with Various Saccharides**  
Rafia Mir, Sujata Sharma, Nagendra Singh, Mau Sinha, A. Ethayathulla, R. Prem Kumar, Punit Kaur and Tej P. Singh
- P21-289 **Specific and non-specific interactions of water molecules between protein and DNA**  
Chin-Yu Chen, Tzu-Ping Ko, Chi-Rung Lee and Andrew H.-J. Wang
- P21-292 **Membrane Protein Crystallization under High Pressure**  
Hiroshi Yoshikawa, Shinya Nakata, Ryota Murai, Tomoya Kitatani, Maki Syou, Hiroaki Adachi, Tsuyoshi Inoue, Hiroyoshi Matsumura, Kazufumi Takano, Satoshi Murakami, Yusuke Mori and Takatomo Sasaki
- P21-295 **Crystal Structure of a Bacteriophage-associated Hyaluronate Lyase**  
Parul Mishra, V. Bhakuni, R. Prem Kumar, Nagendra Singh, Sujata Sharma, P. Kaur and Tej P. Singh
- P21-298 **Design of Specific Peptide Inhibitors of Phospholipase A2: Crystal Structures of two Complexes of Phospholipase A2 with Two Pentapeptides**  
Rishi Somvanshi, Nagendra Singh, Sujata Sharma, Markus Perbandt, Christian Betzel, Sharmistha Dey and Tej Singh

## November 22, Wednesday

- P22-001 **Crystal Structure Analysis of two Aldehyde Substituted Indole Derivatives**  
Palani Kandavelu, Jaisankar P., Srinivasan P.C and Ponnuswamy M.N.
- P22-004 **Structural modulation in the misfit-layered cobalt oxide (CaOH)<sub>k</sub>CoO<sub>2</sub>**  
Masaaki Isobe, Mitsuko Onoda, Mitsuyuki Shizuya, Masahiko Tanaka and Eiji Takayama-Muromachi
- P22-007 **Energy Spectrometer on Diffractometer using Charge-Coupled Device X-ray Detector**  
Hiroshi Abe, Hiroyuki Saitoh, Hironori Nakao, Kazuki Ito and Ken-ichi Ohshima
- P22-010 **Crystallization of n-Hexadecane inside emulsion droplets studied by X-ray Scattering**  
Yuya Shinohara, Tadashi Takamizawa, Satoru Ueno, Isao Kobayashi, Mitsutoshi Nakajima and Yoshiyuki Amemiya
- P22-013 **Reversible thermal gating of photoinduced proton transfer kinetics by cooperative molecular twists in a single crystal**  
Pance Naumov and Kenji Sakurai
- P22-016 **Structural basis for the phase switching of bisaminecopper(II) cations at the thermal limits of lattice stability**  
Pance Naumov, Kenji Sakurai, Toru Asaka and Alexei Belik
- P22-019 **Crystal structure of tricalcium phosphate**  
Yoichi Kawaike, Masatomo Yashima and Masahiko Tanaka
- P22-022 **Design and fabrication of in-situ X-ray diffractometer in Phase- II beam line at IUAC**  
Pawan Kulriya, Fouran Singh, Yogendra Mishra, Amit Kumar, R. Ahuja, Ashok Kothri, R. Dutt, Ambuj Tripathi and D. Avasthi
- P22-025 **Growth process of vapor deposited films of a bisazomethine dye**  
Daisuke Tsuchida, Mie Satoh, Shinya Matsumoto, Takashi Kobayashi, Tetsuya Aoyama and Tatsuo Wada

- P22-028 **XRD applications by using a new area detector**  
Takeyoshi TAGUCHI
- P22-031 **Structural and Dynamical Studies on Protonic Conductor  $K_3H(SeO_4)_2$**   
Fumihito Shikanai, Keisuke Tomiyasu, Ryoji Kiyonagi, Masao Yonemura, Kenji Iwase, Dyah Sulistyantiyas, Tuexun Wurnisha, Kazuhiro Mori, Toru Ishigaki, Itaru Tsukushi, Susumu Ikeda and Takashi Kamiyama
- P22-034 **Photo excited state crystallography of hexanuclear 6-methyl-2-pyridinethiolato copper(I) complex**  
Kimihiro Kimura, Yoshiki Ozawa, Minoru Mitsumi, Koshiro Toriumi and Isamu Kinoshita
- P22-037 **Electron density distribution analysis in the low temperature form of  $LiMn_2O_4$  by X-ray Single-crystal diffraction study**  
Yasuhiko Takahashi, Junji Awaka, Norihito Kijima and Junji Akimoto
- P22-040 **Structural and Physical Properties of Lithium-Ion Deintercalated  $Li_xCoO_2$  Single Crystals**  
Yasuhiko Takahashi, Junji Awaka, Norihito Kijima and Junji Akimoto
- P22-043 **The observation of electron density distribution of thermally excited states in  $CeB_6$  at 430 and 535K**  
Ryoko Makita, Shiro Funahashi, Kiyooki Tanaka, Yoshichika Onuki and Hiroshi Tatewaki
- P22-045 **The development of high-resolution X-ray powder diffractometer using laboratory source for an advanced structural analysis**  
Shinobu Aoyagi, Hiroyuki Suwa, Takeshi Nakashima, Eiji Nishibori and Makoto Sakata
- P22-047 **X-ray and neutron diffraction investigations on electron density distribution in an electride crystals**  
Kiyooki Tanaka, Terutoshi Sakakura, Masashi Watanabe, Yukio Noda, Satoru Matsuishi and Hideo Hosono
- P22-049 **Crystal Structure of the  $[Ru(azpy)_2bpy](PF_6)_2$  Complex (azpy=2-(phenylazo)pyridine, bpy=2,2'-bipyridine)**  
Kanidtha Hansongnern, U. Changsaluk and T-H. Lu

- P22-051 **X-ray structural study of layered compounds  $\text{Co}_x\text{TiS}_2$**   
Takeshi Osakabe, Yasuhiko Takahashi, Takuro Kawasaki and Ken-ichi Ohshima
- P22-053 **Gigantic growth of carbon nanotubes from camphor**  
Mukul Kumar, Naoto Okazaki, Atsushi Iida and Yoshinori Ando
- P22-055 **In-Situ GISAXS Studies on the Evolution of Closed Nanopores in Low-k Organosilicate Dielectric Thin Films**  
Kyeong Sik Jin, Jinhwan Yoon, Kyuyoung Heo and Moonhor Ree
- P22-057 **Lamellar and Crystal Structural Study on Ferroelectric Phase Transition of Vinylidene fluoride-Trifluoroethylene Copolymers by Synchrotron DSC/WAXD/SAXS Simultaneous Measurements**  
H. Masunaga, S. Sasaki, M. Hanesaka, K. Tashiro and M. Takata
- P22-059 **Tetragonal-monoclinic transformation of Na-hollandite**  
Yuichi Michiue
- P22-062 **X-ray twenty-four beam dynamical diffraction in a two-plate crystal cavity of silicon**  
Mau-Sen Chiu, Yu Stetsko and Shih-Lin Chang
- P22-065 **Synthesis, Structure and Luminescence Property of Two Lanthanum Phosphites Hydrate:  $\text{La}_2(\text{H}_2\text{O})_x(\text{HPO}_3)_3$  ( $x=1,2$ )**  
Jing-Tai Zhao, Ding-Bang Xiong, Hao-Hong Chen and Xin-Xin Yang
- P22-068 **In-situ XRD study on the melting process of YBCO thin film with MgO substrate**  
Qunli Rao and Xin Yao
- P22-071 **Molecular Recognition of Aliphatic L-Amino Acids by D-Mandelic acid**  
Taira Kimino, Yukio Takahashi and Isao Fujii
- P22-074 **Neutron Powder Diffraction Studies in  $\text{CaMn}_{1-x}\text{Cu}_x\text{O}_3$  ( $x = 0, 0.20$ )**  
S. Ravi, Manoranjan Kar, S.M. Borah and P.S.R. Krishna

- P22-077 **Synthesis, characterization, and DFT calculations of iridium(III) complexes with tolylterpyridine**  
Naokazu Yoshikawa, Shinichi Yamabe, Hiroshi Takashima, Keiichi Tsukahara, Nobuko Kanehisa and Yasushi Kai
- P22-080 **Liquid structure and mechanical properties of EHD fluid**  
Yuusuke Imai, Hiroshi Abe and Yoshiki Sasaki
- P22-083 **Structural and magnetic studies of atr-based 1-D, 2-D, 3-D frameworks**  
Wei-Lun Ho, Gene-Hsiang Lee, Hwo-Shuenn Sheu and Yu Wang
- P22-086 **Hydrogen Desorption and Absorption Process of NaAlH<sub>4</sub> and Modified NaAlH<sub>4</sub>**  
Chattree Phurat, Nongnuj Muangsin, Pramoch Rangsunvigit, Santi Kulprathipanja and Yindee Suttisawat
- P22-089 **Hydrogen bonding in two solid phases of phenazine-chloranilic acid (1/1) determined at 170 and 93 K**  
Kazuma Gotoh, Tetsuo Asaji and Hiroyuki Ishida
- P22-092 **Crystal and Molecular Structure of 2-(2''-chlorophenoxy)-3,4-dihydro-3-(3'-chloro-4'-fluorophenyl)-2H-[1,3,2] benzoxazaphosphorin 2-oxide**  
Radha Krishna Jadaprolu, Krishnaiah Musali, Y.B. Kiran, Reddy Devendranath C., win Thetmar and Kang P.
- P22-095 **New Microporous Metal-Organic Frameworks with Unusual Structural Features**  
Xiao-Ming Chen
- P22-098 **Crystal Structures, Magnetism, and Spectroscopic Properties of One-dimensional Cyanide-bridged Tb(III)/Dy(III)/Ho(III)/Er(III)-Cr(III) Complexes**  
Takashi Akitsu and Yasuaki Einaga
- P22-101 **Size and Vacancies; Unexpected Phase Transitions in Manganese Perovskites**  
Brendan Kennedy and Qingdi Zhou

- P22-104 **Characterization of niobium substituted potassium tetragonal tungsten bronzes**  
Subrata Roy and Altaf Hussain
- P22-107 **Crystal structure of an organometallic macrocyclic compound**  
Yao-Cheng Shi, Bei-Bei Zhu and Chun-Xia Sui
- P22-110 **Synthesis and Crystal Structures of Novel Zn(II) and Ni(II) Coordination Polymers with 1,4-bis(3-pyridyl)-2,3-diazo-1,3-butadiene Ligands**  
Gene-Hsiang Lee and Hsin-Ta Wang
- P22-113 **Effect of Ga & In Substitution and Swift Heavy Ion Irradiation on Magnetic Properties of Strontium Hexaferrite Crystals**  
Krishen Kumar Bamzai, Balwinder Kaur, Pushkar Nath Kotru, Ravi Kumar and F. Licci
- P22-116 **Immobilization of Rh(PPh<sub>3</sub>)<sub>3</sub>Cl on phosphinated MCM-41 for catalytic hydrogenation and hydroformylation of olefins**  
Shin-Guang Shyu, Hsiu-Mei Lin, Der-Lii Tzou and Shequ-Wen Cheng
- P22-119 **Crystal structure and disorder in the oxide ion conductors Y<sub>1-x</sub>Ta<sub>x</sub>O<sub>1.5+x</sub> (x=0.2 and 0.25)**  
Takayuki Tsuji and Masatomo Yashima
- P22-122 **Crystal structure and textures of the C-type antiferromagnetic manganites by transmission electron microscopy**  
Masahiro Nagao, Toru Asaka, Yutaka Yamauchi, Ryota Hatakeyama, Takuro Nagai, Atsushi Yamazaki, Koji Kimoto, Hideki Kuwahara and Yoshio Matsui
- P22-125 **Structural and Magnetic Study of New LIESST and reverse-LIESST Fe(trz)<sub>1.5</sub>[Au(CN)<sub>2</sub>]<sub>2</sub> Complex**  
Lai-Chin Wu and Yu Wang
- P22-128 **Polymeric Copper(II) Complex Containing Phenanthroline and Bridging Nitrate**  
Panana Kitiphaisalnont and Sutatip Siripaisarnpipat

- P22-131 **Growth and characterization of hollandite-type single crystal**  
Kenjiro Fujimoto, Kenji Takamori and Shigeru Ito
- P22-134 **Order and disorder in heavily Fe-substituted high- $T_c$  superconductors**  
Takashi Mochiku, Yoshiaki Hata, Tuerxun Wuernisha, Kazuhiro Mori, Toru Ishigaki, Takashi Kamiyama, Hiroki Fujii, Hiroshi Yasuoka, Kazuo Kadowaki and Kazuto Hirata
- P22-137 **Structure and phase transition in  $C_5H_{10}NH_2PbI_3$**   
Miwako Takahashi, Yuji Fujii, Takuro Kawasaki, Kataoka Kunimitsu, Masashi Watanabe and Ken-ichi Ohshima
- P22-140 **Approximants for the Al-Co-Si decagonal phase**  
Kazumasa Sugiyama and Hironori Sato
- P22-143 **Systematics of high pressure phase transformation of minerals and compounds containing  $WO_4$  and  $MoO_4$  molecules**  
Shu-Cheng YU, Tony HUANG and Eugene HUANG
- P22-146 **Modulation Structure of Charge Ordering in Nikelates**  
Xiuzhen Yu
- P22-149 **SEM and TEM study of some Wild II cometary particles returned by the NASA Stardust Mission**  
Takashi Mikouchi, Osamu Tachikawa, Kenji Hagiya, Kazumasa Ohsumi and Michael Zolensky
- P22-152 **A new method for characterizing the degree of graphitization of carbon materials by laser Raman spectroscopy**  
Katsumi Suda, Hiromi Ohmiya, Yasuhiro Tanabe and Eiichi Yasuda
- P22-155 **Structural and Thermodynamic Studies on Ferroelectric Molecular Crystal Tricyclohexylmethanol**  
Yasuhisa Yamamura, Hideki Saitoh, Masato Sumita and Kazuya Saito
- P22-158 **An algorithm to solve an n-beam Takagi-Taupin equation for a crystal with an arbitrary shape**  
Kouhei Okitsu, Yoshitaka Yoda, Yasuhiko Imai, Yoshinori Ueji and XiaoWei Zhang

- P22-161 **Sub-micron single crystal structure analysis using micro-focus synchrotron radiation - A development of X-ray pinpoint structure measurement at the SPring-8 (2)**  
 Nobuhiro Yasuda, Haruno Murayama, Jungeun Kim, Yoshimitsu Fukuyama, Yoshiki Ozawa, Kimihiro Kimura, Nobuyuki Kitayama, Shingo Yoshida, Satoshi Wada, Yoshihito Tanaka, Yutaka Moritomo, Shigeru Kimura, Yoshihiro Kuroiwa, Koshiro Toriumi and Masaki Takata
- P22-164 **Synthesis and crystal structure of chloro-hydrido-(6-diphenylphosphanyl-2-hydroxypyridine- $\kappa^2P,N$ )-(6-diphenylphosphanyl-2-pyridonate- $\kappa^2P,N$ )iridium(III) chloroform 1.89-solvate**  
 Tsuneaki Yamagata, Takayuki Miyabayashi, Takeshi Hara and Kazushi Mashima
- P22-167 **Incorporating Transition Metals in Ferroelectric Oxides**  
 Brendan Kennedy, Qingdi Zhou, Scott Mckenzie and Chris Ling
- P22-170 **Angelicaïn : Supramolecular structure generated by O-H...O, C-H...O and C-H... $\pi$  hydrogen bonds, and  $\pi$ - $\pi$  stacking interactions**  
 Sanjeev Goswami, Vivek K. Gupta, R.K. Thappa and S.G. Agarwal
- P22-172 **POLYINFO-A package for selection of aerospace polymers based on crystallographic and related properties**  
 KALYANI VIJAYAN and Mahesh Kumar
- P22-174 **Crystal and molecular structure of 4,5-dimethyl-N-(2-methyl phenyl)-2-[[{(1E)-3,4,5-trimethoxy phenylmethylene] amino}thiophene-3-carboxamide**  
 vasu sriranga vasu, K. A. Nirmala, Deepak Chopra, S. Mohand and J. Saravanan
- P22-176 **Electron charge density study of  $\text{Bi}_4\text{Ti}_3\text{O}_{12}$  and  $\text{Bi}_{3.25}\text{La}_{0.75}\text{Ti}_3\text{O}_{12}$  by MEM/Rietveld analysis**  
 Sayaka Kimura, Su Jae Kim, Chikako Moriyoshi, Yoshihiro Kuroiwa and Yuji Noguchi
- P22-178 **Investigation of the cation ordering in ilmenite-type  $\text{ZnTiO}_3$**   
 Hijiri Kito, Masaki Nakamura, Akira Sato and Haruo Ohashi

- P22-180 **Developing Remote Access for Crystallography**  
Ian M. Atkinson, Douglas du Boulay, Clinton Chee, Kenneth Chiu, Tristan King, Donald F. McMullen, Romain Quilici, Peter Turner and Mathew Wyatt
- P22-182 **Crystal Structure of Catalytic Domain of Japanese Encephalitis Virus NS3 Helicase/Nucleoside Triphosphatase at a Resolution 1.8 angstrom**  
Tetsuo Yamashita, Hideaki Unno, Yoshio Mori, Kohji Moriishi, Tomitake Tsukihara and Yoshiharu Matsuura
- P22-185 **A Modeling Study to Curtail the Action of RNR Enzyme Towards Cancer Therapy**  
Sampath Natarajan and Ponnuswamy Mondikalipudur Nanjappa
- P22-188 **Increasing stability of Papain through structure-based protein engineering**  
Debi Choudhury, Sampa Biswas, Chandana Chakrabarti and J.K. Dattagupta
- P22-191 **The structure of Mcl-1 in complex with the Bim BH3 peptide at 1.55 Å resolution**  
Peter Czabotar, Erinna Lee, Marco Evangelista, David Huang, Walter Fairlie and Peter Colman
- P22-194 **Helical twists of model peptides strongly support our 7/2-helical model for collagen**  
Kenji Okuyama, Chizuru Hongo and Keiichi Noguchi
- P22-197 **How winged helix/forkhead proteins using less conserved residues to regulate diverse DNA sequence**  
Chwan-Deng Hsiao
- P22-200 **Down-puckering of Hyp destabilizes the triple-helical structure**  
Chizuru Hongo, Kenji Okuyama, Keiichi Noguchi, Shutoku Ebisusaki and Norikazu Nishino
- P22-203 **Crystal structure of human Fyn kinase domain complexed with non-specific inhibitor staurosporine**  
Takayoshi Kinoshita, Mamoru Matsubara, Hiroshi Ishiguro, Kouki Okita and Toshiji Tada

- P22-206 **Crystallographic study on two types of threonyl-tRNA synthetases from *Sulfolobus tokodaii***  
Yuichiro Miyashita, Satoru Shimizu, Yoshiteru Sato, Ella Czarina Magat Juan, Kaoru Suzuki, Takeshi Sekiguchi and Akio Takenaka
- P22-209 **A minimum protein-splicing domain designed based on the crystal structure**  
Yudai Ishii, Tetsuo Takahashi and Ryuta Mizutani
- P22-212 **Crystallization and preliminary crystallographic analysis of  $\beta$ -trichosanthin, an isoform of trichosanthin from the root tuber of *Trichosanthe kirilowii***  
Minghuang Chen, Xiaomin Hou, Qi Peng, Feng Yang, Liqing Chen and Mingdong Huang
- P22-215 **Crystal structure of the heme oxygenase complexed with  $\alpha$ -meso hydroxyheme, a high reactive intermediate**  
Masaki Unno and Masao Ikeda-Saito
- P22-218 **Crystal Structure and Substrate Recognition of Aminopeptidase N**  
Yoshitaka Nakajima, Yuko Onohara, Kiyoshi Ito, Yue Xu, Kanako Nakashima, Futoshi Matsubara and Tadashi Yoshimoto
- P22-221 **Crystal structure analyses of S-adenosyl-L-homocysteine hydrolase from *Plasmodium falciparum* complexed with inhibitors**  
Nobutada Tanaka, Yoshio Kusakabe, Ken-ichi Aoki, Masayuki Nakanishi, Yukio Kitade and Kazuo Nakamura
- P22-224 **Structural Analysis of Mutant *E. coli* Dihydroorotase: Role of a Conformational Change in Catalysis**  
Mihwa Lee, Megan Maher, Richard Christopherson and J. Mitchell Guss
- P22-227 **Structural basis for neutral endopeptidase 24.11 recognition by ERM proteins**  
Shin-ichi Terawaki, Ken Kitano and Toshio Hakoshima
- P22-230 **Crystallographic studies of FAD bound form of salicylate hydroxylase from *Pseudomonas putida* S-1**  
Yoshihiko Watanabe, Akiko Kita, Kuniharu Ohnishi, Kenzi Suzuki, Kunio Miki and Yukio Morimoto

- P22-233 **Crystal structure of Nanos**  
Hiroshi Hashimoto, Shigeta Kawaguchi, Naoki Shichijo, Satoru Unzai,  
Keishi Nakamura, Toshiyuki Shimizu, Yutaka Tamaru and Mamoru Sato
- P22-236 **Effective Use of Gel-Tube Method**  
Hiroaki Tanaka, Mari Yamanaka, Koji Inaka, Masaru Sato, Sachiko  
Takahashi, Shigeru Sugiyama, Satoshi Sano, Moritoshi Motohara,  
Tomoyuki Kobahashi and Tetsuo Tanaka
- P22-239 **Chemistry of New Steroidal Antiandrogens and  
5 $\alpha$ -Reductase: 16 $\beta$ -methyl-17 $\alpha$ -propionyloxypregna-4,  
6-diene-3,20-dione**  
MANUEL SORIANO and Eugene Bratoeff
- P22-242 **Introduction of the Protein Data Bank Japan (PDBj)**  
Takashi Kosada, Reiko Igarashi, Yumiko Kengaku, Yasuyo Morita, Kanna  
Matsuura, Masami Kusunoki, Yukiko Shimizu, Reiko Yamashita and  
Haruki Nakamura
- P22-245 **SPRing-8 Structural Biology Beamlines / Current Status of  
Automatic Beamline Operation**  
Go Ueno, Kazuya Hasegawa, Nobuo Okazaki, Hironori Murakami, Raita  
Hirose, Atsushi Nisawa, Takashi Kumasaka and Masaki Yamamoto
- P22-248 **Zeta potential measurements for evaluation the quality of  
protein samples for crystallization**  
Kohei Shiba, Koji Inaka, Shigeru Sugiyama, Kyoko Ogasahara and  
Atsushi Nakagawa
- P22-251 **Structural analyses of substrate-free and substrate-bound  
forms of phycocyanobilin:ferredoxin oxidoreductase**  
Masakazu Sugishima, Yoshinori Hagiwara, Yasuhiro Takahashi and  
Keiichi Fukuyama
- P22-254 **Structure Determination of a novel Phycoerythrin C from a  
hemihedral twinned crystal**  
Punit Kaur, Badrish Soni, A. Ethayathulla, Imtaiyaz Hassan, Savita Yadav,  
Datta Madamwar and Tej Singh

- P22-257 **Control system for high-throughput protein crystallography experiments**  
Yury Gaponov, Yury Gaponov, Naohiro Matsugaki, Nobuo Honda, Kumiko Sasajima, Noriyuki Igarashi, Masahiko Hiraki, Yusuke Yamada and Soichi Wakatsuki
- P22-260 **Crystal structure of the RUN domain of the Rap2 interacting protein x**  
Mutsuko Kukimoto-Niino, Tetsuo Takagi, Ryogo Akasaka, Kazutaka Murayama, Tomomi Uchikubo-Kamo, Takaho Terada, Makoto Inoue, Satoru Watanabe, Akiko Tanaka, Yoshihide Hayashizaki, Takanori Kigawa, Mikako Shirouzu and Shigeyuki Yokoyama
- P22-263 **Crystallographic study of *Pyrococcus horikoshii* tryptophanyl-tRNA synthetase**  
Akiko Mizukawa and Michiko Konno
- P22-266 **Current status of IBARAKI Biological diffractometer in J-PARC - Optimization of design parameters**  
Katsuhiko Kusaka, Takashi Ohhara, Ichiro Tanaka, Nobuo Niimura, Kazuo Kurihara, Takaaki Hosoya, Tomoji Ozeki, Kazuya Aizawa, Yukio Morii, Masatoshi Arai, Makoto Hayashi, Kazuhiro Ebata and Yoshiki Takano
- P22-269 **Crystallographic analysis of CHP1 and DRAK2**  
Youichi Naoe, Kyouhei Arita, Hiroshi Hashimoto, Hiroshi Kanazawa, Mamoru Sato and Toshiyuki Shimizu
- P22-272 **Structural basis of the sphingomyelin phosphodiesterase activity in neutral sphingomyelinase from *Bacillus cereus***  
Hideo Ago, Masataka Oda, Masaya Takahashi, Hideaki Tsuge, Sadayuki Ochi, Nobuhiko Katunuma, Masashi Miyano and Jun Sakurai
- P22-275 **Current status of IBARAKI Biological diffractometer in J-PARC -General View-**  
Ichiro Tanaka, Nobuo Niimura, Takashi Ohhara, Kazuo Kurihara, Katsuhiko Kusaka, Takaaki Hosoya, Tomoji Ozeki, Kazuya Aizawa, Yukio Morii, Masatoshi Arai, Makoto Hayashi, Kazuhiro Ebata and Yoshiki Takano

- P22-278 **Crystal structure of a pro-form of a bacterial leucyl aminopeptidase**  
Satoru Nirasawa, Masataka Horiuch, Nobuo Suzuki, Kiyohiro Takahashi, Fuyuhiko Inagaki and Kiyoshi Hayashi
- P22-281 **Crystal structure of human UDP-GalNAc: polypeptide  $\alpha$ -N-acetylgalactosaminyltransferase 10 (pp-GalNAc-T10)**  
Tomoo Shiba, Tomomi Kubota, Shigemi Sugioka, Sanae Furukawa, Hiromichi Sawaki, Ryuich Kato, Soichi Wakatsuki and Hisashi Narimatsu
- P22-284 **High-Throughput and Automated Protein Crystallography at the Photon Factory**  
Masahiko Hiraki, Ryuichi Kato, Masanori Kobayashi, Yusuke Yamada, Naohiro Matsugaki, Noriyuki Igarashi, Yurii Gaponov and Soichi Wakatsuki
- P22-287 **The crystal structure of a conserved hypothetical protein, TTHA0132 from *Thermus thermophilus* HB8 with homology to the non-histone domain of macroH2A**  
Seiichiro Kishishita, Kazutaka Murayama, Takaho Terada, Mikako Shirouzu, Seiki Kuramitsu and Shigeyuki Yokoyama
- P22-290 **Current Status of Public Beamlines for Protein Crystallography at SPring-8**  
Masahide KAWAMOTO, Kazuya HASEGAWA, Nobutaka SHIMIZU, Hisanobu SAKAI, Tetsuya SHIMIZU, Kunio HIRATA, Atsushi NISAWA and Masaki YAMAMOTO
- P22-293 **Structural insights into the Sec-tRNA(SeC) syntheses in archaea**  
Yuhei Arais, Hiroyuki Oshikane, Shuya Fukai, Dieter Soll, Ryuichiro Ishitani and Osamu Nureki
- P22-296 **Structural studies on the SUF proteins involved in the biogenesis of iron-sulfur clusters**  
Norika Sumi, Kei Wada, Shintaro Kitaoka, Kei Suzuki, Yuko Hasegawa, Yoshiko Minami, Yasuhiro Takahashi and Keiichi Fukuyama
- P22-299 **The Crystallographic Study of Apple Latent Spherical Virus**  
Hisashi Naitow, Masamichi Isogai, Nobuyuki Yoshikawa and Shigeyuki Yokoyama

- P22-301 **Crystal structures of crotocebraneic acid and neocrotocebraneic acid**  
Wilaiwon Tirawanich, Thapong Teerawatananond, Narongsak Chaichit and Amorn Petsom
- P22-303 **Crystallographic Study of *Saccharomyces cerevisiae* Vac8p**  
Yoshiki Nagano, Shuya Fukai and Osamu Nureki
- P22-305 **CCP4 : 6.0 and beyond**  
Charles C. Ballard
- P22-307 **Construction of Comprehensive Protein-Analysis Database and its Applications**  
Ryogo Akasaka, Machiko Hirafuji-Yamaguchi, Akiko Urushibata, Kazutaka Murayama, Chie Takemoto-Hori, Noboru Ohsawa, Mutsuko Kukimoto-Niino, Kanna Motoyama, Mari Aoki, Takaho Terada, Mikako Shirouzu and Shigeyuki Yokoyama
- P22-309 **Crystal Structure of Human Prostacyclin Synthase**  
Chia-Wang Chiang, Hui-Chun Yeh, Lee-Ho Wang and Nei-Li Chan
- P22-311 **Crystal structure of *O*<sup>6</sup>-methylguanine-DNA methyltransferase**  
Masaru Tsunoda and Nakamura Kazuo
- P22-313 **Non-canonical SH3/Pro interface structure of the AMAP1 and cortactin binding**  
Harumi Hosaka, Shigeru Hashimoto, Mayumi Hirose, Ari Hashimoto, Masaki Morishige, Atsuko Yamada, Ken-ichi Akagi, Eiji Ogawa, Chitose Oneyama, Tsutomu Agatsuma, Masato Okada, Hidenori Kobayashi, Hiromi Wada, Hirofumi Nakano, Takahisa Ikegami, Atsushi Nakagawa and Hisataka Sabe
- P22-315 **Crystallization and Structural Analysis of Archaeal Homolog of Ski-2 type RNA helicase from the Hyperthermophilic Archaeon *Pyrococcus horikoshii***  
Takashi Nakashima, Xiaodong Zhang, Yoshimitsu Kakuta and Makoto Kimura

- P22-317 **On A Method of Generating Space Groups and Calculating Structure Factors By Coset Decomposition**  
RYOKO OISHI, Masao Yonemura, Fumihito Shikanai, Shuki Torii, Toru Ishigaki and Takashi Kamiyama
- P22-319 **Crystal structure analyses of reconstituted water-soluble chlorophyll proteins from kale**  
Hiroshi Hara, Hiroyuki Satoh, Isao Oonishi and Akira Uchida
- P22-321 **Structure basis for recognition of the 3'-terminus of aminoacyl-tRNA by Leucyl/Phenylalanyl-tRNA protein transferase**  
Kyoko Suto, Yoshihiro Shimizu and Kozo Tomita
- P22-323 **Structural Studies of a New Class of Binding-Proteins Secreted during the Narrow period of Initial Involution**  
Tej Singh, Devendra Srivastava, Janesh Kumar, Nagendra Singh, Rishi Somvanshi, Sujata Sharma, Sharmistha Dey and Asha Bhushan
- P22-325 **X-ray crystallographic analysis of *CooA* homologue from *Carboxydothemus hydrogenoformans***  
Hirofumi Komori, Sayaka Inagaki, Shiro Yoshioka, Shigetoshi Aono and Yoshiki Higuchi
- P22-327 **The Crystal structure of orotidine 5'-monophosphate decarboxylase from the human malaria parasite *Plasmodium falciparum***  
Keiji Tokuoka, Sudaratana Krungkrai, Yukiko Kusakari, Tsuyoshi Inoue, Hiroaki Adachi, Hiroyoshi Matsumura, Kazufumi Takano, Satoshi Murakami, Yusuke Mori, Yasushi Kai, Krungkrai Jerapan and Toshihiro Horii
- P22-329 **Cation- $\pi$  interaction revealed by crystal structure of thermoalkalophilic lipase: relationship between enzymatic activity and alkali metal cation**  
Hiroyoshi Matsumura, Takahiko Yamamoto, Leow Thean Chor, Abu Bakar Salleh, Tsuyoshi Inoue, Yasushi Kai and Raja Noor Zaliha Raja Abdul Rahman
- P22-331 **X-ray scattering studies on structure of an enzyme protein in solution**  
Kyeong Sik Jin, Sangwoo Jin and Moonhor Ree

## November 23, Thursday

- P23-002 **Isomorphism and Polymorphism of the Crystal Structures of Cholesterol Derivatives**  
Young-Ja Park
- P23-005 **Thermal and Athermal Structure Change of  $\text{Fe}_{3-x}\text{Ti}_x\text{O}_4$  spinel solid solution**  
Takamitsu Yamanaka, Tetsuro Mine, Sachiko Asogawa and Yuki Nakamoto
- P23-008 **X-ray diffraction and XMCD studies for magnetic-related Co oxides**  
Satoshi Sasaki, Norio Shimizu, Takeshi Ohno, Takayasu Hanashima, Koichi Ohkubo, Maki Okube and Takeharu Mori
- P23-011 **A New Large Radius Imaging Plate Camera System for the Diffractometer in BL15XU of SPring-8 for High-resolution and High-throughput Powder Diffraction**  
Masahiko Tanaka, Yoshio Katsuya and Daisuke Nomoto
- P23-014 **Thermally induced saccharinate ligand flips close to ambient temperature**  
Pance Naumov, Gligor Jovanovski and Kenji Sakurai
- P23-017 **Crystal structure of N-(4-fluorophenyl)-2-(((1E)-(4-methoxyphenyl) methylene) amino)-4,5,6,7-tetrahydro-1-benzothiophene-3-carboxamide**  
M. K. Kokila, Dr. Puttaraja, G.N. Anilkumar, S. Mohan and J. Saravanan
- P23-020 **X-ray and Spectroscopic Characterization of Molybdenum doped Lithium and Sodium Tungsten Bronzes**  
KALPANA DEY, Dr. Altaf Hussain and Claus H. Ruscher
- P23-023 **Structure of 1-Cyano, 1-carbethoxy-2- (3'-methoxy-4'-hydroxy) phenyl**  
N. C. Shivaprakash, V. N. Narasimha Murthy, M. K. Sateesh, M. K. Kokila, P. Puttaraja, Geetha M. Kulkarni and M. V. Kulkarni

- P23-026 **Structural and microstructural investigation of tetragonally stabilized ZrO<sub>2</sub> in  $\alpha$ -Al<sub>2</sub>O<sub>3</sub> - ZrO<sub>2</sub> composites: Critical size limit and Oxygen vacancy**  
Apurba Deb, Partha Chatterjee and Siba Prasad Sen Gupta
- P23-029 **PPDA: A program for extracting data from Debye-Scherrer imaging-plate diffractometers**  
James Hester, David Cookson and Brett Hunter
- P23-032 **Crystal Structure of 2-[6-Methylbenzofuran-3-ylmethyl]-5-(morpholin-4-ylmethyl)-6-(4-chlorophenyl)-imidazo [2,1-b][1,3,4]thiadiazole**  
K.V.Arjuna Gowda, Ramakrishna Gowda and Vijay Tiruvankatam
- P23-035 **Interactions between crystallographic domain and magnetic domain in ordered double perovskite**  
Yoshio Matsui, Toru Asaka, Xiuzhen Yu, Yasuhide Tomioka, Yoshio Kaneko, Takuro Nagai, Koji Kimoto, Kazuo Ishizuka and Yoshinori Tokura
- P23-038 **Photo excited state crystallography iodo-bridged dicopper (I) complex**  
Shingo Yoshida, Yoshiki Ozawa, Minoru Mitsumi, Koshiro Toriumi, Nobuhiro Yasuda, Kiyoshi Tsuge, Hiromi Araki and Yoichi Sasaki
- P23-041 **Topological Analysis of Biphenyl**  
Chi-Rung Lee, Chin-Yu Chen, De-Cai Fang and Ting-Hua Tang
- P23-044 **The 4f-EDD quantitative analysis in RB<sub>6</sub> (R=La, Sm) by X-ray diffraction measurement and X-ray AO (atomic orbital) analysis**  
Shiro Funahashi, Kiyooki Tanaka, Fumitoshi Iga and Akira Kunii
- P23-046 **Crystal structure and charge density analysis of the charge- and orbital-ordered phase of La<sub>2-2x</sub>Sr<sub>1+2x</sub>Mn<sub>2</sub>O<sub>7</sub> (x=0.525) using CBED**  
Yoichiro Ogata, Kenji Tsuda, Kazuma Hirota and Youichi Murakami
- P23-048 **Electron density distribution and Topological studies of Copper complex**  
Poomani Kumaradhas, Alvaro De Souza and Tibor Koritzanszky

- P23-050 **Spherical-aberration-corrected HRTEM of Al-Ni-Co decagonal quasicrystals**  
Koh Saitoh, Nobuo Tanaka, Pang Tsai An and Kazuo Ishizuka
- P23-052 **CBED rocking curves of low-order reflections from doped silicon**  
Kenji Tsuda, Hajime Mitsuishi, Masami Terauchi and Kazuo Kawamura
- P23-054 **Structural Analysis of PS-b-PMMA Block Copolymer Thin Films with Grazing Incidence Small-Angle X-ray Scattering**  
Jinhwan Yoon, Byeongdu Lee, Sangwoo Jin, Kyeong Sik Jin, Seung-Yun Yang, Won-Chul Joo, Jin Kon Kim and Moonhor Ree
- P23-056 **In-situ Investigation of Annealing Effect on Higher Order Structure of Polyethylene Thin Films by Synchrotron GISWAXS Measurements**  
Sono SASAKI, Hiroyasu MASUNAGA, Hiroo TAJIRI, Katsuaki INOUE, Hiroshi OKUDA, Atsushi TAKAHARA and Masaki TAKATA
- P23-058 **Crystal Structure of High Pressure Phase of  $MgAl_2O_4$  synthesized at conditions of 2200 K and 41.8GPa**  
Yasuhiro Kudoh, Takahiro Kuribayashi, Yuichiro Sueda and Tetsuo Irifune
- P23-061 **The Crystal Structures of Two Polymeric Silver(I) Complexes with Amino Acids [CANCEL]**  
Li Wang
- P23-064 **Feasibility study of wide-angle incidence X-ray waveguides using surface diffraction**  
Sung-Yu Chen, Chia-Hung Chu, Chien-Liang Chen, Po-Wei Wu, Mou-Sen Chiu, Yu-Chi Shen, M.-H. Hong and Shih-Lin Chang
- P23-067 **Diffusion Path of Oxide Ions in  $La_{0.64}(Ti_{0.92}Nb_{0.08})O_3$**   
Roushown Ali, Masatomo Yashima and Fujio Izumi
- P23-070 **Crystal Structure of the Distorted Pyrochlore  $\alpha-Bi_2Sn_2O_7$**   
Christopher Howard, Ivana Evans, John Evans and Kevin Knight

- P23-073 **Structure-Processing-Property Relationships in Monofilament Fibres of Co/Terpolyesters for Use as Absorbable Surgical Sutures**  
Jintana Siripitayananon, Robert Molloy, Yodthong Baimark and Geoffrey Mitchell
- P23-076 **Molecular Packing and Intermolecular Interactions in Chitosan/Hydrogen Halides Complexes**  
Keiichi Noguchi, Masakazu Kanenari, Kenji Okuyama and Kozo Ogawa
- P23-079 **Preliminary report on the photo emission of spin crossover complexes**  
Yu-Chun Chuang, Jin-Ming Chen and Yu Wang
- P23-082 **Effect of Hot-Drawing on Morphology and Mechanical Property Development in Random and Block Terpolyester Fibres base on L-Lactide,  $\epsilon$ -Caprolactone and Glycolide**  
Wasinee Channuan, Jintana Siripitayananon, Robert Molloy and Geoffrey Mitchell
- P23-085 **Magnetic structural study of Co-doped barium ferrites by the RXMS method**  
Maki Okube, Seiji Ohsawa, Satoshi Sasaki, Takeharu Mori and Takeshi Toyoda
- P23-088 **Pressure-induced structure transition and the pressure dependence of electron density distribution in  $\text{BaTiO}_3$  and  $\text{PbTiO}_3$  perovskite ferroelectrics**  
Hiroaki Sugita, Hiroshi Matsumura, Takamitsu Yamanaka and Yuki Nakamoto
- P23-091 **Molecular structure of Novel Pesticides: Substituted Benzo and Dibenzo [d,f] [1,3,2] dioxaphosphopin 3-oxide (1) and 6-sulphide(11)**  
Musali Krishnaiah, Jadaprolu Radhakrishna, Reddy Suresh C. and Puranik Vedavati G.
- P23-094 **Oxygen non-stoichiometry in layer-misfit cobaltites**  
Chris Ling and Karina Aivazian

- P23-097 **2-D and 3-D X-ray Imaging due to refraction for visualizing soft tissue**  
 Masami Ando, Hiroshi Sugiyama, Anton Maksimenko, Tetsuya Yuasa, Eiko Hashimoto, Shu Ichihara, Kazuyuki Hyodo, Yoshinori Chikaura and Takao Akatsuka
- P23-100 **High temperature x-ray study on a single crystal of humite,  $Mg_7Si_3O_{12}(OH,F)_2$  up to 1023 K**  
 Keiko Sumioka, Takahiro Kuribayashi and Yasuhiro Kudoh
- P23-103 **Photoinduced Reversible Microfibril Formation on a Photochromic Diarylethene Microcrystalline Surface**  
 Yuko Kojima, Kingo Uchida, Norikazu Izumi, Shinichiro Sukata, Shinichiro Nakamura and Masahiro Irie
- P23-106 **Crystal structure and disorder in a Tetrakis (tetraphenyl phosphonium) dodecamolybdate phosphate  $[(PPh_4)_4 Mo_{12}O_{40}P \cdot 3DMF]$**   
 Krishna Chowdhury and Monika Mukherjee
- P23-109 **Effect of clay dispersion on Mechanical, Dynamic Mechanical and Thermal Properties of Vinylester Resin/Clay NanoComposites**  
 Suparna Sengupta, Dipa Ray and Siba Prasad Sengupta
- P23-112 **Isostructural Phase Transition in  $\beta-YbV_4O_8$**   
 Yasushi Kanke, Andrzej Grzechnik and Karen Friese
- P23-115 **Crystal Structure Analysis of Low-Dimensional Nano Crystal**  
 Yasuhiro Takahashi and Kazuaki Okamoto
- P23-118 **Synthesis and Crystal Structure of  $Fe_3(H_2PO_4)_4(PO_4)_2 \cdot (H_3O^+)2H_2O$ , a Novel Iron Phosphate**  
 Hsiu-Mei Lin and Shi-Fang Yeh
- P23-121 **Hydrothermal Synthesis, Crystal structure of Two-Dimensional Cobalt(II) and Nickel(II) Complexes with 4,4'-Bipyridine**  
 Tanwawan Duangthongyou and Sutatip Siripaisarnpipat

- P23-124 **Grain size effects on genesis of moganite and Brazil twin in quartz**  
Koichi Momma, Toshiro Nagase, Yasuhiro Kudoh, Takahiro Kuribayashi and Masahiko Tanaka
- P23-127 **An X-ray study of the modulation in Ga<sub>2</sub>Te<sub>3</sub> with the defect zinc-blende structure**  
Yo Otaki, Yu Yanadori, Yuusuke Seki and Shoji Kashida
- P23-130 **X-ray Structures and Charactrizations of Iron Complexes of Thiocalixarenetetrasulfonate**  
Sachie Shimose, Misato Ichikawa and Haruo Akashi
- P23-133 **Determination of Charge Ordered Structure in (DI-DCNQI)<sub>2</sub>Ag using Synchrotron Radiation X-ray Diffraction**  
Toru Kakiuchi, Yusuke Wakabayashi, Hiroshi Sawa, Tetsuaki Itou and Kazushi Kanoda
- P23-136 **X-ray structural analysis of β-Ga<sub>2</sub>Se<sub>3</sub>**  
Yuu Yanadori, Yo Otaki, Yuusuke Seki and Shoji Kashida
- P23-139 **β to α phase transition in Sn single crystal**  
Miwako Takahashi and Matthias Gutmann
- P23-142 **Host-guest chemistry of resorcinarenes-towards functional cavitands**  
Tayur Guru Row, Mahalakshmi L. and Partha Das
- P23-145 **Magnetic Domain Structure in Canted C-type Manganites**  
Xiuzhen Yu, Yasuhide Tomioka, Yoshio Kaneko, Toru Asaka, Masahiro Nagao, Weizhu Zhang, Koji Kimoto, Takahisa Arima, Yoshinori Tokura and Yoshio Matsui
- P23-148 **Crystal structure of novel layered silicate PLS-3 as a FER-zeolite precursor determined by X-ray powder diffraction**  
Takuji Ikeda, Syunsuke Kayamori, Takaaki Hanaoka and Fujio Mizukami

- P23-151 **Kinetics of crystalline-noncrystalline phase transition of sucrose crystal**  
Taro Fujita, Takahashi Kunimitsu, Takahashi Takahashi and Ken-ichi Ohshima
- P23-154 **Diffraction study of the grain (C2054,0,35,4) obtained by the NASA Stardust Mission**  
Kenji Hagiya, Takashi Mikouchi, Michael Zolensky and Kazumasa Ohsumi
- P23-157 **Electron Density Distributions of Intermolecular N...O Contacts in Crystals of Biphenyl-3,5-diyl bis(t-butyl nitroxide)**  
Masanori Yasui, Shinichiro Mashiyama, Kazuhiro Ozawa, Hiroaki Hosoya, Hirokazu Nishimaki, Gentaro Kurokawa, Takayuki Ishida and Takashi Nogami
- P23-160 **Large enhancement of photocatalytic Activity in Molybdovandate**  
Tayur Guru Row, Giridhar Madras and Sudarshan Mahapatra
- P23-163 **Crystal Structure of 7-methyl [3-(2-(4-Chlorophenyl sulfonyl)) ethenyl]-4H-1-Benzopyran-4-one**  
RaviKumar Raynuthala, Krishnaiah Musali, Zao Oo Than and Kaung P.
- P23-166 **Structures and properties of defect perovskites in the strontium zirconium niobium oxide system**  
Siegbert Schmid and Ivanka Barisic
- P23-169 **Crystal Structure Analysis of Eu<sup>2+</sup>-doped CaAlSiN<sub>3</sub>, a Red Phosphor for White Light-Emitting Diodes**  
Hiroyuki Imura, Takatoshi Seto, Naoto Kijima and Naoto Hirotsuki
- P23-171 **Preparation of Porous LiAl<sub>5</sub>O<sub>8</sub> by Li<sub>2</sub>O and Al<sub>2</sub>O<sub>3</sub> reaction**  
Chumphol BUSABOK, Tatsuo Shikama, Shinji Nagata, Bun Tsuchiya and Kentaro Toh
- P23-173 **Electron Dynamics in the Nanostructure**  
Tri Van Nguyen
- P23-175 **Synthesis and molecular structure of N-2-(4-picoyl)-N'-(6-amino phenyl) thiourea**  
Azadeh Tadjarodi and Nooshin Hafezinejad

- P23-177 **Bond-length fluctuation in the low temperature form of  $\text{LiMn}_2\text{O}_4$**   
Kenji Tateishi and Nobuo Ishizawa
- P23-179 **Thermal vibration behaviors of cations in garnet compounds**  
Akihiko Nakatsuka, Noriaki Nakayama, Hiroki Okudera, Akira Yoshiasa and Kazuake Iishi
- P23-183 **Interaction studies of polygalacturonase with its inhibiting protein through predictive docking**  
Malathy Sony Subramanian Manimekalai and Ponnuswamy Mondikalipudur Nanjappa
- P23-186 **Three dimensional Structure of Glycinin, a 11S Globulin from Peanut (*Arachis hypogaea*)**  
Saraboji Kadhivel, Balasundaresan Dhakshnamoorthy and Ponnuswamy Mondikalipudur Nanjappagounder
- P23-189 **Structure function correlation of multiple cysteine proteases from a tropical plant *Ervatamia coronaria***  
Sampa Biswas, Chandana Chakrabarti, J.K. Dattagupta, Raka Ghosh and Sibani Chakraborty
- P23-192 **Crystal structure and site-directed mutagenesis studies of *Anabaena* sp. CH1 N-acetyl-D-glucosamine 2-epimerase reveal two key histidines for reversible epimerization**  
Wen-Ching Wang, Hsin-Mao Wu, Yen-Chung Lee, Yu-Ning Chang and Wen-Hwei Hsu
- P23-195 **Effect of Sodium Ion on the Structural Phase Transition of Hen Egg-White Lysozyme Crystals**  
Kazuaki Harata and Toshihiko Akiba
- P23-198 **X-ray analyses of 3-hydroxybutyrate dehydrogenase from *Alcaligenes faecalis***  
M. Mominul Hoque, Ella Czarina Juan, Satoru Shimizu, Hiroshi Kondo, M. Tofazzal Hossain, Kaoru Suzuki, Shigeyuki Imamura, Tamotsu Yamamoto, Takeshi Sekiguchi and Akio Takenaka

- P23-201 **X-ray Crystal Structure Analysis of a Collagen Model Peptide (Pro-Hyp-Gly)<sub>3</sub>-Pro-Arg-Gly-(Pro-Hyp-Gly)<sub>4</sub>**  
Tatsuya Morimoto, Mitsuru Haga, Chizuru Hongo, Kenji Okuyama, Keiichi Noguchi and Toshiki Tanaka
- P23-204 **Structural study on full-size acetyltransferase (E2p) of pyruvate dehydrogenase complex from *Thermus thermophilus***  
Keita Kikuchi, Hiroshi Kondo, Ella Juan, Wataru Adachi, Ryoji Masui, Seiki Kuramitsu, Kaoru Suzuki, Takeshi Sekiguchi and Akio Takenaka
- P23-207 **Crystal structure of a splicing precursor of VMA1-derived endonuclease**  
Akihiro Sakai and Ryuta Mizutani
- P23-210 **Estimation of overall atomic displacement parameters from observed data**  
Ayako Nakata and Ryuta Mizutani
- P23-213 **Crystallographic study of thermostable hygromycin B phosphotransferase**  
Daisuke Iino, Yasuaki Takakura, Mika Kuroiwa, Yasuyuki Sasaki, Takayuki Hoshino, Kanju Ohsawa, Akira Nakamura and Shunsuke Yajima
- P23-216 **Crystal Structures of Serine racemase: conformational change implies features of the enzyme .**  
Masaru Goto, Ikuko Miyahara, Takae Yamauchi, Tohru Yoshimura, Nobuyoshi Esaki and Ken Hirotsu
- P23-219 **Tris ion induces conformational change and crystal-packing contraction of porcine pancreatic elastase**  
Asako Yamaguchi, Takayoshi Kinoshita and Toshiji Tada
- P23-222 **Structural insights into broad substrate specificity and catalytic activity of *Thermoplasma acidophilum* aldohexose dehydrogenase**  
Yoshiaki Yasutake, Yoshiaki Nishiya, Noriko Tamura and Tomohiro Tamura
- P23-225 **Structural studies on hydrogenase maturation protein HypE**  
Yasuhiro Shomura and Yoshiki Higuchi

- P23-228 **Crystallographic Study of Selenocysteine Lyase: Strict Substrate Recognition by the Catalytic Cysteine**  
Rie Omi, Suguru Kurokawa, Hisaaki Mihara, Tatsuo Kurihara, Nobuyoshi Esaki, Ikuko Miyahara and Ken Hirotsu
- P23-231 **Crystal structure of a novel human seminal zinc  $\alpha$  - 2 glycoprotein complex with binding protein**  
Imtaiyaz Hassan Md, Vijay Kumar, Sameeta Bilgrami, Punit Kaur, Savita Yadav and T. P. Singh
- P23-234 **Structure of the oncoprotein gankyrin in complex with S6 ATPase of the 26S proteasome**  
Yoshihiro Nakamura, Kazumi Nakano, Takashi Umehara, Eru Adachi, Yoshihide Hayashizaki, Balasundaram Padmanabhan and Shigeyuki Yokoyama
- P23-237 **The crystal structure of the host-guest collagen model peptide (Pro-Pro-Gly)<sub>4</sub>-Hyp-Asp-Gly-(Pro-Pro-Gly)<sub>4</sub>**  
Tatsuya Kawaguchi, Masaki Shimura, Chizuru Hongo, Keiichi Noguchi, Kenji Okuyama, Kazunori Mizuno and Hans Bachinger
- P23-240 **Crystal structures of nucleosidediphosphate kinase from *Pyrococcus horikoshii***  
Kazutaka Murayama, Miyuki Murayama-Kato, Takaho Terada, Mikako Shirouzu and Shigeyuki Yokoyama
- P23-243 **Structural and Functional Studies on Pin1 Mutants**  
Pei Chee Song, Xueji Wu, Jobichen Chacko, J. Sivaraman and Yih-Cherng Liou
- P23-246 **Design of some Non-Steroidal Anti-inflammatory inhibitors to Phospholipase A<sub>2</sub> using docking studies**  
Vaijayanthimala Suryanarayana Rao and Velmurugan Devadasan
- P23-249 **Crystal structures of Halothermothrix orenii  $\alpha$ -amylase at saturated salt concentration provide insights into protein stability at very high salt**  
Sivakumar Neelamegam, Nan Li, Patel Bharat and Swaminathan Kunchithapadam

- P23-252 **Crystal structure of pre-ribosomal RNA processing factor Dim2p from *Pyrococcus horikoshii* OT3 and its interaction with ribosomal RNA**  
Min Ze Jia, Jun Otsuka, Woo Cheol Lee, Koji Nagata and Masaru Tanokura
- P23-255 **Suggestions for improving diffraction data qualities at the undulator beamlines**  
Kunio Hirata, Nobutaka Shimizu, Kazuya Hasegawa and Masaki Yamamoto
- P23-258 **The Crystallization and X-ray Diffraction of the Exo-Arabinanase from *Penicillium Chrysogenum***  
Yuri Sogabe, Takayoshi Kinoshita, Asako Yamaguchi, Tomoya Kitatani, Tatsuji Sakamoto, Hideshi Ihara, Hiroaki Adachi, Hiroyoshi Matsumura, Kazufumi Takano, Satoshi Murakami, Tsuyoshi Inoue, Yusuke Mori and Toshiji Tada
- P23-261 **Development of Online UV-Visible Microspectrophotometer for Protein Crystallography at BL38B1 of SPring-8**  
Nobutaka Shimizu, Kouichi Tomita, Masao Ogaki, Kazuya Hasegawa and Masaki Yamamoto
- P23-264 **Crystal Structure of the Root Effect Fish Hemoglobin, Trout Hb IV bound to ATP molecule**  
Satoru Unzai, Kiyohiro Imai, Sam-Yong Park, Jeremy Tame and Kiyoshi Nagai
- P23-267 **The Crystal Structures of the Pseudouridine Synthases RluC and RluD**  
Kenji Mizutani, Yoshitaka Machida, Satoru Unzai, Jeremy Tame and Sam-Yong Park
- P23-270 **Molecular structure and dynamics of cytoplasmic domain of FlhA, a subunit of the flagellar type III protein export apparatus**  
Yumiko Saijo-Hamano, Katsumi Imada, Tohru Minamino, May Kihara, Akio Kitao and Keiichi Namba

- P23-273 **Performance of the macromolecular crystallography short-gap undulator beam line BL-17A at the Photon Factory**  
Noriyuki Igarashi, Naohiro Matsugaki, Yusuke Yamada, Masahiko Hiraki, Atsushi Koyama, Keiichi Hirano, Toshinobu Miyoshi and Soichi Wakatsuki
- P23-276 **Crystal Structure of Haloalkane Dehalogenase LinB from Sphingomonas paucimobilis UT26 at 0.95 angstrom resolution**  
Matthew Wilce, Aaron Oakley, Martin Klvana, Otyepka Michael, Yuji Nagata and Jiri Damborsky
- P23-279 **X-ray phase-contrast imaging using an x-ray HARP camera**  
Keiichi Hirano, Toshinobu Miyoshi, Noriyuki Igarashi, Soichi Wakatsuki, Tohoru Takeda, Jin Wu, Thet-Thet Lwin, Kenkichi Tanioka, Norifumi Egami, Misao Kubota and Teruo Kawai
- P23-282 **Structural analysis on the human and mouse Galectin-9 N-terminal CRDs reveals flexible mechanism of carbohydrate recognition**  
Masamichi Nagae, Nozomu Nishi, Takeomi Murata, Taichi Usui, Takanori Nakamura, Soichi Wakatsuki and Ryuichi Kato
- P23-285 **Preliminary X-ray crystallographic studies of GLUE domain of mammalian Eap45**  
Satoshi Hirano, Nobuhiro Suzuki, Thomas Slagsvold, Masato Kawasaki, Daniel Trambaiolo, Ryuichi Kato, Harald Stenmark and Soichi Wakatsuki
- P23-288 **Structural analysis of putative transcriptional repressors from Streptomyces coelicolor A3(2) by the S-SAD method**  
Kazuya Kondo, Takeshi Hayashi, Nobuhisa Watanabe and Isao Tanaka
- P23-291 **Crystal Structure Model-Assembly Program Using the Monte Carlo Method**  
Hiroyuki Miura
- P23-294 **Crystal structure of the archaeal transcription termination factor NuaA**  
Rie Shibata, Yoshitaka Bessho, Akeo Shinkai, Madoka Nishimoto, Emiko Fusatomi, Takaho Terada, Mikako Shirouzu and Shigeyuki Yokoyama

- P23-297 **Crystal structures of 6-deoxyclitoriacetal and its derivatives**  
Thapong Teerawatananond, Nustha Kitpratuang, Nattaya Ngamrojnavanich, Wilaiwon Tirawanich, Amorn Petsom and Nongnuj Muangsin
- P23-300 **Biochemical and structural analyses of cooperative inhibition mechanism of 1,2- $\alpha$ -L-fucosidase (AfcA) by deoxyfuconojirimycin and lactose**  
Atsuko Tsuchiya, Masamichi Nagae, Soichi Wakatsuki, Ryuichi Kato, Takane Katayama and Kenji Yamamoto
- P23-302 **Crystal structure of CbiL (CT0388), a methyltransferase involved in anaerobic biosynthesis of vitamin B<sub>12</sub>**  
Kei Wada, Jiro Harada, Hirozo Oh-oka, Hitoshi Tamiaki and Keiichi Fukuyama
- P23-304 **Structural analysis of a DNA tetrahedron by electron cryomicroscopy**  
Takayuki Kato, Russell Goodman, Richard Berry, Andrew Turberfield and Keiichi Namba
- P23-306 **Substrate recognition mechanism of L-lactate oxidase from *Aerococcus viridans* at 2.0 Å resolution**  
Yasufumi Umena, Kazuko Yorita, Takeshi Matsuoka, Akiko Kita, Kiyoshi Fukui, Tomitake Tsukihara and Yukio Morimoto
- P23-308 **Parameters for specification of sharpness in powder diffraction peak shape**  
Takashi Ida
- P23-310 **Development of a next-generation X-ray area detector : X-ray HARP-FEA detector**  
Toshinobu Miyoshi, Soichi Wakatsuki, Noriyuki Igarashi, Naohiro Matsugaki, Yusuke Yamada, Keiichi Hirano, Kazuyuki Hyodo, Masanori Kobayashi, Kenkichi Tanioka, Norifumi Egami, Misao Kubota and Teruo Kawai
- P23-312 **Crystal structure of a novel family 16 endo- $\beta$ -1,3-glucanase from *Nocardiosis* sp. F96**  
Takashi Kumasaka, Guntur Fibriansah, Sumiko Masuda and Satoshi Nakamura

- P23-314 **Crystallographic analysis of SLT1D1 ES complex structure**  
Takamasa Teramoto, Kanako Inada, Youichi Sakakibara, Masahito Suiko,  
Makoto Kimura and Yoshimitsu Kakuta
- P23-316 **The structure and the inhibition of the activity of Human Monoamine Oxidase A**  
Seyoung Son, Masato Yoshimura, Jichun Ma and Tomitake Tsukihara
- P23-318 **Purification and crystallization of photosynthetic reaction-center and light-harvesting I complex from *Rhodospirillum rubrum***  
Takao Okabe, Yuichi Kato, Takashi Kumasaka and Takayuki Odahara
- P23-320 **Crystallization and preliminary X-ray analysis of the bacterial membrane transporters**  
Yoshiki Tanaka, Motoyuki Hattori, Shuya Fukai, Ryuichiro Ishitani and Osamu Nureki
- P23-322 **Crystal Structure of Bovine Lactoperoxidase at 2.3 Å resolution**  
Sujata Sharma, Amit Singh, Kouichirou Shin, Mitsunori Takase, Nagendra Singh and Tej Singh
- P23-324 **Structure and function of new-type exfoliative toxin from *Staphylococcus hyicus***  
Katsuo Katayanagi, Kenji Yamamoto, Yasuyuki Fudaba, Takayuki Yamaguchi and Motoyuki Sugai
- P23-326 **Prototype Structures and Structure Algebra as an Aid to the Refinement of Problem Structures**  
A. David Rae
- P23-328 **Crystal structure and enzyme mechanism of esterase Est1 from an archaeon, *Sulfolobus shibatae***  
Masami Kusunoki, Hideaki Unno, Yasuhiro Oshima, Tokuzo Nishino and Toru Nakayama
- P23-330 **Variation of Measurability of Bijvoet ratios in MAD experiments**  
Gayathri Dasara Raju, Zwart Peter and Velmurugan Devadasan



# **Oral Abstracts**



## Crystal and Functional Engineering for Unique Microporous Materials

Susumu Kitagawa

Department of Synthetic Chemistry and Biological Chemistry, Kyoto University

The recent advent of porous coordination polymers (PCPs) or metal-organic frameworks (MOFs), as new functional microporous adsorbents, has attracted the attention of chemists due to scientific interest in the creation of unprecedented regular nano-sized spaces and in the finding of novel phenomena, as well as commercial interest in their application for storage, for separation and in heterogeneous catalysis.<sup>1-4</sup> One of the advantages of PCPs, as compared with other microporous materials such as activated carbons, is designability, which provides a variety of surface properties based on organic ligands with functional groups, affording the potential to make the pore surfaces hydrophobic, hydrophilic, chiral and so on. This prominent feature leads us to expect that PCPs will show a high adsorption capability for specific molecules. However, few useful concepts and strategies for specific adsorption of smaller molecules have been established to date. Here, we have found superb sorption of C<sub>2</sub>H<sub>2</sub> molecules on the functionalized surface of a PCP and show an enhanced "confinement effect", which can be achieved by precisely and regularly arranged functionalities in the nano-sized pore wall, applicable to a highly stable, selective adsorption system.<sup>5</sup> We have succeeded in obtaining interesting array structures of benzene<sup>6</sup> and O<sub>2</sub><sup>7</sup> molecules and observed their unusual properties in the nanochannel. Recently, we have utilized the regular and tunable nanochannels of PCPs for fields of polymerization, which allows controlled living radical polymerization as well as stereoregulated polymerization of substituted acetylenes,<sup>8</sup> opening up a new dimensions in the field of porous materials.

### References

#### Reviews

- 1) S. Kitagawa *et.al.*, *Bull. Chem. Soc. Jpn. (Accounts)*, **1998**, 71, 1739.
- 2) S. Kitagawa, *et.al.*, *Angew. Chem. Int. Ed.*, **2004**, 43, 2334.
- 3) S. Kitagawa *et.al.*, *Chem. Soc. Rev.* **2005**, 34, 109.
- 4) S. Kitagawa *et.al.*, *Chem. Commun. Feature Article*, 2006, 701.

#### Original Papers

- 5) R. Matsuda, *et.al.*, *Nature*, **2005**, 436, 238.
- 6) R. Matsuda, *et.al.*, *J. Am. Chem. Soc.* **2004**, 43, 14063
- 7) R. Kitaura, *et.al.*, *Science*, **2002**, 298, 2358.
- 8) T. Uemura, *et.al.*, *Chem. Commun.* **2005**, 5968.

## Structural insights into SARS coronavirus proteins

Zihe Rao

Tsinghua University-Institute of Biophysics, CAS Joint Research Group for Structural Biology

Zihe Rao's group has been active in SARS basic research since the 2003 global outbreak, and was the first to determine the crystal structure of a key replicase protein encoded by the SARS coronavirus (SARS-CoV) - the main protease or Mpro - and its complex with an inhibitor. His group has since made a number of important breakthroughs in SARS research, and the major achievements include: wide spectrum inhibitor design targeting coronavirus Mpro; the elucidation of the autocleavage mechanism of coronavirus Mpro; the structures of the spike (S) protein fusion cores from SARS-CoV and MHV; the structure of the super-complex between two SARS non-structural proteins, nsp7 and nsp8; the dodecamer structure of the SARS non-structural protein nsp10; and the hexamer structure of the MHV non-structural protein nsp15, an endoribonuclease. With more than 18 protein and complex structures from SARS-CoV and related coronaviruses to date, Zihe Rao's group has provided important structural insights into coronavirus replication/transcription.

### References:

- [1] Yang, H. et al. & Rao, Z. (2005). *PLoS Biol* **3**, e324.
- [2] Zhai, Y. et al. & Rao, Z. (2005). *Nat Struct Mol Biol* **12**, 980-6.
- [3] Bartlam, M., Yang, H. & Rao, Z. (2005). *Curr Opin Struct Biol* **15**, 664-72.
- [4] Xu, Y. et al. & Rao, Z. (2004). *J Biol Chem* **279**, 30514-22.
- [5] Xu, Y. et al. & Rao, Z. (2004). *J Biol Chem* **279**, 49414-9.
- [6] Xu, Y. et al & Rao, Z. (2004). *Biochemistry* **43**, 14064-71.
- [7] Yang, H. et al. & Rao, Z. (2003). *Proc Natl Acad Sci U S A* **100**, 13190-5.

## **Towards structure determination of human membrane proteins**

So Iwata

Division of Molecular Biosciences, Imperial College London, UK

The results of various genome projects have shown that up to 30% of human proteins occur in cell membranes. Membrane proteins play crucial roles in many biological functions and are of key importance for medicine. Over 50% of commercially available drugs target membrane proteins. In spite of the abundance and importance of membrane proteins there are only 100 unique membrane protein structures in the Protein Data Bank. To address the technical bottlenecks preventing the structure determination of membrane proteins, we have recently started "ERATO human receptor crystallography project" supported by the Japanese Science and Technology Agency. We have also obtained a support from the Wellcome trust to establish an outstation of Imperial College London at the new UK synchrotron Diamond. I will discuss our strategy how to establish the structure determination method of human membrane proteins using these new facilities and its impact on biological sciences, pharmacology and medicine.

## Structures and phase transitions in perovskites - sorting out the subtleties

Christopher J Howard

Institute of Materials and Engineering Science, Australian Nuclear Science and Technology Organisation

The perovskite ( $ABX_3$ ) structure comprises a three dimensional corner-linked array of  $BX_6$  octahedra with  $A$  cations located between. The ideal perovskite is cubic, but most perovskites are distorted variants. The most common distortions are cation displacements and the tilting of  $BX_6$  octahedra. Chemical substitutions resulting, for example, in the presence of more than one chemical species on the  $B$  site, give rise to further structural variability. Though the distortions may be subtle, the transitions between the different structural variants can result in dramatic changes in physical properties, leading to a variety of applications.

The subtlety of the distortions makes for challenging crystallography. In the approach to be described here [1], group theory is used to enumerate the possible space groups and structures, and to analyse the transitions between them. Computer program ISOTROPY [2] is a valuable aid in this endeavour. Experimental techniques used to elucidate structures include synchrotron-based X-ray diffraction and electron microdiffraction. In studies of temperature-induced phase transitions, the combination of group theoretical analysis with very high resolution neutron powder diffraction patterns recorded (using HRPD at ISIS) at fine temperature intervals has proved particularly effective.

The speaker will outline the methodology, and illustrate with recent applications.

- [1] Review article: C J Howard, H T Stokes, *Acta Crystallogr.* A61, 93-111, 2005
- [2] Programs available at: <http://stokes.byu.edu/isotropy.html>

### Structural basis for heme degradation by heme oxygenase

Masakazu Sugishima

Department of Medical Biochemistry, Kurume University School of Medicine

Heme is a well-known prosthetic group utilized for oxygen transport, electron transfer, sensor, and reaction center for many enzymes. It has been classically believed that heme catabolism is important for renewing damaged heme and recovery of iron. Recent progress reveals that the heme degradation is involved in the defense for oxidative stress and the regulation of circadian clock, inflammation, cellular proliferation, and apoptosis. Heme oxygenase (HO) plays a central role for the heme degradation. HO incorporates heme, cleaves the tetrapyrrole moiety of heme, and produces biliverdin IX $\alpha$ , CO, and iron ion using reducing equivalents and O<sub>2</sub> molecules.

The crystal structure of rat heme-HO-1 complex mainly consists of alpha-helices. Heme is sandwiched between two helices (proximal and distal helices). Distal helix is uniquely kinked between the conserved two glycine residues and forms narrow distal pocket. The narrow pocket restricts the orientation of O<sub>2</sub> bound to the heme iron and limits the cleavage site of heme. Because CO produced in HO reaction is an inhibitor, HO should discriminate O<sub>2</sub> and CO. The narrow pocket discriminates CO from O<sub>2</sub> by its preference of the bending angle of the bond between the heme iron and each ligand. Moreover, HO has a hydrophobic cavity at the inner side of the distal pocket. The transient structure of CO-dissociation shows that the CO released from the heme iron is trapped in this hydrophobic cavity. CO released in HO reaction would also initially be trapped in the cavity. Adding ascorbate as an electron donor to the crystal of heme-HO-1 complex, the crystal turns red to green indicating that HO is active even in crystalline state. The structural analysis suggests how biliverdin and iron dissociate from HO.

## **Structure determination of a signaling-competent reelin fragment by X-ray crystallography and electron tomography**

Terukazu Nogi Norihisa Yasui Tomoe Kitao Kenji Iwasaki Junichi Takagi

Institute for Protein Research, Osaka University

Reelin, a gigantic extracellular glycoprotein produced by Cajal-Retzius and other neurons in the cortex, plays a central role in cortical layer formation during mammalian brain development. It was originally identified as a gene product absent in reeler mice exhibiting malformations of the cerebral cortex. It is now accepted that reelin binds to the lipoprotein receptors ApoER2 or VLDLR and initiates a signaling cascade involving phosphorylation of the Dab1 adaptor molecule. Biochemical and structural basis for the reelin-receptor interaction, however, remains poorly understood.

In the present study, we have carried out structural and functional studies on the interaction between reelin and its receptors. Reelin consists of eight tandem repeats, termed reelin repeat, which has a central EGF motif flanked by two homologous subrepeats. It was reported that a fragment of reelin containing reelin repeats three through six, R3-6, is capable of transducing signals in neurons. We have designed and tested a series of deletion constructs of R3-6 for protein production in mammalian cells in order to apply them to structural analysis. As a result, the R3 fragment showed the highest production level, and was subjected to crystallization. The structure of the R3 fragment was solved by X-ray crystallography, and it had a horseshoe-like globular structure with some similarities to carbohydrate binding modules. Moreover, we analyzed the molecular structure of the four-domain fragment, R3-6, by electron micrographic 3D reconstruction, which revealed its elongated rod-like structure. Now we try to determine the 3D structure of a minimum receptor-binding unit and analyze ligand-receptor interaction mode at an atomic level.

## **Synchrotron Protein Crystallography and Structural Proteomics of Protein Transport and Glycosylation**

Soichi Wakatsuki

Structural Biology Research Center, Photon Factory, Institute of Materials Structure Science, High Energy Accelerator Research Organization (KEK), Tsukuba, Ibaraki 305-0801, Japan

Synchrotron X-ray protein crystallography plays critically important roles in structural investigations on macromolecules. A progress report will be presented on our systems approach for developing and operating synchrotron X-ray protein crystallography beam lines at the Photon Factory, Tsukuba. Our instrumentation projects include the new short gap in-vacuum undulator MAD beam line BL-17A, X-ray HARP detector, a large scale crystallization robot, and crystal exchange robots based on the SSRL system. The beam lines provide state-of-the-art, user-friendly experimental environment and are centrally managed.

We also pursue structural proteomics on intracellular transport and post-translational modification of proteins. Our targets are mostly eukaryotic proteins involved in vesicle transport between the ER, the Golgi apparatus and endosomes /lysosomes, post-translational modification of newly synthesized proteins, exocytosis, endocytosis, ubiquitin-dependent protein sorting, and autophagy. Structural results on yeast and mammalian lectins in glycoprotein transport, adapter proteins, Rab proteins and their effectors will be discussed. In addition, more recent examples of ubiquitin recognition by GGA, Tom1, Hrs, and part of the ESCRT II complex will be presented with the emphasis on the recurring structural theme, dual binding of ubiquitin molecules by components of the degradative protein sorting pathway.

Here, the synergy between the synchrotron beam line development and on-site structural biology research activities is quite beneficial. For example, technology developments often originate from and are nurtured by the needs of in-house research while newly developed apparatuses are immediately tested with on-going, often urgent, protein crystallographic projects.

## **Mail-in data collection service at SPring-8 protein crystallography beamline**

Kazuya Hasegawa<sup>1</sup> Nobuo Okazaki<sup>2</sup> Go Ueno<sup>3</sup> Hironori Murakami<sup>4</sup> Yuji Fukumoto<sup>5</sup> Hisanobu Sakai<sup>6</sup> Masaki Yamamoto<sup>7</sup>

SPring-8/JASRI<sup>1</sup> SPring-8/RIKEN<sup>2</sup>

Mail-in data collection is a new service at synchrotron facilities that beamline operator conduct data collection for samples sent from users via the home-delivery services. It's a quite convenient system for most users because they can acquire experimental data with synchrotron radiation without visiting synchrotron facilities. We have already routinely operated mail-in data collection service for academic users at protein crystallography beamline at SPring-8 since September 2005. And, the commercial mail-in service especially targeting pharmaceutical industry has started in July of this year in cooperation with five intermediate private companies.

Characteristic feature of our mail-in service is making use of sample changer SPACE. Users send crystals using a special sample tray for SPACE. Specially developed tool kit is available to mount crystals on the sample tray and to pack it in the dry-shipper. Sample information, experimental conditions, and collected diffraction images are shared between users' laboratory and SPring-8 via a beamline database D-Cha which is composed of relational database and Web interface. Each user gets user account for D-Cha and can only access to the permitted data for that account. Before shipping sample, users attach barcode label indicating 11 digits tray ID on the sample tray and register the ID on D-Cha. By using tray ID, there is no afraid to mix up users' samples at beamline. In commercial mail-in service, users are not asked to disclose details of protein samples except for minimum safety information. Therefore, pharmaceutical companies can apply our service without taking risks of leakage of business secrets.

## Transition Metal Derivatives for SAD method

Atsuo Suzuki Akihito Fukushima Takashi Yamane

Biotechnology, Nagoya University

SAD(Single-wavelength Anomalous Dispersion) method is getting popular in protein crystallography. As an anomalous scatterer for SAD, a selenium atom genetically incorporated into protein is popular. But Se-SAD method requires usage of toxic selenomethionine and synchrotron X-ray. Here we cast a spotlight on transition metals as anomalous scatterers. Some of them are less toxic and suitable for SAD phasing with  $\text{CuK}\alpha$  radiation.

We tested the first series of transition metals, Cr, Fe, Co, Ni, Cu, and Zn. They were introduced into protein crystals by the quick-soak method. Proteinase K and lysozyme were used as test proteins. Diffraction data from transition-metal derivatives were collected at 1.6Å resolution using  $\text{CuK}\alpha$  radiation. Anomalous scatterers were located by the program *SHELXD* and verified by anomalous difference-Fourier maps. Fe and Co were found to bind to both proteins. Using the Fe- or Co-derivative, phase calculation by SAD method and automatic model-building by *ARP/wARP* were easily performed. In the crystals, Fe or Co atoms bind directly to acidic side-chains, or bind to hydrophilic side-chains as octahedral aqua complex.

## **S-SAD phasing at RIKEN structural genomics beamline of SPring-8**

Raita Hirose Yuki Nakamura Tomokazu Hasegawa Akihito Yamano Kensaku Hamada

PharmAcess, Inc.

S-SAD is a phasing method in macromolecular crystallography which uses anomalous signal from sulfur atoms. The method has an advantage over other phasing methods such as MAD and MIR when neither a Se-Met nor a heavy atom is present in the crystal. A disadvantage of SAD, however, is that it is impossible to obtain a unimodal phase probability distribution in principle. In order to resolve the phase ambiguity, it is necessary to combine the SAD approach with density modification and other crystallographic techniques.

Generally, the anomalous signal of sulfur atoms in a protein crystal is so weak that it can readily be buried in background noises and systematic errors. We believe that those noises and errors come mainly from scattering by liquid around the crystal, characteristics of the X-ray detector itself and so on. Therefore, some techniques and modifications to reduce background noises and increasing accuracy of diffraction data are employed to improve success rate of S-SAD phasing.

We examined S-SAD experiments using insulin crystals at BL26B2 in SPring-8, and succeeded in automatic phasing and model building under some specific conditions. For successful datasets, the amount of liquid around the crystal was minimized by mounting crystals on MicroMounts™, a novel crystal mounting device consisted with a nib-shaped Kapton film. Moreover, scattering and absorption by the black paper shading IP's from visible light were greatly reduced by replacing it with a poly-carbonate sheet.

This research was supported by "Program for Strategic Use of Advanced Large-scale Research Facilities of the Ministry of Education, Culture, Sports, Science and Technology."

## **Current status of Macromolecular Crystallography BeamLines at the Photon Factory**

Naohiro MATSUGAKI Masanori Kobayashi Yusuke Yamada Noriyuki Igarashi Masahiko Hiraki Yuri A Gaponov Soichi Wakatsuki

Photon Factory, High Energy Accelerator Research Organization

Macromolecular crystallography (MX) beam lines are required to be more stable, user-friendly and high-throughput according to recent expansion of the field of structural biology. One of the solutions is to automate experiments as many aspects as possible. Increasing users unfamiliar with synchrotron facilities can perform experiments efficiently using well-organized beamline control system, which should be flexible to accept forthcoming technologies and methods. Recent development at currently operated three MX beamlines, NW12A, 5A and 6A at the Photon Factory was mainly focused on various optimizations to bring out the capability of the beamlines.

We have recently installed sample changers in the insertion device beamlines, NW12A and 5A, to reduce the time wasted in the repetition in mounting and dismounting samples on the goniometer. The changers are now under commission and will be available in 2006. Beamline control software was modified to be more stable and functional with a graphical user interface (GUI) through which users can execute all the operations required in MX experiments. The GUI was designed to provide a simple way to complete experiments with minimum steps of intervention. Another control system based on a relational database is under development in parallel, which should allow secure remote access and automatic scheduled experiments together with the sample changer. Due to the database feature, information in the system can be easily tracked and managed.

To extend targets to macromolecules difficult to crystallize in a sufficient size, we have constructed a new micro-focus beamline, 17A, dedicated to diffraction experiments with micron-size crystals. The public operation will commence in 2006, after test experiments using various sizes of crystals.

## Structural Genomics of Mycobacterial Recombination and Repair

Mamannamana Vijayan

Molecular Biophysics Unit, Indian Institute of Science

A major thrust of the mycobacterial structural genomics programme in this laboratory is on recombination and repair. Central to homologous recombination is the RecA protein. The structures of several crystals of RecA from *M. tuberculosis* and *M. smegmatis* and their nucleotide complexes, have been determined (*Nucleic Acids Res.* **28**, 4964-4973, 2000; *Proteins: Structure, Function, Genet.* **50**, 474-485, 2003; *J. Bacteriol.* **185**, 4280-4284, 2003). They provided the first detailed description of RecA-nucleotide interactions and the DNA binding loops in RecA, and brought to light a mechanism for transmitting information on nucleotide binding to the DNA binding region, using a crucially located glutamine residue as a trigger. More recently, the first visualisation of the usually disordered C-terminal stretch has been achieved (*Nucleic Acids Res.* **34**, 2186-2195, 2006). This ordering is accompanied by the generation of a second nucleotide binding site, which communicates with the first in an adjacent molecule, suggesting a new route to allosteric regulation. Single stranded DNA-binding protein (SSB) also plays crucial roles in recombination and repair. Mycobacterial SSB has a novel quaternary structure with a unique dimeric interface which lends it greater stability (*J. Mol. Biol.* **331**, 385-393, 2003; *Acta Cryst. D* **61** 1140-1148, 2005). Also, the length of DNA necessary to wrap around the tetrameric molecule is lower in the mycobacterial proteins than in *E.coli* and human SSBs. The other relevant proteins currently being investigated include RuvA and uracil DNA glycosylase from *M. tuberculosis*.

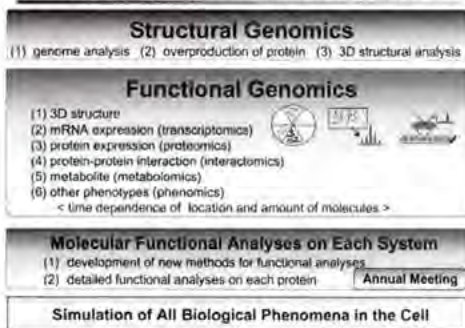
## Progress in the Whole Cell Project of a Model Organism, *Thermus thermophilus* HB8

Akio Ebihara Mayumi Kanagawa Chizu Kuroishi Noriko Nakagawa Ryoji Masui Takaho Terada Mikako Shirouzu Kunio Miki Shigeyuki Yokoyama Seiki Kuramitsu

RIKEN SPring-8 Center, Harima Institute, Japan

The final goal of this research project is the understanding of all fundamental biological phenomena at atomic resolution. As a model organism for the structural and functional studies, an extremely thermophilic bacterium, *Thermus thermophilus* HB8, is very promising because of the small genome size (2 Mbp), the availability of genetic tools for functional analysis, and the thermostability of its proteins (<http://www.thermus.org/>). The complete genome sequence identifies approximately 2,200 genes. Out of them, 1,450 proteins have been overexpressed in *E. coli*, 930 purified, 395 X-ray diffraction data collected, and about 300 structures determined. As part of the functional genomics studies, we have proceeded to analyze mRNA expression (transcriptomics), protein expression (proteomics) and metabolite dynamics (metabolomics) of the wild-type strain and gene disruptants. Such the parallel structural and functional analysis provides a new insight into protein functions as well as a new functional clue to hypothetical proteins. Furthermore, we focus on several sets of proteins involved in a specific metabolism (e.g. transcription, stress response and nucleotide biosynthesis) to investigate how they work as a cellular system.

### Whole Cell Project of *Thermus thermophilus* HB8



*Thermus thermophilus* HB8



Members of Annual Meeting

## Formation of Helical Organic Supramolecular Chains in an Elastic Zincophosphate Lattice

Sue-Lein Wang

Department of Chemistry, National Tsing Hua University

The study reports an interesting photoluminescent elastic zincophosphate lattice in which achiral organic molecules are confined to become chiral or helical supramolecular infinite chains and supramolecular water hexamers are confined to exist in an isolated form. While organic polymers containing dispersed inorganic particles are not uncommon, the subsistence of organic supramolecular infinite entities in inorganic-based matrix has never been reported. The system of NTHU-3 represents the first example that organic supramolecular infinite chains can be prepared in a layered zincophosphate, providing prospect syntheses of hybrid organic-inorganic bio-nanocomposites in phosphates as in layered double hydroxides. Besides, the explicit hydrogen bonding structure retrieved from the  $(\text{H}_2\text{O})_6$  clusters in NTHU-3 is unprecedented and may be of great importance for the derivative properties of bulk ice. We discover that the irremovable template ions in the system are dynamic and may exert pronounced effect on the self-assembly of various organic supramolecular chains between the ZnPO strata, stabilizing the ice-like  $(\text{H}_2\text{O})_6$  clusters in an isolated state, and keeping the recoverable amorphous-to-crystalline property for NTHU-3.

## Crystal Engineering of Microporous Chiral Coordination Polymers based on L-tartrate Ligands

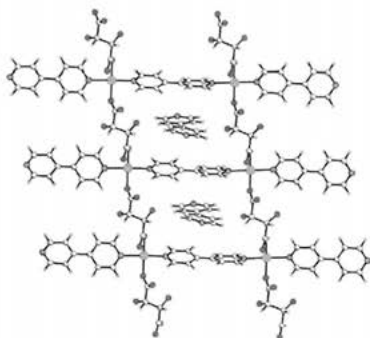
Ian D. WILLIAMS

Chemistry, HKUST

L-tartrate anions can survive hydrothermal synthesis up to 160°C enabling formation of the chiral porous lanthanide tartrates  $[\text{Ln}_2(\text{L-TAR})_3(\text{H}_2\text{O})_2]_3\text{H}_2\text{O}$ . [1] This prompted us to look at the hydrothermal crystal chemistry of a variety of metal tartrate systems, including  $\text{M}^{2+}$ ,  $\text{M}^{3+}$  [2] and vanadium  $\text{M}^{4+}$  ions. In general dimensional and topological control of the crystalline phases formed is exerted through use of elevated temperatures to reduce ancillary ligation. The use of co-ligands can also be employed to engineer the channel size and structure for 3D network polymers, thus the mixed  $[\text{Ln}_2(\text{L-TAR})_2(\text{SUC})(\text{H}_2\text{O})_2]_5.5\text{H}_2\text{O}$  with larger 1D channels can be formed by adding succinate and topomeric open frameworks of  $[\text{Cu}(\text{L-TAR})(\text{bipy})]_3\text{H}_2\text{O}$  or  $[\text{Cu}(\text{L-TAR})(\text{bipy})][\text{bipy}]$  (see fig) can be formed on addition of 4,4'-bipyridine. Stabilities up to 250°C have been found for these microporous frameworks by in situ variable temperature pXRD.

1. S. Thushari, J.A-K. Cha, H. H-Y. Sung, S. S-Y. Chui, I. D. Williams, *Chem. Commun.*, **2005**, 5515.
2. A. S-F. Au-Yeung, J.A-K. Cha, H. H-Y. Sung, S. S-Y. Chui, I. D. Williams, *Inorg. Chem. Commun.*, **2006**, 9, 507.

The RGC is thanked for financial support of this work under grant 6084/02P.



**Crystal Engineering of Isopropylbenzophenone Derivatives and the Morphology Change by Asymmetric Photoreaction**

Hideko Koshima Michitaro Fukano Yuya Ide

Department of Materials Science and Biotechnology, Ehime University

One of the targets of solid state chemistry is development of highly enantioselective reactions. We have achieved several enantiospecific and diastereospecific photocyclization of isopropylbenzophenone derivatives by a cocrystal approach. Most of the reactions were accompanied with the decomposition of initial crystal structures, but a few single-crystal-to-single-crystal reactions were also found. In this Conference, we would like to report our recent research work about the correlation between the structure changes at molecular level and the crystal morphology changes at nanometer level during the reactions.

## Host framework in inclusion compound of 1,1,2,2-tetrakis (4-hydroxyphenyl) ethane, (TEP)

Hidehiro Uekusa<sup>1</sup> Naonori Akai<sup>2</sup> Natsuki Amanokura<sup>3</sup> Masami Kaneko<sup>4</sup>

<sup>1</sup>Department of Chemistry and Materials Science, Tokyo Institute of Technology<sup>1</sup> <sup>2</sup>Department of Chemistry and Materials Science, Tokyo Institute of Technology, Japan<sup>2</sup> <sup>3</sup>Nippon Soda Co., Ltd.<sup>3</sup>

1,1,2,2-tetrakis (4-hydroxyphenyl) ethane (Fig.1, TEP) is an organic host molecule which crystallizes with guest molecules including organic solvents, and a bactericide, 5-chloro-2-methyl-3(2H)-isothiazolone. The TEP molecule has a unique four arms molecular structure, which has terminal OH group for donating/accepting hydrogen bond and phenyl group for weak hydrogen bond and cavity forming.

Crystal structures of five 1:2 host-guest crystals of TEP with methanol, ethanol, acetone, acetonitrile, and methylacetate were analyzed to investigate the host frameworks and their thermal stabilities. In motif (II) and (III) (Fig.2), the TEP host molecules are connected via terminal OH group and making 1D chain, (II), or 2D net, (III), structures. The guests are hydrogen bonded to the host framework. However, motif (I) takes two guest molecules between hosts to form 1D chain structure.

Thermal analyses of crystals indicate that guest molecules in 2D net (III) are removed easily through solvent channels. The guest molecules in the 1D chain framework (II) are confined in a cavity structure, so the leaving temperature is relatively higher. Thus, the crystal stability is well explained by the types of host framework and hydrogen bonding patterns.

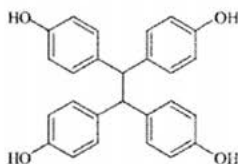


Fig.1 TEP molecule

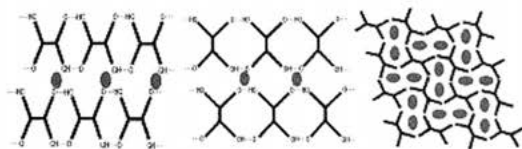


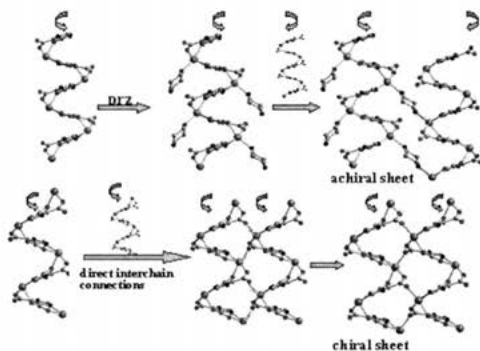
Fig.2 TEP host framework (I), (II), (III)

## The Chirality Transfer Between 1D Helical Chains

Tong-Bu Lu Jin-Zhong Gu Long Jiang Wen-Guan Lu

School of Chemistry and Chemical Engineering, Sun Yat-Sen University

Chirality is of fundamental importance for life and plays a key role in biological systems and pharmacy, as well as in advanced materials. In order to the constructions of homochiral structures containing helical chains, it requires an efficient transfer of stereochemical information between neighboring helices. However, it has not been well understood how homochiral packing of helices in crystals can be induced so far. This presentation is concerned with the constructions of achiral and homochiral compounds containing helical chains.



**Incompatible host-guest strategy to enclathrate discrete water clusters**Tomoji Ozeki<sup>1</sup> Setsuko Nakamura<sup>1</sup> Takuto Yamawaki<sup>1</sup> Katsuhiro Kusaka<sup>2</sup><sup>1</sup>Department of Chemistry and Materials Science, Tokyo Institute of Technology<sup>2</sup> Quantum Beam Science Directorate, Japan Atomic Energy Agency<sup>3</sup>

Many compounds crystallize as hydrated forms when precipitated from aqueous or water-containing solutions. Water plays an important role in constructing such crystals. One extreme example of them is the clathrates of hydrophobic gaseous molecules. Another extreme example may be water clusters enclathrated in hydrophobic environments. We have synthesized discrete water clusters enclathrated in hydrophobic channels composed by the tetraphenylphosphonium cations, which may be regarded as examples of water clusters in hydrophobic environments. The tetraphenylphosphonium cations self-assemble by the C-H...p interactions to form three-dimensional networks, between which polyoxometalate anions are incorporated. However, the sizes and charges of the cations and anions are incompatible and thus void spaces remain unoccupied. These voids lead to the formation of discrete water clusters. In one of these examples, the distribution of the clusters become ordered or disordered depending on the crystallization conditions, resulting in the disappearance/appearance of the diffuse scattering recorded on its single crystal diffraction images.

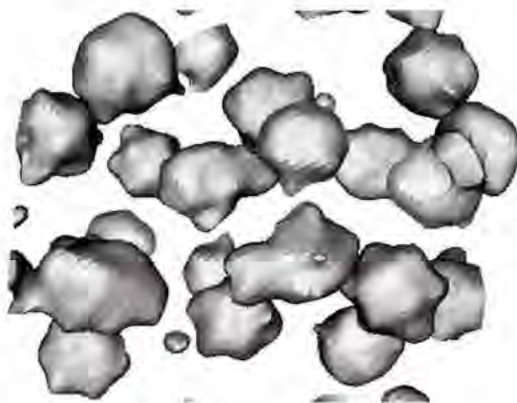


Figure. Electron density distribution of tetradecameric water cluster in  $[(C_6H_5)_4P]_3 [H_5V_{10}O_{26}] \cdot 7H_2O$ .

## Self assembled Nanomaterials Based on Porogenic Water Soluble Calixarenes

Mohamed Makha Colin L Raston Christopher Smith Alex Sobolev

School of Biomedical, Biomolecular and Chemical Sciences, The University of Western Australia

Advances in nanoscale science and engineering suggest that many of the current problems involving molecular separation, sensing, heterogeneous catalysis could be resolved or greatly ameliorated using nanoporosity in self assembled molecular framework. The paper will present recent work on the use of macrocyclic calixarenes sulfonates as molecular platform in conjunction with metal and organic ions of various spatial geometries to construct molecular assemblies of nano dimensions. The assembly process is governed by supramolecular interactions affording new materials such as ionic capsules, molecular solids with extended networks and micellar aggregates. The majority of work in the area is focused on *p*-sulfoantocalix[4]arene and more recently larger *p*-sulfonato-calix[6,8]arenes can also be encouraged to form ionic capsules with phosphonium cations yielding networks of 2D porosity.<sup>1</sup> We also have established the formation of helical structures by the self assembly of *p*-sulfoantocalix[4]arene and Co(III) sepulchrate cation leading to materials with well defined porosity.<sup>2</sup>

1. M. Makha et al. *Chem. Commun.*, 2006, 5, 511-513;

2. M. Makha et al. *Chem. Commun.*, 2006, 9, 950-952.



## High Resolution Powder Diffraction Studies at ESRF

Andy Fitch

ESRF

At the ESRF we have been operating a high resolution powder diffraction beam line for the last ten years. In June 2002 the beam line was moved from its original bending magnet (BM16) to a dedicated undulator source (ID31), giving a large gain in the photon flux over the entire operational energy range of 5 - 60 keV. Recent enhancements include the installation of a robotic sample changer, so that as many as 50 capillary samples can be studied automatically, without intervention by the user, over the temperature range of 80 K -1225 K. In manual mode the range 3.5 K - 1800 K is routinely available.

The beam line is suited to a wide range of studies, particularly powder crystallography where the narrow peak widths maximise the amount of useful information in the diffraction profile. The high flux means that a diffraction pattern can be measured in a few minutes, for strongly-scattering samples, allowing high-resolution studies as a function of multiple temperatures and/or compositions. The high flux can be a problem however, with sensitive specimens, such as organic molecules, suffering radiation damage. Following the seminal work of Von Dreele, powder diffraction studies on proteins have proven feasible, and have been enthusiastically taken up at ESRF. The talk will give a brief overview of the beam line, illustrated by some examples exploiting its high flux and resolution capabilities.

## **IBARAKI Materials Design Diffractometer for J-PARC**

Toru Ishigaki<sup>1</sup> Akinori Hoshikawa<sup>2</sup> Masao Yonemura<sup>3</sup> Takashi Kamiyama<sup>4</sup> Stefans Harjo<sup>5</sup>  
Kazuya Aizawa<sup>6</sup> Takashi Sakuma<sup>7</sup> Yo Tomota<sup>8</sup> Yukio Morii<sup>9</sup> Masatoshi Arai<sup>10</sup> Kazuhiro Ebata<sup>11</sup>  
Yoshiki Takano<sup>12</sup> Takuro Kasao<sup>13</sup>

Quantum Beam Science Directorate, Japan Atomic Energy Agency<sup>1</sup> Institute of Applied Beam Science, Ibaraki University, Japan<sup>2</sup> Neutron Science Laboratory, KEK, Japan<sup>3</sup> Ibaraki Prefecture, Japan<sup>4</sup>

Ibaraki prefecture, the local government of the area for J-PARC site, was decided to build a versatile neutron diffractometer (IBARAKI Materials Design Diffractometer) to promote an industrial application for neutron beam in J-PARC. This diffractometer is planned to be a high throughput diffractometer so that materials engineers and scientists can use it like the chemical analytical instruments in their materials development process. It covers in  $d$  range  $0.18 < d$  (Å)  $< 5$  with  $\Delta d/d = 0.16\%$  at high resolution bank, and covers  $5 < d$  (Å)  $< 800$  with gradually changing resolution at three detector bank (90 degree, low angle and small angle). Typical measuring time to obtain a 'Rietveld-quality' data is several minutes with the sample size of laboratory X-ray diffractometer. To promote industrial application, a utilization system for this diffractometer is required. We will establish a support system for both academic and industrial users who are willing to use neutron but have not been familiar with neutron diffraction. The construction of this instrument was already begun and will be completed in the beginning of 2008, as one of day-one instruments for J-PARC.

**Powder diffraction software: Choosing the right tool for the right job**

Maxim Avdeev

Bragg Institute, Australian Nuclear Science and Technology Organisation

A review of the progress in powder diffraction data analysis, results of synthetic tests and analysis of common and unique features of available software packages, both free and commercial, with the emphasis on neutron diffraction data, both constant wavelength and time-of-flight, will be presented.

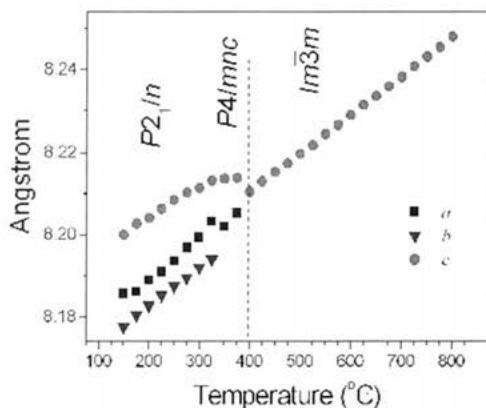
## Neutron and Synchrotron Diffraction Studies on Structural Phase Transitions in 1:3 Ordered Perovskites $\text{Sr}_{4-x}\text{Ba}_x\text{NaSb}_3\text{O}_{12}$

Qingdi Zhou Brendan J Kennedy

School of Chemistry, The University of Sydney

As part of our ongoing studies of the structures and phase transitions in perovskites oxides xx members of the series of 1:3 ordered perovskites of the type  $\text{Sr}_{4-x}\text{Ba}_x\text{NaSb}_3\text{O}_{12}$  have been synthesized and their structures determined using synchrotron X-ray and neutron powder diffraction techniques. At room temperature  $\text{Ba}_4\text{NaSb}_3\text{O}_{12}$  has a cubic structure, where the Na and Sb cations are ordered but there is no tilting of the octahedra. As the average size of the A-site cation decreases tilting of the octahedra is introduced and ultimately  $\text{Sr}_4\text{NaSb}_3\text{O}_{12}$  presents a monoclinic structure in  $C2/c$ . The powder neutron diffraction studies show that the two monoclinic phases of  $C2/c$  and  $P2_1/n$  co-exist at room temperature for samples with x between 1 and 2.5.

Variable temperature synchrotron powder diffraction studies demonstrate that the  $C2/c$  rapidly transforms to  $P2_1/n$  upon heating. A transition from monoclinic  $P2_1/n$  to tetragonal  $P4/mnc$  occurs at  $\sim 350^\circ\text{C}$  for  $\text{Sr}_{2.5}\text{Ba}_{1.5}\text{NaSb}_3\text{O}_{12}$ , and again, a continuous transition to the cubic structure near  $400^\circ\text{C}$  (Fig 1). These experimental results are consistent with a group theoretical analysis of the phase transition in 1:3 ordered perovskites[1].



### References

Howard, C.J. and Stokes, H.T. (2004) *Acta Cryst. B60*, 674-684.

## Single Crystal XRD Pattern Obtained From Magnetically Aligned Powder

Tsune-hisa Kimura<sup>\*</sup> Fumiko Kimura<sup>\*\*</sup> Masashi Yoshino<sup>\*</sup>

Department of Applied Chemistry, Tokyo Metropolitan University<sup>\*</sup> National Institute for Materials Science<sup>\*\*</sup>

There are two major routes to reach the structure determination of a crystal by diffraction methods: a single-crystal analysis and a powder pattern analysis. Each of them has the advantages and disadvantages. For example, the former cannot be applied to some compounds that do not crystallize to sizes large enough suitable for this analysis. The latter is a powerful means because of its wide applicability to any powder samples, but special cares should be paid, for example, to the overlapping of peaks, etc.

In the present paper, we propose the third route that would cover the disadvantages<sup>\*</sup> encountered by the single-crystal and powder methods. We used the magnetic alignment of crystallites to convert powder to a pseudo-single crystal. Crystals belonging to the biaxial crystal system (orthorhombic, monoclinic, triclinic) have three different diamagnetic susceptibility axes, i.e., the easy and hard magnetization axes and the intermediate one. We have developed a new technique by which the easy and hard axes are simultaneously aligned with respect to the laboratory coordinates.[1]

For the demonstration purpose, we used pulverized L-alanine crystallites (orthorhombic).[2] The powder was suspended in a UV curable resin precursor and subjected to a dynamic elliptic magnetic field to achieve 3-D alignment, followed by solidification of the resin. The obtained pseudo-single crystal exhibited the XRD pattern close to that of the original single crystal.

### References

- [1] T. Kimura, M. Yoshino, *Langmuir*, **21**, 4805-4808 (2005).
- [2] T. Kimura, F. Kimura, M. Yoshino, *Langmuir*, **22**, 3464-3466 (2006).

## Structural basis for Rab11-dependent membrane recruitment of FIP3/Arfophilin-1

Tomoo Shiba<sup>1</sup> Hiroshi Koga<sup>2</sup> Hye-Won Shin<sup>2</sup> Masato Kawasaki<sup>2</sup> Ryuichi Kato<sup>2</sup> Kazuhisa Nakayama<sup>2</sup> Soichi Wakatsuki<sup>2</sup>

Structural Biology Research Center, PF, IMSS, KEK, Present address: Graduate School of Arts and Sciences, The University of Tokyo<sup>1</sup> Graduate School of Pharmaceutical Sciences, Kyoto University, Japan<sup>2</sup> Structural Biology Research Center, PF, IMSS, KEK, Japan<sup>3</sup>

Small GTPases belonging to the Ras-like superfamily regulate intracellular membrane trafficking, and ARF and Rab family members participate in multiple stages of trafficking along the exocytic and endocytic pathways. Rab11 is a well-characterized regulator of endocytic and recycling pathways. Recently, a novel family of Rab11-interacting proteins (FIPs) has been identified. FIPs share a highly conserved ~20-amino acid region, termed Rab11-binding domain (RBD), at their C-termini. FIP3/Arfophilin-1 is a dual effector for Rab11 and ARF5/ARF6 involved in membrane delivery from recycling endosomes to the plasma membrane during cytokinesis. Here, we determined the crystal structure of Rab11 in complex with the FIP3-RBD. The structure reveals that the long amphiphilic  $\alpha$ -helix of the FIP3-RBD forms a parallel coiled-coil homodimer, with two symmetric interfaces with two Rab11 molecules (Fig). The hydrophobic side of the RBD helix is involved in homophilic dimerization and mediates the interaction with the Rab11 switch 1 region, whereas the opposite hydrophilic side interacts with the Rab11 switch 2 and is the major factor contributing to the binding specificity.

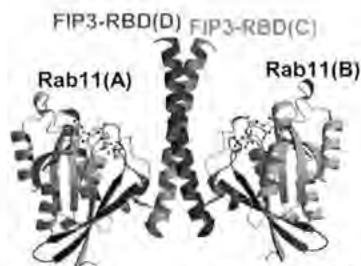


Fig. Crystal structure of Rab11-FIP3-RBD

## Crystal structures and evolutionary relationship of two different lipamide dehydrogenases (E3s) from *Thermus thermophilus*

Hiroshi Kondo<sup>1</sup> Ella Czarina Magat Juan<sup>1</sup> M. Tofazzal Hossain<sup>1</sup> Wataru Adachi<sup>1</sup> Tadashi Nakai<sup>1</sup> Nobuo Kamiya<sup>2</sup> Ryoji Masui<sup>2</sup> Seiki Kuramitsu<sup>2</sup> Kaoru Suzuki<sup>2</sup> Takeshi Sekiguchi<sup>2</sup> Akio Takenaka<sup>1</sup>

Graduate School of Bioscience and Biotechnology, Tokyo Institute of Technology, Midori-ku, Yokohama 226-8501, Japan<sup>1</sup> RIKEN Harima Institute/SPring-8, Hyogo 679-5148, Japan<sup>2</sup> Iwaki-Meisei University, Iwaki, Japan<sup>3</sup>

2-Oxoglutarate dehydrogenase complex (OGDC) and pyruvate dehydrogenase complex (PDC) have similar architectures composed of three proteins, E1, E2 and E3, in which E1 and E2 are substrate-specific while E3 is the common component. However, the E3 gene is classified into either E3o or E3p type, depending on the organisms. Recently, it has been found that a few of organisms possess two E3 genes. They correspond to E3o and E3p, which may bind to the cognate complexes. To compare the two structures, the crystal structures of E3o and E3p from *Thermus thermophilus* have been determined at 1.7 and 1.6 Å resolutions, respectively. The structures of the active sites are highly conserved between the two E3s. Several differences occur on surface residues, which form flexible loops that may be in contact with the different core architectures of the complexes. Ultracentrifugation experiments of E2o and E2p indicate that the cores of OGDC and PDC in *Thermus thermophilus* are cubic (432 symmetry, 24E1:24E2:12E3 composition) and icosahedral (532 symmetry, 60E1:60E2:24E3 composition), respectively. These structural features are similar to those of eucaryotes and Gram-positive prokaryotes, but different from those of Gram-negative prokaryotes where both OGDC and PDC are cubic. We propose that an ancestor operon with a cubic symmetry carrying a set of E1, E2 and E3 genes may have taken the following evolutionary steps: (1) duplication to generate two operons, (2a) disappearance of one of the E3 genes in either operon, or (2b) transformation of the architecture in one of the operons into the icosahedral form, and (3) disappearance of one of the E3 genes in the operon with a cubic architecture.

## Crystal structure of extracellular giant hemoglobin of pogonophoran *Oligobrachia mashikoi*

Nobutaka Numoto<sup>1</sup> Taro Nakagawa<sup>2</sup> Akiko Kita<sup>3</sup> Yuichi Sasayama<sup>4</sup> Yoshihiro Fukumori<sup>5</sup>  
Kunio Miki<sup>6</sup>

Graduate School of Science, Kyoto University<sup>1</sup> Graduate School of Natural Science and Technology, Kanazawa University, Japan<sup>2</sup> Research Reactor Institute, Kyoto University, Japan<sup>3</sup> Institute of Nature and Environmental Technology, Kanazawa University, Japan<sup>4</sup> Natural Science and Technology, Kanazawa University, Japan<sup>5</sup> , Graduate School of Science, Kyoto University, Japan / RIKEN SPring-8 Center at Harima Institution, Japan<sup>6</sup>

Pogonophorans obtain their nutrition mainly from their symbiotic bacteria because they have no mouth or gut. These animals live in sulfide rich seabed and the symbiont is thought to be chemoautotrophic sulfur-oxidizing bacteria. Pogonophorans have 400 kDa extracellular giant hemoglobin (Hb) which can transport oxygen and sulfide simultaneously. The symbiotic bacteria are supplied with sulfide by the giant Hb and afford host organic materials. We have recently determined the crystal structure of an oxygenated giant Hb from pogonophoran *Oligobrachia mashikoi* at 2.85 Å resolution<sup>1</sup>. The structure is hollow-spherical, with outer and inner diameters of about 120 Å and 50 Å, respectively, and composed of a total of 24 globins as a dimer of dodecamer. Crystal structure of the reconstructed Hb dodecamer core complex of annelids giant Hb and vestimentiferan coelomic Hb have also been reported as CO and Oxy form, respectively. These giant Hbs have almost the same dodecameric assemblage and it would be a common unit to pogonophorans, vestimentiferans, and annelids giant Hbs. The structure of pogonophoran Hb suggests sulfide-binding mechanism that free Cys residues bind sulfide by forming a persulfide group and it could be stabilized by aromatic-electrostatic interactions by the surrounding Phe residues.

We also determined the crystal structure of partially oxygenated giant Hb of *O. mashikoi* at higher resolution. The structure of the partially Oxy-Hb is compared with those of other reported Oxy/CO- giant Hbs, especially with that of the Oxy form of *O. mashikoi* Hb.

1) Numoto, N. *et al.*, *Proc. Natl. Acad. Sci. USA*, **102**, 14521-14526 (2005).

## Multiplex formation of repetitive sequences $d([G]_nA)_m$ by non-Watson-Crick pairings

Graduate School of Bioscience and Biotechnology, Tokyo Institute of Technology<sup>1</sup> and IBMC-CNRS, Université Louis Pasteur<sup>2</sup>

Yoshiteru Satō<sup>1</sup>, Kenta Mitomi<sup>1</sup>, Hiromu Sugiyama<sup>1</sup>, Satoru Shimizu<sup>1</sup>, Ella Czarina Magat Juan<sup>1</sup>, Jiro Kondo<sup>2</sup> and Akio Takénaka<sup>2</sup>

We found that DNA fragments with the sequence  $d(gcGA[X]_nAgc)$  ( $X=G$  and  $A$ ) form an base-intercalated duplex and that it is the basic unit for further assembly to form an octaplex. To investigate versatility of multiplex formation,  $d(gcGA[G]_nAgc)$  was crystallized in the two forms:  $P2_12_12_1$  and  $P2_1$ . The crystal structure of the latter form has been determined at 1.8 Å resolution. The two DNA fragments in the asymmetric unit form a duplex. The most interesting finding is that two sheared-type  $G_3:A_6$  and  $A_7:G_2$  pairs, two  $G_5:G_6$  and  $G_6:G_5$  pairs and two sheared-type  $G_7:A_4$  and  $A_8:G_3$  pairs are formed in the major part, which suggests that the duplex is formed by non-WC pairings, though two WC type  $G_1:C_{10}$  and  $C_9:G_8$  pairs occur at both ends (see the figure). Native gel electrophoresis experiments, performed to examine such a possibility, shows that all DNA fragments with  $d(GAG[G]_nGA)$  (where  $n=1-4$ ) form not only duplexes, but also several multiplexes such as quadruplexes, octaplexes, and so on. In human genome, these types of sequences are frequently found in SNPs of purine rich regions. They might have some functions with specific structures. These sequences are crystallized.



Fig. Overall duplex structure of  $d(gcGA[G]_nAgc)$

## Functional interactions of the translation elongation factors.

Anders - Liljas

Molecular Biophysics, Lund University

Structural biology has made an enormous change to the field of translation, particularly due to the crystallographic and EM analysis of the ribosome. However, much remains to be clarified.

The translation factors are needed to get the rate and fidelity required for protein synthesis. They catalyse protein synthesis on the ribosome. Several of the translation factors are GTPases and are structurally and functionally related. EF-Tu and EF-G are the GTPases in the elongation phase of translation. They catalyse irreversible steps in the process. EF-Tu catalyses the binding of a cognate tRNA to the ribosomal A-site. After peptidyl transfer EF-G catalyses the translocation of peptidyl-tRNA from the A- to the P-site.

The translational GTPases are normally inactive enzymes, but at a suitable state, the ribosome activates their inherent capacity to hydrolyse GTP. An important interaction occurs with the ribosomal protein complex (L10<sup>\*</sup>L12<sub>2</sub>) whose structure and function is slowly becoming understood. Through a number of different approaches the conformational dynamics of the factors and their interplay with the ribosome becomes clarified.

## Significance of high Z' structures in crystallization mechanisms

Gautam R. Desiraju

School of Chemistry, University of Hyderabad

Crystal structures with multiple molecules in the asymmetric unit (high Z') have been noted from the earliest days of crystallography. In former times, these structures might have posed problems with structure solution and refinement and in this way, be a nuisance. Today, there are a few of these structures which cast some light on the mechanism of crystallization. In this talk, some polymorphic systems will be described wherein one of the forms has a higher value of Z' and could be a kinetic polymorph. The other has a smaller value of Z' and could be the thermodynamic polymorph. The symmetry independent molecules in the high Z' structure could evolve into symmetry related molecules in the low Z' structure. Both synthons and symmetry could evolve in this process, and a study of the two structures may offer insights into the mechanism of crystallization of small organic molecules.

## **eCrystals: A Route for Open Access to Small Molecule Crystal Structure data**

Michael B Hursthouse<sup>1</sup> Simon C Coles<sup>1</sup> Jeremy G Frey<sup>1</sup> Andrew Milsted<sup>1</sup> Leslie Carr<sup>2</sup> Monica Duke<sup>2</sup> Traugott Koch<sup>2</sup> Elizabeth Lyon<sup>2</sup>

<sup>1</sup>School of Chemistry, University of Southampton <sup>2</sup>School of Electronics and Computer Science, University of Southampton <sup>3</sup>UKOLN, University of Bath, UK<sup>4</sup>

The normal route for the publication of a crystal structure report is coupled with and often governed by the underlying chemistry and is therefore subject to the lengthy peer review process and tied to the timing of the publication as a whole. This bottleneck in the dissemination of crystal structure data hinders the potential growth of databases and the data mining studies that are reliant on these collections. Just 500,000 small unit cell crystal structures are available in the CSD, ICSD & CRYSMET databases, while it is estimated that at least twice this number have been determined in research laboratories and are likely to remain unpublished.

The eBank-UK project (<http://www.ukoln.ac.uk/projects/ebank-uk/>) has established an institutional data repository that supports, manages and disseminates metadata relating to the crystal structure data it contains. The repository (<http://ecrystals.chem.soton.ac.uk>) makes available all the raw, derived and results data from a crystallographic experiment with little further researcher effort after the creation of a normal completed structure in a laboratory archive. This approach allows rapid release of crystal structure data into the public domain, and also provides mechanisms for rapid discovery of the data for further studies and reuse.

The details of the preparation of data, upload process, files supported and automatic report generation will be presented.

## Control of molecular aggregation in inclusion crystals by phase transition

Fumio Toda

Department of Chemistry, Okayama University of Science

Aggregation pattern of molecules in inclusion crystals can easily be controlled by phase transition in the solid state.

Molecular aggregation of a guest molecule in its inclusion complex with a host compound was transferred into a completely different molecular aggregation by a phase transition in the solid state. For example, a photochemically unreactive inclusion crystal of 5-methyl-2-pyridone with 1,3,5-benzenetricarboxylic acid was converted in the solid state into a reactive phase by heating or by contact with MeCN vapor. A racemic complex of *rac*-2,2'-dihydroxy-1,1'-binaphthyl and Me<sub>4</sub>NCl was converted into a conglomerate complex by heating or by contact with MeOH vapor at room temperature. These phase transitions were studied by IR spectra and X-ray analysis.

## Hydrogen Bonded Ladder Structures

Roger - Bishop Vi T. Nguyen Isa Y. Chan Donald C. Craig Marcia L. Scudder

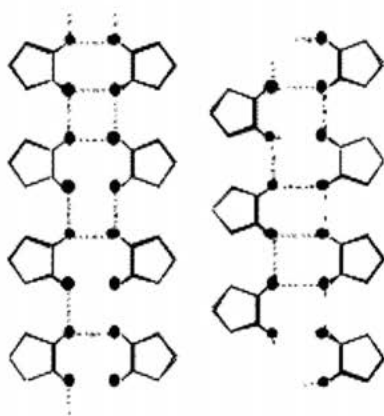
School of Chemistry, University of New South Wales

Certain dialcohols crystallize by means of hydrogen bonding into two parallel strands that are cross-linked by additional hydrogen bonding to form self-assembling ladder structures. If the strands are cross-linked in phase with each other then a step-ladder arrangement is produced. However, if they are cross-linked out-of-phase, then a twisted staircase-ladder results.

There is a strong preference for staircase ladders to contain only one dialcohol enantiomer, even if the starting material is racemic. This paper will describe a new dialcohol capable of forming at least five different staircase-ladder arrangements whose assembly is determined simply by the crystallization conditions employed.

### Reference

V.T. Nguyen, P.D. Ahn, R. Bishop, M.L. Scudder and D.C. Craig, *Eur. J. Org. Chem.*, 4489 (2001).



## Ring-Opening Isomerization: Relationship between Discrete Molecular Architectures and Coordination Polymers

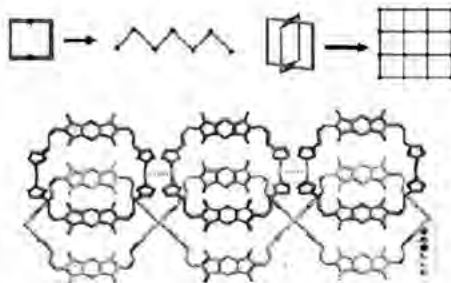
Cheng-Yong Su Zhi-Min Liu Mei Pan

School of Chemistry and Chemical Engineering, Sun Yat-Sen University

The existence of supramolecular isomerism in polymeric structures, which differ not by the building blocks but rather by the arrangement of the building blocks, has received increasing attention recently. Several examples of structural isomerism, conformational isomerism and topological isomerism have appeared in the literature. In contrast, discussions of supramolecular isomers, consisting of the closed and the polymeric isomers, have appeared only recently. Zaworotko<sup>1</sup> demonstrated such isomerism for the case of a discrete molecular hexagon and a polymeric zigzag chain. Another example reported by James<sup>2</sup>, where the coordination polymer  $[M_2L_3]_n$  was obtained from the  $[M_2L_3]$  precursor. It appears that the conversion from the closed structure to the polymeric one inevitably accompanies at least one ring opening. Therefore, we prefer to term this interconversion process as ring-opening isomerism.<sup>3</sup> Here, we would like to introduce some interesting examples which show formation of polymeric structures from the discrete ring or cage precursors.

### References:

- (1) Zaworotko, M. J. etc *J. Am. Chem. Soc.* 2002, 124, 9990;
- (2) James, S. L. etc *Chem. Eur. J.* 2001, 7, 2644.
- (3) Su, C.-Y. etc *Inorg. Chem.* 2003, 42, 5685.  
Supported by the NNSFC (No. 20525310)



## Structures and Non-Linear Optical Properties of Lanthanide Complexes

Wing-Tak Wong

Department of Chemistry, The University of Hong Kong

Multi-photon excitation allows molecules that typically absorb in the ultraviolet region to be excited with red or near-infrared light. The photoluminescence processes from organic-lanthanide complexes are usually induced by an organic chromophore ligand that absorbs incoming light and transfers the excitation energy to the lanthanide ion. Until now, only a few multi-photon processes in organic lanthanide complexes have been observed owing to the limitations of experimental measurements. Although there have been reports on lanthanide complexes containing second harmonic generation; these have been limited and focused just on glassy doped lanthanide materials. We have developed some amide based polymeric lanthanide materials that displayed efficient photo upconversion and/or non-linear optical properties (SHG, THG). Their syntheses, structures and luminescent properties will be discussed.

### References

1. K.-L. Wong, W.-M. Kwok, **W.-T. Wong**, D.L. Phillips, K.-W. Cheah, *Angewandte Chemie International Edition*, 2004, **43**, 4659-4662.
2. K.-L. Wong, G.-L. Law, W.-M. Kwok, **W.-T. Wong**, and D. L. Phillips. *Angewandte Chemie International Edition*, 2005, **44**, 3436-3439.
3. K.-L. Wong, Y.-Y. Yang, G.-L. Law and **W.-T. Wong**, *Advanced Materials*, 2006, **18**, 1051-1054.

## Chirality Scaffolding Crystallization

Department of Life Sciences, Graduate School of Arts and Sciences, The University of Tokyo\*

Kuroda Chiromorphology Team, JST ERATO-SORST\*\*

Reiko Kuroda\* Sayoko Hasebe\* Yoshitane Imai\*\* Tomohiro Sato\*\*

The polymorphism, a phenomenon to have crystals with the same composition but different structure, is of importance in pharmacology, solid-state chemistry, material science etc. Polymorphs usually differ in their chemical and physical properties such as melting point, density and lattice energy. Chiral crystals exhibit favorable properties, but are often meta stable and difficult to obtain selectively. The mechanism and control of polymorphism is not yet well understood. Here, we report a control of polymorphism of 2-arylthio-3-methylcyclohexen-1-one (compound **I**) under various conditions. Four polymorphs, **a - d** (**a, b**: achiral crystals, **c, d**: chiral crystals), were obtained which exhibit similar density and melting point. Crystal **a** is the most stable and was obtained most frequently. When polar solvent with hydroxyl groups was used, crystal **c** was sometime produced. Chirality recognition was observed, when **I** was crystallized in the presence of a chiral organic compound, **II**, where chirality control appears to be achieved in two steps: first, crystal **I-c** with a bigger (001) plane grew on top of the substrate, **II**, which also exposed a unusual crystal face. Then, crystal **I-d** grew on the (001) plane of **I-c**. We named this 'scaffolding crystallization'. Epitaxial growth was observed between the overlayer **I-d** and the substrate **I-c**. Chirality is recognized in both steps, and particularly in the latter step, 100% chirality transfer was achieved. Crystallization from the melt was found to produce different polymorphs depending on the crystallization speed. Various techniques including single or powder crystal X-ray diffractometry, 2D-NMR and DSC are used to analyze the interesting crystallization behaviour.

## **Element- and Site-Specific Phonon Density of States Measured by Nuclear Resonant Inelastic Scattering of Synchrotron Radiation**

Makoto SETO

Research Reactor Institute, Kyoto University, Kumatori-cho, Sennan-gun, Osaka 590-0494

Oscillating properties of the individual atoms in non-equivalent positions in a compound are not necessarily equivalent. Since it is well known that the dynamics of certain atoms in a compound influence the characteristics, to obtain the information on each atomic motion is important. The nuclear resonant inelastic scattering of synchrotron radiation offers element-specific phonon energy spectra. Therefore, it has been applied to a wide variety of scientific fields. In the case of a compound with two or more different states of atoms of the same element, such as mixed Fe valent magnetite, it is very difficult to observe the site-specific phonon densities of states (PDOS) experimentally. However, the combination of the energy and time domain measurements of the nuclear resonant scattering permits the observation of site-specific PDOS. We could measure the site-specific PDOS of Fe atoms in magnetite using nuclear resonant scattering of synchrotron radiation, and this result opened new area of a research. The principal concepts and the experimental results are discussed.

## Inelastic X-Ray Scattering for Investigating Exotic Superconductors

Alfred Q.R. Baron<sup>1,2</sup>

<sup>1</sup>*Materials Dynamics Laboratory, SPring-8/RIKEN*

<sup>2</sup>*Research and Utilization Division, SPring-8/JASRI*

Inelastic x-ray scattering (IXS) is a relatively new method of measuring atomic dynamics in materials at meV energy transfers and 1 to 100 nm<sup>-1</sup> momentum transfers. This range includes phonons in crystalline samples, and excitations in disordered materials (liquids and glasses). The technique affords some unique advantages including access to extremely small samples (<0.01mm<sup>3</sup>, some 5 orders of magnitude smaller than neutron scattering), and easy access to low momentum transfers (important for disordered materials). However, it also pushes the limits of what is possible even at third generation synchrotron sources. The talk will provide a brief introduction to the technique as implemented at BL35XU of SPring-8, with examples from recent work, with a focus on the investigation of electron-phonon coupling in superconductors.

## Theory of Resonant Inelastic X-Ray Scattering in Cuprates

Takami Tohyama<sup>1</sup> Kenji Tsutsui<sup>2</sup> Sadamichi Maekawa<sup>3</sup>

<sup>1</sup>Yukawa Institute for Theoretical Physics, Kyoto University, Kyoto 606-8502, Japan, <sup>2</sup>Yukawa Institute for Theoretical Physics, Kyoto University, Kyoto 606-8502<sup>3</sup> Institute for Materials Research, Tohoku University, Sendai 980-8577, Japan

Cu K-edge Resonant inelastic x-ray scattering (RIXS) in two-dimensional insulating cuprates reveals characteristic momentum dependence of a charge-transfer process from the occupied Zhang-Rice singlet band to the unoccupied upper Hubbard band, i.e., Mott-gap excitation. Using the numerically exact diagonalization technique for finite-size Hubbard cluster, we have proposed that the Mott-gap excitations are seen in the Cu K-edge RIXS even for doped cuprates but with different doping dependence between hole- and electron-doping [1]. Recently we examined theoretically the Cu K-edge RIXS on electron-doped  $\text{Nd}_{2-x}\text{Ce}_x\text{CuO}_4$  and compared with the experimental data obtained in SPring-8. The low-energy spectrum is assigned as the intra-band excitation and is qualitatively similar to the dynamical charge correlation function [2]. These results indicate that the RIXS is a powerful technique to investigate the charge dynamics in the strongly correlated electron systems. We also examine the momentum dependence of Cu L-edge RIXS in insulating cuprates [3]. Using the two-band Hubbard model, we find that charge excitations characteristic of the Cu L-edge RIXS process appear in the spectrum.

[1] T. Tohyama, K. Tsutsui, S. Maekawa, *J. Phys. Chem. Solids* **66**, 2139 (2005).

[2] K. Ishii, K. Tsutsui, et al, *Phys. Rev. Lett.* **94**, 207003 (2005).

[3] K. Tsutsui, H. Yamamoto, T. Tohyama, S. Maekawa, *J. Phys. Chem. Solids* **67**, 274 (2006).

## Low-Energy Charge Excitations by Inelastic X-ray Scattering: From Collective Excitations in Simple Materials to d-d Excitations in Mott Insulators

Yong Cai

National Synchrotron Radiation Research Center

Inelastic X-ray Scattering (IXS) is a powerful experimental technique that provides energy and momentum-resolved information on lattice and charge dynamics of a variety of condensed matters, and offers in particular unique strengths in the study of the low-energy charge excitations of correlated electron systems and the electronic properties of materials under extreme thermal dynamical conditions such as high pressure and extreme temperature. The technique has been widely implemented in third-generation synchrotron radiation sources around the world. The Taiwan Inelastic X-ray Scattering Beamline (BL12XU) at SPring-8 is designed for high-resolution resonant and non-resonant experiments on electronic excitations with energy ranges covering the K (L) absorption edges of most 3d (4f) metals. In this presentation, we will focus on non-resonant studies of low-energy charge excitations of a few archetypal materials, from collective excitations in  $\text{MgB}_2$ , exciton dynamics in organic polymers, to d-d excitations in Mott insulators, recently studied on the beamline, and discuss some of the interesting physics that can be unraveled using the technique. Potential of the technique in high pressure research will also be highlighted.

### References:

- [1] Y.Q. Cai, H.-K. Mao, P.C. Chow, J.S. Tse *et al.*, "Ordering of hydrogen bonds in high-pressure low-temperature  $\text{H}_2\text{O}$ ". *Phys. Rev. Lett.* **94**, 025502 (2005).
- [2] Y.Q. Cai, P.C. Chow, O.D. Restrepo, Y. Takano, *et al.*, "Low-Energy Charge Density Excitations in  $\text{MgB}_2$ : Striking Interplay between Single-Particle and Collective Behavior for Large Momenta", *Cond-Mat* 0605320.
- [3] N. Hiraoka, H. Ishii, I. Jarrige, and Y.Q. Cai, "Inelastic X-Ray Scattering Studies of Low-Energy Charge Excitations in Graphite", *Phys. Rev. B* **72**, 075103 (2005).

## **Evaluation of the experimental conditions for lower energy SAD phasing at the Photon Factory**

Yusuke Yamada Noriyuki Igarashi Tadashi Satoh Naohiro Matsugaki Soichi Wakatsuki

Photon Factory, High Energy Accelerator Research Organization

Recent advancements in the X-ray data-acquisition techniques and phasing algorithms have enabled structure determination using weak anomalous signals from light elements such as sulfur that are naturally present in almost all proteins. This is rapidly becoming a useful technique for high-throughput protein crystallography because it does not require preparation of heavy atom derivatives or Se-Met substituted proteins. This is also a useful technique for the structure determination of membrane proteins of higher organism, because it is quite difficult to produce these proteins in bacteria and Se-Met incorporated variant can not be produced. In the Photon Factory a new insertion device beamline, BL-17A, has been built and the user operation will commence in this October. Because BL-17A is designed with the emphasis on diffraction experiments with microcrystals and lower energy, it is expected to be a useful facility for the structure determination using anomalous signals from light elements. For the successful phasing, it is important to carry out diffraction experiments under an optimal condition. For example, at a lower energy of X-rays, light elements exhibit higher anomalous signals but an absorption effect becomes higher, which not only enhances radiation damages but also deteriorates the data quality. There should be an optimal energy which maximizes the signal-to-noise ratio of anomalous signals. To find out such optimal experimental condition, we carried out our case studies with the crystals of a yeast protein Emp46p as a standard sample and under various experimental conditions, such as X-ray energy, resolution, processing software and so on. We will report the relationship between these experimental conditions and resulting statistics of the SAD phasing.

## On the use of the loopless free crystal mounting method for the longer X-ray S-SAD phasing

Nobuhisa Watanabe

Faculty of Advanced Life Science, Hokkaido University, Sapporo, Japan

Single wavelength anomalous diffraction (SAD) phasing has become a potential tool for protein structure determination. The choice of X-ray wavelength is one of the major decisions required for SAD data collection. In the laboratory, however, we may only choose from several anticathode targets. Considering the phasing using the anomalous signal of sulfur atoms of underivatized native protein, longer wavelength of Cr  $K\alpha$  X-rays (2.29 Å) might be an optimal choice, where the anomalous intensity differences or the Bijvoet ratio becomes about 1% of total reflection intensity, because the  $\Delta f''$  value of sulfur becomes 1.14 e<sup>-</sup> as compared to 0.56 e<sup>-</sup> at Cu  $K\alpha$ . But the Bijvoet difference is still very small and highly accurate data collection is essential. One of the experimental difficulties in using longer wavelengths is the increased absorption. Especially, in standard protein crystallography where the crystal is mounted in a cryoloop with cryo-buffer, X-ray absorption by these materials sometimes prevents the detection of tiny anomalous signals. We have developed a novel loopless free crystal mounting technique to eliminate absorption by the cryo-buffer and cryoloop. This technique increases the precision of the anomalous differences between the Bijvoet mates, and makes the in-house S-SAD method with a Cr  $K\alpha$  X-ray source a very useful tool for high-throughput structure determination. The practical applicability of in-house structure determination using Cr  $K\alpha$  X-rays and the loopless free crystal mounting method was examined using several novel proteins. Proteins from 9.6 kDa to 84 kDa have been solved using this method without any derivatization. In most cases, more than 90% of all the structures were constructed automatically with side chains by use of the SAD phasing method.

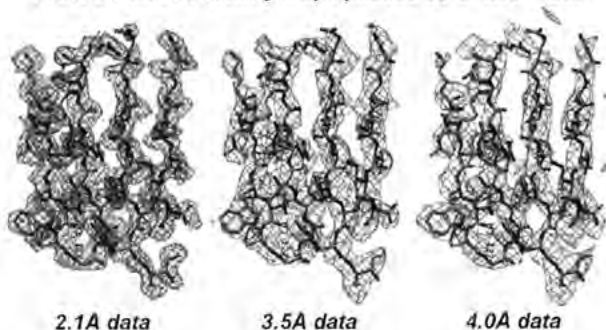
## OASIS applications - SAD phasing and fragment extension at different resolution

Deqiang Yao,<sup>1</sup> Yuanxin Gu,<sup>1</sup> Chaode Zheng,<sup>1</sup> Zhengjiong Lin,<sup>1</sup> Haifu Fan,<sup>1</sup> Nobuhisa Watanabe<sup>2</sup>

<sup>1</sup>Institute of High Energy Physics, Chinese Academy of Sciences<sup>1</sup> Institute of Physics, Chinese Academy of Sciences, P. R. China<sup>1</sup> Faculty of Advanced Life Sciences, Hokkaido University, Japan<sup>2</sup>

Case studies for SAD phasing and fragment extension by OASIS-2004 with  $\sim 2.0\text{\AA}$  data have been reported previously. The present study is to probe the low resolution limit that allows a successful direct-method SAD phasing. Sulfur-SAD data of the 69 kDa protein TT0570 were collected with in-house Cu-K $\alpha$  radiation at 1.8 $\text{\AA}$  resolution. Its truncated subsets at 2.1, 3.5 and 4.0 $\text{\AA}$  resolution were used in the test. The sulfur substructure was solved at each resolution independently. The data has an expected Bijvoet ratio  $\langle |DF| \rangle / \langle F \rangle \sim 0.56\%$ . In the 2.1  $\text{\AA}$  case, a single run of OASIS+DM+ARP/wARP led automatically to a model containing 1178 of the total 1206 residues all docked in sequence. In the 3.5 $\text{\AA}$  case, two cycles iteration of OASIS+DM+RESOLVE (build only) resulted in a model with more than 700 residues, 58 among them were docked in sequence. The corresponding electron density map is traceable by an experienced worker. In the 4.0 $\text{\AA}$  case, a single run of OASIS+DM+RESOLVE (build only) gave a somewhat degraded map, which failed to be improved by further iteration but still provides useful information.

**TT0570 electron density maps phased by OASIS + DM**



**Effective techniques to prepare iodine derivatives for I-SAD phasing by vaporizing iodine labelling (VIL) and hydrogen peroxide VIL (HYPER-VIL)**

Hideyuki Miyatake Tomokazu Hasegawa Akihito Yamano

RIKEN Advanced Development and Supporting Center Biomolecular Characterization Team  
PharmAcess, Inc., Japan

One of the most dominant factors for successful SAD phasing, especially in laboratories, seems to greatly depend on whether we can extract large enough anomalous effects from collected data. Iodine atoms diffract softer X-rays with larger anomalous effects ( $\Delta f''=6.8e'$  for Cu- $K\alpha$ ,  $\Delta f''=12.1e'$  for Cr- $K\alpha$ ), which are comparable to those of conventional heavy atoms such as Pt and Hg. Thus, if we could effectively incorporate iodine atoms into the target native crystals, this will greatly increase the chances of successful phasing by I-SAD using softer X-rays. That because we developed two effective techniques to prepare iodine derivatives, termed as vaporizing iodine labeling (VIL) and hydrogen peroxide VIL (HYPER-VIL), where vapor diffusion of iodine and hydrogen peroxide plays a key role. By the proposed techniques, we can sometimes prepare iodine derivatives with highly occupied binding sites at the *ortho*-positions of tyrosine residues, which contributes sufficient phasing power for structure determination. Details and limitations of the VIL and HYPER-VIL will be discussed.

**Reference**

Miyatake, H., Hasegawa, T. & Yamano, A. (2006). Acta Cryst. D62, 280-289.

## Structure determination of a novel fungal pathogen protein using cobalt SAD phasing with a Cu-rotating anode X-ray generator

Gregor Guncar<sup>1,2</sup>, Ching-I A. Wang<sup>1</sup>, Jade K. Forwood<sup>1,2</sup>, Trazel Teh<sup>1</sup>, Ann-Maree Catanzariti<sup>4</sup>, Horst Schirra<sup>2</sup>, Peter A. Anderson<sup>3</sup>, Jeffrey G. Ellis<sup>4</sup>, Peter N. Dodds<sup>4</sup> and Bostjan Kobe<sup>1,2</sup>

<sup>1</sup>SMMS, University of Queensland, Brisbane Qld 4072, Australia

<sup>2</sup>IMB, University of Queensland, Brisbane Qld 4072, Australia

<sup>3</sup>SBS, Flinders University of South Australia, Adelaide 5001, Australia

<sup>4</sup>Division of Plant Industry, CSIRO, Canberra ACT 0200, Australia

X-ray anomalous scattering from a single cobalt ion was used for phasing of the *Melampsora lini* (flax rust) avirulence protein AvrL567-A. AvrL567-A is a protein from a fungal rust pathogen that induces gene-for-gene based mechanism of plant disease resistance in flax, where it is recognised by plant resistance proteins (L5, L6 and L7). In crystallization trials we observed that AvrL567-A is a cobalt binding protein. Cobalt absorption edge is close to CuK $\alpha$  wavelength, therefore we were able to collect a 2.0 Å resolution single-wavelength anomalous dispersion dataset using a conventional in-house copper rotating anode X-ray generator. Phases calculated using the program Solve were sufficient for Resolve to automatically build most of the structure. Native datasets at 1.7 Å and 1.4 Å resolution were used subsequently to build the rest of the model using program Arp/Warp. The AvrL567-A structure reveals a new  $\beta$ -sandwich-like protein fold and sheds light on the structural basis of recognition specificity of the L proteins for the AvrL567 family members. It also provides insights into possible pathogen-associated functions of the AvrL567 proteins. We demonstrate that Co<sup>2+</sup> can be used for SAD phasing using Cu rotating anode, which is advantageous when synchrotron radiation may not be readily available the method is applicable to proteins binding metals that can be substituted with cobalt.

## Disorder and diffusion path of mobile ions in ionic conductors

Masatomo Yashima

Department of Materials Science and Engineering, Tokyo Institute of Technology

Solid materials that exhibit high ionic conductivity have attracted considerable attention owing to their many applications in solid oxide fuel cells, sensors, catalysts and batteries. The development of better electrolyte materials requires a better understanding of the mechanism of ionic conduction, and crucial to this is a comprehension of the crystal structure at high temperatures where the materials work efficiently. Here we review our recent works on the positional disorder and conduction path of oxide ions in  $\text{Bi}_2\text{O}_3$ ,  $\text{Bi}_{1.4}\text{Yb}_{0.6}\text{O}_3$ ,  $\text{CeO}_2$ ,  $\text{Ce}_{0.93}\text{Yb}_{0.07}\text{O}_{1.96}$ , and  $(\text{La}_{0.8}\text{Sr}_{0.2})(\text{Ga}_{0.8}\text{Mg}_{0.15}\text{Co}_{0.05})\text{O}_{2.8}$  at high temperatures. We describe the conduction path of Li cations in Li-doped lanthanum titanate perovskite  $\text{La}_{0.62}\text{Li}_{0.16}\text{TiO}_3$  at room temperature. These were studied through the nuclear density distribution obtained by a combined technique including a Rietveld refinement and a maximum-entropy method (MEM)-based pattern fitting of the neutron-powder-diffraction data. Neutron-diffraction data were collected using the HERMES and HRPD at JRR-3M, JAEA. We found that the mobile ions in fluorite-type ionic conductors have a complicated disorder spreading over a wide area and shift to the  $\langle 111 \rangle$  directions from the ideal fluorite site at high temperatures. We have demonstrated that the conduction path of oxide ions in the Lanthanum gallate-based compound was not along the straight line between the ideal positions, but exhibited an arc shape away from the B-site cation ( $\text{Ga}_{0.8}\text{Mg}_{0.15}\text{Co}_{0.05}$ ). At 77K, the Li cations in  $\text{La}_{0.62}\text{Li}_{0.16}\text{TiO}_3$  are located at the 2c site (*Cmmm* space group) on the (002) La deficient layer, while at room temperature, they are spread over a wide area and migrate following the  $2c$ - $4f$ - $2c$  or  $2c$ - $2d$ - $2c$  tie line on the (002) layer.

## High-Resolution Neutron and X-ray powder diffraction studies on Phase Transitions in $(1-x)\text{Pb}[(\text{Mg}_{1/3}\text{Nb}_{2/3})\text{O}_3]\text{-xPbTiO}_3$ Ceramics

Akhilesh Kumar Singh<sup>1</sup> Dhananjai Pandey<sup>1</sup> Oksana Zaharko<sup>2</sup> Songhak Yoon<sup>3</sup> Namsoo Shin<sup>4</sup> Sunggi Baik<sup>3</sup>

School of Materials Science and Technology, Institute of Technology, Banaras Hindu University<sup>1</sup> Laboratory for Neutron scattering, Paul Scherrer Institute, CH-5232 Villigen PSI, Switzerland<sup>2</sup> Department of Materials Science and Engineering, Pohang University of Science and Technology, Pohang 790-784, Korea<sup>3</sup> Pohang Accelerator Laboratory, Pohang University of Science and Technology, Pohang 790-784, Korea<sup>4</sup>

Solid solution system  $(1-x)\text{Pb}(\text{Mg}_{1/3}\text{Nb}_{2/3})\text{-xPbTiO}_3$  (PMN-xPT) is technologically important material for piezoelectric transducer and actuator applications due to its very high electromechanical response about the morphotropic phase boundary (MPB) composition. Recently, we have discovered two new monoclinic phases with space groups Cm and Pm in the MPB region, the structure of which was believed to be mixture of rhombohedral and tetragonal phases for decades [A.K. Singh and D. Pandey, Phys. Rev.B **67**,064102(2003)]. In the present work, we have carried out temperature dependent dielectric, piezoelectric resonance frequency and powder diffraction studies on various compositions of PMN-xPT near MPB, which reveals several new phase transitions. Rietveld analysis of the high-resolution neutron and synchrotron x-ray powder diffraction data has been done to characterize different crystallographic phases evolving with composition and temperature near MPB. Our results suggest the presence of a succession of three phase transitions, not reported earlier, corresponding to structural changes from the monoclinic Cm to the monoclinic Pm to the tetragonal to the cubic phases for  $0.26 < x < 0.31$  on heating above room temperature. For the compositions with  $0.30 < x < 0.35$ , phase transitions from monoclinic Pm to tetragonal to cubic phases have been observed on heating above room temperature. The tetragonal compositions close to the MPB transform to monoclinic Pm phase on cooling below room temperature. The implications of these discoveries in terms of the polarization rotation model [H. Fu and R. E. Cohen, Nature **403**, 281(2000), D. Vanderbilt and M. H. Cohen, Phys. Rev. B **63**, 094108 (2001)] for high piezoelectricity of PMN-xPT ceramics are also discussed.

RRB 7A 024101 (2006)

## Structural Phase Transition in $(1-x)\text{Pb}(\text{Fe}_{1/2}\text{Nb}_{1/2})\text{O}_3$ - $x\text{PbTiO}_3$ Ceramics near the Morphotropic Phase Boundary Region

Satendra Pal Singh Akhilesh Kumar Singh Dhananjai Pandey

School of Materials Science and Technology, Institute of Technology, Banaras Hindu University

Lead iron niobate  $\text{Pb}(\text{Fe}_{1/2}\text{Nb}_{1/2})\text{O}_3$  (PFN) is a magnetoelectric material exhibiting paraelectric to ferroelectric and a paramagnetic to antiferromagnetic phase transitions at 385K and 143K, respectively. Further, the solid solution of PFN with  $\text{PbTiO}_3$ , i.e.  $(1-x)[\text{Pb}(\text{Fe}_{1/2}\text{Nb}_{1/2})\text{O}_3]$ - $x\text{PbTiO}_3$  (PFN-xPT), exhibits a morphotropic phase transition similar to that in the well known piezoelectric ceramics like  $\text{Pb}(\text{Zr}_{1-x}\text{Ti}_x)\text{O}_3$  (PZT), and  $(1-x)[\text{Pb}(\text{Mg}_{1/3}\text{Nb}_{2/3})\text{O}_3]$ - $x\text{PbTiO}_3$  (PMN-xPT). The morphotropic phase transition is of special technological interest since the dielectric and piezoelectric responses are known to be maximized near the morphotropic phase boundary (MPB) composition. The MPB has in the past been believed to separate the tetragonal and rhombohedral phase fields. Recently, it has been shown that the tetragonal and rhombohedral phase fields are separated by a thin region of stability of one monoclinic phase ( $M_A$ ) in the MPB region of PZT and two ( $M_B$  and  $M_C$ ) in the PMN-xPT ceramics. In the Present work, we have synthesized pyrochlore phase free PFN-xPT ceramics and studied their structure by powder x-ray diffraction. Rietveld analysis of the powder x-ray diffraction data shows that the MPB in PFN-xPT ceramics lies around  $x = 0.06$ . Our study provides the first experimental evidence for a morphotropic phase transition from a monoclinic phase of  $M_A$  type with  $Cm$  space group to a tetragonal phase with  $P4mm$  space group in the PFN-xPT system. It is proposed that this monoclinic phase persists in the entire composition range  $x < 0.06$ , as evidenced by the presence of anomalous broadening of the 200 profile.

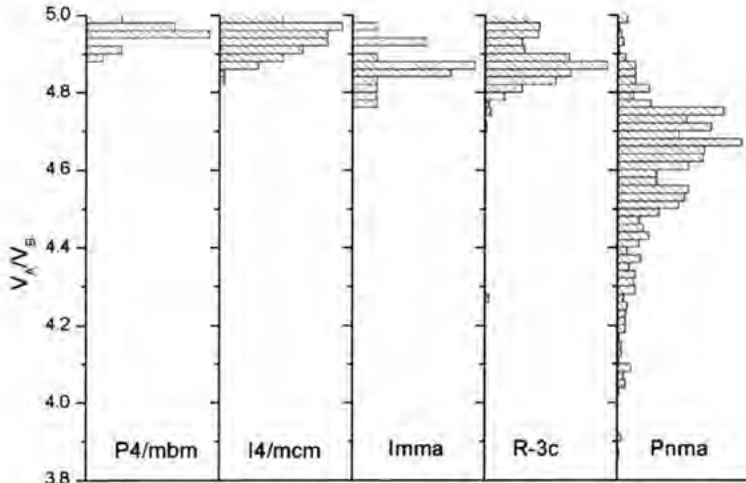
## Perovskites: Sorting Out

Maxim Avdeev

Bragg Institute, Australian Nuclear Science and Technology Organisation

Today relative stability of different modifications of perovskite structure type can be estimated with wide range of methods from simple geometric considerations based on the concept of ionic radii (tolerance factor) and bond valence approach (SPUDS) to energy calculations. However, in general these methods rely on tabulated values of radii, bond valence parameters, interatomic potentials, etc which are well established for room temperature but often unknown for non-standard conditions (high pressure, low/high temperature, etc).

Using a novel analytical approach we investigated crystallographic data for ~1800 perovskites  $ABX_3$  contained in the ICSD (release 2005-2). We show that parameterless method based on the analysis of M-X-M angles and A- and B- site polyhedra volume ratio ( $V_A/V_B$ ) calculated directly from experimental results under any conditions can be used for (a) a unified description of crystal structure evolution during phase transitions according to group-theoretical analysis by Howard&Stokes and (b) estimating critical values at which phase transitions will occur in parametric studies (composition, temperature, pressure, etc). Comparison to other existing approaches and examples will be presented.



Distribution of polyhedra volume ratios by the example of several space groups from the Howard-Stokes diagram.

Results for all other groups will be presented at the conference.

## Crystal Structure and Microwave dielectric properties on the tungstenbronze-type like $\text{Ba}_{6-3x}\text{R}_{8+2x}\text{Ti}_{18}\text{O}_{54}$ Solid Solutions

Hitoshi Ohsato

Materials Science and Engineering, Nagoya Institute of Technology

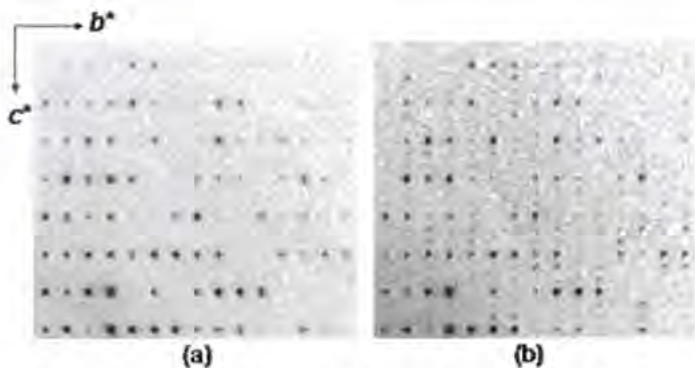
Tungstenbronze-type like  $\text{Ba}_{6-3x}\text{R}_{8+2x}\text{Ti}_{18}\text{O}_{54}$  ( $R$ =rare earth) solid solution reveals simultaneously high dielectric constant  $\epsilon_r$  and high quality factor  $Q$ , proposed as an application for mobile phone. The crystal data in the case of  $R$ =Sm with superlattice doubled of  $c$ -axis are as follows: orthorhombic  $Pbnm$  (No.62),  $a=12.131(13)$ ,  $b=22.271(5)$ ,  $c=7.639(5)$  Å and  $Z=2$ . The fundamental structure is composed of three types of large cation sites: ten  $A1$  rhombic sites in  $2 \times 2$  perovskite blocks, four  $A2$  pentagonal sites and four trigonal sites. The pentagonal and trigonal sites are located among the perovskite blocks. The fundamental structure is expressed by the formula  $[\text{R}_{8+2x}\text{Ba}_{2-3x}\text{V}_x]_{A1}\text{Ba}_{6-3x}\text{R}_{8+2x}\text{Ti}_{18}\text{O}_{54}$  ( $0 \leq x \leq 2/3$ ). Here, V means vacancy. In the  $0 \leq x < 2/3$  composition region, the  $A1$ -sites are occupied mainly by medium-sized  $R$ -ions, and also by a small amount of large Ba-ions. For  $x = 2/3$ , the  $A1$ -sites and  $A2$ -sites are occupied by  $R$ -ions and Ba-ions, respectively.  $A1(1)$ - and  $A1(5)$ -sites are two-cap trigonal prisms with 8 coordination numbers CN,  $A1(2)$ - and  $A1(4)$ -sites are a distorted cubic dodecahedra with 8 CN, and the  $A1(3)$ -site is a three-cap trigonal prism with 9 CN, whereas  $A2(1)$ - and  $A2(2)$ -sites are a two-cap hexahedron with 10 CN. In this study, relationships between crystal structure and microwave dielectric properties are presented. There are three important properties such as dielectric properties, quality factors and temperature coefficient of resonant frequency. We would like to present guidelines for design based on the relationship.

## The Commensurate Modulated Structure of The Thermal Quenching Meta-stable State In Spin Crossover Complex [Fe(abpt)<sub>2</sub>(NCS)<sub>2</sub>]

Chou-Fu Sheu Szu-Miao Chen Shih-Chi Wang Gene-Hsiang Lee Liu Yi-Hung Yu Wang

Department of Chemistry, National Taiwan University

One polymorph (C) of a spin crossover complex [Fe(abpt)<sub>2</sub>(NCS)<sub>2</sub>] ( $T_C = 86$  K) is structurally characterized, the  $c$  axis is tripled to form a commensurate modulated structure in the thermal quenching meta-stable high spin state at 25 K, which is obviously different from that of the thermodynamically stable state at 300 K. The asymmetric unit contains two crystallographic independent iron sites (Fe1 and Fe2), both located at inversion centers. Each iron atom is octahedrally coordinated by six nitrogen atoms: four from two abpt ligands and two from NCS ligands in a trans conformation. The molecular packing around each Fe site is very different. The packing around Fe 1 is similar to that of polymorph A, where neighboring abpt ligands form quasi 1-D chain through  $\pi$ - $\pi$  interaction. On the contrary, the packing around Fe 2, the neighboring abpt are nearly perpendicular to each other, no  $\pi$ - $\pi$  interaction is possible. The reason for phase transition is most likely due to the different anisotropic thermal contraction in the different packing layer. The diffraction evidence of the commensurate structure is shown below, the three dimensional structures will be presented.



The CCD images of **1** at (a) 300 K, (b) thermal quenching to 25 K

## **Recent Advancements in Small Angle X-ray Scattering: Synchrotron Grazing Incidence X-ray Scattering, Specular X-ray Reflectivity and Their Combinations**

Moonhor Ree Jinhwan Yoon Kyuyoung Heo Kyeong Sik Jin Sangwoo Jin Byeongdu Lee Jehan Kim Kwang-Woo Kim

Pohang Accelerator Laboratory, Pohang University of Science & Technology

Conventional small angle X-ray and neutron scattering (SAXS and SANS) have been widely used to determine the large scale features of nanostructures, particularly in bulk specimens. However, these conventional scattering techniques are not applicable to nanostructures supported with substrates or in supported thin films because of their low sensitivity and resolution, which arise for low scattering volumes and when the substrates are much thicker than the nanostructures. Thus, a nondestructive method is required for the quantitative analysis of nanostructures supported with substrates or in supported thin films. In this paper, we describe a nondestructive grazing incidence small angle X-ray scattering (GISAXS) technique, which can produce a high intensity scattering pattern with high statistical significance even for thin films with a thickness of tens of nanometers that are supported with substrates. However, the use of the GISAXS technique is only possible in conjunction with scattering theory development and intensive data analysis because grazing incidence scattering is complicated by reflection and refraction effects that are not found in conventional small angle scattering. Due to these complexities of GISAXS data analysis, the full use of the power of GIXS in the characterization of nanostructure systems has been limited. The GISAXS theory is introduced and its power is demonstrated with quantitative data analyses of various nanostructure systems (for example, nanostructures with and without patterning, and single- and multi-layer nanostructures). Further, the GISAXS technique becomes more powerful when it is used together with specular X-ray reflectivity method.

## Nanostructure and Transition of Polyelectrolyte Brush at the Air/Water Interface by X-ray and Neutron Reflectometry

Hideki Matsuoka

Department of Polymer Chemistry, Kyoto University, Kyoto 615-8510, JAPAN

X-ray and neutron reflectivity techniques (XR and NR) are the unique technique for the *in situ* study on the nanostructure of monolayer on the water surface. In this study, the nanostructure and its transition of ionic amphiphilic diblock copolymer monolayer at the air/water interface by XR and NR. Although the monolayer was expected to consist of hydrophobic layer on the water and polyelectrolyte brush under the water, but it has been clarified that the nanostructure is not so simple by our systematic study; the monolayer consists of hydrophobic layer, polyelectrolyte brush layer and hydrophilic "carpet" layer just in between two layers. The existence of carpet layer is quite new finding, which was become possible by *in situ* reflectivity study. When the hydrophilic block length is short, only carpet layer is formed and no brush layer is formed under the hydrophobic layer. Also, even if hydrophilic chain is long enough, only carpet layer is formed if the brush density is low enough. By systematical investigation with changing the brush density, we have found that there is the "critical brush density" for the transition between "carpet-only" and "carpet + brush layer" structures. The critical brush density was found in the order of  $10^{-1}$  chain per  $\text{nm}^2$  and it decreased with increasing hydrophilic chain length. Also, the nanostructure of the polyelectrolyte brush layer is expected to be very sensitive to salt addition. However, the nanostructure of strongly ionic polyelectrolyte brush layer was not influenced by salt addition up to 0.2 M NaCl condition. This is due to the very high effective ion concentration in the brush layer. Beyond 0.2M NaCl, the monolayer shrunk up and the brush chain also shrunk. Hence, there is also the "critical salt concentration" for the structural transition by salt addition. In addition, the added salt ions in the brush layer were squeezed out by the compression of the monolayer by LB trough. These phenomena could be interpreted by the relative ion concentrations inside and outside the brush layer.

**In-situ observation of forming cell-sized liposome from dry lipid films**

Mafumi Hishida, Hideki Seto, Norifumi L. Yamada<sup>A</sup>, K. Yoshikawa

Department of Physics, Kyoto University, Kyoto 606-8502, Japan

<sup>A</sup>Institute of Materials Structure Science, High Energy Accelerator Research Organization, Tsukuba 305-0801, Japan

Phospholipid molecule is a main constituent of biomembranes. Due to its amphiphilic property, phospholipid molecules usually assemble into multi-lamellar vesicles in water. On the other hand, most of living cells are surrounded by single bilayers of phospholipids. Thus, the methods of creating cell-sized liposome (giant vesicles) are important to investigate model cell systems or for applications such as a drug delivery. However, the mechanisms of forming cell-sized liposome are not fully understood, and only practical recipes are known so far.

From this viewpoint, we have focused on the natural swelling method in which cell-sized liposomes are created spontaneously by a hydration of dry lipid films deposited on a solid substrate. We tried to observe the process of swelling of multi-stacked phospholipids bilayers by means of time resolved small-angle X-ray scattering, because the mean repeat distance  $d$  of lipid bilayers is about 60 Å, and the process usually occur within tens of seconds. All the experiments were done at BL40B2, SPring-8, JASRI, Japan.

The hydration of lipids in the liquid-crystalline phase was found to proceed in 3 stages. In the early stage until about 20 s after hydration, water molecules penetrate between lipid bilayers on a solid substrate, and in the intermediate stage (20-100 s), the lipid bilayers swell about 12 Å and reach a quasi-stable state. In the late stage, lipid bilayers gradually peel off from the stack to form liposome. On the other hand, in the case of a lipid in the gel phase, only the early and intermediate stages are observed. These behaviors correspond to the capacity for the liposome formation depending on the lipid phases. The kinetics of the late stage is discussed in terms of Kramers' formulas.

**SAXS-WAXS study of heterogeneous nucleation of *n*-alkane crystals in O/W emulsion system**

<sup>1</sup>S. Ueno <sup>2</sup>Y. Shinohara, <sup>2</sup>Y. Amemiya and <sup>1</sup>K. Sato

<sup>1</sup>Graduate School of Biosphere Sciences, Hiroshima University, Higashi-Hiroshima 739-8528 Japan.

<sup>2</sup>Graduate School of Frontier Sciences, The University of Tokyo, 5-1-5 Kashiwanoha, Kashiwa, Chiba 277-8561 Japan.

Crystallization in encapsulated system, such as vesicle, liposome, cubosome, emulsion etc., has been studied intensively because it is expected that new polymorphs of various soft materials is crystallized in these systems. In this presentation, interfacial heterogeneous nucleation in oil-in-water (O/W) emulsion will be reported by using simultaneous small-angle and wide-angle X-ray diffraction (SAXS-WAXS) measurement. Crystallization of oil phase in O/W emulsion is controlled by a lot of factors such as temperature, oil droplet size, type of emulsifier, pH etc. *n*-hexadecane-water emulsion system was prepared by high-pressure homogenization techniques. The average droplet size was ~1  $\mu\text{m}$ . Tween 20 was put as an emulsifier. When the high-melting hydrophobic emulsifiers was added to *n*-hexadecane, the model of oil phase in O/W emulsion, the hexagonal and orthorhombic type polymorphs appeared as new polymorphic forms in O/W emulsion together with triclinic type polymorph which was observed only in bulk system. These new polymorphs would be crystallized on the oil-water interface of oil droplets after the added high-melting hydrophobic emulsifiers crystallized. In other words, the high melting emulsifier plays a role of the template for heterogeneous nucleation and following crystal growth of the new polymorphs. These new polymorphs were observed more than 0.1 wt% concentration of the high-melting emulsifiers. On the other hand, no new polymorph was observed without high-melting hydrophobic emulsifiers added in the oil phase of O/W emulsion. However, when we prepared the larger droplet size, such as 30 or 40  $\mu\text{m}$ , of *n*-hexadecane droplet in O/W emulsion system, the transient rotator phase, meaning hexagonal phase, was observed without any high-melting emulsifiers in oil droplet of O/W emulsion. This fact suggests that not only the type and concentration of emulsifiers but also the curvature of oil droplet would strongly affect the heterogeneous nucleation and following crystal growth of oil phase in the O/W emulsion system.

**Study of rubber filled with silica by 2D-USAXS and XPCS**Yuya Shinohara<sup>1</sup>, Hiroyuki Kishimoto<sup>2</sup>, and Yoshiyuki Amemiya<sup>1</sup><sup>1</sup>Graduate School of Frontier Sciences, The University of Tokyo, Chiba 277-8561, Japan<sup>2</sup>SRI R&D Ltd., Hyogo 651-0071, Japan

Carbon black and silica particles are widely used as filler to reinforce rubber. The mechanism of reinforcement, however, has not been clarified yet. The aggregation structure of filler is supposed to be one of the origins of the reinforcement, and now attracts much attention in rubber science. In order to elucidate the role of filler in the reinforcement, it is important to clarify (1) the structure of filler aggregates and (2) their dynamics in rubber. Two-dimensional ultra-small-angle X-ray scattering (2D-USAXS) and X-ray photon correlation spectroscopy (XPCS) are promising tools to investigate filler aggregate structure and filler dynamics, respectively. Filler aggregates show hierarchical anisotropic structure on the order of 0.1 - 10  $\mu\text{m}$ . Conventional scanning-USAXS using Bonse-Hart camera is not appropriate to study the anisotropic structure. Recently, we have developed time-resolved 2D-USAXS at BL20XU, SPring-8 and have investigated the deformation process of aggregated filler in stretched rubber by 2D-USAXS. Also, we have investigated the dependence of the filler dynamics in rubber on temperature, the volume fraction of filler, vulcanization, and the size by XPCS. In this talk, we describe 2D-USAXS and XPCS of rubber filled with silica particles and show their potential for structural analysis.

## Crystallization and evaluation of HEWL crystals at wide range of pH

Wakari Iwai<sup>1</sup> Daichi Yagi<sup>1</sup> Takuya Ishikawa<sup>1</sup> Yuki Ohnishi<sup>1</sup> Ichiro Tanaka<sup>1</sup> Nobuo Niimura<sup>1</sup>

Institute of Applied Beam Science, Ibaraki University<sup>1</sup> Kaken.Co.Ltd.<sup>2</sup>

In the field of high resolution crystal structure analysis of proteins, high quality single crystals are necessary. High quality crystals of hen egg white lysozyme (HEWL) has been grown at different pH and evaluated by Wilson Plot method<sup>1</sup>.

As a crystallization agent, sodium chloride (NaCl) was used by batch method. It has been controlled by adjusting a ratio of phosphoric acid ( $H_3PO_4$ ) and sodium dihydrogen phosphate ( $NaH_2PO_4$ ) at low pH, and a ratio of sodium dihydrogen phosphate ( $NaH_2PO_4$ ) and disodium hydrogenphosphate ( $Na_2HPO_4$ ) at high pH, respectively. The crystallization of HEWL at different pH has been performed by the following method;

- 1) Direct crystallization at a defined pH solution.
- 2) Soaking a crystal grown at a certain easily crystallized pH solution into a defined pH solution.

Direct crystallization was also realized at pH2.5-pH5.5 solution (See the figure.).

The quality of HEWL crystals grown at different pH has been successfully evaluated.



### Reference:

- 1) S.Arai et al, Acta Cryst. D60, (2004)1032-1039

## **Crystallization of DNA oligomers by a simple temperature-control technique**

Toshiyuki Chatake Osamu Matsumoto Tatsuhiko Kikkou

Faculty of Pharmaceutical Sciences, Chiba Institute of Science

The combination of the development of chemical synthesis method for oligonucleotides and the improvement of the X-ray diffraction method has achieved over 500 X-ray structure analyses of nucleic acids in the present two decades. Nevertheless, obtaining single suitable crystals of oligonucleotides is still an empirical technique. During the crystallization, we need to find out the most suitable combination of metal salts and an alcohol as precipitant, and adjust the concentrations of selected chemical reagents to grow better and larger crystals. These steps are trial-and-error procedures, so that they would sometimes require a large effort or end in failure. As the result, a considerable number of three dimensional structures of important nucleic acids haven't been revealed yet.

In this presentation we propose a simple temperature-control method for obtaining single DNA crystals. Two complementary DNA oligomers usually form a double-helical structure by the Watson-Crick base pairing, called as double stranded DNA (dsDNA). Once the temperature rises, these dsDNA are dissociate to be two single stranded DNAs (ssDNA). Since the phosphate groups in ssDNA are exposed into the solvent region, ssDNA is more water soluble than dsDNA. Such change of solubility in the transition from dsDNA to ssDNA is utilized in the present method. In the present investigation, the melting point ( $T_m$ ) of DNA oligomers in the crystallization solution were estimated to be in the range of 333 - 318 K, and the single crystals of these DNA molecules could be obtained by systematically decreasing from 333 to 293 K.

## Crystal Structure and Functional Study of Thalassemic mouse/human Transgenic Hemoglobins.

Chariwat Samanchat<sup>1</sup> Lukana Ngisara<sup>2</sup> Jisnusun Svasti<sup>3</sup> Duangporn Jamsai<sup>4</sup> Suthat Fucharoen<sup>5</sup> Palangpon Kongsaeeree<sup>6</sup>

Department of Chemistry, Center for Protein Structure and Function, Mahidol University<sup>1</sup> Chulabhorn Research Institute, Vibhavadee-Rangsit Highway, Bangkok 10210, THAILAND<sup>2</sup> Department of Biochemistry, Center for Protein Structure and Function, Faculty of Science, Mahidol University and Chulabhorn Research Institute, Vibhavadee-Rangsit Highway, Bangkok 10210, THAILAND<sup>3</sup> Thalassemia Research Center, Institute of Science and Technology for Research and Development, Mahidol University, Salaya Campus, Nakorn Pathom 73170, THAILAND.<sup>4,5,6</sup>

Hemoglobin E (HbE), the most common  $\beta$ -thalassemic disease in Southeast Asia, is caused by a substitution of Glu by Lys at codon 26 of the  $\beta$ -globin gene. Clinically they are very heterogeneous in severity. Individuals homozygous HbE exhibit mild thalassemia, while the combination of HbE with a  $\beta$ -thalassemia mutation exhibit highly variable severity. A novel C57BL/6 Transgenic murine model of HbE were generated by S. Fucharoen's group with knock out mice that had deletions of the  $\beta$ -globin genes in order to create mice expressing chimeric hemoglobin ( $\mu\alpha_2:hu\beta_2^E$ ). Evidently, human  $\beta^E$ -transgene can be expressed and functioned *in vivo*. The transgenic HbE and HbA can be purified to homogeneity with DEAE anion-exchange chromatography. The transgenic hemoglobins were successfully crystallized, the crystals belong to the monoclinic  $P2_1$  space group with unit-cell parameters of  $a=53.81$ ,  $b=151.25$ ,  $c=76.81$  Å and  $\beta=97.38^\circ$  and the same space group with unit cell parameters of  $a=53.60$ ,  $b=148.65$ ,  $c=77.70$  Å and  $\beta=97.67^\circ$  for  $\alpha^m_2/\beta^E_2$  and  $\alpha^m_2/\beta^A_2$ , respectively. The structures were solved by using MR-method and refined to the 2.3 Å resolution. In the transgenic  $\alpha^m_2/\beta^E_2$  structure, Lys26 in human  $\beta^E$ -globin chain lost two H-bonds with Arg30 and His117 with respect to the Glu26 in the normal  $\beta$ -globin. Structural analysis of the difference between both hybrid molecules will be discussed. The structural investigation of transgenic hemoglobin would eventually reveal the involved mechanism in atomic level leading to better understanding of thalassemic mouse model before the development for testing antisense therapy and some antioxidant drugs instead of testing in human.

## Analysis of Crystal Growth of Trigonal Ribonuclease A

Hideaki Takusagawa Masanori Ootaki Shigefumi Yamamura Yoko Sugawara

Graduate School of Fundamental Life Science, Kitasato University

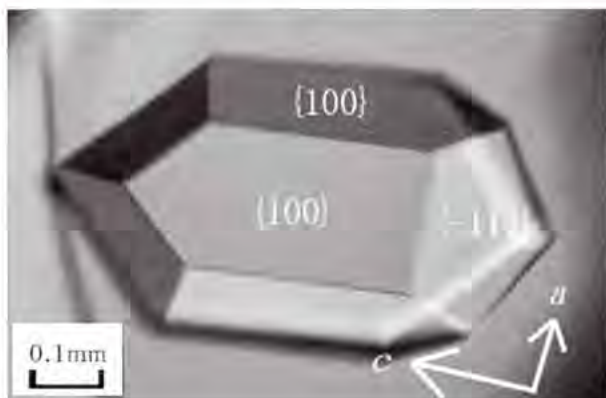
We have started experimental and theoretical analyses of crystal growth of proteins as a basis to regulate crystal shapes and crystal quality. Following the study on cubic insulin, the crystal growth of trigonal bovine pancreatic ribonuclease A (RnaseA) was investigated.

According to the reported crystallization condition [1], crystals of a hexagonal dipyramidal shape were obtained at 298 K and pH 5.5 (Figure 1). Indexes of crystal faces were determined to be  $\{100\}$  and  $\{-111\}$  based on precession photographs and facial angles. The macro-steps which may be attributed to bunching of the spiral steps were observed on  $\{-111\}$  by a differential interference microscope. Under high supersaturation, crystals of a squared shape surrounded by  $\{-111\}$  appeared at 298 K, and they tended to twin. On the other hand, crystals of parallelepiped plates appeared at 308 K.

Surface energies were estimated using the macrobond analysis [2] based on the PDB data of 1RNX. The surface energies of  $\{-111\}$ ,  $\{100\}$ , and  $\{001\}$  increase in this order, which is consistent with the observed crystal shape.

[1] Alexander, A. et al. (1996). *Biochemistry*, **35**, 15962-15972.

[2] Matsuura, Y. & Chernov, A. A. (2003). *Acta Crystallogr.*, **D59**, 1347-1356.



## Purification and crystallization of HutP protein that regulate hut operon of *Bacillus cereus*

Balasundaresan Dhakshnamoorthy<sup>1</sup> Tomoko S. Misono<sup>2</sup> Gopinath C.B. Subash<sup>1</sup> Kumar K.R. Penmetcha<sup>1</sup> Hiroshi Mizuno<sup>2</sup>

Functional Nucleic Acids Group, AIST<sup>1</sup> VALWAY Technology Center, NEC Soft Co. Ltd., Tokyo, Japan<sup>2</sup>

HutP is a 16.2 kDa protein consisting of 148 amino acid residues; HutP also exists in *Bacillus* species, which includes *B. subtilis*, *B. anthracis*, *B. cereus* and *B. halodurans*, with 60% sequence identity. Among these species, HutP of *B. anthracis* and *B. cereus* are 100% homologous in primary sequence. Sequence comparison of the *Bacillus* HutP proteins revealed that the C-terminal amino acid residues are more conserved than the N-terminal residues. Interestingly, the HutP protein binds to the terminator region of the *hut* mRNA and enhances hut structural gene expression only when activated by L-histidine. Several lines of evidences have indicated that HutP regulates the expression of the down-stream genes of the *hut* operon by an anti-termination mechanism. The terminator regions of *hut* operon consisted of at least three UAG repeats (1, 2). To test whether these UAG motifs are important for the HutP recognition, within this genus, we have analyzed the RNA-protein interaction studies, using various biochemical approaches among these species, and found that the HutP specifically recognize UAG repeats. In the present studies, we have identified the important chemical groups within the UAG motif of *hut* mRNA for HutP recognition of *Bacillus cereus*. Furthermore, we have established protocol for the expression, purification and crystallization of HutP protein of *Bacillus cereus*. These studies may reveal the detailed understanding of HutP regulation.

1. Kumarevel *et al.*, Nature 434 (2005) 183-191.
2. Kumarevel *et al.*, NAR 33 (2005) 5494-5502.

## Rare Earth Magnetic Materials: 1-2-2 Intermetallic Compounds

Stewart J Campbell<sup>1</sup> Michael Hofmann<sup>2</sup>

<sup>1</sup>School of Physical, Environmental and Mathematical Sciences, The University of New South Wales, ADFA, Canberra, AUSTRALIA <sup>2</sup>Technische Universitaet Muenchen, FRM II, Garching, Germany

Rare earth (R) magnetic materials are used extensively in society and have numerous technological applications. When combined with transition metal (T) and metalloid (X) elements, rare earth intermetallic compounds, R-T-X, exhibit a wide range of interesting and useful properties. The prime examples are magnets based on the Nd<sub>2</sub>Fe<sub>14</sub>B phase which exhibits the largest energy product (BH) discovered for a magnetic material.

A brief overview of the basic properties of rare earth intermetallic compounds and their applications in modern society will be presented. Interest will then focus on RT<sub>2</sub>X<sub>2</sub>, the 1-2-2 series. RMn<sub>2</sub>X<sub>2</sub> compounds are of particular interest as, unlike most transition metals, the Mn atoms carry a magnetic moment. For example, as LaMn<sub>2</sub>Si<sub>2</sub> is predominantly ferromagnetic and YMn<sub>2</sub>Si<sub>2</sub> antiferromagnetic; compounds of intermediate composition in La<sub>1-x</sub>Y<sub>x</sub>Mn<sub>2</sub>Si<sub>2</sub> exhibit mixed magnetic interactions leading to a complex magnetic phase diagram. RMn<sub>2</sub>(Si,Ge)<sub>2</sub> with R=Yb and Eu exhibit a wide range of unusual properties as well as intermediate valences associated with the transition from a divalent to a trivalent state. An overview of our neutron diffraction investigations of YbMn<sub>2</sub>(Si,Ge)<sub>2</sub> (~1.8-723 K; *p* ~ 0-2.7 GPa) and EuMn<sub>2</sub>(Si,Ge)<sub>2</sub> will also be presented. This has led to a magnetic phase diagram for YbMn<sub>2</sub>Si<sub>2-x</sub>Ge<sub>x</sub> of features consistent with a valence change between the trivalent behaviour of YbMn<sub>2</sub>Si<sub>2</sub> and the divalent-like behaviour of YbMn<sub>2</sub>Ge<sub>2</sub> around *x*<sub>c</sub> ~ 1.6. The volume changes in EuMn<sub>2</sub>Si<sub>2</sub> have been analysed for the first time in terms of the interconfigurational fluctuation model, leading to a valence transition temperature of T<sub>v</sub> ~ 527 K, occupation probabilities for the Eu<sup>2+</sup> state and average Eu<sup>val</sup> values.

## Magnetic structure study on NpTGa<sub>5</sub> (T: Fe, Co, Ni and Rh)

Fuminori HONDA

Advanced Science Research Center, Japan Atomic Energy Agency 1233 Watanuki-machi, Takasaki, Gunma 370-1292, Japan

AnTGa<sub>5</sub> (An: Actinides, T: transition metals) have been receiving increasing attention after the discovery of the heavy fermion superconductivity below 19 K in PuCoGa<sub>5</sub> [1]. Recently, we extend our research activity in neutron scattering for NpTGa<sub>5</sub> (T: Fe, Co, Ni and Rh) compounds in order to get deep insight about the multipolar degree-of-freedom.

We revealed that NpTGa<sub>5</sub> exhibits various antiferromagnetic structures of A-, C-, G-type, ferromagnetic ordering and cant magnetism (Fig.1) [2], which are the reminiscent of manganese perovskites.

The remarkable successive magnetic transition associated with reorientation and considerable increase of magnetic moment found in NpNiGa<sub>5</sub> and NpRhGa<sub>5</sub> is a signature for the change in the 5f electronic states, where the competing interactions of multipoles are expected to play an important role. We also present recent results of the resonant x-ray scattering experiments on NpNiGa<sub>5</sub>, which imply the existence of quadrupole ordering. We will sketch out a diverse electronic properties realized in NpTGa<sub>5</sub> in terms of the competing magnetic and quadrupolar interactions.

[1] J.L. Sarrao, *et al.*, *Nature* **420** (2002) 297.

[2] N. Metoki, *J. Phys. Soc. Jpn.*, **75** (2006) Suppl. p.24 and references therein.

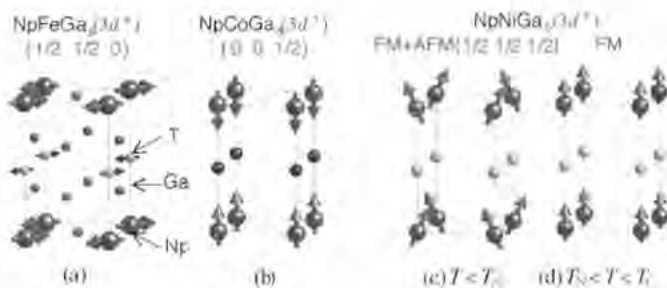


Fig.1 Rich variety of magnetic structures realized in NpTGa<sub>5</sub>.

**Magnetism and unusual behavior of multiferroic hexagonal manganites  $\text{RMnO}_3$** 

Je-Geun Park

Department of Physics, Sungkyunkwan University

Hexagonal manganites  $\text{RMnO}_3$  show ferroelectric transitions at very high temperatures, some of them above 700 K, while they order antiferromagnetically below 100 K. This coexistence of both ferroelectric and antiferromagnetic transitions in a single compound, so-called multiferroic behavior, is a rare phenomenon and has been the subject of recent intensive studies. Another interesting point about the magnetic properties of the rare-earth hexagonal manganites is that the Mn moments form natural two-dimensional edge-sharing triangular networks. Although some of early studies, including neutron diffraction experiments, were carried out in 60s on these materials, with the renewed interests in multiferroic behavior the physical properties of the hexagonal manganites have been reinvestigated. In this talk, we will present our recent works on several hexagonal manganites using both neutron scattering and bulk properties. Key points that will be covered in the talk are: First, we will discuss experimental evidence of spin frustrations observed in both neutron scattering and bulk measurements. Second, we will examine experimental results due to an unusually strong spin-lattice coupling. Third, we will show how the magnetic ground states of  $\text{RMnO}_3$  change upon chemical doping and external pressure.

## Field-induced magnetic phase transitions and the relevance with ferroelectricity in multiferroic compounds of $RMn_2O_5$ ( $R = Er, Ho$ )

Hiroyuki Kimura<sup>1</sup> Shuichi Wakimoto<sup>2</sup> Youichi Kamada<sup>3</sup> Yukio Noda<sup>4</sup> Kazuhisa Kakurai<sup>1\*</sup> Koji Kaneko<sup>5</sup> Naoto Metoki<sup>1</sup> Kay Kohn<sup>1\*</sup>

Institute of Multidisciplinary Research for Advanced Materials, Tohoku University, 2-1-1 Sendai, Miyagi, 980-8577, Japan<sup>1</sup> Japan Atomic Energy Agency, Tokai, Ibaraki, 319-1195, Japan<sup>2</sup> Department of physics, Waseda Univ., Tokyo, 169-8555 Tokai, Japan<sup>3</sup>

A colossal magnetoelectric (CME) effect, has become one of the most important issues in strongly correlated electron systems. A key feature in the CME effect is a multiferroics where a magnetic and a dielectric order coexist. However microscopic relations between magnetic and dielectric properties are not fully understood yet. In this work, we performed neutron diffraction measurements under magnetic field for the multiferroic  $RMn_2O_5$  ( $R = Er, Ho$ ) to clarify the relevance between the field-induced magnetic phase and the dielectric phase. Summary of the results is shown in the Figure. In  $HoMn_2O_5$  the field-induced magnetic phase transition from an incommensurate to a commensurate spin state occurs, where the ferroelectric phase is induced. On the contrary in  $ErMn_2O_5$ , the field-induced magnetic phase transition from the commensurate to the incommensurate spin state occurs where the electric depolarization concomitantly occurs. In both system, there are one to one correspondences between the magnetic and dielectric phase diagrams, indicates that the electric polarization is magnetically induced and the commensurate spin state is indispensable to the ferroelectricity in the multiferroic  $RMn_2O_5$  system.

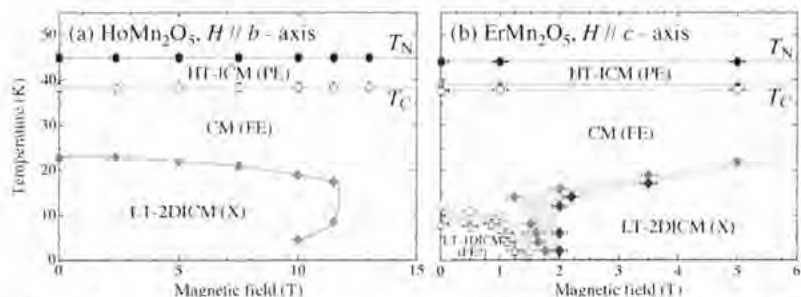


Figure 1: Color online  $H$ - $T$  magnetic phase diagram of (a)  $HoMn_2O_5$  and (b)  $ErMn_2O_5$ . Magnetic field are applied along  $b$ -axis and  $c$ -axis for  $HoMn_2O_5$  and  $ErMn_2O_5$ , respectively. Abbreviations shown in the figure indicate the magnetic and dielectric phases listed below.

HT-ICM (PE): High temperature incommensurate magnetic (Pseudoelectric) phase

CM (FE): Commensurate magnetic (Ferroelectric) phase

LT-IDICM (FE): Low temperature 1-dimensional incommensurate magnetic phase

LT-2DICM (X): Low temperature 2-dimensional incommensurate magnetic (nonferroelectric) phase

## **Extraction of polarisabilities and hyperpolarisabilities from X-ray constrained wavefunctions: applications to a series of NLO compounds**

Dylan Jayatilaka<sup>1</sup>, Andrew Whitten<sup>1</sup>, Paraprathim Munshi<sup>1</sup>, Mark Spackman<sup>1</sup>, Mike Turner<sup>2</sup>, Dima. Yufit<sup>2</sup>, Judith A. K. Howard<sup>2</sup>

Chemistry, University of Western Australia<sup>1</sup>, Chemistry, Durham University, England.<sup>2</sup>

The calculation of polarisabilities and hyperpolarisabilities from X-ray diffraction data on molecular crystals has been previously suggested, but the results have been unconvincing because the approximations made have been quite severe. In this talk we stress the importance of the off-diagonal elements of the density matrix for determining these quantities. Using the Lorentz-factor tensors, we also describe how the polarisability can be used to calculate the refractive index tensor, and the hyperpolarisability can be used to obtain the second order susceptibility tensor, important for non-linear optical (NLO) applications. Two methods are described to obtain these optical properties: one based on the Unsold approximation, another based on coupled-perturbed Hartree-Fock (CPHF) theory. Both methods are based on the use of density matrices obtained from X-ray constrained wavefunctions, but the CPHF method avoids a scaling procedure. The method is applied to a series of molecular crystals which display NLO behaviour: urea, 2-methyl-4-nitroaniline (MNA), 2-(N-nitrophenyl)-L-prolinol (PNP), N-(4-nitrophenyl)-L-prolinol (NPP).

The results will be discussed.

### **References**

A. Whitten, D. Jayatilaka, M. A. Spackman, *Journal of Chemical Physic*

**The MEM Charge density studies from multi high resolution synchrotron powder X-ray diffraction data.**

Eiji Nishibori<sup>1</sup>, Shinobu Aoyagi<sup>1</sup>, Kenichi Kato<sup>1</sup>, Masaki Takata<sup>2</sup>, Makoto Sakata<sup>1</sup>

<sup>1</sup>Applied Physics, Nagoya University, <sup>2</sup>Structural Materials Science Laboratory, Riken

Maximum Entropy Method (MEM) has been widely used for charge studies by X-ray powder diffraction experiments in the materials science field. The MEM is a method for statistical deduction of diffraction data. The MEM density study always requires accurate data with high counting statistics. It is normally difficult to collect high counting statistics in high angular regions in powder data. In order to improve counting statistics of powder diffraction data, we have been developing the both experimental and analytical techniques based on multi powder diffraction data. In this study, we report the MEM charge density studies of Silicon and Diamond from the multi powder diffraction data.

The multi powder data for silicon and diamond were collected at SPring-8, BL02B2. We measured two dataset for one sample at one temperature point. One of the dataset was measured in normal procedure. Another dataset was measured for improvement of counting statistics for high-order reflections.

These data sets were simultaneously analysed. The structure factors for MEM analysis were extracted. The MEM charge densities of silicon and diamond were determined from the extracted structure factors. The covalent bonds of silicon and diamond were clearly revealed by the MEM charge densities. The charge density at bond mid-point is coincided with various theoretical calculations within  $0.1 \text{ e}/\text{\AA}^{-3}$ . The present results show that the multi powder data method is appropriate for accurate charge density by MEM.

**3d-orbital determination of Ni<sup>2+</sup> in NiP<sub>2</sub> crystals by X-ray AO analysis**ZAW WIN<sup>1</sup> Kiyooki Tanaka<sup>2</sup> Ichimin Shirotani<sup>3\*</sup><sup>1</sup>Material Science and Engineering, Nagoya Institute of Technology<sup>2</sup> Muroran Institute of Technology<sup>3</sup>

NiP<sub>2</sub> has a pyrite type structure (Pa3, a=5.46522(5) Å) synthesized by one of the authors under high pressure. Electron density distribution (EDD) of NiP<sub>2</sub> was measured at 100K and 3d-orbital functions of Ni<sup>2+</sup> in the trigonal crystal field was determined keeping the orthonormal relationships among d-orbitals by X-ray AO analysis. In the X-ray AO analysis each atom is divided into sub-shell orbitals, which are treated as pseudo atoms. It enables us analyze the inter-atomic electron transfer even in the non-stoichiometric complexes keeping the electro-neutrality of the unit cell. The data was refined by QNTAO program (K.T.). In order to analyze 3p-orbitals of P atoms on the 3-fold axis sp<sup>2</sup>-like hybridized orbitals were employed. Asphericity of EDD was refined shifting electronic populations, kappas and 3d-orbital functions as well as anharmonic thermal vibration (AHV) terms for 1362 reflections. The R factor reduced to 0.0109 and all parameters converged well. The localized electrons and a contraction of the outermost 3p orbitals change the effective atomic potentials and enhance AHV of constituent atoms. Peaks around Ni<sup>2+</sup> on the deformation density maps were well explained after the AO analysis and d-orbitals, f<sub>i</sub>, expressed in terms of the five basis functions, (b<sub>1</sub>=d<sub>x<sup>2</sup>-y<sup>2</sup></sub>, b<sub>2</sub>=d<sub>z<sup>2</sup></sub>, b<sub>3</sub>=d<sub>yz</sub>, b<sub>4</sub>=d<sub>zx</sub> and b<sub>5</sub>=d<sub>xy</sub>) are determined as,

$$f_1=b_2, f_2=pb_3+qb_4+rb_5, f_3=rb_1+qb_3-pb_4, f_4=-pb_1-rb_4+qb_5, f_5=qb_1-rb_3+pb_5,$$

where p=0.714(5), q= 0.203(5), r=-0.670(4). Orbitals f<sub>1</sub> to f<sub>3</sub> are fully occupied and the electron population on the degenerated orbitals f<sub>4</sub> and f<sub>5</sub> is 1.77(2), indicating that 1.54 electrons are donated from P<sub>2</sub> moiety to Ni making Ni and P<sub>2</sub> almost neutral.

**Combined EXAFS and Neutron Diffraction study of the structure of superionic conducting glasses; AgI-AgPO<sub>3</sub> and Ag<sub>2</sub>S-AgPO<sub>3</sub>**

Abby Scott<sup>1</sup> Shane J Kennedy<sup>1</sup> Evvy Kartini<sup>2</sup>

<sup>1</sup>Bragg Institute, Australian Nuclear Science and Technology Organisation<sup>1</sup> National Nuclear Energy Agency, Tangerang 15314, Indonesia<sup>2</sup>

Selective doping of silver phosphate glass (AgPO<sub>3</sub>) with metal halides, alkali-oxysalts and other glass formers can strongly enhance its electric conductivity. Doping with AgI or Ag<sub>2</sub>S produces exceptionally conductive glass, largely via superionic conduction of silver ions (Ag<sup>+</sup>). In an effort to understand the mechanisms of superionic conduction, the local environment around Ag<sup>+</sup> ions in these glasses has been extensively studied using a wide variety of diffraction and spectroscopic techniques. Unfortunately, due to the disordered nature of glass, no one experimental technique can unambiguously reveal the complete atomic structure.

Our own neutron diffraction study on AgPO<sub>3</sub>, AgI-AgPO<sub>3</sub> and Ag<sub>2</sub>S-AgPO<sub>3</sub> glasses (performed on the HIT-II spectrometer at the spallation neutron source at KEK, Japan) provided excellent information on the modifications to the phosphate network in the doped glasses, but was not able to unambiguously separate the Ag-O, Ag-Ag and Ag-I pair correlations.

Here we report an EXAFS investigation on the same glasses using the Australian National Beamline Facility at the Photon Factory, KEK, Japan. The study was performed at the Ag absorption edge. We compare and contrast the EXAFS with the neutron diffraction results, noting how incorporation of the EXAFS result aids in construction of a more detailed and more accurate model of the structure of these glasses.

## Electrostatic Potential Analysis of the Ferroelectric Phase of BaTiO<sub>3</sub> using Convergent-Beam Electron Diffraction

Kenji Tsuda Michiyoshi Tanaka

Institute of Multidisciplinary Research for Advanced Materials, Tohoku University

We have been developing a method to refine crystal structural parameters using convergent-beam electron diffraction (CBED) (Tsuda and Tanaka, *Acta Cryst.* A55, (1999) 939; Tsuda *et al.*, *Acta Cryst.* A58, (2002) 514; Ogata *et al.*, *Acta Cryst.* A60, (2004) 525). The method is based on the non-linear least-squares fitting between full dynamical calculations and experimental intensities of two-dimensional CBED patterns. The CBED method provides the following advantages for the analysis of ferroelectric materials: (1) The CBED technique allows us to obtain diffraction intensity data from a single domain even though the specimen has a complex ferroelectric domain structure. (2) The direction of ferroelectric polarization can be readily identified from a CBED pattern. (3) CBED directly measures electrostatic potential.

We have applied the present method to the electrostatic potential analysis of the ferroelectric phase of perovskite BaTiO<sub>3</sub>. BaTiO<sub>3</sub> has been extensively studied due to its fundamental and technological importance. Zero-loss filtered CBED patterns were obtained from the ferroelectric phase at room temperature using an energy-filtering transmission electron microscope JEM-2010FEF. The atom positions, anisotropic Debye-Waller factors and Fourier coefficients of the electrostatic potential for low-order reflections were refined using the CBED patterns. The electrostatic potential was obtained by Fourier synthesis.

In the obtained electrostatic potential, the lowest potential valley was found at the position between the nearest-neighbor Ti and O atoms, which is attributed to the covalent bonding electrons between the Ti and O atoms. It is interesting to note that the absorption potential showed a characteristic anomaly in the vicinity of the Ti site.

## Crystal Structure of Mitochondrial Respiratory Membrane Protein Complex II

Fei Sun Xia Huo Yujia Zhai Aojin Wang Jianxing Xu Dan Su Mark Bartlam Zihe Rao

"Tsinghua-IBP Joint Research Group for Structural Biology", Tsinghua University, Beijing 100084,

The mitochondrial respiratory Complex II or succinate:ubiquinone oxidoreductase (SQR) is an integral membrane protein complex in both the tricarboxylic acid cycle and aerobic respiration. The first crystal structure of Complex II from porcine heart was solved at 2.4 Å resolution and its complex structure with inhibitors 3-nitropropionate and 2-thienyltrifluoroacetone (TTFA) was solved at 3.5 Å resolution. Complex II comprises of two hydrophilic proteins, flavoprotein (Fp) and iron-sulfur protein (Ip), and two trans-membrane proteins (CybL and CybS), as well as prosthetic groups required for electron transfer from succinate to ubiquinone. The structure correlates the protein environments around prosthetic groups with their unique midpoint redox potentials. Two ubiquinone binding sites are discussed and elucidated by TTFA binding. The Complex II structure provides a *bona fide* model for study of the mitochondrial respiratory system and human mitochondrial diseases related to mutations in this complex.

## Reorganisation of the pore during gating of inward rectifier K<sup>+</sup> channels

Jacqueline M Gulbis<sup>1</sup> Anling Kuo<sup>2</sup> Jonathan M Elkins<sup>3,4</sup> Declan A Doyle<sup>1,4</sup>

Structural Biology Division, The Walter and Eliza Hall Institute of Medical Research<sup>1</sup> Skirball Institute of Biomedical Medicine, New York University Medical Center<sup>2</sup> Structural Genomics Consortium, University of Oxford, Botnar Research Centre<sup>3,4</sup>

Potassium channels are specialised pores that conduct current, in the form of charged ions, across cell membranes. Their electrical activity depends on the channel adopting alternate physiological conformers correlating with 'closed' and 'open' states. Crystal structures of K<sup>+</sup> channels all have 2 transmembrane helices and a conserved ion filter, but show significant plasticity of the transmembrane pore. It is unclear whether the many conformers observed are specific to channel family or related to gating state.

We set out to investigate the molecular changes occurring during gating, reasoning that if we determine structures of a particular channel in two (or more) conformers we can eliminate this uncertainty.

Two subtly different X-ray structures of a prokaryotic inward rectifier K<sup>+</sup> channel assembly (KirBac3.1) from *Magnetospirillum magnetotacticum* are presented. The KirBac3.1 structures complement that of a close homologue, KirBac1.1, crystallised in an unequivocally non-conducting 'closed' conformation<sup>1</sup>. We observe incremental changes occurring in the pore and intracellular domains, which are likely to reflect distinct stages in the closed-to-open transition. These include movements in the intracellular regions, constriction sites in the pore, rearrangement of the turret and pore helices, site occupancy in the ion selectivity filter, and positioning and ordering of the N-terminus.

- 1 Crystal structure of the potassium channel KirBac1.1 in the closed state. Kuo A, Gulbis J.M., Antcliff JF, Rahman T, Lowe ED, Zimmer J, Cuthbertson J, Ashcroft FM, Ezaki T, Doyle DA. (2003). *Science*, **300**, 1922-6.

**Structural Basis Of GTPase Gate For Protein Import Into Chloroplasts**

Chwan-Deng Hsiao Yuh-Ju Sun Farhad Forouhar Hsou-min Li

Institute of Molecular Biology, Academia Sinica

Protein import into chloroplasts is regulated by the binding and hydrolysis of GTP at two homologous GTPase, Toc34 and Toc159. Toc34, a 34-kDa integral membrane protein, is a member of the Toc (translocon at the outer-envelope membrane of chloroplasts) complex that associates with precursor proteins during protein transport across the chloroplasts outer membrane. Here we report the crystal structure of the cytosolic part of pea Toc34 complexed with GDP and  $Mg^{2+}$  at 2.0 Å resolution. In the crystal, the Toc34 molecules exist as dimers with features resembling the ones found in a small GTPase complexed with a GTPase activating protein (GAP). Gel-filtration, however, revealed that dimeric and monomeric forms of Toc34 coexisted in phosphate saline buffer (pH 7.2) solution. Mutation of Arg128, an essential residue for dimerization, to alanine led to the formation of only a monomeric form whose GTPase activity is significantly reduced compared to that of the wide-type Toc34. These results together with a number of the structural features unique to Toc34, suggest that each monomer acts as a GAP on the other interacting monomer. In addition, the crystal structure of the Toc34 GTP-binding domain suggests that GTP-regulated dimerization of the Toc GTPase domains controls the targeting and translocation of preproteins at the chloroplast envelope.

## Crystal structure of DsbB-DsbA complex revealing a cysteine relocation mechanism

Kenji Inaba<sup>1</sup>, Satoshi Murakami<sup>2</sup>, Mamoru Suzuki<sup>3</sup>, Atsushi Nakagawa<sup>4</sup>, Eiki Yamashita<sup>5</sup>, Kengo Okada<sup>6</sup>, Koreaki Ito<sup>1</sup>

<sup>1</sup>Institute for Virus Research, Kyoto University, <sup>2</sup>Institute for Scientific and Industrial Research, Osaka University, <sup>3</sup>Institute for Protein Research, Osaka University, <sup>4</sup>Nara Institute of Science and Technology

DsbB is an inner membrane protein that transforms oxidizing equivalents of ubiquinone into protein disulfides in *E. coli*. Disulfide bonds generated by DsbB are relayed via DsbA to newly exported proteins. To understand structural basis of this disulfide generating system, we determined the crystal structure of a disulfide-bonded DsbB-DsbA complex having endogenous ubiquinone at 3.7 angstrom resolution. The relatively low-resolution structure was complemented with engineered methionine/selenomethionine signals to enable structural refinement and consequent illumination of the reaction mechanisms. The DsbB portion of the complex was found to possess a transmembrane four-helix bundle and a mobile periplasmic region, which includes a Cys104-containing segment captured by the hydrophobic groove of DsbA and a short horizontal helix juxtaposed with Cys130. While DsbB in resting state contains the Cys104-Cys130 disulfide bond, the intermediate-like DsbB-DsbA complex has Cys104 engaged in the intermolecular disulfide bond with the hyper-reactive Cys30 of DsbA. Remarkably, the residue 130 now proves to be relocated away from Cys104 to the vicinity of Cys41, whose resting partner is Cys44 that we revealed previously to form a thiolate-ubiquinone charge transfer complex during DsbB catalysis. Such a geometrical separation of Cys104 and Cys130 leads to prevention of the backward attack by Cys130 against the Cys30 (DsbA)-Cys104 (DsbB) intermolecular disulfide. Thus, the dynamic repositioning of the periplasmic region is induced when DsbB encounters reduced DsbA, as a mechanism that enables DsbB to oxidize the extremely oxidizing DsbA protein.

## Crystal Structures of Archaerhodopsin-1 and -2

Tsutomu Kouyama Keiko YOSHIMURA Nobuo ENAMI

Department of Physics, Graduate School of Science, Nagoya University

Since bacteriorhodopsin (bR) was discovered in *Halobacterium salinarum*, the number of archaeal retinal proteins for which amino-acid sequences are available have increased to >25. They are classified into three types of rhodopsin according to their physiological functions; i.e., light-driven proton pumps, chloride ion pumps and phototaxis receptors. To elucidate a common structural motif utilized for light-driven proton pumps, we have recently investigated the crystal structures of archaerhodopsin-1 and -2 (aR-1 and aR-2), light-driven proton pumps found in *Halorubrum sp. aus-1 and -2*, which share 55% - 58 % sequence identity with bR [1]. It is found that the proton pathway in the extracellular half (i.e., the proton release channel) is more opened in aR-2 than in aR-1 or bR. This structural difference accounts for a large variation in the  $pK_a$  of the acid purple-to-blue transition among the three proton pumps. All the aromatic residues surrounding the retinal polyene chain are conserved among the three proton pumps, confirming a previous argument that these residues are required for the stereo-specificity of the retinal isomerization. In the cytoplasmic half, the region surrounded by helices B, C and G is highly conserved, while the structural conservation is very low for residues extruded from helices E and F. Structural conservation of the hydrophobic residues located on the proton uptake pathway suggests that their precise arrangement is necessary to prevent a backward flow of proton in the presence of a large pH gradient and membrane potential. An empty cavity is commonly seen in the vicinity of Leu93 contacting the retinal C13 methyl. Existence of such a cavity is required to allow a large rotation of the side chain of Leu93 at the early stage of photocycle, which has been shown to accompany water relocation near the active site.

- [1] N. Enami, K. Yoshimura, M Murakami, H. Okumura, K. Ihara and T. Kouyama., *J. Mol. Biol.*, 358, 675-685 (2006).

## High resolution X-ray diffraction data from 5 micron diameter protein crystals - towards the atomic structure of insect virus polyhedra

Peter Metcalf<sup>1</sup> Fasseli Coulibaly<sup>2</sup> Elaine Y Chiu<sup>3</sup> Hajime Mori<sup>4</sup> Peter Haebel<sup>5</sup> Sascha Guttman<sup>6</sup> Clemens Schulze-Briese<sup>7</sup>

School of Biological Sciences, University of Auckland<sup>1</sup> Kyoto Institute of Technology<sup>2</sup> Alta Pharma AG, Germany<sup>3</sup> Swiss Light Source, Switzerland<sup>4</sup>

Polyhedra are remarkably stable protein microcrystals that form within the cells of insects infected with either of the two viruses Cytoplasmic Polyhedrosis Virus (CPV) or Nucleopolyhedrosis Virus (NPV or baculovirus). Polyhedra are cubic crystals consisting of the virus encoded ~28kD protein polyhedrin. Polyhedra in infected cells also occlude virus particles as the crystals grow and these crystals then become the natural infective form of these viruses after the death and decay of the infected insect. When ingested by insects, polyhedra dissolve in the midgut releasing the occluded virus particles to start a new cycle of infection. We have developed techniques to collect single crystal X-ray diffraction data from 5-7 micron diameter polyhedra using the Swiss Light Source PX1 micro-beam line. The crystals diffract to at most 1.7 Angstrom resolution but decay rapidly in the beam. NPV and CPV crystals have similar unit cell dimensions and symmetry, despite the lack of sequence homology and the different phylogenetic origin of these viruses (CPV is a dsRNA virus and NPV is a dsDNA virus). I will describe our efforts to determine the atomic structure of these micro-crystals.

## Atomic Resolution Crystal Growth in Microgravity

Masaru Sato<sup>1</sup> Hiroaki Tanaka<sup>2</sup> Koji Inaka<sup>3</sup> Sachiko Takahashi<sup>1</sup> Shigeru Sugiyama<sup>3</sup> Mari Yamanaka<sup>2</sup> Satoshi Sano<sup>1</sup> Moritoshi Motohara<sup>1</sup> Tomoyuki Kobayashi<sup>1</sup> Tetsuo Tanaka<sup>1</sup>

Space Environment Utilization Center, Japan Aerospace Exploration Agency<sup>1</sup> Confocal Science Inc.<sup>2</sup> MolLogics Inc.<sup>3</sup>

Highly purified alpha-amylase was crystallized using counter-diffusion technique [1,2] in International Space Station for 13 weeks in Japan Aerospace Exploration Agency's project; JAXA-GCF. It diffracted beyond 0.89Å at SPring-8 beamline BL12B2 using polyethylene glycol (PEG) 8000 as a precipitant without forming cluster-like morphology which was usually observed on the ground-based experiment. The numerical analysis suggested that viscosity of the crystallization solution, caused by PEG, might result in growing highly-ordered protein crystals depending on depletion zone formation around a crystal especially under microgravity [3]. Highly purified lysozyme crystallization experiment was performed using NaCl as a precipitant in which PEG 8000 was purposely added to increase viscosity of the crystallization solution for the enhancement of the effects of microgravity. The crystal diffracted beyond 0.88Å was obtained at SPring-8 beamline BL12B2. Some of the protein samples provided by users for JAXA-GCF project improved the crystal quality using the same strategy.

It may be said that highly purification of the sample and enhancement of the microgravity effects by viscous crystallization solution were effective for obtaining atomic resolution crystals. Proper cryoprotectant was also essential for this purpose.

Such an atomic resolution data can provide more precise data of structural features of target proteins. If microgravity experiments are provided more routinely, crystallization in microgravity environment can become one of the options for obtaining high-quality protein crystals.

- [1] Garcia-Ruiz, J.M. and Moreno, A., *Acta Cryst.*, **D50**, 484, 1994
- [2] Tanaka, H. *et al.*, *J. Synchrotron Rad.*, **11**, 45, 2004
- [3] Tanaka, H. *et al.*, *Ann. N.Y. Acad. Sci.*, **1027**, 10, 2004

**Subatomic resolution crystal structure of subtilisin ALP I from alkalophilic *Bacillus* NKS-21**

Hirofumi Kurokawa` Youhei Yamagata`

Institute of Multidisciplinary Research for Advanced Materials, Tohoku University` Graduate School of Agricultural Science, Tohoku University`

Subtilisin ALP I is produced from alkalophilic *Bacillus* NKS-21 and shows sequence similarity to both the neutral and the alkaline subtilisins. The enzyme is highly sensitive to high alkaline conditions, and the substrate specificity is different from those of well-known subtilisins, such as subtilisin BPN', Carlsberg or Savinase. To characterize its structure and function relationship, subtilisin ALP I is crystallized by batch method in two different space group,  $I4$  with unit-cell parameters  $a = b = 103.6$  Å,  $c = 47.5$  Å and  $P2_1$ , with unit-cell parameters  $a = 45.6$  Å,  $b = 52.2$  Å,  $c = 90.1$  Å,  $\beta = 115.2$  degree.  $I4$  and  $P2_1$  crystals diffract to 1.3 Å, and 0.66 Å resolution, respectively. Initial structure was solved by molecular replacement method by using the coordinates of subtilisin from *Bacillus* sp. KSM-K16 (PDB code 1MPT) as a search model by using the data of  $I4$  crystal. One molecule were found in an asymmetric unit. Using the partially refined model, the structure of  $P2_1$  form ALP I were also determined by molecular replacement method and two molecules were found in an asymmetric unit. Subatomic (0.66 Å) resolution data of  $P2_1$  crystal were measured on beamline BL5A at the Photon Factory (Tsukuba, Japan) using a Quantum 315 CCD detector. Four data scans with different exposure time were performed with single crystal. Total of 3,119,665 reflections were merged and scaled by HKL2000 and 783,190 unique reflections were obtained. The refinement were performed by SHELXL.  $R_{\text{cryst}}$  and  $R_{\text{free}}$  are 0.101 and 0.114, respectively. Most of hydrogen atoms and possible residual valence electron density were observed in hydrogen omit map.

**Atomic resolution crystal structure of iron-bound ovotransferrin N-lobe**

Bunzo Mikami Kimihiko Mizutani Aiko Tanabe Masaaki Hirose

Applied Life Science, Graduate School of Agriculture, Kyoto University

Ovotransferrin, derived from the same gene as chicken serum transferrin, belongs to transferrin family of iron-binding proteins. They are 80 kDa single-chain bilobe proteins possessing one  $\text{Fe}^{3+}$  binding site in each lobe. N- and C- lobes have similar tertiary structures and can be isolated after limited proteolysis. Transferrin transports iron ions in blood, and is imported into the cell as complex with transferrin-receptor, and release iron in the acidic endosome through the domain opening initiated by di-lysine trigger. In order to understand the mechanism of iron release, we have refined the structure of ovotransferrin N-lobe at atomic resolution.

For crystallization, ovotransferrin N-lobe was incubated with  $\text{Fe}^{3+}$  and Na-bicarbonate and concentrated to 18.8 mg/ml. Aliquots were mixed with an equal volume of reservoir solution containing 100 mM Na-HEPES, pH 7.5, 200 mM Na-Acetate, 21-23% PEG3350, and crystallized by hanging-drop vapor diffusion. Red-colored rectangular crystals were obtained. X-ray diffraction data to 0.88 Å resolution were measured at BL38B1 with an imaging plate detector of RIGAKU R-Axis V in SPring-8. Space group of the crystal was  $P2_12_12_1$ , with lattice parameters:  $a = 46.144$ ,  $b = 75.179$ ,  $c = 84.591$  Å. Molecular replacement calculation was succeeded using the structure of holo ovotransferrin N-lobe at low resolution (PDB 1IEJ). Molecular modeling and refinement calculations were performed by Coot and SHELXL.  $R_{\text{cryst}}/R_{\text{free}}$  of anisotropic models without hydrogen and with (riding) hydrogen were 11.32%/13.83% and 10.15%/12.18%, respectively, for reflections between infinity - 0.88 Å. Many hydrogen atoms were observed in hydrogen omit map, and the roles of hydrogen atoms in iron-binding and release were investigated.

## On the Nature of the Superconducting Transition in YBCO

Mohana Yethiraj<sup>1</sup> David K. Christen<sup>2</sup> Masatoshi Arai<sup>3</sup> Yokoo Tetsuya<sup>4</sup> Sonya Crowe<sup>5</sup> Paul McK. Donald<sup>6</sup> Lionel Porcar<sup>7</sup>

Center for Neutron Scattering, Oak Ridge National Laboratory<sup>1</sup> Japan Atomic Energy Agency<sup>2</sup> KEK<sup>3</sup> University of Warwick<sup>4</sup> National Institute of Standards and Technology<sup>5</sup>

Small angle neutron scattering (SANS) is used to probe the flux line lattice (FLL) in type-II superconductors since the neutron has a magnetic moment and can scatter from the magnetic contrast arising from a flux line.

In the high- $T_c$  superconductor YBCO, a transition was observed from a hexagonal FLL at low magnetic field (parallel to the c-axis) to a square configuration at high fields. Also seen was a rapid decrease in the Bragg intensity at low temperature (T). Since the s-wave theory for conventional superconductors predicts little variation in the T-dependence of the Bragg intensity between 0K and  $-T_c/3$ , it has been the general belief that both the symmetry change and the T-dependence behaviour was due to the d-wave nature of high- $T_c$  superconductivity.

However, we observed that the fall-off in intensity with increasing temperature depended on the strength of the applied external field and that excellent fits to this T-dependence could be obtained by simply multiplying the temperature dependence of the familiar Ginzburg-Landau two-fluid model, appropriate for high-kappa materials conventional superconductors, by an exponential factor  $\exp(-aT)$ , with the field-dependent variable 'a' being the only free parameter. Further, comparing the YBCO results to those for another high- $T_c$  material  $(\text{La-Sr})_2\text{CuO}_4$ , we see the orientation of the square FLL is not related to the directions along which nodes exist in the superconducting gap. Finally, the phase diagram of the hexagonal and square FLL arrangement in YBCO is similar to that observed in  $\text{V}_3\text{Si}$ , a conventional superconductor for which non-local effects play a significant role. These observations strongly oppose a d-wave origin for the square-hexagonal FLL symmetry transition in the high- $T_c$  superconductors.

**Orbital order in DyB<sub>2</sub>C<sub>2</sub> and TbB<sub>2</sub>C<sub>2</sub> observed with resonant soft x-ray diffraction.**

A.M. Mulders, U. Staub, V. Scagnoli, S.W. Lovesey, E. Balcar, G. van der Laan, Y. Tanaka, A. Kikkawa, K. Katsumata and J.M. Tonnerre.

Correlation between conduction electrons and electronic orbitals leads to interesting materials properties such as metal-insulator transitions, colossal magneto resistance and superconductivity. Aspheric electronic orbitals, characterized by their quadrupole moment, may order and cause partial charge localization of the conduction electrons or mediate coupling between cooper pairs.

Orbital order in *f* electron materials is dominated by coupling with the lattice (Jahn-Teller) or by indirect Coulomb interactions via the conduction electrons.

The large orbital momentum of the *f* electronic shell also gives rise to a significant influence of higher multipole moments and may lead to hidden order phase transitions as demonstrated in the extensively studied URu<sub>2</sub>Si<sub>2</sub>. Therefore it is important to understand the quadrupolar and higher order multipole pair interactions in these materials.

Resonant and non-resonant Bragg diffraction has been used to study orbital order of DyB<sub>2</sub>C<sub>2</sub> and TbB<sub>2</sub>C<sub>2</sub>. The theoretical description of resonant Bragg diffraction at the Dy *M*<sub>4,5</sub> edge is extended to include the interaction between the 4*f* quadrupole and the 3*d* core state. This leads to the determination of the higher order multipole moments of the Dy 4*f* shell.

TbB<sub>2</sub>C<sub>2</sub> is proposed to exhibit a transition from antiferromagnetic (AFM) to antiferroquadrupolar (AFQ) order in an applied magnetic field. We find that the Tb 4*f* quadrupolar pair interaction depends on the specific orientation of the orbitals as predicted theoretically and can be manipulated with an applied magnetic field.

## Simulation of Diffuse Scattering in Neutron Diffraction Pattern of Superconducting Deuterated Sodium Cobaltate

Mitsuko Onoda<sup>1</sup> Kazunori Takada<sup>1</sup> Dimitri Argyriou<sup>2</sup> Yong Nam Choi<sup>3</sup> Takayoshi Sasaki<sup>1</sup>

Synchrotron X-ray Group, National Institute for Materials Science<sup>1</sup> Hahn-Meithner-Institut, Germany<sup>2</sup> Korea Atomic Energy Research Institute, Korea<sup>3</sup>

Hydrated sodium cobaltate  $\text{Na}(x)\text{CoO}_2 \cdot y\text{H}_2\text{O}$  has been reported to be a superconductor with a  $T(c)$  of about 5 K. Neutron diffraction patterns of deuterated sodium cobaltate show conspicuous diffuse maxima presumed to originate from deuterated sodium part in addition to sharp reflections due to  $\text{CoO}_2$  part. The structure is treated as an interpenetration of two layered subsystem structures,  $\text{CoO}_2$  part ( $a=0.28\text{nm}$ ) and deuterated sodium part ( $a=0.33$ ). A model of short-range order stacking of deuterated sodium parts is expressed using four possible configurations. The sequences, in which neighboring sheets have the same configuration, do not occur, and the other sequences occur with the same probability. Diffuse scattering intensities simulated using the matrix method satisfactorily explain the broad maxima observed in neutron diffraction patterns.

## Structure analysis of lattice modulation of multiferroic compound $YMn_2O_5$ by SR x-ray

Yukio Noda<sup>1</sup>, Hiroyuki Kimura<sup>2</sup>, Youichi Kamada<sup>3</sup>, Yoshihisa Ishikawa<sup>4</sup>, Satoru Kobayashi<sup>5</sup>, Yusuke Wakabayashi<sup>6</sup>, Hiroshi Sawa<sup>7</sup>, Naoshi Ikeda<sup>8</sup>, Kay Kohn<sup>9</sup>

<sup>1</sup>Institute of Multidisciplinary Research for Advanced Materials, Tohoku University, <sup>2</sup>NDESRC, Faculty of Engineering, Iwate University, <sup>3</sup>Photon Factory, Institute Materials Structure Science, KEK, <sup>4</sup>Photon Factory, Institute Materials Structure Science, KEK, <sup>5</sup>Department of Physics, Okayama University, <sup>6</sup>Waseda University

$RMn_2O_5$  ( $R=Y$  and rare earth) are well known multi-ferroic compounds, and they show successive magnetic and ferroelectric phase transitions at about 45K, 40K, 39K, 20K and 10K ( $T_{M1}$ ,  $T_{C1}$ ,  $T_{S1}$ ,  $T_{C2}$ ,  $T_{M2}$ ) associated with the large magneto-electric coupling[1]. The precise structure giving the spontaneous polarization is still unclear at the moment.

We surveyed the existence of superlattice reflections in  $YMn_2O_5$  and  $TbMn_2O_5$  by SR x-ray at Photon Factory BL4C in KEK, and performed the structure analysis at SPring-8 BL02B1. We found very weak superlattice and satellite reflections. The ratio between the fundamental and the superlattice reflection is about  $10^{-6}$ . The lattice modulation wavevector  $\mathbf{q}_l$  was carefully measured, and we found the lattice modulation vector  $\mathbf{q}_l$  is exactly twice of the magnetic propagation vector  $\mathbf{q}_m$ ,  $\mathbf{q}_l=2\mathbf{q}_m$ , in all phases.

The structure analysis of modulation in ferroelectric and magnetically commensurate phase of  $YMn_2O_5$  was carried out. Since we failed to observe the order parameter reflections at  $\mathbf{q}=0$  position, our analysis is limited only to the modulated structure and will not give the final result corresponding to the ferroelectric atomic displacements. The R-factor for fundamental Bragg reflection (304 data points and 22 parameters) is 2.51% and that for weak superlattice reflection (180 data points and 14 parameters) is 7.9%. Obtained atomic displacement shows some characteristic pattern relating to the magnetic spin configuration of  $Mn^{4+}$  and  $Mn^{3+}$  atoms.

### Reference:

- [1] Y. Noda, Y. Fukuda, H. Kimura, I. Kagomiya, S. Matsumoto, K. Kohn, T. Shobu and N. Ikeda, J. Korean Phys. Soc. 42 (2003) S1192.

## Surface X-ray Scattering Study of the Orbital Ordering at a Cleaved Surface of the Layered Manganite $\text{La}_{0.5}\text{Sr}_{1.5}\text{MnO}_4$

Yusuke Wakabayashi<sup>1</sup> Mary H. Upton<sup>2</sup> Stephane Grenier<sup>3</sup> John P. Hill<sup>4</sup> Christie S. Nelson<sup>5</sup>  
Jong-Woo Kim<sup>6</sup> Philip J. Ryan<sup>7</sup> Alan I. Goldman<sup>8</sup> Hong Zheng<sup>9</sup> John F. Mitchell<sup>10</sup>

Synchrotron Radiation Science Div.2, Institute of Materials Structure Science<sup>1</sup> Condensed Matter Physics and Materials Science Department, Brookhaven National Laboratory, USA<sup>2</sup> National Synchrotron Light Source, Brookhaven National Laboratory, USA<sup>3</sup> Ames Lab., Iowa State Univ., USA and Argonne National Laboratory, USA<sup>4</sup> Ames Lab., Iowa State Univ., USA<sup>5</sup> Argonne National Laboratory, USA<sup>6</sup>

Strongly correlated electronic systems exhibit a diverse range of electronic behavior, including the phenomena of orbital ordering --that is a preferential occupancy and orientational alignment of the occupied electronic orbitals. The orbital ordering has been studied a great deal in the manganites. So far, most of this work has been in the form of bulk studies, with very little work performed addressing the role of the surface in orbital order. Very recently, this question has started to attract attention [1-3].

In this study, surface x-ray diffraction measurements on a (001) cleaved surface of the orbitally ordered layered manganite  $\text{La}_{0.5}\text{Sr}_{1.5}\text{MnO}_4$  were performed at X22C and X21 at the NSLS and at 6ID at the APS. We have succeeded in observing crystal truncation rod (CTR) scattering from the orbital ordering for the first time. It allows us to probe the "orbital surface" and its relationship to the crystallographic surface directly. Our striking finding is that the chemical and orbital surfaces are different. Transverse profiles of CTR intensity for chemical surface were as sharp as the instrumental resolution, indicating that the cleaved surface was extremely flat. In contrast, the transverse profile of the CTR intensity from the orbital ordering has two components: One was as sharp as the bulk orbital ordering superlattice reflection, while the other was significantly broader. This implies directly that the surface of the orbital ordering is rough in contrast to the atomically smooth chemical surface.

### References:

- [1] A. Ohtomo *et al.*, *Nature* **419** (2002), 378.
- [2] S. Okamoto and A. J. Millis, *Nature* **428** (2004), 630.
- [3] J.W. Freeland *et al.*, *Nature Materials*. **4** (2005), 62.

**tRNA-dependent amino acid transformation by GatCAB**Akiyoshi Nakamura, Min Yao, Sarin Chimnaronk, Naoki Sakai, and Isao Tanaka

Faculty of Advanced Life Sciences, Hokkaido University, Sapporo, Japan

The formation of Gln-tRNA<sup>Gln</sup> differs among the three domains of life. Most bacteria employ an indirect pathway to produce Gln-tRNA<sup>Gln</sup> by an amidotransferase (Glu-AdT) that acts on the mis-acylated Glu-tRNA<sup>Gln</sup>. Bacterial Glu-AdTs are heterotrimeric proteins composed of A, B, and C subunits, and are named GatCAB. GatCAB converts Glu-tRNA<sup>Gln</sup> into Gln-tRNA<sup>Gln</sup> by initially activating Glu-tRNA<sup>Gln</sup> into  $\gamma$ -phosphoryl-Glu-tRNA<sup>Gln</sup> at the expense of ATP, which is subsequently transamidated into Gln-tRNA<sup>Gln</sup> using ammonia generated by hydrolysis of glutamine. The glutaminase and transamidase reactions are tightly coupled and intrinsically dependent on the binding of Glu-tRNA<sup>Gln</sup> to GatCAB.

In this study, we describe the crystal structures of intact GatCAB complex from *Staphylococcus aureus*, in the apo form, and in the complexes with glutamine, asparagine, Mn<sup>2+</sup> and adenosine triphosphate analog. Based on the structure of GatCAB/glutamine complex, we demonstrated that the glutaminase reaction occurs at the Ser-cis-Ser-Lys catalytic scissors of GatA without the conformational rearrangement of the glutaminase active site. The structure of GatCAB/ADP complex revealed the precise position and environment of the active site at the bottom of the cradle domain of GatB. Two identified catalytic centers for the glutaminase and transamidase reactions are markedly distant but connected by a hydrophilic ammonia channel 30 Å in length. Further, we showed the identity elements essential for discrimination of tRNA<sup>Gln</sup>, and proposed a complete model for the overall concerted reactions to synthesize Gln-tRNA<sup>Gln</sup>.

**Complete crystallographic analysis of the dynamics of CCA-addition**Kozo Tomita<sup>1</sup>, Ryuichiro Ishitani<sup>2</sup>, Shuya Fukai<sup>2</sup>, and Osamu Nureki<sup>2,3</sup><sup>1</sup>AIST<sup>2</sup>Tokyo Institute of Technology<sup>3</sup>SORST

CCA-adding polymerase matures the essential 3'-CCA terminus of tRNA without any nucleic-acid template. However, it remains unclear how a correct NTP is selected in each reaction step and how the polymerization is driven by the protein and RNA dynamics. Here we present complete sequential snapshots of six complex structures of CCA-adding enzyme and four distinct RNA substrates with and without CTP or ATP. The CCA-lacking RNA stem extends by one base pair to force the discriminator nucleoside into the active-site pocket, while it tracks back after the first CMP incorporation. Accommodation of the second CTP clamps the catalytic cleft, inducing a reorientation of the  $\beta$ -turn, which flips C74 to allow CMP acceptance. In contrast, after the second CMP addition, the polymerase and RNA primer are locked in the closed state, which directs the subsequent A-addition. Between the CTP- and ATP-binding stages, the side chain conformation of Arg224 drastically changes, as controlled by the enzyme global motion and primer terminus position, which is likely to achieve the CTP/ATP discrimination depending on the polymerization stage. Throughout the CCA-adding reaction, the enzyme tail domain firmly anchors the tRNA T $\Psi$ C-loop, which ensures accurate polymerization and termination.

## Structure of the Insulin Receptor Ectodomain Homodimer

Michael C Lawrence Neil McKern Victor Streltsov Meizhen Lou Timothy Adams George Lovrecz  
John Bentley Peter Hoyne Maurice Frenkel Colin Ward

Molecular and Health Technologies, CSIRO

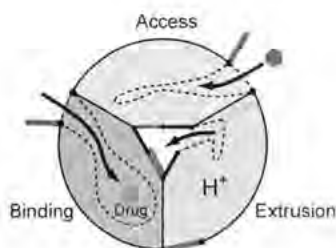
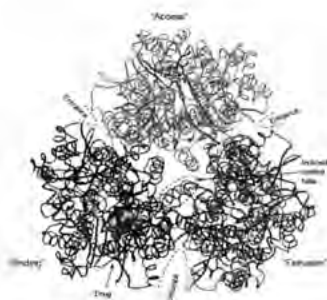
The insulin receptor (IR) is a phylogenetically ancient tyrosine kinase receptor found in organisms as primitive as cnidarians and insects. The key role of the insulin receptor (IR) is in glucose uptake and metabolism by muscle and fat. Dysfunctional IR signaling has been implicated in diseases including type I and type II diabetes, dementia and cancer. The IR exists as two splice variant isoforms IR-A and IR-B. The IR-B isoform is responsible for signaling metabolic responses. In contrast, IR-A signals predominantly mitogenic responses, is the preferentially expressed isoform in several cancers and is capable of binding insulin-like growth factor receptor (IGF-II) with high affinity. Here we present the crystal structure of the IR-A ectodomain dimer. The structure reveals, for the first time, the domain arrangement in the disulphide-linked ectodomain dimer and shows that it adopts a folded-over conformation that places the ligand-binding regions in juxtaposition.

## A functionally rotating mechanism revealed in crystal structures of the multidrug transporter, AcrB, with bound substrates

Satoshi Murakami

Dept.Cell Membrane Biology, Inst. Scientific and Industrial Research, Osaka University

AcrB is a major multidrug efflux transporter in *Escherichia coli* cooperating with an outer membrane channel TolC and a membrane fusion protein AcrA. Here, we describe the new asymmetric crystal structure of AcrB in complex with its substrates. The AcrB-drug complex consists of three protomers, each of which represents one functional state of the transport cycle. Bound substrate was found in the periplasmic domain of one of the three protomers in its voluminous aromatic binding pocket in a multi-site binding mode. The structure clearly revealed that drugs are exported by a three-step functionally rotating ordered binding change mechanism.



## Micro-focus X-ray Diffractometry for Time Resolved Structure Analysis -A Development of X-ray Pinpoint Structural Measurement at the SPring-8 (1)

Haruno Murayama<sup>\*</sup> Nobuhiro Yasuda<sup>\*</sup> Jungeun Kim<sup>\*</sup> Yoshimitsu Fukuyama<sup>\*</sup> Shigeru Kimura<sup>\*</sup>  
Yoshihiro Kuroiwa<sup>\*\*</sup> Kenichi Kato<sup>\*</sup> Yutaka Moritomo<sup>\*\*\*</sup> Yoshihito Tanaka<sup>\*\*\*\*</sup> Koshiro Toriumi<sup>\*\*\*\*\*</sup>  
Masaki Takata<sup>\*\*\*\*\*</sup>

Research and Utilization Division, Japan Synchrotron Radiation Research Institute (JASRI/  
SPring-8)/CREST<sup>\*</sup> Department of Physical Science, Hiroshima University / CREST<sup>\*\*</sup> The  
Graduate School of Pure and Applied Sciences, Tsukuba University / CREST<sup>\*\*\*</sup> RIKEN /  
CREST<sup>\*\*\*\*</sup> Graduate School of Material Science, University of Hyogo / CREST<sup>\*\*\*\*\*</sup> RIKEN/JASRI/  
SPring-8/CREST<sup>\*\*\*\*\*</sup>

The study of dynamic structures is important to characterize nano-materials and their events such as amorphous-crystal change on recording DVD media and photo-induced metal-insulator transition. For these researches, we are developing X-ray pinpoint structural measurement technique, which is XRD measurement system in ~100 nm spatial resolution and ~40 ps time resolution with focusing X-ray by a zone plate.

High brilliant pulse X-ray emanating from insertion device of the SPring-8 is powerful tool for a time resolved measurement using single pulse X-ray. The pinpoint X-ray structural measurement system has been constructed on the high flux beam line using a helical undulator, BL40XU at the SPring-8. About 100nm focused beam can be produced by a high resolution type standard Fresnel zone plate, ZP2, whose Ta thickness is 0.75  $\mu\text{m}$ . For 8 keV X-rays, the ideal X-ray diffraction efficiency is 12 %. To increase X-ray diffraction efficiency, a high flux type, ZP1, whose Ta thickness is 2.5  $\mu\text{m}$ , was designed. The ZP1 achieved the diffraction efficiency up to 20 %. The beam size and flux per unit area of 15 keV X-ray was  $1.4 \times 2.4 \mu\text{m}^2$  and  $3 \times 10^{14}$  photons $\cdot\text{s}^{-1}\cdot\text{mm}^{-2}$ , respectively. In order to align micro-beam with sub-micron size crystal, high precision two circle goniometer, whose decentering error is within  $\pm 100$  nm/360 $^\circ$  were constructed with CCD or IP detector. A femto/picosecond pulse laser (Ti:sapphire oscillator,  $\lambda = 800\text{nm}$ ) system is equipped on the diffractometer for a photo-irradiation pump and probe experiment using X-ray pulse selector. The details of the instruments and performance of the X-ray pinpoint structural measurement system will be presented.

## The Bilbao Crystallographic Server

Mois I. Aroyo<sup>1</sup>, Juan Manuel Perez-Mato<sup>2</sup>, Cesar Capillas<sup>1</sup>, Daniel Orobengoa<sup>1</sup>, Hans Wondratschek<sup>2</sup>

<sup>1</sup>Departamento de Fisica de la Materia Condensada, Universidad del Pais Vasco<sup>1</sup>, Institut fuer Kristallographie, Universitaet Karlsruhe, Germany<sup>2</sup>

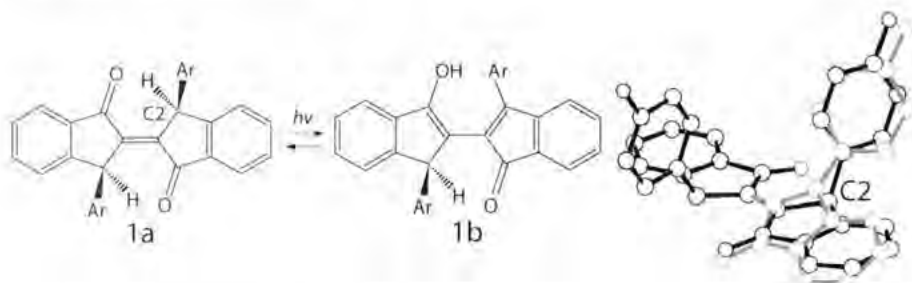
The *Bilbao Crystallographic Server* (<http://www.cryst.ehu.es>) is a free web site with crystallographic databases and programs. It has been operating for almost eight years, and new programs are added regularly. The server is built on a core of databases and the different crystallographic applications are classified in shells. The innermost one is formed by simple retrieval tools which are the interface to the set of databases including the data from *International Tables*, Vols. A, A1 and E. The second shell contains applications which are essential for problems involving group-subgroup relations between space groups. Among them, one can mention programs for determining the different subgroups and supergroups of a given space group type (SUBGROUPGRAPH and SUPERGROUPS) or the splitting of the Wyckoff positions for a group-subgroup pair (WYCKSPLIT). The next shell includes programs on representation theory of space and point groups (REPRES and POINT). Parallel to the crystallographic software the last shell contains more specialized applications of solid-state physics, structural chemistry and crystallography. For example, there exists several tools for the search of pseudosymmetry in crystal structures (PSEUDO, DOPE and BPLOTT), for the determination of selection rules - SAM (Infrared and Raman modes) and NEUTRON (phonon extinction rules in inelastic neutron scattering). SYMMODES carries out a group-theoretical analysis of any structural phase transition, calculating the polarization vectors of the possible primary and secondary symmetry modes and the corresponding isotropy subgroups. TRANPATH, a computer program for studies of structural phase transitions with no direct group-subgroup relation between the two end phases is recently made available on the server.

## Photochromic Reaction Mechanism and Structural Change of trans-Biindenylideneidone Derivatives

Akiko Sekine<sup>\*</sup> Kumiko Aruga<sup>\*</sup> Hidehiro Uekusa<sup>\*</sup> Katsuya Souno<sup>\*\*</sup> Koichi Tanaka<sup>\*\*</sup>

Department of Chemistry and Materials Science, Tokyo Institute of Technology<sup>\*</sup> Department of Applied Chemistry, Kansai University, Japan<sup>\*\*</sup>

It has been reported that trans-biindenylideneidone derivatives show photochromism in the solid state as evidenced by color change, from yellow(**1a**) to red(**1b**), upon irradiation with UV and visible light [1]. However, the crystal structure of the photoproduct (**1b**) is yet unknown. In this paper, in order to clarify the photochromic reaction mechanism of this compound, we present our experimental results concerning crystal structure determination of **1b**. The X-ray analysis of a single crystal of **1a** was performed at 173K before the irradiation. Subsequently, the crystal was irradiated with UV light at room temperature and the X-ray diffraction data was collected under the UV light at 173K. The X-ray analysis result shows that both the reactant (**1a**) and the photoproduct (**1b**) (11.1%) were located as a disordered structure in the red colored crystal. For **1b**, the indenyl and 3-methylphenyl rings are quasi planar. This is due to the proton transfer from C2 to the nearest carbonyl oxygen which causes the change of hybridization from  $sp^3$  to  $sp^2$ . These results suggest that the photochromism is caused by an intramolecular (Norrish Type II) hydrogen transfer reaction.



[1] Koichi Tanaka et al., *CrystEngComm.*, 2004, **6**(2), 1-4

## A study of accurate charge density and bonding nature of $\text{CoSb}_3$ at $T = 10 \text{ K}$ .

Atsuko Ohno<sup>1</sup> Bo B. Iversen<sup>2</sup> Shinobu Aoyagi<sup>3</sup> Eiji Nishibori<sup>4</sup> Makoto Sakata<sup>5</sup> Satoshi Sasaki<sup>6</sup>

Interdisciplinary Graduate School of Science and Engineering, Tokyo Institute of Technology<sup>1</sup>  
 Department of Chemistry, University of Aarhus, Denmark<sup>2</sup> Department of Applied Physics,  
 Nagoya University, Japan<sup>3</sup> Materials and Structures Laboratory, Tokyo Institute of Technology,  
 Japan<sup>4</sup>

Due to the high electrical and low thermal conductivities, the metal-doped  $\text{CoSb}_3$  is a good candidate of practical thermoelectric material. These physical properties must be affected by its bonding nature. It is, therefore, important to study chemical bonding of the metal-doped  $\text{CoSb}_3$ . In this study, an accurate experimental charge density of  $\text{CoSb}_3$  has been determined as the first step by maximum entropy method (MEM) using high-resolution synchrotron powder diffraction data.

The synchrotron powder diffraction experiment was carried out at 10K by a large Debye-Scherrer camera installed at BL02B2, SPring-8. The wavelength of incident X-ray was 0.42066Å. The data were collected from 3 degree to 99 degree with 0.01 degree per step in  $2\theta$ . This covers the d-spacing up to 0.277 Å, which should be called high resolution data in real space. The collected data were firstly analysed by Rietveld refinement. The reliability factors based on weighted profile,  $R_{wp}$ , and, Bragg intensities,  $R_i$ , were 6.0 and 2.5 %, respectively. Then, the MEM analyses were carried out using the structure factors derived from the Rietveld refinement.

The MEM charge density of  $\text{CoSb}_3$  has clearly revealed that there are three types bonding, which are two types Sb-Sb bonding in  $\text{Sb}_2$  ring and the rest is Co-Sb bonding. Judging from the charge density at bond mid-point, Co-Sb bond is stronger than any of two kinds of Sb-Sb bonds in  $\text{Sb}_4$  ring. The present results support the theoretical calculation [1] for the Co-Sb bond. The present study will be easily extended to cover various metal-doped  $\text{CoSb}_3$ .

[1] Lefebvre-Devos *et al.*, Phys. Rev. B 63, 125110 (2001).

## Structural Analysis of Star-Shape Polystyrenes Using Synchrotron X-Ray Scattering

Sangwoo Jin<sup>1</sup>, Tomoya Higashihara<sup>2</sup>, Kyeong Sik Jin<sup>1</sup>, Jinhwan Yoon<sup>1</sup>, Kyuyoung Heo<sup>1</sup>, Jehan Kim<sup>1</sup>, Kwang-Woo Kim<sup>1</sup>, Akira Hirao<sup>2</sup>, Moonhor Ree<sup>1</sup>

<sup>1</sup>Pohang University of Science and Technology, Department of Polymeric and Organic Material, Graduate School of Science and Engineering, Tokyo Institute of Technology<sup>2</sup>

Star-shape polymers have gained great attention because of their interesting properties and potential applications. In the present study, a series of star-polystyrenes with 6-57 arms were synthesized. In addition, linear polystyrenes were purchased. Solutions of each polystyrene sample were prepared at a concentration of 1-4 wt% in tetrahydrofuran, a good solvent and cyclohexane at 35°C, a theta solvent. Small-angle X-ray scattering (SAXS) measurements were conducted at the 4C1 beamline (BL) of the Pohang Accelerator Laboratory. The scattering profiles of the linear polystyrenes were confirmed to reveal the characteristics of a Gaussian coil, which has a Gaussian sphere behaving self-avoiding random walk in the solvent but excluded volume effect in the theta solvent. In comparison, the 6-armed polystyrene reveals scattering profiles varying with a power law of  $q^{-2}$  in the Debye region, and the 57-armed polystyrene exhibits scattering profiles following a power law of  $q^{-4}$  in the Debye region regardless of the good solvent and theta solvent. The other armed polystyrenes show scattering profiles which follow an intermediate power law between those observed for the 6- and 57-armed polystyrenes over the Debye region. All the structural details, which were extracted from the SAXS profiles, will be discussed with considering the chemical nature of the inner and outer parts in the multi-armed polystyrene and the number of arms.

**Structural Study of II-VI Core-Shell Quantum Dots by Synchrotron Anomalous Powder Diffraction and Small Angle X-ray Scattering**

Hwo-Shuenn Sheu Wei-Ju Shih Wei-Tsung Chuang Ying-Huang Lai U-Ser Jeng

Research Division, National Synchrotron Radiation Research Center

The need of nano size materials with bright and stable fluorescence for various applications covering from electro-optics to biology is extensively increasing. The main strategy to increase photoluminescence quantum yield and stability of nanocrystals is to grow a passivating shell on the cores surface. The passivating shell is not only protecting the core from reducing surface degradation but also play a role of charge transition. As opposed to type-I quantum dots (QDs), type-II core-shell QDs have both valence and conduction bands in the core lower than those in the shell materials. Upon electronic excitation, one carrier is predominantly confined to the core, while the other is located at the shell. The rational design and synthesis of the II-VI nanocrystals type-II quantum dots, such as CdS, CdSe, CdTe, ZnS, ZnSe, and ZnTe are reported by P. T. Chou *et al.* In this study, we use synchrotron PXRD and SAXS to elucidate the multiphase structure of the QDs of CdSe, CdTe, and CdTe/CdSe (core-shell). Moreover the anomalous effects around Se, and Zn K-edge are also applied to differentiate the alloy phase from the core-shell multiphase. The well overlapped anomalous SAXS profile for the CdTe/CdSe showed possible two phase structure, with a thin layer of CdSe shell capped on the CdTe core. The mean particle size of CdTe/CdSe is 7.4 nm with 18% polydispersity. The CdSe/ZnTe core-shell structure and other II-VI core shell QDs were also reported.

## Ferroelectric Nanostructures

Songhak Yoon<sup>1</sup>, Hee Han<sup>1</sup>, Yongjun Park<sup>1,2</sup>, Min Gyu Kim<sup>2</sup>, Namsoo Shin<sup>2</sup>, Ran Ji<sup>3</sup>, Dietrich Hesse<sup>3</sup>, Marin Alexe<sup>3</sup>, Kornelius Nielsch<sup>3</sup>, Ulrich Goessele<sup>3</sup>, and Sunggi Baik<sup>1\*</sup>

<sup>1</sup>Department of Materials Science and Engineering

<sup>2</sup>Pohang Accelerator Laboratory Pohang University of Science and Technology, Pohang, Korea

<sup>3</sup>Max Planck Institute of Microstructure Physics, Halle, Germany

A number of synchrotron radiation facilities and their users have been growing rapidly world wide and have feasted new important discoveries and excitement in various scientific and technological areas including materials science, biological science, electronics, environmental engineering, etc. Drastic improvements in time, spatial, energy, and spectroscopic resolutions have been realized in comparison to the conventional light sources and provided strong motivations to revisit many unresolved scientific issues. Ferroelectrics have been one of such issues that have been explored extensively using this new light source in recent years. In this presentation, some of recent attempts and discoveries in studying various issues related to ferroelectric nanostructures including ultra thin films and nano-islands are summarized to demonstrate the unique features and opportunities of synchrotron radiation.

In addition, as an example, our recent study on domain structures in the epitaxial PZT thin films and nano-islands will be described in detail. Evolution of unique domain structures were characterized as a function of film compositions, substrate selection, film thickness, and 2D planar size employed in film fabrication. The c-domain abundance and crystalline quality of the films are studied and quantified by two-dimensional reciprocal space mapping technique in the PLS 3C2 and 10C1 X-ray Scattering Beamlines equipped with *in-situ* high temperature stages and 2C1 X-ray microscopy. Domain switching dynamics are studied by AFM. Attempts have been also made theoretically to establish the correlation with various electrical and thermomechanical factors involved in nano structure processing.

## Grazing incidence x-ray scattering for characterizing advanced nanomaterials

Kazuhiko Omote Yoshiyasu Ito

X-Ray Research Laboratory, Rigaku Corporation

Nowadays, many kinds of surface nanostructures are extensively studied for developing various functional devices, for example, optoelectronics, microelectronics, magnetics, photonics, and so on. Size, shape, and size distributions are crucial for the performance of such nanostructures, quantum effects, magnetic domain size, etc. Grazing incidence surface x-ray scattering is well suited for characterizing such surface nanostructures. It can measure nondestructively without special sample treatments. We have developed an x-ray instrument suited for measuring surface x-ray scattering and diffraction with a laboratory x-ray source. Incident x-rays are focused on the sample surface with a very shallow angle  $\alpha$ , and scattering x-rays are detected both in the out-of-plane (normal) and in-plane (lateral) directions. Angular resolution of the scattered x-rays can be selected by exchanging slit collimation or crystal analyzers. Therefore, we can measure surface structures in the range from nanometer to micrometer. The analysis of the observed data is carried out based on distorted wave Born approximation for taking account of refraction and reflection of x-rays on the surface and interfaces. We will present the results of analysis for several interesting materials, porous low-k dielectric films, magnetic Ni nanoparticles, and some other examples. We have determined the pore size and its distribution in porous low-k film and found anisotropy between the lateral and normal direction by grazing incidence small angle x-ray scattering (GISAXS). Ni nanoparticles in carbon matrix are also characterized by GISAXS and x-ray diffraction (XRD). Particle size determined by GISAXS and crystallite size by XRD agree very well; it indicates every Ni nanoparticle should be a single crystal.

## Interaction between specular reflection and back scattering

Daisuke Arai<sup>1</sup> Shuji Kusano<sup>1</sup> Yousuke Nodumi<sup>1</sup> Mitsuhiro Hashimoto<sup>1</sup> Toshio Takahashi<sup>1</sup>  
Yasuhiko Imai<sup>2</sup> Yoshitaka Yoda<sup>2</sup> Keiichi Hirano<sup>2</sup> Xiao-Wei Zhang<sup>2</sup>

<sup>1</sup>Institute for Solid State Physics, University of Tokyo<sup>1</sup> JASRI/SPring-8, Japan<sup>2</sup> KEK-PF, Japan<sup>2</sup>

We perform the experiment on the Bragg diffraction that the Bragg angle is nearly 90 degrees (back scattering) in the grazing incidence condition that X-rays are totally reflected, and we discuss the results based on the dynamical theory of diffraction. The total reflection occurs when the glancing angle of X-rays is smaller than the critical angle in the grazing incidence condition. Because X-rays penetrate only very little inside the crystal, the total reflection is used for the structure analysis on the surface layer. In the back scattering, because the angular width of the rocking curve becomes comparable to the critical angle, we expect to observe the interaction between the specularly reflected wave and the back scattered wave in the vicinity of the critical angle. Therefore this phenomenon might be applied to the structural analysis of the surface layer for various kinds of crystals in the future.

We think about the diffracting plane perpendicular to the crystal surface. If the glancing angle of incident X-rays on the crystal surface is smaller than the critical angle, the transmitted wave and the diffracted wave can hardly go into the crystal and are reflected outside the crystal. The sample used is a silicon single-crystal with Si(001) surface, and the lattice plane of Si(880) is adopted for back scattering. The glancing angle to the sample surface was changed to observe the rocking curves at each wavelength. The specular reflection and the back scattering were measured at the same time.

The interaction between the specularly reflected wave and the back scattered wave was observed under the grazing incidence conditions at various wavelengths. The experimental results agreed semi-quantitatively with the results calculated by the dynamical theory.

**Conductance and stochastic switching of ligand-supported linear metal atom chains**

Shie-Ming Peng<sup>1</sup> I-Wen Peter Chen<sup>2</sup> Ming-Dung Fu<sup>2</sup> Wei-Hsiang Tseng<sup>2</sup> Jian-Yuan Yu<sup>2</sup> Sung-Hsun Wu<sup>2</sup> Chia-Jui Ku<sup>2</sup> Chun-hsien Chen<sup>2</sup>

<sup>1</sup>Department of Chemistry, National Taiwan University <sup>2</sup>Department of Chemistry, National Tsing Hua University

Molecular wires and switches are projected the elemental building blocks for future electronic applications. Synthesizing one-dimensional molecules and comprehensively understanding their electric characteristics become one of the focus areas of contemporary material research. The growth of this research field is encouraged by discoveries of a strong dependence of electron transport on the length, conjugation, conformation, and substituents of the tailored molecules. While remarkable progress has been achieved during the past decade, most of the knowledge learned has been from conjugated organic molecules whose counterpart, organometallic molecular wires, has been rarely explored. Here we present quantitative measurements of single molecular conductance of one-dimensional multinuclear metal strings ( $[M_n L_m (NCS)_2]$ ,  $M_n = Cr_3, Co_3, Ni_3, Cr_5, Co_5, Ni$ , and  $Cr_7$ ;  $L = \text{oligo-}\alpha\text{-pyridylamine}$ ). The conductance values are found correlated well with the  $d$ -orbital electronic coupling between adjoining metal atoms. Among the strings, *penta*- and *heptachromium* complexes exhibit stochastic switching events. Such multinuclear strings are important in setting up a perfect platform for the fundamental study of metal-metal interactions beyond dinuclear complexes. Crystallographic characterization up to *nonanickel* complex has been achieved and the length of ligands is extended to 11 repetitive pyridylamine units ( $m = 11$ ). While purification and crystallization become increasingly challenging due to the nature of poorer solubility for longer oligomers, preliminary MALDI-MS spectra show that a string of 17 nickel ions ( $m = 7$ ) is obtainable. An understanding of the conduction propagating along the metal chains will advance further towards molecular wires for nanodevices.

## Observation of 2D nanostructures using X-ray reciprocal-lattice space imaging

Osami Sakata<sup>1</sup> Masashi Nakamura<sup>2</sup> Takayuki Watanabe<sup>3</sup> Hiroshi Funakubo<sup>3</sup>

Research Utilization Division, Japan Synchrotron Radiation Research Institute / SPring-8<sup>1</sup> Chiba University<sup>2</sup> Tokyo Institute of Technology<sup>3</sup>

We proposed x-ray reciprocal-lattice space imaging (X-ReSI) as an obvious-at-a-glance analysis method for 1D nanostructures such as NiO nanowires on a sapphire surface[1] and Bi nanolines in Si[2]. The success pushed us to applying X-ReSI to observing 2D structures of a sample surface in solution and a thin film. X-ReSI combined higher-energy and monochromatic synchrotron x-rays in grazing incidence with a 2D detector. An X-ReSI pattern is taken from a sample fixed at an angular position with one-time exposure.

A sample examined was a single-crystal Au (111) working electrode; the reference electrode used was Hg|Hg<sub>2</sub>SO<sub>4</sub>|0.5M H<sub>2</sub>SO<sub>4</sub>. Diffraction patterns were recorded with an imaging plate detector. The 1 1 L and 1 -1 L crystal truncation rods (CTR) were intersected at L=6.3 with the Ewald sphere. A batch of images around the 0 1 6.3 CTR indicates that the surface of the Au electrode was reconstructed. We, moreover, recorded a series of x-ray patterns in the vicinity of a surface structural phase transition between the reconstructed and the bulk-terminated surface. During the transition, change in crystal domain shapes of surface intermediates as well as its smaller lattice distortion was observed.

Other samples were 50 nm- and 3 nm-thick Bi<sub>4</sub>Ti<sub>3</sub>O<sub>12</sub>(100) and (010) films epitaxially grown on TiO<sub>2</sub>(101). Observation of about a hundred spots recorded at a fixed sample position implies that X-ReSI is also applicable for a 2D nanostructure. Similar patterns obtained from the two samples suggest that the sample have the same crystal structure. Measurements were performed at beamline BL13XU, SPring-8. 25 keV x-rays were incident on sample surfaces at an angle of 0.1 degree.

- [1] Sakata et al, Appl. Phys. Lett. 84, 4239 (2004).
- [2] Sakata et al. Phys. Rev. B 72, 121407(R) (2005).

## **Structure of the Munc18c protein involved in insulin-stimulated glucose transport**

Jennifer L Martin<sup>1</sup>, Shu-Hong Hu<sup>1</sup>, Catherine F Latham<sup>1</sup>, Christine L Gee<sup>1</sup>, Michelle Christie<sup>1</sup>, Fred Meunier<sup>1</sup>, David E James<sup>2</sup>

<sup>1</sup>Institute for Molecular Bioscience, University of Queensland, <sup>2</sup>Garvan Medical Research Institute

Membrane trafficking is an essential and regulated process that ensures cellular cargo is delivered to the correct destination in response to the appropriate stimuli. Docking and fusion of target and acceptor membranes are mediated by the formation of SNARE complexes between molecules on both membranes. Regulation of SNARE complex formation is vital and the process is subject to multiple levels of control. Members of the Sec1p/Munc18 (SM) protein family have been implicated in every SNARE-mediated membrane fusion step characterised to date and are thought to tightly control SNARE complex formation. Different SM proteins have been shown to interact with SNAREs via different mechanisms leading to the conclusion that their function has diverged.

We have examined the molecular interactions between Munc18c and its cognate SNARE. These molecules are ubiquitously expressed in mammals and are responsible for plasma membrane vesicle trafficking in muscle and fat cells of the GLUT4 glucose transporter in response to insulin signalling. This system is disrupted in Type II diabetes. Intriguingly Munc18c displays a SNARE binding pattern similar to that described for most other models of SM/SNARE interactions but significantly different to the binding pattern described for its closest relative mammalian Munc18a, that regulates neurotransmitter vesicle trafficking. Here we describe the 3.1Å resolution crystal structure of Munc18c bound to a Syntaxin4 peptide.

## The first structure of myo-inositol oxygenase: An enzyme implicated in Diabetes Mellitus

Peter M. Brown Tom T. Caradoc-Davies James M. Dickson Kerry L. Loomes Garth J.S. Cooper Edward N. Baker

School of Biological Sciences, University of Auckland

Diabetes mellitus (DM) and its complications are associated with altered metabolism of inositol sugars *myo*-inositol (MI) and *D-chiro* inositol (DCI). In animals, catabolism of MI and DCI depends on a highly conserved enzyme *myo*-inositol oxygenase (MIOX), which catalyzes the first committed step of the glucuronate-xylulose pathway. This enzymatic mechanism involves a 4-electron oxidation that appears to be unique in biological systems (1). As MIOX activity increases during hyperglycaemic conditions (2), MIOX inhibition may be a therapeutic strategy to alleviate DM and its complications.

Here, we present the first crystal structure of MIOX at 2.0-Å resolution, in complex with MI. This protein is monomeric with a mostly-helical fold that is distantly related to the HD domain superfamily yet differs from other di-iron oxygenases such as ribonucleotide reductase. Five helices form the structural core and provide 4 His and 2 Asp ligands to result in a novel di-iron center. The MI substrate is coordinated in a bidentate mode to one iron atom. The structure reveals the basis of substrate specificity, insight into the enzyme mechanism and suggests routes for the development of specific MIOX inhibitors.

1. Moskala, R., Reddy, C. C., Minard, R. D. & Hamilton, G. A. (1981) *Biochem. Biophys. Res. Commun.* **99**, 107-113.
2. Nayak, B., Xie, P., Akagi, S., Yang, Q., Sun, L., Wada, J., Thakur, A., Danesh, F. R., Chugh, S. S. & Kanwar, Y. S. (2005) *Proc. Natl. Acad. Sci. USA* **102**, 17952-17957.

## **The Structure of the LIF:LIF Receptor Complex - A Prototype for Receptor Heterodimerisation in the GP130/IL-6 Family**

Thomas PJ Garrett Trevor Huyton Cindy S Luo Mei-zhen Lou Jian-guo Zhang Douglas J Hilton Nicos A Nicola

Structural Biology, Walter and Eliza Hall Institute

The gp130/IL-6 family form the largest known cooperative group of cytokines and receptors, and these molecules act in a wide variety of cell types, including embryonic stem cells, neurones, bone, muscle and breast epithelium. Cell signalling is usually initiated by the cytokine first binding a cytokine-specific non-signalling receptor. Next, signalling subunits are recruited into a high affinity cell-surface complex of between 3 and 6 molecules. In this family, signalling occurs via two distinct mechanisms. Some cytokines, such as IL-6 and IL-11, are capable of signalling via the gp130 receptor alone. However, most require a second signal receptor, such as the leukemia inhibitory factor receptor (LIFR). Questions still remain about the specificity of these multifunctional cytokines and how cytokine-specific signals can be transmitted by relatively few signalling molecules.

We have determined the crystal structure of the LIR:LIFR complex at 4.3 Å resolution which shows a novel contact between the cytokine and an immunoglobulin-like domain of the receptor. This structure is the largest fragment to date of a cytokine receptor and, in combination with previously determined structures and EM studies, it enables us to build an accurate model of the high-affinity heteromeric signalling complex. This structure also reveals how LIF can act a master cytokine and modulate the activity of other cytokines in this family.

## Perspectives of new influenza virus targeted drug design based on human Neu2 sialidase's structure

Leonard M G Chavas<sup>1</sup> Ryuichi Kato<sup>2</sup> Marettta C. Mann<sup>3</sup> Robin J. Thomson<sup>4</sup> Jeffrey C. Dyason<sup>5</sup> Marc von Itzstein<sup>6</sup> Jennifer McKimm-Breschkin<sup>7</sup> Peter M. Colman<sup>8</sup> Paola Fusi<sup>9</sup> Bruno Venerando<sup>10</sup> Guido Tettamanti<sup>11</sup> Eugenio Monti<sup>12</sup> Soichi Wakatsuki<sup>13</sup>

Structural Biology Research Center, PF-IMSS-KEK<sup>1</sup> Griffith University<sup>2</sup> CSIRO<sup>3</sup> WEHI<sup>4</sup> University of Milano-Bicocca<sup>5</sup> University of Milano<sup>6</sup> University of Brescia<sup>7</sup>

Neuraminidases, or sialidases, are glycohydrolytic enzymes widely distributed among species. They catalyze the removal of sialic acid on the non-reducing termini of complex carbohydrates, and act in infection processes, signal transduction, intercellular interactions, glycoconjugate degradation etc. The infectivity of some viruses such as influenza virus is dependent on sialidase's function. Therefore, the influenza virus neuraminidase (NA) is the target of drug designs for clinical treatment of the infection. Within species, sialidases diverge in their amino acid sequences, but assume a similar folding by means of a six bladed beta-propeller, and share an almost identical active site architecture. Consequently, drugs targeted to one virus strain's neuraminidase expectedly acts on other strains as well. Here we report the inhibition studies of the human sialidase Neu2 by NA inhibitors such as Tamiflu, Zanamivir or Peramivir, as indicated by inhibition assays and X-ray structure determinations. As a preliminary result, whereas Tamiflu is inactive against the cytosolic Neu2, Zanamivir and Peramivir considerably affect the human enzyme's activity by entering its active site. These studies open an area of more specific drug developments based on the crystal structures of the complexes.

## Structure of *Plasmodium vivax* P25 and its complex with transmission-blocking antibody

Ajay Kumar Saxena<sup>1</sup>, K Singh<sup>1</sup>, H P Su<sup>1</sup>, M M Klein<sup>1</sup>, A W Stower<sup>1</sup>, A J Saul<sup>1</sup>, G Long<sup>1</sup>, D N Garboczi<sup>2</sup>

School of Life Sciences, Jawaharlal Nehru University, National Institutes of Health<sup>1</sup>

Malaria parasites must infect the mosquito to complete their life cycle. In vertebrates, they inhabit a protected niche inside red blood cells. But when a parasite exits the red blood cell in the mosquito gut, it becomes exposed to the mosquito's digestion and innate immune responses. During the first 24 hours outside the red blood cell, P25 and P28 proteins cover the surface of the parasite, while the parasite develops into a form that can exit the gut. As it moves through the mosquito gut and gut epithelial wall, the abundant P25 and P28 proteins are continually shed from the parasite. Antibodies (and their Fab fragments) against P25 or P28 prevent parasites from exiting the gut without inhibiting locomotion. At present, the mosquito's defenses against *Plasmodium* are under intense study as we realize that only a few vulnerable, yet surviving parasites are responsible for the infection of the mosquito salivary glands. P25 is in clinical trial as a vaccine that will elicit antibodies that block the transmission of malaria.

Our structures reveal the shape of the members of the P25/P28 families of *Plasmodium* proteins and show a loop, at the vertex of the P25/P28 triangle, where antibodies bind that prevent the transmission of malaria through the mosquito. The structures that we describe will stimulate new knowledge of the basic biology of the parasite in the mosquito and the development of drugs and vaccines against the vulnerable mosquito stage of the malaria parasite.

## Anaerobic and Aerobic Structures of Ferredoxin II from *Desulfovibrio Gigas* at Ultrahigh Resolution

Chun-Jung Chen<sup>\*</sup> Yin-Cheng Hsieh<sup>\*\*</sup> Yi-Hung Lin<sup>\*</sup> Yen-Chieh Huang<sup>\*</sup> Ming-Yih Liu<sup>\*</sup>

Life Science Group, National Synchrotron Radiation Research Center<sup>\*</sup> Institute of Bioinformatics and Structural Biology, National Tsing-Hua University, Taiwan<sup>\*\*</sup>

Ferredoxin II (Fd II) is a small electron transfer protein isolated from the strict anaerobic sulfate-reducing bacterium, *Desulfovibrio gigas*. The protein contains 58 amino acids and an iron-sulfur cluster. The cluster [3Fe-4S] spontaneously undergoes conversion to [4Fe-4S] when it is used as an electron mediator in the phosphoroclastic reaction. This two-form interconversion appears to have physiological significance. We have obtained both aerobic and anaerobic Fd II crystals in the high-resolution quality and determined structures independently by the iron single-wavelength anomalous dispersion (Fe-SAD) method using synchrotron radiation X-ray. The structure of aerobic Fd II has been refined to 0.9 Å ultrahigh resolution in space group P2<sub>1</sub>2<sub>1</sub>2. Its [3Fe-4S] cluster is bound with Cys8, Cys14, and Cys50, whereas Cys11 extends away from cluster. Cys18 and Cys42 form a disulfide bridge to maintain the protein folding. Multiple-conformations of residues are also observed in ultrahigh-resolution density map. Five isolated Zn<sup>2+</sup> ions around the protein are bound with Glu, Asn and Asp residues, respectively, which indicates the transition metals, other than iron, could be incorporated into [3Fe-4S] center. On the other hand, the anaerobic Fd II structure from the crystals grown under anaerobic condition has also been refined in different space group C222. The anaerobic structure shows the different iron-sulfur cluster, disulfide bridge conformations, water structures, crystal packing and electron density distribution among activity site. Here we present the structure comparison between aerobic and anaerobic Fd II at ultrahigh resolution which reveals the unique iron storage function and electron transfer mechanism of ferredoxin II from *Desulfovibrio gigas*.

**X-ray Structure of in-situ HIV-1 protease-product complex: observation of a LBHB between catalytic aspartates**

Madhusoodan V Hosur<sup>1</sup> Amit Das<sup>1</sup> Vishal Prashar<sup>1</sup> Smita Mahale<sup>2</sup> Laurence Serre<sup>3</sup> Jean-Luc Ferrer<sup>3</sup>

Solid State Physics Division, Bhabha Atomic Research Centre<sup>1</sup> National Institute for Research in Reproductive Health, India<sup>2</sup> Institut de Biologie Structurale, France<sup>3</sup>

We report here the structure of an *in-situ* complex between HIV-1 protease and the oligopeptide substrate AETF<sup>\*</sup>YVDGAA, which corresponds to the RT-RH junction in the viral polyprotein. The structure refined to 1.65Å resolution against synchrotron data, shows occurrence of the cleavage reaction in the crystal, with the two product peptides still bound in the active site before complete separation. Therefore interactions at the catalytic centre could give an insight into reaction mechanism. Both oxygens of the generated carboxyl group form hydrogen bonds : one to OD2 atom of a catalytic aspartate, and the other to the scissile nitrogen atom. The latter hydrogen bond may indicate protonation of scissile nitrogen by gem-diol hydroxyl. The inner oxygen atoms of the catalytic aspartates in the complex are 2.35Å apart indicating a LBHB. This observation of an LBHB provides the first structural support to the mechanism proposed by Northrop( *Acc. Chem. Res.* 2001, **34**, 790 - 797), which itself is supposed to have resolved decades old uncertainties about aspartyl proteases. Further, atomic configuration of the products may be helpful for the design of mechanism-based inhibitors.

**Structural basis for recognition of high mannose-type glycan by canine cargo receptor VIP36**

Tadashi Satoh<sup>1</sup> Nathan Cowieson<sup>2</sup> Wataru Hakamata<sup>1</sup> Masaaki Kurihara<sup>1</sup> Hiroko Ideo<sup>1</sup>  
Ryuichi Kato<sup>1</sup> Katsuko Yamashita<sup>1</sup> Soichi Wakatsuki<sup>1</sup>

<sup>1</sup>Structural Biology Research Center, Photon Factory, High Energy Accelerator Research Organization (KEK) <sup>2</sup>Institute for Molecular Bioscience, University of Queensland, Australia  
<sup>1</sup>Division of Organic Chemistry, National Institute of Health Sciences (NIHS), Japan <sup>1</sup>Innovative Research Initiatives, Tokyo Institute of Technology, Japan

VIP36, a vesicular-integral protein of 36 kDa, is a family of  $\text{Ca}^{2+}$ -dependent intracellular animal lectins such as ERGIC-53, and functions as a cargo receptor for trafficking certain glycoproteins in the secretory pathway. To investigate the structural basis for the high mannose-type glycoprotein recognition and transport by VIP36, we have determined crystal structures of the carbohydrate recognition domain (CRD) of VIP36, in the absence and presence of  $\text{Ca}^{2+}$  ion and a part of the high-mannose type glycan, i.e.  $\alpha$ -mannose, mannobiose (Man- $\alpha$ -1,2-Man) and mannotriose (Man- $\alpha$ -1,2-Man- $\alpha$ -1,2-Man). We collected a 2.1 Å resolution data set of metal-free VIP36 and a 1.8 Å resolution data set of  $\text{Ca}^{2+}$ -bound VIP36 on PF-AR-NW12A. Moreover, we collected a 1.8 Å resolution data set of VIP36/mannose and a 1.75 Å resolution data set of VIP36/mannobiose on PF-BL5A. As for VIP36/mannotriose, we collected a 2.0 Å resolution data set on PF-AR-NW12A. The structures were solved by the molecular replacement method using the structure of the  $\text{Ca}^{2+}$ -bound p58/ERGIC-53 CRD as a search model. The CRD is composed of a seventeen-stranded antiparallel  $\beta$ -sandwich, and binds one  $\text{Ca}^{2+}$  adjoining the carbohydrate-binding site. The binding of  $\text{Ca}^{2+}$  arranges Asp131, Asn166 and His190 for the proper carbohydrate binding, illustrating its  $\text{Ca}^{2+}$ -dependence mechanism. The mannotriose which corresponds to D1 arm of high-mannose type *N*-glycan is recognized by eight residues through extensive hydrogen bonds and hydrophobic interactions. Our results clearly show that VIP36 functions as a cargo receptor for high-mannose type glycoproteins, and recognizes their D1 arm of the *N*-glycans.

**Structural basis on the catalytic reaction mechanism of novel 1,2- $\alpha$ -L-fucosidase (AfcA) from *Bifidobacterium bifidum***

Masamichi Nagae<sup>1</sup> Atsuko Tsuchiya<sup>2</sup> Takane Katayama<sup>3</sup> Kenji Yamamoto<sup>2</sup> Soichi Wakatsuki<sup>1</sup> Ryuichi Kato<sup>1</sup>

Structural Biology Research Center, IMSS, KEK<sup>1</sup> Division of Integrated Life Science, Graduate School of Biostudies, Kyoto University, Japan<sup>2</sup> Research Institute for Bioresources and Biotechnology, Ishikawa Prefectural University, Japan<sup>3</sup>

A novel 1,2- $\alpha$ -L-fucosidase (AfcA) from *Bifidobacterium bifidum*, which hydrolyzes the  $\alpha$ 1,2 glycosidic linkage of Fuc $\alpha$ 1-2Gal via an inverting mechanism, was isolated recently and classified as a member of a glycoside hydrolase family 95 (GH95). The catalytic activity of AfcA is ascribed to the middle of the polypeptide chain (Fuc domain). The enzymatic activity of the Fuc domain is strongly inhibited by deoxyfuconojirimycin (DFJ), which is an analogue of  $\alpha$ -L-fucose. To elucidate the molecular mechanism of the enzyme, we report the X-ray crystal structures of AfcA Fuc domain in unliganded and complexed forms with DFJ, 2'fucosyllactose (substrate), and fucose and lactose (products) at 1.12-2.10 Å resolution. Overall structure of Fuc domain is composed of four regions: an N-terminal  $\beta$  region, a helical linker, a helical barrel region and a C-terminal  $\beta$  region. The overall domain arrangement is similar to those of maltose phosphorylase from *Lactobacillus brevis* (GH65) and chitobiose phosphorylase from *Vibrio proteolyticus* (GH95). The helical barrel region of Fuc domain shows resemblance to the ( $\alpha/\alpha$ )<sub>6</sub> barrel structure of clan GH-L. In the complex structures, the ligands are deeply buried in the central cavity of the helical barrel region. From the crystal structures and mutational analyses, highly conserved Glu566 is strongly suggested to be the general acid catalyst. However, no carboxylic acid residue is located at the suitable position for the general base catalyst. We propose and discuss a possibly new catalytic reaction mechanism of AfcA based on the structural and biochemical analyses.

## Molecular dynamics in crystals on the basis of X-ray thermal parameters and NQR data in organic and inorganic chlorine compounds

RAMU L Chandramani R

Department of physics, Bangalore University.

Molecular dynamics (Torsional frequencies- $f_t$ ) in several organic and inorganic chlorine compounds have been evaluated on the basis of X-ray thermal parameters and Nuclear Quadrupole Resonance data. NQR Studies gives useful information about the molecular dynamics and phase transitions in solids. Usually the  $f_t$  obtained through NQR data are compared with FT IR/Raman data. The approach here is to evaluate  $f_t$  at room temperature using available data on X-ray thermal parameters.

Temperature factor of an atom for any set of lattice planes (hkl) depends on the inter planar spacing and on the magnitude of vibration perpendicular to the planes. There is an expression [1], which relates general temperature factor, the reciprocal lattice parameters and thermal parameters ( $U_{ij}$ ) expressed in terms of mean square amplitudes ( $\langle\theta^2\rangle$ ) of vibration in  $\text{Pm}^2$ . The NQR motional averaging has been shown to arise from temperature dependent tilting of the z-axis of the EFG tensor. One can therefore estimate  $\langle\theta^2\rangle$  for various C-Cl bond directions, which define the respective z-axis of the EFG tensor using the X-ray thermal parameters.

The  $f_t$  at  $T=300\text{K}$  in the following compounds has been done:

- (1) 3,4 dichlorophenol.
- (2) 4-Chloro-3,5-dimethylphenol.
- (3) 2,5-Dichloroaniline.
- (4) 5-Chloro-2-Pyridone.
- (5) Mercuric Chloride.
- (6) Antimony Trichloride.

The  $f_t$  obtained by X-ray thermal parameters and by NQR data have been compared. The values obtained in both cases are in good agreement. The above approach is a good illustration of the supplementary nature of the data from X-ray studies in relation to NQR studies of compounds in solid state.

### Reference;

- 1). L.Ramu, R.Banu, S.Rani and R.Chandramani. *ACTA PHYSICA POLONICA-A*, 775, Vol-109(2006).

**An intermediate state in phase transition cycles of Na<sub>2</sub>dGMP hydrate**

Shigefumi Yamamura Tadashi Moriguchi Shigetaka Yoneda Yoko Sugawara

School of Science, Kitasato University

The first-order phase transitions of nucleoside and nucleotide hydrates are induced by humidity and temperature changes [1]. We found bifurcation of the phase transition in the case of 2'-deoxyguanosine 5'-monophosphate (Na<sub>2</sub>dGMP), i.e. the tetrahydrate transforms to the anhydrous form A or B [2]. One intermediate state (form M) was observed in the reverse transition from the anhydrous form B to the tetrahydrate. Around room temperature, the anhydrous form B changes to the form M, and then the form M gradually changes to the tetrahydrate. Therefore the form M would be a metastable state. We have successfully determined the crystal structure of the form M.

A single crystal of the form M was obtained by rapid cooling of the anhydrous form B to -100 °C, while the anhydrous form B was prepared by heating the tetrahydrate to 80 °C in a glass capillary. X-ray analysis of the form M was carried out, and the form M was found to be the dihydrate. Water molecules of the form M occupy vacant channel sites between the arrays of dGMP molecules in the anhydrous form B. The arrays of dGMP molecules are maintained in the form M. The conformation of dGMP molecule in the form M is similar to that in the anhydrous form B but largely different from that in the tetrahydrate. It is concluded that the large conformational difference of dGMP molecule between the anhydrous form B and the tetrahydrate plays a key role for the emergence of the intermediate state.

- [1] Urabe *et al.* (1995) *Phys. Rev. B*, **51**, 5666.
- [2] Yamamura *et al.* (2005) *Acta Crystallogr.* **A61**, C326.

**X-ray diffraction analyses of cis-trans photoisomerizaion of olefins**

Jun Harada Mayuko Harakawa Keiichiro Ogawa

Department of Chemistry, The University of Tokyo, Komaba

Cis-trans photoisomerization is one of the most important types of photoreactions, and innumerable studies on the subject have been carried out. The photoisomerization in the solid state, however, has generally been considered difficult to take place, and only limited number of studies has been reported. The nonoccurrence of the reaction in the solid state is believed to be due to the fact that the isomerization involves large changes in the molecular shape, which should be hindered in the crystalline lattice. In this study we succeeded in single-crystal X-ray diffraction analyses of the cis-trans photoisomerizations of small organic molecules in crystals. The structural changes accompanying the reactions were revealed to take place not to disturb the crystalline lattices and in volume-conserving manners. A bicycle-pedal motion, which is another type of volume-conserving molecular motion in crystals, will also be discussed.

## Temperature dependence of crystalline state photo isomerization of an organo-dirhodium dithionite complex

Yoshiki Ozawa<sup>1</sup>, Takae Yonezawa<sup>1</sup>, Tomomi Yokoyama<sup>1</sup>, Minoru Mitsumi<sup>1</sup>, Koshiro Toriumi<sup>1</sup>, Hidetaka Nakai<sup>2</sup>, Yoshihito Hayashi<sup>2</sup>, Kiyoshi Isobe<sup>2</sup>

<sup>1</sup>Graduate School of Material Science, University of Hyogo, <sup>2</sup>Graduate School of Natural Science and Technology, Karazawa University

An organo-dirhodium dithionite complex  $[(C_2Me_5)(\mu-CH_2)_2Rh(O_2SSO_2)](1)$  shows fully reversible photochromism in which one of four terminal oxygen atoms in the side-on type dithionite  $\mu-O_2SSO_2$  moiety is converted to a bridged one to produce geometrical isomer form  $\mu-OSOSO_2$  by visible light illumination in crystalline-state. The reverse reaction occurs thermally at room temperature. During the photoreaction, positional disorders of oxygen atoms were found which indicated geometrical isomers of photoproducts exist. We have tried to analyze time and temperature dependencies of the photo-isomerization process in crystalline state by x-ray structure analyses of the photo illuminated single crystal in order to investigate photo isomerization mechanism.

There are four configurational or conformational isomers of photoproducts (2a, 2b, 2c, 2d) can be generated from the starting complex (1) in the crystal due to combination of geometries of bridged and terminal oxygen atoms. Though all four isomers were found at the initial stage of the reaction, only one isomer (2a) was survived with almost 100% population when the reaction completed after 150 h photo irradiation at 293K. When the photo irradiation was performed at 110 K, all four isomers were generated (but not evenly distributed) and no decreases of populations were observed even after the photoreaction was completed over 90%. These phenomena indicate that conversions between the photoproduct isomers occur with the increase of the population of the most thermally stable isomer (2a) in the crystal cavity.

**Dynamic structural change in the gas adsorption process on microporous coordination polymer**

Yoshiki Kubota<sup>1</sup>, Masaki Takata<sup>2</sup>, Ryolaro Matsuda<sup>3</sup>, Ryo Kitaura<sup>4</sup>, Susumu Kitagawa<sup>5</sup>, Tatsuo C Kobayashi<sup>6</sup>

Department of Physical Science, Osaka Prefecture University<sup>1</sup>, RIKEN SPring-8 Center / JASRI / CREST(JST)<sup>2</sup>, Department of Synthetic Chemistry and Biological Chemistry, Kyoto University<sup>3</sup>, Department of Physics, Okayama University<sup>4</sup>

Metal-organic microporous materials (MOMMs) are the new class of materials with functionalized nano-coordination space and have attracted attention for their application, such as gas storage, gas separation and catalysis. Recently, we reported the highly controlled acetylene accommodation in the nanochannels of MOMM by the in situ synchrotron powder diffraction experiment of gas adsorption and the MEM/Rietveld charge density analysis. While sorption profiles of MOMMs with saturated amounts of guests have been well characterized so far, their intermediate profiles are still unknown. An in-depth understanding of the intermediate state provides us with a feasible design for a porous framework, which changes its structure into one well suited for a desired guest molecules and results in an efficient accommodation system. Therefore, the structural information throughout adsorption phenomena is eagerly required.

Here we report the structure analysis of the intermediate phase in the process of acetylene adsorption in the nanochannels of a MOMM. Crystal lattice was found to expand once in the intermediate phase and contract in the saturated adsorbed phase. Simultaneously the lattice shearing and the rotation of pillar ligand occurred to attain an efficient guest accommodation. These findings will provide us with the guiding principles for a design of gas storage materials for highly reactive gases like acetylene.

## **100ps-Resolved X-ray Diffraction at the NW14A, Photon Factory Advanced Ring**

Shin-ichi Adachi<sup>1</sup>, Shunsuke Nozawa<sup>2</sup>, Ryoko Tazaki<sup>3</sup>, Laurent Guerin<sup>4</sup>, Kohei Ichiyonagi<sup>5</sup>, Matthieu Chollet<sup>6</sup>, Tokushi Sato<sup>7</sup>, Ayana Tomita<sup>8</sup>, Eric Collet<sup>9</sup>, Marylise Buron-Le Cointe<sup>10</sup>, Johan Hebert<sup>11</sup>, Herve Cailleau<sup>12</sup>, Hiroshi Sawa<sup>13</sup>, Hiroshi Kawata<sup>14</sup>, Shin-ya Koshihara<sup>15</sup>

Photon Factory, KEK, ERATO, JST, Japan<sup>1</sup>, Tokyo Institute of Technology, Japan<sup>2</sup>, Universite Rennes 1, France<sup>3</sup>

Time-resolved X-ray experiments using synchrotron radiation sources are becoming general and powerful tools to explore structural dynamics of condensed matters in material and biological sciences. A new insertion device beam line NW14A at the Photon Factory Advanced Ring (PF-AR) was constructed and is now operational for 100ps-resolved X-ray diffraction/scattering and XAFS experiments. The primary scientific targets of the NW14A will be condensed matter systems which can be triggered reversibly by a laser pulse. In particular, photo-induced phase transitions (PIPT) in molecular charge-transfer crystals are one of the main targets of the research. The specifications, the performance and preliminary results of the beam line will be presented.



# Poster Abstracts



## Crystal Structure Analysis of two Aldehyde Substituted Indole Derivatives

Palani Kandavelu<sup>1</sup> Jaisankar P<sup>2</sup> Srinivasan P.C<sup>2</sup> Ponnuswamy M.N.<sup>1\*</sup>

Department of Crystallography and Biophysics, University of Madras<sup>1</sup> Dept. of Organic Chemistry, University of Madras, Guindy Campus, Chennai - 600 025<sup>2</sup> Dept. of Crystallography and Biophysics, University of Madras, Guindy Campus, Chennai - 600 025<sup>1\*</sup>

Indole ring system is present in a number of natural products. The halogenated indole derivatives exhibit antibacterial activity against Gram-positive, Gram-negative bacteria and fungi. Indole derivatives also intercalate with DNA. To establish the structures, the following aldehyde indole derivatives are studied by crystallographic methods.

1. 3-Chloro-1-phenylsulfonyl-1H-indole-2-carbaldehyde (CLPIC) crystallizes in triclinic space group P1 with cell parameters  $a = 8.048(2)\text{\AA}$ ,  $b = 9.568(3)\text{\AA}$ ,  $c = 9.931(3)\text{\AA}$ ,  $\alpha = 79.433(4)$ ,  $\beta = 82.145(4)$ ,  $\gamma = 69.839(4)$ ,  $V = 703.4(4)\text{\AA}^3$ ,  $Z = 2$  and refined to a final R-value of 0.0544.

2. 3-Cyano-1-phenylsulfonyl-1H-indole-2-carbaldehyde (CYPIC) crystallizes in triclinic space group P1 with cell parameters  $a = 9.554(2)\text{\AA}$ ,  $b = 12.193(3)\text{\AA}$ ,  $c = 13.637(3)\text{\AA}$ ,  $\alpha = 103.199(4)$ ,  $\beta = 95.814(4)$ ,  $\gamma = 111.969(4)$ ,  $V = 1403.3(5)\text{\AA}^3$ ,  $Z = 4$  and refined to a final R-value of 0.0862.

In CYPIC, there are two crystallographically independent molecules in the asymmetric unit. The indole ring systems are planar, the dihedral angle formed by the pyrrole and benzo planes are 1.1(1) in CLPIC and 0.5(2) and 2.0(1) for molecules A and B of CYPIC. The molecules stabilized by C-H $\cdots$ O, C-H $\cdots$  $\pi$  and  $\pi\cdots\pi$  types of interactions in addition to van der Waal's forces.

## Isomorphism and Polymorphism of the Crystal Structures of Cholesterol Derivatives

Young-Ja Park

Department of Chemistry, Sookmyung Women's University

We have undertaken 25 crystal structure analyses of cholesteryl ethers, esters and carbonates. Among these crystal structures, (1)cholesteryl ethyl ether, isopropyl ether, hexanoate, heptanoate, pentyl carbonate and hexyl carbonate are isostructural each other, (2)cholesteryl ethyl carbonate(two forms), propyl carbonate, crotonate and crotyl carbonate are isostructural each other, (3)cholesteryl isobutyrate and isobutyl carbonate are isostructural, (4)cholesteryl phenyl acetate and cholesteryl isopropyl carbonate are also isomorphic each other. The cholesteryl 2,4-dichlorobenzoate, ethyl carbonate and butyl carbonate have been crystallized in two polymorphic forms, respectively. The crystal structures of cholesteryl formate, hemisuccinate, aniline, 2,4-dichlorobenzoate, hydrocinnamate, butyl carbonate, methyl ether, methyl carbonate and pentanoate do not belong to any typical packing group and do not show any isomorphism.

Most of crystal structures of cholesterol derivatives are remarkable in forming layer structures, so called monolayer type 1, 2, 3 and bilayer. Typical packing modes will be discussed in terms of isomorphism and polymorphism.

**Valence Transitions and Oxygen Vacancies in  $\text{Ba}_2\text{LnSn}_x\text{Sb}_{1-x}\text{O}_{6-\delta}$** 

Paul J Saines Brendan J. Kennedy

School of Chemistry, The University of Sydney

Double perovskites are of interest due to their wide ranging physical properties, which in many cases can be tuned by suitable chemical substitutions. The electronic and ionic conductivity of perovskites that are either oxygen deficient and/or contain mixed valent cations are of particular interest. The potential for oxygen vacancies to concentrate on a certain site in these materials is of particular interest as it could lead to the development of anisotropic ionic conductivity and hence more efficient electrolytes.

Two series of potentially oxygen deficient double perovskites  $\text{Ba}_2\text{LnSn}_x\text{Sb}_{1-x}\text{O}_{6-\delta}$ ; (Ln = Pr and Nd) have been structurally characterized using a combination of powder neutron and synchrotron X-ray diffraction. The neodymium containing compounds were found to feature a phase transition from rhombohedral to monoclinic symmetry upon partial replacement of the Sb(V) with Sn(IV). Ordering of the resulting oxygen vacancies was observed using neutron diffraction at temperatures of up to 1073 K. The oxygen vacancies in  $\text{Ba}_2\text{NdSnO}_{5.5}$  were found to concentrate on the equatorial sites at ambient conditions shifting to the axial sites at higher temperatures. This rearrangement can be explained using crystal chemistry. By comparison the symmetry of the praseodymium compounds changes from rhombohedral to monoclinic and then to tetragonal with increasing Sn(IV) content. The three B-type cations (Pr, Sb and Sn) are disordered in the tetragonal structure. Thermal-gravimetric and spectroscopic analysis suggest that increasing the tin content results in oxidation of  $\text{Pr}^{3+}$  to  $\text{Pr}^{4+}$  rather than the formation of oxygen vacancies.

**Structural modulation in the misfit-layered cobalt oxide  $(\text{CaOH})_k\text{CoO}_2$** 

Masaaki Isobe Mitsuko Onoda Mitsuyuki Shizuya Masahiko Tanaka Eiji Takayama-Muromachi  
National Institute for Materials Science

Recently, considerable interests have been focused on layered cobalt oxides because of their various unusual physical properties. In particular, unconventional superconductivity in  $\text{Na}_{0.39}\text{CoO}_2 \cdot 1.3\text{H}_2\text{O}$  much stimulates our intellectual curiosity, because origin of the superconductivity seems to be associated with rather unusual spin-triplet-type electron pairing. Following the current research on layered cobalt oxides, new-materials search has intensified. Recently, we succeeded in synthesizing a new misfit-layered cobalt calcium hydroxide system  $(\text{CaOH})_k\text{CoO}_2$  by utilizing high-pressure technique. We report on detailed crystal structure of the compound.

The crystal structure of  $(\text{CaOH})_k\text{CoO}_2$  was analyzed by means of the superspace-group formalism using the synchrotron x-ray diffraction data. The compound belongs to the class of incommensurate composite crystals being isostructural with transition-metal sulfides  $(\text{MS})_x\text{TS}_2$  ( $M=\text{Pb}$ ,  $\text{Gd}$  or  $\text{La}$ ;  $T=\text{Ti}$ ,  $\text{V}$  or  $\text{Cr}$ ;  $x=1.18\text{-}1.27$ ). The structure of the present compound consists of two interpenetrating subsystems: (i)  $[\text{CoO}_6]$  containing triangular lattices formed by edge-sharing  $[\text{CoO}_6]$  octahedra and (ii)  $[\text{CaOH}]$  double-layered rock-salt-type slabs. The two subsystems have incommensurate periodicity along the  $a$ -axis, resulting in modulated crystal structure due to the inter-subcell interaction. We found significant structural modulation realized in the  $[\text{CaOH}]$  subsystem.

**Thermal and Athermal Structure Change of  $\text{Fe}_{3-x}\text{Ti}_x\text{O}_4$  spinel solid solution.**Takamitsu Yamanaka<sup>\*</sup> Tetsuro Mine<sup>\*</sup> Sachiko Asogawa<sup>\*</sup> Yuki Nakamoto<sup>\*\*</sup>Earth and Space Science, Osaka University<sup>\*</sup> Center for Quantum Science and Technology, Osaka University<sup>\*\*</sup>

$\text{Fe}_{3-x}\text{Ti}_x\text{O}_4$  continuous solid solutions have a spinel structure ( $Fd3m$ ). Various pressure-induced transforms have been reported into  $\text{CaMn}_2\text{O}_4$  ( $Pbcm$ ),  $\text{CaTi}_2\text{O}_4$  ( $Bbmm$ ), or  $\text{CaFe}_2\text{O}_4$  ( $Pnma$ ) structure. Using synchrotron radiation we performed high-pressure single-crystal structure analyses with diamond anvil cell up to 15GPa and powder diffraction experiments up to 60GPa. The cubic-to-tetragonal transition pressure of decreases with increasing Ti content. The transition was induced from the tetragonal distortion due to the Jahn-Teller effect of  $\text{Fe}^{2+}$  at the tetrahedral site. But the spinel with less than  $x=0.6$  does not transform. Structure refinements of  $\text{Fe}_2\text{TiO}_4$  were executed at various pressures at room temperature and at low-temperatures down to -170C at ambient pressure. All least-squares analyses are converged to  $R=0.015\text{--}0.04$  at low temperature and  $0.03\text{--}0.09$  at high pressure. The transition to the low-temperature tetragonal phase takes place at -110C. The  $c/a$  ratio is  $0.9982(4)$  at 11.43GPa at room temperature and  $0.9967(5)$  at -170C at ambient pressure. Base on the high-spin state condition, degeneracy of  $e_g$  orbit at the tetrahedral site for  $\text{Fe}^{2+}$  under high-pressure or low-temperature condition prefers electronic state on  $d_{z^2}$  orbit to  $d_{x^2-y^2}$ , inducing the tetragonal distortion with  $c/a < 1$ . Difference Fourier maps of  $\text{Fe}_2\text{TiO}_4$  reveal the electron density of  $d_{z^2}$  state in  $e_g$  electrons of  $\text{Fe}^{2+}$ . Another high-pressure phase of orthorhombic structure of  $\text{Fe}_2\text{TiO}_4$  was found at 30GPa and the structure was determined to be  $\text{CaTi}_2\text{O}_4$ -type structure by Reitveld method. In addition, we found a new higher-pressure polymorph for specimens with  $x=0.8$  and  $1.0$  at 59GPa and 45GPa, respectively. We could not confirm the phase for specimens  $x=0.7$ .

## Crystal structure of the parent misfit-layered cobalt oxide $[\text{Sr}_2\text{O}_2]_q\text{CoO}_2$

Takuro Nagai<sup>1</sup>, Kei Sakai<sup>2</sup>, Maarit Karppinen<sup>3</sup>, Toru Asaka<sup>4</sup>, Koji Kimoto<sup>5</sup>, Atsushi Yamazaki<sup>6</sup>, Hisao Yamauchi<sup>7</sup>, Yoshio Matsui<sup>8</sup>

<sup>1</sup>High Voltage Electron Microscopy Station, National Institute for Materials Science, Materials and Structures Laboratory, Tokyo Institute of Technology, Japan; <sup>2</sup>Laboratory of Inorganic and Analytical Chemistry, Helsinki University of Technology, Finland; <sup>3</sup>Advanced Nano Characterization Center, National Institute for Materials Science, Japan; <sup>4</sup>Department of Resources and Environmental Engineering, Waseda University, Japan

The crystal structure of a new Sr-Co-O phase was investigated through high-resolution electron microscopy (HREM) techniques [1]. We synthesized a sample in evacuated and sealed quartz ampoules at 850 °C from a mixture of  $\text{SrO}_2$  and  $\text{Co}_3\text{O}_4$  powders with the ratio of 1:1 for Sr and Co. Electron diffraction (ED) measurement together with energy dispersive x-ray spectroscopy (EDS) analysis showed that the sample contains an unknown Sr-Co-O ternary phase with monoclinic symmetry and the cation ratio of Sr/Co = 1. A layered structure with a regular stacking of a  $\text{CdI}_2$ -type  $\text{CoO}_2$  sheet and a rock-salt-type  $\text{Sr}_2\text{O}_2$  double-layered block was observed in the HREM images; the phase is the parent of the more complex misfit-layered cobalt oxides of  $[\text{M}_m\text{A}_2\text{O}_{m+2}]_q\text{CoO}_2$  with the formula of  $[\text{Sr}_2\text{O}_2]_q\text{CoO}_2$ , i.e.  $m = 0$  as shown in the figure. It was also revealed that the misfit parameter  $q$  is 0.5, namely, the two sublattices of the  $\text{CoO}_2$  sheet and the  $\text{Sr}_2\text{O}_2$  block coexist to form a commensurate composite structure. We proposed a structural model with monoclinic  $P2_1/m$  symmetry, which was supported by simulations of ED patterns and HREM images based on dynamical diffraction theory.

[1] T. Nagai et al., J. Solid State Chem. 179, 1898 (2006).

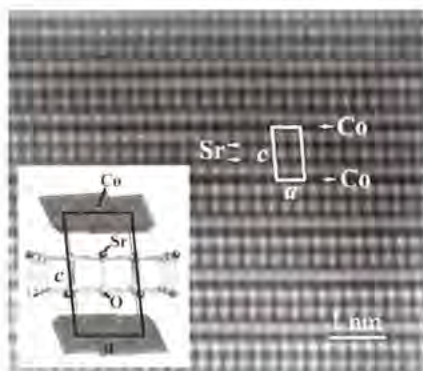


Fig. High-resolution image and structural model of the parent misfit-layered cobalt oxide  $[\text{Sr}_2\text{O}_2]_q\text{CoO}_2$ .

## Energy Spectrometer on Diffractometer using Charge-Coupled Device X-ray Detector

Hiroshi Abe<sup>1</sup> Hiroyuki Saitoh<sup>2</sup> Hironori Nakao<sup>3</sup> Kazuki Ito<sup>4</sup> Ken-ichi Ohshima<sup>5</sup>

Department of Materials Science and Engineering, National Defense Academy<sup>1</sup> Synchrotron Radiation Research Center, Japan Atomic Energy Research Institute<sup>2</sup> Department of Physics, Tohoku University<sup>3</sup> Laboratory for Structural Biochemistry, RIKEN Harima Institute SPring-8 Center<sup>4</sup> Institute of Materials Science, University of Tsukuba<sup>5</sup>

A charge-coupled device (CCD) X-ray detector for inelastic X-ray scattering was installed at the beamline BL-4C of the Photon Factory at the High Energy Accelerator Research Organization in Japan<sup>1</sup>. A wavelength-dispersive X-ray spectrometer was mounted on a 6-circle diffractometer. Energy spectra were obtained by the CCD X-ray detector and curved highly oriented pyrolytic graphite for analyzer. By combination of energy spectroscopy and diffraction, real time data acquisition both of the momentum and energy transfer was performed simultaneously.

Considering the optical geometry, it was found that each channel position is not proportional to the scattered energy. Therefore, we introduced the equation from scattering angle to energy. After data correction, calculated X-ray energy was in good agreement with the observed ones. The accuracy of energy correction was found to be within 1 eV. The energy resolution was experimentally determined by using observed peak width on the corrected energy scale of CCD X-ray detector. Experimental energy resolution,  $\Delta E$ , in the beam optics was 20 eV.

### Reference

- 1) H. Abe et al., to be published in J. Appl. Cryst. (2006).

**X-ray diffraction and XMCD studies for magnetic-related Co oxides**

Satoshi Sasaki<sup>\*</sup> Norio Shimizu<sup>\*</sup> Takeshi Ohno<sup>\*</sup> Takayasu Hanashima<sup>\*</sup> Koichi Ohkubo<sup>\*</sup> Maki Okube<sup>\*</sup> Takeharu Mori<sup>\*\*</sup>

Materials and Structures Laboratory, Tokyo Institute of Technology<sup>\*</sup> Photon Factory, KEK, Japan<sup>\*\*</sup>

Co ions in ferrites, which are notable to be ferrimagnetic at room temperature, give strong magnetic moments through the super exchange interaction between the tetrahedral and octahedral sites. Since the spinel structure has the geometrical frustration of a pyrochlore type, site occupancy between Fe and Co ions and the valence and spin states are key factors to control the physical properties. On the other hand, an intermediate-spin state of Co ions can be stabilized  $\text{Co}^{3+}$  or  $\text{Co}^{4+}$  with the strong Co 3d- O 2p hybridization in perovskite structures. Nonmagnetic  $\text{LaCoO}_3$  transforms to paramagnetic with the spin-crossover phenomenon around  $T = 100$  K. By substituting Sr for La,  $(\text{La},\text{Sr})\text{CoO}_3$  becomes ferromagnetic. A combination study of x-ray diffraction, XANES and XMCD at Co K absorption edges has been carried out to determine the valence and spin states of Co ions at PF-BL-3A and BL-10A. Compositional dependence on the valence state of Co ions has been examined for cubic spinel of  $\text{Fe}_x\text{Co}_{3-x}\text{O}_4$  ( $x = 0, 0.8, 1.0, 1.1, 1.4, 1.8, 2.0$  and  $2.1$ ) and rhombohedral perovskite of  $\text{La}_{1-x}\text{Sr}_x\text{CoO}_3$  ( $x = 0, 0.2, 0.3, 0.4, 0.5$  and  $0.6$ ). The present study suggests (1) mixing of two spin states of Co ions in Fe cobaltite, (2) the existence of an intermediate-spin state of  $\text{Co}^{3+}$  in  $\text{LaCoO}_3$  and (3) the double-exchange interaction between  $\text{Co}^{3+}$  and  $\text{Co}^{4+}$  in La-Sr-Co oxide.

## X-ray reflectometry and diffraction study of Co(Pt)/AlN annealed multilayer film

Takashi Harumoto<sup>\*</sup> Yasuaki Hodumi<sup>\*\*</sup> Yoshio Nakamura<sup>\*\*</sup>

Department of Metallurgical Engineering, Tokyo Institute of Technology<sup>\*</sup> Dept. of Metallurgy and Ceramics Science, TokyoTech, Japan<sup>\*\*</sup>

Structure analysis of a Co(Pt)/AlN multilayer film has been performed by X-ray reflectometry and diffraction. A layer structure is fabricated at room temperature on fused silica glass. Each layer consists of polycrystalline AlN with thickness of 10nm and Co-Pt fcc solid solution (hereafter denoted by Co(Pt)) with thickness of 2 nm, and the layers are stacked 5 times and then capped by AlN with 10 nm thickness. The specimen was annealed at 400°C.

Preliminary diffraction study has shown that the film shows strong preferred orientation of (001) for AlN and (111) for fcc Co(Pt). Figure 1 shows the X-ray diffraction profiles of low angle ( $2\theta=0$  to  $11^\circ$ ) region and medium angle ( $2\theta=34$  to  $46^\circ$ ) region. At the medium angle region, strong peak located at the left is the 002 reflection of AlN and broad and wavy peak is the 111 reflection of Co(Pt), which indicates the formation of superlattice even after heat treatment. At the low angle region, we can recognize total reflection and diffraction peaks indexed by 1 to up 18th. From diffraction data, we can successfully analyze the multilayer; period of superlattice is 15.0 nm, thickness of Co(Pt) layer is 2.7 nm, average refractivity of the S.L. is  $1-1.6 \times 10^{-5}$ , roughness of is 2.0 nm.

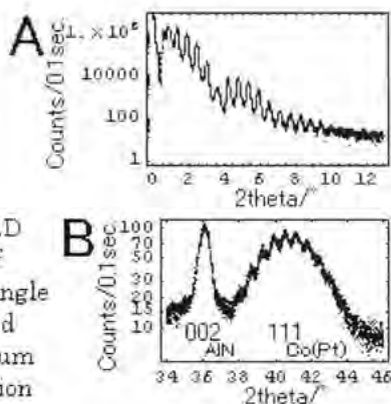


Fig. 1 XRD profiles of (A) low angle region and (B) medium angle region

## Crystallization of *n*-Hexadecane inside emulsion droplets studied by X-ray Scattering

Yuya Shinohara<sup>a</sup> Tadashi Takamizawa<sup>a</sup> Satoru Ueno<sup>b</sup> Isao Kobayashi<sup>c</sup> Mitsutoshi Nakajima<sup>c</sup> Yoshiyuki Amemiya<sup>a</sup>

Department of Advanced Materials Science, University of Tokyo<sup>a</sup> Hiroshima University<sup>b</sup> National Food Research Institute, Japan<sup>c</sup>

Crystallization inside emulsion droplets now attracts attention due to its possibility to control the polymorph inside the droplets. Recent study suggests that the interfacial heterogeneous nucleation at the oil-water interface have large effects on the process of crystallization in oil-in-water (O/W) emulsion droplets and that a transient rotator phase of *n*-Hexadecane (C16), so called rotator phase, play a vital role of crystallization of C16 inside the emulsion droplets. In the present study, we investigated the effect of the droplet size and the type of hydrophobic part of surfactant on the crystallization of C16 in O/W emulsions by using combined measurement of time-resolved two-dimensional (2D) small-angle x-ray scattering (SAXS), wide-angle x-ray scattering (WAXS) and DSC. It was observed that the crystallization into the rotator phase and stable triclinic crystal were greatly influenced by the hydrophobic base of the surfactant and the size of droplet. Effects of the oil-water interface on the crystallization were also studied by microbeam 2D SAXS-WAXS. By scanning microbeam x-ray ( $5\ \mu\text{m} \times 5\ \mu\text{m}$ ) over a crystallized droplet, we investigated the orientation of crystals in a single emulsion droplet. The result shows that the C16 molecules align their axes parallel to the hydrophobic base of the surfactant, and that the difference of the hydrophobic part of surfactant leads to a change of crystal size in droplets. These results also strongly suggest that the surfactant at oil-water interface play a precursor role for the crystallization.

## **A New Large Radius Imaging Plate Camera System for the Diffractometer in BL15XU of SPring-8 for High-resolution and High-throughput Powder Diffraction**

Masahiko Tanaka<sup>1</sup> Yoshio Katsuya<sup>2</sup> Daisuke Nomoto<sup>2</sup>

WEBRAM / SPring8, National Institute for Materials Science<sup>1</sup> SPring-8 Service Co. Ltd.,<sup>2</sup>

A new large radius imaging plate (IP) system for high-resolution and high-throughput powder X-ray diffraction has been developed for the 2-axis diffractometer at BL-15XU, which is an undulator beamline of SPring-8. An IP cassette that has a cylinder surface shape with a radius of 954.9mm is set on the 2-theta arm of the diffractometer normal to the incident X-ray. This system has Debye-Scherrer geometry and the diffracted X-rays from the sample filled into glass capillary placed at the center of the diffractometer are recorded on the IP. The IP size is 200\*400mm and an IP covers 24 degrees of the 2-theta. To collect one data set, several exposures are necessary while changing the 2-theta and overlapping the 2-theta ranges. The separately collected data are translated to 2-theta-intensity format and are connected by comparing the peak intensity included in the overlapped area. The diffraction data is read out by Fuji Film BAS-2500 with pixel resolution of 50 micrometers. One pixel equals 0.003 degrees of the 2-theta. The exposure time is less than 120 seconds for most samples and the readout time is about 3 minutes, thus the total measurement time for one powder diffraction pattern is less than 20 minutes. The 2-theta errors caused by inconsistency of the sample position and rotation center of the 2-theta are corrected by an external standard. The angular resolution of this system was evaluated by comparing the FWHM of 111 reflection of NBS-Si. The observed FWHM was 0.011 degrees and the value is smaller than that of the powder diffractometer with Ge(111) analyzer at a bending magnet beamline of 2nd generation synchrotron. This new system has achieved twenty-times faster powder diffraction improving the high resolution of current synchrotron powder diffractometer.

## Observation of the photoinduced phase transition of the spin-Peierls organic radical crystal TTTA with powder photodiffraction

Pance Naumov<sup>1</sup>, Jonathan P. Hill<sup>2</sup>, Masahiko Tanaka<sup>3</sup>, Kenji Sakurai<sup>4</sup>

<sup>1</sup>ICYS, National Institute for Materials Science, National Institute for Materials Science, Tsukuba, Ibaraki, Japan, <sup>2</sup>WEBRAM, SPring-8, National Institute for Materials Science, Sayo, Hyogo, Japan, <sup>3</sup>X-ray Physics Laboratory, Quantum Beam Center, National Institute for Materials Science, Tsukuba, Ibaraki, Japan, <sup>4</sup>

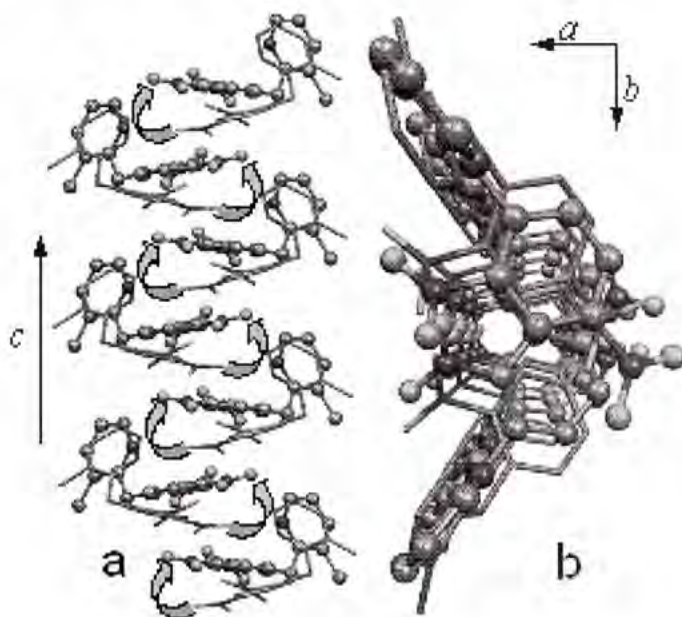
We report on the first direct observation of photoinduced domain formation by photocarrier doping of the stable organic radical TTTA (1,3,5-trithia-2,4,6-triazapentalenyl), which exhibits unusually large thermal hysteresis width of 75 K of the paramagnetic-to-diamagnetic phase transition around room temperature. For that purpose, a setup for powder photodiffraction was developed, composed of a second harmonic pump (532 nm) of Nd:YAG laser coupled with powder diffractometer using synchrotron radiation as probe at the beamline BL15XU at the 8 GeV third generation synchrotron SPring-8. Lowering of the lattice symmetry by thermally induced and photoinduced formation of structural domains of two different phases was observed. Both phases can be decayed by thermal treatment. The results show, for the first time, that the photoinduced and the thermally induced phases in this open-shell spin-Peierls system are structurally different, in accordance with the different proposed mechanisms for their creation.

## Reversible thermal gating of photoinduced proton transfer kinetics by cooperative molecular twists in a single crystal

Pance Naumov<sup>1</sup> Kenji Sakurai<sup>2</sup>

<sup>1</sup>ICYS, National Institute for Materials Science<sup>1</sup> X-ray Physics Laboratory, Quantum Beam Center, National Institute for Materials Science, Tsukuba, Japan<sup>2</sup>

By cooperative twisting of alternating molecules from the adjacent columns, the structure and the kinetics of the photoinduced nitro-assisted proton transfer of 3-methyl-2-(2',4'-dinitrobenzyl)pyridine can be reversibly gated in a single crystal over a hysteresis gap of 10-11 K close to ambient temperature [1].



### Reference

Ref.: P. Naumov, K. Sakurai, *Crystal Growth & Design*, 2006, **5**, 1699.

## Thermally induced saccharinate ligand flips close to ambient temperature

Pance Naumov<sup>\*</sup> Gligor Jovanovski<sup>\*\*\*</sup> Kenji Sakurai<sup>\*\*\*</sup>

ICYS, National Institute for Materials Science<sup>\*</sup> Institute of Chemistry, Faculty of Science, Sts. Cyril and Methodius University, Skopje, Macedonia<sup>\*\*</sup> X-ray Physics Laboratory, Quantum Beam Center, National Institute for Materials Science, Tsukuba, Ibaraki, Japan<sup>\*\*\*</sup>

The *N*-saccharinate ligand of tetrakis(imidazole)tetrakis(saccharinato)dicopper(II) (**1**) features an acutely short carbonyl bond [1.103(6) Å] [1], which is incompatible with the bridging carbonyl group, other saccharinates [2], the analogous cadmium compound [3], infrared [5] and Raman data [6], bond-order and theoretical calculations [2], and is beyond values expected for electronically-induced effects. Structure re-determination [7] at 298 K showed that the anomaly is due to a minor (1/8) superimposed pseudo-mirror component.

The diffraction and thermal data [8] show that a small portion of the axial *N*-saccharinate ligands in single crystals of **1** flip around the coordination bond, changing the ratio of the two overlapped mirror-plane isomers.

### References:

- (1) Liu, S.-X.; Huang, J.-L.; Li, J.-M. *Acta Cryst.* **1991**, C47, 41.
- (2) Naumov, P.; Jovanovski, G. *Struct. Chem.* **2000**, 11, 19.
- (3) Li, Y.; Ke, Y.; Wang, Q.; Wu., X. *Cryst. Res. Technol.* **1997**, 32, 481.
- (4) Naumov, P.; Jovanovski, G. *Acta Chim. Slov.* **1999**, 46, 389.
- (5) Naumov, P.; Jovanovski, G. *Spectrosc. Lett.* **1999**, 32, 237.
- (6) Naumov, P.; Jovanovski, J. *Raman Spectrosc.* **2000**, 31, 475.
- (7) Naumov, P.; Jovanovski, G.; Hu, S.-Z.; Suh, I.-H.; Abdul Razak, I.; Chantrapromma, S.; Fun, H.-K.; Ng, S.-W. *Acta Cryst.* **2001**, C57, 1016.
- (8) P. Naumov, G. Jovanovski, K. Sakurai, *Cryst. Growth Des.* **2006**, 6, 815.

**Ab-initio Structure Determination of 1-(2-Hydroxy-5-methoxy-4-methyl-phenyl)-ethanone and 1-(2-Benzyloxy-5-methoxy-4-methyl-phenyl)-ethanone from Laboratory X-ray Powder Data.**

Swastik Mondal Monika Mukherjee

Department of Solid State Physics, Indian Association for the Cultivation of Science

*Ab-initio* structure determination of two hydroxy acetophenone derivatives, 1-(2-Hydroxy-5-methoxy-4-methyl-phenyl)-ethanone (**1**) and 1-(2-Benzyloxy-5-methoxy-4-methyl-phenyl)-ethanone (**2**), has been carried out from laboratory X-ray powder diffraction data. Intensity data were collected on a Bruker D8 Advance powder diffractometer using monochromatic  $\text{CuK}_{\alpha 1}$  radiation selected with an incident beam germanium monochromator with a step size of  $0.02^\circ$  ( $2\theta$ ) and counting time  $25 \text{ sec}^{-1}$ . Both compounds, (**1**) and (**2**), belonged to the monoclinic system with space group  $P2_1/c$  [ $a = 8.66(3)$ ,  $b = 13.75(5)$ ,  $c = 8.13(3) \text{ \AA}$ ,  $\beta = 108.27(4)^\circ$  for (**1**) and  $a = 12.15(2)$ ,  $b = 16.41(2)$ ,  $c = 7.45(1) \text{ \AA}$ ,  $\beta = 102.99(1)^\circ$  for (**2**)]. The crystal structures have been solved by the direct space parallel tempering approach and refined by the Rietveld method. Final Rietveld refinement of the structures converged to  $R_p = 0.0886$ ,  $R_{wp} = 0.1145$  for (**1**) and  $R_p = 0.0989$ ,  $R_{wp} = 0.1447$  for (**2**) respectively. The molecule of (**1**) is essentially planar with the substituted methoxy carbon and keto oxygen atoms slightly deviating from the plane of the central benzene ring. The structure of (**2**) reveals that the molecule has two planar fragments constructed by methyl-phenyl and benzyloxy groups. There were strong indications of intra and inter molecular hydrogen bonds ( $\text{D} \cdots \text{A}$  distance  $< 3.6 \text{ \AA}$ ,  $\text{D} - \text{H} \cdots \text{A} > 110^\circ$ ) stabilizing the molecular structures of (**1**) and (**2**).

## Structural basis for the phase switching of bisaminecopper(II) cations at the thermal limits of lattice stability

Pance Naumov<sup>1</sup>, Kenji Sakurai<sup>2</sup>, Toru Asaka<sup>3</sup>, Alexei A. Belik<sup>1,3</sup>

<sup>1</sup>ICYS, National Institute for Materials Science, X-ray Physics Laboratory, National Institute for Materials Science, Tsukuba, Ibaraki, Japan<sup>1</sup>, <sup>2</sup>HVEMS, National Institute for Materials Science, Tsukuba, Ibaraki, Japan<sup>2</sup>, <sup>3</sup>National Institute for Materials Science, Tsukuba, Ibaraki, Japan<sup>3</sup>

The structural grounds of the decrease of point and lattice symmetries coupled with switching of the exchange interaction in single crystals of highly strained, coordinationally unsaturated bisdiaminecopper(II) cation are described [1,2]. The combined magnetic susceptibility and X-ray diffraction results indicate that the interplay between the inherent vibronic instability and ligand field strain imposed by moderately flexible, coordinationally shielding ligands, enables effective switching of the pseudo-Jahn-Teller  $d^9$  centers between states with different exchange interaction in the low-temperature regime, and valence orbital orientation and coordination geometry in the high-temperature regime. Within the low-temperature hysteresis region, the phase transition can be also induced by excitation of the ligand-to-metal charge transfer bands, resulting in overall shrinkage of the lattice. The compound is a prototype of weakly electronically coupled one-dimensional Jahn-Teller systems which can undergo phase transitions induced by light, in addition to heating, cooling and change of pressure, and it represents a prospective basis for the design of switching materials capable of multimode external control.

### Reference

- [1] P. Naumov, K. Sakurai, T. Asaka, A. A. Belik, S. Adachi, J. Takahashi, S. Koshihara, *Inorg. Chem.* 2006, **45**, 5027.
- [2] P. Naumov, K. Sakurai, T. Asaka, A. A. Belik, S. Adachi, J. Takahashi, S. Koshihara, *Chem. Comm.* 2006, 1491.

**Crystal structure of N-(4-fluorophenyl)-2-[[[(1E)-(4-methoxyphenyl)methylene] amino] -4,5,6,7-tetrahydro-1-benzothiophene-3-carboxamide**

M K Kokila<sup>a</sup>, Dr. Puttaraja<sup>a</sup>, G.N. Anilkumar<sup>b</sup>, S. Mohan<sup>c</sup>, J. Saravanan<sup>c</sup>

<sup>a</sup>Department of Physics, Bangalore University; <sup>b</sup>Department of Physics, M S Ramaiah College of Arts, Science & Commerce, Bangalore, India; <sup>c</sup>PES College of Pharmacy, Bangalore, India

The title compound, is one of the series of Schiff bases of 2-amino-3-(N-chlorophenyl-carboxamido)-4,5,6,7-tetrahydro-benzothiophenes and was found to exhibit antibacterial and antifungal activities. Various derivatives of thiophenes and Schiff bases are known to possess different biological activities, such as antitubercular, bacteriostatic and antifungal activities. Sulfur containing Schiff bases are the most effective. The crystal structure of the compound has been determined in order to study the role of organic fluorine in crystal engineering.

The compound  $C_{23}H_{21}FN_2O_2S$ , crystallizes under Triclinic system, P-1 space group,  $a = 8.6363(1)$  Å,  $b = 11.0660(14)$  Å, and  $c = 11.8153(15)$  Å,  $\alpha = 67.874(3)^\circ$ ,  $\beta = 81.656(2)^\circ$ ,  $\gamma = 70.473(2)^\circ$ ,  $V = 985.62(15)$  Å<sup>3</sup>,  $Z = 2$ ,  $\mu = 0.196$  mm<sup>-1</sup>, &  $D = 1.38$  gcm<sup>-3</sup>. The three dimensional intensity data were collected using Bruker Smart CCD diffractometer using graphite monochromated  $MoK_{\alpha}$  radiation.

The structure was solved by direct methods using SIR92 program and refined using full-matrix least squares on  $F^2$  to an R value of 0.07 using SHELXL-97 Program for 2256 reflections with  $I > 2\sigma(I)$ . The molecules are packed in layers along b-axis and are stabilized by intermolecular C-H...O interactions.

## Isostructural relationship of $(Rb_2H_2O)C_2O_4$ to $(Ti_2)C_2O_4$ : substitution of one water molecule for two lone electron pairs

Takuya Echigo Mitsuyoshi Kimata

Earth Evolution Sciences, Life and Environmental Sciences, University of Tsukuba

The crystal-chemical and mineralogical significance of the substitution between water molecules  $(H_2O)^0$  and lone electron pair (LEP) were discussed. Fig. 1 shows that  $(Rb_2H_2O)C_2O_4$  is basically isostructural with  $(Ti_2)C_2O_4$ . Comparison between interlayer spaces occupied by  $(H_2O)^0$  and LEP in these two structures revealed the first uncharged substitution:  $(H_2O)^0 \rightleftharpoons 2 \times LEP$ , where the directions of the latter occupants are opposite to each other, and nearly perpendicular to a dipole direction of the former. Two LEPs of  $Ti^{IV}$  work like a dipole moment of the  $(H_2O)^0$  in  $(Rb_2H_2O)C_2O_4$ .

Large and hard cations ( $K^+$ ,  $Rb^+$ ,  $Cs^+$  and  $Sr^{2+}$ ) commonly constitute part of hydrous aluminosilicate minerals, the structures of which suggest that incorporation of  $(H_2O)^0$  into their crystal structures stabilizes their minerals. On the other hand, soft cations with LEP ( $Ti^{IV}$ ,  $Pb^{2+}$ ,  $Sn^{2+}$ ,  $Sb^{3+}$ , and  $Bi^{3+}$ ) are incorporated mainly into sulfide minerals and not into silicate ones, and the former crystal structures suggest that sulfur anion can moderate the polyhedral distortion caused by the LEP. In conclusion,  $(H_2O)^0$  and LEP play key roles in forming the crystal structures of minerals containing nonvolatile incompatible elements, occurring at the very end of magmatism.

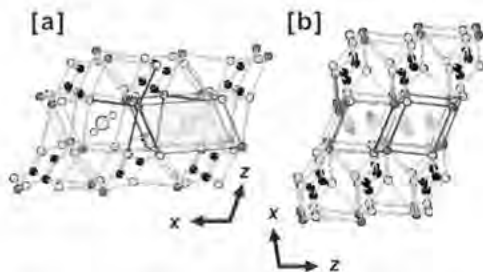


Fig. 1 Crystal structure of [a]  $(Rb_2H_2O)C_2O_4$  and [b]  $(Ti_2)C_2O_4$  (Nagy et al. 2005)

## Crystal structure of tricalcium phosphate

Yoichi Kawaike<sup>\*</sup> Masatomo Yashima<sup>\*</sup> Masahiko Tanaka<sup>\*\*</sup>

Department of Materials Science and Engineering, Tokyo Institute of Technology<sup>\*</sup> National Institute for Materials Science, Japan.<sup>\*\*</sup>

Tricalcium phosphate ( $\text{Ca}_3(\text{PO}_4)_2$ , TCP) has at least three polymorphs, i.e., the  $\beta$ -,  $\alpha$ -, and  $\alpha'$ -phases, depending on temperature. The  $\beta$ -TCP with a rhombohedral structure (space group  $R\bar{3}c$ ) is stable up to 1125 degrees C. The monoclinic  $\alpha$ -TCP, which has a complicated crystal structure with the space group of  $P2_1/a$ , is stable between 1125 degrees C and 1430 degrees C, and can be maintained to room temperature as a metastable phase. The  $\alpha'$ -TCP is stable above 1430 degrees C and unable to survive quenching to room temperature. In the present work, unit-cell parameters of the  $\alpha$ -TCP has been investigated using high-resolution synchrotron powder diffraction and the Rietveld method. The diffraction experiment was conducted at 29 degrees C with a transmission mode at the 15XU experimental station of SPring-8, Japan. Precise unit-cell parameters of the  $\alpha$ -TCP were obtained,  $a=12.8328(1)$ ,  $b=27.1958(1)$ ,  $c=15.1656(1)$ ,  $\alpha=\gamma=90$  deg. and  $\beta=126.2070(5)$  deg. Calculated density of  $\alpha$ -TCP (2.8945 g/cm<sup>3</sup>) is smaller than that of  $\beta$ -TCP, indicating the "looser" structure of  $\alpha$ -TCP. This "looser" structure is consistent with the higher reactivity of the  $\alpha$ -TCP in water.

## X-ray and Spectroscopic Characterization of Molybdenum doped Lithium and Sodium Tungsten Bronzes

KALPANA RANI DEY<sup>1</sup>, Dr. Altaf Hussain<sup>2</sup>, Claus H. Ruscher<sup>3\*</sup>

<sup>1</sup>School of Environmental Science and Management, Independent University, Department of Chemistry, University of Dhaka, Bangladesh; <sup>2</sup>Institute of Mineralogy, University of Hannover, Germany; <sup>3</sup>

In the present investigation powder samples of  $\text{Li}_{0.1}\text{Mo}_y\text{W}_{1-y}\text{O}_3$  ( $x = 0.1, 0.4$ , and  $y = 0.02, 0.4$ ) and  $\text{Na}_{0.6}\text{Mo}_y\text{W}_{1-y}\text{O}_3$  ( $x = 0.6$  and  $y = 0.05, 0.25$ ) have been prepared by solid state reaction in evacuated silica tubes with synthesis temperature  $700^\circ\text{C}$ . From X-ray powder diffraction pattern of  $\text{Li}_{0.1}\text{Mo}_y\text{W}_{1-y}\text{O}_3$  system, it is observed that with increasing Mo content the proportion of  $\text{PTB}_{\text{tet}}$  decreases and a phase of orthorhombic symmetry increases with a small amount of impure phase  $\text{Li}_2\text{W}_2\text{O}_{12}$ . This X-ray result is supported by IR absorption spectra of the samples. Whereas, in the system  $\text{Li}_{0.4}\text{Mo}_y\text{W}_{1-y}\text{O}_3$  the proportion of  $\text{PTB}_{\text{cubic}}$  phase reduces with increasing molybdenum content. In presence of small amount of Mo, a  $\text{Li}_2\text{W}_2\text{O}_{12}$  type phase is formed along with  $\text{PTB}_{\text{cubic}}$  phase.

From the X-ray powder diffraction patterns of  $\text{Na}_{0.6}\text{Mo}_y\text{W}_{1-y}\text{O}_3$  system, a  $\text{PTB}_{\text{cubic}}$  phase is observed with  $y = 0.1$ . However, for  $y > 0.1$  an extra phase of  $\text{Na}_2\text{Mo}_2\text{O}_7$  is also observed along with  $\text{PTB}_{\text{cubic}}$  phase.

**An analysis of the different behavior displayed by OMCTS and 6CB molecules confined between mica surfaces**Fabio Pichierri<sup>1</sup> Masashi Mizukami<sup>2</sup> Kenichi Kusakabe<sup>2</sup> Kazue Kurihara<sup>2</sup><sup>1</sup>COE Laboratory, Tohoku University<sup>2</sup> IMRAM, Tohoku University<sup>2</sup>

Recent experiments performed with the shear force resonance method have shown that the octamethyl-cyclotetrasiloxane (OMCTS) and 4-cyano-4'-hexylbiphenil (6CB) molecules behave differently when confined between mica surfaces [1]. Whereas the resonance peak of 6CB decreased under compression that of OMCTS did not change in the range of applied pressures. Furthermore, upon further compression OMCTS molecules were completely removed from the gap whereas this did not happen with the 6CB molecules under the same pressure conditions. These results were interpreted by taking into account the differences in the interaction between these two molecules and mica surface as well as the differences in the intermolecular interactions that operate within these two liquids. Here we present an analysis of the molecule-surface and molecule-molecule interactions with the aid of electronic structure calculations. The latter indicate that 6CB is characterized by a large dipole moment (~4 Debye) which is likely to affect both the interaction with mica and the structuring process via the formation of dimers. Also, plausible models of these two liquids confined in nanometer-scale spaces are constructed by using the available crystallographic data.

**Reference**

- [1] M. Mizukami, K. Kusakabe, K. Kurihara, *Progr. Colloid Polym. Sci.* 128 (2004) 105.

## **Design and fabrication of in-situ X-ray diffractometer in Phase- II beam line at IUAC**

Pawan K Kulriya Fouran Singh Yogendra Y Mishra Amit Kumar R Ahuja Ashok Kothri R N Dutt  
Ambuj Tripathi D K Avasthi

Materials Science Group, Inter-University Accelerator Centre, New Delhi

The X-ray diffraction (XRD) techniques are highly used in studies of phase transformation, surface/Interface modification, ion beam induced epitaxial crystallization, nano phase synthesis and modification. The XRD (Model D8 Advance) was acquired from Bruker AXS German and installed in the phase-II beam line at Inter-University Accelerator Centre (IUAC), New Delhi, India. To design an in-situ XRD, a vacuum chamber was fabricated at workshop of the IUAC. This XRD chamber consists of two window, sealed with Kapton foil, for incident and reflected X-rays. The electropolished chamber is pumped by a turbo molecular pump and a vacuum of  $5 \times 10^{-5}$  torr was obtained. Two beam pipes were fabricated and electropolished. The XRD chamber was interfaced to the beam line using two gate valves and a bellow. The alignment of the sample holder to the beam line was done using a theodolite. A lifting mechanism system that can lift the vacuum chamber up to a height of 200 mm, was fabricated. To avoid any damage of the x-ray tube and detector, two SS guide rods are provided. The in-situ testing of XRD was done by using 90MeV Ni beam with a 15 UD Pelletron Accelerator at IUAC. The in-situ XRD monitoring of the growth of the Au nano particles was undertaken. It was observed that the particle size increases as the fluence increases from  $1 \times 10^{13}$  to  $1 \times 10^{14}$  ions/cm<sup>2</sup>.

## Structure of 1-Cyano, 1-carbethoxy-2-(3'-methoxy-4'-hydroxy) phenyl

N C Shivaprakash<sup>1</sup> V N Narasimha Murthy<sup>2</sup> M K Sateesh<sup>2</sup> M K Kokila<sup>3</sup> P Puttaraja<sup>3</sup> Geetha M Kulkarni<sup>3</sup> M V Kulkarni<sup>3</sup>

<sup>1</sup>Department of Instrumentation, Indian Institute of Science, Bangalore<sup>2</sup> Ballistics Division, Forensic Science, Bangalore, India<sup>3</sup> Department of Physics, University of Bangalore, Bangalore, India<sup>4</sup> Department of Chemistry, University of Karnatak, Dharwad, India<sup>5</sup>

The title compound has been taken up for study as it shows Non-Linear Optical (NLO) properties with an electron withdrawing group at one end and electron donating group at the other, with an extended conjugation in between. The crystal structure has been determined at room temperature. Needle like crystals of the compound crystallize in monoclinic system, space group  $P2_1/n$  with cell dimensions  $a=10.646(3)\text{\AA}$ ,  $b=9.351(4)\text{\AA}$ ,  $c=12.647(5)\text{\AA}$ ,  $\beta=97.13(3)^\circ$  and  $Z=4$ . The structure was solved by direct method and refined by full-matrix least squares method to a final  $R=0.046$  for 1993 observed reflections.

The molecule as a whole is almost planar, the methoxy group makes a dihedral angle of  $0.7^\circ$  with the planar phenyl ring. The two armed conjugated side chain possesses a linear C-C=N chain and a zig-zag ester group. The torsion angle  $C4-O4-C5-C6=174.1(3)^\circ$  indicates an anti-*peri* planar relationship between the carbonyl carbon and the methoxy group. The C=O bond is *syn* to the ester group about the C-O. The molecules are held by strong O-H $\cdots$ O, C-H $\cdots$ O and C-H $\cdots$ N inter and intra molecular hydrogen bonds. The details will be discussed in this paper.

**Characterization of arsenic accumulating minerals in the iron sediments by SR  $\mu$ -XRF imaging,  $\mu$ -XAFS and XRD.**

Satoshi Endo<sup>\*</sup> Izumi Nakai<sup>\*</sup> Akiko Hokura<sup>\*</sup> Yasuhiro Kato<sup>\*\*</sup> Yasuko Terada<sup>\*\*\*</sup>

Department of Chemistry, Tokyo University of Science<sup>\*</sup> Department of Geosystem Engineering, University of Tokyo, Japan<sup>\*\*</sup> Research & Utilization Division, JASRI, JAPAN<sup>\*\*\*</sup>

When the arsenic containing minerals are decomposed with mine wastewater during the mining activity, arsenic is leached from the minerals to the environments. Recently, some researchers have found phenomena where arsenic concentration in the wastewater decreased without artificial treatments and the quality of the wastewater could be controlled by natural factors. To understand how arsenic is removed from wastewater, we have analyzed the iron precipitates collected from the floor of water stream by utilizing synchrotron radiation (SR) X-ray techniques and revealed elemental distribution and identified the minerals.

Rocks composed of the iron precipitates were collected from the stream floor located in Gunma pref. The samples were embedded with resin and fixed to the quartz glass plate, and then grounded to 10 microns in thickness. For SEM observation, the samples were further treated by etching with 3% HF and with ultrasonic cleaner for 10 minutes. The samples were analyzed by SR  $\mu$ -XRF (X-ray fluorescence) imaging and  $\mu$ -XAFS (X-ray absorption fine structure) at BL37XU, SPring-8. The beam size was ca.  $1 \times 1 \mu\text{m}^2$ . The samples were also subjected to SR-XRD (X-ray diffraction) analysis at BL-4A, Photon Factory and SEM observation.

The SR- $\mu$ -XRF imaging showed that high level of arsenic accumulated in the iron precipitates as dots with typical radius of ca. 20 microns. The  $\mu$ -XAFS results showed that arsenic exists as arsenate form and is coordinated by four oxygen atoms at 1.7 Å. It was observed that arsenic-accumulating points have peculiar spherical structures. Furthermore, SR-XRD patterns showed that these structures consisted of strengite ( $\text{FePO}_4 \cdot 2\text{H}_2\text{O}$ ). Consequently, it has been found that arsenic accumulated in strengite via ion exchange with  $\text{PO}_4$ .

## Growth process of vapor deposited films of a bisazomethine dye

Daisuke Tsuchida<sup>1</sup> MieI Satoh<sup>2</sup> Shinya Matsumoto<sup>3</sup> Takashi Kobayashi<sup>4</sup> Tetsuya Aoyama<sup>5</sup> Tatsuo Wada<sup>6</sup>

Graduate School of Environment and Information Sciences, Yokohama National University<sup>1</sup> Faculty of Education and Human Sciences, Yokohama National University, Japan<sup>2</sup> Department of Physics and Electronics, Osaka Prefecture University, Japan<sup>3</sup> Supramolecular Science Laboratory, RIKEN(The Institute of Physical and Chemical Research), Japan<sup>4</sup>

A bisazomethine dye, *N,N'*-bis-[4-(*N,N*-diethylamino)benzylidene]diaminomaleonitrile (DE2), is known to form J-aggregates in vapor deposited films depending on the film thickness. The J-aggregate films also include non-aggregate forms, and this has become a problem in its applications to optoelectronic devices. The growth of DE2 thin films was then studied to obtain its complete J-aggregate films. The analysis was carried out from the morphological point of view by using AFM. Vapor deposited films were prepared by vacuum deposition onto a slide glass at various film thicknesses. The rate was controlled to be 0.01, 0.1 and 1.0 nm/s.

The J-aggregates appear when the films are deposited at a rate of 0.1 nm/s and their thickness is more than 100 nm. AFM observation showed that the J-aggregate films showed heterogeneous texture composed of prismatic grains and unclear grain boundaries. The J-aggregates were found to be a metastable phase and are considered to form in the grain boundaries and on the grain surfaces. In the film deposited at a rate of 0.01 nm/s, clear crystal grains formed as is the case of 0.1 nm/s. However the J-aggregate formation was not observed in the thick films. At this rate, supersaturation is considered to be too small to form metastable J-aggregates. On the other hand, large supersaturation resulted in many nucleation in the film deposited at a rate of 1.0 nm/s. The substrates were covered by many small crystal grains and they doesn't grow up to large ones as increasing film thickness. The J-aggregate formation was not observed in the thick film at this rate. This result indicates that the J-aggregates cannot form on such small crystal grains. The present study shows that both nucleation and growth processes are important for the J-aggregate formation.

**Structural and microstructural investigation of tetragonally stabilized ZrO<sub>2</sub> in  $\alpha$ -Al<sub>2</sub>O<sub>3</sub> - ZrO<sub>2</sub> composites: Critical size limit and Oxygen vacancy**Apurba Kanti Deb<sup>1</sup> Partha Chatterjee<sup>2</sup> Siba Prasad Sen Gupta<sup>1</sup><sup>1</sup>Department of Materials Science, Indian Association for the Cultivation of Science<sup>2</sup> Department of Physics, Vivekananda Mahavidyalaya, Haripal, Hooghly 712405, India<sup>2</sup>

A detailed study on the phase stability of ZrO<sub>2</sub> in the tetragonal phase at room temperature and near its transformation temperature and its structural and microstructural features in the  $\alpha$ -Al<sub>2</sub>O<sub>3</sub> matrix has been conducted using X-ray structural and microstructural refinement using Rietveld method, TEM, FTIR and Raman spectroscopy. It is observed that the tetragonal ZrO<sub>2</sub> is stabilized in an alumina matrix up to a wt. fraction of ~ 0.58. The crystallite size (54 nm), obtained from the X-ray diffraction analysis, is in accordance with TEM studies (65 nm). The size value is well above the critical size limit as reported in the literature. It is found that microstrains play a role in the stabilization process. A detailed structural analysis reveals that the tetragonal distortion for t-ZrO<sub>2</sub> in the composites is similar to that of pure t-ZrO<sub>2</sub>, no indication of Al<sub>2</sub>O<sub>3</sub>-ZrO<sub>2</sub> solid solution formation from X-ray and FTIR study was obtained. The Rietveld refinement discloses oxygen deficiency in t-ZrO<sub>2</sub>. Thus in conclusion for size-stabilized t-ZrO<sub>2</sub> the critical size limit is proposed to be ~ 54 nm and that the stabilization process is also influenced by other factors such as oxygen vacancy, microstrain.

## Crystal growth and structure refinement of spinel-type $\text{Li}_4\text{Ti}_5\text{O}_{12}$

Kunimitsu Kataoka<sup>\*</sup> Yasuhiko Takahashi<sup>\*\*</sup> Norihito Kijima<sup>\*\*</sup> Junji Akimoto<sup>\*\*\*</sup> Ken-ichi Ohshima<sup>\*\*\*</sup>

University of Tsukuba, AIST<sup>\*</sup> AIST<sup>\*\*</sup> University of Tsukuba<sup>\*\*\*</sup>

Single crystal growth and structural characterization of  $\text{Li}_4\text{Ti}_5\text{O}_{12}$  were originally determined by Deschanvres et al. in 1971 [1]. However, the precise structural properties have not been determined yet. In the present study, we report crystal and electronic structures of  $\text{Li}_4\text{Ti}_5\text{O}_{12}$  using the single-crystal X-ray diffraction data.

Single crystals of the spinel-type  $\text{Li}_4\text{Ti}_5\text{O}_{12}$  were grown by a flux method. A colorless octahedral-shaped crystal was obtained, as shown in the figure. The crystal structure and electron density distribution of the  $\text{Li}_4\text{Ti}_5\text{O}_{12}$  have been studied by X-ray structure analysis and maximum entropy method (MEM) using single-crystal X-ray diffraction data at room temperature. The cubic lattice parameter ( $a = 8.355(4)$  Å), determined by a least-squares refinement using 25 strong reflections, and the space group  $Fd\bar{3}m$  have been confirmed by the present single-crystal X-ray diffraction data. The structure was refined to the conventional values of  $R = 3.3\%$  and  $wR = 5.4\%$  using 209 independent reflections. From the results of the single-crystal MEM analysis, a strong covalent bonding was clearly found between the Ti and O atoms in  $\text{Li}_4\text{Ti}_5\text{O}_{12}$ .



### Reference

- [1] A. Deschanvres, B. Raveau and Z. Sekkal, *Mat. Res. Bull.* 6, 699, (1971)

## XRD applications by using a new area detector

Takeyoshi TAGUCHI

X-ray research laboratory, Rigaku Corporation

A state-of-art semiconductor technology based area X-ray detector, namely D/teX-25, has recently been developed for high-speed and high-sensitivity X-ray diffraction analysis of materials. An XRD system equipped with a conventional 2-kW X-ray source and a D/teX-25 detector has been used to collect ultra-fast XRD patterns at a maximum speed of 160 degree in 2theta per minute, more than 30 times faster than a conventional speed of 5 degree in 2theta per minute with a scintillation or a proportional counter. This is particularly useful for dynamic and/or *in-situ* studies. The ultra high-speed data collection makes time-resolved experiments possible. An XRD system equipped with a D/teX-25 detector can be used also for in-line quality control when manufacturing and monitoring a very large number of samples in a day are required.

In addition to high-speed data collection, the D/teX-25 detector can provide two-dimensional X-ray diffraction data. Two-dimensional XRD data are known to have an advantage over conventional one-dimensional XRD data. This includes rapid detection/evaluation of preferred orientation and study of particle-size distribution in a sample. Examples of the XRD measurements with a D/teX-25 detector will be given.



## **PPDA: A program for extracting data from Debye-Scherrer imaging-plate diffractometers**

James R Hester<sup>1</sup> David J Cookson<sup>2</sup> Brett A Hunter<sup>3</sup>

<sup>1</sup>Australian Beamline, Australian Synchrotron Research Program<sup>2</sup> Australian Synchrotron Research Program, Australia<sup>3</sup> Australian Nuclear Science and Technology Organisation, Australia

The Australian National Beamline Facility (ANBF) includes a large Debye-Scherrer camera equipped with Weissenberg screens and a translatable Image Plate (IP) holder. This allows up to 30 powder data strips to be recorded on a single set of IPs. PPDA (short for Python Powder Data Analyse) has been developed over the last 10 years for extracting the powder data contained in the exposed strips on these IPs.

PPDA is able to read and display raw IP data from various sizes and generations of IP scanners, and has been tested with data from the APS, SPring-8 and the ANBF. An intelligent algorithm will automatically detect and extract strips with nominal angular scale, but if beam registration marks (e.g. SPring-8 BL02) or embedded fiducial data (e.g. ANBF, KEK-BL20B) are available the angular scale can be calibrated prior to strip extraction. Data can be output in formats suitable for LHPM/Rietica and GSAS, as well as simple columnar format suitable for input to a spreadsheet program, and CIF. The output CIF can be configured to include general beamline information (e.g. monochromator-sample distance, beam divergence).

Output angles can optionally include corrections for IP rotation introduced in the IP scanner, with the rotation angle determined either from the beam registration marks or fiducial markers.

PPDA is a portable program written in Python with the Tkinter toolkit, and has been tested on Windows and Linux platforms. It is freely available from <http://anbf2.kek.jp/ppda/ppdapage.html>.

## Low temperature XRD analysis of BaTiO<sub>3</sub>

Koichi Ishibashi Kazuyosi Arai Ryuji Matsuo Katsuhiko Inaba

Design, Rigaku corporation

Barium Titanate (BaTiO<sub>3</sub>) is one of the functional oxide materials with a Perovskite-type structure, and used in various industrial applications, such as piezoelectric actuators, ferroelectric random access memories, so on. Successive structural phase transitions have been reported, resulting from a slight shift of cationic position in oxygen-surrounding polyhedra with varying temperature. Though tremendous studies are conducted focusing on phase transitions at high temperature between the paraelectric phase and the ferroelectric phase, its behaviour at low temperature has not been fully understood.

We have developed a new X-Ray Diffraction analysis system(SmartLab RIGAKU Co.) with a low temperature chamber, which will be applicable to XRD measurement both for powder specimen and for films on substrates.

A specially-designed hemispherical-domed X-ray window covering a sample chamber with heating/cooling system enables XRD measurements for films along the directions of stacking sequences (Out-of-Plane direction) and also along the directions within the surface planes (In-Plane direction). Together with this configuration of sample chamber and the specially designed goniometer system with horizontal sample mounting both for Out-of-Plane and In-Plane XRD measurement, anisotropic behaviour of lattice expansion/compression of films on substrates will be easily analyzed.

We will report results of XRD analyses at low-temperature for BaTiO<sub>3</sub> samples comparing powder specimen and BaTiO<sub>3</sub> films on substrates.

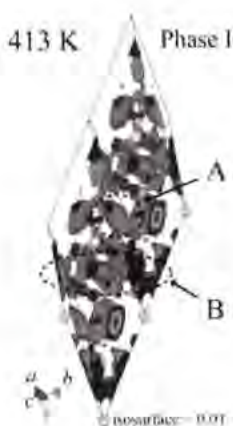
## Structural and Dynamical Studies on Protonic Conductor $K_3H(SeO_4)_2$

Fumihito Shikana<sup>1</sup> Keisuke Tomiyasu<sup>1</sup> Ryoji Kiyonagi<sup>2</sup> Masao Yonemura<sup>3</sup> Kenji Iwase<sup>4</sup> Dyah Sulistyantyas<sup>5</sup> Tuerxun Wurnisha<sup>6</sup> Kazuhiro Mori<sup>7</sup> Toru Ishigaki<sup>8</sup> Itaru Tsukushi<sup>9</sup> Susumu Ikeda<sup>10</sup> Takashi Kamiyama<sup>11</sup>

<sup>1</sup>Institute of Materials and Structure Science, High Energy Accelerator Research Organization<sup>2</sup> Intense Pulsed Neutron Source Division, Argonne National Laboratory, USA<sup>3</sup> Graduate school of Engineering and Science, Ibaraki University, Japan<sup>4</sup> Research Reactor Institute, Kyoto University, Japan<sup>5</sup> Quantum Beam Science Directorate, Japan Atomic Energy Agency, Japan<sup>6</sup> Faculty of Engineering, Chiba Institute of Technology, Japan<sup>7-11</sup>

Hydrogen-bonded typed crystals of  $M_3X(YO_4)_2$  have attracted much attention due to interesting phenomena in the high-temperature region. Most of the crystals undergo phase transition in the high-temperature, and show over 100 times higher electric conductivities than those at the room-temperature. It has been considered that the higher conductivities were due to the proton transfer in the crystals.

Crystal structures of protonic conductor  $K_3H(SeO_4)_2$  in the phase I (conducting phase) and phase II (room-temperature phase) have been determined using a time-of-flight (TOF) neutron diffractometer VEGA.  $SeO_4$  tetrahedra in the phase I were rotationally displaced with the occupancy 1/3 and the crystal structure in the phase II was remain locally. Proton distribution maps were obtained from the maximum entropy method (MEM) describe that the amount of the proton in a hydrogen bond were decline from 87.3 % to 21.4 % with increasing the temperature and 13.4 % of protons exist at inter-layer space. Incoherent quasi-elastic neutron scattering experiments performed by LAM80-ET spectrometer yield the QENS spectra of conducting protons. Proton diffusion constants are estimated as  $1.9(1) \times 10^{-10} \text{ m}^2/\text{s}$  at 393 K and  $2.1(3) \times 10^{-10} \text{ m}^2/\text{s}$  at 413 K respectively.



**Crystal Structure of 2-[6-Methylbenzofuran-3-ylmethyl]-5-(morpholin-4-ylmethyl)-6-(4-chlorophenyl)-imidazo [2,1-b][1,3,4]thiadiazole.**

K.V.Arjuna Gowda<sup>1</sup>, Ramakrishna Gowda<sup>2</sup>, Vijay Tiruvenkatam<sup>1</sup>

<sup>1</sup>Department of Physics, M.V.J. College of Engineering, Bangalore-67<sup>2</sup> Department of SSCU, IISc., Bangalore-560 012 India

The title compound belongs to a class of compounds referred to as imidazo[2,1-b]thiadiazoles with substituents at C-2, C-5, C-6. The 5-substituted imidazothiazoles are known for wide range of biological activities. In view of the importance of naturally occurring oxygen heterocycles it was planned to synthesize derivatives of the above system possessing a benzofuran moiety at C-2 bridged by a methylene group. The aim of the present study is to recognize the presence of weak Cl...Cl interaction in the solid structure of the compound. It was also contemplated to understand the conformation of the morpholine ring in this compound. The compound crystallizes as colourless plates in orthorhombic with space group  $P2(1)2(1)2(1)$  and cell dimensions  $a=10.2467\text{\AA}$ ,  $b=11.6297\text{\AA}$  and  $c=19.8524\text{\AA}$ . The structure was solved by SHELX-97 program (Sheldrick 1997) and refined to a R factor of 0.0521. The details of weak interactions are discussed in this paper.

## Structural Analysis of Chrysocolla by Anomalous X-ray Scattering (AXS) Coupled with Reverse Monte Carlo (RMC) Simulation

Yasutaka Takemaru<sup>1</sup> Kazumasa Sugiyama<sup>2</sup> Masatoshi Saito<sup>1\*</sup>

<sup>1</sup>Department of Earth and Planetary Science, The University of Tokyo; <sup>2</sup>Department of Radiological Technology, School of Health Sciences, Niigata University, Japan\*

Chrysocolla is found in the oxidized zone of copper deposits associated with malachite, azurite, cuprite, or native copper. Chrysocolla was believed to be the mixture of crystalline Cu and Cu oxide, as well as amorphous silica [1]. The main purpose of this study is to provide the quantitative structural information of such chrysocolla by using the anomalous X-ray scattering (AXS) measurement coupled with reverse Monte Carlo (RMC) simulation.

The X-ray scattering profiles of a chrysocolla sample  $((\text{CuO})_{0.5}(\text{SiO}_2)_{0.6}(\text{H}_2\text{O})_{1.1}; D_n=2.2\text{Mg/m}^3)$  were measured at the Cu K-absorption edge and the observed energy dependence in scattering intensities was employed in order to obtain the environmental radial distribution function (RDF) around Cu. The ordinary RDF analysis was also carried out by using Mo K $\alpha$  radiation. The obtained RDFs clearly suggest that the correlation distances of the nearest neighbor Si-O and Cu-O are around 0.16nm and 0.20nm, respectively. These distances are similar to those of SiO<sub>2</sub> and CuO<sub>2</sub> in diopside (Cu<sub>4</sub>Si<sub>6</sub>O<sub>18</sub>·6H<sub>2</sub>O), and the structural information around Cu is consistent with that obtained by XAFS study, in particular [2]. However, the RMC simulation indicates that the average coordination numbers of the nearest oxygen around Si and Cu were approximately three and four, respectively. These results could be explained by introducing the unusual SiO<sub>3</sub> coordination found in Si<sub>10</sub>O<sub>13</sub>H<sub>10</sub>, only.

### References

- [1] F.V.Chukhrov, B.B.Zvyagin, A.I.Gorshkov, L.P.Ermilova & E.S.Rudnitskaya, *Izvest. Akad. Nauk SSSR, Ser. Geol.*, **6**(1968)29.
- [2] D.A.McKeown: *J. Non-Crystalline Solids*, **180**(1994)1.

## Photo excited state crystallography of hexanuclear 6-methyl-2-pyridinethiolato copper(I) complex.

Kimihiko Kimura<sup>\*</sup> Yoshiki Ozawa<sup>\*</sup> Minoru Mitsumi<sup>†</sup> Koshiro Toriumi<sup>†</sup> Isamu Kinoshita<sup>\*\*</sup>

Graduate School of Material Science, University of Hyogo<sup>\*</sup> Graduate School of Material Science, Osaka City University<sup>\*\*</sup>

Hexanuclear 6-methyl-2-pyridinethiolato copper(I) [Cu<sub>6</sub>(6-mpyt)<sub>6</sub>] crystals show highly luminescence whose color changes from red (room temperature) to green-blue (liquid nitrogen temperature) with a decrease in temperature, i.e., luminescence thermochromism. The assignments of intense luminescence bands of these multinuclear-copper(I) compounds are complicated because weak interacted multi-copper centered (CC) transition is often concurrent with common Cu(I) to ligand charge transfer transition. We have tried direct observation of photo-induced geometrical change of the complex by using the photo excited state crystallographic technique in order to figure out the luminescence characteristics of this compound.

Single crystal X-ray diffraction experiments were performed by using the low-temperature vacuum X-ray camera at SPring-8 BL02B1 beamline. Full intensity data of both under light irradiated and non-irradiated conditions were collected at 25 K and 150 K by the multiple-exposure IP method. He-Cd CW laser (442 nm 100 mW, 325 nm 30 mW) was used for photo-excitation of the crystal. Photo-difference Fourier syntheses base on ( $|F_{on}| - |F_{off}|$ ) show positive and negative peaks pairs around the Cu atoms. This result indicates that the trigonally compressed octahedral Cu<sub>6</sub> core is shrank toward perpendicular to the -3 axis.

### Reference

- [1] H.Xie et al., *J.Phys.Chem.B*, **2005**, 109, 9339-9345.
- [2] Y.Ozawa et al., *Chem.Lett.*, **2003**,32, 62-63.

## Interactions between crystallographic domain and magnetic domain in ordered double perovskite

Yoshio Matsui<sup>1</sup> Toru Asaka<sup>1</sup> Xiuzhen Yu<sup>2</sup> Yasuhide Tomioka<sup>3</sup> Yoshio Kaneko<sup>4</sup> Takuro Nagai<sup>5</sup>  
Koji Kimoto<sup>6</sup> Kazuo Ishizuka<sup>7</sup> Yoshinori Tokura<sup>8</sup>

Advanced Electron Microscopy Group, National Institute for Materials Science<sup>1</sup> Spin Super Structure Project, ERATO-JST, Japan<sup>2</sup> Correlated Electron Research Center (CERC), AIST, Japan<sup>3</sup> HREM Research, Inc., Japan<sup>4</sup> Department of Physics, University of Tokyo, Japan<sup>5</sup>

Ordered double perovskite,  $AE_2\text{FeMoO}_6$  ( $AE = \text{Ca, Sr and Ba}$ ), has two kinds of ions, i.e.  $\text{Fe}^{3+}$  and  $\text{Mo}^{5+}$ , at the B site in the perovskite-type structure. The  $\text{Fe}^{3+}$  and  $\text{Mo}^{5+}$  ions are ordering in manner of rock-salt type structure. In the magnetic aspects, the local spins on the  $\text{Fe}^{3+}$  ( $S = 5/2$ ) and  $\text{Mo}^{5+}$  ( $S = 1/2$ ) ions couple antiferromagnetically. This leads to ferrimagnetism. This system contains essentially a crystallographic antiphase-domain structure which is caused by a spatial distribution of the Fe/Mo ordering. It has been reported that the antiphase boundary (APB) plays a role of the magnetic domain wall (MDW) where the spins couple antiferromagnetically [1]. Concerning the interactions between APB and MDW, Yu *et al.* have demonstrated the direct observation of the pinning effect of MDW at APB in  $\text{Ba}_2\text{FeMoO}_6$  by combined use of dark-field imaging and Lorentz transmission electron microscopy (LTEM)[2]. Here, we report detail research of the crystallographic antiphase domain and magnetic domain structures for a single crystal of  $\text{Ba}_2\text{FeMoO}_6$ , by semi-quantitative LTEM observation.

We observed bending and branching of the MDW at the APB. In addition, the MDWs perfectly coincide with the APBs in most parts of the observed area. We found that the magnetic domain corresponds one-to-one with antiphase domain at many regions. Besides, it was revealed that the magnetic nanodomains formed at the short-range Fe/Mo ordering region. We consider that the magnetic nanodomains were formed by restriction of coherent magnetic ordered region due to the crystallographic short-range ordering, and fragmentation of magnetic domain and spatial fluctuation of local magnetic moments on the APB.

### Reference

- [1] H. Q. Yin *et al.* J. Appl. Phys. **87**, 6761 (2000).
- [2] X. Z. Yu *et al.* J. Elect. Microsc. **54**, 61 (2005).

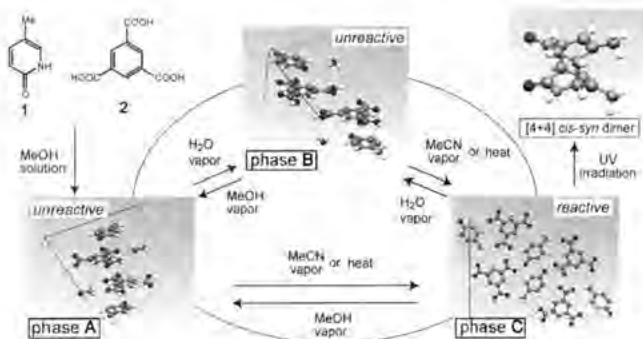
## Vapor induced solid-state phase transition and photoreactivity change investigated by *ab initio* powder crystal structure determination

Kotaro Fujii<sup>1</sup>, Yasunari Ashida<sup>1</sup>, Hidehiro Uekusa<sup>1</sup>, Hirano Shinya<sup>2</sup>, Shinji Toyota<sup>2</sup>, Fumio Toda<sup>2</sup>

<sup>1</sup>Department of Chemistry and Materials Science, Tokyo Institute of Technology, <sup>2</sup>Department of Chemistry, Okayama University of Science, JAPAN

Inclusion complex crystal of 5-methyl-2-pyridone (**1**) and trimesic acid (**2**), exhibits variety of solid-state phase transitions induced by solvent vapor contact. Thus, modification of the photoreactivity of pyridone molecules in crystal is expected. A 1:1:1 inclusion complex of **1**, **2** and MeOH (phase **A**; unreactive) was transformed to the unreactive phase **B** by water vapor contact. But both **A** and **B** were transformed by MeCN vapor contact or by heating to photoreactive phase **C** and [4+4] *cis-syn* dimer molecule was obtained by UV irradiation. The structure of **B** and **C** were successfully determined by *ab initio* powder crystal structure analysis in spite of the disintegration to powder crystalline state during phase transition.

Phase **B** is formed after crystalline solvent exchange of MeOH for H<sub>2</sub>O and the structure resembles to **A**. Both are unreactive due to lack of suitable pyridone molecules arrangement. Phase **C** has a reactive distance (3.84 Å) and an arrangement to produce *cis-syn* dimer. This arrangement was achieved by turning of a pyridone molecule about 180° during removal of the solvent molecule.



## Electron density distribution analysis in the low temperature form of $\text{LiMn}_2\text{O}_4$ by X-ray Single-crystal diffraction study

Yasuhiko Takahashi Junji Awaka Norihito Kijima Akimoto Junji

Advanced Manufacturing Research Institute, National Institute of Advanced Industrial Science and Technology (AIST)

In the past few years, the lithium transition metal oxides have been extensively studied as cathode materials for rechargeable lithium-ion batteries, since these can be reversibly deintercalated and reintercalated by lithium ions at high potential. Recently, special attention has been paid to the spinel-type lithium manganates,  $\text{LiMn}_2\text{O}_4$ , due to its economical and environmental advantages.

$\text{LiMn}_2\text{O}_4$  presents a first order structural transition around room temperature. Above the transition temperature, it has the cubic spinel structure with  $Fd\bar{3}m$  space group. The crystal structure of the low temperature form has been investigated with the orthorhombic symmetry and  $Fddd$  space group by using the neutron powder diffraction method. However, the mechanism of structural transition has not been clarified yet. Recently, we have succeeded in the synthesis of  $\text{LiMn}_2\text{O}_4$  single crystals by a flux method [1], and revealed the precise crystal and electronic structures of the cubic  $\text{LiMn}_2\text{O}_4$  [2]. In this presentation, we demonstrate the precise crystal structure determination of low temperature form [3] and electron density distribution of  $\text{LiMn}_2\text{O}_4$  by single-crystal X-ray diffraction method and Maximum Entropy Method using program PRIMA. In the electron density analysis of orthorhombic  $\text{LiMn}_2\text{O}_4$  experimentally, some different tendency could be observed for  $\text{Mn}^{3+}\text{-O}_6$  and  $\text{Mn}^{4+}\text{-O}_6$  octahedral bonding natures which results were comparable the result of bond valence sum results [3]. These tendencies were comparison to the theoretical DFT calculations using program Wien2K and similar results were confirmed in this study.

### Reference

- [1] J. Akimoto et al., *Chem. Mater.* **12** (2000) 3246.
- [2] Y. Takahashi et al., *J. Phys. Soc. Jpn.* **72** (2003) 1483.
- [3] J Akimoto et al., *Solid State Ionics* **172** (2004) 491.

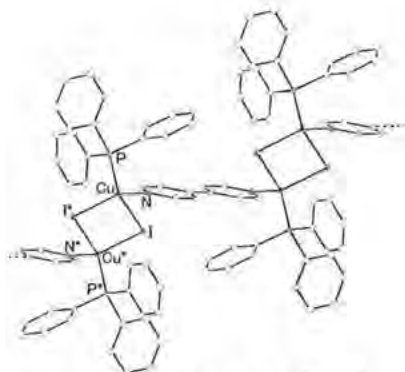
### Photo excited state crystallography iodo-bridged dicopper (I) complex.

Shingo Yoshida<sup>1</sup> Yoshiki Ozawa<sup>1</sup> Minoru Mitsumi<sup>1</sup> Koshiro Toriumi<sup>1</sup> Nobuhiro Yasuda<sup>2</sup> Kiyoshi Tsuge<sup>3</sup> Hiromi Araki<sup>3</sup> Yoichi Sasaki<sup>3</sup>

<sup>1</sup>Graduate School of Material Science, University of Hyogo, Japan <sup>2</sup>Synchrotron Radiation Research Institute<sup>2</sup> <sup>3</sup>Graduate School of Science, Hokkaido University, Japan<sup>3</sup>

A luminescent dicopper(I) complex  $[\text{Cu}_2\text{I}_2(\text{PPh}_3)_2(4,4'\text{-bpy})]_n$  ( $\text{bpy}=\text{C}_{10}\text{H}_8\text{N}_2$ ) consists of  $\{\text{Cu}_2\text{I}_2\}$  planer units, which are bridged by diimine ligands constructing an infinite chain structure. The assignments of emission bands of the oligo-copper compounds are complicated because the weak interacted multi-copper centered charge transfer is often concurrent with the common Cu(I) to ligand charge transfer. We've tried to observe geometrical distortion in the excited state of the complex by crystallographic technique in order to figure out this emission nature.

Single crystal X-ray diffraction experiments were performed by using the low-temperature vacuum X-ray camera at SPring-8 BL02B1 beamline. Full intensity data of both under light irradiated and non-irradiated conditions were collected by multiple-exposure method. Two CW laser light, 442nm on the absorption band and 532nm on its tail, were used. Photo-difference Fourier syntheses for the 442nm irradiation show that a small portion of two I atoms in  $\{\text{Cu}_2\text{I}_2\}$  unit shift toward close to each other, while two Cu atoms tend to shift apart from each other. No significant peak was observed for the 532nm case.



Structure of  $[\text{Cu}_2\text{I}_2(\text{PPh}_3)_2(4,4'\text{-bpy})]$

#### Reference

- [1] Tsuge et al., *Inorg. Chem.*, 2005, **44**, 9667.
- [2] Ozawa Y et al., *Chem. Lett.*, 2003, **32**, 62.

## Lattice parameter determination by using fitting in Hough space of CBED pattern

Yosifumi Yasuda Koh Saito

Department of Crystalline Materials Science, Nagoya University

The convergent-beam electron diffraction (CBED) method, which uses a nanometer-size electron probe, is a powerful tool for characterizing crystal structures in nanometer region. The method provides a diffraction pattern composed of reflection discs. The 000 disc shows dark lines, along which higher-order Laue zone (HOLZ) reflections satisfy the Bragg conditions. Since the positions of the dark lines (HOLZ lines) are sensitive to the variation of lattice parameters, lattice parameters can accurately be determined by comparing experimental HOLZ line positions with simulated ones. So far, distances between HOLZ line intersections have been used as a criterion of the fit of the experimental and simulated patterns [1,2]. However, it needs a cumbersome procedure to get intersections of many HOLZ lines and to sum up their distances.

In this paper, we propose a simple method to fit experimental and simulated HOLZ line positions using the Hough transform [2]. Since a HOLZ line is transformed into a spot by the Hough transform, the fit of HOLZ line positions in CBED patterns correspond to the fit of spot patterns in the Hough transforms. We define the error sum of squares (chi-sq.) as a sum of the distances between experimental and simulated Hough spots. Lattice parameters, acceleration voltage are determined by minimizing chi-sq. The kinematical approximation with an acceleration voltage correction is used for simulating HOLZ line positions to reduce a computing cost. The process of finding the best fit is automated by using Powell's method. We confirmed that the accuracy is a few 0.0001 nm from a [107] GaAs pattern, which is comparable to the intersection method.

### References

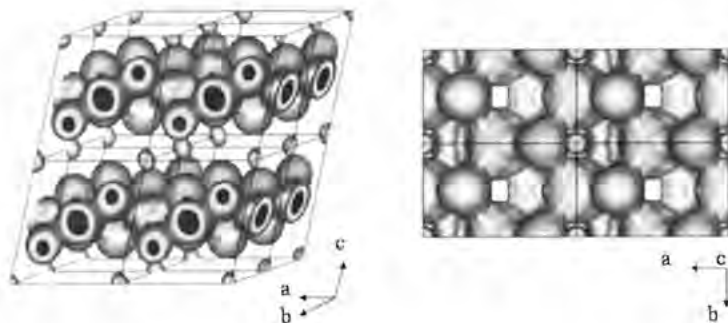
- [1] J. M. Zuo, Ultramicrosc., 41, 211 (1992).
- [2] S. Kraemer and J. Mayer, J. Microsc., 194, 2 (1999).

## Structural and Physical Properties of Lithium-Ion Deintercalated $\text{Li}_x\text{CoO}_2$ Single Crystals

Yasuhiko Takahashi Junji Awaka Norihito Kijima Junji Akimoto

Advanced Manufacturing Research Institute, National Institute of Advanced Industrial Science and Technology (AIST)

Lithium cobalt dioxide,  $\text{LiCoO}_2$ , has been used industrially as the positive electrode material for lithium-ion rechargeable batteries. In almost of the experimental studies reported to date, sintered or pressed powder samples or the corresponding polycrystalline thin films are used. In an experiment using such samples, much of information on the anisotropy is lost. In the recent of our study, we have succeeded in the growth of  $\text{LiCoO}_2$  single crystals and determined the crystal structure by single-crystal X-ray diffraction method. In this study, the structural and physical properties of  $\text{Li}_x\text{CoO}_2$  were investigated using the chemically and electrochemically oxidized  $\text{Li}_x\text{CoO}_2$  single crystal samples. Compositional dependence of the in-plane electrical resistivity in  $\text{Li}_{0.5}\text{CoO}_2$  has been clarified. Metallic conductivity in  $\text{Li}_{0.5}\text{CoO}_2$  single crystal has been successfully measured for the first time. The lithium-ion and vacancy ordering structure and electron density distribution in  $\text{Li}_{0.5}\text{CoO}_2$  has been precisely determined by single-crystal X-ray diffraction and Maximum Entropy Method using program PRIMA (Fig.). And also calculate the electronic structure of  $\text{Li}_x\text{CoO}_2$  using DFT calculations and the results were compared with the experimental results.



## Topological Analysis of Biphenyl

Chi-Rung Lee<sup>1</sup> Chin-Yu Chen<sup>2</sup> De-Cai Fang<sup>3</sup> Ting-Hua Tang<sup>3</sup>

<sup>1</sup>Department of Chemical Engineering, Minghsin University of Science and Technology, Institute of Chemistry, Academia Sinica, Taiwan<sup>2</sup> <sup>3</sup>Department of Chemistry, Beijing Normal University, Beijing<sup>3</sup>

H-H interaction is shown in the quantum theory of atoms in molecules. The molecular electron densities are obtained both from X-ray diffraction data at low temperature and from a periodic density functional theory calculation. Intra and intermolecular interactions of biphenyl is investigated in terms of topological analyses. The features of the deformation densities, Laplacian distributions, bond paths, and atomic domains are shown to describe the variety bonding. All the interactions are verified by the location of the bond critical point and its associated topological properties. From the experimental multipole model and theoretical results, di-hydrogen bonds can be verified by molecular graph, and the related interactions energies could be discussed by calculations.

**Crystal and molecular structure investigation of cis-(+)-3-Acetoxy-2-(4-methoxyphenyl)-4-oxo-2,3,4,5-tetrahydro-1,5-benzothiazepine-1-oxide**A. David Stephen<sup>1</sup>, K. A. Nirmala<sup>2</sup>, N. Kalyanam<sup>3</sup>, P. Kumaradhas<sup>4</sup>

<sup>1</sup>Department of Physics Periyar University, <sup>2</sup>Department of Physics, Bangalore University, Bangalore-560 056, India, <sup>3</sup>Sabinsa Corporation, Deerpark Drive Suit, Monmouth Junction, NJ 00852, USA, <sup>4</sup>

The title compound [C<sub>18</sub>H<sub>17</sub>NO<sub>5</sub>S] is a (+) form of cis(±) mixture<sup>1</sup> and it is a diltiazem<sup>2</sup> related compound. Diltiazem is a benzothiazepine calcium-channel blocking agent. This is a part of our work on a series of 1, 5-benzothiazepine compounds to understand the geometrical effect and the nature of hydrogen bonding interaction by varying the different substituents with parent skeleton using x-ray analysis. The title compound crystallizes in orthorhombic space group P2<sub>1</sub>2<sub>1</sub>2, with a = 9.271(1) Å, b = 11.838(1) Å, c = 15.836(2) Å, Z = 4, V = 1738.0(3) Å<sup>3</sup> and F(000) = 752. The structure has been determined using SHELX-97 program suit. The least-square refinement gave residual index  $R(F) = 0.042$ ,  $wR(F) = 0.111$  for 1733 observed reflections. The molecular packing is stabilized by hydrogen bonding. The amide group forms strong hydrogen bond with the symmetrically sitting neighboring molecules in the crystal. The molecules are linked into an infinite chain through hydrogen bonds. The seven-membered ring is distorted showing twist-boat conformation. The methoxyphenyl group significantly deviated from planarity.

**Reference**

- [1] Kumaradhas, P. and Nirmala, K.A. Acta Cryst. (1996), C52, 1259.
- [2] Kojic-Prodic, B., Ruzic-Toros, Z. and Sunjic, V. Helv. Chim. Acta. (1984), 67, 916.

## The observation of electron density distribution of thermally excited states in CeB<sub>6</sub> at 430 and 535K

Ryoko Makita<sup>1</sup> Shiro Funahashi<sup>2</sup> Kiyooki Tanaka<sup>3</sup> Yoshichika Onuki<sup>4</sup> Hiroshi Tatewaki<sup>5</sup>

<sup>1</sup>Graduate School of Materials Science & Engineering, Nagoya Institute of Technology, Gokisocho, Showa-ku, Nagoya, Japan  
<sup>2</sup>Graduate School of Materials Science & Engineering, Nagoya Institute of Technology, Gokisocho, Showa-ku, Nagoya, Japan  
<sup>3</sup>Graduate School of Science, Osaka University, Japan  
<sup>4</sup>Graduate School of Natural Science, Nagoya City University, Japan

Most of the properties of materials are determined by electrons. The electron density distribution (EDD) of excited states have not yet been observed. The observation of EDD is useful for revealing relations between physical properties and electronic states and will help control physical properties.

CeB<sub>6</sub> crystal has 4f(j=5/2)  $\gamma_7$  and  $\gamma_8$  (ground state). In the previous study<sup>[1]</sup>, just significant amount of electrons exist in  $\gamma_7$  orbital of CeB<sub>6</sub> at 298K. The excitation energy between  $\gamma_7$  and  $\gamma_8$  is reported to be 530K - 560K<sup>[2]</sup>. Therefore the aim of present study is to observe EDD of excited states of CeB<sub>6</sub> and to pioneer accurate measurements of EDD at high temperature.

X-ray intensity measurement is performed by 4-circle diffractometer keeping multiple diffraction effect minimum and CeB<sub>6</sub> single-crystal is heated by furnace up to 430K and 535K. The furnace equipped with a brass cylinder and a spiral Pt wire is put on chi circle of our diffractometer keeping the N<sub>2</sub>-gas flow rate constant by KOFLOC 8300.

The reflection data are refined by the least-squares method (QNTAO by K.Tanaka). Spin-orbital interaction was taken into account and scattering factors calculated from relativistic atomic orbital were used. The EDD was divided into sub-shells and electron-population and expansion/contraction of each orbital were refined keeping the unit cell electrically neutral together with anharmonic vibration parameters.

We investigate states of electron occupied  $\gamma_7$  and  $\gamma_8$  orbital at 430K and 535K, and verify EDD of thermally excited states of CeB<sub>6</sub> are observed at 430K and 535K.

### Reference

- [1] K.Tanaka and Y.Onuki, *Acta Cryst.* **B58**, 423-436(2002)
- [2] E.Zirngiebl et al, *Phys.Rev.* **B30**, 4052-4054(1984)

## The 4f-EDD quantitative analysis in $RB_6$ ( $R=La, Sm$ ) by X-ray diffraction measurement and X-ray AO (atomic orbital) analysis

Shiro Funahashi<sup>1</sup> Kiyooki Tanaka<sup>2</sup> Fumitoshi Iga<sup>3</sup> Akira Kuni<sup>4</sup>

<sup>1</sup>Graduate School of Materials Science and Engineering, Nagoya Institute of Technology  
<sup>2</sup>Omohi College, Graduate School of Materials Science and Engineering, Nagoya Institute of Technology, Japan  
<sup>3</sup>Graduate School of Advanced Sciences of Matter, Hiroshima University  
<sup>4</sup>Graduate School of Science and faculty of Science, Tohoku University

Generally, it was thought difficult to observe EDD (electron density distribution) of compound containing heavy atoms and analyze 4f-EDD quantitatively. Tanaka et al. (2002) [1] succeeded in 4f-electron EDD analysis in  $CeB_6$  ( $Ce; f^1$ ) by X-ray AO analysis. EDD of isomorphous  $RB_6$  ( $R=La; f^0, Sm; f^5$ ) crystals,  $LaB_6$  and  $SmB_6$ , were measured at four temperatures. To establish 4f-EDD can be measured and be analyzed based on a quantum-mechanical models. Furthermore, we consider the relation of physical properties and EDD of each sample.

Oxford Cryostream system was employed for low-temperature measurements. For reducing absorption correction and extinction, samples were made spherical with radius about 35  $\mu m$ , and measurement was performed keeping multiple diffraction effect minimum. Analysis based on a quantum-mechanical model was carried out employing a weak-field model considering spin-orbit interaction by a least-square method (QNTAO by Tanaka).

We see in Fig.1 negative areas originating from 4f  $j=5/2 \gamma_7$  along  $\langle 111 \rangle$  near the center are reduced after aspherical refinement (population of  $\gamma_7$  ;from 5/6 to 0.34(14)). We report a more detailed result in this conference.

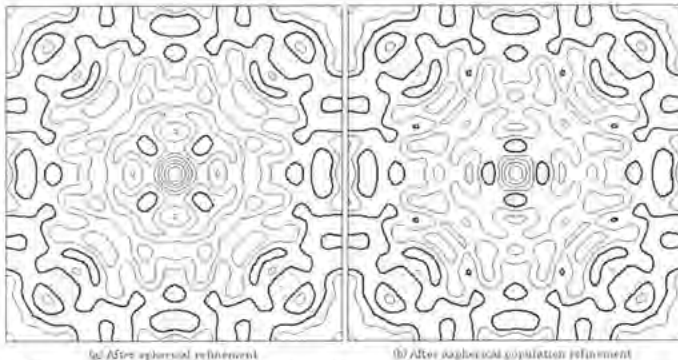


Fig.1 (a) (b) 4f-Electron EDDs for the  $SmB_6(000)$  layers at 100K  
 Contours are given at intervals of 0.2  $e/\text{\AA}^3$ . Broad and dashed lines are zero and negative values respectively.

### Reference

- [1] K.Tanaka and Y.Onuki, *Acta Cryst.* **B58**, 423-436(2002)

## The development of high-resolution X-ray powder diffractometer using laboratory source for an advanced structural analysis

Shinobu Aoyagi Hiroyuki Suwa Takeshi Nakashima Eiji Nishibori Makoto Sakata

Department of Applied Physics, Nagoya University

Recently, advanced structural analyses, such as charge density analysis and ab-initio structure determination, from powder sample have been carried out in the wide range of materials science fields. These studies require high-resolution X-ray powder diffraction data with high counting statistics compared to conventional powder structural refinement. There are large demands for a powder diffractometer available to the advanced structural analysis based on laboratory X-ray source. In this study, we developed a high-resolution powder diffractometer with Imaging Plate (IP) as a detector using laboratory source.

The detailed specs of the diffractometer are as follows. The X-ray source is Rigaku ultraX 18, an 18 kW rotating anode generator, with a Mo target. The X-ray optics consists of a curved graded multilayer mirror (MM) and two Ge channel-cut monochromators (CCM). Three different optical systems, MM, MM with one CCM and MM with two CCM, are available. The X-ray intensities for each optical system at sample position are approximately  $\sim 10^9$  for MM,  $\sim 10^7$  for MM with one CCM and  $\sim 10^6$  for MM with two CCM, cps. Diffraction pattern is recorded on a curved IP, which can simultaneously collect a wide d-spacing range ( $> 0.58$  Å).

We measured powder diffraction data of various kinds of materials by the diffractometer in MM with one CCM optical system. The whole powder pattern of diamond, including 222 forbidden reflection due to the bonding electron, was collected by 24 hours X-ray exposure. Ab-initio structure determination including hydrogen atoms of cytidine was successfully carried out from the data collected by 2.5 days exposure. The present results indicate that our diffractometer has an ability to collect a powder data for the advanced structural analysis in a few days.

## Crystal structure and charge density analysis of the charge- and orbital-ordered phase of $\text{La}_{2-2x}\text{Sr}_{1+2x}\text{Mn}_2\text{O}_7$ ( $x=0.525$ ) using CBED

Yoichiro Ogata<sup>1</sup> Kenji Tsuda<sup>2</sup> Kazuma Hirota<sup>3</sup> Youichi Murakami<sup>4</sup>

<sup>1</sup>Institute of Multidisciplinary Research for Advanced Materials, Tohoku University; <sup>2</sup>Institute for Solid State Physics, University of Tokyo, Japan; <sup>3</sup>Department of Physics, Graduate School of Science, Tohoku University, Japan

We developed a method to refine crystal structural parameters and charge density using convergent-beam electron diffraction (CBED) and applied the method to some materials. We have applied the method to  $\text{La}_{2-2x}\text{Sr}_{1+2x}\text{Mn}_2\text{O}_7$  (LSMO327) ( $x=0.525$ ) which is a charge-ordering material and shows a phase separation phenomenon.

LSMO327 has a bi-layered perovskite structure with space group  $I4/mmm$  at room temperature. Recently, the phase separation between the A-type antiferromagnetic phase (A-phase) and the CE-type charge- and orbital-ordered phase (CE-phase) was found in the range of  $x=0.5-0.6$  of LSMO327 at temperature 150-210 K by using neutron diffraction and resonant X-ray scattering experiments. In the present study, we have observed the domain structure of the phase separation in LSMO327 ( $x=0.525$ ) using dark-field electron microscopy, and have analyzed the crystal structure and charge density using CBED.

The dark-field images were taken at 160 K with accelerating voltage 200 kV using an electron microscope JEM-2000FX. The domain size of CE-phase was about 2  $\mu\text{m}$ . The CBED experiments were carried out using an energy-filter electron microscope JEM-2010FEF at 160 K at an accelerating voltage 100 kV, the space groups of the A-phase and CE-phase being determined to be  $I4/mmm$  and  $Bbmm$ , respectively. The lattice constants of the CE-phase were determined to be  $a=5.4993$  Å,  $b=10.999$  Å and  $c=20.090$  Å from higher-order Laue zone (HOLZ) lines in the CBED patterns. An initial structure model for the refinement was constructed from simulations of CBED intensities with systematically varying atom positions and Debye-Waller factors.

## X-ray and neutron diffraction investigations on electron density distribution in an electride crystals

Kiyooki Tanaka<sup>1</sup>, Terutoshi Sakakura<sup>1</sup>, Masashi Watanabe<sup>2</sup>, Yukio Noda<sup>3</sup>, Satoru Matsuishi<sup>1</sup>,  
Hideo Hosono<sup>1</sup>

Graduate School of Engineering, Nagoya Institute of Technology<sup>1</sup>, Institute of Multidisciplinary Research for Advanced Materials, Tohoku University, Japan<sup>2</sup>, Materials and Structures Laboratory, Tokyo Institute of Technology, Japan<sup>3</sup>

A typical cement material  $12\text{CaO}\cdot 7\text{Al}_2\text{O}_3$  (C12A7) is an first 'electride' stable at room temperature formed by removing two O atoms from cages leaving four electrons ( $[\text{Ca}_{24}\text{Al}_{48}\text{O}_{64}]^{4+}(4e^-)$ ). The unusual crystal was investigated by X-ray and neutron diffraction (ND) methods to find the location of the four electrons in crystallographic cages and to assess the O atoms were extracted from the cage, respectively. The ND study revealed a peak on the 2-fold axis connecting two Ca atoms at about 0.75 Å from a Ca atom (Ca1). The crystal structure revealed that small amount of Ca atoms (Ca2) locate there (about 3% of Ca1). X-ray diffraction on the other hand exhibited two large peaks of 10.5 and 6.2  $\text{e}\text{\AA}^{-3}$  on the 2-fold axis at 0.4 (peak A) and 0.75 Å from the Ca atom, respectively. The second peak disappeared when Ca2 was assigned to the position but O atoms could not occupy the site indicating they were extracted completely from the cage. X-ray AO analysis as well as anharmonic vibration (AHV) analysis were then carried out dividing each atom into sub-shells, which enabled us to keep the electro-neutrality of the unit cell. It reduced peak A to 6.2  $\text{e}\text{\AA}^{-3}$  and made the analysis of temperature factor of Ca2 possible, which further reduced the peak to 3.0  $\text{e}\text{\AA}^{-3}$ . Significant AHV of Ca1 indicates that peak A is due to electrons which do not belong to any Ca orbitals. The remaining Peak A was integrated to be 0.083e corresponding to 3.98e in the unit cell. These facts supports strongly that the present compound is an electride.

## Electron density distribution and Topological studies of Copper complex

Poomani Kumaradhas<sup>1</sup> Alvaro De Souza<sup>2</sup> Tibor Koritzanszky<sup>3</sup>

Department of Physics, Periyar University<sup>1</sup> Department of Chemistry, University of Witwatersrand, Johannesburg, South Africa<sup>2</sup> Department of Chemistry, Middle Tennessee State University, USA<sup>3</sup>

The presence of copper atom in structures exhibit variety of unusual properties, for instance, superconductivity in naval material<sup>1</sup> Cu<sub>2</sub>O and so on. These properties are mainly attributed to the chemical bonding, therefore, tremendous attention being paid on understanding the bonding nature of Cu atom in different environment. We are studying, electron density distribution of a series of metal complexes to understand the nature of chemical bonding and topological characteristics of the bonds. The title copper complex molecule crystallizes in monoclinic C2/c space group. The x-ray intensity data were collected at 110 K using SMART 1K CCD area detector with Mo K $\alpha$  radiation up to the resolution  $(\sin\theta/\lambda)_{\max} = 1.1 \text{ \AA}^{-1}$ . The structure of the molecule has been determined using SHELXS97 program package. In the molecule, the copper atom is sitting at two fold axis symmetry and coordinated in a square planar geometry consisting of two N atoms and two O atoms. The multipole refinement<sup>2</sup> and the bond topological analysis of static densities were performed using the XD<sup>3</sup> suit program. The results will be presented.

### Reference

- [1] Thomas Lippmann and Jochen R. Schneider. Acta Cryst. A56, (2000), 575.
- [2] Hansen, N.K. and Coppens, P. Acta Cryst. A, (1978), 48, 188.
- [3]. Koritzanszky, T.; Richter, T.; Macchi, P.; Volkov, A.; Gatti, C.; Howard, S.; Mallinson, P.R.; Farrugia, L.; Su, Z. and Hansen, N.K: XD: a Computer Program Package for Multipole Refinement and Topological Analysis of Electron Densities from Diffraction Data (2003).

**Crystal Structure of the [Ru(azpy)<sub>2</sub>bpy](PF<sub>6</sub>)<sub>2</sub> complex (azpy=2-(phenylazo)pyridine, bpy=2,2'-bipyridine)**Kanidtha - Hansongnern<sup>\*</sup> U. Changsaluk<sup>\*</sup> T-H Lu<sup>\*\*</sup>Department of Chemistry, Prince of Songkla University<sup>\*</sup> National Tsing Hua University, Hsinchu, Taiwan<sup>\*\*</sup>

The complex of [Ru(azpy)<sub>2</sub>bpy](PF<sub>6</sub>)<sub>2</sub> (azpy = 2-(phenylazo)pyridine, bpy = 2,2'-bipyridine) was synthesized by reaction between  $\alpha$ -[Ru(azpy)<sub>2</sub>Cl<sub>2</sub>] and 2,2'-bipyridine in water-ethanol mixture. The characterization of this complex was studied by FAB-mass spectrometry and infrared spectroscopy. In addition, the X-ray crystal structure of the complex was also determined. The coordination geometry of ruthenium(II) was distorted octahedral with coordinating from two N-donor atoms of bpy and four N-donor atoms of two azpy units. The Ru-N(pyridine) bonds of bpy were longer than the Ru-N(pyridine) distances in azpy. In this complex the N-N distances of azpy ligands were slightly longer than that of the free azpy ligand.

## Spherical-aberration-corrected HRTEM of Al-Ni-Co decagonal quasicrystals

Koh Saitoh<sup>1</sup> Nobuo Tanaka<sup>2</sup> Pang Tsai An<sup>3</sup> Kazuo Ishizuka<sup>4</sup>

<sup>1</sup>EcoTopia Science Institute, Nagoya University<sup>2</sup> Institute of Multidisciplinary Research for Advanced Materials, Tohoku University, Japan<sup>3</sup> HREM Research Inc., Japan<sup>4</sup>

Quasicrystals (QCs) have a complex structural order, which are neither of ordinary crystals due to their non-crystallographic rotational symmetry, nor of amorphous solids by their long range order. Many electron microscope studies have been performed for various types of QCs and have provided valuable structural information of the QCs [1-3]. Hiraga *et al.* first took high-resolution transmission electron microscope (HRTEM) images of decagonal quasicrystals (DQC) at an accelerating voltage of 400kV [2]. The images show the arrangement of atom-clusters and atoms inside the cluster in atomic resolution. However, the 400 kV HRTEM has a problem that the high-energy electron beam inevitably introduces severe damages. 200 kV HRTEM is considered to be desirable for avoiding such beam induced damages. However, the resolution of the 200kV images is not sufficient to resolve all the atomic columns of QCs, even though the current highest-resolution objective lens is used.

In the present study, spherical aberration ( $C_s$ ) corrected HRTEM [4,5] was applied to DQC. A significant improvement of the resolution from that with  $C_s$ -uncorrected 200kV HRTEM was observed. When  $C_s$  was set at nearly 0  $\mu\text{m}$  ( $\pm 1 \mu\text{m}$ ) and the defocus was at a slightly negative value (underfocus), the images appear to be very similar to those taken at 400kV by Hiraga *et al.* Exit plane wave reconstruction was applied to defocus series of  $C_s$ -corrected HRTEM images [6].

### Reference

- [1] K. Hiraga and D. Shindo: *Mater. Trans. JIM* **31** (1990) 567.
- [2] K. Hiraga, et al.: *Mater. Trans JIM* **32** (1991) 308.
- [3] K. Tsuda, et al.: *Jpn. J. Appl. Phys.* **32** (1993) 129.
- [4] M. Haider, et al.: *Ultramicrosc.* **75** (1998) 53.
- [5] N. Tanaka, et al.: *J. Electron Microsc.* **52** (2003) 69.
- [6] R.R. Meyer, et al., *Ultramicrosc.* **92** (2002) 89.

**X-ray structural study of layered compounds  $\text{Co}_x\text{TiS}_2$** 

Takeshi Osakabe<sup>1</sup> Yasuhiko Takahashi<sup>2</sup> Takuro Kawasaki<sup>1</sup> Ken-ichi Ohshima<sup>1</sup>

<sup>1</sup>Graduate School of Pure and Applied Sciences, University of Tsukuba<sup>2</sup> National Institute of Advanced Industrial Science and Technology(AIST)

The transition metal dichalcogenides and their intercalation compounds have layered type structures and are regarded as two-dimensional solids. They have been studied due to their interesting physical and chemical properties and their potential applications. It is important to understand the relationship between the structure and the properties. It is peculiar that the c-axis lattice spacing in  $\text{Co}_x\text{TiS}_2$  is decreasing with increasing the Co content. We have, therefore, performed X-ray structural determinations for the single crystals of  $\text{Co}_x\text{TiS}_2$  ( $x=1/4, 1/3$ ), which were grown by the chemical vapor transport method using iodine as a transport gas. The X-ray intensity data were collected with the use of four circle diffractometer AFC7(Rigaku) at room temperature.

Space groups of  $\text{Co}_x\text{TiS}_2$  ( $x=1/4, 1/3$ ) are P-3m1(164) and P-31c(163) of the trigonal system, respectively. Co atoms have two kinds of ordered structure depending on their composition. The cell constants  $a=7.148$ ,  $b=7.148$ ,  $c=11.88\text{\AA}$  ( $x=1/4$ ),  $a=5.8798$ ,  $b=5.8798$ ,  $c=11.2579\text{\AA}$  ( $x=1/3$ ) were refined.

Co atoms occupy the octahedral sites in the van der Waals gap. As the Co composition increases, the van der Waals gap layer becomes narrow. The results of maximum entropy method analysis show the covalent bonding between Ti and S atoms, and between Co and S atoms.

**CBED rocking curves of low-order reflections from doped silicon**Kenji Tsuda<sup>1</sup>, Hajime Mitsui<sup>1</sup>, Masami Terauchi<sup>1</sup>, Kazuo Kawamura<sup>2</sup><sup>1</sup>Institute of Multidisciplinary Research for Advanced Materials, Tohoku University, <sup>2</sup>Fujitsu Ltd.

Determination of strain distributions in devices with a nanometer-scale spatial resolution has become a crucial issue in semiconductor technologies. Lattice strains of semiconductor devices have been investigated using higher-order Laue zone (HOLZ) line patterns in convergent-beam electron diffraction (CBED) disks. We report here another promising way to detect strains using CBED rocking curves of low-order reflections.

Terauchi *et al.* found anomalously high intensities in rocking curves of CBED patterns of the 004 reflection for arsenic-doped silicon with doping concentration of less than 1 at.% [Terauchi *et al.*: *J. Electron Microsc.* 52 (2003) 441]. Such high intensities can never be expected from scattering power of the doped As atoms of less than 1 at.%. In order to clarify the origin of the anomalous intensities, CBED rocking curves of low-order reflections have been investigated with various doping amounts, ion-implantation conditions and specimen preparation methods, using an energy-filter transmission electron microscope. Simulations of CBED patterns were performed using models with different types of strains based on dynamical diffraction theories. Kato's statistical dynamical theory for X-ray diffraction [Kato: *Acta Cryst.* A36 (1980) 763.] was first applied to electron diffraction.

As a result of these analyses, it has been revealed that the anomalously high intensities in the rocking curves are reproduced by two types of strains: (i) statistically-distributed local strains and (ii) lattice bending caused by strain relaxation in thin TEM lamella. Both types of the strains originate from doped atoms, interstitial atoms and clusters induced by ion implantation. Thus the CBED rocking curves of low-order reflections can be used as a new probe to detect strains.

## Gigantic growth of carbon nanotubes from camphor

Mukul Kumar Okazaki Naoto Iida Atsushi Ando Yoshinori

Materials Science and Engineering Department, Meijo University

Camphor, a well-valued material in biotechnology, is successfully brought to nanotechnology. The first report of carbon nanotubes (CNTs) from a tree product, camphor, was made by our group in 2001 [1]. Since then, we remained involved with this regenerative source of CNTs and established the conditions for growing multiwall nanotubes (MWNTs) [2,3] single-wall nanotubes (SWNTs) [4] and vertically aligned nanotubes [5] on quartz and silicon plates by a simple CVD technique. As-grown CNTs have shown appreciable field emission properties [6]. Recently, using iron-cobalt bimetallic catalyst impregnated in mesoporous zeolite powder, we have been able to grow MWNTs at a temperature as low as 550°C, whereas SWNTs could be grown at 850-900°C [7]. The exciting new feature of our work is that, apart from the high purity (88%) of as-grown MWNTs, camphor-to-CNT production yield is 50%, which is incomparably higher than that of any other CNT precursor reported so far. Camphor-grown CNTs have relatively higher graphitization and negligible amorphous carbon. And quite recently, we have found the conditions to grow attractive CNT architecture on quartz or silicon substrate that are useful in device fabrication. The technique involves thin patterning of iron or nickel on the substrates as a growth guide, while ferrocene is used as a catalyst.

### Reference

1. M. Kumar et al, *Internat. Symposium on Nanocarbons, Nagano, Japan (Nov. 14-16, 2001) Extended Abstract*, 244-245.
2. M. Kumar et al, *Molecular Crystals Liquid Crystals* **387** (2002) 117.
3. M. Kumar et al, *Diamond & Related Materials* **12** (2003) 998.
4. M. Kumar et al, *Diamond & Related Materials* **12** (2003) 1845.
5. M. Kumar et al, *Chem. Phys. Lett.* **374** (2003) 521.
6. M. Kumar et al, *Chem. Phys. Lett.* **385** (2004) 161.
7. M. Kumar et al, *Carbon* **43** (2005) 533.

## Structural Analysis of PS-*b*-PMMA Block Copolymer Thin Films with Grazing Incidence Small-Angle X-ray Scattering

Jinhwan Yoon<sup>1</sup>, Byeongdu Lee<sup>1</sup>, Sangwoo Jin<sup>1</sup>, Kyeong Sik Jin<sup>1</sup>, Seung-Yun Yang<sup>1</sup>, Won-Chul Joo<sup>1</sup>, Jin Kon Kim<sup>1</sup>, Moonhor Ree<sup>1</sup>

<sup>1</sup>Pohang University of Science and Technology, Department of Chemical Engineering, Pohang University of Science and Technology

Thin films of block copolymer with well defined nanostructure have recently received considerable attention for their potential nano-fabrication application. In these applications, controlling the morphology of the block copolymer thin film, particularly the orientation and ordering of the phase-separated microdomain, is essential. For characterizing the structures and observing the morphology and orientation of the block copolymer thin films, microscopy tools such as transmission electron microscopy, scanning electron microscopy and atomic force microscopy are commonly used. With these tools, images such as those that show local structures near the surface have been obtained, thus enabling discussion of the underlying physics. From the viewpoint of fabrication, this approach is often sufficient, but from the scientific point of view, X-ray scattering & Diffraction results are required, because only they provide information on a larger scale at high resolution. Grazing incidence small-angle X-ray scattering (GISAXS) has emerged as a powerful technique for characterizing internal structure of thin film. The X-ray beam impinges at a grazing angle onto the sample slightly above the critical angle, so that the film is still fully penetrated by X-ray. Analytical solutions of GISAXS patterns based on the distorted wave Born approximation have been developed to describe the complicated reflection and refraction effects, which are not found in conventional Transmission SAXS. Here, we attempted the quantitative analysis of the two-dimensional GISAXS patterns of polystyrene-*b*-polymethylmethacrylate (PS-*b*-PMMA) diblock copolymer films deposited on silicon substrates with derived GISAXS formula for hexagonal cylinder with preferred orientation, which were obtained with synchrotron radiation sources. The analysis of the GISAXS patterns was successfully carried out, and we found that PS-*b*-PMMA thin films deposited on silicon substrates contain cylinder microdomain perfectly oriented normal to the substrate surface.

## In-Situ GISAXS Studies on the Evolution of Closed Nanopores in Low-k Organosilicate Dielectric Thin Films

Kyeong Sik Jin Jinhwan Yoon Kyuyoung Heo Moonhor Ree

Pohang University of Science & Technology

Porous organosilicate materials have recently attracted much interest due to their potential application as low dielectric constant (low- $k$ ) interdielectrics. In particular, much effort has been directed towards the development of low- $k$  porous organosilicate dielectric thin films via the templated polycondensation of their soluble precursors in the presence of a thermally-labile, organic polymeric porogen. Pores are subsequently formed in the resulting dielectrics through the sacrificial thermal decomposition of the porogens in the range 350-400°C. However, the tendency of porogens to aggregate in organosilicates has limited the ability to reduce the pore size and porosity of the resulting dielectrics, making them unsuitable for use in advanced integrated circuits patterned with small feature sizes. The formation of porous films from an organosilicate precursor polymer/porogen composite is a complex procedure since the matrix precursor readily undergoes crosslinking while the porogen undergoes thermal degradation. In order to understand the structure of pores in the porous film, it is necessary to investigate their generation during the porous dielectric film process. Pore structure evolution during porous film process has rarely been investigated. In this study, we present the *in-situ* grazing incidence small angle X-ray scattering (GISAXS) study of the evolution of nanopores during porous dielectric film formation in a composite film containing polymethylsilsesquioxane (PMSSQ) precursor and star-shaped four-armed poly( $\epsilon$ -caprolactone) porogen in various compositions. Using a synchrotron X-ray source, *in-situ* GISAXS measurements were carried out during thermal treatment of the PMSSQ/porogen composite films to 400°C in vacuum, and continued during the subsequent cooling of the resulting porous films. In addition, thermogravimetric analysis and electron microscopy measurements were performed. Detailed analyses of the measured two-dimensional GISAXS data were accomplished using a recently developed GISAXS formula.

## In-situ Investigation of Annealing Effect on Higher Order Structure of Polyethylene Thin Films by Synchrotron GISWAXS Measurements

Sono SASAKI<sup>1</sup>, Hiroyasu MASUNAGA<sup>1</sup>, Hiroo TAJIRI<sup>1</sup>, Katsuaki INOUE<sup>1</sup>, Hiroshi OKUDA<sup>2</sup>, Atsushi TAKAHARA<sup>3</sup>, and Masaki TAKATA<sup>4</sup>

<sup>1</sup>Japan Synchrotron Radiation Research Institute (JASRI) / SPring-8, Hyogo 679-5198, Japan ;

<sup>2</sup>International Innovation Center, Kyoto University, Kyoto 606-8501 Japan; <sup>3</sup>Institute for Materials Chemistry and Engineering, Kyushu University, Fukuoka 812-8581, Japan; <sup>4</sup>The RIKEN Harima Institute / SPring-8, Hyogo 679-5198, Japan.

We have investigated lamellar stacking structure of melt-crystallized and annealed high-density polyethylene (HDPE) thin films with a thickness of ca. 400 nm prepared on silicon wafers by synchrotron grazing-incidence small-angle and wide-angle X-ray scattering (GISWAXS) measurements at the BL40B2 in SPring-8. Figure 1 shows in-situ GISWAXS patterns measured for a melt-crystallized HDPE thin film in a stepwise annealing process. Scattering peaks relating to the long period, the average distance between stacked crystalline lamellae, were measured only in the in-plane direction near Yoneda peak of the grazing-incidence small-angle X-ray scattering (GISAXS) patterns. On the other hand, the orthorhombic (110) and (200) reflections of oriented HDPE crystals were measured in the out-of-plane direction of the grazing-incidence wide-angle X-ray scattering (GIWAXS) patterns. It was revealed that crystalline lamellae were stacked in the parallel direction to the film surface and the long period increased from ca. 25 nm to ca. 30 nm in a stepwise annealing process. Within a lamella, molecular chains were packed regularly and the chain axis (the *c* axis) was relatively oriented parallel to the film surface.

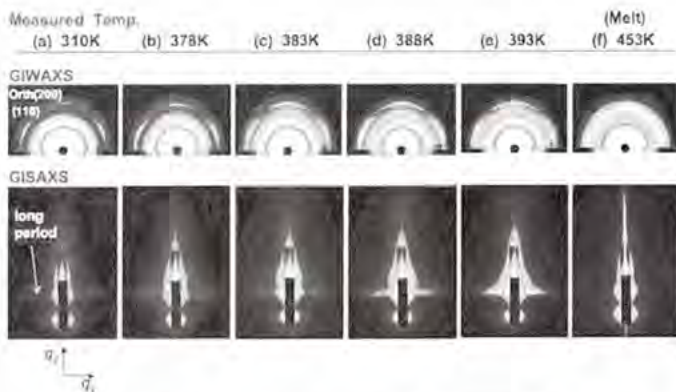


Figure 1. GIWAXS and GISAXS patterns measured at the incident angle of X-ray beams:  $\theta$  of 0.13 deg. for a melt-crystallized HDPE thin film in the initial state at 310 K, in the stepwise annealed state at 378 K, 383 K, 388 K and 393 K, and in the melt state at 453 K, respectively.

## Lamellar and Crystal Structural Study on Ferroelectric Phase Transition of Vinylidene fluoride-Trifluoroethylene Copolymers by Synchrotron DSC/WAXD/SAXS Simultaneous Measurements

H. Masunaga<sup>1</sup>, S. Sasaki<sup>1</sup>, M. Hanesaka<sup>2</sup>, K. Tashiro<sup>2</sup>, M. Takata<sup>1,3</sup>

<sup>1</sup>Japan Synchrotron Radiation Research Institute (JASRI) / Spring-8, Hyogo 679-5198 Japan;

<sup>2</sup>Graduate School of Engineering Toyota Technological Institute, Nagoya 468-8511, Japan;

<sup>3</sup>The RIKEN Harima Institute / Spring-8, Hyogo 679-5198, Japan

Vinylidene fluoride-trifluoroethylene (VDF-TrFE) copolymers show the ferroelectric phase transition at a Curie transition temperature. For the sample with VDF contents higher than 80 mol %, the transition occurs between the polar crystalline forms I, II and the nonpolar high-temperature phase. It has been found that the structural change in crystal lattice affects not only the inside of the crystalline lamella but also the morphological change of stacked lamellae drastically. However, the morphological change and its relation with the crystal structural change have not yet been clarified at all. In this work, we will report the experimental data concerning the simultaneous measurements of DSC/WAXD/SAXS during the heating and cooling processes of VDF 82% copolymer samples.

Simultaneous measurements of DSC, WAXD and SAXS were carried out at BL40B2 of Spring-8. WAXD and SAXS patterns from the sample were detected for 30 sec at 5 min-intervals in the heating and cooling processes at a rate of 1°C/min. In the heating process for the melt-quenched sample, the relative intensity of the reflection from the form II decreases and that from the HT phase increases instead in the endothermic temperature region of the DSC thermogram. On the other hand, the mean lamellar thickness and the long period of stacked lamellae, which were estimated from the one-dimensional electron density correlation function of SAXS profiles from the sample, increased largely and slightly due to thermal expansion, respectively. DSC/WAXD/SAXS data suggested that the phase transition from II to the HT phase enhanced lamellar thickening without large change in lamellar stacking distance.

## Crystal Structure of High Pressure Phase of $\text{MgAl}_2\text{O}_4$ synthesized at conditions of 2200 K and 41.8GPa

Yasuhiro Kudoh<sup>1</sup> Takahiro Kuribayashi<sup>1</sup> Yuichiro Sueda<sup>1,2</sup> Tetsuo Irifune<sup>2</sup>

Graduate School of Science, Tohoku University<sup>1</sup> Geodynamics Research Center, Ehime University<sup>2</sup>

The specimen used in this study was a single crystal of high pressure phase of  $\text{MgAl}_2\text{O}_4$  synthesized using a multi-anvil apparatus at conditions of 2200 K and 41.8 GPa and quenched to ambient condition by Sueda et al. (2004). EDS analysis showed that the specimen has a chemical composition of ideal formula  $\text{MgAl}_2\text{O}_4$  within the limit of experimental error. Sets of X-ray diffraction intensities were measured with a single crystal of  $47 \times 47 \times 24$  micron using synchrotron radiation at the beam line BL-10A, Photon Factory, High Energy Accelerator Research Organization, Tsukuba, Japan. The wave length,  $\lambda = 0.7009$  Å was calibrated by the unit cell constants of a ruby standard crystal ( $a = 4.76099(6)$  Å,  $c = 12.99625(35)$  Å). The crystallographic data obtained are: orthorhombic,  $a = 2.781(3)$  Å,  $b = 9.183(3)$  Å,  $c = 9.383(3)$  Å,  $V = 239.6(3)$  Å<sup>3</sup>. The systematic absences and  $N(Z)$  test for a center of symmetry indicated the centrosymmetric space group  $Cmcm$  (No.63). From the total of 2043 reflections measured in the sphere of  $\sin\theta/\lambda = 1.00$  Å<sup>-1</sup>, 1264 symmetry-independent reflections were obtained by averaging the symmetry equivalent intensities in Laue group  $mmm$  ( $R_{int} = 11\%$ ). The crystal structure is isostructural with  $\text{CaTi}_2\text{O}_6$  and refined to an  $R = 8.7\%$  ( $R_w = 8.3\%$ ) with anisotropic temperature factors. The calculated density value  $3.94$  g/cm<sup>3</sup> is 10% larger than  $3.578$  g/cm<sup>3</sup> value of spinel,  $\text{MgAl}_2\text{O}_4$  which is the stable phase at ambient condition. The Mg atom is surrounded by 8 oxygen atoms with the average Mg-O distance being  $2.246(4)$  Å. The Al atom is surrounded by 6 oxygen atoms with the average Al-O distance being  $1.921(3)$  Å which is comparable to the  $1.926$  Å value of spinel.

## Tetragonal-monoclinic transformation of Na-hollandite

Yuichi Michiue

Quantum Beam Center, National Institute for Materials Science

Na-hollandite is a candidate for the one-dimensional Na ion conductor, as the frequency-independent conduction was observed by impedance spectroscopy measurements [1]. In the present study, hollandite structures were obtained in the pseudobinary system  $\text{NaCrO}_2\text{-TiO}_2$  (*i.e.*  $\text{Na}_x\text{Cr}_x\text{Ti}_{8-x}\text{O}_{16}$ ) of the composition range  $1.7 \leq x \leq 2.0$  at 1350 C. The symmetry of the samples at room temperature was tetragonal for  $x=1.7$  and 1.75, and monoclinic for  $x=1.8$  and above. Furthermore, single crystals of monoclinic hollandite  $\text{Na}_2\text{Cr}_2\text{Ti}_6\text{O}_{16}$  were grown and the structure refinement has been carried out using an X-ray diffraction technique. The space group was  $I2/m$  and cell parameters were  $a=10.2385(11)$ ,  $b=2.9559(9)$ ,  $c=9.9097(11)\text{\AA}$ , and  $\beta=90.545(9)$ . There are three characteristics in  $\text{Na}_2\text{Cr}_2\text{Ti}_6\text{O}_{16}$  related to tetragonal-monoclinic transformation of hollandite structures; (i) distortion of the framework structure, (ii) deformation of the Na ion distribution in the tunnel, and (iii) different Cr/Ti ratios between the two metal sites in the framework structure. The first one is common in hollandite structures showing the tetragonal-monoclinic transformation. The second one was observed in the low-temperature phase of  $\text{Na}_x\text{Cr}_x\text{Ti}_{8-x}\text{O}_{16}$  ( $x=1.7$ ) [2] and more prominent in  $\text{Na}_2\text{Cr}_2\text{Ti}_6\text{O}_{16}$ . The third one was first pointed out in this study.

### Reference

- [1] S. Yoshikado, Y. Michiue, Y. Onoda, and M. Watanabe, *Solid State Ionics* **136/137**, 371-374 (2000).
- [2] Y. Michiue, A. Sato, and M. Watanabe, *J. Solid State Chem.* **145**, 182-185 (1999).

## Crystal structure analysis and microwave dielectric properties of $\text{LaAlO}_3\text{-SrTiO}_3$ solid solutions

Yumi Inagaki<sup>1</sup> Shotaro Suzuki<sup>1</sup> Isao Kagomiya<sup>1</sup> Ken-ichi Kakimoto<sup>1</sup> Hitoshi Ohsato<sup>1</sup> Katsuhiro Sasaki<sup>2</sup> Kotaro Kuroda<sup>2</sup> Takeshi Shimada<sup>2</sup>

<sup>1</sup>Department of Materials Science and Engineering, Nagoya Institute of Technology, Nagoya University<sup>2</sup> NEOMAX Co. LTD.,

Microwave dielectric properties have been much investigated for wireless and telecommunicating applications. In particular, one kinds of band-pass-filter, high temperature superconductive filters, exhibits minimum insertion loss, which is an important for wireless communicating systems for next generations. However, there is a problem that the loss of the filters increases with dielectric loss of substrates printing strip lines. It has been found that  $(\text{La}_{1-x}\text{Sr}_x)(\text{Al}_{1-x}\text{Ti}_x)\text{O}_3$  solid solutions improve the dielectric loss compared to  $\text{LaAlO}_3$ , which is a typical substrate for the HTS filters. Therefore, the single crystal of  $(\text{La}_{1-x}\text{Sr}_x)(\text{Al}_{1-x}\text{Ti}_x)\text{O}_3$  is promising an appropriate substrates for high performance HTS filters. In this study, we try to prepare the single crystal of  $(\text{La}_{1-x}\text{Sr}_x)(\text{Al}_{1-x}\text{Ti}_x)\text{O}_3$  ( $x = 0.005, 0.2$ ) by using a floating zone method and investigate the relationship between the crystal structure and the microwave dielectric properties of the  $(\text{La}_{1-x}\text{Sr}_x)(\text{Al}_{1-x}\text{Ti}_x)\text{O}_3$ . As a result of the X-ray structure analysis,  $(\text{La}_{0.8}\text{Sr}_{0.2})(\text{Al}_{0.8}\text{Ti}_{0.2})\text{O}_3$  exhibits the cubic ( $Pm-3m$ , A-221) structure, whereas the crystal structure of  $\text{LaAlO}_3$  is trigonal ( $R-3m$ , A-166). It is suggested that  $(\text{La}_{1-x}\text{Sr}_x)(\text{Al}_{1-x}\text{Ti}_x)\text{O}_3$  solid solutions change their crystal structures from trigonal to cubic with increasing  $x$ . In additions, we investigated the difference in crystal structure between  $\text{LaAlO}_3$  and  $(\text{La}_{0.8}\text{Sr}_{0.2})(\text{Al}_{0.8}\text{Ti}_{0.2})\text{O}_3$ . We consider that the increase of the dielectric constant is related to the site volume of  $\text{BO}_6$  octahedra and the the  $Q \times f$  value is related to response for external force.

## The Crystal Structures of Two Polymeric Silver(I) Complexes with Amino Acids

Li Wang

Department of Chemistry, Central China Normal University

$\alpha$ -Amino acids are interesting biological ligands with multiple functional groups, which display variant coordination modes under different chemical environment.<sup>[1]</sup> The studies of silver(I) complexes have been mostly related to their antiethylene and antimicrobial activities.<sup>[2]</sup> Two novel polymeric silver(I) complexes, namely  $[\text{Ag}(\text{L-phenylalaninato})]_n$ , **1** and  $\{[\text{Ag}(\text{L-argininato})\text{NO}_3]_n$ , **2** have been synthesized and structurally characterized by x-ray crystallography. The compound **1** is a one-dimension polymer along the [100] direction, with the Ag (I) cation coordinated by one carboxylate oxygen atom of the L-Phenylalanine ligand and one amido nitrogen atom from the other asymmetric unit (Ag--N=2.146(8) Å and Ag--O=2.148(9) Å ). In compound **2**, Ag(I) is also two-coordinated by one amino N atom of the L-Arginine ligand, one O atom of another carbonyl group L-Arginine ligand( Ag--O and Ag--N are 2.147(2) Å and 2.156(3) Å ), the N-Ag-O bonding units are repeated.

### References

- 1 O. Yamauchi, A. Odani and M. Takani, *J. Chem. Soc., Dalton Trans.*, **2002**, 3411.
- 2 K. Nomiya and H. Yokoyama, *J. Chem. Soc., Dalton Trans.*, **2002**, 2483.

## **X-ray twenty-four beam dynamical diffraction in a two-plate crystal cavity of silicon**

Mau-Sen Chiu<sup>\*</sup> Yu P Stetsko<sup>\*\*</sup> Shih-Lin Chang<sup>\*</sup>

Department of Physics, National Tsing Hua University<sup>\*</sup> National Synchrotron Radiation Research Center<sup>\*\*</sup>

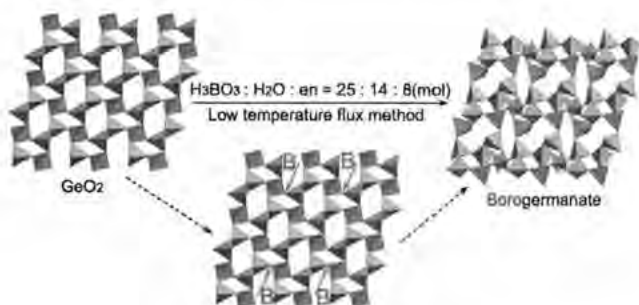
The theoretical approach of using a Cartesian coordinate representation for polarization based on the dynamical theory is applied to the back diffraction of Si (12 4 0) in a two-plate cavity at 14.4388 keV. At this photon energy, simultaneous twenty-four beam diffraction consisting of nine coplanar reflections occurs. Also the interference due to Fabry-Perot type resonance produces intensity undulation in both transmitted and back-reflected beams. In order to understand the wavefield distribution and interaction of 24-beam diffraction with the resonant X-rays, the geometry of the dispersion surface, linear absorption coefficients, wavefield intensity, and excitation of mode are calculated. The calculated intensity distributions of the transmitted and back-reflected beams are in good agreement with the observed ones. Details about the interaction between the multiply diffraction X-rays and cavity resonant photons will be reported.

## A New Ammonium Borogermanate Made of Infinite Chain Building Blocks Synthesized by Flux Method

Crystal Research Center, Shanghai Institute of Ceramics, CAS' Shanghai Institute of Ceramics,  
Jing-Tai Zhao' Ding-Bang Xiong'' Hao-Hong Chen'' Man-Rong Li'' Xin-Xin Yang''

Chinese Academy of Science, China''

A new microporous borogermanate  $\text{NH}_4[\text{BGe}_2\text{O}_9]$  has been synthesized by a molten boric acid flux method with "reagent" quantities of water in which  $\text{GeO}_2$ , en,  $\text{H}_2\text{O}$  and  $\text{H}_3\text{BO}_3$  (5 : 8 : 14 : 25) were heated together at 513 K for 4 days. It is noteworthy that the high viscosity of reactive medium and the quantity of water play important role in the formation of the compound. The structure consists of  $\{\text{Ge}_6\text{O}_{18}\}_n$  chains, further linked together via  $\text{BO}_3$  tetrahedra, forming a three-dimensional open framework with intersecting channel systems including 1-D ten-membered rings (MRs) channels. Interestingly, the infinite chains  $\{\text{Ge}_6\text{O}_{18}\}_n$  as building block, built of alternate four- and six-MRs made of vertex-sharing  $\text{GeO}_4$  tetrahedra.



### Reference

- [1] Li, Y. F.; Zou, X. D. *Angew. Chem. Int. Ed.*, **2005**, *44*, 1212.
- [2] Li, M. R.; Liu, W.; Ge, M. H.; Chen, H. H.; Yang, X. X.; Zhao, J. T. *Chem. Comm.*, **2004**, 1272.

## **Feasibility study of wide-angle incidence X-ray waveguides using surface diffraction**

Sung-Yu Chen<sup>\*</sup> Chia-Hung Chu<sup>\*</sup> Chien-Liang Chen<sup>\*</sup> Po-Wei Wu<sup>\*</sup> Mou-Sen Chiu<sup>\*</sup> Yu-Chi Shen<sup>\*</sup>  
M.-H. Hong<sup>\*\*</sup> Shih-Lin Chang<sup>\*</sup>

Department of Physics, National Tsing Hua University<sup>\*</sup> Department of Materials Science and Engineering, National Tsing Hua University, Hsinchu 300, Taiwan, R.O.C.<sup>\*\*</sup>

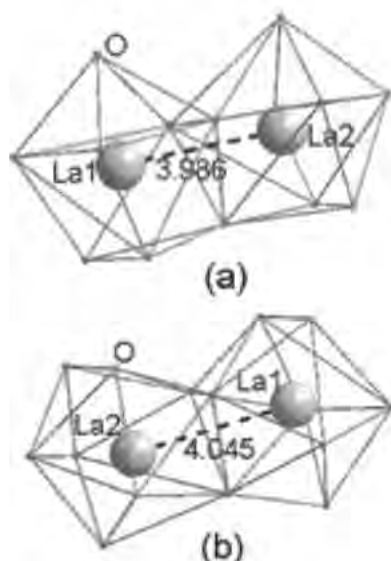
Grazing incidence X-ray waveguides have been most studied because of its simple geometry and applicability for all photon energies. However, wide-angle incidence waveguides are also essential for modern X-ray optics, as far as coupling/guiding X-ray beams into a given direction are concerned. In order to investigate the possibility of making wide-angle incidence waveguides for hard X-rays, we prepare waveguides on silicon (001) wafers by using X-ray lithographic technique. The shapes of the waveguides are 150 $\mu\text{m}$  high and 2cm long with different widths ranging from 5 to 100 $\mu\text{m}$  and the distance between the adjacent waveguides is 3mm. The silicon waveguides are plated with gold on top and by sides. The X-ray wide-angle incidence Bragg surface (113) diffraction from the (001) silicon using synchrotron radiation at 8.878keV clearly shows the guiding and preserving effects of X-rays inside the 1.5 dimensional waveguides. Details of this investigation will be discussed.

## Synthesis, Structure and Luminescence Property of Two Lanthanum Phosphites Hydrate: $\text{La}_2(\text{H}_2\text{O})_x(\text{HPO}_3)_3$ ( $x=1,2$ )

Jing-Tai Zhao<sup>1</sup> Ding-Bang Xiong<sup>2</sup> Hao-Hong Chen<sup>1</sup> Xin-Xin Yang<sup>1</sup>

<sup>1</sup>Crystal Research Center, Shanghai Institute of Ceramics, CAS<sup>1</sup> Shanghai Institute of Ceramics, Chinese Academy of Science, China<sup>1</sup>

Two new lanthanum phosphites hydrate,  $\text{La}_2(\text{H}_2\text{O})(\text{HPO}_3)_3$  (**a**) and  $\text{La}_2(\text{H}_2\text{O})_2(\text{HPO}_3)_3$  (**b**) were synthesized by hydrothermal method. Their crystal structures were determined by X-ray single crystal method (**a**, monoclinic,  $C2/c$  (No.15);  $a=20.820(5)\text{\AA}$ ,  $b=6.717(2)\text{\AA}$ ,  $c=14.123(3)\text{\AA}$ ,  $\beta=101.261(3)$  deg.,  $V=1937.0(8)\text{\AA}^3$ ;  $Z=8$ ; **b**, triclinic,  $P-1$  (No. 2);  $a=8.168(3)\text{\AA}$ ,  $b=8.439(2)\text{\AA}$ ,  $c=9.337(3)\text{\AA}$ ,  $\alpha=115.641(3)$  deg.,  $\beta=98.655(3)$  deg.,  $\gamma=105.124(3)$  deg.,  $V=533.87(1)\text{\AA}^3$ ,  $Z=2$ ). Both crystal structures present three-dimensional open framework structures containing channels, and **a** adopts intersecting type. In the two structures, the face-sharing dimers of  $\text{LaO}_n$  ( $n=8, 9$ ) were observed. Furthermore, both of the two compounds doped with  $\text{Ce}^{3+}$  showed intensive broad emission band around 340nm under UV excitation.



## Flux Synthesis of New Bis(Salicylato)borates

Alex S-F Au-Yeung Mingmei Wu Gavin K-C Wan Herman H-Y Sung Ian D Williams

Chemistry, HKUST

Molten boric acid 'flux' synthesis has been used for the preparation of borate-rich clusters [1] and porous frameworks[2]. We recently found the use of boric acid flux conditions can lead to new bis(salicylato)borate compounds by this HT method, through direct reaction of boric acid and salicylic acids and either inorganic or organic bases. For example use of Li(OH) results in  $\text{Li}[(\text{BSal}_2)(\text{H}_2\text{O})]$  in a new material with a double-chain structure and with potential applicability for Li batteries. Organic molecular salts can also be prepared such as  $[\text{pizp-H}_2][\text{BSal}_2]_2$  (see fig) by reaction of piperazine, salicylic and boric acid. The importance of the flux condition is emphasized since use of hydrothermal conditions through water addition leads to reduced yields and in the organic case the simple salt  $[\text{pizp-H}_2][\text{Sal-H}]_2$  is formed with no boron incorporation.  $[\text{Sal} = (\text{C}_7\text{H}_5\text{O}_2)]^2$



### Reference

1. I. D. Williams, M. Wu, H. H-Y. Sung, X. X. Zhang and J. Yu, Chem. Commun., **1998**, 2463.
  2. J. L. Rowsell, N. J. Taylor, L. F. Nazar, J. Amer. Chem. Soc., **2002**, 124, 6522
- The RGC is thanked for financial support of this work (grant 6043-05)

**Diffusion Path of Oxide Ions in  $\text{La}_{0.64}(\text{Ti}_{0.92}\text{Nb}_{0.08})\text{O}_3$** Roushown Ali<sup>1</sup> Masatomo Yashima<sup>2</sup> Fujio Izumi<sup>1</sup><sup>1</sup>Quantum Beam Center, National Institute for Materials Science<sup>2</sup> Department of Materials Science and Engineering, Tokyo Institute of Technology, Japan<sup>1,2</sup>

Solid oxides that exhibit high ionic conductivity have received special attention in recent years owing to their potential applications in both batteries and fuel cells. To develop and exploit better oxide-ion conductors, we need to understand the mechanism of diffusion of mobile ions at high temperature where the materials work efficiently. In this study, we have studied the crystal structure and pathway of oxide-ion conduction in an A-site deficient perovskite-type oxide,  $\text{La}_{0.64}(\text{Ti}_{0.92}\text{Nb}_{0.08})\text{O}_3$ , at high temperature by neutron powder diffraction.

Densities of coherent-scattering lengths in  $\text{La}_{0.64}(\text{Ti}_{0.92}\text{Nb}_{0.08})\text{O}_3$  ( $P4/mmm$ ) have been determined by whole-pattern fitting based on the maximum-entropy method (MPF) from neutron powder diffraction data measured at 496°C, 1008°C and 1358°C. The combination of RIETAN-2000 and PRIMA were used for MPF. Oxide ions located at a 4*i* site are disordered along <100> and <010> directions. These oxide ions tend to be localized near the 4*i* site with decreasing temperature while they spread over a wide space near the (001) plane. The diffusion path of oxide ions was clearly visualized in a density map obtained for the (001) plane from the diffraction data measured at 1358°C. The equi-density level of the position intermediate between the oxygen atoms was 0.1 fm Å<sup>-3</sup> and 0.05 fm Å<sup>-3</sup> at 1358°C and 1008°C, respectively, whereas it was practically null at 496°C. The appreciable increases in nuclear densities between the oxide ions with increasing temperature shows that oxide ions responsible for ionic conduction migrate near lines connecting these oxide ions.

**In-situ XRD study on the melting process of YBCO thin film with MgO substrate**Qunli Rao<sup>\*</sup> Xin Yao<sup>\*\*</sup>Instrumental Analysis Center, Shanghai Jiao Tong University<sup>\*</sup> Department of Physics, Shanghai Jiao Tong University<sup>\*\*</sup>

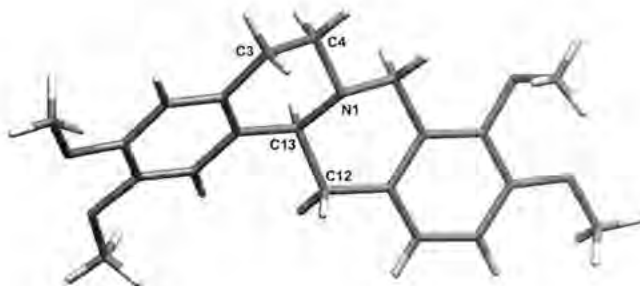
In order to study the superheating phenomenon during the melting process of  $\text{YBa}_2\text{Cu}_3\text{O}_{7-\delta}$  (YBCO) thin films, in-situ XRD measurements were explored around the peritectic temperature ( $T_p$ ) of YBCO with a high temperature sample stage. As the temperature heating up from 850 °C to 1250°C, several phase transformations take place in the YBCO thin-film on an MgO substrate. XRD analysis shows that  $\text{Ba}_2\text{Cu}_3\text{O}_{5.9}$  phase was formed at the temperature 1100°C, which indicates YBCO thin film can be substantially superheated above its  $T_p$  (1050°C). In addition,  $\text{Ba}_2\text{Cu}_3\text{O}_{5.9}$  has a certain oriented relationship with its parent phase YBCO.

## Hydrothermal Crystallization of Salts and Adducts of Tetrahydropalmatine (THP) - A Component From Traditional Chinese Medicine

Fanny L-Y Shek<sup>1</sup> Wan-Yee Wong<sup>1</sup> Herman H-Y. Sung<sup>1</sup> Hong Xue<sup>2</sup> Ian D. Williams<sup>2</sup>

Chemistry, HKUST<sup>1</sup> Department of Biochemistry, HKUST, Hong Kong<sup>2</sup>

Derived from various Traditional Chinese Medicinal herbs, Tetrahydropalmatine THP  $C_{21}H_{25}NO_4$  (below) is a dopamine receptor antagonist used as anti-anxiolytic agent (H. Xue, HKUST 2004). It is a chiral molecule and can occur as both rac and active (-)-form. We have looked at forming salts of this through hydrothermal crystallization, for enhanced stability, solubility and possible chiral resolution of the isomer forms. A wide range of salts have been prepared using various organic acids. Chiral resolution appears possible using D-tartaric acid. Examination of the forms from rac-THP with various benzoic acids shows an interesting solid state pKa phenomenon. For acidic benzoates proton transfer to the nitrogen occurs and a salt is formed, but less acidic ones form a neutral molecular adduct with N---HO H-bond. This switch is found for the 4-Cl and 4-Br derivatives at pKa ca 4.0. Finally hydrothermal reaction allows hydrolytic stability of drug molecules to be assessed. Long time hydrothermal reaction (6d, 110°C) of either rac- or (-)-THP eventually leads to the new oxidation product Dihydropalmatine (DHP)  $C_{21}H_{23}NO_4$  in good yield and purity. The RGC is thanked for financial support of this work (grant HKUST 6084/02P).



## Crystal Structure of the Distorted Pyrochlore $\alpha$ - $\text{Bi}_2\text{Sn}_2\text{O}_7$

Christopher J Howard<sup>1</sup>, Ivana R Evans<sup>2</sup>, John S O Evans<sup>2</sup>, Kevin S Knight<sup>3</sup>

<sup>1</sup>Institute of Materials and Engineering Science, Australian Nuclear Science and Technology Organisation, <sup>2</sup>Department of Chemistry, University of Durham, UK, <sup>3</sup>ISIS Facility, Rutherford Appleton Laboratory, UK

Bismuth stannate,  $\text{Bi}_2\text{Sn}_2\text{O}_7$ , was recognised as a distorted pyrochlore some fifty years ago[1], but a satisfactory crystal structure solution has hitherto proved elusive. At temperatures above about 700C it was thought to have the ideal pyrochlore structure, at lower temperatures a face-centred cubic structure on a doubled (21.4) unit cell, which at room temperature showed a tetragonal distortion to a large (15.08 by 21.5 ) body-centred tetragonal structure[2]. There were various reports in the literature on the higher temperature phases [3,4], but refinements of the room temperature structure in the preferred tetragonal space group  $I-4c2$ , were never satisfactory. Recently, direct space methods were applied to the problem [5]. The structure was solved on the accepted 15.08 by 21.5 tetragonal cell, but turned out to be monoclinic in  $Pc$ , with 176 atoms in the asymmetric unit. A problem evident in this solution, however, is the large number of space group allowed reflections that are not observed. The solution presented here is based on a successful indexing of the X-ray and neutron diffraction patterns on a smaller  $C$ -centred monoclinic cell, implying only 22 atoms in the asymmetric unit. The higher temperature phases need to be re-examined in the light of this work.

### Reference

- [1] R S Roth, J. Res. Natl. Bur. Std 56, 17-25, 1956.
- [2] R D Shannon, J D Bierlein, G A Jones, A W Sleight, J. Phys. Chem. Solids 41, 117-122, 1980.
- [3] R J Jones, K S Knight, J. Chem. Soc. Dalton, 1997, 2551-2555
- [4] B J Kennedy, Ismunander, M M Elcombe, Mater. Sci. Forum 278-281, 762-767, 1998,
- [5] I R Evans, J A K Howard, J S O Evans. J. Mater. Chem. 13, 2098-2103, 2003.

**Molecular Recognition of Aliphatic L-Amino Acids by D-Mandelic acid**Taira Kimino<sup>1</sup> Yukio Takahashi<sup>2</sup> Isao Fujii<sup>1</sup><sup>1</sup>Biological Science and Technology, Tokai University<sup>2</sup> Daito Chemical Co. Ltd.<sup>2</sup>

The production of non-naturally occurring-amino acids has great importance in the pharmaceutical industry. An aqueous solution of racemic compound and optically pure mandelic acid [MAN] has been applied in the diastereomer salt separation. Although MAN is widely used in the resolution of such amino acids, the crystal structures of alanine, phenylalanine and methionine recognized by MAN have only been studied. From the limited information, the MAN molecules have been considered to recognize the hydrophilic groups of amino acid by its hydrophilic groups, and pack in a specific way to form hydrophobic and hydrophilic layers that are well separated. The MAN molecules mainly stabilized the hydrophobic layers by the CH... $\pi$  interactions among phenyl groups and the hydrophobic groups of amino acids.

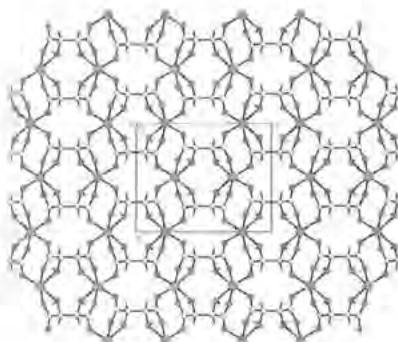
We recently reported that the chiral interface (or surface) between hydrophobic and hydrophilic layers formed by MAN strongly recognizes the chirality of L-cysteine. In this study, we focused to disclose the varieties of chiral interface formed by MAN molecules, especially on the size of hydrophobic pocket. The complexes of L-2-aminobutanoic acid, L-norvaline and L-norleucine with D-MAN were examined by X-ray analysis to disclose the fashion of interactions between the L-amino acids and D-MAN. It reveals that the chiral interface plays an important role for the molecular recognition by MAN, which allows fractional crystallization of the aliphatic chain amino acids.

## Dimensional and Structural Control of Magnesium Tartrate Coordination Polymers

Pokka K-C. Pang John A-K Cha Andy L-F Leung Herman H-Y Sung Alvin W-H Siu Yu-fong Yen Ian D Williams

Chemistry, HKUST

Hydrothermal synthesis of the chiral porous lanthanide tartrates  $[\text{Ln}_2(\text{L-TAR})_3(\text{H}_2\text{O})_3]3\text{H}_2\text{O}$  [1] as well as indium tartrates [2] prompted us to look at the group 2 analogues. Reaction of magnesium acetate with L-tartaric acid, *rac* D/L-tartaric acid or *meso*-tartaric acid under a variety of conditions was studied in-depth and a variety of phase types  $[\text{Mg}(\text{TAR})(\text{H}_2\text{O})_x]\text{H}_2\text{O}_y$  with variable hydration and dimensionality discovered. For L-tartrate at lower temperatures the 2D sheet polymer  $[\text{Mg}(\text{L-TAR})(\text{H}_2\text{O})_2]$  **1** is formed, whilst temperatures to 180°C yield  $[\text{Mg}(\text{L-TAR})]\text{H}_2\text{O}$  **2**, a tetragonal phase with small aquated micropores. Compound **1** smoothly and irreversibly converts to an anhydrous phase  $[\text{Mg}(\text{L-TAR})]$  **3** (see fig) in a single crystal-single crystal transformation. This new phase type **3**, has a different topology from isomeric **2**. Despite the phase diversity all tartrate binding to  $\text{Mg}^{2+}$  is dominated by 1,2-chelation of a carboxylate oxygen and the b-hydroxy group.



### Reference

1. S. Thushari, J.A-K. Cha, H. H-Y. Sung, S. S-Y. Chui, I. D. Williams, *Chem. Commun.*, **2005**, 5515.
2. A. S-F. Au-Yeung, J.A-K. Cha, H. H-Y. Sung, S. S-Y. Chui, I. D. Williams, *Inorg. Chem. Commun.*, **2006**, 9, 507. The RGC is thanked for financial support of this work under grant 6084/02P.

**Structure-Processing-Property Relationships in Monofilament Fibres of Co/Terpolyesters for Use as Absorbable Surgical Sutures**

Jintana Siripitayananon<sup>1</sup>, Robert Molloy<sup>2</sup>, Yodthong Baimark<sup>3</sup>, Geoffrey R. Mitchell<sup>4</sup>

<sup>1</sup>Department of Chemistry, University of Chiang Mai, Biomedical Polymers Technology Unit, Department of Chemistry, Faculty of Science, Chiang Mai University, Chiang Mai 50200, Thailand<sup>2</sup>, <sup>3</sup>Polymer Science Centre, University of Reading, Reading RG6 6AF, UK<sup>4</sup>

Co/terpolymers of L-lactide,  $\epsilon$ -caprolactone and glycolide are biodegradable and have potential for use as absorbable monofilament surgical sutures. Both random and segmented triblock co/terpolymers of various compositions were melt spun at slow speeds into cooled water to obtain almost completely "quenched amorphous" monofilament as-spun fibres. Combinations of hot-drawing and annealing steps under different conditions of rate, temperature and time were employed to increase crystallinity and molecular orientation. The processed fibres were then characterized using DSC and XRD. A novel approach using a series of spherical harmonic functions to represent XRD patterns enabled the molecular orientation to be evaluated. Mechanical (tensile) properties of the fibres were determined and related as far as possible to their physical morphologies. The results showed that the block copolymers had more potential to be developed as absorbable monofilament sutures than the random copolymers. As an example, the tensile strength of an L-lactide :  $\epsilon$ -caprolactone (79:21 mol %) block copolymer fibre tested at 25°C, as obtained from its stress-strain curve, was found to be about 94% of that of a commercial 'PDS II' monofilament surgical suture of similar size (size 2-0) tested under identical conditions.

**Neutron Powder Diffraction Studies in  $\text{CaMn}_{1-x}\text{Cu}_x\text{O}_3$  ( $x = 0, 0.20$ )**S Ravi<sup>1</sup>, Manoranjan Kar<sup>2</sup>, S.M. Borah<sup>3</sup>, P.S.R Krishna<sup>4</sup>

Department of Physics, Indian Institute of Technology Guwahati, Guwahati-781 039<sup>1</sup>, Centre for Nanotechnology, Indian Institute of Technology Guwahati, Guwahati, India<sup>2</sup>, Solid State Physics Division, Bhabha Atomic Research Centre, Mumbai-400 085, India<sup>3,4</sup>

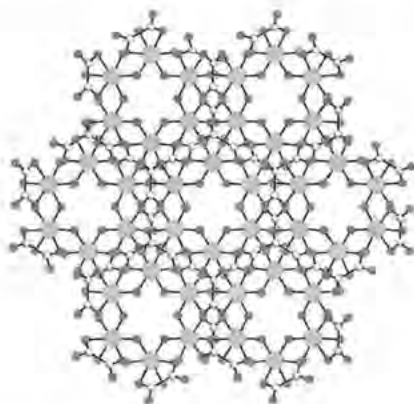
$\text{CaMn}_{1-x}\text{Cu}_x\text{O}_3$  compounds have been prepared in single phase form for  $x = 0$  to 0.30 by following solid state route. The X-ray diffraction (XRD) patterns recorded at room temperature could be analyzed using  $Pbnm$  space group. AC susceptibility measurements show that these materials exhibit antiferromagnetic transitions with Neel temperature  $T_N = 125\text{K}$ . The Neutron Powder Diffraction (NPD) patterns were recorded for  $x = 0$  and 0.20 samples at different temperatures down to 11K. All the observed crystallographic peaks could be refined to  $Pbnm$  space group by using Rietveld refinement technique and no structural transition has been observed down to 11K. The lattice parameters for  $x = 0$  and 0.20 samples at room temperature (300K) are found to be  $a=5.264$ ,  $b=5.275$  &  $c=7.451\text{\AA}$  and,  $a=5.267$ ,  $b=5.280$  &  $c=7.459\text{\AA}$  respectively. An additional peak at  $2\theta = 16.7^\circ$  has been observed below  $T_N$  and its intensity was found to increase with decrease in temperature. It could be indexed to magnetic (101) plane. The magnetic structure has been refined by assuming the propagation vector  $k = (0,0,0)$ , since the magnetic peaks appear exactly on crystallographic plane. The magnetic ordering is found to be G-type arrangement. The magnetic moment of Mn ions was refined and its temperature variation shows a magnetic ordering at  $T = T_N$ . The typical value of magnetic moment of Mn ion is  $2.69\mu_B$  for  $x = 0$  sample at 11K.

## Group 13 Tartrate and Oxalate Hydroxides

Herman H-Y. Sung Alex S-F Au-Yeung Pokka P-K Pang Ian D Williams

Chemistry, HKUST

Hydrothermal synthesis of the chiral porous lanthanide tartrates  $[\text{Ln}_2(\text{L-TAR})_3(\text{H}_2\text{O})_2]3\text{H}_2\text{O}$  [1] prompted us to look at the chemistry of the group 13 analogues. Hydrothermal reaction of indium hydroxide or acetate with L-tartaric acid or racemic D/L-tartaric acid at  $160^\circ\text{C}$  for 2 days affords respectively **1**  $[\text{In}(\text{L-TAR})\text{H}_2\text{O}]0.5\text{H}_2\text{O}$  which contains tartrate trianions and has a 2D structure and **2**  $[\text{In}(\text{OH})(\text{D/L-TAR})]$ , with a microporous 3D framework that undergoes phase transformation at *ca.*  $150^\circ\text{C}$ . [2] Starting from indium nitrate and L-tartaric acid under similar conditions afford the novel microporous phase  $[\text{In}(\text{OH})(\text{C}_2\text{O}_4)(\text{H}_2\text{O})]$  **3**. This has an open 3D structure with microchannels along the hexagonal *c*-axis. The gallium analog is related and also non-centric  $P6_3$  but has an anhydrous framework  $[\text{Ga}(\text{C}_2\text{O}_4)(\text{OH})]$  **4**. (see fig) The properties of these phases and their preparation directly from oxalic acid are under investigation.



### Reference

1. S. Thushari, J.A-K. Cha, H. H-Y. Sung, S. S-Y. Chui, I. D. Williams, *Chem. Commun.*, **2005**, 5515.
2. A. S-F. Au-Yeung, J.A-K. Cha, H. H-Y. Sung, S. S-Y. Chui, I. D. Williams, *Inorg. Chem. Commun.*, **2006**, *9*, 507.

The RGC is thanked for financial support of this work (grant 6084/02P)

## Molecular Packing and Intermolecular Interactions in Chitosan/Hydrogen Halides Complexes

Keiichi Noguchi<sup>1</sup> Masakazu Kanenari<sup>2</sup> Kenji Okuyama<sup>3</sup> Kozo Ogawa<sup>4</sup>

Instrumentation Analysis Center, Tokyo University of Agriculture and Technology<sup>1</sup> Faculty of Technology, Tokyo University of Agriculture & Technology<sup>2</sup> Graduate School of Science, Osaka University<sup>3</sup> Research Institute for Advanced Science and Technology, Osaka Prefecture University<sup>4</sup>

In order to elucidate the intermolecular interactions involved in complex formation of chitosan with hydrogen halides, crystal structures of chitosan/HBr and chitosan/HI complexes were analyzed based on X-ray fiber diffraction data collected using synchrotron radiation source (BL40B2, SPring-8, Hyogo, Japan). The packing models were refined using the linked-atom least-squares method. The final *R*-values were 0.192 for 93 observed spots (HBr complex) and 0.193 for 44 observed spots (HI complex). Both crystals are isomorphous and belong to the space group *P*21. The unit cell constants are *a* = 9.299(9), *b* = 9.504(8), *c*(fiber axis) = 10.41(1) Å and  $\beta$  = 106.93(8) deg, and *a* = 9.46(2), *b* = 9.72(2), *c*(fiber axis) = 10.33(2) Å and  $\beta$  = 105.1(2) deg for HBr and HI complexes, respectively. The chitosan chain adopts 2/1-helical structure that is a typical conformation for  $\beta$ -D-(1 $\rightarrow$ 4)-linked polysaccharides. The unit cell contains four glucosamine residues (two polymer chains) and four halide ions. The halide ions are aligned along the *c*-axis at intervals of about 5Å and are surrounded by four polymer chains. In an asymmetric unit, there are two halide ions. One ion accepts three hydrogen bonds from N2 nitrogen atoms. The other one participates in one hydrogen bond from N2 and two hydrogen bonds from O6 oxygen atoms. In addition, the chitosan chains are linked by N-H...O and C-H...O hydrogen bonds along the *b*-axis. In the hydrated form of chitosan, water molecules form a columnar structure along the chain direction. The sites of halide ions in the complex crystals are similar to those of the water molecules in the hydrated form. Therefore, it was suggested that the water column was used as a path of halide ions during the complex formation.

## Synthesis, characterization, and DFT calculations of iridium(III) complexes with tolylterpyridine

Naokazu Yoshikawa<sup>\*</sup> Shinichi Yamabe<sup>\*\*</sup> Hiroshi Takashima<sup>\*</sup> Keiichi Tsukahara<sup>\*</sup> Nobuko Kanehisa<sup>\*\*\*</sup> Yasushi Kai<sup>\*\*\*</sup>

Chemistry, Nara Women's University<sup>\*</sup> Department of Chemistry, Nara University of Education<sup>\*\*</sup> Department of Applied Chemistry, Graduate School of Engineering, Osaka University<sup>\*\*\*</sup>

Three polypyridine iridium(III) complexes in the form of  $[\text{IrCl}(\text{L})(\text{tterpy})]^{2+}$  were newly prepared (L=phen (**1**), dpphen(**2**), and dmbpy(**3**)). Reference complexes  $[\text{IrCl}(\text{bpy})(\text{tterpy})]^{2+}$  (**4**) and  $[\text{Ir}(\text{L})_2]^{3+}$  (L= tterpy (**5**) and terpy (**6**)) were also prepared. They were synthesized by using a microwave oven and were characterized by ESI MS, UV-vis spectroscopy, and cyclic voltammograms(CV). Abbreviations of the ligands are phen = 1,10-phenanthroline, dpphen = 4,7-diphenyl-1,10-phenanthroline, bpy = 2,2'-bipyridine, dmbpy = 4,4'-dimethyl-2,2'-bipyridine, tterpy = 4'-(4-tolyl)-2,2':6',2"-terpyridine and terpy= 2,2':6',2"-terpyridine. The X-ray structures of the two complexes, **5**, and **6** were also obtained. In CV, all the  $[\text{IrCl}(\text{L})(\text{tterpy})]^{2+}$  complexes showed that the first reduction occurred at around -1.27 V, which was attributed to the reduction of tterpy ligand in  $[\text{IrCl}(\text{L})(\text{tterpy})]^{2+}$ . The electronic properties of **3**, **5**, and **6** complexes were studied using the B3LYP functional. Optimized geometries were compared to the experimentally observed structures. Excited triplet and singlet states were examined using time-dependent density functional theory (TDDFT). The calculated energies of the lowest triplet state and lowest singlet state in the two complexes were in good agreement with experimental absorption spectra. All complexes in the form of  $[\text{IrCl}(\text{L})(\text{tterpy})]^{2+}$  showed that LUMOs were localized on the tterpy ligand. It was found that  $[\text{IrCl}(\text{L})(\text{tterpy})]^{2+}$  emitted an intense phosphorescence at room temperature. The spectroscopic and electrochemical results were discussed correlatively.

## Correlations between interface structures and magnetic properties of Co/Cu multilayers sputter-grown on Ta buffers

Kotaro Ishiji Hiroo Hashizume

Photon Factory, High Energy Accelerator Research Organization

Interface structures are a crucial factor influencing the magnetic properties of metal multilayers. For magnetic applications, large magnetoresistance (MR) ratio and low saturation field are desirable. To investigate the correlation between interface structures and magnetic properties, we prepared five Co/Cu multilayers on Ta buffer of varying thickness  $t_{Ta}$  = 30-500 nm by a magnetron sputtering. As  $t_{Ta}$  grows, the buffer surface becomes rough, which is duplicated onto the Co/Cu interface. We thus controlled the roughness,  $\sigma_{Co/Cu}$ , from 0.6 to 1.0 nm in rms values. With increasing  $\sigma_{Co/Cu}$ , the peak MR ratio decreases, but the rate of decrease is not uniform (Fig. 1). AFM images of the buffer surfaces show that the abrupt decrease of the peak MR ratio and coupling energy  $J$  in the 0.7-0.9 nm range of  $\sigma_{Co/Cu}$  is concomitant with the growth of large grains of 80-100 nm in in-plane size. It is considered that superparamagnetic particles and the orange peel effect are produced by the presence of the grain.

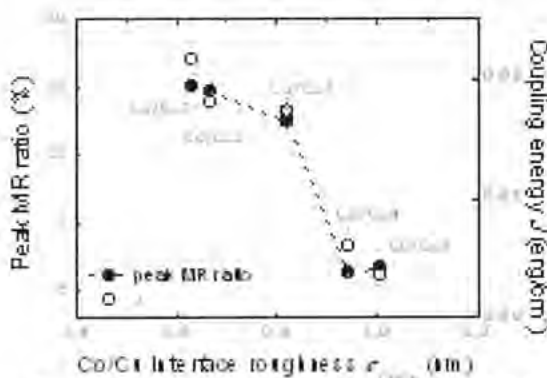


Fig. 1 Variations of peak MR ratio and interlayer coupling energy  $J$  with interface roughness  $\sigma_{Co/Cu}$  for multilayered Co/Cu.

## Preliminary report on the photo emission of spin crossover complexes

Yu-Chun Chuang<sup>†</sup> Jin-Ming Chen<sup>\*\*</sup> Yu Wang<sup>‡</sup>

Department of Chemistry, National Taiwan University<sup>†</sup> National Synchrotron Radiation Research Center, Hsinchu, Taiwan<sup>\*\*</sup>

Spin crossover (SCO) complexes are considered to be one of the potential molecular switch materials. The spin state of the metal ion in such complexes could be switched between high spin (HS) and LS (low spin) state by changing in temperature, pressure or by light irradiation. The Light induced excited spin state trapping (LIESST) phenomenon is associated with pumping electron from LS to metastable HS state with laser irradiation of proper wavelength. Such phenomenon is our special concern due to its potential applications in the future. Evolutions of electronic configuration accompanied with spin transitions were studied for several Fe SCO systems by x-ray absorption spectroscopy at both Fe K- and L-edge. The  $L_{2,3}$ -edge XAS is a powerful fingerprint of the electronic structure for 3d-transition-metal center. An unexpected excitation to HS state was recorded at ca. 8K with soft x-ray irradiation. Similar finding was reported before, where they propose a so called "SOXIESST" (soft X-ray induced excited spin state trapping) process. Nevertheless, the energy is too high to be fitted in the same scheme for the LIESST scheme, where the excitation is mainly through the metal ligand charge transfer band. The photo emission spectrum out of the soft x-ray excitation on the system is therefore designed in order to unravel the mechanism of the LS to HS process. An emission peak at about 430nm is observed at 8K for three different Fe SCO complexes. In addition, the emission spectrum seems highly dependent on the intensity of the incident beam. We therefore propose that the emission line at 430 nm is the one which is responsible for the LIESST process. Detail analysis for the emission spectra will be discussed.

## Liquid structure and mechanical properties of EHD fluid

Yuusuke Imai Hiroshi Abe Yoshiki Sasaki

Department of Materials Science and Engineering, National Defense Academy

Electrohydrodynamics (EHD) phenomenon is known to be liquid convection caused by applied electric field. In particular, the convection depends on the applied voltage and inhomogeneous electric field. In spite of experimental progress, mechanism of EHD convection is still unclear. Therefore, we clarify the liquid structure under high voltage by X-Ray diffraction method. For instance, it is considered that the intermolecular interaction plays an important role with macroscopic convection of EHD fluids.

In this study, we measured X-Ray diffraction patterns of EHD fluids, which are molecular liquids as an insulator. The liquids possess high performance as an actuator. In NMR experiment, each molecular liquid had isomer obviously. It is possible to form cluster under high voltage in two kinds of isomer.

In X-Ray diffraction method, the scattered intensities increased with increasing the applied voltage, although X-Ray diffraction patterns were similar to each other. At least, it is predicted that cluster population is proportional to the applied voltage.

## Spin crossover phenomenon of $\mu$ -bpt dinuclear one- dimensional complexes with different bridge ligands

Szu-Miao Chen Yu Wang Sheu Chou Fu Chen Ko Wa Lee Gene Hsiang

Department of Chemistry, National Taiwan University

$[\{\text{Fe}^{\text{II}}(\mu\text{-bpt})(\text{NCS})\}_2(\text{bipy}) \text{CH}_3\text{OH}]$  (bpt = 3,5-bis(pyridin-2-yl)-1,2,4-triazole) synthesized successfully by one-step solvo-thermal syntheses represents the first example of an one dimensional dinuclear iron(II) spin-crossover compound which exhibits an abrupt two-step spin transition at 130 K. The zigzag chain structure containing a dinuclear Fe complexes bridged by 4,4'-bipy ligand. It has only one unique Fe site in the asymmetric unit. However, when it undergoes a spin transition, the spin transition corresponds to only half of the total amount of Fe content. The unit cell doubled at and below 130 K, thus two Fe centers can be different, namely a [HS -LS] pair of Fe(II) dinuclear complexes in the asymmetric unit. The LIESST phenomenon was observed with proper light irradiation (532 nm, power 10 mW cm<sup>-2</sup>) at 25 K. It is characterized with XRD, XANES, IR spectra and SQUID. The typical change of  $-0.2 \text{ \AA}$  in Fe-N bond lengths is also observed during the LIESST process.

The other similar one-dimensional zigzag dinuclear Fe(II) complex bridged by a shorter ligand, pyrazine,  $[\{\text{Fe}^{\text{II}}(\mu\text{-bpt})(\text{NCS})\}_2(\text{pyrazine})]$  is also synthesized and characterized. The complex shows quite different magnetic property, in which the spin transition takes place gradually at  $T_c \sim 120 \text{ K}$ . The structures of this complex both at HS and at LS state will be presented. The comparison between these two dinuclear complexes as well as other similar structures will be discussed.

**Effect of Hot-Drawing on Morphology and Mechanical Property Development in Random and Block Terpolyester Fibres base on L-Lactide,  $\epsilon$ -Caprolactone and Glycolide**

Wasinee Channuan<sup>\*</sup> Jintana Siripitayananon<sup>\*</sup> Robert Molloy<sup>\*</sup> Geoffrey R Mitchell<sup>\*\*</sup>

Biomedical Polymers Technology Unit, Department of Chemistry, Chiang Mai University<sup>\*</sup>  
Department of Physics and Polymer Science Centre, University of Reading, UK<sup>\*\*</sup>

Terpolymers of L-lactide (LL),  $\epsilon$ -caprolactone (CL) and glycolide (G) were synthesized for use as absorbable surgical sutures. Random ( $M_w = 61,000$ ) and block terpolymers ( $M_w = 47,000$ ) with a composition ratio of LL:CL:G  $\approx$  75:20:5 mol % were studied for comparison. The crystallization behaviour of the terpolymers was investigated by 4-circle X-ray diffractometry, optical microscopy, and confirmed by DSC. The results showed that the block terpolymer crystallized at a higher rate of about twice that of the random due to the greater regularity of its end-blocks but gave approximately the same maximum level of crystallinity. As-spun fibres of the terpolymers produced by melt spinning were almost completely amorphous with low crystallinity and molecular orientation. Hot-drawing under various conditions was employed to improve their mechanical properties. The analysis results from WAXD and DSC demonstrated that hot-drawing to a higher draw ratio induced molecular orientation and crystallization without any changes in the crystal structure within the fibre. The lamellar thickness of both terpolymers was invariant while the width increased with draw ratio, although the random fibre contained thinner crystallites. From mechanical testing, all tensile properties of the block terpolymer hot-drawn fibres were found to be better than those of the random fibres. The superior tensile strength of the block terpolymer fibre was attributed to its larger crystal size, higher crystallinity, lamellar stack structure, and greater molecular orientation in both the crystalline and amorphous phases.

## Structural and magnetic studies of atr-based 1-D, 2-D, 3-D frameworks

Wei-Lun Ho<sup>\*</sup> Gene-Hsiang Lee<sup>\*</sup> Hwo-Shuenn Sheu<sup>\*\*</sup> Yu Wang<sup>\*</sup>

Department of Chemistry, National Taiwan University<sup>\*</sup> National Synchrotron Radiation Research Center, Hsinchu, Taiwan<sup>\*\*</sup>

New iron(II) coordination polymers, 1-D  $\{[\text{Fe}(\text{atr})_2(\mu\text{-atr})(\text{H}_2\text{O})_2](\text{BF}_4)_2 \cdot 4\text{H}_2\text{O}\}_n$  atr = trans-4,4'-azo-1,2,4-triazole), 2-D  $\{\text{Fe}(\mu\text{-admtr})(\mu\text{-}4,4'\text{-bipyridine})(\text{NCS})_2\}_n$  (admtr= trans-4,4'-azo-3,5-dimethyl-1,2,4-triazole) and 3-D  $\{[\text{Fe}(\mu\text{-atr})_3](\text{BF}_4) \cdot 2\text{H}_2\text{O}\}_n$  have been synthesized and characterized. The crystal structure of 1-D and 3-D compounds have similar formula, but contain two types of coordination: In 1-D compound the coordination of Fe contains two water, two terminal atr ligands, and one bridging atr ligand, while in 3-D compound the metal coordination contains three bridging atr ligands between iron centers, resulting in an interpenetrated structure. Powder X-ray Diffraction of dehydrated 1-D compounds shows that it actually turns into 3-D structure, which is confirmed by the corresponding magnetic behavior being changed from paramagnetic to a spin crossover at 290K. We can also presume that the path of structural transformation from the 1-D and 3-D crystal structure.

In another 2-D structure, the Fe coordination contains one methyl-substituted atr bridging ligand, one 4-4'-bipyridine bridging ligand, and two NCS anions. The 2-D compound shows a structural phase transition at 105K. At room temperature, the iron is at the center of inversion ( $Z=1$ , in  $P-1$ ), while at 120K, it is not ( $Z=2$ , in  $P-1$ ) with  $c$ -axis doubled. The SQUID measurement indicates that there is a weak ferromagnetic interaction below 50K.

## **Fabrication and characterization of Electrodeposited Aluminum Nanocrystalline**

Delphic Chen Han-Hong Wang Jui-Chao Kuo

Department of Materials Science and Engineering, National Cheng Kung University

In this study, nanocrystalline aluminum was prepared by direct current electrodeposition method. The aluminum chloride and dimethylsulfone mixture were used as the electrolyte for the electrodeposition process. The influence of current density did on the electrodeposited layers was discussed in this study. The grain size of the electrodeposited layer produced by different current density was calculated from the broadening peak of the Xray diffraction peak with Scherrer's Formula. On the other hand, the microstructure of the electrodeposited layer was determined by the Xray diffraction and further texture analysis was conducted by pole figure analysis. The elemental composition of the electrodeposited layer was examined with the EDS and the surface was observed by the SEM. Microvickers test was used to determine the hardness of the sample from different current density conditions. In addition to the above analyses, the morphology of coatings was investigated by using nano-focus.

## Magnetic structural study of Co-doped barium ferrites by the RXMS method

Maki Okube<sup>1</sup>, Seiji Ohsawa<sup>2</sup>, Satoshi Sasaki<sup>1</sup>, Takeharu Mori<sup>3</sup>, Takeshi Toyoda<sup>4</sup>

<sup>1</sup>Materials and Structures Laboratory, Tokyo Institute of Technology<sup>1</sup>, Interdisciplinary Graduate School of Science and Engineering, Tokyo Institute of Technology, Japan<sup>2</sup>, Photon Factory, Institute of Materials Structure Science, KEK, Japan<sup>3</sup>, Industrial Research Institute of Ishikawa, Japan<sup>4</sup>

Resonant X-ray magnetic scattering (RXMS) has attracted much interest as a useful tool to determine the magnetic structures associated with specific electronic states. The magnetic resonance even at the  $K$  absorption edge is useful to arise from the spin-orbit coupling. We have carried out synchrotron RXMS studies for single crystals of ferrimagnetic M-type barium ferrites at the Fe  $K$  edge at the BL-3A of Photon Factory. Diffraction experiments at  $\lambda = 1.7406 \text{ \AA}$  ( $E = 7122.8 \text{ eV}$ ) gave a magnetic satellite peak for  $0\ 0\ 8+(2/3)$  of  $\text{BaCoTiFe}_{10}\text{O}_{19}$  at  $T = 100 \text{ K}$ , which disappeared at  $200 \text{ K}$ . It was interpreted from the neutron work as a magnetic helix propagated along the hexagonal  $c$  axis. This shows that magnetic intensity can be resonantly excited at the Fe  $K$ .

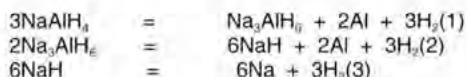
M-type barium ferrite has five independent Fe sites in a hexagonal-ferrite structure, which are well described as a sequence of spinel  $fcc$  block of  $(\text{Fe}_6\text{O}_8)^{2+}$  and  $hcp$  block of  $(\text{BaFe}_2\text{O}_{11})^{2-}$ . In this study, the crystal structure with spin orientation has been determined based on the difference between observed and calculated asymmetry ratios. Diffraction profiles were measured with right- and left-circularly polarized X-rays at  $\lambda = 1.7406$  and  $1.7390 \text{ \AA}$ . A diamond (001) phase retarder was used to produce the circular polarization near the 111 Bragg condition in the asymmetric Laue case. The observed asymmetrical ratios  $DR_{\text{obs}}$  were obtained through the RXMS measurements. The structure factors and  $DR_{\text{calc}}$  was estimated through magnetic structural models by related to the charge, resonant, magnetic and resonant magnetic scatterings for more than 30 Bragg reflections. Finally, the spin orientations were evaluated through the difference of  $DR_{\text{obs}} - DR_{\text{calc}}$ .

## Hydrogen Desorption and Absorption Process of NaAlH<sub>4</sub> and Modified NaAlH<sub>4</sub>

Chattree Phurat<sup>\*</sup> Nongnuj Muangsin<sup>\*</sup> Pramoch Rangsunvigit<sup>\*\*</sup> Santi Kulprathipanja<sup>\*\*\*</sup> Yindee Suttisawat<sup>\*\*</sup>

Chemistry, Chulalongkorn<sup>\*</sup> Petroleum and Petrochemical College, Chulalongkorn University<sup>\*\*</sup>  
UOP LLC<sup>\*\*\*</sup>

NaAlH<sub>4</sub> doped with 4mol% of HfCl<sub>3</sub> showed the maximum hydrogen capacity of 5.5wt%. It was obtained from the first desorption and dropped to 2.2-2.6wt% after that. The drawback of the doped-NaAlH<sub>4</sub> is the reported loss of stability upon cycling. The reason for this seems to be due to the incomplete rehydrogenation in the second step (Na<sub>3</sub>AlH<sub>6</sub> to NaAlH<sub>4</sub>). This, in turn, might be explained by (i) the reduction availability of Al due to the formation of large Al crystallites, possibly accompanied by coating of the Al particles by NaAlH<sub>4</sub> and (ii) the formation of Hf-Al alloy, resulting in its reduced effectiveness. In this work, we purpose to reduce the formation of Hf-Al alloy and large Al crystallites by adding porphyrins Al/Hf complex into the doped sodium alanate system. The mechanism and result of hydrogen desorption/absorption were investigated by X-ray diffraction and Rietveld refinement method.



### Reference

- [1] B. Bogdanovic, M. Schwickardi, *J. Alloys Comp.* 1(1997), 253-254.
- [2] D. Sun, S.S. Srinivasan, G. Chen, C. Jensen, *J. Alloys Comp.* 373(2004), 11-2, 265-269.
- [3] A.G. Haiduc, H.A. Stil, M.A. Schwarz, P. Paulus, J.J.C. Geerlings, *J. Alloys Comp.* 393(2005), 252-263.

**Small imperfection causes a very small molecule to pack in a very large cell: Sodium saccharinate 1.875 hydrate with unit cell of 15.6 nm<sup>3</sup>**

Pance Naumov<sup>1</sup> Gligor Jovanovski<sup>2</sup> Orhideja Grupce<sup>3</sup> Branko Kaitner<sup>4</sup> David A. Rae<sup>5</sup> Seik Weng Ng<sup>6</sup>

ICYS, National Institute for Materials Science<sup>1</sup> Institute of Chemistry, Faculty of Science, Sts. Cyril and Methodius University, Skopje, Macedonia<sup>2</sup> Department of Inorganic Chemistry, University of Zagreb, Zagreb, Croatia<sup>3</sup> Australian National University, Caberra, Australia<sup>4</sup> Department of Chemistry, University of Malaya, Malaysia<sup>5</sup>

The structure of the common artificial sweetener sodium saccharinate, with one of the largest unit cells for a small, nearly planar organic anion such as the saccharinate, was determined for the first time from laboratory X-ray diffraction data. The formally  $^{15/8}$  hydrate crystal is composed of 64 formula units and represents an eight-fold occupational and displacive modulation of a  $C2/m$  parent structure with 8 formula units. The lack of one water molecule in the hypothetical dihydrate crystal  $\text{Na}(\text{C}_7\text{H}_4\text{NO}_3\text{S}) \cdot 2\text{H}_2\text{O}$  and the respective structural misfit result in eight-fold expansion of the aperiodicity and the formula  $\text{Na}_{64}(\text{C}_7\text{H}_4\text{NO}_3\text{S})_{64} \cdot 120\text{H}_2\text{O}$ . Due to the extensive disorder, the compound can be considered a frozen intermediate state between complete disorder of a concentrated solution of the salt and the completely ordered triclinic  $\text{Na}(\text{C}_7\text{H}_4\text{NO}_3\text{S}) \cdot 2/3\text{H}_2\text{O}$ , which crystallizes as stable hydrate from ethanol.

**Reference**

P. Naumov, G. Jovanovski, O. Grupce, B. Kaitner, A. D. Rae, S. W. Ng, *Angew. Chem., Int. Ed. Engl.* 2005, **44**, 1251.

**Pressure-induced structure transition and the pressure dependence of electron density distribution in BaTiO<sub>3</sub> and PbTiO<sub>3</sub> perovskite ferroelectrics**Hiroaki Sugita<sup>1</sup> Hiroshi Matsumura<sup>1</sup> Takamitsu Yamanaka<sup>2,3</sup> Yuki Nakamoto<sup>2,3</sup><sup>1</sup>Department of Earth and Space Science, Graduate School of science, Osaka University<sup>2</sup> Center for Quantum Science and Technology under Extreme Conditions, Osaka University, Japan<sup>3</sup>

BaTiO<sub>3</sub> and PbTiO<sub>3</sub> perovskite are known as ferroelectrics at ambient conditions, and are used as electronic materials in various fields. Both have phase transitions by applying pressure, from tetragonal structure (*P4mm* *Z*=1) to cubic structure (*Pm3m* *Z*=1). The former is a ferroelectric phase, and the latter a paraelectric phase.

In order to understand a change of a dipole moment, dielectric efficiency and dielectric capability under high-pressure or low-temperature conditions, we carried out electron density analysis by single crystal diffraction experiment using synchrotron radiation and diamond-anvil cell (DAC).

BaTiO<sub>3</sub> and PbTiO<sub>3</sub> single crystals are synthesized by a flux method. We used a modified Merrill and Bassett type DAC for generating pressure. We conducted single-crystal X-ray diffraction experiment at ambient temperature under pressure from 0.0001GPa to 5GPa in BaTiO<sub>3</sub>, from 0.0001GPa to 9.3GPa in PbTiO<sub>3</sub>. Moreover in BaTiO<sub>3</sub>, we executed an experiment at low temperatures (20°C--170°C) and ambient pressure, and further at various low temperature under compression.

We determined a dipole moment by electron density and radius distribution between atoms at each pressure. This study revealed a pressure dependence of anisotropy of a dipole moment of BaTiO<sub>3</sub> accompanied by successive phase transitions; cubic to tetragonal to orthorhombic to rhombohedral at low temperatures.

## Hydrogen bonding in two solid phases of phenazine-chloranilic acid (1/1) determined at 170 and 93 K

Kazuma Gotoh<sup>1</sup> Tetsuo Asaji<sup>2</sup> Hiroyuki Ishida<sup>1</sup>

<sup>1</sup>Department of Chemistry, Faculty of Science, Okayama University <sup>2</sup>Department of Chemistry, College of Humanities and Sciences, Nihon University<sup>3</sup>

Horiuchi et al. [1, 2] have revealed that the title compound,  $C_{12}H_8N_2 \cdot C_6H_2O_4Cl_2$ , has a ferroelectric phase (space group  $P2_1$ ) below 253 K, in which the phenazine and chloranilic acid molecules are arranged alternately through O-H...N hydrogen bonds to form a one-dimensional supramolecular structure. Recently, Saito et al. [3] reported two phase transitions at 136 and 146 K by heat capacity measurements. The low temperature phases were also detected by NQR measurements [4, 5]. In the present study, we have determined the crystal structure in the low-temperature phase stable below 136 K and re-determined the structure in the ferroelectric phase in order to clarify the hydrogen bonding scheme in each phase. In both phases the compound crystallizes in the space group  $P2_1$ . These structures are essentially same, except for the H atoms involved in the hydrogen bonds formed between the base and the acid. In the ferroelectric phase, H atoms in the hydrogen bonds are attached to O of the acid as reported by Horiuchi et al., but one H atom (H4) was found to have a considerably large  $U_{iso}$  value compared to that of the other H atom (H2), suggesting that atom H4 is disordered in the hydrogen bond. On the other hand, in the low temperature phase the H atom corresponding to atom H4 was found to be attached to N, which implies that proton transfer of one of the two H atoms of the acid to the base occurs in this phase.

### Reference

- [1] Horiuchi et al. (2005). *Nat. Mater.* 4, 163-166.
- [2] Horiuchi et al. (2005). *J. Am. Chem. Soc.* 127, 5010-5011.
- [3] Saito et al. (2006). *J. Phys. Soc. Jpn.*, 75, 033601-1-3.
- [4] Asaji et al. (2006). *J. Mol. Struct.* 791, 89-92.
- [5] Watanabe et al. (2006). Annual Meeting of Chem. Soc. Jpn., Tokyo, Japan, 2PC-021.

## A new 3-D incommensurate structure in the Bi-Re-O system

Neeraj Sharma Chris D Ling

School of Chemistry, University of Sydney

Here we report the discovery and characterisation of a new phase in the Bi-Re-O system that exhibits rare three-dimensionally incommensurate structural and compositional modulations. The phase has the cubic fluorite-type substructure of the high-temperature form of bismuth oxide,  $d\text{-Bi}_2\text{O}_3$ . Rhenium becomes the latest in a series of transition metal dopants known to give rise to 3-D incommensurate modulations in bismuth oxides, the others being Nb(V), Ta(V), Mo(VI), and Cr(VI)[1],[2],[3]. Electron and X-ray powder diffraction data indicate a modulation vector of  $\sim 0.29 < 111 >^*_{\text{F}}$ , and energy-dispersive X-ray analysis using scanning electron microscopy indicate a Bi-Re ratio of  $\sim 5.9:1$ . These results suggest that the new phase has more in common with the Mo(VI) and Cr(VI) doped bismuth oxides than with the Nb(V) and Ta(V) cases, suggesting an oxidation state of Re(VI). This is backed up by magnetic susceptibility data that shows a weak antiferromagnetic signal below  $\sim 150$  K, attributable to interactions among the single unpaired  $d$  electrons of Re(VI). Further investigations to confirm the valence state of rhenium are ongoing and will be presented along with further structural data.

### References

1. R. L. Withers, et al.  
*Atomic Modulation Functions, Periodic Nodal Surfaces and the three-dimensional incommensurately modulated  $(1-x)\text{Bi}_2\text{O}_3 \cdot x\text{Nb}_2\text{O}_5$ ,  $0.06 < x < 0.23$ , solid solution.*  
*Z. Kristallogr.*, 1999. **214**: p. 296-304.
2. C. D. Ling, et al.  
*A review of bismuth-rich binary oxides in the systems  $\text{Bi}_2\text{O}_3\text{-Nb}_2\text{O}_5$ ,  $\text{Bi}_2\text{O}_3\text{-Ta}_2\text{O}_5$ ,  $\text{Bi}_2\text{O}_3\text{-MoO}_3$ , and  $\text{Bi}_2\text{O}_3\text{-WO}_3$ .*  
*J. Solid State Chem.*, 1998. **137**: p. 42-61.
3. M. Valldor, et al.  
*A new high-temperature cubic fluorite-type phase  $\text{Mo}_{0.16}\text{Bi}_{0.84}\text{O}_{1.74}$  with a rare 3-D incommensurate modulation.*  
*J. Solid State Chem.*, 2000. **152**: p. 573-576.

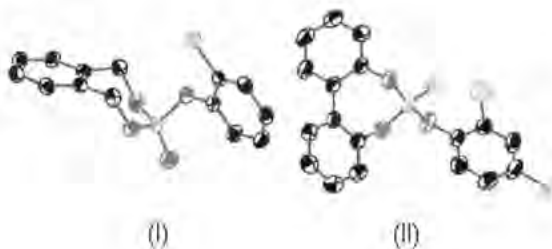
## Molecular structure of Novel Pesticides: Substituted Benzo and Dibenzo [d,f] [1,3,2] dioxaphosphopin 3-oxide (1) and 6-sulphide(11).

Musali Krishnaiah<sup>1</sup> Jadaprolu Radhakrishna<sup>2</sup> Reddy Suresh C<sup>3</sup> Puranik Vedavati G<sup>4</sup>

<sup>1</sup>Department of Physics, Sri Venkateswara University, Tirupati<sup>2</sup> Department of Physics, Sri Venkateswara University, Tirupati - 517 502<sup>3</sup> Department of Chemistry, Sri Venkateswara University, Tirupati - 517 502<sup>4</sup> Center For Materials Characterisation, National Chemical Laboratory, Pune<sup>5</sup>

Organophosphorus heterocycles with phosphoryl unit exhibit significant physiological activity depending on their size, electrophilic character of phosphorus, the strength of the bond p-x and steric nature of the substituents. These compounds find applications as pesticides, nerve gases, antioxidants and as stabilizers in polymer and oil industries. The structures P2,<sub>c</sub> & P2,<sub>n</sub> of the title compounds are determined to know the effect of substituents on the conformation of dioxaphosphepine ring.

The dioxaphosphepine rings exhibit twist - chair form for the former where as a distorted boat conformation for the later. Fusion of the phosphepine ring to the biphenyl system causes strain, as evidenced by both widening and compression of the endocyclic angles in the heterocyclic ring.



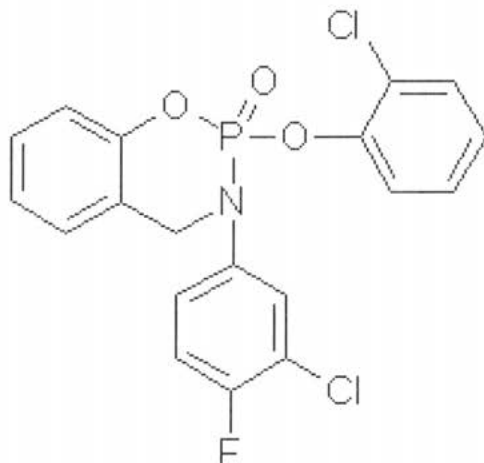
## Crystal and Molecular Structure of 2-(2''-chlorophenoxy)-3,4-dihydro-3-(3'-chloro-4'-fluorophenyl)-2H-[1,3,2] benzoxazaphosphorin 2-oxide

Radha Krishna Jadaprolu<sup>1</sup> Krishnaiah Musali<sup>2</sup> Y.B Kiran<sup>3</sup> Reddy Devendranath C<sup>4</sup> win Thetmar<sup>5</sup> Kannig P<sup>6</sup>

Department of Physics, Sri Venkateswara University, Tirupati<sup>1</sup> Department of Physics, S.V. University, Tirupati, India<sup>2</sup> Department of Chemistry, S.V. University, Tirupati, India<sup>3</sup> Department of Physics, Yangon University, Myanmar<sup>4,5,6</sup>

Orgnophosphorus compounds are widespread in nature and they have unique multifaceted applications as insecticides, anticancer agents and lubricating oil additives and polymer stabilizers. The title compound has both antimicrobial and pesticidal activity, which promoted us to undertake crystal structure determination to know the influence of the substituents on the conformation of the heterocyclic ring.

In the title compound  $C_{19}H_{13}Cl_2FN O_3P$ , the six-membered phosphorin ring exhibits a sofa conformation with phosphoryl O atom occupying an equatorial and chlorophenoxy group in an axial position. The P=O distance is 1.446(2)Å and the average length of the three P --- O bonds is 1.574(2) Å. The chlorophenoxy ring is oriented at an angle of 36.2(1) to the heterocyclic phosphorin ring. Crystals obtained from 2-propanal by slow evaporation are monoclinic, space group  $P2_1/n$  with cell parameters  $a=6.731(2)$ ,  $b=18.652(3)$  and  $c=15.045(3)$  Å;  $\beta=101.9(3)$ ,  $V=1847.7(7)$  Å<sup>3</sup>. The structure was solved by direct methods and refined by full matrix least squares using SHELXL-97 to final values of  $R = 0.0598$  and  $R_w = 0.1642$ .

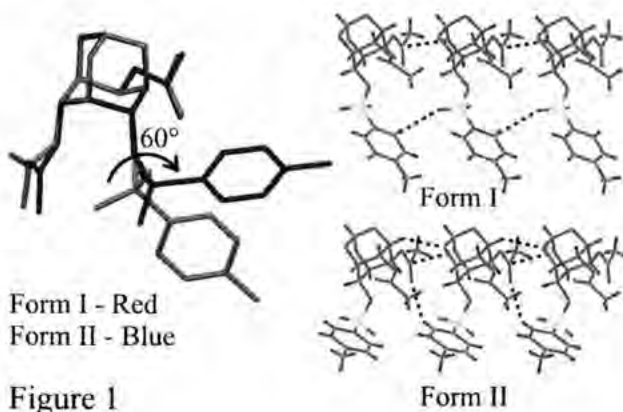


## Identical One Dimensional Molecular Assembly in Conformational Polymorphs of Racemic 2,4-di-*O*-Acetyl 6-*O*-Tosyl -*myo*-Inositol 1,3,5-Orthoformate

K Manoj<sup>1</sup> R G Gonnade<sup>1</sup> M M Bhadbhade<sup>1</sup> M S Shashidhar<sup>2\*</sup>

Center for Materials Characterization, National Chemical Laboratory<sup>1</sup> Division of Organic Synthesis, National Chemical Laboratory<sup>2</sup>

Polymorphism, the ability of a molecule to exist in more than one crystal form, has great implications in chemical industries especially in drugs and pigments. We have reported polymorphic<sup>1</sup> and pseudopolymorphic<sup>2</sup> behaviour in various *myo*-inositol derivatives. The title compound 1) showed polymorphic modifications under different crystallization conditions. Compound 1 gave orthorhombic, Pbc<sub>a</sub> crystals (Form I) when crystallized from chloroform-petroleum ether mixture, whereas crystals from ethyl acetate-petroleum ether mixture were monoclinic, P2<sub>1</sub>/c (Form II. Crystal structure analysis revealed that the two forms are conformational polymorphs with C6-*O*-tosyl group adopting two different conformations (Figure 1). An interesting feature in both the forms is the formation of an almost isostructural string linked by O (orthoester)C=O (acetate) interactions, the deviation arising from different C-HO contacts made by the tosyl group in the two forms (Figure 1). These one-dimensional rows, however, are stitched differently to yield dimorphs.



### References:

- (1) Gonnade, R. G.; Shashidhar, M. S.; Bhadbhade, M. M. *Chem. Commun.* **2004**, 2530.
- (2) Manoj, K.; Gonnade, R. G.; Bhadbhade, M. M.; Shashidhar, M. S. *Cryst. Growth & Des.* **2006**, 6, 1485.

## Oxygen non-stoichiometry in layer-misfit cobaltites

Chris D Ling Karina Aivazian

School of Chemistry, The University of Sydney

Misfit layered cobaltites have attracted considerable recent attention due to their promising thermoelectric [1] and colossal magnetoresistive (CMR) properties [2]. Their defining structural feature is the stacking of alternating layer types along the  $c$  axis: a hexagonal  $Cd_2$ -type layer of edge-sharing  $CoO_6$  octahedra (subsystem 1); and 3 or 4 tetragonal NaCl-type metal oxide layers (subsystem 2). A mismatch between these two layers along the  $b$  axis (and also along the  $a$  axis in some compounds) means that the structures of these oxides must be described as an incommensurately modulated composite.

One of the most intensively studied misfit layered cobaltites is  $[Ca_2CoO_3][CoO_2]_q$ , commonly known by its approximate stoichiometry  $Ca_3Co_4O_9$ . The so-called misfit parameter  $q = b_1/b_2 \sim 1.62$  is defined in terms of the  $b$  axes of subsystems 1 and 2. It was recently shown by chemical analysis and thermogravimetry that " $Ca_3Co_4O_9$ " contains a significant number of oxygen anion vacancies in concentrations that depend strongly on synthetic conditions [3, 4]. Here we report the results of a synchrotron XRD and neutron powder diffraction study aimed at determining the precise location of these oxygen vacancies, and in particular, within which subsystem they principally reside. This has a direct bearing on the oxidation states of cobalt in each layer, and hence on the physical and magnetic properties of the material.

### Reference

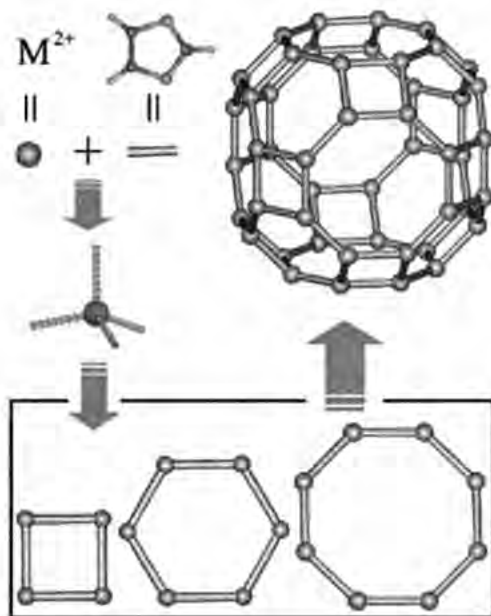
- [1] S. Li, R. Funahashi, I. Matsubara, et al., *Chemistry of Materials* 12 (2000) 2424.
- [2] A. C. Masset, C. Michel, A. Maignan, et al., *Physical Review B* 62 (2000) 166.
- [3] M. Karppinen, H. Fjellvåg, T. Konno, et al., *Chemistry of Materials* 5 (2004) 2790.
- [4] Y. Morita, J. Poulsen, K. Sakai, et al., *Journal of Solid State Chemistry* 177 (2004) 3149.

## New Microporous Metal-Organic Frameworks with Unusual Structural Features

Xiao-Ming Chen

School of Chemistry and Chemical Engineering, Sun Yat-Sen University

In this report, our new strategies using simple bent exo-bidentate and exo-tridentate ligands such as imidazoles and triazoles to generate a series of microporous metal-organic frameworks (MOFs) will be presented [1-4]. A series of crystal structures of the MOFs exhibiting unusual zeolitic topologies, dynamic structures driven by water absorption/desorption, window opening/closing configurations will be reported, along with the structural tuning of the porous sizes and shapes by using different kinds of bridging ligands.



### Reference

- [1] Zhang J.-P., Zheng S.-L., Huang X.-C., Chen X.-M., *Angew. Chem. Int. Ed.* **2004**, *43*, 206.
- [2] Zhang, J.-P.; Lin, Y.-Y.; Huang, X.-C.; Chen, X.-M., *J. Am. Chem. Soc.* **2005**, *127*, 5495.
- [3] Huang X.-C., Zhang J.-P., Chen X.-M., *J. Am. Chem. Soc.* **2004**, *126*, 13218.
- [4] Huang, X.-C.; Lin, Y.-Y.; Zhang, J.-P.; Chen, X.-M., *Angew. Chem. Int. Ed.* **2006**, *45*, 1557.

## Crystal structure and optical properties of $(\text{Ga}_{1-x}\text{Zn}_x)(\text{N}_{1-x}\text{O}_x)$ oxynitride photocatalyst ( $x = 0.13$ )

Yong Phat<sup>1</sup> Masatomo Yashima<sup>2</sup> Kazuhiko Maeda<sup>3</sup> Kentaro Teramura<sup>3</sup> Tsuyoshi Takada<sup>3</sup> Kazunari Domen<sup>1</sup>

Department of Materials Science and Engineering, Tokyo Institute of Technology<sup>1</sup> Department of Materials Science and Engineering, Tokyo Institute of Technology, Japan<sup>2</sup> Department of Chemical System Engineering, The University of Tokyo, Japan<sup>3</sup>

Overall water-splitting using a photocatalyst is an attractive solution for the supply of clean and recyclable hydrogen energy. Although a number of photocatalysts have been proposed, most function only in the ultraviolet region (e.g.,  $\text{TiO}_2$ ). While photocatalysts such as doped  $\text{TiO}_2$ ,  $\text{Ta}_3\text{N}_5$ ,  $\text{TaON}$  and  $\text{LaTiO}_3\text{N}$  function under visible light, these materials are not able to achieve overall water splitting. Recently, Maeda *et al.* [1] reported the solid solution of GaN and ZnO  $((\text{Ga}_{1-x}\text{Zn}_x)(\text{N}_{1-x}\text{O}_x))$  as a new type of oxynitride photocatalyst that is capable of overall water splitting under visible light. Here we report the crystal structure and optical properties of  $(\text{Ga}_{0.87}\text{Zn}_{0.13})(\text{N}_{0.83}\text{O}_{0.16})$  [2]. This material was demonstrated to absorb visible light at wavelengths of up to ca. 500 nm, and to exhibit photoluminescence at around 650 nm (1.9 eV) even at room temperature. The Rietveld analyses of neutron powder diffraction data of the  $(\text{Ga}_{0.87}\text{Zn}_{0.13})(\text{N}_{0.83}\text{O}_{0.16})$  ( $P6_3mc$ ) confirmed that the oxygen substitutes for nitrogen in the crystal structure, and may be responsible for the desirable optical properties of  $(\text{Ga}_{0.87}\text{Zn}_{0.13})(\text{N}_{0.83}\text{O}_{0.16})$  as a photocatalyst for visible light-driven overall water splitting. The nuclear density mapping revealed the structure to be free of interstitial sites and large disorder.

### Reference

- [1] K. Maeda *et al.*, *J. Am. Chem. Soc.* **127**(2005) 8286.  
 [2] M. Yashima *et al.*, *Chem. Phys. Lett.*, **416** (2005) 225.

**2-D and 3-D X-ray Imaging due to refraction for visualizing soft tissue**

Masami Ando<sup>\*</sup> Hiroshi Sugiyama<sup>\*\*</sup> Anton Maksimenko<sup>\*\*</sup> Tetsuya Yuasa<sup>\*\*\*</sup> Eiko Hashimoto<sup>\*\*\*\*</sup> Shu Ichiyama<sup>\*\*\*\*\*</sup> Kazuyuki Hyodo<sup>\*\*</sup> Yoshinori Chikaura<sup>\*\*\*\*\*</sup> Takao Akatsuka<sup>\*\*\*</sup>

DDS Center, Research Institute for Science and Technology, Tokyo University of Science<sup>\*</sup>  
Institute of Materials Structure Science, High Energy Accelerator Research Organization<sup>\*\*</sup>  
Yamagata University<sup>\*\*\*</sup> Graduate University of Advanced Studies<sup>\*\*\*\*</sup> National Nagoya Hospital<sup>\*\*\*\*\*</sup>  
Kyushu Institute of Technology<sup>\*\*\*\*\*</sup>

X-ray optics and algorithm in order to obtain 2-dimensional and 3-dimensional images of soft tissue has been successfully developed. We would like to first propose an x-ray optics named x-ray dark-field imaging for achieving high contrast 2-dimensional image. The system comprises an asymmetric-cut monochromator-collimator to obtain an extremely highly parallel incident beam onto object and a Laue type angular analyzer (Laa) to only deduce refraction component from the object. By selecting the specific thickness of Laa one can obtain such condition that the forward diffraction has no intensity at  $W=0$  where  $W$  means the angular parameter of the Bragg diffraction due to the x-ray dynamical diffraction theory. Using this condition only the refraction component from object can pass through Laa that has a function of angular filtering. Thus soft tissue such as breast cancer, lung cancer and articular cartilage at joint can be successfully visualized with say  $10\ \mu\text{m}$  spatial resolution. Furthermore we have attempted at development of an algorithm to be able to reconstruct x-ray image due to refraction. Application of this novel algorithm to DCIS (ductal carcinoma in-situ) breast cancer one can obtain a 3-dimensional arrangement of ductus lactiferi (milk duct), its wall, calcification and its surrounding atmosphere with say  $50\ \mu\text{m}$  spatial resolution. The detailed x-ray optics, the spatial resolution and content of the algorithm will be discussed in the presentation.

## Crystal Structures, Magnetism, and Spectroscopic Properties of One-dimensional Cyanide-bridged Tb(III)/Dy(III)/Ho(III)/Er(III)-Cr(III) Complexes.

Takashi Akitsu Yasuaki Einaga

Department of Chemistry, Keio University

Recently, we have discovered the first photo-induced magnetization phenomenon of 3d-4f cyanide-bridged bimetallic assemblies,  $\text{Ln}(\text{DMF})_4(\text{H}_2\text{O})_2\text{M}(\text{CN})_6 \cdot \text{H}_2\text{O}$  ( $\text{Ln} = \text{Nd}$ ;  $\text{M} = \text{Fe}, \text{Co}$ ) [1]. In contrast to conventional photo-induced electron transfer for cyanide-bridged 3d-3d transition metal complexes, the photo-induced magnetization for 3d-4f complexes was suggested to be due to structural distortion of cyanide-bridge ligands as well as lattice strain of the crystals. In order to elucidate the relationship between molecular or crystal structures and their electronic properties, we have developed metal-substituted complexes exhibiting various dimensionality such as bimetallic complexes, one-dimensional chains, and two-dimensional sheets systematically. In the present paper, we will report on new one-dimensional chain structures, magnetism, and IR, electronic, and XPS spectroscopic properties of,  $\text{Ln}(\text{DMF})_4(\text{H}_2\text{O})_2\text{Cr}(\text{CN})_6 \cdot \text{H}_2\text{O}$  ( $\text{Ln} = \text{Tb}, \text{Dy}, \text{Ho}, \text{and Er}$ ) complexes.

Because of lanthanoid contraction, four complexes are isostructural in  $P2_1/a$  showing gradual differences in both cell parameters and Ln-N bond lengths or Ln-N-C bond angles. Only Dy and Er complexes could be solved as  $P2_1/c$ , though structural similarity between  $P2_1/c$  and  $P2_1/a$  complexes was proved by powder pattern simulation. The detailed electronic properties in the solid state will be presented later.

### Reference

- [1] G. Li, T. Akitsu, O. Sato, and Y. Einaga, *J. Am. Chem. Soc.*, **125**, 12396 (2003).

## Supramolecular Structure of Cocrystallized Catechol and Hexamine

Kadsada Sala Kenneth J. Haller

School of Chemistry, Institute of Science, Suranaree University of Technology, Nakhon Ratchasima

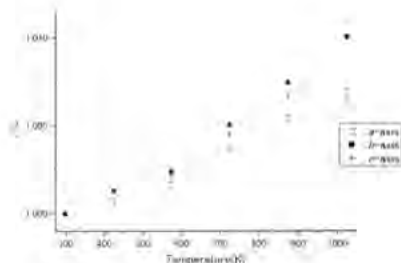
Computers and computational algorithms have increased in power, and consequently X-ray crystallography has been able to provide precise three-dimensional structures of more and more complex materials. This has opened two related new frontiers in solid state materials research on molecular compounds: one, supramolecular structure, deriving from the chemistry of noncovalent interactions (weak bonding interactions), and two, cocrystallization studies, allowing detailed examination of weak interactions between different molecular species in the condensed phase. These studies have become important in pharmaceutical chemistry where they allow study of potential drug interactions that may help to tailor drug molecules to fight specific diseases and may have applications in drug manufacturing. The current work reports the preparation of the 2:1 cocrystal of catechol (1,2-benzenediol) and hexamine (hexamethylenetetraamine), and the characterization of the resulting supramolecular material by single crystal X-ray analysis. The structure consists of one-dimensional chains of alternating catechol and hexamine molecules utilizing all the strong hydrogen bond donors of the catechol molecules and all the strong hydrogen bond acceptors of the hexamine molecules. Interactions between chains are by weaker noncovalent interactions. Details of the supramolecular structure will be discussed.

## High temperature x-ray study on a single crystal of humite, $\text{Mg}_7\text{Si}_3\text{O}_{12}(\text{OH},\text{F})_2$ up to 1023 K

Keiko Sumioka Takahiro Kuribayashi Yasuhiro Kudoh

Department of Mineralogy, Petrology and Economic Geology, graduate school of Science, Tohoku University

The specimen used in this study was a natural humite from Tilley Foster mine, U. S. A.. Chemical composition determined by electron micro probe analyzer (JEOL, JXA-8800M) yields the formula,  $(\text{Mg}_{6.46}\text{Fe}_{0.37}\text{Ti}_{0.03}\text{Mn}_{0.02})_{\Sigma 6.88}\text{Si}_{3.00}\text{O}_{12}(\text{F}_{0.93}\text{OH}_{0.95}\text{O}_{0.06})_{2.00}$ . The unit cell parameters and x-ray diffraction intensities of a single crystal of  $180 \times 250 \times 250 \mu\text{m}^3$  placed in a silica capillary at 296K, 423 K, 573 K, 723 K, 873 K and 1023 K were measured by an imaging plate x-ray diffractometer (RIGAKU, R-Axis IV) equipped with rotating anode ( $\text{MoK}\alpha$ , 50kVx89mA) and a U-shaped resistance heater (Huber; High temperature attachment Type 231). The thermal expansion coefficients along the crystal axes up to 1023 K are  $\alpha_a = 9.4(3) \times 10^{-6} \text{ K}^{-1}$ ,  $\alpha_b = 12.9(2) \times 10^{-6} \text{ K}^{-1}$  and  $\alpha_c = 11.9(3) \times 10^{-6} \text{ K}^{-1}$ . The expansion coefficients are in the order  $\alpha_b > \alpha_c > \alpha_a$  indicating that the thermal expansion coefficient of the direction perpendicular to the closest packing oxygen layer is smallest (Figure). The structure refinement were carried out using SHELEXL 97 (Sheldrick, 1997). The residual indexes (%) at 296K, 423 K, 573 K, 723 K, 873 K and 1023 K were 2.06, 2.85, 2.90, 2.55, 2.78 and 3.37, respectively.



## Size and Vacancies; Unexpected Phase Transitions in Manganese Perovskites

Brendan J Kennedy Qingdi Zhou

School of Chemistry, The University of Sydney

Manganese containing perovskites have been extensively studied in recent years because of their potential applications as catalysts and magnetoresistive sensors. As is observed in numerous other systems, most manganese perovskites do not exhibit the ideal cubic structure but rather have a distorted variant. The physical and electronic properties of the manganese perovskites are sensitive to the structural distortion and the actual stoichiometry and in some cases the distorted perovskites undergo thermally induced phase transitions.

Using a combination of high resolution synchrotron X-ray and neutron powder diffraction we have studied solid solutions of the type  $\text{Sr}_{1-x}\text{Ca}_x\text{MnO}_3$ . For  $x$  greater than 0.45 the materials all adopted an orthorhombic structure in  $Pbnm$  at room temperature. The diffraction pattern for  $\text{Sr}_{0.6}\text{Ca}_{0.4}\text{MnO}_3$  showed the presence of two phases, tetragonal in  $I4/mcm$  and orthorhombic in  $Pbnm$ . Heating this to 573 K yielded a single phase ( $I4/mcm$ ) structure. This behaviour is indicative of a first order  $Pbnm$  to  $I4/mcm$  transition. Variable temperature structural studies of  $\text{Sr}_{0.5}\text{Ca}_{0.5}\text{MnO}_3$  show a similar first order  $Pbnm$  to  $I4/mcm$  transition with extensive two-phase region. Above 573 K the sample is tetragonal ( $I4/mcm$ ) and this undergoes a continuous transition to cubic near 850 K. We find no evidence for an intermediate  $Imma$  phase and suggesting the behaviour of the first row transition metal perovskites  $\text{AMO}_3$  is different than the analogous heavier second and third row oxides such as  $\text{SrZrO}_3$  or  $\text{SrRuO}_3$ . Further we find the phase transition behaviour is very sensitive to the environment of the study with both the transition temperature and the nature of the transition being highly influence by oxygen nonstoichiometry.

## Correlation between H<sub>2</sub> gas sensitivity and structure of *o*-,*m*- and *p*-dipyridyldiketopyrrolopyrroles as viewed from the electron delocalization within the molecule and the crystal structure

Tsuyoshi Hirota Tomohiko Imoda Hiroo Takahashi Jin Mizuguchi

Department of Applied Physics, Graduate School of Engineering, Yokohama National University

We have previously developed a high-sensitive H<sub>2</sub> gas sensor utilizing a high-proton affinity of *p*-dipyridyldiketopyrrolopyrrole (*p*-DPPP). The sensor exhibits a remarkable reduction of the electrical resistivity by two orders of magnitude under 0.05 % H<sub>2</sub> due to protonation at the *para*-site of the pyridyl ring. The present outstanding result motivated us to further investigate *o*- and *m*-derivatives in order to achieve an even better performance. However, the performance of these isomers was extremely poor. For this reason, the present investigation has been made in order to clarify the mechanism of the poor sensitivity from the standpoint of the electron delocalization (*i.e.* electron conduction) within the molecule as well as the electron hopping from one molecule to another (*i.e.* structure problem). As for the electron delocalization in *p*-DPPP, the change in electron density at the *para*-site (due to *e.g.* protonation) is found to be well propagated throughout the molecule, while those at the *o*- and *m*-sites are ineffective. This explains why *p*-DPPP is much superior for H<sub>2</sub> gas sensors to *o*- and *m*-DPPPs. Another support is also given by the structure analysis of *o*-, *m*-, and *p*-derivatives. The N atom of the pyridyl ring (that serves as the antenna for protonation) remains unbounded (*i.e.* free) in *p*-DPPP and is capable of accepting protons. On the other hand, the N atoms are totally blocked by the formation of NH...N hydrogen bonds in *o*- and *m*-DPPPs. The above molecular and crystallographic considerations lead us to conclude that *p*-DPPP is, by far, advantageous to H<sub>2</sub> sensors over *o*- and *m*-DPPPs.

## Photoinduced Reversible Microfibril Formation on a Photochromic Diarylethene Microcrystalline Surface

Yuko Kojima<sup>1</sup>, Kingo Uchida<sup>2</sup>, Norikazu Izumi<sup>3</sup>, Shinichiro Sukata<sup>4</sup>, Shinichiro Nakamura<sup>5</sup>, Masahiro Irie<sup>6</sup>

<sup>1</sup>Yokohama Laboratory, Mitsubishi Chemical Group Science And Technology Research Center, Inc., <sup>2</sup>Department of Materials Chemistry, Faculty of Science and Technology, Ryukoku University and CREST, Japan Science and Technology Corporation, <sup>3</sup>Mitsubishi Chemical Group Science and Technology Research Center, Inc. and CREST, Japan Science and Technology Corporation, <sup>4</sup>Department of Chemistry and Biochemistry, Graduate School of Engineering, Kyushu University

Diarylethene derivatives are promising artificial photoresponsive molecules that show reversible transformation between open- and closed-ring isomers with different absorption spectra. Recently we found photoinduced wettability changes based on the morphology changes of a photochromic diarylethene crystal and thin film.

Here we report a new photoinduced surface morphology change, which provides superhydrophobic properties that is obtained by the photoinduced reversible formation of fine fibril structures on coated microcrystalline surfaces. The origin of reversible fibril formation is the photoisomerization of a photochromic diarylethene, 1,2-bis(2-methoxy-5-trimethylsilylthien-3-yl)perfluorocyclopentene (**1**) molecule of thin film. The reversible surface morphology changes of **1** were followed by SEM. (Fig. 1)

X-ray single crystal analysis of open- (**1o**) and closed-ring (**1c**) isomers and powder X-ray diffraction measurement were carried out to discover the microfibril composition. The X-ray results indicate that the fibril crystal formed on the film grew up freely from the crystal lattice of the open-ring isomer. We will discuss the reversible microfibril formation mechanism by a phase diagram and structures of **1o** and **1c** crystals.

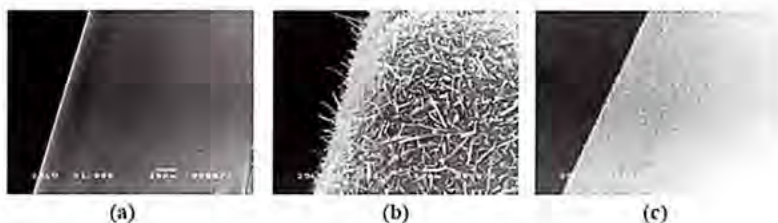


Fig. 1. SEM images of reversible surface morphology changes of **1**.

- (a) The crystalline surface of **1o**
- (b) After UV light (254nm) irradiation (a) and storage in dark for 24 hrs.
- (c) After visible light ( $\lambda > 500$  nm) irradiation on (b)

## Characterization of niobium substituted potassium tetragonal tungsten bronzes

Subrata Chandra Roy Altaf Hussain

Department of Chemistry, University of Dhaka

Tungsten bronzes,  $M_xWO_{3-x}$ , are well known non-stoichiometric ternary metal oxides where M is typically an electropositive metal and  $0 < x < 1$ . Among tungsten bronzes, the alkali metal tungsten bronzes are extensively studied compounds. Fully oxidized, isostructural phases termed as bronzoids,  $M_xNb_yW_{1-y}O_3$ , and partially oxidized bronzes of alkali metals have also been reported.

In our present investigation, powder samples of potassium tetragonal tungsten bronzes (TTB),  $K_xWO_3$ , and niobium substituted TTB,  $K_xNb_yW_{1-y}O_3$ , were prepared by the conventional solid-state method at 800°C. The powder samples were characterized by X-ray powder diffraction technique.

XRD patterns of  $K_{0.50}WO_3$  and  $K_{0.55}WO_3$  show TTB phase while the sample with composition  $K_{0.45}WO_3$  shows a mixture of TTB and hexagonal tungsten bronzes (HTB) phases.

Attempts to substitute Nb in  $K_{0.45}WO_3$  result mixtures of HTB and TTB phases and with  $y > 0.1$  the TTB phase disappears giving rise to an orthorhombic phase along with HTB. While for the systems  $K_{0.50}Nb_yW_{1-y}O_3$  and  $K_{0.55}Nb_yW_{1-y}O_3$  a single phase of TTB is observed upto  $y = 0.05$  and  $y = 0.07$  respectively. Further substitution of Nb in these compositions results mixture of TTB and HTB phases.

## Structural Systematics of Complexes of Lanthanoid Picrates with Unidentate O-donor Ligands

Eric J Chan<sup>1</sup> Allan H White<sup>2</sup> Brian W Skelton<sup>1</sup> Jack M Harrowfield<sup>2</sup>

Chemistry, University of Western Australia<sup>1</sup> Chemistry, University of Western Australia, Australia<sup>2</sup> ISIS, Universite Louis Pasteur, Strasbourg, France<sup>3</sup>

Structures as determined by single crystal X-ray methods for lanthanoid(III) compounds for series of simple homoleptic species with diverse ligands frequently display variations entailing a diminution in coordination number ('C.N.'), a consequence of the variation in the size of the atoms/ions due to the 'lanthanoid contraction'. A change from C.N. nine to eight is common, clearly separating compounds of the light/early' or heavy/'later' metal atoms. Earlier work on the complexes of the lanthanoid(III) picrates arose out of the exploration of simple reagents which might usefully exploit lanthanoid ion properties for purposes such as solvent extraction. They are also of potential synthetic utility because of their relatively high solubility in apolar solvents. Present work includes a systematic structural study of hydrated lanthanoid picrate complexes (including those of yttrium) with a selection of dipolar aprotic solvent ligands, namely trimethylphosphate ('tmp'), dimethylsulfoxide ('dmsO'), hexamethylphosphoramide ('hmpa'), *N,N'*-dimethylacetamide ('dma'), *N*-methylpyrrolidinone ('nmp') and octamethylpyro phosphoramidate ('ompa'), all liquids at room temperature and all unidentate. The introduction of polycyclic aromatic nitrogen base ligand complexes, namely 1,10-phenanthroline ('phen') and 2,2':6',2''-terpyridyl (tpy) resulted in further novel mixed ligand compounds. This work aims not only to establish structural 'domains of existence' with a concomitant consideration of the associated stereochemistry for these related series of rare earth complexes, but, also, to enhance our understanding of metal ion solvation and the interactions of aromatic groups within these types of crystal structures.

**Crystal structure and disorder in a Tetrakis (tetraphenyl phosphonium) dodecamolybdate phosphate [(PPh<sub>4</sub>)<sub>4</sub> Mo<sub>12</sub>O<sub>40</sub>P. 3DMF]**

Krishna Chowdhury Monika Mukherjee

Department of Solid State Physics, Indian Association for the Cultivation of Science

The polyoxomolybdates with alpha-Keggin structure form an important class of compounds, which can accommodate several guest moieties in the anionic cavity, and the use of different counter cations makes these system capable of forming supramolecular assembly. The molecular structure of the title complex consisting of [Mo<sub>12</sub>O<sub>40</sub>P]<sup>4-</sup> anions, tetraphenyl phosphonium (PPh<sub>4</sub>)<sup>+</sup> cations and solvent DMF molecules has been determined from single crystal X-ray analysis data. The structure was solved by the direct methods and refined to an R value of 0.0702. The polyoxoanion shows the disordered alpha-Keggin structure. The PO<sub>4</sub> group was orientationally disordered over two positions related by an inversion center. The anionic structure of the complex has a central P atom surrounded by a cube of eight oxygen atoms and the Mo atoms are situated at the corners of a regular cubooctadron. The polyoxoanion [Mo<sub>12</sub>O<sub>40</sub>P]<sup>4-</sup>, thus consists of a central PO<sub>4</sub> tetrahedron surrounded by four corner-sharing Mo<sub>3</sub>O<sub>13</sub> units; the three edge-sharing MoO<sub>6</sub> octahedra form as almost spherical unit with an approximate diameter 7.07 . The packing arrangements in the complex can be visualized as systems of polyoxometalate units forming channels along the y-direction into which infinite columns of (PPh<sub>4</sub>)<sup>+</sup> cations and solvent DMF molecules are placed.

**Crystal structure of an organometallic macrocyclic compound**

Yao-Cheng Shi Bei-Bei Zhu Chun-Xia Sui

School of Chemistry, Yangzhou University

The title compound,  $C_{23}H_{22}FeN_4O_2$ , was synthesized from the acylation of 1, 1'-bis(5-methyl-1*H*-pyrazolyl)ferrocene. The compound crystallizes in triclinic space group *P*-1 with unit cell parameters:  $a = 7.3830(15)\text{\AA}$ ,  $b = 11.4020(19)\text{\AA}$ ,  $c = 13.3750(15)\text{\AA}$ ,  $\alpha = 112.310(17)^\circ$ ,  $\beta = 94.390(18)^\circ$ ,  $\gamma = 108.06(2)^\circ$ ,  $Z = 2$ . The crystal structure has been determined using direct methods and refined by full-matrix least-squares to a final *R* value of 0.0502 for 3776 observed reflections. There is one independent molecule in an asymmetric unit. By double C-H $\cdots$ O hydrogen bonds, molecules of the title compound are linked into a [010] chain [H10 $\cdots$ O1' = 2.49\AA, C10 $\cdots$ O1' = 3.369(5)\AA, C10-H10 $\cdots$ O1' = 157^\circ; H14 $\cdots$ O2' = 2.57\AA, C14 $\cdots$ O2' = 3.494(5)\AA, C14-H14 $\cdots$ O2' = 173^\circ; symmetry code: (i)  $x, y-1, z$ ].

**X-ray structural study of manganese intercalated titanium disulfides**

Takuro Kawasaki Ken-ichi Ohshima

Institute of Materials Science, University of Tsukuba

Transition-metal intercalated titanium disulfides  $M_xTiS_2$  have various structures and characteristic physical properties depending on the kind or composition of intercalant M. There are several structural reports on  $M_xTiS_2$ , but no systematic structural study of  $Mn_xTiS_2$  has done until now. Single crystals of  $Mn_xTiS_2$  were grown in evacuated silica tubes by chemical vapor transport method using iodine as a transport gas. X-ray intensity data were collected at room temperature with the use of an automatic four circle diffractometer. Crystal structures of  $Mn_xTiS_2$  ( $x=0, 0.19, 0.26$ ) were refined and final R-factors are 3.7%, 3.8%, 2.9% where numbers of independent reflections are 576, 464, 307, respectively. The space group of  $Mn_xTiS_2$ , P-3m1, is the same as that of  $TiS_2$ . Mn atoms occupy octahedral sites in the van der Waals gap randomly. The electron density distributions for the layered compounds by the maximum entropy method have revealed that the covalent bonding exists between Ti and S atoms. On the other hand, no covalent electrons were found between Mn and S atoms. It is understood that Mn atoms show ionic character in the compounds. X-ray diffuse scattering measurements were also performed. The diffuse intensity maxima appeared at  $(1/2 \ 1/2 \ 1/2)$ ,  $(1/2 \ 0 \ 1/2)$ ,  $(0 \ 1/2 \ 1/2)$  and its equivalent positions. This reveals that intercalated Mn atoms have a short-range ordering three-dimensionally. We have tried to obtain Warren-Cowley's short-range order parameter for understanding of structural fluctuation in the compound.

## **Effect of clay dispersion on Mechanical, Dynamic Mechanical and Thermal Properties of Vinylester Resin/Clay NanoComposites**

Suparna Sengupta<sup>\*</sup> Dipa Ray<sup>\*\*</sup> Siba Prasad Sengupta<sup>\*</sup>

Materials Science, Indian Association for the Cultivation of Science<sup>\*</sup> Department of Polymer Science & Technology, University College of Science and Technology, University of Calcutta, 92 A.P. C Road, Kolkata 700009, India.<sup>\*\*</sup>

Vinylester resin matrix composites were fabricated with 1%, 3% 5% and 10 weight% loading of organoclay respectively. The composite samples were subjected to various characterization techniques like X ray Diffraction, Flexural testing, Dynamic Mechanical Analysis, Thermogravimetric analysis, Differential Scanning Calorimetric analysis and Scanning Electron Microscopy. The clay samples as well as the clay/resin composites were investigated with X ray Diffraction studies. From the shift in the peak positions and the change in d-spacing values, it was evident that there was intercalation in the 3% and 10% composites, whereas some exfoliation occurred in the 1% and the 5% composites. The flexural strength and the breaking energy of all the composites were decreased compared to the unfilled resin, but there was an increase in flexural modulus value by 13%. From the dynamic mechanical analysis of the 3% and the 5% composites, it was observed that exfoliation (in 5% composites) raised the clay-resin interaction significantly, leading to an increase in the loss modulus value with a higher glass transition temperature compared to that of the intercalated sample (3% composites). Thermal degradation behaviour was also improved in the exfoliated sample compared to the intercalated one.

**Synthesis and Crystal Structures of Novel Zn(II) and Ni(II) Coordination Polymers with 1,4-bis(3-pyridyl)-2,3-diazo-1,3-butadiene Ligands**

Gene-Hsiang Lee Hsin-Ta Wang

Institute of Organic and Polymeric Materials, National Taipei University of Technology

Two novel coordination polymers with 1D metal-organic frameworks (MOFs) have been synthesized by reacting 1,4-bis(3-pyridyl)-2,3-diazo-1,3-butadiene (**L**) with zinc dichloride. Both compounds have the same repeating unit  $[\text{ZnLCl}_2]_n$  of a distorted tetrahedral Zn(II) center coordinated by two chlorides and two pyridyl nitrogen atoms of two bridging bisonodentate ligands. These two complexes show different structural conformations, with one forming a helical chain crystallized in an orthorhombic space group  $Pna2_1$  with  $a = 7.9652(3)$ ,  $b = 21.4716(7)$ ,  $c = 8.2491(3)\text{\AA}$ ,  $V = 1410.81(9)\text{\AA}^3$  and  $Z = 4$  and the other producing a square-wave chain crystallized in a monoclinic space group  $P2_1/n$  with  $a = 9.1752(3)$ ,  $b = 14.5976(4)$ ,  $c = 10.3666(3)\text{\AA}$ ,  $\beta = 98.231(2)^\circ$ ,  $V = 1374.16(7)\text{\AA}^3$  and  $Z = 4$ . When  $\text{Ni}(\text{NO}_3)_2$  was used instead of  $\text{ZnCl}_2$  under the same reaction conditions, a new 3D metal-organic coordination polymer,  $[\text{Ni}_2(\text{L})_3(\text{NO}_3)_4\text{EtOH}]_n$  was obtained. This compound shows the monoclinic system, space group  $P2_1/c$  with  $a = 16.3181(10)$ ,  $b = 14.9976(8)$ ,  $c = 19.6917(11)\text{\AA}$ ,  $\beta = 98.360(2)^\circ$ ,  $V = 4768.0(5)\text{\AA}^3$ ,  $Z = 4$ . The Ni(II) ion lies in the distorted octahedral environment with three bridging ligands and two nitrate anions, and also an ethanol guest molecule occupies of a ca.  $6.7 \times 8.5\text{\AA}^2$  cavity.

## Search for the new Pb-free solder materials

Son Van Phung Akira Fujitsuka Ken-ichi Ohshima

Institute of Materials Science, University of Tsukuba

Environmental and health concerns of lead have increased the pressure towards the development of new Pb-free solders. Japan Electronics and Information Technology Industries Association (JEITA) defines Pb-free solder as the one in which Pb concentration is less than 0.1% of the total weight. We have been searching for the new Pb-free solder materials. The hardness, electrical resistivity and the melting point of Sn-Ag, Sn-Cu and Sn-Ag-Cu solders have been measured and compared with the eutectic Sn-Pb solder as a reference alloy. The results have clearly shown that the Pb-free solder has higher melting temperature, higher hardness and higher electrical resistivity than eutectic Sn-Pb solder. For improving the performance of the Pb-free solder, the carbon black was added into Sn-Ag solder under the high-pressure (5.5GPa) at 1200 °C. The X-ray diffraction data have shown the presence of carbon black in the composite solder. From the differential scanning calorimetry (DSC) data the melting temperature of the composite solder was found to be unchanged with adding the carbon black.

## Isostructural Phase Transition in $\beta$ -YbV<sub>4</sub>O<sub>8</sub>

Yasushi Kanke<sup>\*</sup> Andrzej Grzechnik<sup>\*\*</sup> Karen Friese<sup>\*\*</sup>

Advanced Nano Materials Laboratory, National Institute for Materials Science<sup>\*</sup> Departamento Física Materia Condensada, Universidad del País Vasco, Spain<sup>\*\*</sup>

The  $\alpha$ - and  $\beta$ -phases of MV<sub>4</sub>O<sub>8</sub> (M=Y<sup>3+</sup>, Yb<sup>3+</sup>) are composed of essentially identical V<sub>4</sub>O<sub>8</sub> octahedral frameworks and differ only in the arrangement of the trivalent cations [1,2]. As a consequence, the one-dimensional disorder and the co-existence of the two polytypic modifications is frequently observed [3,4]. Magnetic susceptibility [4] and specific heat measurements show an anomaly for  $\beta$ -YV<sub>4</sub>O<sub>8</sub> at approximately 190 K. Due to magnetic impurities, the corresponding measurements could not be carried out on  $\beta$ -YbV<sub>4</sub>O<sub>8</sub>.

The diffraction intensities of  $\beta$ -YbV<sub>4</sub>O<sub>8</sub> have been measured on a single crystal in the temperature range from 290 K to 100 K at the *Single Crystal Diffraction* Beamline at the Institute for Synchrotron Radiation, Anka, Karlsruhe, Germany. The space group symmetry (space group A21/d11 with lattice parameters a=9.030(5), 21.44(3), c=5.752(2) at 290K, [1]) does not change in the whole temperature range, yet significant discontinuities in the lattice parameters indicate an isostructural phase transition between 200 and 175 K. Atomic coordinates also show significant and discontinuous changes, which can most probably be attributed to a different tilting of the octahedral framework before and after the phase transition. Another striking change concerns the anisotropic displacement parameters of part of the oxygen atoms, as the longest axes of the displacement ellipsoids clearly change their orientation.

### References

- [1] Y. Kanke, K. Kato (1997), Chem. Mater. 9, 141-147.
- [2] K. Kato, Y. Kanke, K. Friese (1997), Z. Krist. 212, 110-114.
- [3] K. Friese, O. Jarchow, K. Kato, Y. Kanke (1997), Z. Krist. 212, 859-863.
- [4] M. Onoda, A.-C. Dhaussy, Y. Kanke (2003), Acta. Cryst. B59, 429-438.

## Effect of Ga & In Substitution and Swift Heavy Ion Irradiation on Magnetic Properties of Strontium Hexaferrite Crystals.

Krishen Kumar Bamzai<sup>1</sup> Balwinder Kaur<sup>1</sup> Pushkar Nath Kotru<sup>1</sup> Ravi Kumar<sup>2</sup> F Licci<sup>3</sup>

Department of Physics, University of Jammu<sup>1</sup> Inter University Accelerator Centre, Aruna Asif Ali Marg, New Delhi-110067 (India)<sup>2</sup> Institute of Maspec, Italy<sup>3</sup>

Hexagonal ferrites, which is represented by  $\text{MeFe}_{12}\text{O}_{19}$  (where Me=Ba, Sr or Pb) belongs to a class of ferromagnetic oxides. Attempt to improve the magnetic properties of these ferrites was done by substituting  $\text{Fe}^{3+}$  ions with some non magnetic ions (i.e., Ga, In, Sc & Al). These substitutions lead to drastic variation in the magnetic structures of hexaferrites. Substitution of  $\text{Fe}^{3+}$  cations leads to a reduction of the strong uniaxial magnetic anisotropy. The substitution of Ga & In in Sr hexaferrite crystals of the type  $\text{SrGa}_x\text{In}_y\text{Fe}_{12-(x+y)}\text{O}_{19}$  (where  $x = 0, 5, 7, 9$ ;  $y = 0, 0.8, 1.3, 1.0$ ) decreases the value of magnetization which is attributed to shifting of collinear magnetic order to a non collinear one. Reduction of magnetization is also explained as a result of the occupation of the crystallographic sites of  $\text{Fe}^{3+}$  ions by  $\text{Ga}^{3+}$  &  $\text{In}^{3+}$ . Changes in their magnetic structures can also be brought about by swift heavy ions. Swift heavy ions in the MeV range causes modifications in the materials which entirely changes their magnetic structure. 50 MeV  $\text{Li}^{3+}$  ion irradiation decreases the value of magnetization irrespective of whether the crystals are Ga & In substituted or unsubstituted. The results are interpreted in terms of occurrence of a paramagnetic doublet in crystals replacing magnetic sextuplet as a result of irradiation. Substitution of Ga & In in Sr hexaferrite decreases the value of anisotropy field as well as anisotropy constant. Irradiation with  $\text{Li}^{3+}$  ions increases the value of  $H_a$  for both substituted as well as unsubstituted crystals. Substitution with Ga & In also decreases the value of Curie temperature ( $T_c$ ) but the irradiation with  $\text{Li}^{3+}$  ions does not affect the  $T_c$  of either substituted or pure  $\text{SrFe}_{12}\text{O}_{19}$  crystals.

## New Series of Oxalato-Gallophosphate Structures Containing Transition Metal Centers

Wen-Ming Chang Sue-Lein Wang

Department of Chemistry, National Tsing-Hua University

The synthesis of organic-inorganic hybrid materials by incorporating appropriate organic ligands into the inorganic frameworks has been the subject of intense research. One class of organic-inorganic hybrid frameworks is based on oxalate and phosphate in which the metal centers are coordinated by two types of ligands. In the search for new varieties of frameworks, we further incorporate transition metals into the oxalato-gallophosphate structures. Along this line, five novel organic-inorganic hybrid mixed-metal oxalatophosphates,  $(C_3H_{12}N_2)_2[(VO)_2(ox)Ga_2(PO_4)_4]$  (**1**),  $(C_{10}H_{28}N_4)[(VO)_2(ox)Ga_2(PO_4)_4] \cdot 2H_2O$  (**2**),  $(C_7H_{21}N_3)_{0.5}(H_2O)[Mn(H_2O)_2Ga_4F_2(ox)(PO_4)_4] \cdot 4H_2O$  (**3**),  $(C_5H_{14}N_2)[Mn(H_2O)_2Ga_4F_2(ox)(PO_4)_4] \cdot 3H_2O$  (**4**) and  $(C_4H_{16}N_3)[MnGa_2(ox)_2(HPO_4)_2(PO_4)]$  (**5**) ( $ox = C_2O_4^{2-}$ ) were successfully synthesized under mild hydrothermal conditions. They were characterized by single-crystal X-ray diffraction, magnetic susceptibility and TG analysis. The vanadium compounds **1** and **2** are layered whereas the manganese compounds **3**, **4**, and **5** are 3D materials. The oxalate anion can act as a bis-bidentate ligand in all five compounds and also as a mono-bidentate ligand in **5**. Besides homo bi-octahedral units of  $M'_2(ox)O_6$  ( $M' = (VO)$  for **1** and **2**,  $(GaF)$  for **3** and **4**), we observe the first hetero chelating  $MnGa(ox)O_8$  unit, formed of an unusual  $Mn^{VI}O_6$  trigonal prism and a  $GaO_6$  octahedron, and unique trimeric polyhedral  $Mn(H_2O)_2(GaF)_2O_{12}$  and  $MnGa_2O_{16}$  units. The fundamental frameworks for **1-5** effectively display a series that are constructed from a substructure of 1D or 2D with a four ring linker and/or  $Mn^{2+}$  ions into 2D or 3D structures. The hetero metals have imposed magnetic property to the  $Ga(ox)PO$  lattices and led to the first well-defined M-X-Ga ( $X = O, F$ ) bonds ever observed in the metal phosphate chemistry.

## Crystal Structure Analysis of Low-Dimensional Nano Crystal

Yasuhiro Takahashi Kazuaki Okamoto

Department of Macromolecular Science, Osaka University

Crystal structure analyses of one dimensional crystals which are of the stacking of layers and two dimensional crystal which is of the regular array of cylinders were carried out by the small angle scatterings and three kinds of the least-squares methods. One-dimensional crystal: the lamellar phase of polystyrene-poly2-vinylpyridine block copolymer was interpreted by the electron density of the disordered rectangular form. One-dimensional crystal: the stacking of polyethylene single crystals was interpreted by the electron density of the disordered trapezium. Two-dimensional crystal: the cylinder phase of polystyrene-polyethylenebutylene-polystyrene block copolymer was interpreted by the electron density of the disordered cylinder.

## Immobilization of $\text{Rh}(\text{PPh}_3)_3\text{Cl}$ on phosphinated MCM-41 for catalytic hydrogenation and hydroformylation of olefins

Shin-Guang Shyu<sup>1</sup> Hsiu-Mei Lin<sup>2</sup> Der-Lii Tzou<sup>1</sup> Shequ-Wen Cheng<sup>1</sup>

<sup>1</sup>Institute of Chemistry, Academia Sinica<sup>2</sup> Institute of Bioscience and Biotechnology, National Taiwan Ocean University<sup>2</sup>

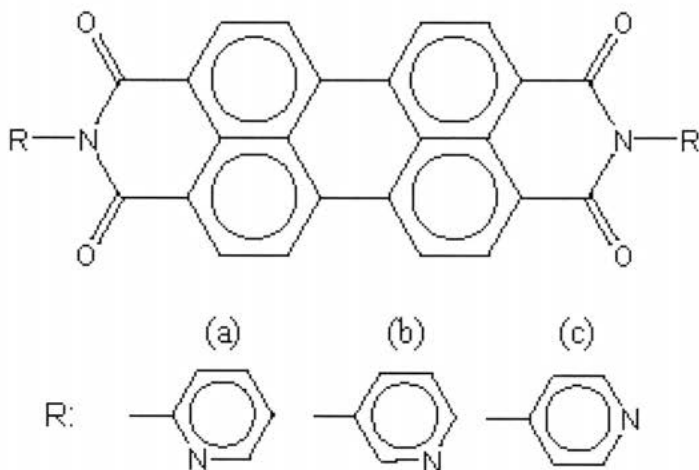
The complex  $\text{Rh}(\text{PPh}_3)_3\text{Cl}$  immobilized on MCM-41 modified with  $(\text{OEt})_3\text{Si}(\text{CH}_2)_3\text{PPh}_2$  results in a stable hydrogenation catalyst with turn over frequency (TOF) three times higher than that of  $\text{Rh}(\text{PPh}_3)_3\text{Cl}$  in the hydrogenation of cyclohexene. Powder X-ray, BET pore size measurement **and** solid state  $^{29}\text{Si}$  NMR were used to characterize the morphology of the catalyst. Solid state  $^{31}\text{P}$  NMR and EXAFS analyses of Rh were carried out to investigate the structure of the immobilized Rh catalyst. EXAFS analyses show a Rh to Rh interaction at 3.0 Å indicating a possible dimer structure without Rh-Rh metal-metal bonding. After hydrogenation, a Rh-Rh interaction at 2.6 Å was observed indicating the presence of a Rh-Rh metal-metal bonding.

## Hydrogen gas sensors based upon perylene-imide derivatives with pyridyl rings

Kazuyuki Sato Kazuyuki Hino Hiroo Takahashi Jin Mizuguchi

Department of Physics, Yokohama National University

We have recently developed a  $H_2$  gas sensor utilizing a high proton affinity of diketodi pyridylpyrrolopyrrole (*para*-DPPP). Protonation is found to bring about remarkable reduction of the electrical resistivity and this effect has been applied to  $H_2$  gas sensors. In the present investigation, we extend our idea to a larger chromophore such as a perylene-imide skeleton in order to improve the sensor characteristics. We have synthesized novel perylene-imide derivatives connected directly with proton accepting pyridyl rings. The two N atoms of the pyridyl rings which work as proton acceptors are found to remain unbonded (*i.e.* free) in the solid state according to X-ray analysis and are thus available for protonation necessary for  $H_2$  gas sensors. The present sensors exhibit a significant change in electrical resistivity by about three orders of magnitude even under 0.05 %  $H_2$  and a higher sensitivity by one order of magnitude as compared with that of *p*-DPPP. Furthermore, these sensors are found to operate reversibly at room temperature and are scarcely influenced by ambient gases such as  $CH_4$ , CO,  $CO_2$ , NO,  $SO_2$ ,  $CH_3OH$ ,  $C_2H_5OH$  and  $H_2O$  moisture.



**Synthesis and Crystal Structure of  $\text{Fe}_3(\text{H}_2\text{PO}_4)_4(\text{PO}_4)_2 \cdot (\text{H}_3\text{O}^+)2\text{H}_2\text{O}$ , a Novel Iron Phosphate**

Hsiu-Mei Lin Shi-Fang Yeh

Institute of Marine Bio Technology, National Taiwan Ocean University

A new iron phosphate,  $\text{Fe}_3(\text{H}_2\text{PO}_4)_4(\text{PO}_4)_2 \cdot (\text{H}_3\text{O}^+)2\text{H}_2\text{O}$ , has been synthesized under hydrothermal conditions. The resulting product consists of light purple plate-shaped crystals of the title compound. Its structure has been determined by single crystal X-ray diffraction. Crystal data: triclinic, space group  $P-1$ ,  $a = 7.1545(2)$ ,  $b = 8.8195(2)$ ,  $c = 9.4368(2)$  Å,  $\alpha = 64.849(1)$ ,  $\beta = 70.215(1)$ ,  $\gamma = 69.386(1)$  degree,  $V = 491.8(3)$  Å<sup>3</sup>,  $Z = 2$ , and  $R1(Rw) = 0.027(0.075)$ . Crystal data were collected on a Simens CCD diffractometer with Mo K $\alpha$  ( $\lambda = 0.7103$  Å) at room temperature. There are two unique iron atoms in the crystal structure, having octahedral oxygen coordination,  $\text{FeO}_6$  octahedral are linked together via corners of  $\text{PO}_4$  tetrahedral to form a three-dimensional network. Within this network are hollows that are occupied by oxonium ions, lie on crystallographic twofold axis. The synthesis and crystal structure of the title compound will be presented.

**Crystal structure and disorder in the oxide ion conductors  $Y_{1-x}Ta_xO_{1.5+x}$  ( $x=0.2$  and  $0.25$ )**

Takayuki Tsuji Masatomo Yashima

Department of Materials Science and Engineering, Tokyo Institute of Technology

We report the results of a neutron powder diffraction study of the  $Y_{0.8}Ta_{0.2}O_{1.7}$  and  $Y_{0.75}Ta_{0.25}O_{1.75}$  compounds at room temperature.  $Y_{0.8}Ta_{0.2}O_{1.7}$  and  $Y_{0.75}Ta_{0.25}O_{1.75}$  materials were prepared by solid-state reactions. Neutron-diffraction data for both samples were collected at 299K on a multi-detector fixed wavelength powder diffractometer (HERMES) installed at the JRR-3M research reactor of the Japan Atomic Energy Association (JAEA), by the Institute for Materials Research, Tohoku University. A neutron beam with a 1.8207 angstrom unit wavelength was obtained by the (3 3 1) plane of a Ge monochromator. The diffraction data were analyzed by the Rietveld method, maximum entropy method (MEM) and MEM-based pattern fitting, in order to refine crystal parameters and to investigate the nuclear density distribution. The diffraction pattern of  $Y_{0.8}Ta_{0.2}O_{1.7}$  exhibited a background with a complicated profile shape due to diffuse scattering. Thus, we subtracted the background using a computer program PowderX before the Rietveld analysis. In the orthorhombic  $Y_{0.75}Ta_{0.25}O_{1.75}$  compound, the Y and Ta atoms were ordered and the oxide ions were localized at around the stable position. On the contrary, in the defect fluorite-type cubic  $Y_{0.8}Ta_{0.2}O_{1.7}$  material, the Y and Ta atoms were disordered and the oxide ions exhibited a large spatial distribution. The large distribution of oxide ions is responsible for the high oxygen diffusion constant and conductivity at high temperatures.

## Crystal structure and microwave dielectric properties of Ni substituted cordierite ceramics

Mio Terada<sup>1</sup>, Keizou Kawamura<sup>2</sup>, Isao Kagomiya<sup>1</sup>, Ken-ichi Kakimoto<sup>1</sup>, Hitoshi Ohsato<sup>1</sup>

<sup>1</sup>Department of Materials Science and Engineering, Nagoya Institute of Technology, Materials Research & Development Div. General R & D Laboratories, Taiyo Yuden Co., Ltd., Japan

Cordierite ( $\text{Mg}_2\text{Al}_4\text{Si}_5\text{O}_{18}$ ) is characterized by a lower dielectric constant ( $\epsilon_r$ ) and lower temperature coefficient of resonance frequency ( $\tau_f$ ) among the systems of  $\text{MgO-Al}_2\text{O}_3\text{-SiO}_2$ .  $\epsilon_r$  of cordierite ceramics prepared by standard solid state reaction method showed 6.19 and its  $\tau_f$  exhibited -24 ppm/ $^\circ\text{C}$ , which was more close to zero compared to other isotropic silicates. However, quality factor ( $Q_f$ ) value is relatively lower compared to more isotropic silicate such as forsterite, diopside, etc. This study investigated an effect of Ni substitution to improve the  $Q_f$  value. In addition, we discuss relationship between the crystal structure of the Ni substituted cordierite and microwave dielectric properties, particularly  $Q_f$  from the viewpoint of crystal structure refined by Rietveld analysis.  $(\text{Mg}_{1-x}\text{Ni}_x)_2\text{Al}_4\text{Si}_5\text{O}_{18}$  with no secondly phase was obtained in the compositions range of  $x = 0 - 0.1$ . Furthermore substitution of Ni caused presence of the secondary phase.  $\epsilon_r$  of  $(\text{Mg}_{1-x}\text{Ni}_x)_2\text{Al}_4\text{Si}_5\text{O}_{18}$  solid solution slightly increased with increasing the composition  $x$ . The  $\tau_f$  were almost comparable in the range from  $x = 0.05$  to  $0.2$ . On the other hand, the  $\tau_f$  abruptly shifted toward negative value with increasing  $x$  from  $0.3$  to  $0.5$ . The  $Q_f$  value increased with substituting a small amount of Ni and the highest  $Q_f$  value of 99,110 GHz was obtained at the composition  $x = 0.1$ . According to Rietveld analysis, hexagonal rings composed of corner sharing  $(\text{Si,Al})\text{O}_4$  tetrahedron in the  $(\text{Mg}_{0.9}\text{Ni}_{0.1})_2\text{Al}_4\text{Si}_5\text{O}_{18}$  are more isotropic than that of the  $\text{Mg}_2\text{Al}_4\text{Si}_5\text{O}_{18}$ , suggesting that the  $Q_f$  value is improved with the slight variation of the hexagonal rings.

## Hydrothermal Synthesis, Crystal structure of Two-Dimensional Cobalt(II) and Nickel(II) Complexes with 4,4'-Bipyridine

Tanwawan Duangthongyou Sutatip Siripaisarnpipat

Department of Chemistry, Kasetsart University

Two coordination polymers, 4,4'-bipyridine complexes of cobalt (1) and nickel (2) have been synthesized by hydrothermal reactions. Complex 1 crystallizes in monoclinic system with space group  $C_2$  and complex 2 crystallizes in triclinic system with space group  $P1$ . In complex 1, the 4,4'-bipyridine ligands bridge between cobalt atoms constructing a motif of 1-D polymeric chain. Each 1-D polymeric chain attracts each other through an intermolecular hydrogen bond between water and 4,4'-bipyridine forming layers. Two uncoordinated 4,4'-bipyridine molecules are between these layers. The crystal structure of complex 2 consists of two polymeric cationic chains of  $[Ni(4,4'-bpy)]_n^{2+}$  which connect to each other through another bidentate 4,4'-bipyridine forming a square of composition  $[Ni(\mu-4,4'-bpy)]_4$ . Consequently, the ladder type polymeric chain is obtained. Two uncoordinated 4,4'-bipyridine molecules are clathrated in the square cavities.

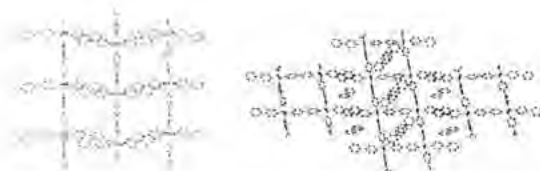


Figure 1 Packing diagram of compound 1 and 2

## Crystal structure and textures of the C-type antiferromagnetic manganites by transmission electron microscopy

Masahiro Nagao<sup>1</sup>, Toru Asaka<sup>2</sup>, Yutaka Yamauchi<sup>3</sup>, Ryota Hatakeyama<sup>4</sup>, Takuro Nagai<sup>5</sup>, Atsushi Yamazaki<sup>6</sup>, Koji Kimoto<sup>7</sup>, Hideki Kuwahara<sup>8</sup>, Yoshio Matsui<sup>9</sup>

Advanced Nano Characterization Center, National Institute for Materials Science / Waseda University<sup>1</sup>, National Institute for Materials Science<sup>2</sup>, Sophia University<sup>3</sup>, Waseda University<sup>4</sup>,  
National Institute for Materials Science<sup>5</sup>, National Institute for Materials Science<sup>6</sup>, National Institute for Materials Science<sup>7</sup>, National Institute for Materials Science<sup>8</sup>, National Institute for Materials Science<sup>9</sup>

Perovskite manganites have a wide variety of electronic/magnetic structures depending on the interplay among spin, charge, orbital, and lattice degrees of freedom. In  $\text{Nd}_{1-x}\text{Sr}_x\text{MnO}_3$ , various electronic/magnetic ground states such as a ferromagnetic and an antiferromagnetic charge order state appear. Among these series, there have been few studies of the C-type antiferromagnetic phase which has 1D-like orbital chain structure, although the other magnetic structures have been studied extensively to understand the properties of the manganites such as colossal magnetoresistance, charge/orbital order. Here we show the crystal structure and the textures of the C-type antiferromagnetic phase for single crystals of  $\text{Nd}_{1-x}\text{Sr}_x\text{MnO}_3$  ( $x=2/3, 3/4, 4/5$ ) by means of transmission electron microscopy.

The electron diffraction (ED) patterns of  $x=2/3, 3/4$ , obtained at room temperature and 82K, indicated tetragonal  $I4/mcm$  structure corresponding to the previous neutron diffraction study. In contrast, the ED pattern of  $x=4/5$  demonstrated the emergence of diffuse scattering around 460K at the forbidden reflections points for  $I4/mcm$  structure. The diffuse scattering changed into the sharp spot at the vicinity of Neel temperature,  $\sim 300\text{K}$ . The observation provides the evidence for the presence of a different structure from  $I4/mcm$ .

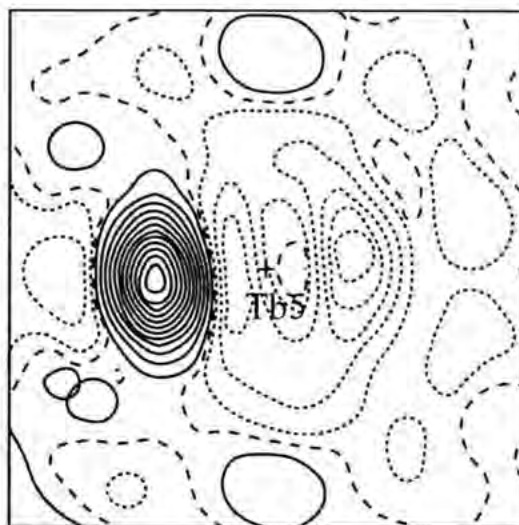
We carried out dark-field imaging in order to elucidate the detail of the structural phase transition. In the high-temperature paramagnetic phase, the nanometer-scale domains with another structure embedded in  $I4/mcm$  matrix were observed. The nanodomains evolved to become large in size with decreasing temperature. Eventually, the other structure was replaced  $I4/mcm$  phase at Neel temperature. This behavior would be regarded as the diffuse phase transition.

## Synchrotron X-ray Single-Crystal Structure Analysis of Partially-Disordered $Tb_3RuO_7$

Tsuyoshi Suwa<sup>\*</sup> Nobuo Ishizawa<sup>\*</sup> James R. Hester<sup>\*\*\*</sup>

Nagoya Institute of Technology<sup>\*</sup> ANBF<sup>\*\*\*</sup>

A series of  $Ln_3MO_7$  crystals composed of trivalent lanthanide (Ln) and pentavalent transition metal (M=Ru, Os) oxides is structurally characterized by the presence of infinite single chains of corner-linked  $MO_6$  octahedra embedded in the matrix of Ln and O atoms. This series has attracted attention because of its interesting electrical and magnetic properties. The series shows a polymorphism. A noncentrosymmetric orthorhombic  $P2_1nb$  modification has been recently found in addition to the centrosymmetric  $Cmcm$ . The present study revealed that the  $Tb_3RuO_7$  crystals grown from the  $SrCl_2$ - $Ru_2O_5$ - $Tb_2O_3$  system form the  $P2_1nb$  structure with partially disordered Tb positions. Single-crystal diffraction data were collected using synchrotron X-rays of 0.6886Å at the Photon Factory, Tsukuba. Presence of residual electrons near Tb5 in the figure ( $2 e/\text{Å}^3$  intervals,  $2.1 \times 2.1 \text{ Å}^2$  section perpendicular to  $a$ ) suggested a positional disorder of the atom. The least-squares refinement, assuming split atom sites for Tb5 and Tb6, yielded a final  $R_2$  value of 0.017 for 7559 independent reflections. Nine and five percents of Tb atoms are slightly displaced from the regular Tb5 and Tb6 positions by 0.323(5) and 0.395(6) Å, respectively.



## Grain size effects on genesis of moganite and Brazil twin in quartz

Koichi Momma<sup>1</sup> Toshiro Nagase<sup>2</sup> Yasuhiro Kudoh<sup>3</sup> Takahiro Kuribayashi<sup>4</sup> Masahiko Tanaka<sup>5</sup>

Institute of Mineralogy, Petrology, & Economic Geology, Tohoku University<sup>1</sup> The Tohoku University Museum, Japan<sup>2</sup> Institute of Mineralogy, Petrology, & Economic Geology, Tohoku University, Japan<sup>3</sup> BL15XU/SPRing8, National Institute for Materials Science, Japan<sup>4</sup>

Brazil twin in microcrystalline quartz was studied by using Rietveld analysis of X-ray powder diffraction and Raman spectroscopy. Genesis of Brazil twin and moganite in microcrystalline quartz varieties has long been argued. However, effects of surface energy on their occurrence have never been studied so far.

Crystallite size and anisotropic lattice strain of natural and synthetic quartz was refined by Rietveld analysis of synchrotron X-ray powder diffraction data. The lattice strain along  $\langle 101 \rangle^*$  is largest in all microcrystalline samples, which are different in origins, crystallite size, and texture. On the other hand, the lattice strain is isotropic in macroscopic samples. The anisotropic lattice strain increases with decreasing size of the crystallite. Axial ratio ( $c/a$ ) also decreases with an increase in lattice strain and with a decrease in crystallite size. Quantitative analysis of moganite contents in microcrystalline silica samples was carried out by Raman spectroscopy. The result reveals that the samples having large lattice strain contain high amount of moganite, and that the lattice strain along  $\langle 101 \rangle^*$  is caused by Brazil twin. A sample synthesized from Al-doped silica gel has larger lattice strain than those of non-doped samples. A synthesis from Fe-doped silica gel has the same lattice strain as those of non-doped samples. The correlation between the Brazil twin and crystallite size shows that the surface energy is the driving force for the formation of Brazil twin in microcrystalline quartz. Although ferric iron is believed to be a cause of Brazil twin, its role in microcrystalline quartz is negligibly small compared to the surface energy.

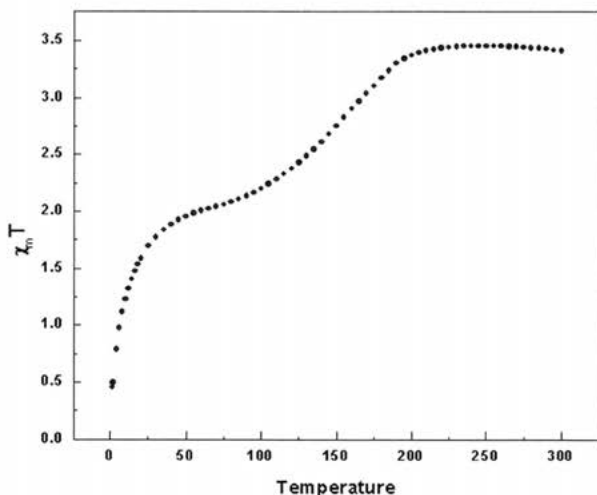
## Structural and Magnetic Study of New LIESST and reverse-LIESST $\text{Fe}(\text{trz})_{1.5}[\text{Au}(\text{CN})_2]_2$ Complex

Lai-Chin Wu Yu Wang

Department of Chemistry, National Taiwan University

The spin transition between high spin (HS) and low spin (LS) state of metal with  $d^4$ - $d^7$  electronic configuration has been studied for several dozen years. Spin transition phenomenon can be induced by temperature, pressure, and even light. Light induced spin change was called light-induced excited state spin trapping (LIESST). Cooperative effect is an important effect. Usually, abrupt spin transition and spin transition with hysteresis loop happened with strong cooperative effect. Hofmann-like structure is always with relative strong such effect.

A new spin transition complex  $\text{Fe}(\text{trz})_{1.5}[\text{Au}(\text{CN})_2]_2$  was synthesized. The magnetic property was studied by SQUID magnetometer. The magnetic property shows half and gradual spin transition which was found between 200K to 80K with  $T_c$  around 155K, followed with anti-ferromagnetic interaction until the temperature down to 1.8K. This phenomenon is also reflected on C=N stretching of IR spectrum. Two peaks can be assigned for LS and HS at wave number, 2135 and 2167  $\text{cm}^{-1}$ , respectively. Interestingly, the strength of two C=N stretching is changed when we light the sample with 532 and 808 nm laser at about 10K. It shows LIESST and reverse-LIESST properties, respectively.



**Atomic Short-Range Order in Disordered Pd<sub>2</sub>Mn Alloy**Yin Suo<sup>\*</sup> Rokuro Miida<sup>\*\*</sup> Toetsu Shishido<sup>\*\*\*</sup> Ken-ichi Ohshima<sup>\*</sup>Institute of Materials Science, University of Tsukuba<sup>\*</sup> Center of General Education and Humanities, Tokyo University of Science, Japan<sup>\*\*</sup> Institute for Materials Research, Tohoku University, Japan<sup>\*\*\*</sup>

Pd-Mn alloy system has complicated phases and structures. It presents  $\alpha_1$ ,  $\beta_1$ ,  $\beta_2$ , and  $\beta_3$  phases among 20-60 at. % Mn [1]. There are few reports on  $\beta_2$  phase (Pd<sub>2</sub>Mn) [2], so that more detailed X-ray diffraction experiments should be performed for understanding of the structural characteristics. We have, therefore, measured the X-ray diffuse scattering intensity distributions from a single crystal of disordered Pd<sub>2</sub>Mn alloy, whose specimen was quenched into iced water from 1000°C. Cigar-like intensity distributions along the [010] direction at (100) and other equivalent positions were observed, which are due to an atomic short-range order (ASRO). With using Borie-Sparks' method, the ASRO intensity was separated from the total diffuse scattering intensities. Warren-Cowley ASRO parameters were determined up to the 50th neighbor. It is of characteristic that the values of  $\alpha(l00)$  parameters ( $l = \text{even number}$ ) are larger than those of the others. The X-ray diffraction intensity data for a specimen, annealed at 600°C, were also collected to determine the average structure of  $\beta_2$  phase.

**Reference**

- [1] R. Miida, T. Tajima, D. K. Saha, M. Y. Wey, D. Watanabe and K. Ohshima: Materials Transactions, 45, 9 (2004) 2822.
- [2] G. Kadar, E. Kren and M. Marton: J. Phys. Chem. Solids, 33 (1972) 212.

## An X-ray study of the modulation in $\text{Ga}_2\text{Te}_3$ with the defect zinc-blende structure

Yo Otake<sup>1</sup> Yu Yanadori<sup>1</sup> Yuusuke Seki<sup>1</sup> Shoji Kashida<sup>2\*</sup>

<sup>1</sup>Graduate School of Science and Technology, Niigata University<sup>2</sup> Department of Environmental Science, Niigata University, Japan<sup>\*</sup>

The 3-6 compound semiconductor  $\text{Ga}_2\text{Te}_3$  crystalizes into the zinc-blende structure, where one-third of its cation sites is vacant in order to satisfy the chemical valency. Hanada et al. reported from electron diffraction study that if  $\text{Ga}_2\text{Te}_3$  is annealed at temperature just below its melting point, vacancies are gathered at every ten layer.

We prepared three types of  $\text{Ga}_2\text{Te}_3$  samples, 1) cooled down slowly 2) quenched 3) annealed. Detailed X-ray intensity data were collected on a four-circle diffractometer. Weak diffuse streaks appeared between main reflections along the [111] directions and satellite reflections appeared near the main reflections. The crystal 1) shows satellite reflections at  $q=(0.085, 0.05, 0.0)$ . An extinction rule was observed: around the (100) type main reflections, satellites appeared only at planes perpendicular to the [100] direction.

An asymmetry exists between a pair of satellites centered about the main reflection. The intensity of the higher angle satellite is stronger than that of the low angle counterpart. These data indicate that the crystals have long period incommensurate structures, with transverse type modulation coupled with vacancies.

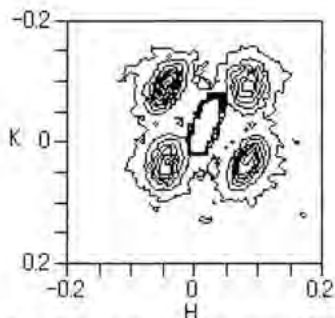


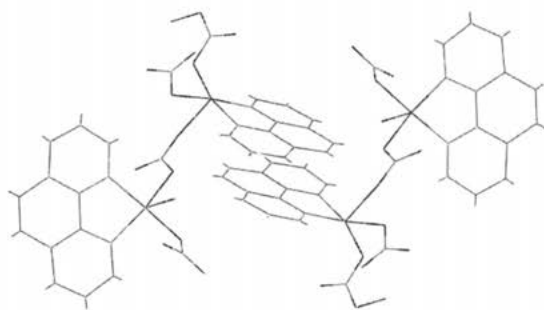
Fig. Satellites in H-K plane near (004) main reflection. They appeared at  $q=(0.06, 0.06, 0)$ .

## Polymeric Copper(II) Complex Containing Phenanthroline and Bridging Nitrate

Panana Kitiphaisalnont Sutatip Siripaisarnpipat

Department of Chemistry, Kasetsart University

The bridging complex  $[\text{Cu}(\text{phen})(\text{NO}_3)(\mu\text{-NO}_3)_2]_n$  has been synthesized by adding  $\text{Cu}(\text{NO}_3)_2 \cdot 2\text{H}_2\text{O}$  solution in to a methanol solution of ligand. The reaction mixture was stirred at room temperature. After one day, a blue crystalline product was obtained. The single crystal X-ray data was collected on SMART CCD detector. The crystal are in monoclinic system of space group  $P2(1)/n$  with  $a = 8.79470(10)$ ,  $b = 9.1099(2)$ ,  $c = 17.1963(3)\text{\AA}$ ,  $\alpha = 90$ ,  $\beta = 101.8200(10)$ ,  $\gamma = 90$ ,  $T = 293(\text{K})$ ,  $R1 = 0.0279$ . The crystal structure consists of polymeric structure of  $[\text{Cu}(\text{phen})(\text{NO}_3)(\mu\text{-NO}_3)_2]_n$ . The coordination geometry around copper atom is distorted square pyramid. One bridging nitrate is at the equatorial plane, the other at the axial position. The crystal packing shows that it is one dimensional (1D) polymeric structure. Two 1D chain lie in opposite directions in such a way that  $\pi$ - $\pi$  interaction between two phenanthroline was observed.

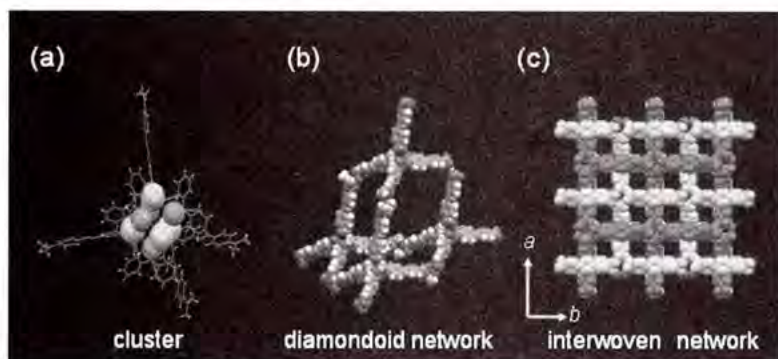


## Connection of Supramolecular Clusters with Triphenylmethylamine Disulfonate

Shinji Uehara Norimitsu Tohnai Ichiro Hisaki Mikiji Miyata

Graduate School of Engineering, Osaka University

Hydrogen-bonded supramolecular synthons represent a primary tool for crystal engineering. Recently, we have reported that organic salts composed of four carboxylic acids and four bulky triphenylmethylamines construct a cluster like a cubane through hydrogen bonds. Moreover, we succeeded in forming clusters with ammonium monosulfonates (Fig.1a), which resemble those of the carboxylate, possess discrete hydrogen-bonded networks, and shape such as a tetrapod. Here we show a connection of the supramolecular clusters with ammonium disulfonates. The connection has two kinds of networks. The one is 4-fold diamondoid network (Fig.1b). The crystals have large channel-type spaces where various organic molecules are included. The other is interwoven network (Fig.1c). The disulfonic acid molecules in latter network are considerably bent by packing force.



## X-ray Structures and Characterizations of Iron Complexes of Thiacalix-arenetetrasulfonate

Sachie Shimose Misato Ichikawa Haruo Akashi

Research Institute of Natural Sciences, Okayama University of Science

Recently, we have reported the structure of Tetrasodium thiacalix[4]arenetetrasulfonate ( $H_4TCAS$ )[1]. Odo and co-workers found that some metal complexes of  $H_4TCAS$  attached on ionexchangers showed peroxidase-like catalytic activity[2]. This prompted us to make single crystals of metal complexes of  $TCAS$  for the structure analyses. We succeeded in the preparation of micro crystals of Fe(III) complex of  $TCAS$ . A blue thin plate-like crystal of  $K_2[Fe(H_2TCAS)(H_2O)_2] \cdot 8H_2O$ (**1**), selected for data collection, was mounted in the cold nitrogen stream (105 K) of RAXIS IV(Rigaku Corp.). The compound was found to crystallize in the orthorhombic space group *Pcab* with  $a = 18.552(1)$  Å,  $b = 18.7287(8)$  Å,  $c = 25.550(2)$  Å,  $V = 8863.1(9)$  Å<sup>3</sup>. The structure analysis of **1** revealed that the iron atom is located in a distorted octahedral site. The iron atom is bound to three oxygen atoms and one sulfur atom of the  $TCAS$ . This is the first example of the  $H_4TCAS$  ligand attached directly to the Fe(III) moiety. Second-sphere coordination compounds,  $K[Fe(H_2O)_6](H_4TCAS)$  and  $K_2[Fe(H_2O)_6](H_4TCAS)$ , will also be reported.

### Reference

- [1] Akashi H., et al., *Acta Cryst.*, 2003, **E59**, m336.
- [2] Odo J., et al., *Anal. Sci.*, 2004, **20**, 707.

## Growth and characterization of hollandite-type single crystal

Kenjiro Fujimoto Kenji Takamori Shigeru Ito

Department of Pure and Applied Chemistry, Tokyo University of Science

Hollandite-type compounds are represented by a general chemical formula  $A_xM_yN_{8-y}O_{16}$  ( $x < 2$ ,  $y < 2$ ); where usually A = alkali or alkaline earth ions, M = di- or trivalent cations, and N = tetravalent cations. The structure has a tetragonal symmetry and contains tunnels extended along the unique axis with about 0.3 nm in period. This type of framework structure consists of double chains of  $(M,N)O_6$  octahedra edge-shared with adjacent ones. In the K-M-Ti-O hollandite-type compounds (M: Al, Ga etc.), these compounds have been studied as a one-dimensional fast ion conductor of alkali ions [1] and nuclear waste immobilizers [2,3] so far. In this study, K-(Fe or Ga)-Sn-O hollandite-type single crystals were grown in order to obtain crystallographic information and physical property by flux method. A mixture of  $(K_2O)_x(MoO_3)_y(B_2O_3)_z$  system was used for flux composition. Needle like single crystal aggregate, about 3mm long and 60 $\mu$ m thickness, were collected by cooling down from 1623K to 1273K at 1.5-2.0K/hr.

### Reference

- [1] S. Yoshikado, T. Ohachi, I. Taniguchi, Y. Onoda, M. Watanabe and Y. Fujiki, Solid State Ionics 9-10,1305, (1983).
- [2] A. E. Ringwood, S. E. Kesson, N. G. Ware, W. Hibberson and A. Major, Nature 278, 219, (1979).
- [3] H. Mitamura, S. Matsumoto, M. W. A. Stewart, T. Tsuboi, M. Hashimoto, E. R. Vance, K. P. Hart, Y. Togashi, H. Kanazawa, C. J. Ball and T. J. White, J. Am. Ceram. Soc. 77(9), 2255, (1994).

## Investigation on structural Phase Transition in Langbeinites

Tayur N Guru Row Diptikanta Swain

Solid State and Structural Chemistry Unit, Indian Institute of Science

The occurrence of a phase transition in a solid alters several material properties. Measurement of a particular property across the phase transition using sophisticated techniques provides insights into the nature of phase transition. Ferroic phase transitions in crystals usually involve a change of the space group symmetry. The langbeinite family of sulfates is well known for their ferroelectrics and ferroelastic phase transition with temperature. Langbeinites are categorized into three types, type-I, type-II and type-III. Type-I langbeinites exhibit series of phase transition from cubic to orthorhombic and to monoclinic crystal systems, Type-II exhibits phase transition from cubic to orthorhombic modifications and Type-III does not exhibit any phase transition with the temperature in the range 293K to 80K. We have investigated two new compounds in the langbeinite family,  $\text{Rb}_2\text{Mn}_2(\text{SO}_4)_3$  and  $(\text{NH}_4)_2\text{Mn}_2(\text{SO}_4)_3$  at various temperature to cover the entire range of phase transition.  $\text{Rb}_2\text{Mn}_2(\text{SO}_4)_3$  shows a phase transition from cubic (P2,3) at 293K to orthorhombic (P2,2,2<sub>1</sub>) at 80K via a monoclinic (P2<sub>1</sub>) 140K crystal system, where as  $(\text{NH}_4)_2\text{Mn}_2(\text{SO}_4)_3$  shows a phase transition from cubic(P2,3) at 293K to monoclinic (P2<sub>1</sub>) at 120K via orthorhombic (P2,2,2<sub>1</sub>) at 80K crystal system. The features of the crystal structures across the phase transition regime will be presented.

## Determination of Charge Ordered Structure in $(DI\text{-}DCNQI)_2\text{Ag}$ using Synchrotron Radiation X-ray Diffraction

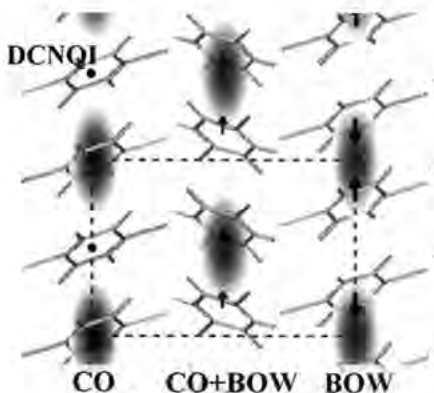
Toru Kakiuchi<sup>1</sup> Yusuke Wakabayashi<sup>1</sup> Hiroshi Sawa<sup>2</sup> Tetsuaki Ito<sup>3</sup> Kazushi Kanoda<sup>4</sup>

<sup>1</sup>Department of Materials Structure Science, The Graduate University for Advanced Studies<sup>1</sup>  
<sup>2</sup>Institute of Materials Structure Science, High Energy Accelerator Research Organization, Japan<sup>2</sup>  
<sup>3</sup>Department of Applied Physics, University of Tokyo, Japan<sup>3</sup>

Recently, charge ordering (CO) phenomena are attracting considerable attention. Many investigations about CO materials have been performed in order to make clear how the electronic correlation stabilizes CO state.

Organic salt  $(DI\text{-}DCNQI)_2\text{Ag}$ , a typical pseudo one-dimensional electronic structure material, is one of such CO materials.[1] Although Hiraki *et al.* proposed Wigner crystal type of CO as the ground state based on their NMR measurement,[2] the CO structure is still unsolved because the real crystal has complicated three-dimensional interaction.

We have conducted a full-structure analysis in order to clarify the CO structure in this compound. The measurement was made at BL1A at the Photon Factory, KEK, Japan with using imaging plate Weissenberg camera attached with displax. Obtained low-temperature structure shows that the CO coexists with bond order wave (BOW) accompanied with dimerization. This is due to frustration among the DCNQI column. In spite of the peculiar structure, charge distribution (black clouds in the figure show charge rich area schematically) was concluded as a simple body centered Wigner crystal.



### Reference

- [1] H. Seo and H. Fukuyama, J. Phys. Soc. Jpn. 66 1249(1997)  
 [2] K. Hiraki and K. Kanoda, Phys. Rev. Lett. 80 4737(1998)

## Order and disorder in heavily Fe-substituted high- $T_c$ superconductors

Takashi Mochiku<sup>1</sup> Yoshiaki Hata<sup>2</sup> Tuerxun Wuernisha<sup>3</sup> Kazuhiro Mori<sup>4</sup> Toru Ishigaki<sup>5</sup> Takashi Kamiyama<sup>6</sup> Hiroki Fujii<sup>7</sup> Hiroshi Yasuoka<sup>8</sup> Kazuo Kadowaki<sup>9</sup> Kazuto Hirata<sup>10</sup>

<sup>1</sup>Superconducting Materials Center, National Institute for Materials Science<sup>1</sup> Department of Applied Physics, National Defense Academy, Japan<sup>2</sup> Institute of Materials Structure Science, High Energy Accelerator Research Organization, Japan<sup>3</sup> Research Reactor Institute, Kyoto University, Japan<sup>4</sup> Quantum Beam Science Directorate, Japan Atomic Energy Agency, Japan<sup>5</sup> Institute of Materials Science, University of Tsukuba<sup>6-10</sup>

Although most of high- $T_c$  superconductors with light substitution of transition metal exhibit superconductivity, the heavily substituted compounds do not exhibit superconductivity even after annealing under high oxygen pressures, which is considered to promote superconductivity due to charge introduction. However, superconductivity was discovered around 50 K in heavily Fe-substituted high- $T_c$  superconductor  $\text{FeSr}_2\text{YCu}_2\text{O}_{6+d}$ , which was annealed in an  $\text{N}_2$  atmosphere and subsequently in an  $\text{O}_2$  atmosphere. Neutron powder diffraction study shows that  $\text{N}_2$ -annealing causes ordering of Cu and Fe, and that  $\text{O}_2$ -annealing supplies the charge on the  $\text{CuO}_2$  sheets. We have also found a superstructure in the samples  $\text{N}_2$ -annealed within a particular temperature range. It has the  $\text{CoSr}_2\text{YCu}_2\text{O}_7$ -type superstructure with the  $\text{FeO}_4$  tetrahedron, due to not only atomic ordering of Cu and Fe but also oxygen ordering. The formation of the  $\text{FeO}_4$  tetrahedron is important for exhibiting superconductivity in heavily Fe-substituted compounds, because Cu can be not substituted for Fe in the  $\text{FeO}_4$  tetrahedron and the formation of the  $\text{FeO}_4$  tetrahedron promotes atomic ordering of Cu and Fe to exhibit superconductivity. However, since the formation of the  $\text{FeO}_4$  tetrahedron is not promoted by  $\text{N}_2$ -annealing in Nd-substituted compound  $\text{FeSr}_2\text{NdCu}_2\text{O}_{6+d}$  with larger lattice size than  $\text{FeSr}_2\text{YCu}_2\text{O}_{6+d}$ , exhibiting superconductivity is dependent on lattice size in this system.

## Chiral Recognition of Racemic Alcohols in Lattice Inclusion Compounds

Kazuaki Aburaya Ichiro Hisaki Norimitsu Tohnai Mikiji Miyata

Department of Material and Lifescience, Osaka University

Chiral recognition in inclusion crystals is of interest not only in resolution of racemate but also in crystal engineering and supramolecular chemistry. Though many artificial hosts have been developed for chiral recognition of alcohols in the crystalline state, there are few examples in which small alcohols have been included with high enantioselectivity [1]. Especially, in the case of secondary alcohols, it is difficult to recognize chirality due to the subtle structural differences between the enantiomers as implied by four-location model [2]. Bile acid derivatives include various alcohols within channel-like chiral cavities created by the host molecules. Therefore a systematic study of chiral recognition of secondary alcohols can be carried out.

We describe here chiral recognition of various alcohols in the inclusion compounds of bile acid derivatives such as 3-epicholic acid (**ECA**), 3-epideoxycholic acid (**EDCA**) and cholamide (**CAM**). The host compounds showed enantioselective inclusion for many aliphatic and aromatic alcohols. These enantioselectivity varied from poor to excellent depending on combination of a host and a guest. For example, crystallization of **CAM** from racemic 2,2-dimethyl-3-hexanol (**1**) showed selective inclusion of (*S*)-**1** with as high as 98% enantiomeric excess (ee). On the other hand, crystallization of **CAM** from racemic 2-methyl-3-hexanol (**2**) showed inclusion of (*S*)-**2** with 19% ee. The chiral recognition mechanism of these inclusion compounds will be examined on the basis of X-ray crystallographic analyses.

### Reference

- [1] Y. Imai, T. Sato, R. Kuroda *Chem. Commun.* **2005**, 3289-3291.
- [2] K. Kato, K. Aburaya, Y. Miyake, K. Sada, N. Tohnai, M. Miyata *Chem. Commun.* **2003**, 2872-2873.

### X-ray structural analysis of $\beta$ -Ga<sub>2</sub>Se<sub>3</sub>

Yuu Yanadori<sup>\*</sup> Yo Otaki<sup>\*</sup> Yuusuke Seki<sup>\*</sup> Shoji Kashida<sup>\*\*</sup>

Environmental Science and Technology, Niigata University Graduate School of Science and Technology<sup>\*</sup> Faculty of Science, Niigata University, Japan<sup>\*\*</sup>

Ga<sub>2</sub>Se<sub>3</sub> has a zinc-blende type structure, where in order to satisfy the valence condition, one-third of the cation sites is vacant. From X-ray powder diffraction study, the vacancy ordered phase,  $\beta$ -Ga<sub>2</sub>Se<sub>3</sub> is reported to have a monoclinic structure,  $a=6.6608$ ,  $b=11.6516$ ,  $c=6.6491\text{\AA}$ , and  $\beta=108.840$  ( $Z=4$ ). In this study using single crystal samples we have performed X-ray structural analysis.

The X-ray precession photographs show zinc-blende type main reflections and weak reflections at  $1/3(220)c$ ,  $1/6(111)c$ , where  $c$  means the ideal cubic lattice. Diffuse streaks are also observed which is centered on main Bragg peaks and elongated along the  $\langle 111 \rangle$  direction. From the reciprocal unit cell vectors,  $a^*=1/3(1-11)c$ ,  $b^*=2/3(1-10)c$  and  $c^*=1/6(111)c$ , we concluded that the crystal is triclinic  $a=1/2(-1-12)c$ ,  $b=3/2(10-1)c$ ,  $c=3(110)c$ ,  $\alpha=60.0465$ ,  $\beta=125.285$  and  $\gamma=149.97$  ( $Z=6$ ).

Intensity data were collected on Huber four-circle diffractometer, and the structure analysis was done using the heavy-atom method. Since the crystal is composed of multiple twins, we have used only the satellite reflections. The synthesized partial Patterson function shows that three of the six vacant cation sites are located along the (011) axis (Fig. 1).

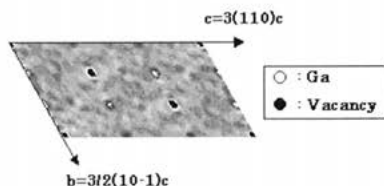


Fig.1 Position of Ga vacancies in the (100) plane.

**Structure and phase transition in  $C_5H_{10}NH_2PbI_3$** 

Miwako Takahashi<sup>1</sup> Yuji Fujii<sup>2</sup> Takuro Kawasaki<sup>2</sup> Kataoka Kunimitsu<sup>2</sup> Masashi Watanabe<sup>3</sup>  
Ken-ichi Ohshima<sup>1</sup>

<sup>1</sup>Institute of Materials Science, University of Tsukuba<sup>1</sup> Graduate School of Pure and Applied Sciences, University of Tsukuba, Japan<sup>2</sup> Institute of Multidisciplinary Research for Advanced Materials, Tohoku University, Japan<sup>3</sup>

The structure and phase transition in the one-dimensional semiconductor  $C_5H_{10}NH_2PbI_3$  has been investigated by using x-ray and neutron single crystal diffraction methods.  $C_5H_{10}NH_2PbI_3$  has a lead-based inorganic-organic perovskites structure consisting of semiconducting parts which are composed of one-dimensional chains of face-sharing lead-iodide octahedra and barrier parts composed of  $C_5H_{10}NH_2^+$  molecules. It has been shown by Raman scattering that the structure undergoes successive phase transitions below the room temperature which involves rotational/orientational ordering of the organic  $C_5H_{10}NH_2^+$  parts. However, its precise structure has not been determined even for the room temperature. The aim of the present study is to clarify the structural change and its effects on the electronic state in the phase transition of  $C_5H_{10}NH_2PbI_3$ . By combining the data obtained by x-ray and neutron single crystal diffraction, its structural model at room temperature including positional information for Hydrogen and Nitrogen atoms is proposed. The temperature- and pressure- induced phase transitions in  $C_5H_{10}NH_2PbI_3$  have also been investigated. The temperature variation of neutron diffraction patterns shows drastic changes below 250K, indicating a symmetrical change of the structure takes place at around 250K. The lattice constant for b-axis shows large contraction of 5.84% at this temperature together with the expansion of a- and c- axis of 0.51 and 1.54 %, respectively. These changes indicate that the phase transition induced by rotational and orientational ordering of  $C_5H_{10}NH_2^+$  molecules, as predicted by Raman scattering, occurs around 250K. The structural model below 250K is now under consideration and will be presented.

## Processing and characterization of ferroelectric nanostructures

Songhak Yoon<sup>1</sup> Hee Han<sup>1</sup> Yongjun Park<sup>2</sup> Min Gyu Kim<sup>2</sup> Namsoo Shin<sup>2</sup> Ran Ji<sup>3</sup> Dietrich Hesse<sup>4</sup>  
 Marin Alexe<sup>4</sup> Kornelius Nielsch<sup>4</sup> Ulrich Goeessele<sup>4</sup> Sunggi Baik<sup>1</sup>

Department of Materials Science and Engineering, Pohang University of Science and Technology, KOREA<sup>1</sup> Pohang Accelerator Laboratory, Pohang University of Science and Technology, Korea<sup>2</sup> Max Planck Institute of Microstructure Physics, Germany<sup>3</sup>

This presentation will focus on recent findings related to the process and analysis of ferroelectric nano-materials. In the first example, the influence of lattice expansion on the crystal structural changes of the BaTiO<sub>3</sub> nanoparticles have been studied by X-ray diffraction and X-ray absorption near edge structure via synchrotron radiation. BaTiO<sub>3</sub> nanoparticles are synthesized by hydrolysis and condensation of mixed isopropanol solution of barium hydroxide octahydrate and titanium (IV) isopropoxide. The BaTiO<sub>3</sub> nanoparticles synthesized without additional water showed anomalous lattice expansion and high tetragonality. As extra water is introduced and its amount is increased, Rietveld analysis confirms that the crystal structures of BaTiO<sub>3</sub> nanoparticles change gradually from tetragonal to cubic structure. Change in peak intensities at the titanium pre-edge region in XANES also indicates that highly distorted TiO<sub>6</sub> octahedra are gradually relaxed with water addition.

In the second example, well-ordered Pb(Zr<sub>0.2</sub>Ti<sub>0.8</sub>)O<sub>3</sub> nanostructures with the lateral size ranging from 400 nm to 100 nm were fabricated on SrRuO<sub>3</sub> bottom electrode on SrTiO<sub>3</sub> single crystal substrate using laser interference lithography (LIL) process combined with pulsed laser deposition. Transmission electron microscopy confirmed that (001)-oriented PZT nanostructures were grown epitaxially on (001)-oriented single crystal substrate covered with epitaxial SrRuO<sub>3</sub> (001) bottom electrode layer. Anisotropic ferroelectric properties of each PZT nanostructure were characterized by scanning force microscopy and the evolution of domain structures as a function of thickness and width of PZT nano-islands was characterized by reciprocal space mapping using synchrotron X-ray diffraction.

**$\beta$  to  $\alpha$  phase transition in Sn single crystal**Miwako Takahashi<sup>1</sup> Matthias J Gutmann<sup>2</sup><sup>1</sup>Institute of Materials Science, University of Tsukuba<sup>2</sup> ISIS Facility, CLRC Rutherford Appleton Laboratory, U.K.

It is well known that Sn undergoes a phase transition from its usual metallic phase (beta phase) to lower temperature phase (alpha phase). Alpha Sn has the diamond structure and is a semiconductor. Beta Sn has a body-centered tetragonal structure and is metallic. The thermodynamic temperature of the transition is 13C at atmospheric pressure, however, beta Sn does not transform readily into alpha Sn below 13C. The rate of transition only becomes significant after considerable undercooling, and long periods are necessary to allow alpha Sn to nucleate. Up to now, a detailed microscopic description of this phase transition has not been available. The aim of our study is to understand the mechanism and kinetics of the transition. Neutron diffraction experiments were performed with the beta Sn single crystals to observe a change in diffraction pattern for the beta to alpha phase transition. In the measurement, characteristic rod-like diffuse scattering has been observed in the beta phase. The detail structure and temperature dependence were investigated by using four-circle single crystal diffractometer FINDER at JRR-3M. It was found that the diffuse intensities strongly depend on temperature and distributed around the z.b., thus the origin is considered as temperature diffuse scattering (TDS) with two-phonons process. The intensity distribution was calculated for the 2nd TDS and was found to reproduce the observed diffuse scattering well. The time dependence of the structure in the process of transition was also investigated by using pulsed single crystal diffractometer SXD at ISIS. The results of the structural analysis will also be presented.

## Approximants for the Al-Co-Si decagonal phase

Kazumasa Sugiyama Hironori Sato

Department of earth and Planetary Science, The University of Tokyo

Since the addition of transition metals and silicon into an Al matrix involves the formation of a variety of intermetallic phases which contribute to special mechanical strength and high thermal and electrical conductivity, the ternary phase diagram of Co-Al-Si system was extensively studied [1,2]. On the other hand, much attention has been paid to the Al-Co alloy system because a large number of quasi-crystalline phases together with their approximants have been found in their Al-rich region. The ternary system of Al-Co-Si is also classified in this category [3].

The crystal structures of approximant structures; f-AlCoSi (*Pnma*;  $a=1.3859(1)\text{nm}$ ,  $b=2.3019(1)\text{nm}$ ,  $c=0.7322(1)\text{nm}$ ,) and W-AlCoSi (*Cm*;  $a=3.9658(4)\text{nm}$ ,  $b=0.8139(1)\text{nm}$ ,  $c=2.3658(2)\text{nm}$ ,  $b=90.02(1)^\circ$ ) grown in the Al-rich region of the Al-Co-Si system, were analyzed by the single crystal X-ray diffraction. Both compounds exhibit surprisingly large unit cells and complex structures. In particular, the structure of W-AlCoSi phase is isostructural with W-AlCoNi phase by providing a fundamental atomic arrangement for the columnar atom cluster observed commonly in the Al-Co-Ni decagonal quasicrystals[4]. The structure of f-AlCoSi phase serves an unique columnar structural unit similar to those found in the approximants of  $\text{Al}_3\text{Mn}$ [5] and  $\text{Al}_3\text{Pd}$ [6].

### Reference

- [1] K.W.Richter & D.T.Gutierrez, *Intermetallics* **12**(2005)848.
- [2] K.W.Richter, Y.Prots & Y.Grin, *Inorg. Chem.* **44**(2005)4576.
- [3] J.Menon & C.Suryanarayana, *Mater. Trans. JIM* **30**(1989)878.
- [4] K.Sugiyama, S.Nishimura & K.Hiraga, *J. Alloy Comp.*, **342**(2002)65.
- [5] K.Hiraga, M.Kaneko, Y.Matsuo & S.Hashimoto, *Philos. Mag.* **B67**(1993)193.
- [6] Y.Matsuo & K.Hiraga, *Philos. Mag. Lett.*, **70**(1994)155.

## Structural and magnetic studies on $\text{CuMPT}_6$ (M= 3d elements) ternary alloys

Ejaz Ahmed Yuji Fuji Miwako Takahashi Hiroshi Iwasaki Ken-ichi Ohshima

Institute of Materials Science, University of Tsukuba

We have already identified the crystal structure of newly designed  $\text{CuMPT}_6$  (M=3d elements) alloys by X-ray, electron and neutron diffraction methods [1, 2]. In the analysis, a double step ordering without any change of cubic symmetry was firstly discovered for  $\text{CuMnPt}_6$  alloy. In order to obtain more quantitative information on structure and magnetism of the alloys, we have performed in-situ X-ray diffraction, electrical resistivity and magnetic susceptibility measurements. First, the transition temperatures from disordered to  $\text{Cu}_3\text{Au}$  type ordered phases were determined in a temperature range from 750 °C for M=Mn to 1010 °C for M=Fe. Secondly, the values of the resistivity were determined as  $(5\sim 7)\times 10^{-5}$  ohm-cm except for M = Mn with  $6\times 10^{-4}$  ohm-cm. Thirdly, a general trend in magnetic properties is as follows: paramagnetic - spinglass like - ferromagnetic - paramagnetic with increasing atomic number. The nature of the magnetism is not much affected by the structural phase changes in the present alloys, though a little change is observed in  $T_c$  or  $T_g$  due the structural phase change. The original nature of the magnetism in the ternary  $\text{CuMPT}_6$  alloys remains the same as in the binary  $\text{MPT}_3$  one. We believe that the unpaired electrons in 3d-elements are responsible for the magnetic properties of  $\text{CuMPT}_6$  alloys.

### Reference

- [1] M. Takahashi, A. K. Das, R. Nakamura, H. Iwasaki, T. Shishido and K. Ohshima: J. Phys. Soc. Jpn. 75 (2006) 013601-1.
- [2] A. K. Das, R. Nakamura, M. Takahashi, H. Iwasaki, T. Shishido and K. Ohshima: J. Phys. Soc. Jpn. 75 (2006) 024604.

**Host-guest chemistry of resorcinarenes-towards functional cavitands**

Tayur N Guru Row Mahalakshmi L. Partha Pratim Das

Solid State and Structural Chemistry Unit, Indian Institute of Science

Design of functional materials via molecular recognition and self assembly is a topic of ongoing interest. Such studies on cavitands like resorcinarenes show the generation of novel supramolecular architecture stabilized by weak intermolecular interactions. In this context, we report our studies of the host molecule C-methylcalix[4]resorcinarene(**1**) with guest molecules 2,2-bipyridine(**2**), 1,4-diazabicyclooctane(**3**), coumarin(**4**), coumarin and 4,4-bipyridine (**5**). The compounds **2** and **4** crystallize in monoclinic system [*C2/c*,  $a=37.3084(43)$ ,  $b=12.7857(14)$ ,  $c=25.0057(29)$ ,  $\beta=131.496(2)$  and  $a=15.5206(21)$ ,  $b=14.4806(19)$ ,  $c=21.0803(29)$ ,  $\beta=109.378(2)$  respectively]whereas **3** crystallizes in a Tetragonal [*P4(2)n*],  $a=b=21.1519(10)$ ,  $c=15.7507(16)$ ] and **5** in a Triclinic system[*(P-1)*,  $a=12.0821(36)$ ,  $b=13.3291$ ,  $c= 16.8730(50)$ ,  $\alpha=93.197(5)$ ,  $\beta=100.739(5)$ ,  $\gamma=101.409(5)$ ]. The conformation of the host molecule changes with the nature of the guest for e.g., in **1** and **2** the cone conformation is retained whereas in compounds **3** and **4** the host conformation changes to a partial cone or an open basket. Detailed structural analysis and nature of various intermolecular forces that constitute the packing modes in these complexes will be discussed.

**Systematics of high pressure phase transformation of minerals and compounds containing  $WO_4$  and  $MoO_4$  molecules**

Shu-Cheng --- YU' Tony HUANG' Eugene HUANG''

Department of Earth Sciences, Cheng-Kung University' Chung-Chou Institute of Technology, TAIWAN''

Tetrahedron is a very fundamental structural unit in a vast number of terrestrial mineral species. Tetrahedral unit of  $SiO_4$ ,  $SO_4$  and  $PO_4$  are commonly occurred in most of the rock-forming minerals. Their high pressure structures and phase transformation have been well documented. In the present study, we extend and summarize the high pressure X-ray diffraction and Raman scattering analyses to the minerals and compounds containing  $WO_4$  and  $MoO_4$  tetrahedral components.

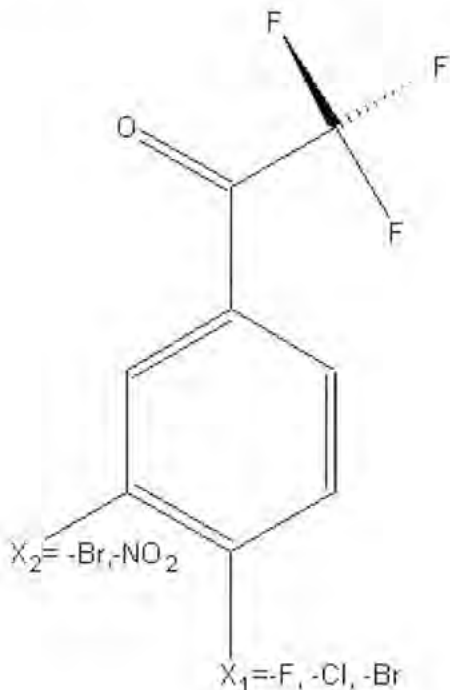
Tungstates and molybdates of Ca, Sr, Pb and Ba all adopt a scheelite structure at the ambient conditions. Scheelite ( $CaWO_4$ ) transforms from  $I4_1/a$  symmetry to an  $I2/a$  symmetry of the fergusonite structure at a pressure of about 10 GPa. The phase transformation pressures for the molybdates series,  $CaMoO_4$ ,  $SrMoO_4$ ,  $PbMoO_4$ , and  $BaMoO_4$ , decrease with increasing the cationic radii. The similar relationship was also observed for the tungstates series only when  $PbWO_4$  was excluded. The detailed spectroscopic and structural characteristics of these two series as a function of pressure will be discussed.

## Variability in Halogen Interactions: In-situ cryocrystallization of low melting substituted trifluoroacetophenones.

Deepak Chopra<sup>1</sup> Vijay Thiruvengadam<sup>2</sup> Tayur Narasimha Row<sup>1</sup>

<sup>1</sup>Solid State and Structural Chemistry Unit, Indian Institute of Science<sup>2</sup> Solid State and Structural Chemistry Unit Indian Institute of Science India<sup>2</sup>

*In-situ* cryo-crystallization of low melting halogenated trifluoroacetophenones reveals the features of short halogenhalogen and halogenoxygen contacts acting cooperatively with weak but highly directional C-HO and C-HF contacts. Studies based on Cambridge structural database indicate directional preferences in halogenhalogen and halogen...oxygen short contacts. Intra-molecular C-HF contacts lock the trifluoroacetophenone moiety conformationally to provide the basic building block.



## Magnetic Domain Structure in Canted C-type Manganites

Xiuzhen Yu<sup>1</sup> Yasuhide Tomioka<sup>2</sup> Yoshio Kaneko<sup>3</sup> Toru Asaka<sup>4</sup> Masahiro Nagao<sup>5</sup> Weizhu Zhang<sup>6</sup> Koji Kimoto<sup>7</sup> Takahisa Arima<sup>8</sup> Yoshinori Tokura<sup>9</sup> Yoshio Matsui<sup>10</sup>

Advanced Electron Microscopy Group, National Institute for Materials Science,<sup>1</sup> Correlated Electron Research Center, AIST, Japan<sup>2</sup> Spin Super Structure Project, ERATO, JST, Japan<sup>3</sup> Advanced Electron Microscopy Group, NIMS, Japan<sup>4</sup> Institute of Multidisciplinary Research for Advanced Materials, Tohoku Univ., Japan<sup>5</sup> Department of Applied Physics, Univ. of Tokyo, Japan<sup>6</sup>

The doped perovskite manganite  $RE_{1-x}AE_xMnO_3$  ( $RE$ : a rare earth element;  $AE$ : an alkaline element) has been attention to the colossal magnetoresistance properties [1, 2], which strongly correlate to the coupling among charge, orbital and spin. In order to study the magnetic properties for the canted C-type antiferromagnetic (AF) materials [1], such as  $RE_{0.4}Sr_{0.6}MnO_3$  ( $RE$ : Sm, Eu), magnetic domain structure was studied using the Lorentz TEM. Figure 1 shows the magnetic domain structure of  $Sm_{0.4}Sr_{0.6}MnO_3$  at 20 K. Fresnel image and transport-of-intensity equation [3] image reveal that the 180 degrees magnetic domains exist in the(010) thin crystal. The easy magnetization direction was found to be along the  $a_c$ -axis ( $a_c$ : the axis of cubic perovskite structure). Furthermore, it was found the local crystalline defects and twins of the sample decrease the magnetic domain size. This result is useful for understanding the magnetic property of the canted C-type AF manganites.

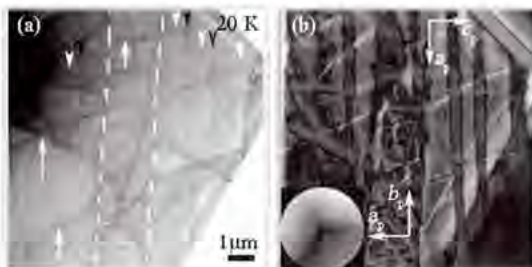


Fig 1 Magnetic domain structure images of  $Sm_{0.4}Sr_{0.6}MnO_3$  at 20 K.

(a) Fresnel Lorentz image. White and black lines (indicated by white and black triangles) correspond to magnetic domain walls. The local crystalline defects are indicated by white arrows. (b) Magnetization distribution images obtained by the transport-of-intensity equation (TIE) method. The directions of magnetizations are represented by the color wheel. The  $a_p$  and  $c_p$  indicate cubic perovskite crystalline directions. (c) Schematic of the spin arrangement in  $Sm_{0.4}Sr_{0.6}MnO_3$  at 20 K. The color arrows present the spin directions.

### Reference

- [1] Colossal Magnetoresistive Oxides, edited by Y. Tokura (Gorden and Breach Science Publisher, 2000).
- [2] Y. Tomioka *et al.* Appl. Phys. Lett. **70** (26), 3609 (1997).
- [3] V. V. Volkov and Y. Zhu, Phys. Rev. Lett., **91** (2003) 043904.

## Modulation Structure of Charge Ordering in Nikelates

Xiuzhen Yu

Advanced Electron Microscopy Group, National Institute for Materials Science,

Charge ordering (CO) is an important phenomenon of physics in the correlated electron systems [1]. In manganites, the CO state can be controlled by the solid solution of the perovskite A-site where rare-earth (RE) ions and alkaline-earth (AE) ions locate. The CO correlation is suppressed by the A-site randomness that originates from ionic-radius-variance-induced local distortions [2]. In this work, we have investigated the relation of the CO state and the variance  $\sigma$  in A-site ionic radii in  $RE_{2-x}AE_xNiO_4$  ( $x = 1/3$ ) (RE: Pr, Sm; AE: Sr, Ca). The single crystals were prepared by the floating-zone method [3]. For TEM observations, the samples were thinned by argon-ion milling. Selected-area electron diffraction (SAED) patterns were obtained by the transmission electron microscope (Hitachi HF-3000S). By analyzing the SAED patterns of  $RE_{2-x}AE_xNiO_4$  ( $x = 1/3$ ), we found that the CO state depends strongly on the variance in A-site ionic radii. The modulation wave number  $\delta d$  and the half-width at half-maximum (HWHM) of the superlattice spot have been plotted as a function of the variance in A-site ionic radii  $\sigma$ . It is obvious that the HWHM increases with increasing the  $\sigma$ , while  $\delta d$  exhibits the contrary behavior. The results indicate that the CO instability and correlation length decrease when  $\sigma$  increases. Namely, the CO state is suppressed by the A-site randomness in the nikelates, just as observed previously in manganites.

### Reference

- [1] Colossal Magnetoresistive Oxides, edited by Y. Tokura (Gordon and Breach Science Publisher, 2000).
- [2] Y. Tomioka *et al.*, Phys. Rev. B. 70 (2004) 14432.
- [3] S. Seki *et al.*, to submit.

## A Tunable Solid-State Luminescence System Consisting of 4,4''-Terphenyldisulfonic Acid and 1,2,4,5-Tetracyanobenzene with Aliphatic Amines

Keisuke Inoue Norimitsu Tohnai Ichiro Hisaki Mikiji Miyata

Department of Material and Life Science, Graduate School of Engineering, Osaka University

### [INTRODUCTION]

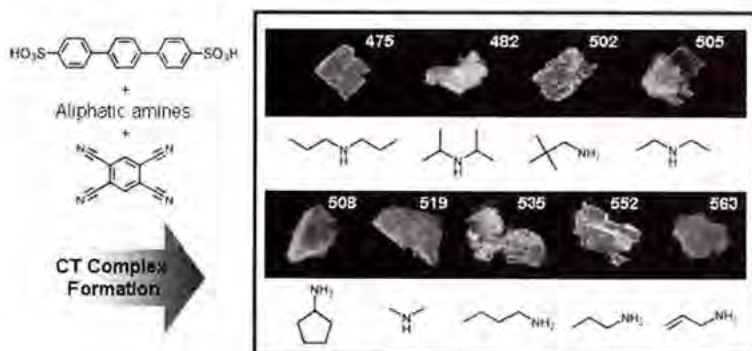
Solid-state organic luminescence has been the focus of considerable interest because of their various availabilities in the applied fields. In this work, we prepared CT complex crystals composed of 4,4''-terphenyldisulfonic acid (TPDS), various aliphatic amines, and 1,2,4,5-tetracyanobenzene (TCNB) (Figure shown at the bottom), here we elucidated the correlation between the photophysical properties and crystal structures.

### [EXPERIMENTS]

CT complex crystals were prepared by mixing TPDS, the amines and TCNB in methanol/acetnitrile with a 1:2:1 molar ratio. We investigated the crystals by fluorescence spectroscopy and single crystal X-ray structure analysis.

### [RESULTS and DISCUSSION]

First, it was revealed that the crystals showed wide spread luminescence ( $\lambda_{\text{max}} = 475\text{-}563$  nm) corresponding to difference of the amines (Figure shown at the bottom). Next, the crystal structures were classified into 4 groups by single crystal X-ray structure analysis. Consequently we found the luminescence of CT complex crystals depended on relative alignments between TPDS and TCNB, which are is controlled by the amines.



## Crystal structure of novel layered silicate PLS-3 as a FER-zeolite precursor determined by X-ray powder diffraction

Ikeda Takuji Syunsuke Kayamori Takaaki Hanaoka Fujio Mizukami

Research Center for Compact Chemical Process, National Institute of Advanced Industrial Science and Technology

Recently, a new zeolite synthetic method by the topotactic conversion using zeolitic layered silicates is interested and produced novel framework zeolites, e.g., Nu-6(2)(NSI), RUB-41(RRO), RUB-24(RWR) and CDS-1(CDO). On the other hand, layered silicate PREFER, which have been known as the first example by the above method, can be converted to FER zeolite. In this work, we report that a novel layered silicate PLS-3, which has a similar framework topology to PREFER[1], was synthesized from H-formed layered silicate kanemite by steam assisted solid-state reaction. Crystal structure of PLS-3 was determined by the *ab-initio* analysis using X-ray powder diffraction data. PLS-3 was successfully converted to siliceous zeolite CDS-3 with FER-topology by carefully calcination.

X-ray powder diffraction data were collected on a Bruker D8-ADVANCE Vario-1 using monochromatic Cu K $\alpha$  radiation and modified Debye-Scherrer geometry. Lattice constants and space group were  $a = 13.9937(10)$  Å,  $b = 7.4170(6)$  Å,  $c = 22.337(2)$  Å and  $Pnmm$  (No.58). The partial atomic coordinates obtained by the direct method analysis were introduced as a starting model for a Rietveld refinement using the RIETAN-2000 program system.

The framework structure of PLS-3 is a very similar to that of PREFER, but the lattice constant of  $c$ -axis was relatively shorten ca. 3 Å. Chemical composition was estimated to be  $\text{Si}_{16}\text{O}_{66}(\text{OH})_8 \cdot 2.4(\text{TEAOH}) \cdot 8(\text{H}_2\text{O})$  calculated from refined occupancy factors. Both TEAOH and water molecules were intercalated into an interlayer.

### Reference

- [1] L. Schreyeck, P. Caullet, J. C. Mougénel, J. L. Guth, B. Marler, *Stud. Surf. Sci. Catal.*, 105, 1949 (1997).

**SEM and TEM study of some Wild II cometary particles returned by the NASA Stardust Mission**Takashi Mikouchi<sup>1</sup> Osamu Tachikawa<sup>2</sup> Kenji Hagiya<sup>3</sup> Kazumasa Ohsumi<sup>4</sup> Michael Zolensky<sup>5</sup><sup>1</sup>Department of Earth and Planetary Science, University of Tokyo<sup>2</sup> Graduate School of Life Science, University of Hyogo<sup>3</sup> High Energy Accelerator Research Org. (KEK)<sup>4</sup> NASA Johnson Space Center<sup>5</sup>

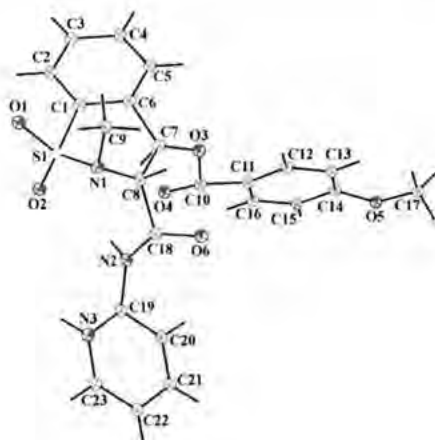
Stardust is a NASA comet sample return mission that successfully returned the Wild II cometary particles in Utah, USA on Jan. 15, 2006. We studied several naked particles and microtomed sections by Hitachi S-4500 SEM and JEOL JEM-2010 TEM for mineralogy and crystallography as a part of preliminary examination teams. The size of Wild II particles ranges from <1 to 30 micrometers. Most analyzed samples were contaminated with silica aerogel used for the capture of cometary particles in space. These samples are composed of an amorphous silica-rich phase with scattered ~100 nm particles of iron metal and iron sulfides. It is likely that these particles were formed by high temperature during the capture process. There are some areas enriched in Mg, suggesting the presence of mafic silicates. We could also find some crystalline materials such as olivine and pyroxene that were identified by electron diffraction of TEM and electron back-scatter diffraction of SEM. Most of crystalline phases are small (up to 1 micrometer), but their diffraction patterns are sharp, suggesting good crystallinity. It is interesting that both olivine and pyroxene show a fairly wide range in Mg-Fe ratios (atomic Mg/(Mg+Fe) = 0.6-1.0). Although most pyroxenes were low-Ca pyroxenes (orthopyroxene), small amounts of Ca-rich pyroxene (augite) were also detected. The presence of mafic silicates suggests that some Comet Wild II particles were formed near the sun at high temperature and then transformed to a cold comet formation region away from the sun by some process such as X-wind in the solar nebula.

## Ab-initio structure determination of 4-O-(4-methoxybenzoyl)-2-methyl-N-(2-pyridyl)-2H-1,2-benzothiazine-3-carboxamide-1,1-dioxide from laboratory X-ray powder diffraction data

Santu Chakraborty<sup>1</sup> Soumen Ghosh<sup>2</sup> Sarbani Pal<sup>1\*</sup> Alok Kumar Mukherjee<sup>2</sup>

<sup>1</sup>Department of Physics, Jadavpur University<sup>2</sup> Department of Chemistry, MNR Post Graduate College, Kukatpally, Hyderabad, India<sup>\*\*</sup>

The synthesis and ab-initio structure determination of 4-O-(4-methoxybenzoyl)-2-methyl-N-(2-pyridyl)-2H-1,2-benzothiazine-3-carboxamide-1,1-dioxide have been performed to study the role of enolic hydroxyl group present in piroxicam on its anti-inflammatory effects. X-ray powder diffraction data were collected on a Bruker D8-Advance powder diffractometer equipped with monochromated  $\text{CuK}_{\alpha 1}$  radiation ( $\lambda = 1.5406\text{\AA}$ ) over an angular range  $4-90^\circ(2\theta)$  with step size  $0.02^\circ(2\theta)$  and counting time  $25\text{ S}^{-1}$  per step. Indexing of the diffraction pattern revealed a triclinic system with cell parameters  $a=8.518(5)$ ,  $b=10.224(6)$ ,  $c=14.356(6)\text{\AA}$ ,  $\alpha=72.8(1)^\circ$ ,  $\beta=70.8(1)^\circ$  and  $\gamma=68.8(1)^\circ$ . The structure solution was performed in direct space (parallel tempering mode) with space group  $P-1$  using the program *FOX*. The final Rietveld refinement converged to  $R_F=0.0546$ ,  $R_{w0}=0.0726$ , respectively. The molecule contains three essential planar parts with small deviations of the methoxy oxygen and pyridine nitrogen atom from the corresponding least-squares planes. Strong intermolecular  $\text{N-H}\cdots\text{O}$ ,  $\text{C-H}\cdots\text{O}$ , and  $\text{C-H}\cdots\text{N}$  hydrogen bonds connects the molecules into three-dimensional supramolecular network.



## **Kinetics of crystalline-noncrystalline phase transition of sucrose crystal**

Taro Fujita<sup>1</sup>, Takahashi Kunimitsu<sup>2</sup>, Takahashi Takahashi<sup>3</sup>, Ken-ichi Ohshima<sup>2</sup>

<sup>1</sup>Microphase.Co.,Ltd<sup>1</sup>, Institute of Materials Science, University of Tsukuba, Japan<sup>2</sup>, National Institute of Advanced Industrial Science and Technology, Tsukuba 305-8565, Japan<sup>3</sup>

Sugar, whose principal ingredient is the sucrose, is one of functional materials for developing the battery of environmental intention by using the relation among the enzyme, the micro-organism, and the photocatalyst technology. However, melting points among sucrose crystals with high purity are occasionally different from each other and the melting points quoted from references range 433K to 464K. It has been assumed that a little impurity and moisture content in the sample caused different melting points in addition to the method how to grow the specimen. There are few X-ray structural reports on microscopic phenomena of the melting, though macroscopic observations of the melting point were performed with the use of differential scanning calorimetry and optical microscope. We have measured in-situ X-ray diffraction intensities for the sucrose until the melting point. When temperature was kept constant, the intensity decreased rapidly after retarding time, which is corresponding to starting the melting ( $t_m$ .) The relation between  $t_m$  and the holding temperature is not monotonous decrease with increasing the temperature, but has the minimum around 160°C. Present study gives an important information of understanding the melting point described above.

## A new method for characterizing the degree of graphitization of carbon materials by laser Raman spectroscopy

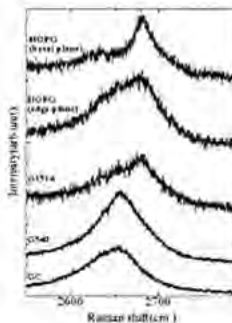
Katsumi Suda<sup>1</sup> Hiromi Ohmiya<sup>1</sup> Yasuhiro Tanabe<sup>2</sup> Eiichi Yasuda<sup>1</sup>

<sup>1</sup>Materials and Structures Laboratory, Tokyo Institute of Technology<sup>2</sup> Department of Chemical Engineering, Nagoya University

Raman spectroscopy is used for the characterization of the local structures of carbon materials. The degree of graphitization of the materials is usually estimated by the ratio of intensities of D band (1360  $\text{cm}^{-1}$ ) and G band (1580  $\text{cm}^{-1}$ ). However, the ratio shows disagreement with powder X-ray diffractometry and depends on the orientation of the sample. In this study, a method to characterize the carbon materials using 2D band (2600-2700  $\text{cm}^{-1}$ ) is investigated.

Raman spectra of highly orientated pyrolytic graphite (HOPG), glassy carbon, non-graphitizable carbon, and so on, were measured using Jobin-Yvon T64000 spectrometer with two different laser excitations (514.5 nm and 647.1 nm). Figure 1 shows the Raman spectra near 2D bands obtained with 514.5 nm excitation. The 2D band of highly graphitized carbon material (such as HOPG) is consisted of two peaks independent with the orientation of the sample, however the band of glassy carbon (GC) consisted of only one broad peak. It indicated that the shape of 2D band spectra reflects the structure of carbon materials and the method can be used to characterize the carbon materials.

The authors acknowledge profs H. Kaburagi and A. Yoshida, Musashi Institute of Technology, for valuable suggestions.



## Anomalous bonding behavior in Racemic 1,1'-Bi-2,2'-naphtholbiscarbonate

Tayur N Guru Row<sup>1</sup>, Sosale Chandrasekhar<sup>2</sup>, Susanta Kumar Nayak<sup>1</sup>, Guruprasad Kulkarni<sup>1</sup>

Solid State and Structural Chemistry Unit, Indian Institute of Science, Department of Organic Chemistry, IISc, India<sup>1</sup>

Structure determination at room temperature of the compound 1,1'-Bi-2,2'-naphtholbiscarbonate indicated that one of the terminal C-C bond length is unusually short [C-C=1.31Å]. The modalities of such a short bond length has been analyzed by collecting the data sets initially at 393K and later at on the same crystal at 150K and 90 K respectively. The results suggest that the short bond length is not a consequence of the disorder in the two atoms due to large thermal vibrations, but due to positional disorder at the two sites. At 90K, the positional disorder is fully visible and the refinement strategies adopted will be outlined.

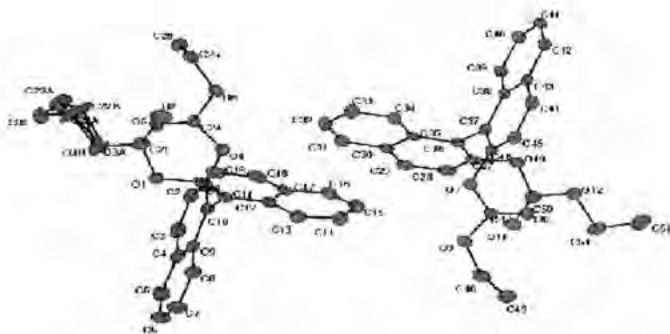


Figure: Ortep diagram of 50% probability at 90K.

## Diffraction study of the grain (C2054,0,35,4) obtained by the NASA Stardust Mission

Kenji Hagiya<sup>1</sup> Takashi Mikouchi<sup>2</sup> Michael E Zolensky<sup>3</sup> Kazumasa Ohsumi<sup>4</sup>

Graduate School of Life Science, University of Hyogo<sup>1</sup> Department of Earth and Planetary Science, University of Tokyo, Japan<sup>2</sup> NASA Johnson Space Center, U.S.A.<sup>3</sup> High Energy Accelerator Research Org. (KEK), Japan<sup>4</sup>

One of the Comet Wild-II particles (C2054,0,35,4) collected by the NASA Stardust Mission was analyzed by X-ray diffraction method. The sample with about 10 micrometers in size was attached to the end of a thin glass fiber. Diffraction experiment was carried out using the microbeam diffraction system placed at BL-4B1 of PF, KEK. The incident beam is limited to 1.6 micrometer in diameter by a micro-pinhole set just upstream of the sample. Laue photograph was successfully taken on an imaging plate by 30 minutes exposure using polychromatic X-ray of synchrotron radiation operated at energy of 2.5GeV.

All Laue spots are well indexed by three domains of one olivine and two orthopyroxenes. The axial ratio of each domain is refined based on the positions of Laue spots, shown in the table. It is shown that the olivine is conceived to be forsterite according to the Vegard's law. The structure refinement including site occupancies of Mg and Fe of olivine was carried out based on the diffraction intensities of Laue spots. The obtained value of Fe/(Mg+Fe) is around 0.11. This value is compatible with the results obtained from the axial ratio. The structure of orthopyroxene was also refined, and the value of Fe/(Mg+Fe) is also around 0.11.

	olivine	orthopyroxene	orthopyroxene
<i>a/b</i>	0.46526(6)	2.0719(3)	2.0673(12)
<i>c/b</i>	0.58608(8)	0.5900(2)	0.5885(4)
No. spots	224	261	32

Table. Observed axial ratio.

## Structural and Thermodynamic Studies on Ferroelectric Molecular Crystal Tricyclohexylmethanol

Yasuhisa Yamamura<sup>\*</sup> Hideki Saitoh<sup>\*\*</sup> Masato Sumita<sup>\*</sup> Kazuya Saito<sup>\*</sup>

Department of Chemistry, University of Tsukuba<sup>\*</sup> Molecular Analysis and Life Science Center, Saitama University<sup>\*\*</sup>

Tricyclohexylmethanol (TCHM) is a tertiary alcohol with three cyclohexyl groups, i.e. methanol substituted by three cyclohexyl groups. The crystal structure at room temperature is triclinic P-1 with two molecules in a unit cell [1]. The two molecules form a dimer through a hydrogen bond. Each hydroxyl group of the two molecules lies at the center of the dimer. The hydroxyl group of TCHM is, thus, not able to build a network structure like other ferroelectric crystals with hydrogen bond network, e.g.  $\text{KH}_2\text{PO}_4$  (KDP). Crystalline TCHM undergoes a phase transition at 103 K and has a spontaneous polarization at low temperature phase [2]. That is, TCHM shows ferroelectricity at low temperature phase, though no hydrogen bond network exists. However, detail of the phase transition is not clear. To clarify the mechanism of the phase transition, we investigate the structural and thermodynamic properties on TCHM in this study.

An anomaly was detected at 103 K in the heat capacity of TCHM. This anomaly is due to the paraelectric-ferroelectric phase transition of TCHM. Our x-ray diffraction experiment on a single crystal suggests that the direction of tandem hydroxyl groups with hydrogen bond in dimer is disordered in two possible orientations at room temperature. In this case, entropy of transition is expected to be  $1/2 R \ln 2$  ( $= 2.9 \text{ J K}^{-1} \text{ mol}^{-1}$ , because of the two orientations per one dimer). The expected entropy is comparable to the resultant excess entropy ( $1.9 \text{ J K}^{-1} \text{ mol}^{-1}$ ). We will discuss the mechanism of the paraelectric-ferroelectric phase transition of TCHM.

### References

- [1] P. Sgarabotto and F. Ugozzoli, *Acta Cryst.* **C44**, 674 (1988).
- [2] P. Szklarz and G. Bator, *J. Phys. Chem. Solid*, **66**, 121 (2005).

**Structural analyses of two N-[(3'-aryl) prop-2'-ynyl]-N, N'-1, 2-phenylene di-p- tosylamides: Supramolecular structure formed by N-H...O, C-H...O, C-H...pi;(arene) interactions.**

Soumen Ghosh Alok Kumar Mukherjee

Department of Physics, Jadavpur University

Quinoxiline systems have been an integral part in many naturally occurring substances, and exhibit important pharmacological activities. In this context, N-[(3'-aryl) prop-2'-ynyl]-N, N'-1,2-phenylene di-p-tosylamides,  $C_{27}H_{24}N_2S_3O_4$  (I) and  $C_{29}H_{25}N_2S_3O_4Cl$  (II) have been synthesized, and X-ray crystallographic analyses were undertaken. Both compounds crystallize in a triclinic system, space group P-1 with  $a = 9.0592(6)$  Å,  $b = 10.3757(7)$  Å,  $c = 14.2600(9)$  Å,  $\alpha = 74.623(1)^\circ$ ,  $\beta = 82.903(1)^\circ$ ,  $\gamma = 78.481(1)^\circ$  (I) and  $a = 8.8039(8)$  Å,  $b = 11.8783(11)$  Å,  $c = 13.1957(12)$  Å,  $\alpha = 87.633(1)^\circ$ ,  $\beta = 77.257(2)^\circ$ ,  $\gamma = 81.915(2)^\circ$  (II). Intensity data were collected on a Bruker SMART-CCD diffractometer using graphite monochromated  $MoK_\alpha$  radiation ( $\lambda = 0.7107$  Å). The crystal structures have been solved by direct methods and refined by full matrix least-squares technique on  $F^2$  to  $R = 0.0423$  for (I) and  $R = 0.0399$  for (II) using SHELX 97. Both compounds consist of a planar phenylenediamine part (C8-C13, N1, N2) with a substituted prop-2-ynyl group [C21-C27, S3 in (I) and C21-C29, Cl1 in (II)] at N1 and two p-tosyl moieties (C1-C7, S1, O1, O2 and C14-C20, S2, O3, O4) at N1 and N2 positions, respectively. The molecular packings stabilized by C-H...O, N-H...O and C-H...pi;(arene) interactions, leading to a three- and a two dimensional architecture in (I) and (II), respectively.

## Electron Density Distributions of Intermolecular N...O Contacts in Crystals of Biphenyl-3,5-diyl bis(*t*-butyl nitroxide)

Masanori Yasui Shinichiro Mashiyama Kazuhiro Ozawa Hiroaki Hosoya Hirokazu Nishimaki Gentaro Kurokawa Takayuki Ishida Takashi Nogami

Department of Applied Physics and Chemistry, The University of Electro-Communications

The title compound gave two crystalline phases (a- and b-phase). Though this biradical molecule has a triplet ground state, the a-phase crystals exhibit unusual diamagnetic properties. The very large intermolecular antiferromagnetic interactions between N-O radical moieties are ascribed to the diamagnetic properties.(1) In order to study these strong intermolecular interactions, the experimental electron density distributions were examined using the atoms-in-molecule method. The multipole refinements were successfully completed using the program XD to give R value of 0.034 for observed 10249 reflections up to  $2\theta=100^\circ$ . Both N-O radical moieties have short intermolecular contacts with those of another molecules related by the center of symmetry to form infinite chains in the crystals. The N...O distances are 2.3051(8) and 2.3418(8) Å. The topological analysis of the electron densities gave bond critical points and bond paths between the N...O contacts. The total energy densities at the BCPs ( $H_{cp}$ ) are -6 and -4 kJ/mol. These values mean that the intermolecular N...O interactions are "covalent". This observation is consistent with the strong intermolecular antiferromagnetic interactions.

The crystals of another polymorph (b-phase) have no intermolecular N...O interactions and exhibits paramagnetic properties.(2) Charge density studies of b-phase crystals were also carried out. Theoretical studies of electron densities for a-phase structure are now in progress. The comparison of the experimental and theoretical electron densities between two phases will be presented.

### Reference

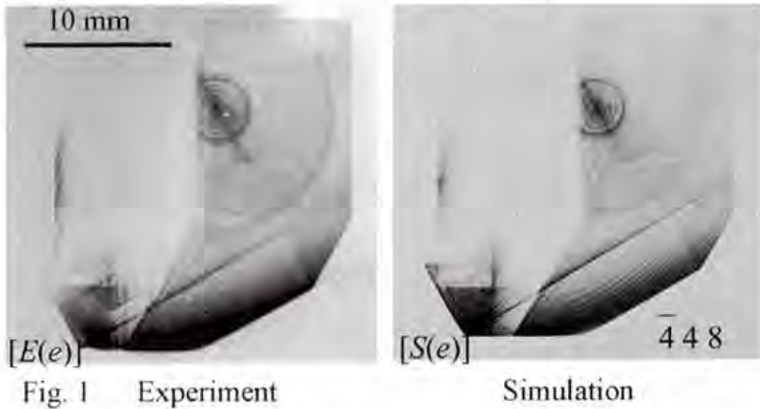
- (1) Kurokawa, G., *et al.* (2004) *Chem. Phys. Lett.* **392**, 74.
- (2) Nishimaki, H., *et al.* (2006) *Chem. Mater.* To be published.

## An algorithm to solve an $n$ -beam Takagi-Taupin equation for a crystal with an arbitrary shape

Kouhei Okitsu<sup>\*</sup> Yoshitaka Yoda<sup>\*\*</sup> Yasuhiko Imai<sup>\*\*</sup> Yoshinori Ueji<sup>\*\*\*</sup> XiaoWei Zhang<sup>\*\*\*</sup>

School of Engineering, The University of Tokyo<sup>\*</sup> Japan Synchrotron Radiation Research Institute<sup>\*\*</sup> Graduate School of Frontier Sciences, The University of Tokyo<sup>\*\*\*</sup> Photon Factory, KEK<sup>\*\*\*</sup>

The Takagi-Taupin equation has been extended to  $n$ -beam cases (Okitsu, K (2003). *Acta Cryst.* **A59**, 235-244.) where  $n$  is 3, 4, 5, 6, 8 or 12, taking into account the polarization effect, correctly. A new algorithm numerically to solve the new theory has also been developed. X-ray six-beam pinhole topographs with a parallel-sided floating zone silicon crystal have been experimentally obtained with the incidence of X-rays whose polarization state was controlled by using a 'four-quadrant phase retarder system' (Okitsu, K. *et al.* (2002). *Acta Cryst.* **A58**, 146-154.). They agreed quantitatively with computer-simulated images using the new algorithm based on the new theory (Okitsu, K. *et al.* (2006). *Acta Cryst.* **A62**, 237-247.). Figure. 1 shows 4 4 8-reflected images of experimentally obtained and computer-simulated six-beam pinhole topographs with a channel-cut floating zone silicon crystal, which reveals that the new theory and algorithm can calculate correctly an  $n$ -beam wave field excited in a crystal with an arbitrary shape. The polarization state of X-rays for Fig. 1 was left-screwed circular. A further advanced  $n$ -beam Takagi-Taupin equation and an algorithm to solve it that are applicable to arbitrary number of  $n$  will also be mentioned.



## Two methods of preparation of Silver nanoparticles in 3-18 nm scale

Asal Kiazadeh<sup>\*</sup> Azadeh Tadjarodi<sup>\*\*</sup>

chemistry department, iran university of science and technology<sup>\*</sup> iran of science and technology university<sup>\*\*</sup>

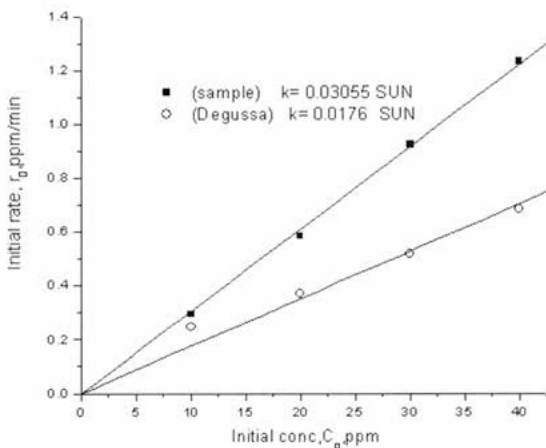
**Abstract** :Silver nanoparticles were synthesis in aqueous solution with  $\text{NaBH}_4$  and in alcoholic solution with  $\text{CH}_3\text{OH}$  . In order to keep the silver particles in the nanometer range , polyvinylpyrrolidone (PVP) was used . The alcohol served both as solvent and reducing agent for silver ions and cause of slow reaction rate . The synthesis was carried out by microwave .The results were confirmed with TEM images and UV-Vis spectrum.

## Large enhancement of photocatalytic Activity in Molybdovandate

Tayur N Guru Row<sup>1</sup> Giridhar Madras<sup>2</sup> Sudarshan Mahapatra<sup>1</sup>

Solid State and Structural Chemistry Unit, Indian Institute of Science<sup>1</sup> Department of Chemical Engineering, Indian Institute of Science, INDIA<sup>2</sup>

A new Cerium molybdovandate ( $\text{CeMo}_x\text{V}_{1-x}\text{O}_4$ ) has been synthesized, which depicts 50% enhancement in photo catalytic behavior compared to the commercial catalyst, Degussa (P-25). The compound crystallizes in a tetragonal zircon structure, space group  $I4_1/amd$ , with  $a = 7.3733(4)$  and  $c = 6.4909(4)$  and  $Z = 4$ . The crystal structure has been analyzed with powder X-ray diffraction, FTIR and UV-Visible spectroscopy. Particle sizes are in the range of 200-300 nm as seen by scanning electron microscopy and energy dispersive X-ray analysis indicates the formation of  $\text{CeMo}_x\text{V}_{1-x}\text{O}_4$ . Thermal analysis of this solid shows stability up to 1100C. Photocatalysis with respect to several organic compounds and dyes has been investigated both with UV and in sunlight. In accordance with the UV-Vis absorption spectra, the compound shows excellent properties under visible light as compared to UV irradiation. Experimental details related to water splitting and high temperature, high-pressure oxidative dehydrogenation of different organic compounds will be presented.



## Sub-micron single crystal structure analysis using micro-focus synchrotron radiation - A development of X-ray pinpoint structure measurement at the SPring-8 (2)

Nobuhiro Yasuda<sup>1</sup> Haruno Murayama<sup>2</sup> Jungeun Kim<sup>3</sup> Yoshimitsu Fukuyama<sup>4</sup> Yoshiki Ozawa<sup>5</sup> Kimihiro Kimura<sup>6</sup> Nobuyuki Kitayama<sup>7</sup> Shingo Yoshida<sup>8</sup> Satoshi Wada<sup>9</sup> Yoshihito Tanaka<sup>10</sup> Yutaka Moritomo<sup>11</sup> Shigeru Kimura<sup>12</sup> Yoshihiro Kuroiwa<sup>13</sup> Koshiro Toriumi<sup>14</sup> Masaki Takata<sup>15</sup>

Research and Utilization Division, Japan Synchrotron Radiation Research Institute (JASRI/SPring-8) / CREST<sup>1</sup> Graduate School of Material Science, University of Hyogo / CREST<sup>2</sup> Department of Inorganic Materials, Tokyo Institute of Technology<sup>3</sup> RIKEN / CREST<sup>4</sup> The Graduate School of Pure and Applied Sciences, Tsukuba University / CREST<sup>5</sup> Department of Physical Science, Hiroshima University / CREST<sup>6</sup> RIKEN / JASRI / CREST<sup>7</sup>

X-ray pinpoint structure measurement is the research project carried out at the SPring-8. The purpose is to develop an advanced X-ray measurement technique in nano-meter spatial scale and/or pico-second time scale by using the pulse characteristics, high brilliance and high efficiency of third generation synchrotron radiation X-ray.

One of the key techniques of the project is "the sub-micron single crystal structure analysis technique", which can be attained by applying "high brilliance micro-focus technique". This technique shall not only allow the single crystal structure analysis even from single grain of powder sample for powder X-ray diffraction, but also enables us to investigate dynamics of chemical reaction and phase transition caused by applied field within sub-micron scale domain of device and materials.

The high-precision diffractometer system was developed and installed at BL40XU beamline. The main features for single crystal analysis are (1) zone plate X-ray focusing up to 1 $\mu$ m at sample point, (2) a high precision goniometer system which realize sample rotation within  $\pm 100$ nm/360deg., and (3) CCD detector for 2 dimensional data collection.

To achieve the technique for the sub-micron single crystal structure analysis, the intensity data measurements were applied for 2 x 2 x 2 $\mu$ m<sup>3</sup> cytidine (C<sub>9</sub>H<sub>13</sub>N<sub>3</sub>O<sub>5</sub>) and 500 x 500 x 500nm<sup>3</sup> BaTiO<sub>3</sub> single crystals. By the one hour  $\omega$ -oscillation measurements with the total oscillation range of 180 deg., data collection and structure analyses have succeeded. The reliability factors of the present refinements were R<sub>1</sub>=6.4% for cytidine and 4.8% for BaTiO<sub>3</sub>, respectively.

Details of the data collection and structure analysis and precision of the refined structures will be discussed in the presentation.

**Crystal structure of the photo-excited state of three-coordinated gold(I) complex**Manabu Hoshino<sup>1</sup> Hidehiro Uekusa<sup>2</sup> Yoshiki Ozawa<sup>1</sup> Koshiro Toriumi<sup>1</sup><sup>1</sup>Department of Chemistry and Materials Science, Tokyo Institute of Technology<sup>2</sup> Graduate School of Material Science, University of Hyogo, Japan

The three-coordinated Au(I) complexes are highly interested as new EL material. The spectroscopic and theoretical studies on these complexes suggested that the emission is due to the large structural distortion of the complexes induced by photo-excitation. In order to investigate the emission and the structural distortion relationship, the photo-excited molecular structure of three-coordinated Au(I) complex, [AuCl(PPh<sub>3</sub>)<sub>2</sub>], was determined by single crystal X-ray structural analysis.

X-ray diffraction intensity data were collected in the dark (Light-off) and under the irradiation with UV excitation light (Light-on) condition in the laboratory system. Comparing the molecular structure of Light-off and Light-on states, all Au-P, Au-Cl bonds were found to be shortened (Au-P = -0.0065(5) Å & -0.0076(5) Å, Au-Cl = -0.0052(5) Å). These bonds shortening were clearly explained by electric excitation (assigned antibonding bonding). More precise diffraction intensity data of Light-off and Light-on states were collected by multiple-exposure IP method using low-temperature vacuum X-ray camera at SPring-8 BL02B1 beamline. Photo-difference Fourier map showed that the Au atom was slightly shifted toward the farther phosphor atom within a molecule by photo-excitation. This asymmetric shift of Au atom was also observed in the laboratory system. In conclusion, the structural distortion on the photo-excited state of [AuCl(PPh<sub>3</sub>)<sub>2</sub>] includes two types of structural change, the bond shortening and the asymmetric shift of Au atom.

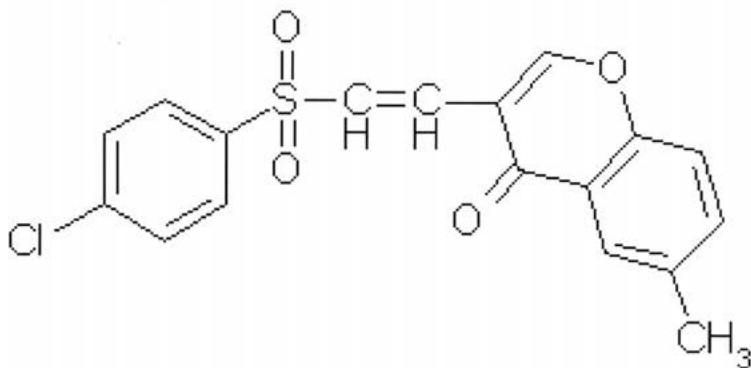
### Crystal Structure of 7-methyl [3-(2-(4-Chlorophenyl sulfonyl)) ethenyl]-4H-1-Benzopyran-4-one

RaviKumar Raynuthala<sup>1</sup> Krishnaiah Musali<sup>2</sup> Zaoo Oo Than<sup>3</sup> Kaung P<sup>4</sup>

Department of Physics, Sri Venkateswara University<sup>1</sup> Department of Physics, Sri Venkateswara University, Tirupati<sup>2</sup> Department of Physics, Yangon University, Myanmar<sup>3</sup>

Sulfones display activity as antibacterial and antifungal agents. Dapsone has been proven to be effective against leprosy and diasone is found to be highly effective against streptococci and pneumococci infections. The antifungicidal activity of some unsaturated sulfones has been found to be dependent upon substituent and stereochemical effect.

In the title compound  $C_{17}H_{14}ClO_4S$ , contains three nearly planar segments (the benzopyranone group, the chlorophenyl ring and the ethene group). The sulfonyl plane is inclined at  $52.8(2)^\circ$  to the plane of the chlorophenyl group and at  $48.9(2)^\circ$  to the plane of the benzopyranone group. Crystals obtained from 2-propanal by slow evaporation are monoclinic,  $a=12.91(7)$ ,  $b=9.708(6)$  and  $c=14.372(4)$  Å  $\beta=112.54(2)^\circ$   $V=1655.1(3)$  Å<sup>3</sup>,  $M_w = 360.81$ ,  $\lambda(\text{MoK}\alpha)=0.71073$  Å. The structure was solved by direct methods and refined by full matrix least squares using SHELXL-97 to final values of  $R = 0.0791$  and  $R_w = 0.2703$  for 2794 symmetry independent reflections collected using Bruker Smart diffractometer.



**Synthesis and crystal structure of chloro-hydrido-(6-diphenylphosphanyl-2-hydroxypyridine- $\kappa^2P,N$ )-(6-diphenylphosphanyl-2-pyridonate- $\kappa^2P,N$ )iridium(III) chloroform 1.89-solvate**

Tsuneaki Yamagata Takayuki Miyabayashi Takeshi Hara Kazushi Mashima

Department of Chemistry, Graduate School of Engineering Science, Osaka University

A tridentate ligand of 6-diphenylphosphanyl-2-pyridonate (pyphos) ligand has three coordination sites, O, N, and P, supported linearly by the rigid pyridone ring. The pyphos ligand acts as coordination sites for arrangements more than two kinds of transition metals in a linear manner. The 6-diphenylphosphanyl-1*H*-pyridin-2-one/6-diphenylphosphanyl-2-hydroxypyridine tautomer system is known to dimerize in aprotic solvents to form predominantly the symmetrical pyridone dimer through hydrogen bonding, and the Ruthenium and Rhodium complexes having 2-pyridone/2-hydroxypyridine or analogous ligands serve as effective catalyses. We synthesized and crystallized the title complex, containing hydrido, chloro, 6-diphenylphosphanyl-2-hydroxypyridine (pyphosH), and 6-diphenylphosphanyl-2-pyridonate (pyphos) ligands. The structure of the iridium(III) metal centre adopts a distorted octahedron. The N-H bond of the pyphosH ligand is oxidatively added to an iridium atom. The two P and N atoms of the pyphosH and pyphos ligands lie the *cis* coordination in the basal plane. An intramolecular O-H...O hydrogen bond between pyphosH and pyphos ligands is observed. Spectroscopic data show the presences of the hydrogen bond and the magnetically equivalent phosphorous atoms. Therefore the proton exchange in the O-H...O hydrogen bond would occur in the solution.

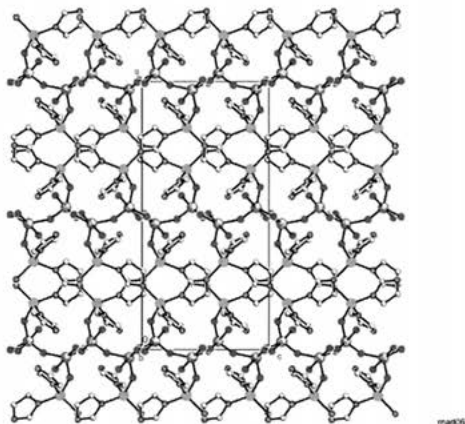
## Synthesis and Structures of Organically Modified Zinc Vanadates

Samroeng Krachodnok<sup>1</sup> Kittipong Chainok<sup>1</sup> Kenneth J. Haller<sup>2</sup> Herman H-Y. Sung<sup>1</sup> Fanny L-Y. Shek<sup>1</sup> Ian D. Williams<sup>1</sup>

<sup>1</sup>School of Chemistry, Suranaree University of Technology<sup>2</sup> Department of Chemistry HKUST Hong Kong

Exploration of the structural chemistry of organically modified zinc vanadates has been carried out through hydrothermal crystallization reactions of various organic bases with zinc acetate and vanadium pentoxide ( $V_2O_5$ ) under different conditions of pH, stoichiometry, temperature, time and concentration. A wide variety of product types have been found in which either organic or complex cations crystallize with anionic vanadate chains for example  $[ZnIm_4][VO_3]_2$ , or vanadate clusters as in  $2[Zn(2-Melm)_4]_2[2Melm-H][V_{10}O_{28}]$ . Alternatively the organo-zinc and vanadate components may be connected as in the network solids  $[Zn(en)(VO_3)_2]$ , or  $[Zn(Im)(Im)VO_3]$  containing  $[Im]^-$  anions (shown in Fig). Finally even discrete molecular species such as  $\{[Zn(2-Melm)_{3/2}V_4O_{12}]\}$  which is composed of a cyclotetranvanadate ring with two pendant zinc tris-imidazolyl groups can be isolated in phase pure form.

The Thai Research Fund (2002 RJG PhD scholarship to S.K.) and RGC (HK) are thanked for financial support of this work.



## Structures and properties of defect perovskites in the strontium zirconium niobium oxide system

Siegbert Schmid Ivanka Barisic

School of Chemistry, University of Sydney

The  $\text{Sr}_x\text{NbO}_3$ ,  $0.7 < x < 1$ , solid solution with niobium in oxidation states +IV and +V for  $x < 1$ , has been reported to adopt the ideal cubic perovskite structure across the whole solid solution field. Despite intensive searching when data were collected on good quality single crystals no additional reflections were detected. This indicates random ordering between strontium and vacancies on the perovskite A sites. Since niobium and zirconium are able to occupy positions in a structure at random, it was expected that a similar solid solution might be formed if niobium +IV is replaced by zirconium +IV. Therefore an investigation was undertaken in the SrO-ZrO<sub>2</sub>-Nb<sub>2</sub>O<sub>5</sub> system to see whether an analogous solid solution is indeed formed. The composition range of  $\text{Sr}_{0.7+x}\text{Zr}_{0.4+2x}\text{Nb}_{0.6-2x}\text{O}_3$  has been investigated in detail (as well as the Hf and Ta analogues) and specimens synthesised with  $0.01 < x < 0.30$ . X-ray and neutron powder diffraction patterns have shown that while there is an underlying pseudo cubic perovskite sub-structure the symmetry for all investigated compositions is lowered to tetragonal or orthorhombic. The low strontium content end member of the solid solution appeared to adopt cubic symmetry (in accordance with the laboratory X-ray and electron diffraction data), however, profile fitting clearly showed that the phase is actually tetragonal. The rest of the solid solution requires symmetry lowering to orthorhombic to fit the patterns satisfactorily. It now appears that there is no complete solid solution from  $\sim 0.01 < x < 0.3$ , but rather a series of smaller solid solutions the extent of which needs to be carefully examined.

## Incorporating Transition Metals in Ferroelectric Oxides

Brendan J Kennedy Qingdi Zhou Scott Mckenzie Chris Ling

School of Chemistry, The University of Sydney

There is considerable practical and fundamental interest in developing multiferroic materials that exhibit the unusual co-existence of ferroelectricity and ferromagnetic and display coupling between these. One strategy to prepare such oxides is to incorporate transition metals into ferroelectric oxides such as the Aurivillius oxides. In the present presentation we shall describe recent efforts to prepare such oxides. Two systems shall be presented in some detail, firstly we describe a novel method to prepare high quality samples of the three layered oxides  $\text{ASrBi}_2\text{Nb}_2\text{TiO}_{12}$  A = Ca, Sr or Ba using the pre-formed intermediates  $\text{ABi}_2\text{Nb}_2\text{O}_9$  and  $\text{SrTiO}_3$ . The room temperature structures were refined using synchrotron X-ray and Neutron powder diffraction data in the orthorhombic space group B2cb. This symmetry arises as a consequence of cooperative tilting of the BO6 octahedra in the  $[\text{ASrNb}_2\text{TiO}_{10}]^{2-}$  perovskite-like slabs and a polar displacement of the cations. The structure is characterized by extensive cation disorder but lacks appreciable oxygen vacancies. Next we will describe efforts to replace the Ti with paramagnetic ions such as Cr, Mn and Fe. Here we find there is a limit to the amount of the transition metal that can be incorporated with the high quality samples of the type  $\text{Sr}_2\text{Bi}_2\text{Nb}_{2.5}\text{M}_{0.5}\text{O}_{12}$  being prepared. The structures of these oxides will be described.

**Charge density distribution of iron atoms on  $[\text{Fe}(\text{II})(\text{bpy})_3][\text{Fe}(\text{II})_2(\text{ox})_3]$  complex**

Jey Jau Lee` Yu Wang`

National Synchrotron Radiation Research Center` Department of Chemistry, National Taiwan University, Taipei, Taiwan, R.O.C`

Charge density distribution and bond characterization have been investigated on a polymeric 3D complex  $[\text{Fe}(\text{II})(\text{bpy})_3][\text{Fe}(\text{II})_2(\text{ox})_3]$ , in terms of accurate single crystal diffraction at 100K. The 3D framework is made by iron complex  $\text{Fe}(\text{II})_2(\text{ox})_3^{2-}$  in a porous network, which is encapsulated with isolated iron complex of  $\text{Fe}(\text{II})(\text{bpy})_3^{2+}$  inside the cage. Each asymmetric unit contains two different spin state  $\text{Fe}^{2+}$  atoms: a high spin and a low spin states coordinated to six oxygen and six nitrogen atoms respectively.

The experimental approach is based on the multipole model formalism refinement on the diffraction data. The purpose of this work is to compare the charge density distributions at the iron site with a high spin (HS) and a low spin (LS) configuration. The expected differences in the electron density distribution around the iron site will be demonstrated.

There are significant differences at the iron center between HS and LS sites shown in the deformation density maps and in the VSCC derived from the Laplacian. The apparent asphericity in electron density of the LS species is not observed in that of the HS case. The VSCC of the high spin state is approximately spherical; in contrast, the VSCC of the LS case indicates a clear octahedral feature with six local charge concentrations around the iron center. This difference between two spin states can be best illustrated by the isovalue surfaces of Laplacian will be showed.

## Crystal Structure Analysis of $\text{Eu}^{2+}$ -doped $\text{CaAlSiN}_3$ , a Red Phosphor for White Light-Emitting Diodes

Hiroyuki Imura<sup>1</sup>, Takatoshi Seto<sup>1</sup>, Naoto Kijima<sup>1</sup>, Naoto Hirosaki<sup>2</sup>

<sup>1</sup>Mitsubishi Chemical Group Science and Technology Research Center, INC., National Institute for Materials Science<sup>2</sup>

The  $\text{Eu}^{2+}$ -doped  $\text{CaAlSiN}_3$  ( $\text{CaAlSiN}_3:\text{Eu}^{2+}$ ) was developed as a new red phosphor for the white light-emitting diodes (LEDs) by Uheda et al. [1]

The emission spectra of  $\text{CaAlSiN}_3:\text{Eu}^{2+}$  excited by blue (460nm) or violet (405nm) light has a broad emission band around 650 nm, but the band center and the intensity change as the  $\text{Eu}^{2+}$ -concentration increase in  $\text{CaAlSiN}_3:\text{Eu}^{2+}$ .

We studied the crystal structures about 5 kinds of  $\text{CaAlSiN}_3:\text{Eu}^{2+}$  which have different  $\text{Eu}^{2+}$ -concentration,  $\text{Eu}_x\text{Ca}_{1-x}\text{AlSiN}_3$  ( $x=0.004, 0.008, 0.010, 0.060, 0.200$ ), by the Rietveld analysis in order to reveal the relationship between the  $\text{Eu}^{2+}$ -concentration and the crystal structure in  $\text{CaAlSiN}_3:\text{Eu}^{2+}$ .

The crystal system of  $\text{CaAlSiN}_3:\text{Eu}^{2+}$  is the orthorhombic and the space group is Cmc21(No.36). The lattice parameters are  $a=9.7784(1)\text{\AA}$ ,  $b=5.6388(1)\text{\AA}$  and  $c=5.0529(1)\text{\AA}$  in case of  $\text{Eu}_x\text{Ca}_{1-x}\text{AlSiN}_3$  ( $x=0.004$ ). The Si and Al are located in the same crystallographic 8b site and form the tetrahedron of  $\text{SiN}_4$  and  $\text{AlN}_3$  type. The  $\text{Ca}^{2+}$  ions are located in the 4a site surrounded by 5 nitrogen-ligands which form the apex of the  $\text{SiN}_4$  and  $\text{AlN}_3$  tetrahedrons. The  $\text{Eu}^{2+}$  ions, luminescent center are substituted with a part of the 4a site. Rietveld analysis was carried out in the following restrictions. : The ratio of  $\text{Ca}^{2+}$  and  $\text{Eu}^{2+}$  in the 4a site is equal to  $x$ -value in  $\text{Eu}_x\text{Ca}_{1-x}\text{AlSiN}_3$ . The fractional coordinates of  $\text{Ca}^{2+}$  and  $\text{Eu}^{2+}$  are equivalent in each other.

It was confirmed that the  $b$  and  $c$ -axis length increase, but  $a$ -axis length hardly change and also it was suggested that the 4a site occupancies decrease and the average distances between the 4a site and the surrounding ligands lengthen as the  $\text{Eu}^{2+}$ -concentration increase.

### Reference

- [1] K. Uheda et al., *Electrochem. Solid-State Lett.*, 9 (2006) H22.

**Angelicaïn : Supramolecular structure generated by O-H...O, C-H...O and C-H... $\pi$  hydrogen bonds, and  $\pi$ - $\pi$  stacking interactions**Sanjeev Goswami<sup>1</sup> Vivek K. Gupta<sup>2</sup> R.K. Thappa<sup>3</sup> S.G. Agarwal<sup>4</sup><sup>1</sup>Department of Applied Physics, M.B.S. college of Engineering and Technology<sup>2</sup> Natural Products Chemistry Division, Regional Research Laboratory, India<sup>3</sup>

The compound angelicaïn (2-hydroxymethyl-5-hydroxy-10,11-dihydro-11(S)-(1-hydroxy-1-methylethyl)-2H-furo[2,3-g]-4H-1-benzopyran-4-one, C<sub>15</sub>H<sub>16</sub>O<sub>6</sub>) isolated from *Angelica archangelica* Linn. has been a seat of various biological activities and natural occurrence. The crystal structure of angelicaïn has been determined from X-ray diffraction data using direct methods. The compound crystallizes into monoclinic space group P2<sub>1</sub> with unit cell parameters : a=11.647(1)Å, b=7.268(1)Å, c=17.680(2)Å,  $\beta$ =105.54(2)°, Z = 4. The structure has been refined by full-matrix least-squares to a final R value of 0.038 for 2834 observed reflections. The structure contains two crystallographically independent molecules, A and B, in the asymmetric unit which are almost identical in geometry. The benzopyran moiety is planar and the furan ring has a C11-envelope conformation. In both the molecules, an intramolecular O-H...O hydrogen bond forms a pseudo-six membered ring. In the crystal structure, molecules A and B interact through O-H...O and  $\pi$ - $\pi$  interactions, forming a dimer and further forming double chains along diagonal of the unit cell. The double chains are extended through C-H...O and C-H... $\pi$  interactions forming a supramolecular structure.

## Preparation of Porous $\text{LiAl}_5\text{O}_8$ by $\text{Li}_2\text{O}$ and $\text{Al}_2\text{O}_3$ reaction

Chumphol BUSABOK Tatsuo Shikama Shinji Nagata Bun Tsuchiya Kentaro Toh

Shikama's Laboratory, Institute for Materials Research, Tohoku University

The porous  $\text{LiAl}_5\text{O}_8$  fabricated by reaction bonded sintering.  $\text{Li}_2\text{O}$  (0.5 mm) and  $\text{Al}_2\text{O}_3$  (0.3 mm) powder were used for starting materials. Two type of powder mixed by 1:9, 3:7, 5:5 by mole in the water for 6 hours and dried for  $100^\circ\text{C}$  for 10 hours. The dried power shaped by uniaxial pressing to form 10 mm diameter disk specimens. The disk specimen sintered at temperature  $1300^\circ\text{C}$ ,  $1400^\circ\text{C}$  and  $1550^\circ\text{C}$ , respectively for 2 hours. The sintered specimens were observed by SEM and phase characterized by X-ray diffractometry. Pore size distribution of specimens were measured by mercury porosimetry technique. Porosity measured by Achimedes method.

The x-ray diffraction results of specimens which were prepared by reaction bonded sintering from 1 : 9 by mole of  $\text{Li}_2\text{O}$  :  $\text{Al}_2\text{O}_3$  were shown  $\text{LiAl}_5\text{O}_8$  peaks. Specimens, 3:7 and 5:5 by mole were shown  $\text{LiAl}_5\text{O}_8$  peaks and  $\text{LiAlO}_2$  peak. Increasing of  $\text{LiAlO}_2$  peak depend on amount of  $\text{Li}_2\text{O}$  increase. Pore size distribution of specimens were sintered at  $1300^\circ\text{C}$  there are 40.86 % porosity and pore size distribute between 0.08-8.00 mm and 0.12 mm as a median pore. Sintered temperature,  $1400^\circ\text{C}$ , there are 43.88 % porosity, pore size distribute as two range 0.08-8.00 mm and 80-110 mm and 0.12 as a median pore. The higher temperature sintering specimens,  $1550^\circ\text{C}$ , there are 35.56 % porosity and pore size distribute between 0.08-10.00 mm and 0.16 as a median pore. When we compare pore size distribution by ratio of  $\text{Li}_2\text{O}$  and  $\text{Al}_2\text{O}_3$ , 1:9 by mole was more homogeneous pore than other ratio.

## **POLYINFO-A package for selection of aerospace polymers based on crystallographic and related properties**

KALYANI VIJAYAN Mahesh Kumar

Materials Science Division, National Aerospace Laboratories, Bangalore

POLYINFO enables property-specific selection of polymers used in aerospace. POLYINFO has two components viz., a database POLYSEARCH and a selection module POLYSELECT. Aerospace polymers have stringent requirements on their properties. Good thermal resistance, excellent mechanical properties, light weight are few examples of such requirements. As is well known, properties are closely related to crystal structural characteristics. Indeed, several hard and soft sources providing information on the crystallographic properties of polymers in general, are available. However, databases which combine crystallographic data with mechanical properties and other user-relevant information like decomposition temperature, service temperature, suppliers etc are perhaps not many. The authors have developed the database POLYSEARCH which includes data on crystallographic, mechanical and miscellaneous properties, exclusively for aerospace polymers (Access from [www.nal.res.in](http://www.nal.res.in)). To select polymers with specific properties from POLYSEARCH, in its stand-alone mode, the user has to survey the entire database. To simplify this procedure, a selection module POLYSELECT which enables property-specific selection/identification has been developed. For example, all polymers belonging to the monoclinic crystal system can be identified by a simple click on the 'monoclinic' grouping button. Similar, selection modules based on other properties have been included in POLYSELECT. POLYINFO hyperlinks POLYSEARCH and POLYSELECT.

## Electron Dynamics in the Nanostructure

Tri Van Nguyen

Institute of Engineering Physics, Hanoi University of Technology

From the experimental results with ESR in combination with other methods on many different material and biomedical systems of Nano level, numerous effects concerning the peculiar behaviours of the active Electrons (the odd Electrons) very distinct from the ones in the normal crystalline materials have been revealed. These effects stand in close connection with the fundamental properties of the materials such as the stereo-conformation, the conductivity, the biomedical activity. Just these achieved results have led to elaborating a new model-conception for the Dynamics of Electron in the Nanostructure.

On the basis of this model, the revealed phenomena and effects as well as the nano-micromechanisms concerning the particular properties and technological factors of some specific material and biomedical systems can be thoroughly interpreted.

This paper briefly presents some fundamental conceptions of the Dynamics of Electron in the Nanostructure and some typical applications cases as illustrative examples for the peculiar phenomena in some special materials and living bodies, such as the persisting of the fivefold aperiodic structures, the nanomechanism of the superconductivity in YBCO compounds, the called "non-pumping laser effect", etc.

This research was supported by the National Research Program "New Materials", the National Basic Research Program in Natural Sciences and other Research Programs.

## Crystal and molecular structure of 4,5-dimethyl-N-(2-methyl phenyl)-2-[[[(1E)-3,4,5-trimethoxy phenylmethylene]amino]thiophene-3-carboxamide

vasu sriranga vasu<sup>1</sup> K. A. Nirmala<sup>2</sup> Deepak Chopra<sup>3</sup> S. Mohand<sup>4</sup> J. Saravanan<sup>5</sup>

Physics Department, Vivekananda Degree college, Malleshwaram west, Bangalore -560055, Bangalore University<sup>1</sup> Department of Physics, Bangalore University, Bangalore 560 056, Karnataka, India<sup>2</sup> Solid State and Structural Chemistry Unit, Indian Institute of Science, Bangalore 560 012, Karnataka, India<sup>3</sup> PES College of Pharmacy, Hanumanthanagar, Bangalore 560 050, Karnataka, India<sup>4</sup>

The title compound shows promising antibacterial activity against *subtilis aureus*, *Escherichia coli* compared with Ampicillin. The structure was determined by direct methods using SHELXS-97 and refined to a final R-value 0.045. In the title compound, the geometry of the thiophene ring is planar and is in good agreement with the data obtained for thiophene by electron diffraction. The o-toluidine is in the gauche position. The angle between thiophene and o-toluidine is 59.24(2)°. The S-C bond distances are not equal due to delocalisation. The methyl group of the p-methoxy connected to oxygen is not in the plane and is deviated from the phenyl plane by 0.095(1). The methyl groups attached at m-positions point away from each other. The inclination angles in the methoxy parts are not equal due to steric environment. The bond distances in the methoxy groups agree with values observed in other methoxy benzene derivatives. The non-planar part of the molecule i.e., o-toluidine is characterised by the torsion angle 72.84(2)° indicating the conformation of the o-toluidine is bent in the compound.

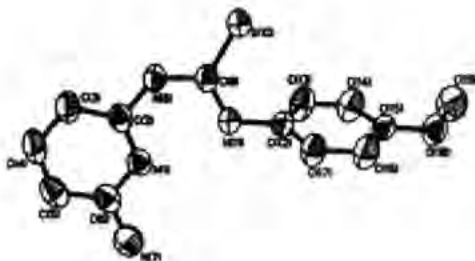
The molecular structure is primarily stabilized by intra-molecular N-H...O interactions forming pseudo-six membered S(6) ring forming hydrogen bonded pattern. The crystal packing is governed by a diverse set of C-H...O and  $\pi$ ... $\pi$  interactions. The dimers form a ring described by graph set analysis (12).

## Synthesis and molecular structure of N-2-(4-picolyl)-N'-(6-amino phenyl) thiourea

Azadeh Tadjarodi Nooshin Hafezinejad

Faculty of Chemistry, Iran University of Science and Technology(IUST)

Thioheterocyclic compounds are very interesting ligands because they are able to coordinate to many metals and biological materials by their sulfur and nitrogen atoms. These compounds show potent anti-HIV activity and biological activity and also are suitable for fabrication of selective membrane sensors for monitoring low level of lanthanids. In this work, the reaction between 2,6-diamino pyridine and 4-methoxy phenyl isothiocyanate in 95% EtOH led to formation of N-2-(4-picolyl)-N'-(6-amino phenyl) thiourea. On cooling and reducing the volume, white powder formed. The result compound was characterized by IR, <sup>1</sup>H, <sup>13</sup>C-NMR spectra, elemental analysis and single crystal X-ray diffraction. We obtained crystals of compound by recrystallization of this powder in ethanol and acetone solution (1:1). The crystal system of this compound is monoclinic with space group P2<sub>1</sub>/c and 4 molecules per unit cell. The intramolecular and intermolecular hydrogen bonding interactions of this compound was confirmed by <sup>1</sup>H-NMR and single crystal X-ray diffraction.



**Electron charge density study of  $\text{Bi}_4\text{Ti}_3\text{O}_{12}$  and  $\text{Bi}_{3.25}\text{La}_{0.75}\text{Ti}_3\text{O}_{12}$  by MEM/Rietveld analysis**Sayaka Kimura<sup>1</sup> Su Jae Kim<sup>2</sup> Chikako Moriyoshi<sup>1</sup> Yoshihiro Kuroiwa<sup>1</sup> Yuji Noguchi<sup>2</sup><sup>1</sup>Department of Physical Science, Hiroshima University<sup>2</sup> Research Center for Advanced Science and Technology, University of Tokyo, Japan

Lead-free materials have attracted much attention for the application to FeRAM. Bismuth layer-structured ferroelectric  $\text{Bi}_4\text{Ti}_3\text{O}_{12}$  (BIT), which consists of  $(\text{Bi}_2\text{O}_2)^{2+}$  layer and  $(\text{Bi}_2\text{Ti}_3\text{O}_{10})^{2-}$  perovskite layer, is one of the candidates due to its large spontaneous polarization. One of the problems to be overcome is, however, that BIT does not have a sufficient endurance for repetitive switching of its polarization states. Recently La-substituted BIT, that is  $\text{Bi}_{3.25}\text{La}_{0.75}\text{Ti}_3\text{O}_{12}$  (BLT), has been reported to be fatigue-free. To clarify the La/Bi substitution effect and the origin of the fatigue-free characteristics of BLT, we performed synchrotron radiation (SR) powder diffraction experiment of BIT and BLT.

Powder diffraction data were obtained at BL02B2 in SPring-8 using the large Debye-Scherrer camera equipped with an imaging plate as a two-dimensional detector. High-energy X-rays (35 keV) were used in this experiment. High-energy SR powder diffraction has advantages of being free of problems of extinction and absorption effects, and is quite useful for samples such as  $\text{Bi}_4\text{Ti}_3\text{O}_{12}$  and  $\text{Bi}_{3.25}\text{La}_{0.75}\text{Ti}_3\text{O}_{12}$  consisting of an extremely heavy element Bi and a light element O. The crystal structure parameters and electron charge density distributions of BIT and BLT were determined by the MEM/Rietveld analysis.

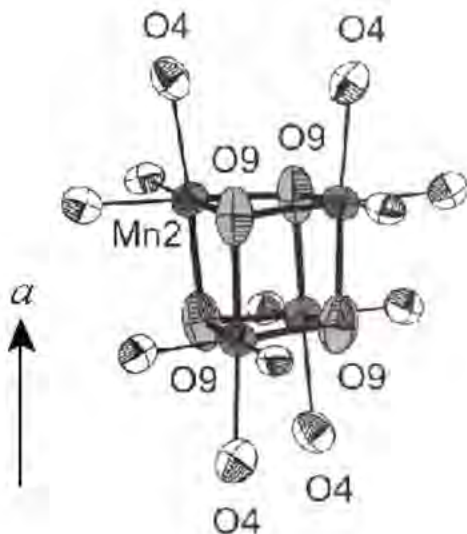
We confirmed that La atoms substitute for Bi atoms only in the perovskite layer, as has been reported. An orbital hybridization between Bi-O in the perovskite layer along the *a*-axis was observed for BIT, whereas in BLT, in addition to the hybridization, another hybridization along the *b*-axis in the perovskite layer was revealed. We conclude that this hybridization stabilizes oxygen and induces the fatigue-free property in BLT.

## Bond-length fluctuation in the low temperature form of $\text{LiMn}_2\text{O}_4$

Kenji Tateishi<sup>1</sup>, Nobuo Ishizawa<sup>2</sup>

<sup>1</sup>Gifu Prefectural Ceramics Research Institute<sup>1</sup>, Ceramics Research Laboratory, Nagoya Institute of Technology<sup>2</sup>

Crystals of  $\text{LiMn}_2\text{O}_4$  undergo a first order structural phase transition near the room temperature. The high temperature (HT) form adopts a normal spinel-type structure (cubic,  $Fd\bar{3}m$ ) with the octahedral sites populated statistically with heterovalent  $\text{Mn}^{III}$  and  $\text{Mn}^{IV}$  in the equal ratio. The low temperature (LT) form adopts a  $3 \times 3 \times 1$  superstructure (orthorhombic,  $Fddd$ ) with respect to the HT form, containing  $\text{Mn}^{1III}$ ,  $\text{Mn}^{3III}$ ,  $\text{Mn}^{4IV}$ ,  $\text{Mn}^{5V}$  and intervalent  $\text{Mn}_2$  atoms. The synchrotron X-ray single-crystal electron-density analysis revealed a large anisotropy of the atomic displacement parameters of the O9 and O4 atoms. This suggests an occurrence of the bond-length fluctuation along the pseudo-tetragonal Jahn-Teller distortion parallel to the  $a$  axis in the heterocubane  $\text{Mn}_2\text{O}_9$  cluster which presumably shares three electrons among four  $e$ -parentage orbitals of  $\text{Mn}^{2+}$  and behaves as a core of Zener-type polaron. The heterocubane  $\text{Mn}_2\text{O}_9$  clusters are isolated with each other and embedded in an ordered way in the charge-ordered matrix containing  $\text{Mn}^{1III}$ ,  $\text{Mn}^{3III}$ ,  $\text{Mn}^{4IV}$  and  $\text{Mn}^{5V}$ . The transition between the LT and HT forms of  $\text{LiMn}_2\text{O}_4$  can thus be regarded as an order-disorder transition of the Zener-type polarons.



**Investigation of the cation ordering in ilmenite-type  $\text{ZnTiO}_3$** Hijiri Kito<sup>1</sup> Nakamura Masaki<sup>2</sup> Sato Akira<sup>2</sup> Ohashi Haruo<sup>2</sup>

<sup>1</sup>Superconducting Materials Group, Nanoelectronics Research Institute, National Institute of Advanced Industrial Science and Technology (AIST) <sup>2</sup>National Institute for Materials Science (NIMS)

$\text{ZnTiO}_3$  single crystals have been synthesized by the grain growth technique under 3.5 Gpa at 1123 K using the program controlled high pressure apparatus for the first time. The crystal structure of  $\text{ZnTiO}_3$  was confirmed by X-ray diffraction data at room temperature. The final refinement using the 528 reflections converged into  $R=0.027$  and  $wR=0.035$ . The  $\text{ZnTiO}_3$  crystallizes R-3 (No.148) space group symmetry and it is an ilmenite-type structure. Lattice parameters are  $a = 0.50778(2)$  nm,  $c = 1.39238(4)$  nm and unit cell volume is  $V=0.31091(2)$  nm<sup>3</sup> (formula units  $Z=6$ ). Temperature-dependence of the magnetic susceptibility for the polycrystalline sample indicated that no magnetic ordering appears above 4.2 K and exhibits Curie-Weiss like profiles at low temperature.

## Thermal vibration behaviors of cations in garnet compounds

Akihiko Nakatsuka<sup>1</sup> Noriaki Nakayama<sup>2</sup> Hiroki Okudera<sup>2</sup> Akira Yoshiasa<sup>3</sup> Kazuake Iishi<sup>1</sup>

<sup>1</sup>Graduate school of Science and Engineering, Yamaguchi University<sup>1</sup> Department of Earth Sciences, Kanazawa University, Japan<sup>2</sup> Department of Earth Sciences, Kumamoto University, Japan<sup>3</sup>

Garnets can accommodate various cations, which occupy tetrahedral, octahedral and dodecahedral sites. These three types of coordination polyhedra link in a complex manner by sharing edges and corners with each other. We have reported that the repulsions between cations across the shared edges of polyhedra contribute greatly to the structural stability of garnets. In the present study, we investigated the relationship between the cationic thermal vibration behaviors and the cation-cation repulsions. Consequently, we found that the ratios  $\text{RMSD}_{x,z}/\text{RMSD}_{x,o}$  and  $\text{RMSD}_{z,x}/\text{RMSD}_{z,o}$  have the negative correlations with the repulsions between tetrahedral and dodecahedral cations, where  $\text{RMSD}_{x,z}$  and  $\text{RMSD}_{z,x}$  are the root mean square displacements (RMSD) of dodecahedral and tetrahedral cations in the tetrahedral-dodecahedral directions, respectively;  $\text{RMSD}_{x,o}$  and  $\text{RMSD}_{z,o}$  are the RMSD's of dodecahedral and tetrahedral cations in the respective cation-oxygen directions. In most of reported garnets, the  $\text{RMSD}_{x,z}$  and  $\text{RMSD}_{z,x}$  are smaller than  $\text{RMSD}_{x,o}$  and  $\text{RMSD}_{z,o}$ , respectively, which indicates that the repulsions between tetrahedral and dodecahedral cations are stronger than the interactions between dodecahedral cation and oxygen and between tetrahedral cation and oxygen. On the other hand, only  $\text{NaPb}_2\text{M}_2\text{V}_3\text{O}_{12}$  ( $M = \text{Mg}, \text{Co}, \text{Ni}$ ) vanadate garnets among the investigated garnets are in the opposite situation. Moreover, in these vanadate garnets, the repulsions between adjacent dodecahedral cations and between dodecahedral and octahedral cations are remarkably weak, which yields the unusually long dodecahedral-dodecahedral and octahedral-dodecahedral shared edges.

## Developing Remote Access for Crystallography

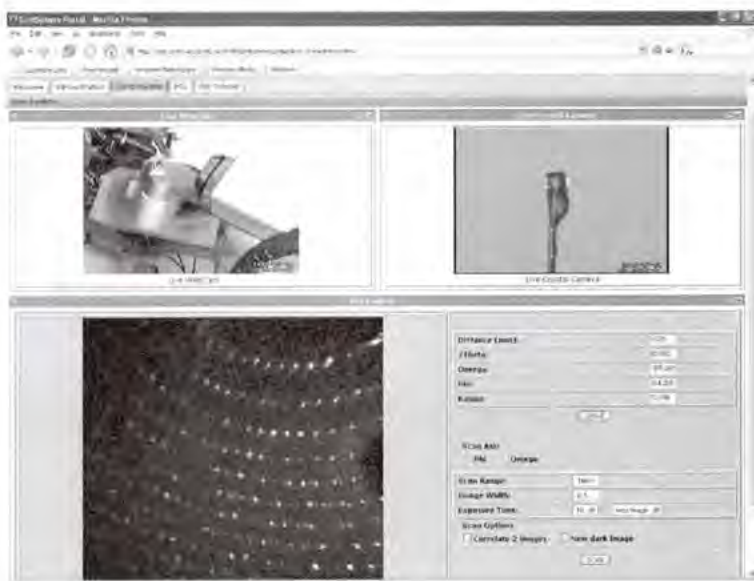
Ian M. Atkinson,<sup>1</sup> Douglas du Boulay,<sup>2</sup> Clinton Chee,<sup>2</sup> Kenneth Chiu,<sup>3</sup> Tristan King,<sup>1</sup> Donald F. McMullen,<sup>4</sup> Romain Quilici,<sup>2</sup> Peter Turner,<sup>2</sup> Mathew Wyatt.<sup>1</sup>

<sup>1</sup>School of Information Technology, James Cook University, Townsville, QLD 4811, Australia.

<sup>2</sup>Department of Chemistry, University of Sydney, Sydney, NSW 2006, Australia. <sup>3</sup>Computer

Science Department, SUNY Binghamton, Binghamton, NY, USA. <sup>4</sup>The Pervasive Technology Labs, Indiana University, Bloomington, IN 47404 USA.

Crystallography provides an ideal domain for the research and development of e-Research tools and techniques. A multi-institution collaboration is developing a sophisticated remote instrument and data access system using Grid and web services technologies. The system builds on the Common Instrument Middleware Architecture (CIMA) project from Indiana University. Storage Resource Broker (SRB) technology is used for Grid data storage, and the Kepler workflow system is introduced for added flexibility and functionality. A feature rich portal is being developed that provides remote instrument control and data inspection. Instrument control is being augmented with an instrument simulation system for training and strategy evaluation.



## A New-Generation DDL : Evolving discipline dictionaries for the structural sciences

Syd Hall<sup>a</sup>, Nick Spadaccini<sup>b</sup>, John Westbrook<sup>c</sup>

<sup>a</sup>School of Biomedical & Chemical Sciences, Univ. of Western Australia. <sup>b</sup>School of Computer Science & Software Engineering, Univ. of Western Australia, <sup>c</sup>Protein Data Bank, Rutgers Univ., New Jersey, USA. E-mail: Sydney.Hall@uwa.edu.au

COMCIFS decided at the 2005 Florence Congress to use the *StarDDL* [1] approach as a basis for a new dictionary definition language that facilitates the better integration of the discipline dictionaries used to define data in the structural sciences [2].

Existing CIF dictionaries are written using two dictionary definition languages known as *DDL1* and *DDL2* [2]. These have a similar syntax but are sufficiently different to inhibit the integration of dictionaries and an efficient approach to developing common CIF browsers and validators. A new proposed DDL supports existing definition approaches while extending the semantic content in data definition (e.g. it provides method expressions for relating items) and enabling more-precise data validation and evaluation paradigms. The use of the new DDL will extend data definition facilities without requiring changes to the large body of existing CIF data files.

This paper will describe the draft attributes for the DDL and how these may be used to enrich and integrate CIF dictionaries.

- [1] Spadaccini, N., Hall, S.R., and Castleden, I.R. Relational Expressions in STAR File Dictionaries 2000 *J Chemical Information and Computer Science* **40**, 1289-1301.
- [2] International Tables for Crystallography (2005). Volume G, *Definition and exchange of crystallographic data*, edited by S.R. Hall & B. McMahon. Heidelberg: Springer.

**Crystal Structure of Catalytic Domain of Japanese Encephalitis Virus NS3 Helicase/Nucleoside Triphosphatase at a Resolution 1.8 angstrom**

Tetsuo Yamashita<sup>1</sup> Hideaki Unno<sup>2</sup> Mori Yoshio<sup>1</sup> Moriishi Kohji<sup>1</sup> Tsukihara Tomitake<sup>3</sup> Matsuura Yoshiharu<sup>1</sup>

Research Institute for microbial diseases, Department of molecular virus, Osaka University<sup>1</sup>  
Institute for Protein Research, Research Center for structural and function proteomics, Osaka University, Japan<sup>2</sup>  
Institute for Protein Research, Department of Protein crystallography, Osaka University, Japan<sup>3</sup>

Mosquito-borne flaviviruses have a single stranded and positive-sense RNA as a genome and are classified into two serocomplexes, Japanese encephalitis virus (JEV) and dengue virus (DEN), and unclassified yellow fever virus (YFV). The flavivirus NS3 proteins are composed of two domains, the N-terminal protease and the C-terminal helicase/nucleoside triphosphatase catalytic domains, which are essential for viral replication. The crystal structures of the helicase domains of DEN and YFV have been recently elucidated. To obtain more insight in the structure of the flavivirus helicases, we determined the crystal structure of JEV helicase domain. The purified samples were crystallized by a hanging drop vapour-diffusion method. A single crystal was obtained by the reservoir solution containing 15% ethanol, 100mM Tris-HCl (pH7.0) and 4% pentaerythriol etoxylate (3/4 EO/OH). Data obtained by the beamline BL44XU of Spring-8 (Harima, Japan) using Mac Science DIP6040 imaging plate were processed with the program HKL2000 and the crystal structure was determined by a molecular replacement method. The 3D structures of JEV NS3 helicase domain at 1.8 angstrom were well conserved with those of DEN and YFV. In the comparison of flavivirus helicases, the active site topology of helicase of JEV, DEN and YFV is conserved well, but only HCV helicase is distant away from Walker motif A of other flavivirus helicase. In addition, the detail analysis of the active site residues of JEV NS3 helicase domain by using mutagenesis will be discussed.

## **Interaction studies of polygalacturonase with its inhibiting protein through predictive docking**

Malathy Sony Subramanian Manimekalai Ponnuswamy Mondikalipur Nanjappa

Department of Crystallography and Biophysics, University of Madras

Polygalacturonase (PG) is an enzyme involved in the biochemical conversion of pectins, which actively participate in softening process during fruit ripening. PGs are produced by plants and its pathogens. Microbial PGs facilitate the penetration of plant tissues by both bacteria and fungi. Plant cells as a way of host defense mechanism towards the invading pathogens express polygalacturonase inhibiting proteins (PGIPs) which are specific, reversible, saturable, high-affinity "receptors" for fungal PGs. Plant PGIPs interact with endo-PGs from fungi, but do not appear to have an effect on those of bacterial or plant origin. In this study the question of how PGs of plant origin may escape the recognition by PGIP and maintain their functionality in the presence of them through predictive docking at the molecular level is addressed. The docking was carried out using GRAMM program. The structures used for the study are: fungal PG (PDB ID:1czf ); since 3D structure of any plant PGs are unavailable, PG from tomato was predicted using homology modeling; structure of tomato PGIP is also not available and so was modeled. From this study the non-competitive mode of binding was proved and it also clearly demonstrates the differential recognition of plant PG and fungal PG by plant PGIP. From the predicted complex of the fungal PG and the PGIP the mode of inhibition could be explained at the molecular level. The detailed methodology adopted and the results obtained will be presented.

**Purification, Crystallization and Preliminary analysis of Hemoglobin from Turkey (*Meleagiris gallopova*) and Domestic Pigeon (*Columba livia*)**

Charles Packianathan Sundaresan Sigamani Neelakandan Kamariah Palani Kandavel Ponnuswamy Mondikalipudur Nanjapa goundar

Department of Crystallography and biophysics, University of Madras

Hemoglobin is an oxygen carrier protein in the red cells of the blood in mammals and other animals. The purification of the hemoglobins from both the sources were achieved by using the ion exchange column chromatography DEAE-Cellulose as the column material and the single peak of activity through SDS-PAGE electrophoresis. The hemoglobin crystals obtained by hanging drop vapor diffusion by using PEG 3350 as the precipitant in the reservoir. The data were collected using mar345image plate with the crystal to detector system of 100 mm at 293 K. The crystals of both the samples belong to orthorhombic space group P2<sub>1</sub>2<sub>1</sub>2, and the cell dimensions are: a = 66.458 Å, b = 79.957 Å, c = 104.131 Å for turkey and a = 79.658 Å, b = 81.787 Å, c = 82.232 Å for pigeon. Evaluation of crystal packing parameter indicated that the lattice could accommodate one molecule per asymmetric unit (Matthews coefficient for turkey is 2.16(V<sub>m</sub>(Å/Da)) and pigeon is 2.09 (V<sub>m</sub>(Å/Da)) with the solvent contents are 43.13% and 41.26%). The structure solutions were obtained by molecular replacement method using Graylag goose hemoglobin (PDB id: 1FAW) as the starting model, using the program AmoRe implemented in CCP4 suite. The solution resulted in a conventional crystallographic R-factor of 33.0% and correlation coefficient of 77.5% for turkey and 35.1% and 75.7% for pigeon hemoglobin. The refinement of both the hemoglobins are underway using Refmac5.0.

## **A Modeling Study to Curtail the Action of RNR Enzyme Towards Cancer Therapy**

Sampath Natarajan Ponnuswamy Mondikalipudur Nanjappa

Department of Crystallography and Biophysics, University of Madras

Ribonucleotide reductase(RNR) is a ubiquitous cytosolic enzyme, responsible for converting ribonucleotides into deoxyribonucleotides, the eventual substrates for DNA polymerase and also repairs DNA in all living cells. Thus cell division makes it a potential target for designing drug to inhibit cell growth in cancer therapy. This cell division is performed with the help of free radicals, which is from tyrosine residue. An increased interest in RNR as a target for cancer therapy is seen ever since the human RNR is regulated by p53 enzyme. The p53 enzyme actively suppresses the tumor formation but on mutation it leads to several forms of cancer. As much as over 80% of the human tumors have been found to contain mutations in p53 enzyme and the cancer cells would die if the normal RNR were inhibited. This appears to be a good strategy but unfortunately the picture seems to be more complicated. A new strategy to kill the cancer cells would be a specific inhibitor, which inhibits the RNR-R2 enzyme which is crucial to cancer cells after DNA damage since they cannot induce the p53R2 due to lack of p53. Therefore an understanding of the molecular mechanism of RNR is essential for the design of new cytostatic drugs. The inhibitor must be a radical scavenger to destroy the tyrosyl radical or iron metal scavenger (which affects the iron center). In this view the modeling studies on human RNR-R2 were made to understanding the interaction with radical scavengers through the docking studies. Further more, the radical mechanism of action of inhibitors will be proposed. In addition to this how the metal scavenger drugs are better than radical scavenger drugs to curtail action of RNR enzyme will be discussed in details.

### **Three dimensional Structure of Glycinin, a 11S Globulin from Peanut (*Arachis hypogaea*)**

Saraboji Kadhivel Balasundaresan Dhakshnamoorthy Ponnuswamy Mondikalipur  
Nanjappagounder

Department of Crystallography and Biophysics, University of Madras

Seed storage proteins of grain crops meet the major dietary protein requirement of over half of the world population and play a major nitrogen source for the developing plant. Most of the plant seeds contain 11S globulins as major storage proteins for their nutrition. Large quantities of storage proteins are accumulated in developing seeds of leguminous plants that function as a reserve of carbon and nitrogen used during germination and early growth. A Glycinin, 11S globulin, is one of the major storage proteins in peanut and accounts for about 50% of the total seed proteins. Thus, glycinin plays an important role in the properties of food made from peanut. The protein glycinin was purified from the globulin fraction of peanut seed and the crystal structure was determined at 3.5Å resolution. The crystals grown under 30%MPD are rhombohedral with space group R3. The overall fold of the present model is consistent with the storage protein structures and this fold comes under the cupin superfamily domain. The crystal structure shows that the hexamer has 32-point group symmetry formed by face-to-face stacking of two trimers and these trimers are stabilized by hydrophobic, electrostatic and hydrogen bonding interactions. The inter and intra-chain disulphide bonds conserved in the 11S globulin family are clearly observed.

## Crystal Structures of the dTDP-4-keto-2,3,6-trideoxy-3-aminohexose Reductase (DnmV) from *Streptomyces peucetius*: Implications for the Inhibition and Catalytic Mechanisms

Yi-Wei Chang<sup>1</sup> Chih-Chien Wu<sup>2</sup> Yuh-Ju Sun<sup>1</sup> Hsien-Tai Chiu<sup>2</sup> Chwan-Deng Hsiao<sup>3\*</sup>

Department of Life Science & Institute of Bioinformatics and Structural Biology, National Tsing Hua University<sup>1</sup> Institute of BioMedical Science, National Chiao Tung University, Taiwan<sup>2</sup> Institute of Molecular Biology, Academia Sinica, Taiwan<sup>3\*</sup>

Daunorubicin (DNR) and its C-14-hydroxylated derivative doxorubicin (DXR) which produced by *Streptomyces peucetius* are clinically important anti-tumor agents in the treatment of a number of malignancies including leukemia, non-Hodgkin lymphoma, and breast cancer. Like many microbial secondary metabolites, DNR and DXR require a deoxyhexose component for their biological activity. The biologically important deoxy-sugar in this case is the 2,3,6-trideoxy-3-aminohexose daunosamine. According to the well characterized biosynthetic pathway of these two anti-tumor components, the last step of daunosamine biosynthesis is performed by the thymidine diphospho-4-keto-2,3,6-trideoxy-3-aminohexose reductase (DnmV). Here, two complex crystal structures of DnmV were determined. One is a binary complex structure in which DnmV coupled with cofactor NADP, and another is a ternary complex structure in which DnmV coupled with cofactor NADP and inhibitor thymidine diphosphate. These two complex structures provide insights into the conformation of DnmV and help us to elucidate the detail inhibition mechanism of TDP. Furthermore, modeling of the saccharide moieties of the substrate in the active site based on the DnmV/NADP/TDP ternary complex structure allows us to propose a detailed catalytic mechanism for DnmV. These studies should lead to facilitate efforts to engineer strains that produce larger quantities of more capable and more valuable microbial metabolites.

## Increasing stability of Papain through structure-based protein engineering

Debi Choudhury Sampa Biswas Chandana Chakrabarti J.K. Dattagupta

Crystallography & Molecular Biology Division, Saha Institute of Nuclear Physics

Proteases constitute one of the important groups of industrial enzymes. Amongst the proteases, the cysteine proteases are of considerable commercial importance due to their strong proteolytic activity against a broad range of substrates. The widely studied member of this group is Papain, which has immense industrial and pharmaceutical applications, for which it is desirable that papain has higher stability. High stability is of economic advantage because of reduced enzyme turnover, higher reaction rates, and lesser microbial contamination. The kinetic stability of many proteins has been improved by rational design. One strategy for identifying stabilizing mutations involves comparison of more stable homologous proteins with less-stable ones.

In our laboratory we have solved the three dimensional structures of a few naturally occurring highly stable plant cysteine proteases of papain-family. Based on these three dimensional structures and amino acid sequence patterns we have attempted to design a papain molecule, which will have enhanced stability with negligible compromise in its catalytic activity. For this, the 40 kDa *wild type* papain precursor has been cloned, overexpressed in *E. Coli* as inclusion bodies, purified and refolded. Site-directed mutagenesis attempts are in progress on this recombinant papain to obtain the desired stability.

**Structure function correlation of multiple cysteine proteases from a tropical plant *Ervatamia coronaria***

Sampa Biswas Chandana Chakrabarti J.K. Dattagupta Raka Ghosh Sibani Chakraborty

C and M B Division, Saha Institute of Nuclear Physics, Kolkata-64

Proteases represent a single class of enzymes which plays an important role in physiological processes and in the commercial field. The papain-like cysteine proteases (family C1A) from plants have been described as catalysts in many physiological processes and are involved in the plant defense mechanism against pathogens and insects. The existence of multiple genes (30 genes in Arabidopsis genome) for this family in a single species and their product, executing similar catalytic mechanism, need to be explored. Fortunately this protease family includes members having long history of structural and functional analysis which makes them an ideal subject for structural genomics project of plant. Three such proteases Ervatamin A, B, and C (from the same source) have been isolated and purified from the latex of the tropical plant *Ervatamia coronaria*, biochemically, biophysically characterised and three-dimensional structures solved by the X-ray diffraction method. They have been cloned for sequence analysis and future protein engineering project on these enzymes. Though their basic catalytic mechanism and overall folding are similar, they differ in overall charges (pI values), stability and substrate specificity. The amino acid sequence comparison and finally three dimensional structures of these proteases explain how nature tailored array of enzymes known to be involved in defense mechanism to cope with the diverse need in environmental stress. This will also address the question of functional redundancy and evolution of catalytic mechanism for closely related members of a multigene family in plants.

## **Crystal Structure of the Human FOXK1a-DNA Complex and Its Implications on the Diverse Binding Specificity of Winged Helix/Forkhead Proteins**

Kuang-Lei Tsai<sup>1</sup> Cheng-Yang Huang<sup>1</sup> Chia-Hao Chang<sup>2</sup> Yuh-Ju Sun<sup>3</sup> Woei-Jer Chuang<sup>2</sup> Chwan-Deng Hsiao<sup>1</sup>

<sup>1</sup>Institute of Molecular Biology, Academia Sinica<sup>1</sup> Department of Biochemistry, National Cheng Kung University, College of Medicine, Taiwan<sup>2</sup> Institute of Bioinformatics and Structural Biology, National Tsing Hua University, Taiwan<sup>3</sup>

Interleukin enhancer binding factor (ILF) is a human transcription factor and a new member of the winged helix/forkhead family. ILF can bind to purine-rich regulatory motifs such as the human T-cell leukemia virus-long terminal region and the interleukin-2 promoter. Here we report the 2.4 Å crystal structure of two DNA binding domains of ILF (FOXK1a) binding to a 16-bp DNA duplex containing a promoter sequence. Electrophoretic mobility shift assay studies demonstrate that two ILF-DNA binding domain molecules cooperatively bind to DNA. In addition to the recognition helix recognizing the core sequences through the major groove, the structure shows that wing 1 interacts with the minor groove of DNA, and the H2-H3 loop region makes ionic bonds to the phosphate group, which permits the recognition of DNA. The structure also reveals that the presence of the C-terminal  $\alpha$ -helix in place of a typical wing 2 in a member of this family alters the orientation of the C-terminal basic residues (RKRRPR) when binding to DNA outside the core sequence. These results provide a new insight into how the DNA binding specificities of winged helix/forkhead proteins may be regulated by their less conserved regions.

## **The structure of Mcl-1 in complex with the Bim BH3 peptide at 1.55 Å resolution**

Peter E Czabotar Erinna F Lee Marco Evangelista David C Huang Walter D Fairlie Peter M Colman

Structural Biology, Walter & Eliza Hall Institute

Mcl-1 is a member of the Bcl-2 family of proteins. These proteins are important in the regulation of programmed cell death, a process known as apoptosis. Apoptosis is essential for the development of multicellular organisms. Inappropriate regulation of apoptosis occurs during tumour formation and thus is an important target for cancer therapy.

Bim regulates the anti-apoptotic activity of Mcl-1 via its BH3 domain. We have crystallised the Mcl-1:Bim BH3 complex and determined its structure to 1.55 Å resolution. We seek to exploit unique structural aspects of the complex by eventually identifying ligands that are able to bind Mcl-1 selectively and which might therefore have utility in treating cancers such as multiple myeloma where Mcl-1 expression is essential for the survival of the cancer cells.

**Crystal structure and site-directed mutagenesis studies of *Anabaena* sp. CH1 *N*-acetyl-D-glucosamine 2-epimerase reveal two key histidines for reversible epimerization**

Wen-Ching Wang<sup>1</sup> Hsin-Mao Wu<sup>1</sup> Yen-Chung Lee<sup>2</sup> Yu-Ning Chang<sup>1</sup> Wen-Hwei Hsu<sup>2</sup>

Department of Life Science, National Tsing Hua University<sup>1</sup> Institute of Molecular Biology, National Chung Hsing University, Taichung, Taiwan<sup>2</sup> Institute of Molecular and Cellular Biology and Department of Life Science, National Tsing Hua University, Hsinchu, Taiwan<sup>1</sup>

*N*-Acetyl-D-glucosamine 2-epimerase (GlcNAc 2-epimerase) catalyzes the reversible epimerization between *N*-acetyl-D-glucosamine (GlcNAc) and *N*-acetyl-D-mannosamine (ManNAc). We report here the 2.0 Å resolution crystal structure of the GlcNAc 2-epimerase from *Anabaena* sp. CH1. The structure demonstrates an  $(\alpha/\alpha)_6$  barrel fold, which shows structural homology with porcine GlcNAc 2-epimerase as well as a number of glycoside hydrolase enzymes and other sugar-metabolizing enzymes. One side of the barrel structure consists of short loops involved in dimer interactions. The other side of the barrel structure is comprised of long loops containing six short beta-sheets, which enclose a putative central active-site pocket. Site-directed mutagenesis of conserved residues near the *N*-terminal region of the inner alpha helices shows that R57, H239, E308, and H372 are strictly required for activity. E242 and R375 are also essential in catalysis. Based on the structure and kinetic analysis, H239 and H372 may serve as the key active site acid/base catalysts. These results suggest that the  $(\alpha/\alpha)_6$  barrel represents a robust fold for presenting active-site residues in a cleft at the *N*-terminal ends of the inner alpha helices, thus forming a fine-tuned catalytic site in GlcNAc 2-epimerase.

**Structural and biochemical characterization of circadian clock related protein Pex in *Synechococcus* sp. Strain PCC 7942**

Kyouhei Arita<sup>1</sup> Kumiko Igari<sup>2</sup> Mayuko Akaboshi<sup>2</sup> Toshiyuki Shimizu<sup>2</sup> Hiroshi Hashimoto<sup>2</sup>  
Shinsuke Kutsuna<sup>2</sup> Mamoru Sato<sup>2</sup>

Graduate School of Engineering, Kyoto University<sup>1</sup> Yokohama city university/International  
Graduate School of Arts and Sciences<sup>2</sup>

Circadian clocks are self-sustained biochemical oscillators. The oscillator of *Synechococcus elongates* is constituted by the products of the *Kai* genes (*KaiA*, *KaiB*, and *KaiC*). *KaiC* auto-phosphorylation cycle robustly oscillates in the cell with 24 hr period and is essential for basic timing process of the cyanobacterial circadian clock. Recently, *period extender* (*pex*), whose deficient mutant shows short period phenotype, was also isolated as a resetting-related gene. In fact, *pex* mRNA and *pex* protein (Pex) increase in dark period, and the *pex* mutant subjected diurnal light-dark cycles showed phase-advance of the rhythm by 3 h. Furthermore, disruption of *pex* gene in cyanobacteria cell leads to greatly enhancement of *KaiA* gene activity. To more fully understand the molecular mechanism involved in regulation of circadian clock oscillation in cyanobacteria, we have determined the crystal structure of Pex in *Synechococcus* sp. Strain PCC 7942 at 1.8 Å resolution. Pex has a winged-helix motif in the mid portion similar to that of several DNA binding proteins. Pex dimerizes in a unique fashion compared with other winged-helix DNA binding proteins. Electrophoretic Mobility Shift Assay of Pex with DNA containing *KaiA* promoter sequence demonstrates that Pex has DNA binding activity and specifically recognize *KaiA* promoter sequence. Mutation analysis shows that Pex uses the winged-helix region to recognize DNA. Our structural and biochemical data suggest Pex potentially regulates *KaiA* expression levels by interaction with the *KaiA* promoter region as a negative transcriptional regulator.

## Helical twists of model peptides strongly support our 7/2-helical model for collagen

Kenji Okuyama<sup>\*</sup> Chizuru Hongo<sup>\*</sup> Keiichi Noguchi<sup>\*\*</sup>

Department of Macromolecular Science, Osaka University<sup>\*</sup> Tokyo University of Agriculture and Technology<sup>\*\*</sup>

During the last five decades, the 10/3-helical model proposed by Rich and Crick was believed to be the molecular structure of collagen. Although we proposed the different structural model (7/2-helix) based on the single crystal structure of collagen-model peptide (1977), this was only accepted as the structure of model peptides, but not accepted as the structural model for collagen. However, we recently demonstrated that both the 7/2- and 10/3-helical models can explain quantitatively the X-ray diffraction data from native collagen. In this study, we investigated helical twists of 2,163 triplets of the collagen-model peptides found in single crystal structures analyzed at high resolutions. The histogram of helical twists (Fig.1) shows that the center of the distribution (52.6°) agrees very well with the helical twist (51.4°) of the ideal 7/2-helix, while there is no indication of even a very small peak around 36° which corresponds to the ideal twist angle for the 10/3-helical model. These evidences strongly indicated a preference for the 7/2-helical conformation rather than the now prevailing Rich & Crick (10/3-helical) model.

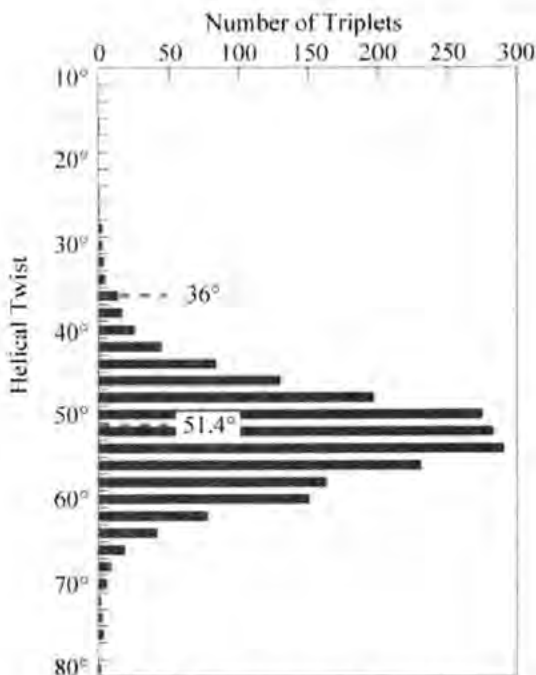


Fig.1 Distribution of helical twists

## Effect of Sodium Ion on the Structural Phase Transition of Hen Egg-White Lysozyme Crystals

Kazuaki Harata Toshihiko Akiba

Biological Information Research Center, National Institute of Advanced Industrial Science and Technology

Crystal-to-crystal phase transition induced by dehydration is observed when a triclinic or monoclinic lysozyme crystal is slowly desiccated. We have determined crystal structures at atomic resolution before and after the transition and reported that the phase transition is associated with the binding (triclinic crystal) or release (monoclinic crystal) of a sodium ion in the loop region Ser60-Leu75 [1, 2]. A monoclinic crystal soaked in a saturated NaCl solution was hard to transform completely in 24 hours by dehydration in a nitrogen gas stream with 263K. In this crystal, a sodium ion was fully bound to the loop region with a distorted octahedral coordination. On the other hand, a crystal soaked in a saturated KCl solution was easily transformed in an hour. The sodium ion bound to the loop region was replaced with a water molecule in the KCl soaked crystal although the structure of the loop region is still in the sodium bound form. The phase transition is accompanied with the structural transformation of the loop region from the sodium-bond form to the water-bound form. The binding of the sodium ion stabilizes the loop structure and seems to prevent the change to the water-bound form.

### Reference

- [1] K. Harata & T. Akiba. (2004). *Acta Cryst.*, D60, 630.
- [2] K. Harata & T. Akiba. (2006). *Acta Cryst.*, D62, 375.

**Coupling crystallography with kinetic studies leads to identification of a previously unknown binding pocket**

Nyssa Drinkwater<sup>1</sup> Christine L Gee<sup>2</sup> Joel D Tyndall<sup>3</sup> Gary L Grunewald<sup>4</sup> Wu Qian<sup>5</sup> Michael J McLeish<sup>6</sup> Jennifer L Martin<sup>1</sup>

Institute for Molecular Bioscience, The University of Queensland<sup>1</sup> National School of Pharmacy, University of Otago<sup>2</sup> Department of Medicinal Chemistry, The University of Kansas<sup>3</sup> College of Pharmacy, University of Michigan<sup>4</sup>

Phenylethanolamine *N*-Methyltransferase (PNMT), as the enzyme that synthesises adrenaline in the central nervous system has been the target of structure-based inhibitor design for 25 years. Recently, on the basis of computational studies, inhibitors predicted to be too large to occupy the PNMT active site surprised researchers by maintaining high levels of potency. X-ray crystallographic structures of the enzyme:inhibitor complexes now show the reasons for this include dramatic movements of key active site residues and rigid body movements of nearby alpha helices. The described conformational changes reveal a previously unknown binding cavity, and result in a doubling in volume of the ligand-binding pocket. Furthermore, kinetic and mutational analysis shows that these major structural changes occur at relatively minor energetic cost. Presented here is a detailed structural, mutational, and kinetic study characterising the described structural perturbations. This research now has implications towards emerging techniques of drug design and development including virtual screening of compounds and fragment-based lead discovery.

## How winged helix/forkhead proteins using less conserved residues to regulate diverse DNA sequence

Chwan-Deng Hsiao

Institute of Molecular Biology, Academia Sinica

Winged helix/forkhead proteins have shown to have similar binding specificity to the core sequence. In addition, these proteins have conserved amino acid sequences in the putative recognition helix. This raises an intriguing question as how proteins use conserved residues to recognize distinct core sequences. To date, more than 200 winged helix/forkhead proteins have been identified but only two forkhead protein/DNA complexes have been reported. Prior to this study, little is known about how winged helix/forkhead proteins recognize diverse DNA sequence. We report here a 3-D crystal structure of human FOXK1a bound to a 16-base pair DNA duplex containing promoter sequence (1). This complex structure provides a new insight into that how the DNA-binding specificities of winged helix/forkhead proteins may be regulated by their less conserved regions. The present structural study also offers the first view of a cooperative binding of ILF to DNA that contains the core sequence. The cooperativity of ILF can arise through DNA conformability in the absence of strong protein-protein interactions. The structural evidence present here was also consistent with our biochemical data.

### Reference

- (1) Tsai, K.-L., Huang, C.-Y., Chang, C.-H., Sun, Y.-J., Chuang, W.-J. and Hsiao, C.-D.\* (2006). Crystal structure of the human FOXK1a/DNA complex and its implications on the diverse binding specificity of winged helix/forkhead proteins. *J. Biol. Chem.* (in press)

### X-ray analyses of 3-hydroxybutyrate dehydrogenase from *Alcaligenes faecalis*

M. Mominul Hoque<sup>1</sup> Ella Czarina M. Juan<sup>1</sup> Satoru Shimizu<sup>1</sup> Hiroshi Kondo<sup>1</sup> M. Tofazzal Hossain<sup>1</sup> Kaoru Suzuki<sup>2</sup> Shigeyuki Imamura<sup>3</sup> Tamotsu Yamamoto<sup>3</sup> Takeshi Sekiguchi<sup>3</sup> Akio Takenaka<sup>1</sup>

Graduate School of Bioscience and Biotechnology, Tokyo Institute of Technology<sup>1</sup> College of Science and Engineering, Iwaki-Meisei University, Iwaki, Japan<sup>2</sup> Asahi Kasei Corporation, Japan<sup>3</sup>

3-Hydroxybutyrate dehydrogenase (3-HBDH) is an NAD-dependent enzyme for reversible conversion between D-3-hydroxybutyrate and acetoacetate. These ketone bodies are important energy sources, but their excess level causes ketoacidosis. 3-HBDH is useful for diagnostic analysis of ketone bodies in diabetes mellitus. To elucidate the reaction mechanism, we started X-ray analyses of 3-HBDH from *Alcaligenes faecalis* and its complex with NAD. Two crystal forms (I and II) of 3-HBDH and an NAD-containing crystal (III) were obtained by the hanging drop vapor-diffusion method at 293 K. Diffraction data were collected at 100 K with synchrotron radiation at PF(Tsukuba, Japan). Crystal data are  $a=77.3$ ,  $b=118.8$ ,  $c=118.7\text{\AA}$ ,  $\beta=93.8^\circ$  and  $P2_1$ , for I,  $a=119.0$ ,  $b=121.4$ ,  $c=165.3\text{\AA}$  and  $P2_12_12_1$  for II, and  $a=165.5$ ,  $b=165.9$ ,  $c=152.9\text{\AA}$ , and  $C222$ , for III. The preliminary structure of I was solved by the molecular replacement method, and the atomic parameters have been refined at 2.19 Å resolution to  $R=22\%$  and  $R_{\text{free}}=29\%$ . The asymmetric unit contains two tetrameric enzymes composed of the four subunits arranged with non-crystallographic 222 symmetry. Each subunit has a Rossmann fold for NAD binding.



A ribbon drawing of 3-HBDH composed of the four subunits.

**A new class of oxidoreductases: structure and function of DsbA3 from *Wolbachia pipientis***

Mareike Kurz<sup>1</sup> Begona Heras<sup>1</sup> Inaki Iturbe-Ormaetxe<sup>1</sup> Scott O'Neill<sup>2</sup> Jenny Martin<sup>1</sup>

<sup>1</sup>Institute for Molecular Bioscience, University of Queensland<sup>2</sup> School for Integrative Biology, University of Queensland, Australia<sup>1</sup>

The correct folding of proteins into their secondary, tertiary and quaternary structure is essential in order to attain a native functional conformation. Many secreted proteins are structurally stabilized by intramolecular disulfide bridges, which, linked in the correct way, are essential for activity and stability. For prokaryotes, the mechanism of disulfide bond formation is well characterised only for the Gram-negative  $\gamma$ -proteobacteria *Escherichia coli*. Its folding system is composed of two pathways, the oxidizing and the isomerizing pathway. DsbA and DsbB introduce disulfide bonds into proteins (oxidative pathway), while DsbC and DsbD catalyse the rearrangement of mismatched cysteines (isomerizing pathway).

Can findings from studies on *E. coli* be translated to other bacteria? To address this question a comprehensive analysis of DsbA-like sequences over the entire bacterial kingdom was performed. Based on the results from this study we infer that the classical *E. coli*-like DsbA is present only in the  $\gamma$ -proteobacteria subclass and that at least two other DsbA classes exist. We have provisionally named these classes 2 and 3.

Two DsbA proteins from the  $\alpha$ -proteobacteria *Wolbachia pipientis*, DsbA3 and DsbA4, were chosen for further study. DsbA3 is a class 3 DsbA, characterized by the presence of a second conserved pair of cysteines in the sequence. DsbA4 is a hybrid DsbA with an *E. coli*-like active site (Cys-Pro-His-Cys) and sequence motifs characteristic of Dsb isomerases. Structural and biochemical characterization of these proteins will be presented.

## Down-puckering of Hyp destabilizes the triple-helical structure

Chizuru Hongo<sup>1</sup> Kenji Okuyama<sup>2</sup> Keiichi Noguchi<sup>3</sup> Shutoku Ebisusaki<sup>4</sup> Norikazu Nishino<sup>5</sup>

<sup>1</sup>Department of Macromolecular Science, Graduate School of Science, Osaka University  
<sup>2</sup>Department of Macromolecular Science, Graduate School of Science, Osaka University, Japan  
<sup>3</sup>Instrumentation Analysis Center, Tokyo University of Agriculture & Technology, Japan  
<sup>4</sup>Faculty of Engineering, Kyushu Institute of Technology, Japan

Collagen is a major fibrous protein in animal body. Its amino acid sequence is usually assumed to be  $(\text{Gly-X-Y})_n$ , where X and Y positions are frequently occupied by a proline (Pro) and a 4(*R*)-hydroxyproline (Hyp), respectively. These features enable collagen molecules to form a stable triple-helical structure. Especially, Hyp in the Y position facilitates this helical formation. However, it was also known that Hyp in the X position destabilizes the helix.

In this study, the puckering of Hyp in the X position was investigated by using a host-guest peptide,  $(\text{Pro-Pro-Gly})_4\text{-Hyp-Pro-Gly-(Pro-Pro-Gly)}_4$  (hereafter OPG). X-ray data collections were performed at BL40B2 of the SPring-8. The structure was analyzed at 1.36 Å resolution. In this structure, Hyp in the X position adopted a down-puckering in spite of energetically stable up-puckering and formed van der Waals stacking interactions with Pro in the Y positions of the adjacent strand (Fig. 1). These interactions are available only when imino acids in the X and Y positions adopt down- and up-puckerings, respectively. Although there is some compensation by the Pro(X):Hyp(X) interaction, the major factor to destabilize the OPG helix seems to be the unfavorable down-puckering of Hyp.

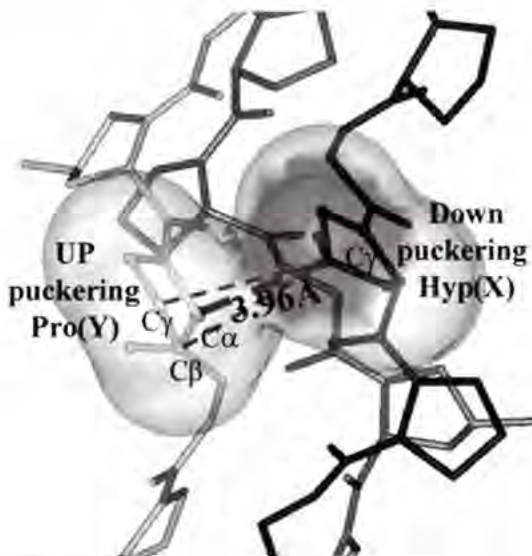


Fig. 1 Pro(Y):Hyp(X) stacking interaction of OPG

## X-ray Crystal Structure Analysis of a Collagen Model Peptide (Pro-Hyp-Gly)<sub>3</sub>-Pro-Arg-Gly-(Pro-Hyp-Gly)<sub>4</sub>

Tatsuya Morimoto<sup>1</sup> Mitsuru Haga<sup>2</sup> Chizuru Hongo<sup>3</sup> Kenji Okuyama<sup>4</sup> Keiichi Noguchi<sup>5</sup> Toshiki Tanaka<sup>6</sup>

<sup>1</sup> Department of Macromolecular Science, School of Science, Osaka University<sup>1</sup> Department of Biotechnology and Life Science, Graduate School of Engineering, Tokyo University of Agriculture & Technology, Japan<sup>2</sup> Department of Macromolecular Science, Graduate School of Science, Osaka University, Japan<sup>3</sup> Instrumentation Analysis Center, Tokyo University of Agriculture & Technology, Japan<sup>4</sup> Department of Materials Science and Engineering, Graduate School of Engineering, Nagoya Institute of technology, Japan<sup>5,6</sup>

The amino acid sequence of collagen is designated by the repetition of Gly-X-Y triplet. It is well known that Hyp in the Y position stabilizes the triple-helical structure of collagen. Recently, Brodsky and co-workers reported that the host guest peptide with Gly-Pro-Arg sequence as a guest showed a similar helix-coil transition temperature compared with that of Gly-Pro-Hyp sequence. In order to investigate stabilization mechanism of the Gly-Pro-Arg sequence, the host-guest peptide, (Pro-Hyp-Gly)<sub>3</sub>-Pro-Arg-Gly-(Pro-Hyp-Gly)<sub>3</sub> (hereafter PRG), was synthesized and its crystal structure was analyzed at 1.45 Å resolution by using synchrotron radiation (SPRING-8).

No substantial difference in the main chain conformation was observed between triple-helical structures of the PRG peptide and previously analyzed (Pro-Hyp-Gly)<sub>11</sub>. In the triple-helix of the PRG peptide, the side chain of Arg seems to stabilize its structure in two ways. One is van der Waals interactions between the long side chain of Arg and several parts of the adjacent chain (Fig1). The other is water-mediated hydrogen bonds between one of three nitrogen atoms in the Arg side chain and one of oxygen atoms in the same chain or in the adjacent chain.

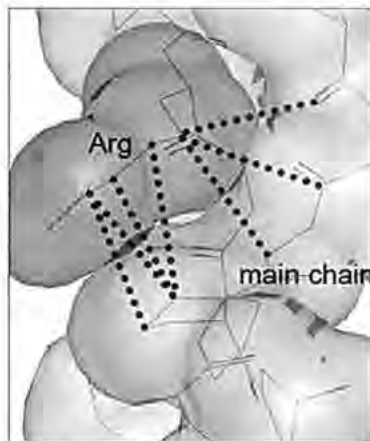


Fig. 1 Inter-chain van der Waals interactions between Arg and adjacent chain.

## Crystal structure of archaeal photolyase with two FAD molecules

Masahiro Fujihashi<sup>1</sup> Nobutaka Numoto<sup>2</sup> Kobayashi Yukiko<sup>1</sup> Akira Mizushima<sup>1</sup> Masaya Tsujimura<sup>2</sup>  
Akira Nakamura<sup>1</sup> Yutaka Kawarabayashi<sup>1</sup> Kunio Miki<sup>1</sup>

Department of Chemistry, Graduate School of Science, Kyoto University<sup>1</sup> National Institute of Advanced Industrial Science and Technology, Japan<sup>2</sup> Department of Chemistry, Graduate School of Science, Kyoto University / RIKEN SPring-8 Center, Harima Institute, Japan<sup>3</sup>

UV exposure on DNA molecules induces serious DNA lesions. CPD (cyclobutane pyrimidine dimer) photolyase repairs CPD type of lesion by using the energy of visible light. This enzyme possesses two chromophores; one catalyzes the CPD repair reaction and the other works as an antenna pigment that harvests photon energy. The catalytic cofactor of all known photolyases is FAD, whereas the light harvesting cofactor is either MTHF (5,10-methenyltetra hydrofolate) or 8-HDF (8-hydroxy-5-deaza-riboflavin). Three crystal structures of photolyases from *E. coli*, *A. nidulans*, and *T. thermophilus* have been determined; however, no archaeal photolyase structure is presently available. A similarity search of archaeal genomic data indicated the presence of a homologous gene, ST0889, on *Sulfolobus tokodaii* strain 7. The crystal structure of the ST0889 protein is superimposed very well on the three known photolyase including the catalytic cofactor FAD, suggesting that the protein functions as a photolyase. Surprisingly, another FAD molecule is found at the position of the light harvesting cofactor. This second FAD is well accommodated in the crystal structure. Recent work indicates that FMN enhances Tt-photolyase activity. These facts suggest that FAD works as a novel light harvesting cofactor of photolyase. In addition, two of the four CPD recognition residues in the crystal structure of An-photolyase are not found in the ST0889 protein. An archaeal photolyase from *S. tokodaii* might utilize a different mechanism to recognize the CPD from that of An-photolyase.

**Crystal structure of human Fyn kinase domain complexed with non-specific inhibitor staurosporine**Takayoshi Kinoshita<sup>1</sup> Mamoru Matsubara<sup>2</sup> Hiroshi Ishiguro<sup>3</sup> Kouki Okita<sup>3</sup> Toshiji Tada<sup>1</sup><sup>1</sup>Department of Biological Science, Graduate School of Science, Osaka Prefecture University  
<sup>2</sup>Faculty of Bioenvironmental Science, Kyoto Gakuen University<sup>3</sup> Carna Bioscience<sup>3</sup>

The tyrosine kinase Fyn is a member of the Src kinase family. Besides the role of Fyn in T cell signal transduction in concert with Lck, its excess activity in the brain is involved with conditions such as Alzheimer's and Parkinson's diseases. Therefore, inhibition of Fyn kinase may help counteract these nervous system disorders.

The truncated kinase domain (260-537) was overexpressed in the baculovirus expression system using *Sf21* insect cells and purified using His Trap HP, Mono Q and Superdex 200 columns (GE Amersham Biosciences). The non-specific inhibitor staurosporine was suspended into the protein solution, and the complex solution was incubated at 277 K. Hexagonal-plate crystals of the complex were obtained at 277 K using a reservoir solution of 1.15 M ammonium phosphate dibasic, 0.2 M NaCl and 0.1 M imidazole buffer, pH 8.0. After dipping into Paratone-N oil (Hampton Research), the crystals were frozen using a nitrogen gas stream at 100 K. Diffraction data were collected at a wavelength of 1.0 Å using the synchrotron radiation at Photon Factory beamline NW12A. X-ray diffraction data were processed and scaled using the program HKL2000 (HKL). We solved the crystal structure of the complex at 2.8 Å resolution using the program AMoRe.

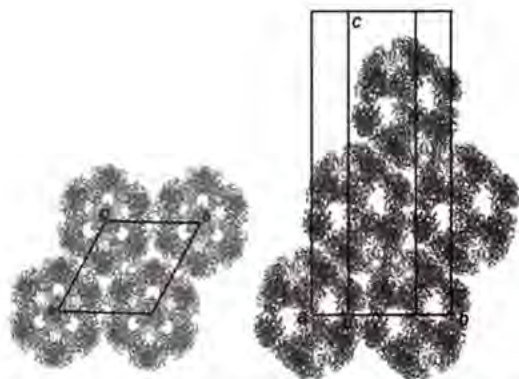
Staurosporine binds to the ATP-binding site of Fyn in a similar manner as in the Lck- and Csk- complexes. The structural basis for staurosporine binding to three protein tyrosine kinases, Fyn, Lck, and Csk may help in the development of new selective Fyn kinase inhibitors.

## Structural study on full-size acetyltransferase (E2p) of pyruvate dehydrogenase complex from *Thermus thermophilus*

Keita Kikuchi<sup>1</sup> Hiroshi Kondo<sup>1</sup> Ella C.M. Juan<sup>1</sup> Wataru Adachi<sup>1</sup> Ryoji Masui<sup>2</sup> Seiki Kuramitsu<sup>3</sup> Kaoru Suzuki<sup>4</sup> Takeshi Sekiguchi<sup>5</sup> Akio Takenaka<sup>1</sup>

<sup>1</sup>Graduate School of Bioscience and Biotechnology, Tokyo Institute of Technology, RIKEN Harima Insutitute/SPring-8, Japan <sup>2</sup>Iwaki-Meisei University, Japan<sup>3,4,5</sup>

Pyruvate dehydrogenase complex (PDC) is composed of multiple copies of three enzymes E1, E2 and E3, in which E2s form the central core. There are two types of the architectures depending on organisms; one is composed of 60 subunits of E2 (with 532 symmetry), and the other of 24 subunits (with 432 symmetry). In this study, ultracentrifugation experiments were performed at first to clarify the architecture of E2 from *Thermus thermophilus* (Tt-E2). The resulting sedimentation coefficient corresponds to 60 copies of Tt-E2, suggesting that the core structure is similar to those of eukaryotes and Gram-positive prokaryotes despite *Thermus thermophilus* being Gram-negative bacteria. To determine the structure, Tt-E2 was crystallized by the hanging-drop vapor diffusion method. X-Ray diffraction data at 11 Å resolution were collected with synchrotron radiation at PF. The initial phases were successfully solved by molecular replacement assuming 532 symmetry. The crystal structure was refined with ncs constraints. The unit cell has the following dimensions,  $a=b=215$  Å and  $c=543$  Å with the space group R32. As shown in the figure, the icosahedral Tt-E2s are reasonably packed in the unit cell.



Packing diagrams of icosahedral Tt-E2ps in the unitcell, viewed down along the c axis (left) and along the a<sup>\*</sup> axis (right)

**Crystal structures of M11L in the presence and absence of a Bak BH3 domain: structural insight into virus-mediated inhibition of apoptosis**

Marc Kvansakul Mark Van Delft Walter D Fairlie Jacqui M Gulbis David CS Huang Peter M Colman

Structural Biology Division, The Walter and Eliza Hall Institute of Medical Research

Programmed cell death (apoptosis) is a critically important mechanism that enables multicellular organisms to eliminate damaged, infected or unwanted cells. The Bcl-2 family of proteins, which contains both pro- and antiapoptotic members, plays a central role in regulating apoptosis. The two pro-apoptotic members Bax and Bak are activated in response to apoptotic stimuli and play a pivotal role by triggering the release of pro-death factors by a series of unknown conformational events that result in mitochondrial membrane permeabilization (MMP). In healthy cells, Bax and Bak are held in check by anti-apoptotic family members such as Bcl-2, Bcl-X<sub>L</sub> and Mcl-1. Apoptotic stimuli result in the release of pro-apoptotic BH-3 only proteins (e.g. Bim, Noxa, Bid) that neutralize anti-apoptotic Bcl-2, Bcl-X<sub>L</sub> and Mcl-1, thus freeing Bak and Bax to cause MMP.

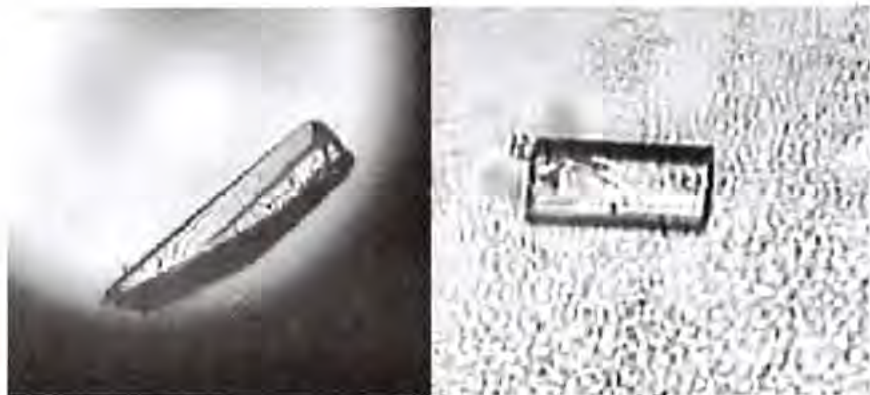
Apoptosis is recognised as a key innate immunity defence mechanism, and viruses have developed different strategies to ensure their survival in the face of host immune responses. Viral Bcl-2 homologs are deployed by Kaposi Sarcoma and Eppstein Barr virus to prevent cells from apoptosis during infection. Myxoma virus (MV), a member of the poxvirus family, encodes a multitude of anti-apoptotic proteins, but lacks an obvious Bcl-2 homologue. The MV protein M11L has been identified as a major virulence factor that localises to the outer mitochondrial membrane, and has been shown to inhibit apoptosis. We have determined the crystal structures of free M11L and M11L in complex with a Bak 26-mer peptide and investigated the anti-apoptotic properties of M11L. Our analysis provides new insight into the mechanism by which MV subverts host apoptosis to ensure virus survival.

## Crystallographic study on two types of threonyl-tRNA synthetases from *Sulfolobus tokodaii*

Yuichiro Miyashita<sup>1</sup>, Satoru Shimizu<sup>1</sup>, Yoshiteru Sato<sup>1</sup>, Ella Czarina Magat Juan<sup>1</sup>, Kaoru Suzuki<sup>2</sup>, Takeshi Sekiguchi<sup>2</sup>, Akio Takenaka<sup>1</sup>

<sup>1</sup>Graduate School of Bioscience and Biotechnology, Tokyo Institute of Technology, <sup>2</sup>College of Science and Engineering, Iwaki-Meisei University, Iwaki, Japan

Threonyl-tRNA synthetase (ThrRS) maintains the highest fidelity in protein synthesis by selective-editing of the misacylated aa-tRNAs. The structural architecture of the N-terminal editing domain, catalytic domain and anticodon-binding domain are highly conserved in bacteria and eukaryotes. In archaea *Sulfolobus tokodaii*, however, the two different genes (ST0966 and ST2187) have been found for ThrRS. Such a two-gene system was also found in *Sulfolobus solfataricus*. In the latter case, the gene products compensate each other (one for aminoacylation and the other for editing) to complete the reaction. To clarify the reaction mechanism, ST0966 and ST2187 were expressed in *E. coli* and the corresponding proteins were purified. Crystallization conditions were surveyed at room temperature by the hanging-drop vapor diffusion method. X-Ray data were collected at 100 K with synchrotron radiation of PF. The figure shows the crystals obtained. The ThrRS (ST2187) crystal diffracts at 2.3 Å resolution with the space group  $P222$ , and the cell parameters  $a=60.3$ ,  $b=68.0$  and  $c=134.4$  Å. The crystal structure has been solved by MAD phasing using zinc-containing crystals and Se-Met derived crystals.



Crystals of ThrRS(ST2187) (left) and ThrRS(ST0966) (right)

**Crystal structure of a splicing precursor of VMA1-derived endonuclease**

Akihiro Sakai Ryuta Mizutani

Department Applied Biochemistry, Tokai University

Protein splicing is a post-translational process in which an internal segment (intein) excises itself out of a precursor with concomitant ligation of the two flanking peptides (extein). Crystallographic analyses have been performed for recombinants of the *VMA1*-derived endonuclease (VDE) bearing N- and C-extein residues. The crystal structure of the X10SSS recombinant (with mutations C284S / H362N / N737S / C738S) showed that the extein peptides were connected to the intein via *trans* peptide bonds, while X10SNS (C284S / H362N / C738S) underwent splicing in the crystal lattice. These results suggest that N737 is essential for the protein splicing reaction.

Expression systems of VDE precursors bearing mutation N737S were prepared by cloning mutant genes derived from pTYB1 carrying a VDE allele into the *NdeI-BamHI* site of the expression vector pET-17b. The VDE precursor with single mutation (N737S) or double mutation (N737S / C738A) was purified by anion-exchange and gel-filtration chromatography. In the SDS-PAGE analysis, each purified protein gave a single 53-kDa band corresponding to the splicing precursor. This band was resistant to reducing agents, indicating that the single mutation N737S inhibits thioester formation in the initial N-S acyl shift step of the protein splicing. The N737S protein was crystallized in the presence of metal ions. Diffraction data to 3 Å resolution were collected by a laboratory diffractometer. The initial model obtained by the molecular replacement method using the X10SSS-VDE structure as a search molecule was subjected to the crystallographic refinement. Electron density maps of the splicing sites indicate that the existence of the extein peptides connected to the intein.

## First Results of Axiom 200, a High-speed, Photon-counting X-Ray Area Detector

Martin Adam<sup>1</sup> Matt Benning<sup>2</sup> Yacouba Diawara<sup>2</sup> Roger Durst<sup>2</sup> Bram Schierbeek<sup>2</sup>

<sup>1</sup>Bruker AXS B.V. <sup>2</sup>Bruker AXS Inc., Madison WI, USA

Axiom 200: A new type of imaging detector for X-ray crystallography based on resistive microgap technology will be described. The Axiom 200 exhibits a number of compelling advantages over the conventional, analog detectors such as CCD's and image plates. The Axiom 200 is a pure digital photon-counter and thus exhibits true single-photon sensitivity with essentially zero intrinsic noise and zero frame readout dead time. This allows it to acquire both very long exposures on weakly diffracting samples without data degradation and also extremely fast exposures for time resolved experiments. It also demonstrates a very high counting rate. With an active area of 20 cm and a spatial resolution better than 100 microns the Axiom 200 can resolve over 400 diffraction orders. Also, the Axiom 200 is extremely robust and has no internal dead areas. Because of the short read-out time the Axiom can be used in shutter-free mode, where the shutter is only opened once at the start of the experiment and closed again at the end of the experiment. The high sensitivity and low noise make the Axiom 200 a good candidate for SAD phasing experiments. Results of high quality data collections and successful S-SAD phasing will be shown.



## A minimum protein-splicing domain designed based on the crystal structure

Yudai Ishii Tetsuo Takahashi Ryuta Mizutani

Department Applied Biochemistry, Tokai University

The protein splicing reaction has been exploited to allow peptide ligation or excision to proceed *in vivo* and *in vitro*. Miniaturization of the splicing domain would facilitate these protein splicing applications to the larger peptide targets. Crystallographic studies have been performed for recombinants of the *VMA1*-derived endonuclease intein (VDE) bearing N- and C-extein residues. The dodecapeptide-motif domain of VDE is responsible for the endonuclease activity and not required for the protein splicing reaction. This endonuclease domain is connected to the splicing domain with antiparallel beta strands. In the present study, the endonuclease domain is replaced with a beta-turn designed from the crystal structure, giving a minimum protein that undergoes splicing reaction.

Synthesized oligonucleotide fragments corresponding to the beta-turn were inserted to the *HindIII* - *SacI* site of the VDE allele of the pET expression vectors. The obtained VDEdelta463-699 with the wild-type sequence and VDEdelta463-699 bearing a mutation N737S were expressed and recovered from the supernatant of the *Escherichia coli* lysate. In the SDS-PAGE analysis, the VDEdelta463-699(wt) recombinant gave a product band, while VDEdelta463-699(N737S) gave a precursor band, indicating that the N737S recombinant is a minimum analog of the protein splicing precursor, and that the shortcut linkage forms an expected turn structure. The VDEdelta463-699(N737S) protein was purified by ammonium sulfate precipitation and cation chromatography procedures. Crystallization of the purified protein underway will lead to precise elucidation of the reaction mechanism of protein splicing.

## Estimation of overall atomic displacement parameters from observed data

Ayako T Nakata Ryuta Mizutani

Department of Applied Biochemistry, Tokai University

Overall atomic displacement parameters represent average displacement of atoms over the whole crystal entities which contribute diffraction. The Wilson plot is known as the primary method for the estimation of the overall isotropic displacement parameter and absolute scaling from observed data. This plot utilizes the logarithmic fall-off property of observed intensity in the higher resolution. Results of statistical analysis indicate that the Wilson plot gives displacement parameter lower than model average, since high resolution data largely depend on atoms with small displacements.

It has been reported that the overall isotropic displacement parameter can be estimated from the Gaussian profile of the origin peak of the Patterson function. The Patterson origin peak represents a sum of self vectors of electron densities, and is computed from the entire observed data. This method, called Patterson scaling, principally gives displacement parameters deviated from model, since the Patterson function is a Fourier transform of a product of the atomic scattering factor and the Debye-Waller factor, resulting in deterioration of shape of the origin peak giving deviated displacement parameters.

Assuming the static atomic electron density has spherical symmetry in average, overall atomic displacement can be determined from the Patterson origin distortion from that calculated using the static models. The origin peak distortion is computed from a Patterson-like function  $P_E(r) = \text{Int. } \{|E(h)T(h)|^2 \exp(-2\pi i \cdot hr)\} dv^*$ , where  $E(h)$  is the normalized structure factor and  $T(h)$  the Debye-Waller factor. Overall isotropic and anisotropic displacement parameters can be estimated from a plot of  $P_E(r)$ , giving the best agreement with structure model.

## **Developments In High-Throughput Crystallography For the Home Laboratory**

Martin Adam, Matthew Benning, Sue Byram

Bruker AXS B.V., Bruker AXS Inc., Madison, WI, USA

Recent trends in macromolecular crystallography have dictated the development of methods that facilitate high throughput experiments, specifically at synchrotron sources. Equally as important but often less emphasized in the success of these experiments are the procedures that take place in the home laboratory. From crystallization to characterization, advances in technology have not only improved high-throughput applications but also extended capabilities at home.

This presentation will focus on recent developments in Bruker AXS hardware, such as Crystal Farm, Bruno, X8 Proteum and AXIOM 200, that are key to high-throughput experiments in the home laboratory.

**Crystallization and preliminary crystallographic analysis of  $\beta$ -trichosanthin, an isoform of trichosanthin from the root tuber of *Trichosanthe kirilowii***Minghuang Chen<sup>\*</sup> Xiaomin Hou<sup>\*</sup> Qi Peng<sup>\*</sup> Feng Yang<sup>\*</sup> Liqing Chen<sup>\*\*</sup> Mingdong Huang<sup>\*</sup>State Key Laboratory of Structural Chemistry, Fujian Institute of Research on the Structure of Matter, Chinese Academy of Sciences<sup>\*</sup> Department of Chemistry, Graduate Programs of Biotechnology, Chemistry and Materials Science, University of Alabama in Huntsville<sup>\*\*</sup>

Trichosanthin (TCS) is a type 1 Ribosome inactivity protein which was first isolated from the root tuber of *Trichosanthe kirilowii* Maxim and crystallized by Chinese scientists. TCS has been crystallized from barbital buffer, using  $\text{NaNO}_3$  as precipitant, the crystals belong to space group C2 with cell parameters  $a=75.60 \text{ \AA}$ ,  $b=75.44 \text{ \AA}$ ,  $c=88.36 \text{ \AA}$ ,  $\beta=99.50^\circ$ . TCS has also been crystallized from citrate buffer with KCl as precipitant, the crystals belong to space group P2<sub>1</sub>,2<sub>1</sub>,2<sub>1</sub>, with cell parameters  $a=38.305 \text{ \AA}$ ,  $b=76.225 \text{ \AA}$ ,  $c=79.213 \text{ \AA}$ . Crystalline TCS has multiple pharmacological properties including abortifacient, anti-tumor and anti-HIV. When the crystallized TCS was further purified using Mono-S column, two distinct protein peaks were designated as  $\alpha$ - and  $\beta$ -TCS according to the reverse order of elution from the Mono-S column, the minor peak was labelled  $\beta$ -TCS, which had an area less than 20% in total. Both  $\alpha$ - and  $\beta$ -TCS showed a single band with an apparent molecular weight of 27 kDa by SDS-PAGE. ESI-MS analysis indicated that the molecular weight of  $\beta$ -TCS is 27143 Da slightly less than that of  $\alpha$ -TCS, 27167 Da. Highly purified  $\beta$ -TCS has been crystallized using KCl as precipitant. The crystals belong to space group P2<sub>1</sub>,2<sub>1</sub>,2<sub>1</sub> with cell parameters  $a=38.244 \text{ \AA}$ ,  $b=86.934 \text{ \AA}$ , and  $c=135.785 \text{ \AA}$ , and have two molecules in the asymmetric unit. A data set to 1.6  $\text{\AA}$  resolution was collected with synchrotron source.

We are grateful for financial support from NSFC (No.39970872) and NSF of Fujian Province (C97052).

## Crystallographic study of thermostable hygromycin B phosphotransferase

Daisuke Iino<sup>1</sup>, Yasuaki Takakura<sup>1</sup>, Mika Kuroiwa<sup>1</sup>, Yasuyuki Sasaki<sup>1</sup>, Takayuki Hoshino<sup>1</sup>, Kanju Ohsawa<sup>1</sup>, Akira Nakamura<sup>1</sup>, Shunsuke Yajima<sup>1</sup>

Department of Bioscience, Tokyo University of Agriculture<sup>1</sup>, Division of Integrative Life Sciences, Graduate School of Life and Environmental Sciences, University of Tsukuba<sup>1</sup>

Bacteria elaborate the systems to survive antibiotics in various ways, and in turn, by using them the selection markers to clone genes have been developed as tools for molecular biology. Hygromycin B is one of the aminoglycoside antibiotics and targets ribosome to kill eukaryotic cells as well as prokaryotic ones. On the other hand, hygromycin B phosphotransferase (Hph) inactivates this antibiotic using ATP, thus this gene, especially that from *Escherichia coli*, has been used as a selection marker in many host-vector systems, including plants and animals. However, the tertiary structure of this protein has never been reported.

Recently, we have obtained a mutant Hph useful as a selection marker in a thermophilic bacterium, *Thermus thermophilus*, by the directed evolution<sup>1)</sup>. The mutant protein, Hph5, contains five amino acid substitutions, and shows an increased thermostability of about 16 deg *in vivo* and *in vitro*, compared with the wild type protein.

The Se-Met substituted protein was crystallized using the hanging-drop vapour-diffusion method. The crystal grew to dimensions of 0.2 x 0.2 x 0.2 mm in a couple of days. The data was collected at 2.1-Å resolution at BL-5A, Photon Factory (Tsukuba, Japan). The crystal belongs to space group  $P3_221$ , with unit cell parameters of  $a = b = 71.0$  Å,  $c = 125.0$  Å, and an asymmetric unit contains one monomer of Hph5 (340 residues). The data was processed by Mosflm, and the initial phase was obtained using the program SOLVE followed by the density modification with RESOLVE. RESOLVE also successfully traced the density to build the initial model with about 70% of total residues. Further modeling and refinement are currently continuing.

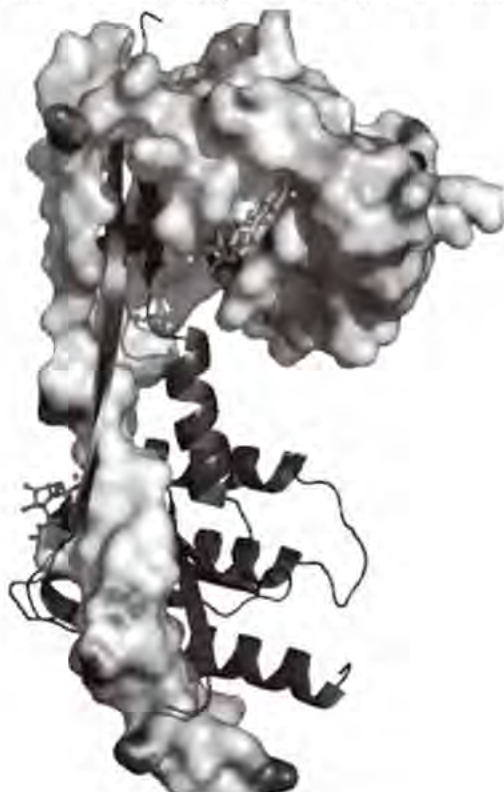
1) Nakamura, A *et al.* *J Biosci Bioeng* 2005, **100**,158-63.

**Rab27b structure swaps under GDP binding**

Leonard M G Chavas<sup>1</sup> Seiji Torii<sup>2</sup> Hironari Kamikubo<sup>3</sup> Masato Kawasaki<sup>1</sup> Kentaro Ihara<sup>1</sup> Ryuichi Kato<sup>1</sup> Mikio Kataoka<sup>3</sup> Tetsuro Izumi<sup>2</sup> Soichi Wakatsuki<sup>1</sup>

Structural Biology Research Center, PF-IMSS-KEK<sup>1</sup> Department of Molecular Medicine, IMCR, Gunma University<sup>2</sup> Graduate School of Material Science, NAIST<sup>3</sup>

Members of the Rab family of small GTPases regulate membrane traffic within the cell by recruiting their specific effectors in a nucleotide-dependent manner. The Rab27 subfamily consists of Rab27a and Rab27b, which share 70% sequence identity. By interacting with a large set of effector proteins such as melanophilin and granuphilin, both Rab27a/b regulate exocytosis of secretory lysosomes. Here we report the crystallographic structure determination of mouse Rab27b, solved from three distinct lattices in complex with GDP. Surprisingly, Rab27b-GDP exists in an open conformation, stabilized through dimerization by means of domain swapping in the crystals. The high flexibility of the switch domains might be the basis of such unfastening of the enzyme. In contrast, small-angle X-ray scattering measurements demonstrated a monomer form of the enzyme in solution both in its GDP- and GTP-bound states. Potential roles of the dimerization of the inactive Rab27b-GDP along its GTPase cycle will be discussed.



**Crystal structure of the heme oxygenase complexed with  $\alpha$ -meso hydroxyheme, a high reactive intermediate.**

Masaki Unno Masao Ikeda-Saito

Institute of Multidisciplinary Research for Advanced Materials, Tohoku University

Heme oxygenase (HO) catalyzes the regiospecific oxidation of heme to biliverdin with concomitant liberation of CO and iron. In its catalytic cycle, HO first binds one equivalent of heme to form a ferric heme-HO complex. The first electron donated from the reducing substrate converts the heme iron to the ferrous state. Then O<sub>2</sub> binds to reduced 5-coordinate heme to form a meta-stable oxy complex. One-electron reduction of the oxy ferrous form generates a ferric hydroperoxo complex, which self-hydroxylates the alpha *meso*-carbon of the porphyrin ring. The latter reaction is different from what occurs in P450 enzymes, in which the O-O bond of the hydroperoxo complex is heterolytically cleaved to generate an actively hydroxylating, ferryl (Fe<sup>4+</sup>=O) intermediate. Ferric alpha *meso*-hydroxyheme is then converted to biliverdin by multiple oxidoreductive steps involving a verdoheme intermediate.

To understand the unique mechanism of HO catalysis at atomic level, we have engaged in crystallographic analysis of its reaction intermediates. Recently, we solved the structure of the hydroxyheme-bound HO from *Corynebacterium diphtheriae* at 1.5 Å resolution. The occupancy of hydroxyl group bound to alpha *meso*-carbon is approximately 0.9. This high reactive intermediate was trapped by X-ray induced photo reduction and crystal annealing techniques. The binding distance between alpha *meso*-carbon and O atom of hydroxyl group is 1.25 Å, indicative that the structure dominantly exists in a keto form.

In the conference, we report the detailed structure of the hydroxyheme-bound HO and how to trap such a high reactive intermediate in crystals with high occupancy. We also discuss the HO reaction mechanism.

**Crystal Structures of Serine racemase: conformational change implies features of the enzyme.**

Masaru Goto<sup>1</sup> Ikuko Miyahara<sup>2</sup> Takae Yamauchi<sup>3</sup> Tohru Yoshimura<sup>4</sup> Nobuyoshi Esaki<sup>3</sup> Ken Hirotsu<sup>1</sup>

Department of Biochemistry, Osaka Medical College<sup>1</sup> Department of Chemistry, Osaka City University, Japan<sup>2</sup> Institute of Chemical Research, Kyoto University, Japan<sup>3</sup> Department of Applied Molecular Bioscience, Nagoya University, Japan<sup>4</sup>

D-serine is present at high levels in the mammalian brain including the central nervous system, higher than even some common amino acids, and is an endogenous ligand of the glycine site of *N*-methyl D-aspartate receptors. In glial cells, D-serine is synthesized by a serine racemase (SerR), a pyridoxal phosphate (PLP)-dependent enzyme enriched in astrocytes in mammalian brain, while its degradation is carried out by a D-amino acid oxidase. SerR has been shown previously to possess two distinct catalytic activities. In addition to the conversion of L-serine to D-serine, SerR catalyzes the alpha, beta-elimination of water from both stereoisomers of serine. It was reported that ATP together with magnesium is a physiological activator and enhances the racemase activity by tenfold. *S. pombe* gene homologous (sSerR) to mouse SerR was overexpressed in *E. coli*. The enzyme was purified and crystallized. Crystal structures of sSerR in its unliganded form, the complex with the activator analog (AMP-PCP) and the complex with serine in the closed form have been determined at 1.7, 1.9, and 1.7 Å resolution, respectively. The enzyme is a homodimer, and each subunit is divided into small and large domains. Superposition of the unliganded onto the closed forms reveals significant differences including a large conformational change at the domain level. The small domain rotates by about 20 degrees and approaches the large domain to close the active site. Interestingly, the substrate serine bound to the active site makes a covalent bond with PLP and the catalytic lysine and enhancer AMP-PCPs are bound to the subunit interface away from the active-site PLP.

## Water-mediated crystal transformation of D-xylose isomerase

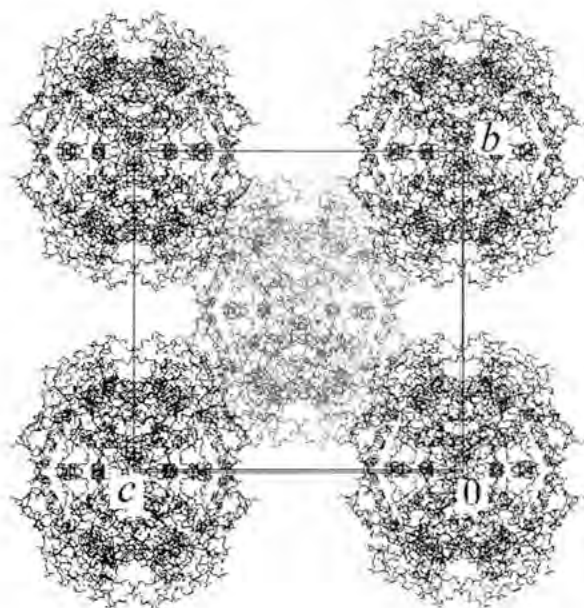
Masanori Ootaki<sup>1</sup>, Hiroyuki Konosu<sup>2</sup>, Hideaki Tagusagawa<sup>1</sup>, Shigefumi Yamamura<sup>1</sup>, Yoko Sugawara<sup>1</sup>

<sup>1</sup>Graduate School of Fundamental Life Science, Kitasato University, <sup>2</sup>School of Science, Kitasato University

There have been several reports on water-mediated crystal transformations of proteins, which offer valuable information on the role of hydration in crystals. D-xylose isomerase from *Streptomyces olivochromogenes* form a tetramer and crystallizes in the orthorhombic system with space group of  $I222$  (crystal A) or  $P2_12_12_1$  (crystal B) [1,2]. We found that the single crystal transformation of crystal A proceeds at 84% relative humidity. The estimated water content was reduced from 56% to 46% associated with the transformation. Precession photographs showed that the space group changed from  $I222$  to  $P2_12_12_1$ . The changes of cell parameters  $a$ ,  $b$ , and  $c$  are approximately 1%, 15%, and 3%, respectively. The cell parameters after the transition are similar to those of crystal B. Large shrinkage along the  $b$  axis is understandable from the crystal packing of crystal A (Figure 1 based on the PDB data of 1XIB). The transformation from  $I222$  to  $P2_12_12_1$  would be explained by rotational displacement of tetramers at  $(0,0,0)$  and  $(1/2, 1/2, 1/2)$  to the opposite direction around the two fold axes parallel to the  $c$  axis.

[1] H. L. Carrell *et al.* (1984) *J. Biol. Chem.* **256**, 3230-3236.

[2] G. K. Farber *et al.* (1987) *Protein Eng.* **1**, 459-466.



## Crystal Structure and Substrate Recognition of Aminopeptidase N

Yoshitaka Nakajima Yuko Onohara Kiyoshi Ito Yue Xu Kanako Nakashima Futoshi Matsubara Tadashi Yoshimoto

Graduate School of Biomedical Sciences, Nagasaki University

Aminopeptidase N (APN; EC 3.4.11.2) from *Escherichia coli* is a zinc peptidase, member of peptidase family M1. This enzyme possesses broad-substrate specificity and prefers substrates of N-terminal Arg, Lys, and Ala residues. It is noteworthy that the enzyme shows a little activity against peptides with an N-terminal Pro residue. In order to clarify catalytic and substrate-recognition mechanism of APN, we investigated this enzyme using X-ray crystallography.

The structure of ligand-free form and enzyme-bestatin, -amastatin, -L-leucine complex were determined at 1.50, 1.60, 1.65, and 1.55 Å resolution, respectively. The enzyme is composed of four domains: an N-terminal  $\beta$ -domain (Met1-Asp193), a catalytic domain (Phe194-Gly444), a middle  $\beta$ -domain (Thr445-Trp546), and a C-terminal  $\alpha$ -domain (Ser547-Ala870). The structure of the catalytic domain exhibits similarity to thermolysin, and a metal binding motif (HEXXHX<sub>18</sub>E) is found in the domain. The zinc ion is coordinated by His297, His301, Glu320, and a water molecule. The groove on the catalytic domain that contains the active site is covered by the C-terminal  $\alpha$ -domain, and a large cavity is formed inside the protein. However, there existed a small hole at the center of the C-terminal  $\alpha$ -domain. The amino terminus of bestatin, amastatin, and L-leucine was recognized by residues Glu121 and Glu264, which are located in the N-terminal and catalytic domains, respectively. Glu298 and Tyr381, located near the zinc ion, are considered to be involved in peptide cleavage. A difference revealed among the ligand-free form and three complexes indicated that Met260 functions as a cushion to accept substrates with different amino terminal sizes, resulting in the broad substrate specificity of this enzyme.

**Tris ion induces conformational change and crystal-packing contraction of porcine pancreatic elastase**

Asako Yamaguchi Takayoshi Kinoshita Toshiji Tada

Graduate School of Science, Osaka Prefecture University

Porcine pancreatic elastase (PPE) was crystallized under the new sulphate-free conditions containing 0.3 M NaCl and 50 mM tris(hydroxymethyl)aminomethane (TRIS)/HCl at pH 7.0. The crystal structure determined at 1.5 Å resolution had a unique conformation in four regions which contained loop portions. A chloride ion bound near the catalytic triad instead of a sulphate ion in 1QNJ, a typical PPE crystal structure. However, the chloride ion did not affect the configuration of the catalytic triad. A TRIS molecule bound to the S4 and S5 subsites in the place of the adjacent molecule in the 1QNJ crystal and played a significant role in the structural change of the region. Subsequently, the distortion in this region may have induced the conformational changes in the other three regions. The fact that TRIS and these four regions made a diagonal line in the *ac* plane may have affected the crystal-packing contraction along the *a* and *c* axes in the crystal compared to the typical crystal.

## **Crystal structure of bispecific antibody R310 against modified protein and DNA with oxidized lipids**

Sohei Ito<sup>1</sup> Mitsugu Akagawa<sup>2</sup> Koji Uchida<sup>1\*</sup>

<sup>1</sup>Department of Food and Nutritional Sciences, University of Shizuoka<sup>2</sup> Graduate School of Bioagricultural Sciences, Nagoya University, Japan<sup>\*</sup>

The aldehydes are important mediators of cell damage and can disrupt important cellular functions and can cause mutations. 4-Hydroxy-2-nonenal (HNE) is a major product of lipid peroxidation and is largely responsible for the cytopathological effects during oxidative stress. Upon reaction with protein, HNE predominantly reacts with nucleophilic amino acids and leads to the formation of stable Michael adducts.

We created monoclonal antibody (mAb) R310, which can enantioselectively recognize the HNE-histidine adducts, and demonstrated the both epitopes *in vivo*. To better understand the anti-HNE immune response, we undertook a detailed comparison of the primary structure of these mAbs and discovered that the presence of anti-R mAb R310 was homologous to anti-DNA autoantibodies, the hallmark of systemic lupus erythematosus. And the mAb R310 crossreacted with the dsDNA and oligo deoxyguanosine to some extent. On the basis of these findings, we evaluated the structural identity of mAb R310 with the anti-DNA mAbs by x-ray crystallographic analysis. Crystallization of mAb R310 Fab fragment with HNE-histidine adduct shows that the adduct binds to a hydrophobic pocket in the groove, consisting of six CDRs. Comparison of the structure of R310 to that of the anti-DNA Fab, which has been shown to bind oligonucleotides by making stacking interactions between tyrosine residues and the bases, revealed a common structural motif that could be a fundamental aspect of DNA recognition by Abs. The Ab primarily binds the HNE-histidine adduct by sandwiching between hydrophobic residues. The spatial distribution of these hydrophobic amino acids makes these residues to bind to DNA in the same way as the anti-DNA mAbs, allowing the bases to form sequence-specific hydrogen bonds with the protein.

## Crystal structure analyses of S-adenosyl-L-homocysteine hydrolase from *Plasmodium falciparum* complexed with inhibitors

Nobutada Tanaka<sup>1</sup>, Yoshio Kusakabe<sup>1</sup>, Aoki Ken-ichi<sup>1</sup>, Masayuki Nakanishi<sup>1</sup>, Yukio Kitade<sup>2</sup>, Kazuo T Nakamura<sup>1</sup>

<sup>1</sup>School of Pharmaceutical Sciences, Showa University; <sup>2</sup>Department of Biomolecular Science, Faculty of Engineering, Gifu University

The human malaria parasite *Plasmodium falciparum* is responsible for the death of more than a million people each year. The emergence of strains of malarial parasite resistant to conventional drug therapy has stimulated searches for antimalarials with novel modes of action. S-Adenosyl-L-homocysteine hydrolase (SAHH) is a regulator of biological methylations. *Plasmodium falciparum* SAHH (PfSAHH) inhibitors are expected to provide a new type of chemotherapeutic agent against malaria. Despite the pressing need to develop selective PfSAHH inhibitors, only the mammalian SAHH structures were available. We have determined the crystal structure of PfSAHH complexed with the reaction product adenosine (Ado) [Tanaka *et al.*, *J. Mol. Biol.* **343**, 1007-1017 (2004)]. Knowledge of the structure of the Ado complex in combination with a structural comparison with *Homo sapiens* SAHH (HsSAHH) revealed that a single substitution between the PfSAHH (Cys59) and HsSAHH (Thr60) accounts for the differential interactions with nucleoside inhibitors.

Recent studies suggest that introduction of a fluorine atom at the 2-position of a carbocyclic adenine nucleoside derivative improves the selectivity index between HsSAHH and PfSAHH inhibition. To obtain an insight into structural basis for selective inhibition of SAHHs by the inhibitors, structural analyses of PfSAHH complexed with the selective inhibitors are essential.

Here we present the crystal structure analysis of PfSAHH complexed with a selective inhibitor, 2-fluoronoraristeromycin (Tanaka *et al.*, in preparation).

**Structural insights into broad substrate specificity and catalytic activity of *Thermoplasma acidophilum* aldohexose dehydrogenase**Yoshiaki Yasutake<sup>1</sup> Yoshiaki Nishiya<sup>2</sup> Noriko Tamura<sup>1</sup> Tomohiro Tamura<sup>1</sup><sup>1</sup>Research Institute of Genome-based Biofactory, National Institute of Advanced Industrial Science and Technology (AIST) Tsuruga Institute of Biotechnology, Toyobo Co. Ltd, Japan<sup>2</sup>

The aldohexose dehydrogenase from the thermoacidophilic archaeon *Thermoplasma acidophilum* (AldT) is an enzyme that belongs to the short-chain dehydrogenase/reductase (SDR) superfamily, and catalyzes the oxidation of C1 hydroxyl of various monosaccharides such as D-mannose and D-xylose, with a preference of NAD<sup>+</sup> rather than NADP<sup>+</sup> as a cofactor. Most of the functionally related enzymes in the SDR superfamily are found in *Bacillus* species and display the highest activity for D-glucose. In contrast, AldT exhibits very low activity for D-glucose but the highest activity against D-mannose. To date, AldT is the only enzyme known to display an efficient NAD<sup>+</sup>-dependent dehydration activity against D-mannose. Although several crystal structures of the SDR family enzymes were determined, no structural information regarding the monosaccharide-recognition mechanism is available. It is of interest to investigate how these enzymes discriminate between various monosaccharides, particularly D-glucose and its C2 epimer D-mannose. AldT crystallized in space group  $P3_221$  with unit-cell dimensions of  $a = b = 82.0$  and  $c = 138.7$  Å, and the structures of AldT in ligand-free form, cofactor complex, and substrate complex were determined by the molecular replacement method using *Bacillus megaterium* glucose dehydrogenase as a search model. The AldT monomer forms a single domain structure with an unexpected long C-terminal tail, and assembles into intertwined tetramer having a 222 point-group symmetry. The details of the structure, structural mechanism of cofactor and monosaccharide recognition, and the significance of the C-terminal tail of the enzyme will be presented.

## **Isolation, Purification and Crystallization of Ribosome inactivating protein from Barley (*Hordeum vulgare*)**

Etti Sundaresan Karthe Ponnuraj Shanmugam Guruswamy

Department of Crystallography and Biophysics, University of Madras

Ribosome-inactivating proteins (RIPs) are cytotoxic *N*-glycosidases identified in plants, fungi, and bacteria. RIPs inhibit protein synthesis by virtue of their enzymatic activity, selectively cleaving a specific adenine residue from a highly conserved, surface-exposed, stem-loop (S/R loop) structure in the 28S rRNA of ribosomes. RIP's are usually classified into two groups: type I and type II. Type I (or single-chain) RIP's are unable to enter intact cells and thus are only capable of intoxicating cell-free systems. Type I RIP's are thought to be better candidates than type II RIP's for constructing immunotoxins because they lack their own cell recognition and binding ability. RIP from barley seeds, belonging to the type I category, inactivates eukaryotic ribosomes *via* a mechanism identical to that of ricin A-chain. Like many other type I RIP's, it is a basic protein with *pI* of above 9.0. The mature polypeptide chain, consisting of 280 amino-acid residues, has a molecular mass of about 30 kDa. The isolation and purification of RIP from barley seeds was done by a simple procedure of Ammonium sulphate precipitation and ion exchange column chromatography using CM-Sephadex as the column material and the single peak of the protein was confirmed by 15% SDS-PAGE gel electrophoresis. The micro crystals of RIP obtained by hanging drop vapor-diffusion method using PEG 4000 as the precipitant in reservoir. Improving the quality of crystals is in progress.

## Structural Analysis of Mutant *E. coli* Dihydroorotase: Role of a Conformational Change in Catalysis.

Mihwa Lee<sup>1</sup> Megan J. Maher<sup>2</sup> Richard I. Christopherson<sup>1</sup> J. Mitchell Guss<sup>2</sup>

School of Molecular and Microbial Biosciences, University of Sydney<sup>1</sup> Division of Biomolecular Sciences, Imperial College, London, SW7 2ZA, UK<sup>2</sup>

Dihydroorotase (DHOase) is a zinc metalloenzyme that catalyses the reversible cyclization of *N*-carbamyl-L-aspartate (CA-asp) to L-dihydroorotate (DHO) in the *de novo* pyrimidine biosynthetic pathway. Two different conformations of a surface loop (residues 105-115) are found in the dimeric *E. coli* DHOase crystallized in the presence of L-DHO [1-2]. The loop asymmetry mirrors that of the active site contents of the two subunits: DHO is bound in the active site of one subunit and CA-asp in the other active site. In the CA-asp-bound subunit, the surface loop reaches in towards the active site and makes hydrogen bonds with the bound substrate, whereas the loop forms part of the surface of the protein in the DHO-bound subunit. To investigate the relationship between the structural states of the loop and the catalytic mechanism, 8 mutant forms of DHOase including deletion of the entire loop were generated and characterized structurally and kinetically. In the presence of L-DHO, some of these mutants first formed tetragonal crystals with one monomer in the asymmetric unit with the loop in the "out" conformation. In contrast, the wild type enzyme formed orthorhombic crystals with a dimer in the asymmetric unit with one loop in and one out. The tetragonal crystals were extremely unstable and disintegrated shortly after formation, followed by the growth of orthorhombic crystals from the remnants of the tetragonal crystals. This transformation has been explored by using a product analogue instead of L-DHO in the crystallization. The close relationship between the catalytic state of DHOase and the importance of the loop movement will be discussed based on the kinetic and structural analyses.

1. Thoden, *et al.* (2001) *Biochem*, 40, 6989
2. Lee, *et al.* (2005) *J Mol Biol*, 348, 523

**Structural studies on hydrogenase maturation protein HypE**

Yasuhito Shomura Yoshiki Higuchi

Department of Life Science, University of Hyogo, Graduate School of Life Science

Hydrogenases are essential proteins in most microorganisms. The enzymes catalyze reversible oxidation of molecular hydrogen into protons and electrons. The members can be divided into a few classes according to the metal content of the active site. [NiFe] hydrogenases, a class of the members, are characterized by the [NiFe] cluster and the synthesis of the dimetallic center involves the products of at least six genes, hyp (hydrogenase pleiotropic genes) A, B, C, D, E and F. Of these, HypE and HypF are required for the synthesis of cyanide, one of the non-protein ligand for the iron, with using carbamoylphosphate as a substrate. Cyanide is known to be highly toxic to most of the organisms and the complexity of the dimetallic center implies the involvement of the sophisticated mechanism catalyzed by the HypE-HypF machinery. HypF first transfers carbamoyl moiety from carbamoylphosphate to the C-terminal cysteine in HypE, and subsequently, the carbamoyl residue is decarboxylated into thiocyanate *per se*. It is now open as to how ATP hydrolyses (both HypE and F have ATPase activity) are coupled to the reactions and whether the two enzymes cooperatively catalyze the reaction or not. To this end, we solved the crystal structure of HypE. The detail of the atomic structure and the proposed mechanism of the ATP-dependent dehydration reaction will be reported.

**ADP-Ribose Pyrophosphatase from *Thermus thermophilus* HB8, as A Target for Time-Resolved X-Ray Crystallography**Kentarō Kai<sup>1</sup> Ikuko Miyahara<sup>1</sup> Noriko Nakagawa<sup>2</sup> Seiki Kuramitsu<sup>2</sup> Nobuo Kamiya<sup>3</sup><sup>1</sup>Graduate School of Science, Osaka City University<sup>2</sup> Graduate School of Science, Osaka University, Japan<sup>3</sup> Graduate School of Science, Osaka City University, Japan<sup>3</sup>

ADP-ribose pyrophosphatase (ADPRase) from *Thermus thermophilus* (*Tt*) HB8 is a member of the nudix family proteins that distribute widely in nature and metabolize many kinds of nucleotide diphosphates. *Tt*-ADPRase catalyzes the divalent metal ion-dependent hydrolysis of ADP-ribose (ADPR) to AMP and ribose 5'-phosphate. The crystal structures of ADPRase have been reported including the ternary complex with divalent metal ions and ADPR (Yoshida, S. *et al.* (2004) *J. Biol. Chem.* 279, 37163-74). The complex crystals were obtained in acetate buffer out of catalytically optimum condition pH 6-7. Two metal binding sites, MI and MII, were involved in the metal coordination scheme around ADPR in the reaction cavity. We continued to improve the ternary complex crystal with Zn (II) ions and ADPR, and succeeded to determine the structure at 1.6Å resolution using X-ray diffraction data collected at the PF. When the pH value was increased slightly to pH4.7, an additional Zn ion was newly found at the third metal binding site, MIII, interacting with the ADPR phosphate and the Glu82 carboxylate. A water molecule bridging two Zn ions at MI and MIII is a candidate of nucleophile which is stereochemically suitable in the inline mechanism of the nucleotide diphosphate hydrolysis. The ternary complex crystal will be a potential target for time-resolved X-ray crystallography to prove the reaction mechanism proposed, if the catalytic reaction in the crystalline state could be triggered by the pH shift toward the optimum condition pH 6-7. We are at present investigating the protocol for the pH shift in crystal, and may present more detailed reaction mechanism of ADPRase, based on the results from both of the static and time-resolved structure analyses.

## Structural basis for neutral endopeptidase 24.11 recognition by ERM proteins

Shin-ichi Terawaki<sup>1</sup> Ken Kitano<sup>2</sup> Toshio Hakoshima<sup>1\*</sup>

<sup>1</sup>Structural Biology Laboratory, Nara Institute of Science and Technology<sup>2</sup> Structural Biology Laboratory, Nara Institute of Science and Technology, Japan. CREST, JST, Japan<sup>\*</sup>

ERM (Ezrin/Radixin/Moesin) proteins act as a cytoplasmic cross-linker that mediates formation of membrane-associated cytoskeletons by binding both actin filaments and cytoplasmic parts of membrane proteins. Members of this family possess the conserved N-terminal regions, which contain the FERM (Four point one and ERM) domain consisting of about 300 residues. The FERM domain recognizes the cytoplasmic tails of several adhesion molecules such as CD44, CD43 and ICAMs that are classified to type I membrane proteins. Recently, the FERM domain of ERM proteins has been shown to bind to a type II membrane protein, neutral endopeptidase (NEP), which inactivates G protein coupled receptors (GPCRs) by cleaving neuropeptides such as bombesin and neurotensin through the C-terminal extracellular metallopeptidase domain that belongs to the M13 family of zinc peptidases. The NEP-ERM interaction suppresses the cell adhesion by competing with the interaction between hyaluronane receptor CD44 and ERM proteins, while it is obscure how the FERM domain recognizes the N-terminal cytoplasmic tail of NEP that possesses the opposite peptide polarity to type I membrane protein CD44. Here, we determined the crystal structure of the radixin FERM domain complexed with the N-terminal NEP cytoplasmic peptide at 3.2 Å resolution. In the FERM-NEP complex, the NEP peptide locates at a long shallow groove on PTB (phosphotyrosine binding domain)-like subdomain C. This poster presents structural insight into the type II membrane protein recognition by the FERM domain and the suppression of cell adhesion through the interaction of NEP with the FERM domain.

## Crystallographic Study of Selenocysteine Lyase: Strict Substrate Recognition by the Catalytic Cysteine

Rie Omi<sup>1</sup> Suguru Kurokawa<sup>1</sup> Hisaaki Mihara<sup>1</sup> Tatsuo Kurihara<sup>1</sup> Nobuyoshi Esaki<sup>1</sup> Ikuko Miyahara<sup>2</sup> Ken Hirotsu<sup>1</sup>

<sup>1</sup>Institute for Chemical Research, Kyoto University<sup>2</sup> Department of Chemistry, Graduate School of Science, Osaka City University, Osaka, Japan

Selenocysteine lyase (SCL), which is a pyridoxal 5'-phosphate (PLP) dependent enzyme, catalyzes the beta-elimination of L-selenocysteine to yield L-alanine and selenium. The reaction mechanism involves formation of an enzyme-bound cysteine-perselenide intermediate (Cys-S-Se) and the conserved cysteine residue (Cys375) is essential for catalysis. SCL is specific for L-selenocysteine and has no activity for L-cysteine, therefore it is known as the key enzyme in the specific selenium-delivery pathway for selenoprotein synthesis. In order to elucidate the strict discrimination between selenium and sulfur by SCL, we have determined the three-dimensional structures of native SCL and L-cysteine complex at 1.8 Å and 1.9 Å, respectively.

Overall and active site structure of SCL is similar to those of cysteine desulfurases which catalyze the same type of reaction as SCL but act on both cysteine and selenocysteine. Why SCL does not show activity on cysteine? In the case of SCL/L-cysteine complex structure, not the amino group of L-cysteine but the thiol group is located close to the C4A of PLP in the active site. This indicates that L-cysteine is incorporated into the active site but can not make an external aldimine with PLP. In addition, spectrum analysis shows that Cys375 plays an important role in the recognition of the L-selenocysteine. The mechanism for discrimination between selenium and sulfur by Cys375 will be presented on the basis of the structural comparison between SCL and cysteine desulfurase.

## Structural analysis of Tollip C2 domain

Masato Akutsu<sup>1</sup>, Masato Kawasaki<sup>2</sup>, Yohei Katoh<sup>3</sup>, Ryuichi Kato<sup>4</sup>, Kazuhisa Nakayama<sup>5</sup>, Soichi Wakatsuki<sup>1</sup>

<sup>1</sup>Department of Materials Structure Science, The Graduate University for Advanced Studies, <sup>2</sup>Structural Biology Research Center, PF, IMSS, KEK, Japan, <sup>3</sup>Graduate School of Pharmaceutical Sciences, Kyoto University, Japan

Tollip (Toll-interacting protein) was initially identified as a negative regulator of the interleukin1 signaling pathway. Tollip consists of TBD (Tom1 binding domain) at the N-terminal, followed by a C2 domain and a ubiquitin binding CUE (Coupling of ubiquitin conjugation to ER degradation) domain at the C-terminal.

Tollip localizes on the endosomal membrane through the interaction between the C2 domain phosphoinositides. This interaction is thought to play an important role for endosomal trafficking of ubiquitinated proteins.

We have determined the crystal structure of Tollip C2 domain at 2.4Å resolution. The crystal belongs to the hexagonal space group  $P6_3$  with cell constants of  $a = b = 59.3\text{Å}$  and  $c = 199.1\text{Å}$ . The crystal structure reveals that the Tollip C2 domain is an anti-parallel  $\beta$ -sandwich and belongs to the Type II topology. There is a conventional anion binding site at the concave side of the  $\beta$ -sandwich core, and three basic residues around this site are involved in the interaction with a sulfate ion in the crystal structure. This sulfate binding site is a possible binding site for phosphoinositides.



**Crystallographic studies of FAD bound form of salicylate hydroxylase from *Pseudomonas putida* S-1**

Yoshihiko Watanabe<sup>\*</sup> Akiko Kita<sup>\*</sup> Kuniharu Ohnishi<sup>\*\*</sup> Kenzi Suzuki<sup>\*\*\*</sup> Kunio Miki<sup>\*\*\*\*</sup> Yukio Morimoto<sup>\*</sup>

Research Reactor Institute, Kyoto University<sup>\*</sup> Department of Microbiology, School of Pharmacy, Hokuriku University<sup>\*\*</sup> Department of Chemistry, Faculty of Science, Kanazawa University<sup>\*\*\*</sup> Department of Chemistry, Graduate School of Science, Kyoto University<sup>\*\*\*\*</sup>

Salicylate (*o*-hydroxybenzoate) hydroxylase from *Pseudomonas putida* S-1, consisting of 421 amino acid residues, catalyzes the decarboxylative hydroxylation of salicylate to catechol and CO<sub>2</sub>, with a 1:1:1 stoichiometry. It is a flavin-dependent monooxygenase containing 1 mol of FAD per mol of enzyme with a molecular weight of 54,000. The enzyme is a unique monooxygenase that catalyzes the hydroxylation with decarboxylation of salicylate or deformylation of salicylaldehyde. To understand the reaction mechanism and the substrate recognition system, it is important to determine the crystal structure of salicylate hydroxylase. We have reported the crystallization of apo-form salicylate hydroxylase previously<sup>(1)</sup>. We report here the crystallographic studies of FAD bound form (holo-form) of salicylate hydroxylase from *Pseudomonas putida* S-1. The crystals of holo-form enzyme were obtained by vapor diffusion method using ammonium sulfate as a precipitant and 2-methyl-2,4-pentanediol as an additive reagent at the room temperature. The crystal was grown to a maximal size of 0.7 x 0.3 x 0.3 mm. The crystals belong to hexagonal space group of  $P6_2$  or  $P6_4$ , with unit-cell dimension of  $a=b=141.7$  Å,  $c=62.0$  Å. The crystals diffracted X-ray beyond 2.7 Å resolution. Assuming one molecule per asymmetric unit, the crystal volume per unit molecular mass,  $V_m$ , is calculated to be 3.3 Å<sup>3</sup>/Da. The crystal structure analysis is in progress. The comparison of the structures between apo- and holo- enzyme will be discussed.

(1) T. Yabuuchi, K. Suzuki, T. Sato, K. Ohnishi, E. Itagaki, and Y. Morimoto, *J. Biochem.* 119, 829 (1996).

**Crystal structure of a novel human seminal zinc  $\alpha$  - 2 glycoprotein complex with binding protein**

Imtaiyaz Hassan Md Vijay Kumar Sameeta Bilgrami Punit Kaur Savita Yadav T.P Singh

Biophysics, All India Institute of Medical Sciences

ARITRASKZinc  $\alpha$ -2 glycoprotein (ZAG) has molecular weight 39 kDa and it is present in human body fluids such as blood plasma, seminal plasma, saliva, sweat and cerebrospinal fluid. It is induced by glucocorticoids and androgens in breast cancer cell lines indicating its role in the progression of mammary diseases including breast cancer. It is also implicated in stimulation of lipolysis in adipocytes, activation of GTP dependent adenylate cyclase that leads to the activation of multiple cellular pathways, down regulation of tumor proliferation, ribonuclease activity as well as a carrier protein. Although it is present in semen in high concentration, structure and function relationship is not yet clearly understood. We have purified a naturally occurring complex of ZAG with a protein subunit from human seminal plasma by using chromatographic techniques. The protein complex was at 20°C from PEG 9000 at pH 5.6. The crystals belong to tetragonal space group P4<sub>2</sub>,2 with unit cell dimensions a = b = 132.1 Å and c = 74.2 Å. The structure has been determined using molecular replacement method with plasma ZAG ( PDB Id: 1ZAG) as the model. It has three domains and the structure folds into a V-shaped groove which can ideally bind to another protein molecule. Two long  $\alpha$  - helical domains ( $\alpha$  1 and  $\alpha$  2) form the sides of the groove whereas the base is formed by the  $\beta$  pleated sheet domain. The protein molecule complexed to ZAG is composed of 106 amino acid residues and has predominately a  $\beta$ -pleated sheet structure. The two proteins bind strongly through large contact surfaces.

## **A 3D visualization system, VESTA, for electronic and structural analysis**

Koichi Momma<sup>1</sup> Fujio Izumi<sup>2</sup>

<sup>1</sup>Institute of Mineralogy, Petrology, & Economic Geology, Tohoku University<sup>2</sup> Quantum Beam Center, National Institute for Materials Science, Japan<sup>3</sup>

Though many structure-drawing programs are available nowadays, only few can deal with both structural models and electron/nuclear densities resulting from diffraction data and simulation. Then, we have developed a new computer program, VESTA (Visualization for **E**lectronic and **S**tructural **A**nalysis), for three-dimensional visualization of pixel data and structural models. VESTA represents crystal structures as ball-and-stick, space-filling, polyhedral, wireframe, stick, dot-surface, and thermal-ellipsoid models. Electron/nuclear densities, wave functions, and electrostatic potentials are visualized as isosurfaces, bird's-eye views, and two-dimensional maps. VESTA has a feature of surface colorization to show the electrostatic-potential value at each point on isosurfaces. Translucent isosurfaces and/or slices can be overlapped with a structural model. VESTA allows us to handle a virtually unlimited number of objects such as atoms, bonds, polyhedra, and polygons on isosurfaces. Drawing boundaries can be specified with lattice planes and ranges along *x*, *y*, and *z* axes. General equivalent positions can be transformed from conventional to non-conventional settings using a transformation matrix. Interatomic distances and bond angles on which restraints are imposed in Rietveld analysis with RIETAN-FP are easily visualized through close cooperation between VESTA and ORFFE.

## Crystal structure of Nanos

Hiroshi Hashimoto<sup>1</sup> Shigeta Kawaguchi<sup>1</sup> Naoki Shichijo<sup>1</sup> Satoru Unzai<sup>1</sup> Keishi Nakamura<sup>2</sup>  
Toshiyuki Shimizu<sup>1</sup> Yutaka Tamaru<sup>2</sup> Mamoru Sato<sup>1</sup>

<sup>1</sup>Yokohama City University<sup>2</sup> Mie University<sup>2</sup>

The germ cell is the only cell descended to the next generation. It has the totipotency that invents all soma and germ cells again. In general, germ cell precursor move to conceptacle and then the precursor differentiates to germ cell. It is, however, unclear about the formation mechanism of germ cell, translational control plays crucial role to express proteins in differentiation of germ cell, because transcription is absent in later stages of germ cell differentiation and does not resume until some time in early development. Nanos and Pumilio proteins are translational repressor and they play significant role in formation of germ cell. They bind nanos response element (NRE) in 3'-UTR of mRNA and repress translation of the target mRNA. Crystal structures of Pumilio and the complex with NRE were determined, previously. Although these structures reveal interaction between Pumilio and NRE, no structural insight of Nanos is known. In this work, we determined the crystal structure of Nanos. The structure of Nanos will provide a clue to reveal the mechanism of translational control by Nanos and Pumilio.

Crystals of Nanos were obtained by hanging drop vapor diffusion method using polyethylene glycol as a precipitant. Nanos is Zinc finger protein and contains two CCHC motifs. Thus, the crystal structure of Nanos was determined by single wavelength anomalous dispersion (SAD) technique using zinc atom. Initial phases were determined with the program SOLVE and were improved with the program RESOLVE. The initial model was build by the program O. The structure refinement is now in progress using the programs CNS and REFMAC.

**Structure of the oncoprotein gankyrin in complex with S6 ATPase of the 26S proteasome**

Yoshihiro Nakamura<sup>1</sup>, Kazumi Nakano<sup>1</sup>, Takashi Umehara<sup>1</sup>, Eru Adachi<sup>1</sup>, Yoshihide Hayashizaki<sup>1</sup>, Balasundaram Padmanabhan<sup>2</sup>, Shigeyuki Yokoyama<sup>1</sup>

<sup>1</sup>RIKEN Genomic Sciences Center, <sup>2</sup>RIKEN GSC, Riken Harima Inst., Grad. Sch. of Sci., Univ. of Tokyo

Tumorigenesis is mainly regulated by both oncoproteins and tumor-suppressors in G1-S transition during the cell cycle. In this regulatory pathway, one of the key factors is the retinoblastoma tumor-suppressor protein (pRb). pRb binds to the transcription factor E2F which is required for the expression of genes involved in G1-S transition and inhibits its transactivation function. The hyperphosphorylation of pRb by cyclin-dependent kinase 4 and 6 (CDK4/6) leads to the release of E2F from the Rb-E2F complex and degradation of Rb by the proteasome via a ubiquitin-dependent pathway. Rb phosphorylation by CDK4/6 is regulated mainly by proteins containing ankyrin repeats: gankyrin (Gann ankyrin: Gann means cancer in Japanese) for positive regulation and INK4 (CDK4/6 inhibitor) for negative regulation, in addition to cyclin for activating CDK4/6. Recent studies have proposed that gankyrin is also one of the subunit of 19S non-regulatory particle of the proteasome, and is likely to interact with the S6 ATPase subunit. To understand the functional role of gankyrin in the proteasome, we have initiated the project on structure and functional analysis of gankyrin complexed with S6 ATPase.

The protein complex, gankyrin- C-term domain of S6 ATPase, was co-expressed, purified to homogeneity, crystallized and determined its tertiary structure at 2.4 Å resolution. The gankyrin contains seven ankyrin repeats with crescent shape like structure. The C-terminal domain of S6 ATPase which possess mainly alpha-helices, binds to gankyrin at the region containing the ankyrin repeats 3, 4, 5 and 6. Biochemical studies based on the crystal structure revealed that gankyrin recognizes pRb both in the presence or absence of S6 ATPase.

**Crystallization and preliminary X-ray studies of a ferredoxin-NAD(P)+ reductase from the green sulfur bacterium *Chlorobium tepidum***Norifumi Muraki<sup>1</sup>, Daisuke Seo<sup>2</sup>, Tomoo Shiba<sup>1</sup>, Hidehiro Sakurai<sup>1</sup>, Genji Kurisu<sup>1</sup><sup>1</sup>Department of Life Sciences, University of Tokyo, Graduate School of Natural Science and Technology, Kanazawa University, Japan

Ferredoxin-NAD(P)+ reductase (FNR) from the green sulfur bacterium *Chlorobium tepidum* consists of 360 residues and a flavin adenine dinucleotide. The native enzyme is dimeric with the molecular mass of 90,000Da. *C. tepidum* FNR sequence identifies the thioredoxin reductase-like protein but differs from the FNRs from oxygen evolving photosynthetic organisms (Seo *et al.*, 2002). In order to determine the structure-function relationship of this interesting FNR, we have crystallized the *C. tepidum* FNR by hanging drop vapor diffusion method at 293 K (Figure) and crystallographically characterized the FNR crystals. Diffraction data to 2.4 Å resolution were collected using synchrotron radiation. The crystals belong to the space group of C222<sub>1</sub>. Assuming two molecules in the asymmetric unit, the Matthews coefficient ( $V_M$ ) was calculated to be 2.6 Å<sup>3</sup>/Da, corresponding to a solvent content of 53.2 %. Non-crystallographic symmetry (NCS) of crystals was explored with self-rotation functions using the program POLARFN in the CCP4 program suite, giving no significant peaks. The NCS peaks might overlap the peaks from crystallographic symmetry. The structure determination using heavy atom derivatives is now in progress.

**Figure** Crystal of *Chlorobium tepidum* FNR

## Effective Use of Gel-Tube Method

Hiroaki Tanaka<sup>1</sup> Mari Yamanaka<sup>2</sup> Koji Inaka<sup>3</sup> Masaru Sato<sup>4</sup> Sachiko Takahashi<sup>1</sup> Shigeru Sugiyama<sup>5</sup> Satoshi Sano<sup>6</sup> Moritoshi Motohara<sup>7</sup> Tomoyuki Kobahashi<sup>8</sup> Tetsuo Tanaka<sup>9</sup>

Confocal Science Inc.<sup>1</sup> MolLogics Inc.<sup>2</sup> Japan Aerospace Exploration Agency<sup>3</sup>

Gel-Tube [1] is a simplified method for a protein crystallization using counter-diffusion technique, based on gel-acupuncture method [2]. In the Gel-Tube method, a gel in a silicon tube, through which protein and precipitant solution diffuse each other from the opposite direction, is attached to the end of a capillary. The crystallization can be controlled not only by the concentrations of protein and crystallization solution but also the length and the diameter of the gel-tube. We have applied this method for microgravity experiment since 2004, yielding high quality crystals with high probability and high reproducibility.

If the vapor-diffusion method is preliminarily used, an optimized crystallization condition can be estimated. In some cases, crystals of higher quality grew in the Gel-Tube method not only in microgravity but also in ground-based experiment. Post-diffusion of ligand slowly to the crystal in the capillary makes this method suitable for making protein-ligand complex. Using 1-dimensional (1-D) simulation [1], the diffusion process inside the capillary can be estimated, so that the crystallization condition can be optimized in a short time and the Gel-Tube method can work more effectively. We will show the 1-D simulation of various kinds of precipitant and new method for controlling diffusion in a capillary.

[1] Tanaka, H. *et al.*, *J. Synchrotron Rad.*, **11**, 45-48, 2004

[2] Garcia-Ruiz, J.M. and Moreno, A., *Acta Cryst.*, **D50**, 484-490, 1994

## The crystal structure of the host-guest collagen model peptide (Pro-Pro-Gly)<sub>4</sub>-Hyp-Asp-Gly-(Pro-Pro-Gly)<sub>4</sub>

Tatsuya Kawaguchi<sup>1</sup> Masaki Shimura<sup>2</sup> Chizuru Hongo<sup>1</sup> Keiichi Noguchi<sup>3</sup> Kenji Okuyama<sup>1</sup> Kazunori Mizuno<sup>3</sup> Hans Peter Bachinger<sup>3</sup>

<sup>1</sup>Department of Macromolecular Science, Graduate School of Science, Osaka University  
<sup>2</sup>Department of Biotechnology and Life Science, Graduate School of Engineering, Tokyo University of Agriculture and Technology  
<sup>3</sup>Department of Biochemistry and Molecular Biology, Oregon Health & Science University

The crystal structure of the host-guest collagen model peptide, (Pro-Pro-Gly)<sub>4</sub>-Hyp-Asp-Gly-(Pro-Pro-Gly)<sub>4</sub>, was determined at 1.02Å resolution ( $R = 0.128$ ,  $R_{free} = 0.159$ ) by using synchrotron radiation (PF BL6A). The crystal belongs to  $P2_1$  space group with cell parameters of  $a = 31.59$ ,  $b = 21.71$ ,  $c = 39.15$  Å, and  $\beta = 100.17^\circ$ . The asymmetric unit contains one molecule which consists of three peptide strands and forms a collagen-like triple-helical structure. Although the helical twist of each residue ranges from  $36^\circ$  to  $66^\circ$ , the average values in the host ( $49.0^\circ$ ) and the guest ( $52.6^\circ$ ) parts agree very well with that for the ideal 7/2-helical model. Although Hyp residues in the X position of the (Hyp-Hyp-Gly)<sub>n</sub> ( $n=9, 10$ ) were reported to adopt up-puckering, Hyp in the guest triplet of the present peptide adopts a down-puckering. The lateral packing structure of this peptide showed the quasi-hexagonal packing, which was usually observed for the Pro-Hyp-Gly sequence-rich peptides.

Two Asp residues in a triple helix were found to form hydrogen-bondings with Asp residues in the adjacent helices and the third Asp was found to interact electrostatically with N-terminal of the adjacent staggered molecule.

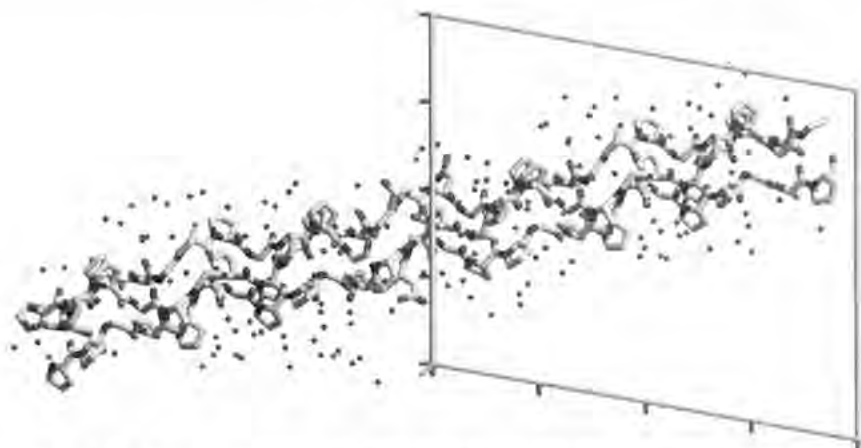


Figure 1. Final structure of (Pro-Pro-Gly)<sub>4</sub>-Hyp-Asp-Gly-(Pro-Pro-Gly)<sub>4</sub>

**Crystal structure of Formin Homology 2 domain of human DAAM1**

Shuya Fukai<sup>1</sup> Masami Yamashita<sup>2</sup> Tomohito Higashi<sup>3</sup> Yusuke Sato<sup>2</sup> Ryutarō Shirakawa<sup>3</sup> Toru Kita<sup>3</sup> Hisanori Horiuchi<sup>3</sup> Osamu Nureki<sup>1</sup>

Center for Biological Resources and Informatics, Tokyo Institute of Technology<sup>1</sup> Department of Biological Information, Tokyo Institute of Technology, Japan<sup>2</sup> Department of Cardiovascular Medicine, Kyoto University, Japan<sup>3</sup>

Formin proteins nucleate and elongate the unbranched actin filament under the regulation by the GTP-dependent interaction with the Rho/Rac GTPases. They are conserved beyond species and characterized by the formin homology domains, FH1 and FH2. FH1 binds with profilin, and enhances the elongation rate. FH2 forms a ring-shaped dimer in a head-to-tail manner, and processively moves towards the barbed end of the actin filament to catalyze the actin polymerization. Dishevelled-associated activator of morphogenesis (DAAM) is a Rho-regulated formin implicated in the actin organization during neuronal development. In this study, we determined the crystal structure of the human DAAM1 FH2 dimer at 2.8 Å resolution, and performed a structure-based mutagenic analysis. This is the first FH2 dimer structure that is represented without an aid of the crystallographic symmetry. Two DAAM1 FH2 molecules were associated in a head-to-tail manner, and formed a rectangular ring in contrast to the parallelogram-shaped ring of yeast Bni1p FH2. Furthermore, the orientation of the DAAM1 FH2 ring was basically different from that of the Bni1p FH2 ring. Docking analysis using the structure of the yeast Bni1p FH2 in the complex with the filament-like actin showed that the present DAAM1 FH2 dimeric ring adopts a contracted conformation, which could cap the barbed end of the actin filament. These structural analyses suggested the functional importance of the length of the linker region, which connects the N-terminal "lasso" region and the C-terminal "core" region. This was shown by the polymerization assays using a series of FH2 mutants with various linker lengths. We propose the "expanded and contracted" stair-stepping model for the actin polymerization by FH2.

## Chemistry of New Steroidal Antiandrogens and 5 $\alpha$ -Reductase: 16 $\beta$ -methyl-17 $\alpha$ -propionyloxypregna-4,6-diene-3,20-dione

MANUEL SORIANO Eugene Bratoeff

Departamento de Bioquímica, Instituto de Química, Universidad Nacional Autónoma de México

Benign prostatic hyperplasia and prostate cancer are androgen-dependent diseases which afflict a large percentage of males over the age of fifty and are usually treated by surgery. Dihydrotestosterone, a 5 $\alpha$ -reductase metabolite of testosterone, has been implicated as a causative factor in the progression of these diseases. It has also been determined that dihydrotestosterone interacts more efficiently with the androgen receptors than testosterone. This fact indicates that the logical step in the treatment of these diseases should be the inhibition of the 5 $\alpha$ -reductase enzyme or the blockage of the dihydrotestosterone-receptor formation. Crystals of 16 $\beta$ -methyl-17 $\alpha$ -propionyloxypregna-4,6-diene-3,20-dione are orthorhombic and space group  $P2_12_12_1$ . The unit-cell dimensions are  $a = 7.397(1)$ ,  $b = 11.061(1)$ ,  $c = 27.266(3)$ ,  $V = 2230.7(5)\text{\AA}^3$ ,  $D_x = 1.187\text{ g/cm}^3$ , and  $Z = 4$ . The molecule consists of three six-membered rings and one five-membered ring, all *trans* fused. The six-membered rings A, B and C occur in a distorted envelope, a distorted half chair and a chair conformations, respectively. Ring D occurs in a conformation between an envelope and a half chair. The bond lengths and angles are normal. The stereochemistry of the title compound is as follows: C8- $\beta$ H is *trans* to C9- $\alpha$ H; C9- $\alpha$ H is *trans* to C10- $\beta$ CH<sub>3</sub>; C13- $\beta$ CH<sub>3</sub> is *trans* to C14- $\alpha$ H; C13- $\beta$ CH<sub>3</sub> is *cis* to C17- $\alpha$ (COCH<sub>3</sub>); and C16- $\beta$ CH<sub>3</sub> is *trans* to C17- $\alpha$ [OCO(CH<sub>2</sub>)<sub>3</sub>CH<sub>2</sub>Br]. The molecules in the crystal are packed at normal van der Waals distances.

1. E. Bratoeff, M. Cabeza, E. Ramirez, Y Heuse and E. Flores, *Curr. Med. Chem.*, **2005**, 12, 927.

## Crystal structures of nucleosidediphosphate kinase from *Pyrococcus horikoshii*

Kazutaka Murayama<sup>1</sup>, Miyuki Murayama-Kato<sup>2</sup>, Takaho Terada<sup>2</sup>, Mikako Shirouzu<sup>2</sup>, Shigeyuki Yokoyama<sup>3</sup>

<sup>1</sup>Biomedical Engineering Research Organization, Tohoku University, <sup>2</sup>RIKEN, Genomic Sciences Center, Japan, <sup>3</sup>Department of Chemistry, University of Tokyo, Japan

Nucleosidediphosphate kinase (NDPK) transfers the  $\gamma$ -phosphate of nucleosidetriphosphate to nucleosidediphosphate.



NDPK shows low selectivity for nucleotide bases. The enzyme catalyzes this reaction among variety of nucleosides as the phosphate donor and acceptor. We determined high-resolution structures of NDPK from *Pyrococcus horikoshii* to reveal the mechanism of the catalysis reaction.

The protein was synthesized by the cell-free system and co-crystallized with purin nucleotides (ADP, ATP, ATP analog, GDP, and GTP analog). Crystals were obtained from the same condition of the native crystal (unliganded form), although two space groups appeared, depending on the co-crystallized substrates. The reflection data were measured at 2.0-1.7Å resolution using in-house diffractometer with CuK $\alpha$  radiation. Structure determinations were conducted by molecular replacement method using the unliganded form of the enzyme (PDB code: 2CWK).

All crystal forms include two molecules in an asymmetric unit, forming a homodimer. Furthermore, the dimers are arranged by three-fold axis to form a hexamer. Analytical ultracentrifuge measurement also showed that the molecular weight of this protein is around 105kDa, which supports hexamer formation. In the complex structures, bases (guanine/adenine) were stabilized by stacking interaction with Phe63. The electron densities of diphosphate groups in ADP or GDP were clear. However,  $\beta$ - and  $\gamma$ -phosphate of NTP analogs could not identified from electron density. This result suggest that binding affinity for NTP and NDP are different, and the different affinity may play an important role for binding and release during catalytic reaction.

## The oligomerization state of SKD1 is regulated by ATP

Michio Inoue<sup>1</sup>, Masato Kawasaki<sup>1</sup>, Hironari Kamikubo<sup>2</sup>, Mikio Kataoka<sup>2</sup>, Ryuichi Kato<sup>1</sup>, Tamotsu Yoshimori<sup>1</sup>, Soichi Wakatsuki<sup>1</sup>

<sup>1</sup>PF, IMSS, KEK<sup>1</sup>, Grad. School of Materials Sci., NAIST, Japan<sup>2</sup>, Res. Inst. for Microbial Dis., Osaka Univ., Japan<sup>3</sup>

Yeast *vps* mutants have been isolated by their vacuolar morphologies which differ significantly from that of the wild-type. Among them, class E *vps* mutants possess an exaggerated form of a pre-vacuolar endosome-like compartment. Recently, an ESCRT (endosomal sorting complex required for transport) model is proposed for MVB (multivesicular body) sorting by the class E Vps proteins in yeast. SKD1 (suppressor of K<sup>+</sup> transport growth defect 1), which belongs to the AAA (ATPases associated with diverse cellular activities) type ATPase family, is identified as a mouse homologue of class E Vps protein, Vps4. SKD1 interacts with several ESCRT proteins and plays an important role in the MVB vesicle formation.

It has been reported that AAA family proteins alter their oligomerization states between monomer and hexamer depending on ATP hydrolysis. We overproduced and purified recombinant mouse SKD1 protein and found that SKD1 shows two different oligomerization states in solution by size exclusion chromatography and small angle X-ray scattering. To elucidate the molecular mechanism of SKD1 in detail, X-ray crystallographic study of SKD1 has been performed. At present, the resolution is up to 3.5 Å and an AAA motif ( $\alpha$ / $\beta$  and  $\alpha$  subdomains), a  $\beta$ -domain and a C-terminal  $\alpha$ -helical region could be identified. (N-terminal region is disordered and not defined). Based on the current structure and the solution experiments, we will discuss the relationship between the crystal structure and the oligomerization state regulated by ATP.

## Introduction of the Protein Data Bank Japan (PDBj)

Takashi Kosada<sup>1</sup> Reiko Igarashi<sup>2</sup> Yumiko Kengaku<sup>2</sup> Yasuyo Morita<sup>2</sup> Kanna Matsuura<sup>2</sup> Masami Kusunoki<sup>2</sup> Yukiko Shimizu<sup>2</sup> Reiko Yamashita<sup>2</sup> Haruki Nakamura<sup>2</sup>

Institute for Protein Research, Osaka University<sup>1</sup> Institute for Protein Research, Osaka University, Japan, Japan Science and Technology Agency.<sup>2</sup>

The Protein Data Bank (PDB) is the sole international public repository for three dimensional structure data of biological macromolecules and serves for supporting essential biological sciences. Macromolecular structures in the PDB help to solve crystallographic structure determination. In 1999, the Protein Data Bank Japan (PDBj) was founded at the Institute for Protein Research, Osaka University, to accept and process PDB entries in Asia and Oceania with collaboration of RCSB. The PDBj enhances the PDB capabilities and has performed the following activities:

1. PDB search web site [1].
2. PDB deposition site [1].
3. FTP download site [1].
4. Process and Release of Deposited entries.
5. Exploiting an XML format database[2], a 3D viewer, and secondary databases[3].

The PDBj, RCSB and MSD-EBI have formed the world wide Protein Data Bank (wwPDB) on 2003[4]. The mission of the wwPDB is to maintain a single archive of macromolecular structural data that is freely and publicly available to the global community.

Convenient methods of finding particular entries from such many entries and the deposition method including the above list 1. to 5. will be presented here. Also the statistics of recent refinement information and expression system will be shown.

The PDBj processed 1586 entries for 2006 in a year. The PDBj would like to solicit you to deposit your entries through the PDBj deposition site.

## References

1. All PDBj sites can access through <http://www.pdbj.org/>
2. XML-based Protein Structure Search Service (xpss:<http://www.pdbj.org/xpss/>).
3. Kinoshita, K., Nakamura, H. (2004) *Bioinformatics* 20, 1329-1330.
4. Berman, H., Henrick, Kim., and Nakamura, H. (2002) *Nat. struct. biol.* 12, 979-1024.

## Structural and Functional Studies on Pin1 Mutants

Pei Chee Song<sup>1,2</sup>, Xueji Wu<sup>3</sup>, Jobichen Chacko<sup>1</sup>, J. Sivaraman<sup>1</sup>, Yih-Cherng Liou<sup>1\*</sup>

<sup>1</sup>Department of Biological Sciences, <sup>2</sup>Department of Biochemistry National University of Singapore, 117543, Singapore<sup>3</sup>Xiamen University, China \*Corresponding author; email: dbslyc@nus.edu.sg

Peptidyl-prolyl isomerase Pin1 is an essential protein in regulating entry into mitosis by catalyzing the conformational change of a number of critical proteins. So far, more than 50 Pin1 targets have been identified, suggesting that Pin1 may play an important role in a diverse array of cellular processes including cell cycle control, transcription and splicing regulation, DNA replication checkpoint control, DNA damage response, neuronal survival, and germ cell development. Moreover, Pin1 function has been implicated in several human diseases. Notably, overexpression of Pin1 is prevalently found in many human cancers; whereas its inhibition induces apoptosis and contributes to neuronal death in Alzheimer's disease. Structurally and functionally, Pin1 is a novel prolyl isomerase and specifically catalyzes *cis/trans*-isomerization of proline in the sequence of phosphorylated Ser/Thr-Pro. Although the first structure of Pin1 has been reported in 1997 along with the short peptide substrate complex (4 to 7 residues), very little are known about its catalytic mechanism and its interaction with the biological substrates. Therefore, in our current studies, we have focused on the structural and functional studies on Pin1 mutants. Several mutants' crystal structures and *in vitro* peptide binding assay combined with functional studies in mammalian cells have been carried out. Together, these studies provide a deeper understanding of how Pin1 interacts with its biological target proteins and perhaps is eventually leading to effective drug design.

## The crystal structure of cellulase module Cel44A from *Clostridium thermocellum*

Yu Kitago<sup>1</sup> Shuichi Karita<sup>2</sup> Nobuhisa Watanabe<sup>1</sup> Kazuo Sakka<sup>3</sup> Isao Tanaka<sup>1</sup>

Division of Biological sciences, Graduate School of Science, Hokkaido University<sup>1</sup> Major of Sustainable Resource Science, Graduate School of Bioresources, Mie University, Japan<sup>2</sup> Major of Sustainable Resource Science, Graduate School of Bioresources, Mie University, Japan<sup>3</sup>

Cellulosome is the huge multiprotein complex that consists of the noncatalytic scaffolding protein and the various enzymatic proteins. The cellulosomal enzymatic proteins contain many kinds of cellulases such as endoglucanases, xylanases, mannanases, cellobiohydrolases, glucosidases, etc. This variety of enzymatic proteins makes it possible to degrade crystalline cellulose quite efficiently. In these enzymatic proteins, enzymes that belong to glycoside hydrolase family (GH family) 44 appear in some celulytic bacteria's cellulosome, and those had been only known as its endoglucanase, lichenase, xylanase and xyloglucanase activity.

This study aims to reveal the detailed structure and mechanisms of the GH family 44 enzymes by X-ray crystallographic study of Cel44A from *Clostridium thermocellum*. Cel44A was overexpressed, purified and crystallized. The X-ray diffraction datasets of the wild type and the E186Q mutant complexed with various substrates were collected at SPring-8 and Photon Factory. The primary phases were solved by the MAD method using zinc ion, and the refinement procedure is performed at 0.96 Å resolution. The revealed structure shows that Cel44A consists of TIM-like barrel domain and b-sandwich domain, and suggests that two glutamic acid residues, Glu186 and Glu359, work as catalytic residues. The catalytic ability of these two residues is confirmed by biological assay of each mutant, E186Q and E359Q. The wild type and E186Q mutant structures complexed with various substrates show the substrate recognition mechanisms and the pyranose ring distortion at the subsite -1. These structural characters of Cel44A indicate that GH44 belongs to the clan GH-A, and that Cel44A's reaction is classified in retaining type hydrolysis.

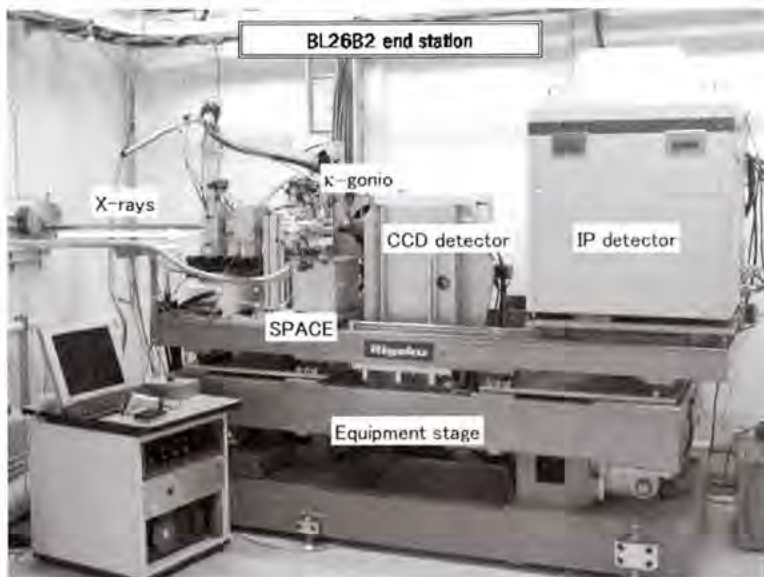
## SPring-8 Structural Biology Beamlines / Current Status of Automatic Beamline Operation

Go Ueno<sup>\*</sup> Kazuya Hasegawa<sup>\*\*</sup> Nobuo Okazaki<sup>\*\*\*</sup> Hironori Murakami<sup>\*\*\*\*</sup> Raita Hirose<sup>\*\*\*\*\*</sup> Atsushi Nisawa<sup>\*</sup> Takashi Kumasaka<sup>\*\*\*\*\*</sup> Masaki Yamamoto<sup>\*</sup>

RIKEN SPring-8 Center, RIKEN<sup>\*</sup> SPring-8/JASRI<sup>\*\*</sup> SPring-8 Service Co.<sup>\*\*\*</sup> PharmAcess Inc.<sup>\*\*\*\*</sup> Tokyo Institute of Technology<sup>\*\*\*\*\*</sup>

Structural genomics research projects progressing worldwide have been accelerated by high throughput protein crystallography with the automation of beamlines at synchrotron radiation facilities. Here in SPring-8, the automatic system to execute successive diffraction experiments with sample auto-changer SPACE [1] was developed at RIKEN Structural Genomics Beamlines (BL26B1 & BL26B2). The operation software BSS [2] provides the intuitive GUI and centralized control of beamline instruments with the networked client-server architecture. In 2005, more than twenty crystals a day have been constantly delivered and screened at BL26B2, at rates of 5 min/sample, and seven data sets in daily average have been constantly collected. Up to now, a public beamline BL38B1 (Structural Biology Beamline III) and another beamline in SPring-8, other than BL26s, and also five laboratories inside and outside SPring-8 have implemented SPACE robotic system to carry out the automated data collection.

- [1] Ueno, G., Hirose, R., Ida, K., Kumasaka, T. and Yamamoto, M. (2004). J. Appl. Cryst. 37, 867-873.  
 [2] Ueno, G., Kanda, H., Kumasaka, T., and Yamamoto, M. (2005). J. Synchrotron Rad. 12, 380-384.



## **Design of some Non-Steroidal Anti-inflammatory inhibitors to Phospholipase A<sub>2</sub> using docking studies**

Vaijayanthimala Suryanarayana Rao Velmurugan Devadasan

Crystallography and Biophysics, University of Madras

Understanding the protein-ligand interactions is a crucial step in structure-based drug design. Starting with the three-dimensional structure, docking and virtual screening are often carried out to evaluate the enzyme-ligand complexes. Phospholipase A<sub>2</sub> (PLA<sub>2</sub>) is a well-known target for anti-inflammatory therapy. An automated molecular docking (AutoDock 3.0) was applied to a series of Non-steroidal Anti-inflammatory inhibitors with PLA<sub>2</sub> enzyme. In the present study the target protein chosen is PLA<sub>2</sub> from snake venom. We aim to develop new inhibitors that fit specifically into PLA<sub>2</sub> with specific chemical groups, using docking algorithms/softwares. Moreover, the stability of the resulting complexes has been assessed by the bound conformation and the estimated binding energies of these compounds. The current results provide the model for the binding of Non-steroidal Anti-inflammatory inhibitors to PLA<sub>2</sub> and assist the design of more potent or selective analogs since the binding energies between PLA<sub>2</sub> and some of these compounds are comparable to those complexes for which X-ray crystal structures are reported.

## Crystal structures of the CERT START domain in complex with ceramides and specific inhibitors reveal recognition and transport mechanisms of ceramides.

Norio Kudo<sup>\*</sup> Keigo Kumagai<sup>\*\*\*</sup> Soichi Wakatsuki<sup>\*\*</sup> Masahiro Nishijima<sup>\*\*</sup> Kentaro Hanada<sup>\*\*</sup> Ryuichi Kato<sup>\*</sup>

Structural Biology Research Center, Photon Factory, Institute of Materials Structure Science, High Energy Accelerator Research Organization (KEK)<sup>\*</sup> Department of Biochemistry and Cell Biology, National Institute of Infectious Diseases, Japan<sup>\*\*</sup>

Ceramide is synthesized at the endoplasmic reticulum (ER), and transferred to the Golgi apparatus where ceramide is converted to sphingomyelin. The major pathway of this transport is mediated by CERT, a cytosolic 68-kDa protein, in a nonvesicular manner. The C-terminal ~250 amino acid residues of CERT form a START domain catalyzing intermembrane transfer of ceramide (1).

Here we present crystal structures of the CERT START domain in the apo-, C<sub>6</sub>-, C<sub>16</sub>-, and C<sub>18</sub>-ceramides bound forms at 1.4-2.2 Å resolution. The overall structure is a compact  $\alpha/\beta$  structure with a long tunnel, where one ceramide molecule is buried in the complex structures. Two long hydrophobic chains of ceramide are arranged along the tunnel lined with hydrophobic amino acids, while the amide and hydroxyl groups of ceramide interact with specific amino acid residues via a hydrogen bond network. Mutations of these residues impaired the ceramide transfer activity of the CERT START domain.

We also determined the crystal structures of CERT START domain in complex with antagonists of CERT, HPA-12, 13, 14, 15 and 16, at 1.7 - 2.3 Å resolution (2). Interestingly, the hydrogen bond network between HPA and the protein is slightly different from that between ceramide and the protein. There are no drastic conformational changes between the apo and the ceramide or antagonists bound structures. We will discuss how the CERT START domain can specifically recognize ceramide and its antagonists.

(1) Hanada. *et al.*, (2003) *Nature* **426**, 803-

(2) Kumagai *et al.*, (2004) *J. B. C.* **280**, 6488-

HPA-12: (1*R*,3*R*)-*N*-(3-hydroxy-1-hydroxymethyl-3-phenylpropyl)dodecamide

## **Zeta potential measurements for evaluation the quality of protein samples for crystallization.**

Kohei Shiba<sup>1</sup>, Koji Inaka<sup>2</sup>, Shigeru Sugiyama<sup>2</sup>, Kyoko Ogasahara<sup>1</sup>, Atsushi Nakagawa<sup>1</sup>

<sup>1</sup>Scientific Instrumentation Business Div., Sysmex Corporation, Mol Logics, Japan, <sup>2</sup>Institute for Protein Research, Osaka University, Japan

Recent progress in structure determination of proteins allows us to reveal the interactions of protein molecules at atomic level. NMR and X-ray crystallography are widely used for determination of the three-dimensional structure of the proteins in detail. In both techniques, preparation of good samples is now the most difficult and important step. In addition, crystallization of the sample is required for X-ray crystallography. However, it is often met the serious problem that the crystals cannot easily be obtained, after enormous number of trials of crystallization has been attempted. Gel-electrophoresis, such as SDS-PAGE and Native-Page, gel-filtration and dynamic light scattering measurement are often used for evaluation of quality of samples and these measurements sometimes used for evaluation of possibility of crystallization. However, these measurements are not the magic bullet for evaluation of possibilities of crystallization.

Zeta potential is often used for judging the dispersion stability of colloidal or some other nano-particles. Roughly speaking, the zeta potential shows surface potential effecting around the particles. Zeta potentials at stable dispersion condition of the particles often show the values higher than  $+25\text{mV}$ .

We will report here the results of Zeta potential measurement of proteins for estimation of the quality of the samples and relationship between Zeta potential and quality of crystals.

**Crystal structures of *Halothermothrix orenii*  $\alpha$ -amylase at saturated salt concentration provide insights into protein stability at very high salt**

Sivakumar Neelamegam<sup>1</sup> Nan Li<sup>2</sup> Patel KC Bharat<sup>3</sup> Swaminathan Kunchithapadam<sup>4</sup>

PROTEOMICS, Invitrogen Bioservices India Pvt Ltd<sup>1</sup> Institute of Molecular and Cell Biology, Singapore<sup>2</sup> Griffith University, Brisbane<sup>3</sup>

Adaptations of proteins to extreme conditions are very important for the survival of extremophiles and have been the subject of study at the atomic level for many years. However, the adaptations of proteins to poly-extreme condition have not been studied in detail so far. Here we report the crystal structure of a protein, AmyA, a secretory  $\alpha$ -amylase isolated from *Halothermothrix orenii*, which is both halophilic and thermophilic. The crystal structure was determined at 4.7 M NaCl salt concentration at 1.83 Å resolution. To our knowledge this is the most concentrated salt solution from which a protein has been crystallized. We observe surprising structural features, which are likely to be the molecular determinants responsible for the extreme stability of AmyA. AmyA lacks the conserved acidic surface, which is considered essential for protein stability at high salinity. When compared to the AmyA structure at low salt, changes in side chain conformations were observed that impart stability to the protein over a wide range of salt concentrations. AmyA binds to more calcium ions and chloride ion when compared to its low salt structure. The structure at high salt reveals novel calcium and chloride binding sites. These studies provide valuable insight into the structural elements that contribute to the stability of AmyA at both physical and chemical extremes and their functional implications.

## Rational Design of a Novel Molecular Switch for Nano-Biotechnology

Mohammad S Yousef<sup>1,2,3,4</sup> Nicole Bischoff<sup>1</sup> Collin Dyer<sup>1</sup> Walt Baase<sup>1</sup> Brian Matthews<sup>1</sup>

Structural Biology Group, KEK, PF<sup>1</sup> University of Zurich<sup>1</sup> University of California Santa Barbra<sup>2</sup>  
HHMI, University of Oregon<sup>3,4</sup>

We have designed a molecular switch in a T4 lysozyme construct that controls a large-scale translation of a duplicated helix. As shown by crystal structures of the construct with the switch on and off, the conformational change is triggered by the binding of a ligand (guanidinium ion) to a site that in the wild-type protein was occupied by the guanidino head group of an Arg. In the design template, a duplicated helix is flanked by two loop regions of different stabilities. In the "on" state, the N-terminal loop is weakly structured, whereas the C-terminal loop has a well defined conformation that is stabilized by means of non-covalent interactions with the Arg head group. The truncation of the Arg to Ala destabilizes this loop and switches the protein to the "off" state, in which the duplicated helix is translocated approximately 20 Angstrom. Guanidinium binding restores the key interactions, restabilizes the C-terminal loop, and restores the "on" state. Thus, the presence of an external ligand, which is unrelated to the catalytic activity of the enzyme, triggers the inserted helix to translate 20 Angstrom away from the binding site. The results illustrate a mechanism for protein evolution in which a sequence duplication followed by a point mutation can lead to the establishment of new functions. Moreover, a fluorescence-based optical method was developed to detect the ligand-triggered helix translation in solution.

### References,

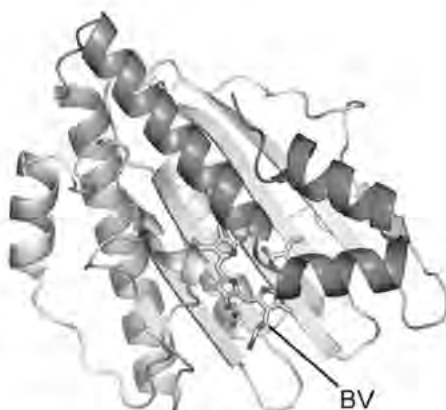
(Yousef *et. al*, 2004,2006)

## Structural analyses of substrate-free and substrate-bound forms of phycocyanobilin:ferredoxin oxidoreductase

Masakazu Sugishima<sup>\*</sup> Yoshinori Hagiwara<sup>\*\*</sup> Yasuhiro Takahashi<sup>\*\*</sup> Keiichi Fukuyama<sup>\*\*</sup>

Department of Medical Biochemistry, Kurume University School of Medicine<sup>\*</sup> Department of Biology, Graduate School of Science, Osaka University, Japan<sup>\*\*</sup>

Phytobilins are linear tetrapyrrole compounds used as pigments for light-harvesting (phycobiliproteins) and photoreceptor (phytochromes) proteins in O<sub>2</sub> producing photosynthetic organisms, such as cyanobacteria and plants. Phytobilins are biosynthesized from biliverdin (BV), a catabolite of heme, by ferredoxin-dependent bilin reductases (FDBRs). Phycocyanobilin:ferredoxin oxidoreductase (PcyA) one such FDBR, is a new class of radical enzymes that require neither cofactors nor metals, and serially reduces the vinyl group of the D-ring and A-ring of BV using four-electrons from ferredoxin to produce phycocyanobilin. We have determined the crystal structure of substrate-bound and substrate-free forms of cyanobacterial PcyA, the first tertiary structure in FDBRs. PcyA folds into three-layer alpha/beta/alpha sandwich and BV is located between the beta-sheet and C-terminal alpha-helices. The structure of substrate-free form of PcyA is similar to that of substrate-bound form, but the charge distribution and the active site structure slightly differ. Recognition of substrate and ferredoxin and reaction mechanism to control the serial reductions of the D- and A-rings of BV will be presented.



Ribbon drawing of substrate-bound form of PcyA

**Crystal structure of pre-ribosomal RNA processing factor Dim2p from *Pyrococcus horikoshii* OT3 and its interaction with ribosomal RNA**

Min Ze Jia Jun Otsuka Woo Cheol Lee Koji Nagata Masaru Tanokura

Department of Applied Biological Chemistry, University of Tokyo

The eukaryotic rRNA processing factor Dim2p is required for the cleavage of rRNA precursors at processing sites  $A_2$  to generate the pre-20S rRNA. Its homologs are distributed from archaea to metazoa. In this study, we have solved the crystal structure of PH-Dim2p (Dim2p from *Pyrococcus horikoshii* OT3) at 2.0-Å resolution. The PH-Dim2p molecule contains two KH domains, KH-1 and KH-2, which have dissimilar molecular surfaces in terms of electrostatic potentials. Binding assays have shown that PH-Dim2p shows no sequence preference in target rRNA molecules and that only KH-1 binds 16S rRNA while KH-2 does not. Based on the crystal structure of PH-Dim2p and the binding assay data, we have constructed a putative model of the PH-Dim2p and ribosomal RNA complex.

## **The Development of Nervous System in Drosophila; a Structural Approach.**

Mohammad S Yousef, Brian Matthews

Structural Biology Group, KEK, PF HHMI, University of Oregon

We used X-ray crystallography to study the interaction between the *Drosophila* transcription factor "Prospero" and its non-canonical DNA target. Prospero is a cell fate determinant that is essential in directing the neuron stem cells toward differentiation.

Knowledge of the crystal structure of the complex (protein homeodomain/DNA) identifies key residues on the protein that are responsible for making specific contacts with the DNA. The structure also reconciles the two reportedly distinct DNA sequences that have been proposed as transcriptional target for Prospero. We proposed a mechanism by which Prospero controls the fate of developing neural cells in *Drosophila*. To confirm the proposed mechanism, we are working on the structural determination of longer segments of Prospero with and without the target DNA.

### **Reference:**

(Yousef et al, 2005)

**Structure Determination of a novel Phycoerythrin C from a hemihedral twinned crystal**

Punit Kaur<sup>1</sup>, Badrish R. Soni<sup>2</sup>, A. S. Ethayathulla<sup>1</sup>, Imtaiyaz Hassan<sup>1</sup>, Savita Yadav<sup>1</sup>, Datta Madamwar<sup>2</sup>, Tej P. Singh<sup>1</sup>

Department of Biophysics, All India Institute of Medical Sciences, New Delhi<sup>1</sup>; PG Department of Biosciences, Sardar Patel University, Vallabh Vidyanagar -388 120, Gujarat, INDIA<sup>2</sup>

Phycobiliproteins belong to a fluorescent family of light harvesting proteins which are components of the photosynthetic mechanism in Cyanobacterium. Phycoerythrin C, a phycobiliprotein, isolated from the blue green algae absorbs light and is the first protein involved in the transfer of energy to the photoactive reactions localized in the thylakoid membrane. They are composed of two structural subunits, alpha and beta which aggregate to form trimers, tetramers or hexamers with an additional gamma-subunit. All the subunits have different numbers of chromophores which are classified according to their spectral differences as phycocyanobilin (PCB), phycoerythrin (PEB) and phycourobilin (PUB). Phycobiliproteins have earlier been reported as dimers, tetramers or hexamers. This is the first crystal structure where the phycoerythrin C has crystallized as a single alpha-subunit. The crystal diffracted to 2.5Å resolution and could unambiguously be indexed in both orthorhombic and monoclinic space groups. The diffraction data indicated the presence of twinning in monoclinic space group  $P2_1$  with unit cell dimensions  $a = 57.3\text{Å}$ ,  $b = 83.7\text{Å}$ ,  $c = 62.5\text{Å}$  and  $\beta = 90.2^\circ$ . The structure was solved by molecular replacement with two molecules of the alpha-subunit in the asymmetric unit. The twinning fraction was estimated to be 0.49. The structure refined to  $R_{\text{cryst}} = 23.0$  and  $R_{\text{free}} = 28.1$ . The alpha-subunits in the present phycoerythrin are shorter at the N-terminus by 31 residues and have 132 amino acid residues unlike other phycoerythrins which have 164 residues. The structure predominantly comprises of alpha-helices with the chromophore (phycourobilin) units.

## **Suggestions for improving diffraction data qualities at the undulator beamlines**

Kunio Hirata<sup>1</sup>, Nobutaka Shimizu<sup>2</sup>, Kazuya Hasegawa<sup>3</sup>, Masaki Yamamoto<sup>4</sup>

<sup>1</sup>Division of Synchrotron Radiation Instrumentation, RIKEN/SPring-8, <sup>2</sup>JASRI/SPring-8, <sup>3</sup>RIKEN/SPring-8, <sup>4</sup>JASRI/SPring-8

Precisions of diffraction data crucially govern qualities of entire structural analyses of target protein molecules in protein crystallography. This is especially true for data collection at undulator beamlines, where we often face up to difficulties in collecting good data because of 'source-specific' problems.

Generally, high flux and highly collimated X-rays available at undulator beamlines are believed to provide us 'the best quality datasets' from a view point of the fundamental crystallographic statistics compared with other radiation sources. It is true in most cases, but sometimes the source badly affects data qualities because of radiation damages and narrow rocking profiles of diffracted spots, and so on.

We conducted more than 100 diffraction data collections using several species of cryo-cooled protein crystals at the undulator beamline BL41XU at SPring-8 under various experimental conditions in order to demonstrate dominant parameters for the best data acquisition. Experimental conditions were modified by choosing several beam sizes, exposure times, oscillation widths, oscillation repetition times and pixel resolution of the CCD detector. All of the datasets were processed with several data reduction suites, such as HKL2000, MOSFLM/SCALA, XDS and DENZO/SCALA. Comparing statistical and crystallographic parameters among these datasets, key conditions governing precisions of diffraction data will be discussed.

## New mechanism for broad substrate-specificity of enzymes

Teruya Nakamura<sup>1</sup> Hiroyuki Kamiya<sup>2</sup> Masaki Mishima<sup>3\*</sup> Sachiko Toma<sup>4</sup> Shinji Ikemizu<sup>5</sup> Masahiro Shirakawa<sup>6</sup> Yusaku Nakabeppu<sup>7</sup> Yuriko Yamagata<sup>8</sup>

Graduate School of Pharmaceutical Sciences, Kumamoto University<sup>1</sup> Graduate School of Pharmaceutical Sciences, Hokkaido University<sup>2</sup> Department of Chemistry, Tokyo Metropolitan University<sup>3</sup> Graduate School of Engineering, Kyoto University<sup>4</sup> Medical Institute of Bioregulation, Kyushu University<sup>5</sup>

Oxidized nucleotides cause replicational and transcriptional errors because of their misincorporations into DNA and RNA. In oxidized nucleotides, 8-oxo-dGTP and 2-oxo-dATP are known to induce frequent transversion mutations. *E. coli* MutT specifically hydrolyzes 8-oxo-dGTP to 8-oxo-dGMP and prevents the A:T to C:G transversion caused by 8-oxoguanine. On the other hand, human MutT homolog-1 (hMTH1) protein has broad substrate-specificity for several oxidized purine nucleotides such as 8-oxo-dGTP, 2-oxo-dATP and 8-oxo-dATP. Mice lacking the *mth1* gene exhibit an increased occurrence of spontaneous carcinogenesis especially in the liver, and to a lesser extent, in the lung and stomach, thus suggesting that the accumulation of oxidized purine nucleotides triggers such malignant transformation *in vivo*.

In addition to the determination of the solution structure of hMTH1 (apo form)<sup>\*</sup>, we have solved the crystal structures of hMTH1 in complexes with 8-oxo-dGMP, 8-oxo-dGTP and 2-oxo-dATP. The hMTH1-8-oxo-dGMP and hMTH1-8-oxo-dGTP structures compared with the previously determined MutT-8-oxo-dGMP structure reveal the structural basis of the difference in substrate-specificity for 8-oxo-dGTP between hMTH1 and MutT. The hMTH1-2-oxo-dATP and hMTH1-8-oxo-dGTP structures suggest that hMTH1 recognizes the different oxidized purine nucleotides by the exchange of the protonation site in the neighboring aspartate residues. This is the first mechanism found for broad substrate-recognition of enzymes. This mechanism is supported by our mutational studies.

<sup>\*</sup> Mishima *et al.*, *J. Biol. Chem.* 279, 33806-33815 (2004)

## **Control system for high-throughput protein crystallography experiments**

Yury Alexandrovich Gaponov Naohiro Matsugaki Nobuo Honda Kumiko Sasajima Noriyuki Igarashi Masahiko Hiraki Yusuke Yamada Soichi Wakatsuki

Structural Biology Research Center, Photon Factory, KEK, Japan

An integrated client-server control system (PCCS) with a unified relational database (PCDB) has been developed for high-throughput protein crystallography experiments on synchrotron beamlines. The major steps in protein crystallographic experiments (purification, crystallization, crystal harvesting, data collection, and data processing) are integrated into the software. All information necessary for performing protein crystallography experiments is stored in the PCDB database (except raw X-ray diffraction data, which is stored in the Network File Server). To allow all members of a protein crystallography group to participate in experiments, the system was developed as a multi-user system with secure network access based on TCP/IP secure UNIX sockets. Secure remote access to the system is possible from any operating system with X-terminal and SSH/X11 (Secure Shell with graphical user interface) support. Currently, the system covers the high-throughput X-ray data collection stages. Experimental schedule is created and stored in the database in advance or at beamline (using the database editor PCDBEditor or the StepWizard procedure of user's control application PCCTools) and can be executed at once or step-by-step allowing to correct the experiment strategy. The crystal changing and centering are automated. To increase the efficiency of the high-throughput experiment the beamline equipment operations are performed in parallel, when it is possible. The source code of the main PCCS applications and modules is written in C/C++. The main operating system is Linux. PCDB database was built using MySQL software. The system is being commissioned at BL5A and NW12A beamlines (PF, PF-AR, KEK, Tsukuba, Japan).

## The Crystallization and X-ray Diffraction of the Exo-Arabinanase from *Penicillium chrysogenum*

Yuri Sogabe<sup>1</sup>, Takayoshi Kinoshita<sup>1</sup>, Asako Yamaguchi<sup>1</sup>, Tomoya Kitatani<sup>1</sup>, Tatsuji Sakamoto<sup>2</sup>, Hideshi Ihara<sup>3</sup>, Hiroaki Adachi<sup>4</sup>, Hiroyoshi Matsumura<sup>5</sup>, Kazufumi Takano<sup>6</sup>, Satoshi Murakami<sup>7</sup>, Tsuyoshi Inoue<sup>8</sup>, Yusuke Mori<sup>9</sup>, Toshiji Tada<sup>1</sup>

Department of Biological Science, Osaka Prefecture University<sup>1</sup>, Graduate School of Life and Environmental Sciences, Osaka Prefecture University, Japan<sup>2</sup>, Graduate School of Engineering, Osaka University, Japan / SOSHO Inc., Japan / CREST, JST, Japan<sup>3</sup>, The Institute of Scientific and Industrial Research, Osaka University, Japan / SOSHO Inc., Japan / CREST, JST, Japan<sup>4</sup>

Arabinanase hydrolyzes the  $\alpha$ -1,5-L-arabinofuranoside linkage of arabinan which is widely distributed in plant walls. The crystal structures of three arabinanases have revealed that the enzymes have a common unique fold consisting of five  $\beta$ -sheets, each of which is made up of four antiparallel  $\beta$ -strands. *Penicillium chrysogenum* exo-arabinanase (Abnx) releases arabinobiose from the nonreducing terminus of arabinan. Abnx has a completely different primary structure from other arabinanases so far isolated. We have initiated an X-ray structure analysis of Abnx to clarify the three-dimensional structure and molecular mechanisms of the novel enzyme.

The recombinant Abnx was expressed in *E. coli*. The purified enzyme was crystallized by 2.0 M ammonium sulfate as a precipitant using the hanging-drop vapor diffusion method. The crystals diffracted to a maximum resolution of 3.2 Å and belonged to the tetragonal system,  $P4_22$  with unit cell parameters of  $a = b = 166.4$  and  $c = 401.2$  Å. The crystal was estimated to include over eight Abnx molecules in the asymmetric unit. Thus, we have attempted to improve the diffraction quality of the crystals and/or to obtain new crystal forms by the mutational surface engineering and the laser-irradiation technique. The latter technique gave a new crystal in 30% MPD solution. The crystal diffracted beyond 1.5 Å resolution and belonged to the orthorhombic system,  $P2_12_12_1$ , with unit cell parameters of  $a = 66.6$ ,  $b = 76.9$  and  $c = 79.3$  Å. Assuming one protein molecule in the asymmetric unit, the  $V_M$  value is  $2.4 \text{ \AA}^3 \text{Da}^{-1}$ . A search for heavy-atom derivatives is currently under way for structure determination by isomorphous replacement method.

## Crystal Structure of Phospholipase A<sub>2</sub> Complex with Indomethacin at 1.4 Å Resolution Reveals a Non-Competitive Ligand-Binding Site within the Hydrophobic Channel

Nagendra Singh<sup>1</sup> R. Prem Kumar<sup>1</sup> Sujata Sharma<sup>1</sup> Marcus Perbandt<sup>2</sup> Punit Kaur<sup>1</sup> Christian Betzel<sup>2</sup> Tej P. Singh<sup>1</sup>

Biophysics, All India Institute of Medical Sciences<sup>1</sup> Department of Biochemistry and Molecular Biology, University of Hamburg c/o DESY, Building 22a, 22603 Hamburg, Germany<sup>2</sup>

Inhibition of synthesis of pro-inflammatory eicosanoids by an anti-inflammatory agent indomethacin has been attributed to its action against the enzymes which are involved in the eicosanoids biosynthesis pathway particularly cyclo-oxygenase. In the first step of this pathway, phospholipase A<sub>2</sub> (PLA<sub>2</sub>) hydrolyzes acyl group at C2 of phospholipids and produces arachidonic acid which serves as a substrate for cyclooxygenase. Therefore, synthesis of eicosanoids will also be inhibited if the supply of precursor fatty acid is reduced by blocking the action of enzyme PLA<sub>2</sub>. It was reported that indomethacin inhibits the action of PLA<sub>2</sub> in an unusual way but its mode of action and the precise site of binding in the hydrophobic channel are not known. Therefore, it is of great interest to analyze the detailed three-dimensional structure of PLA<sub>2</sub> complex with indomethacin. The initial binding studies using SPR indicated the value of  $1.3 \times 10^{-6}$  M for the dissociation constant (K<sub>d</sub>). The crystal structure of the PLA<sub>2</sub> complex with indomethacin was determined at 1.4 Å resolution and refined to an R<sub>cryst</sub> factor of 18.8% (R<sub>free</sub> factor of 20.2%). The final model contains 944 protein atoms, 25 atoms of indomethacin, 235 water molecules and 4 sulfate ions. The structure revealed the site of binding of indomethacin at a different location in the hydrophobic channel than the conventional site occupied by PLA<sub>2</sub> inhibitors. Indomethacin carboxylic group oxygen atom O1 interacts with Asp 49 and His 48 through catalytic water molecule while O2 forms an ionic interaction with Lys 69. In order to be able to form these interactions, indomethacin is oriented parallel to helices H2 and H3. This is a novel site and thus it is of utmost importance for improving the design of PLA<sub>2</sub> inhibitors.

**Crystal structure of the RUN domain of the Rap2 interacting protein x**

Mutsuko Kukimoto-Niino<sup>1</sup>, Tetsuo Takagi<sup>1</sup>, Ryogo Akasaka<sup>1</sup>, Kazutaka Murayama<sup>2</sup>, Tomomi Uchikubo-Kamo<sup>1</sup>, Takaho Terada<sup>1</sup>, Makoto Inoue<sup>1</sup>, Satoru Watanabe<sup>1</sup>, Akiko Tanaka<sup>1</sup>, Yoshihide Hayashizaki<sup>1</sup>, Takanori Kigawa<sup>1</sup>, Mikako Shirouzu<sup>1</sup>, Shigeyuki Yokoyama<sup>2</sup>

<sup>1</sup>Genomic Sciences Center, RIKEN Tohoku University Biomedical Engineering Research Organization, Japan; <sup>2</sup>Graduate School of Science, The University of Tokyo, Japan

Rap2 interacting protein x (RPIPx) is a homolog of RPIP8, a specific effector of the Rap2 GTPase of the Ras family. The N-terminal region of RPIP8, which contains the RUN domain, interacts with Rap2. Using cell-free synthesis and NMR, we determined that the region encompassing residues 83-255 of mouse RPIPx, which is 40-residues larger than the predicted RUN domain (residues 113-245), is the minimum fragment that forms a correctly folded protein. This fragment, the RPIPx RUN domain, interacted specifically with Rap2B *in vitro*, in a nucleotide-dependent manner. The crystal structure of the RPIPx RUN domain was determined at 2.0 Å resolution, by the multiwavelength anomalous dispersion (MAD) method. The RPIPx RUN domain comprises eight anti-parallel  $\alpha$ -helices, which form an extensive hydrophobic core, followed by an extended segment. This structure is distinct from any other known Ras/Rap-binding domain. The residues in the core region are highly conserved, suggesting the conservation of the RUN-domain fold among the RUN domain-containing proteins. The residues forming a positively charged surface are conserved between RPIP8 and its homologs, suggesting that this surface is important for Rap2 binding. In the crystal, the putative Rap2 binding site of the RPIPx RUN domain interacts with the extended segment in a segment-swapping manner.

## Development of Online UV-Visible Microspectrophotometer for Protein Crystallography at BL38B1 of SPring-8

Nobutaka Shimizu<sup>1</sup>, Kouichi Tomita<sup>2</sup>, Masao Ogaki<sup>3</sup>, Kazuya Hasegawa<sup>4</sup>, Masaki Yamamoto<sup>5</sup>

<sup>1</sup>Research and Utilization Division, Structural Biology Group, Japan Synchrotron Radiation Research Institute, <sup>2</sup>PHOTON Design Co., <sup>3</sup>EPL Inc., <sup>4</sup>SPring-8/JASRI, <sup>5</sup>SPring-8/JASRI, RIKEN SPring-8 Center

The high intensity X-ray of synchrotron radiation gives the radiation damage to a protein crystal. It is difficult to evaluate the damage through structural analysis, and is necessary to obtain the complementary information of the damage against the X-ray diffraction experiment. UV-visible spectroscopy is one of good techniques for obtaining the information of amino acids in the protein. Especially, Trp and Tyr have absorption around 280 nm unlike other amino acids. Moreover, since proteins which bind with metal atoms and organic small molecules have absorption in the visible region, the change of specific position in the protein might be clarified. We developed online UV-Vis. microspectrophotometer at BL38B1 of SPring-8 to analyze the state of protein in the crystal to which X-ray was irradiated.

This spectrophotometer employed a difference dispersive double monochromator mounted by Czerny-Turner type in order to acquire high brightness in UV region and reject stray light (PDPT0320, PHOTON design). Two types of diffraction gratings (53006BK01-150R and 53006BK01-280R, Newport) were installed into the monochromator. Mercury-Xeon lamp (L2423, Hamamatsu Photonics) and the photomultiplier (R374, Hamamatsu Photonics) are selected as a light source and a detector, respectively. In the preliminary test using solution samples and ND filters, the absorption spectra were able to be measured up to ~ 3.0 OD from 250 to 700 nm. We will introduce the feature of this spectrophotometer and the measurement results of crystals on the poster.

**Crystal Structures of the complexes of C-terminal lobe of lactoferrin with NSAIDs : Structural basis of the prevention of NSAID induced gastropathy by lactoferrin revealed**

Mau Sinha Sujata Sharma Nagendra Singh Tej P Singh

Department of Biophysics, All India Institute of Medical Sciences

Non steroidal anti-inflammatory drugs (NSAIDs) are the most commonly prescribed drugs for various inflammatory disorders. However, use of NSAIDs is accompanied by risk of upper and lower gastrointestinal (GI) complications, some of which can be serious or even fatal. Lactoferrin is an 80 kDa glycoprotein found in various biological fluids which consists of two homologous lobes each containing a single ferric ion. The C-terminal molecular half (C-lobe) of bovine lactoferrin was produced proteolytically. It consists of Tyr 342 to Ser 676 and Leu 681 to Phe 686. The structures of the complexes of C-lobe have been determined with three NSAIDs ; aspirin, indomethacin and diclofenac. These structures have revealed three additional zinc binding sites and a new site for the binding of NSAIDs. These results indicate new roles of lactoferrin C-lobe in regulating the roles of zinc ions and exhibits its potential of sequestering the NSAIDs in the human body. The structures of C-lobes also revealed a new role for the N-terminal residues of C-lobe which were involved in the interactions with N-lobe at the interface in the intact lactoferrin. The three potential glycosylation sites at Asn 368, Asn 476 and Asn 545 in the C-lobe are indeed glycosylated and contain 13 sugar residues. These structures reveal the mechanism by which lactoferrin is effective at preventing NSAID-induced intestinal injury.

## Crystallographic study of *Pyrococcus horikoshii* tryptophanyl-tRNA synthetase

Akiko Mizukawa Michiko Konno

Department of Chemistry, Ochanomizu University

The codon for Trp is one kind and three bases of anticodon CCA of tRNA<sup>Trp</sup> bind on three regions of tryptophanyl-tRNA synthetase (TrpRS), respectively. It is predicted that residues recognize bases of anticodon are conserved, since this enzyme existed from the origin of life and selects only one kind of anticodon. The comparison of the reported crystal structures between *Bacillus stearothermophilus* TrpRS and human TrpRS reveals difference of the orientation of an anticodon-binding  $\alpha$ -helix domain against a catalytic domain. In order to clarify the binding region of the three bases of anticodon of tRNA through comparison with these proteins, we tried crystal structure analysis of *Pyrococcus horikoshii* TrpRS (Ph TrpRS).

Ph TrpRS is about 45.3kD and has 386 residues. Ph TrpRS gene was cloned into plasmid pET28c (Novagen) and over expressed in *E. coli* strain BL 21 (DE3) codon plus (Stratagene). To remove proteins of *E. coli* as early as possible, supernatant of sonicated cells was heated on 70°C for 30 minutes. Then TrpRS was purified by three steps; Ni-NTA Superflow column, RESOURCE Q column and Hi-Trap Heparin column. We tried crystallization by the hanging or sitting drop vapor diffusion technique at 20°C and obtained about 2  $\mu$ m microcrystals from drops containing 2  $\mu$ l of the protein (10 mg/mL), 2  $\mu$ l of a reservoir solution (1.6 M (NH<sub>4</sub>)<sub>2</sub>SO<sub>4</sub>, 0.2 M NaCl, 5 mM MgCl<sub>2</sub>, Tris-HCl pH 8.5-7.4) and 0.2  $\mu$ l of additive solution (0.1 M SrCl<sub>2</sub>).

## Crystal Structure of the Root Effect Fish Hemoglobin, Trout Hb IV bound to ATP molecule

Satoru Unzai<sup>1</sup> Kiyohiro Imai<sup>2</sup> Sam-Yong Park<sup>1</sup> Jeremy Tame<sup>1</sup> Kiyoshi Nagai<sup>1\*</sup>

<sup>1</sup>Protein Design Laboratory, Yokohama City University<sup>1</sup> Faculty of Engineering, Hosei University, Japan<sup>2</sup> MRC Laboratory of Molecular Biology, UK<sup>3</sup>

Blood from the trout *Oncorhynchus mykiss* (formerly *Salmo irideus*) contains four distinct hemoglobins (Hbs). Trout Hb IV makes up roughly 65% of the total Hb component and it is characterized by the Root effect, an unusually strong dependence of oxygen affinity on pH. Below pH 6 this Hb binds oxygen weakly and non-cooperatively. This allows discharge of oxygen into the swim bladder by the secretion of lactic acid into the blood in the gas gland.

In addition to protons, intracellular Hb function is also mediated by organic phosphates. Erythrocytes of teleost fish use ATP, GTP, or IHP (inositol hexaphosphate) as allosteric effectors. Addition of ATP tends to decrease both the overall oxygen affinity and the cooperativity of trout Hb IV.

Here we report the crystal structure of met form trout Hb IV bound to ATP, refined to 1.70 Å resolution. Electron density corresponding to ATP was found in the cleft between the two beta chains. Although the trout Hb IV was met form, its quaternary structure was very similar to that of deoxy (T state) trout Hb I, another trout Hb component. Because the crystal was formed at low pH (pH 5.5) and in the presence of ATP it appears that the T state was strongly stabilized. The position of the ATP molecule in the trout Hb IV central cavity is deeper than that of DPG molecule in the deoxy human Hb A. In fish Hbs, the Asp residue in position beta-NA2 was suggested to form contacts with ATP, however, the side chain points into solvent and does not make contact with ATP or other amino acid residues in the trout Hb IV structure.

## Refinement of high resolution X-ray structure; the case of Taka-amylase A and Lysozyme

Akifumi Higashiura<sup>1</sup>, Hiroaki Tanaka<sup>2</sup>, Koji Inaka<sup>3</sup>, Masaru Sato<sup>4</sup>, Shigeru Sugiyama<sup>5</sup>, Sachiko Takahashi<sup>6</sup>, Mari Yamanaka<sup>7</sup>, Moritoshi Motohara<sup>8</sup>, Satoshi Sano<sup>9</sup>, Tomoyuki Kobayashi<sup>10</sup>, Mamoru Suzuki<sup>11</sup>, Tetsuo Tanaka<sup>12</sup>, Atsushi Nakagawa<sup>13</sup>

<sup>1</sup>Institute for Protein Research, University of Osaka<sup>2</sup>, Japan Space Forum<sup>3</sup>, Maruwa Food Industries, Inc.<sup>4</sup>, Japan Aerospace Exploration Agency<sup>5-13</sup>

Recently, high brilliance and small divergence synchrotron beam lines, X-ray data collection at low temperature and technical advances in crystallographic analysis have significantly improved the resolution of X-ray crystallography. In this study Taka-amylase A and lysozyme were used as a model protein for high resolution X-ray crystallography. Taka-amylase A crystals were grown in microgravity environment (JAXA-GCF project) and lysozyme crystals were grown in the ground. Data collections were performed using synchrotron radiation from SPring-8 beamline BL12B2, BL44XU and Photon Factory beamline BL-5A. Two data sets were collected for high- and low-resolution data to avoid the saturation of high intensity diffraction. The high-resolution diffraction data of Taka-amylase A were observed to 0.94Å and lysozyme were 0.75Å. The data were integrated, scaled and merged using the *DENZO* and *SCALEPACK* programs. Taka-amylase A crystals belong to space group  $P2_12_12_1$ , with the cell dimensions  $a=50.4\text{Å}$ ,  $b=67.4\text{Å}$ ,  $c=130.5\text{Å}$  and lysozyme crystals were  $P1$ ,  $a=26.7\text{Å}$ ,  $b=31.0\text{Å}$ ,  $c=33.7\text{Å}$ ,  $\alpha=89.21$ ,  $\beta=72.5$ ,  $\gamma=67.7$ . The overall  $R_{\text{merge}}$  based on intensities for all data of Taka-amylase A was 7.7% with its completeness of 97.6% against data to 1.0Å and lysozyme was 4.7%, 88.0%. Refinement was carried out by *SHELX* programs. The refinement of Taka-amylase A and lysozyme were proceeding against data to 1.0Å and 0.80Å respectively. An  $R$  factor and *free-R* factor of Taka-amylase A was 13.1%, 16.1% and lysozyme was 12.6%, 14.8%. These high-resolution structures were providing us more reliable geometric and conformational properties of the protein.

## Current status of IBARAKI Biological diffractometer in J-PARC - Optimization of design parameters

Katsuhiro Kusaka<sup>1</sup> Takashi Ohhara<sup>2</sup> Ichiro Tanaka<sup>3</sup> Nobuo Niimura<sup>4</sup> Kazuo Kurihara<sup>5</sup> Takaaki Hosoya<sup>6</sup> Tomoji Ozeki<sup>7</sup> Kazuya Aizawa<sup>8</sup> Yukio Morii<sup>9</sup> Masatoshi Arai<sup>10</sup> Makoto Hayashi<sup>11</sup> Kazuhiro Ebata<sup>12</sup> Yoshiki Takano<sup>13</sup>

Quantum Beam Science Directorate (QuBS), Japan Atomic Energy Agency (JAEA)<sup>1</sup> Department of Biomolecular Functional Engineering, Ibaraki University, Japan<sup>2</sup> Institute of Applied Beam Science, Ibaraki University, Japan<sup>3</sup> Department of Chemistry and Materials Science, Tokyo institute of technology, Japan<sup>4</sup> Department of planning, Ibaraki prefectural government, Japan<sup>5-13</sup>

Ibaraki prefectural government in Japan has started to construct the TOF neutron biological diffractometer for industrial use at BL03, Materials and Life science facility, J-PARC. The diffractometer is designed so that it can measure sample crystals with maximum cell dimension of 135 angstrom. It is necessary to achieve the efficiency which is more than 50 times larger than the present high performance diffractometer BIX-4 (JRR-3, JAEA, Japan) in order to pioneer a new basic life science fields as well as applied industries.

To realize this performance, the diffractometer will be installed on a coupled moderator has more intense peak and integrated intensity but wider pulse shape than a decoupled one. It is expected that some neighbor Bragg spots will overlap partially each other along the time axis. The overlapping of Bragg spots should be considered for the determination of optic parameters and it is necessary to de-convolute the overlapped spots with faster algorithm and higher accuracy. The three original simulation programs of TOF diffraction data with designed parameters of the diffractometer were developed to obtain information of spot-overlapping, completeness of Bragg spots and spot profiles along the time axis. The consideration of important designed parameters (divergence of incident neutron beam at a sample position, the distance between sample and detector surface and the detector arrangement) focused on biological macromolecular and the strategy of de-convoluting overlapped spots will be reported based on the simulation results by using the programs mentioned as above.

## The Crystal Structures of the Pseudouridine Synthases RluC and RluD

Kenji Mizutani Yoshitaka Machida Satoru Unzai Jeremy R. H. Tame Sam-Yong Park

Protein Design Laboratory, Yokohama City University

The most frequent modification of RNA, the conversion of uridine bases to pseudouridines, is found in all living organisms and often in highly conserved locations in ribosomal and transfer RNA. RluC and RluD are homologous enzymes which each convert three specific uridine bases in *Escherichia coli* ribosomal 23S RNA to pseudouridine: bases 955, 2504, and 2580 in the case of RluC and 1911, 1915, and 1917 in the case of RluD. Both have an N-terminal S4 RNA binding domain. While the loss of RluC has little phenotypic effect, loss of RluD results in a much reduced growth rate. We have determined the crystal structures of the catalytic domain of RluC, and full-length RluD. The S4 domain of RluD appears to be highly flexible or unfolded and is completely invisible in the electron density map. Despite the conserved topology shared by the two proteins, the surface shape and charge distribution are very different. The models suggest significant differences in substrate binding by different pseudouridine synthases.

## Loop and scaffold of serine protease inhibitors: role in religation and specificity

Susmita Khamrui Jhimli Dasgupta Jiban K Dattagupta Udayaditya Sen

Crystallography and Molecular Biology Division, Saha Institute of Nuclear Physics

The scaffold of serine protease inhibitors plays a significant role in the process of religation that resists proteolysis of the inhibitors compared to a substrate. To examine the structural element responsible for 'prevention of proteolysis', we have targeted a conserved scaffolding Asn residue of WCI and mutated it with residues having different shapes and charges like Gly, Ala, Thr, Leu and Gln. Results of structural and biochemical studies performed on these mutants prompted us to conclude that the side chain of spacer Asn not only fits snugly into the concave space of the reactive site loop cavity but also its ND2 atom forms hydrogen bonds with P2 and P1' carbonyl O at either side of the scissile bond holding the cleaved products together for religation. Data base analysis allowed us to identify such spacer asparagines in 5 other families of serine protease inhibitors with similar disposition of their ND2 atom suggesting that Asn mediated religation is prevalent for serine protease inhibitors<sup>1</sup>. In another approach, to examine the role of scaffold in broader sense, two chimeric proteins are planned to prepare with loops of trypsin inhibitors like ETI and STI on the scaffold of WCI. As a first step towards this approach, we prepared a P1 mutant (Leu to Arg) of WCI that strongly inhibits trypsin with a  $K_i$  value comparable to ETI and STI and structure of this mutant (L65R) at 2.15 Å provides a clue to this altered inhibition<sup>2</sup>. More over structure of the complex (2.6 Å) between L65R and trypsin provides intricate details of this strong inhibition<sup>3</sup>. Structural results of the Asn mutants, P1 mutant and complex of it with trypsin along with their biochemical data will be presented here.

1. *Biochemistry* (2006) **45**:6783
2. *BBA*. (2005) **1752**:65
3. Manuscript under preparation

## Crystallographic analysis of CHP1 and DRAK2

Youichi Naoe<sup>1</sup> Kyouhei Arita<sup>1</sup> Hiroshi Hashimoto<sup>1</sup> Hiroshi Kanazawa<sup>2</sup> Mamoru Sato<sup>1</sup> Toshiyuki Shimizu<sup>1</sup>

<sup>1</sup>International Graduate School of Arts and Sciences, Yokohama City University, <sup>2</sup>Department of Biological Science, Graduate School of Science, Osaka University, Japan

CHP1 (Calcineurin B homologous protein 1), is a calcium binding EF-hand protein and shows substantial sequence similarity (~39% identity) with the CNB (Calcineurin B subunit). CHP1 was the essential cofactor of NHEs (Na<sup>+</sup>/H<sup>+</sup> exchangers), which catalyze the electroneutral influx of extracellular Na<sup>+</sup> and efflux of intracellular H<sup>+</sup>. CHP1 also binds to DRAK2 (DAP kinase related apoptosis inducing protein kinase 2) and significantly reduced its kinase activity calcium dependently. Interestingly CHP1 binding region of NHE1 and DRAK2 shows little sequence similarity. We have determined crystal structure of calcium-bound CHP1 from rat at 2.2 Å resolution. The overall folding topology of the protein is similar to that of the regulatory B subunit of calcineurin. CHP1 contains a hydrophobic pocket on the opposite side of the protein to the EF-hands. The hydrophobic pocket has been implicated in multiple ligand binding. DRAK2 is a Ser/Thr kinase which belongs to DAP (Death associated protein) kinase family. Today, DAP kinase family has five members which can induce apoptosis depend on its kinase activity. Recently, DRAK2 is thought to regulate the TCR (TCell responses) activation threshold during thymocyte selection. But its target molecules and physiological role remains unknown. To clarify the function and the regulation mechanism of DRAK2 by CHP1, we tried to determinate three dimensional structure of DRAK2. We express, purify and crystallize the kinase domain of DRAK2.

We also performed CHP1 and DRAK2 binding experiment by taking size exclusion chromatography and ultracentrifugation. We confirmed that CHP1 strongly bind to DRAK2.

**Molecular structure and dynamics of cytoplasmic domain of FlhA, a subunit of the flagellar type III protein export apparatus.**

Yumiko Saijo-Hamano<sup>1</sup>, Katsumi Imada<sup>2</sup>, Tohru Minamino<sup>2</sup>, May Kihara<sup>3</sup>, Akio Kitao<sup>4</sup>, Keiichi Namba<sup>1</sup>

JST, ICORP<sup>1</sup>, Graduate School of Frontier Biosciences, Osaka University, JAPAN and ICORP, JST<sup>2</sup>, Department of Molecular Biophysics and Biochemistry, Yale Univ<sup>3</sup>, Institute of Molecular and Cellular Biosciences, Univ. of Tokyo and CREST, JST<sup>4</sup>

The bacteria flagellum has the type III protein export apparatus as one part of the basal body. It selectively translocates flagellar axial proteins into the central channel of the flagellum. The export apparatus consists of six integral membrane components (FlhA, FlhB, FliO, FliP, FliQ and FliR) and three cytoplasmic components (FliH, FliI and FliJ). Genetic and biochemical information are available for some of these proteins. However, the export mechanism is not clear except that the energy released by ATP hydrolysis by FliI is used for the export process. FlhA from *Salmonella* is an integral membrane component of the flagellar specific type III protein export apparatus. It consists of an N-terminal transmembrane domain (FlhATM) and a C-terminal cytoplasmic domain (FlhAC). We solved a 2.8 Å crystal structure of FlhAC, which is composed of one elongated linker region continued from FlhATM and four subdomains (ACD1, ACD2, ACD3 and ACD4). We thought that FlhAC could conformational change from the structure, therefore we carried out molecular dynamics simulation of FlhAC. The simulation showed that FlhAC periodically repeated conformational change to open and then closed state using two hinges between ACD1 and ACD3, and ACD3 and ACD4. And also substitution mutations of key residues interacting between the subdomains failed to complement to motility of flhA-null mutant. These results suggest that the fluctuation of conformational change is important to function of FlhAC. The crystal structure, together with the result of multicopy effects of N-terminal half of FlhAC to motility of wild-type cell and previous studies, suggest that linker region and ACD1 act as holding soluble export apparatus components, probably FliI, which is a ATP-ase.

## **Crystal structure of goat lactoperoxidase at 3.5 Å resolution**

Amit K. Singh E.S. Ethayathulla Nagendra Singh Sujata Sharma Tej P. Singh

Department of Biophysics, All India Institute of Medical Sciences, New Delhi

Lactoperoxidase is a heme containing enzyme that catalyzes the inactivation of various micro-organisms. The crystal structure of goat lactoperoxidase was determined as part of the programme of structural and functional studies of antimicrobial secretory glycoproteins such as lactoperoxidases and lactoferrins. The structure has been refined to an R-factor of 0.177. The protein is crystallized in space group P1 with two molecules in the unit cell. Thus, the structure contains two identical crystallographically independent molecules. Their conformations are also formed essentially identical. Both molecules contain one calcium ion in each with pentagonal bipyramidal geometries. The structure has also revealed a number of halide binding sites. The structure contains two cis-prolines. It is essentially an alpha-helical protein with a little beta structure. The central core region contains the heme binding site which is composed of five alpha-helices. The heme porphyrin ring is considerably distorted from planarity. Heme is covalently linked to protein via Asp94 and glu242. A proximal ligand to the heme iron atom has been identified as His336 which in turn is hydrogen bonded to Asn421. On the distal side of the heme group, His95 and Arg239 are likely to participate directly in the catalytic mechanism in a manner analogous to the distal histidine and arginine of the non-homologous enzyme cytochrome C peroxidase.

**Structural basis of the sphingomyelin phosphodiesterase activity in neutral sphingomyelinase from *Bacillus cereus***

Hideo Ago<sup>1</sup>, Masataka Oda<sup>2</sup>, Masaya Takahashi<sup>3</sup>, Hideaki Tsuge<sup>4</sup>, Sadayuki Ochi<sup>5</sup>, Nobuhiko Katunuma<sup>6</sup>, Masashi Miyano<sup>7</sup>, Jun Sakurai<sup>8</sup>

Structural Biophysics Laboratory, RIKEN SPring-8 Center, Harima Institute<sup>1</sup>, Faculty of Pharmaceutical Science, Tokushima Bunri University, Japan<sup>2</sup>, Institute for Health Sciences, Tokushima Bunri University, Japan<sup>3</sup>, School of Medicine, Fujita Health University, Japan<sup>4</sup>

Sphingomyelinase (SMase) from *Bacillus cereus* (*Bc*-SMase) hydrolyzes sphingomyelin (SM) to phosphocholine and ceramide in a divalent metal ion dependent manner. *Bc*-SMase is a homologue of mammalian neutral SMase (nSMase), and mimics the actions of the endogenous mammalian nSMase in causing differentiation, development, aging and apoptosis. Thus *Bc*-SMase may be a good model for the poorly characterized mammalian nSMase. The metal ion activation of sphingomyelinase activity of *Bc*-SMase was in the order of  $\text{Co}^{2+} \gg \text{Mn}^{2+} \gg \text{Mg}^{2+} \gg \text{Ca}^{2+} \gg \text{Sr}^{2+}$ . The first crystal structures of *Bc*-SMase bound to  $\text{Co}^{2+}$ ,  $\text{Mg}^{2+}$  or  $\text{Ca}^{2+}$  were determined. The water bridged double divalent metal ions at the center of cleft in both the  $\text{Co}^{2+}$  and  $\text{Mg}^{2+}$  bound forms was concluded to be the catalytic architecture require for sphingomyelinase activity. In contrast, the architecture of  $\text{Ca}^{2+}$  binding at the site showed only one binding site. A further single metal binding site exists at one side edge of the cleft. Based on the highly conserved nature of the residues of the binding sites, the crystal structure of *Bc*-SMase with bound  $\text{Mg}^{2+}$  or  $\text{Co}^{2+}$  may provide a common structural framework applicable to phosphohydrolases belonging to the DNase I like folding superfamily. In addition, the structural features and site directed mutagenesis suggest that the specific b-hairpin with the aromatic amino acid residues participates in binding to the membrane-bound SM substrate.

## Performance of the macromolecular crystallography short-gap undulator beam line BL-17A at the Photon Factory

Noriyuki Igarashi Naohiro Matsugaki Yusuke Yamada Masahiko Hiraki Atsushi Koyama Keiichi Hirano Toshinobu Miyoshi Soichi Wakatsuki

Photon Factory, IMSS, KEK

Four new short straight sections were created as part of the "Straight-Section Upgrade Project" of the Photon Factory during a six-month shutdown in the first half of FY2005. A new short-gap undulator, SGU#17, was designed for one of the short straight sections. With the high brilliance beam derived from SGU#17, we have proposed two advances in the field of structural biology: micro-crystal structure analysis and structure determination using softer X-rays.

After the completion of BL-17A, we successfully delivered the first beam on Oct 7, 2005. Then, we started alignment and commissioning of the beam line. The preliminary performance is as follows. The focused beam size (FWHM) with the K-B mirror system is about  $32.9 \mu\text{m}$  (V) x  $234 \mu\text{m}$  (H). The photon flux at 12.4 keV after the collimation slit of 100, 40 and  $20 \mu\text{m}^2$  are  $7.7 \times 10^{10}$ ,  $2.2 \times 10^{10}$  and  $6.7 \times 10^9$  photons/sec, respectively. This preliminary result is about 60 % of the expected performance and it could be improved by optimizing the setting of the undulator and beam line optics.

A single-axis diffractometer was designed with the final goal of 100 to 200 nm rotation error for micron-size crystals. We started test experiments in April of 2006. We will describe the optical design and preliminary performance of the beam line, and the results of the test experiments using small crystals and softer X-rays.

The BL-17A is still under improvement although very promising results have already been obtained. Further optimization of the optics, stabilization of the beam position by feedback system and tuning of the diffractometer will be integrated into the user friendly experimental environment, and micron-crystal structure analysis and structure determination using softer X-ray will become routine at the BL-17A.

**Sugar recognition by lactoferrin: Crystal structure of the complex formed between C-lobe of bovine lactoferrin and a pentasaccharide at 2.38 Å resolution**

Rishi Jain Nagendra Singh Talat Jabeen Sujata Sharma Asha Bhusan Tej P Singh

Department of Biophysics, All India Institute of Medical Sciences

Lactoferrin is an 80 kDa iron-binding glycoprotein. The single polypeptide chain of 691 amino acid residues is folded into two globular N-lobe and C-lobe. The present study reports the crystal structure of the complex of a proteolytically generated bovine C-lobe by proteinase K with a pentasaccharide at 2.38 Å resolution. The crystal belongs to space group  $P2_1$ , with unit cell dimensions  $a = 62.9$ ,  $b = 50.5$ ,  $c = 65.8$ ,  $\beta = 107.5^\circ$ . Final model contains 2605 protein atoms; 1  $\text{Fe}^{3+}$ , 3  $\text{Zn}^{2+}$  and 1  $\text{CO}_3^{2-}$  ions, 13 sugar residues (N-linked), 5 NAG residues and 276 water molecules. There were three zinc atoms were observed at sites involving Tyr342, His588, and Glu659. This is the first time that a novel ligand binding site has been observed in lactoferrins. The pentasaccharide binds at a very distinct site. This site is located near C-terminal end of the C-lobe, which is formed by residues Leu651, Gly652, Thr430, Tyr660, Thr663, Glu659, and Lys498. The pentasaccharide interacts with C-lobe residues. The main feature of the present structure is the presence of a pentasaccharide at a novel binding site on C-lobe of the bovine lactoferrin. The site is formed by a number of hydrophobic and polar residues. The pentasaccharide forms extensive hydrogen bonding interactions with the protein molecule. The main residues involved in the interactions are Leu 651, Gly 652, Thr 430, Tyr 660, Glu 659, Thr 663 and Lys 498. The pentasaccharide fits exactly in the shape of the new binding site. The binding of pentasaccharide can explain several function of lactoferrin which involved interactions with surface sugar molecules on other proteins. This site is most probably involved in protein-protein interaction with other molecules.

## Current status of IBARAKI Biological diffractometer in J-PARC -General View-

Ichiro Tanaka<sup>1</sup> Nobuo Niimura<sup>1</sup> Takashi Ohhara<sup>2</sup> Kazuo Kurihara<sup>2</sup> Katsuhiro Kusaka<sup>2</sup> Takaaki Hosoya<sup>2</sup> Tomoji Ozeki<sup>3</sup> Kazuya Aizawa<sup>3</sup> Yukio Morii<sup>3</sup> Masatoshi Arai<sup>3</sup> Makoto Hayashi<sup>3</sup> Kazuhiro Ebata<sup>3</sup> Yoshiki Takano<sup>3</sup>

College of Engineering, Ibaraki University<sup>1</sup> JAEA, Japan<sup>2</sup> Tokyo Institute of Technology<sup>3</sup> Ibaraki Prefectural Government<sup>3</sup>

Ibaraki Prefectural Government in Japan has started to construct a TOF neutron diffractometer for biological macromolecules for industrial use at J-PARC. The diffractometer is designed to cover the sample crystals which have their cell edges up to around 150 Å. It is expected to measure more than 100 samples per year if they have 2mm<sup>3</sup> in crystal volume according to simple calculation. The efficiency is more than 50 to 100 times larger than the present high performance diffractometers, BIX-4 in JRR-3 reactor in JAEA. To realize this performance, a coupled moderator (intense neutrons, but broad pulse in time resolution) was selected. In addition, two important and key items should be developed; a new detector with high spatial resolution and a special software to de-convolute overlapped spots in data reduction. The detector uses ZnS:Ag<sup>6</sup>LiF scintillator with wavelength-shift-fiber (WLSF) system. And the software has been designed using simple-profile-fitting method. The current status of these developments will be reported with an idea of system to promote industrial uses.

The figure shows an illustration of the diffractometer; camera distance is 0.45m.



**Crystal Structure of Haloalkane Dehalogenase LinB from *Sphingomonas paucimobilis* UT26 at 0.95 Angstrom resolution.**

Matthew CJ Wilce<sup>1</sup> Aaron J Oakley<sup>2</sup> Martin Klvana<sup>3</sup> Otyepka Michael<sup>4</sup> Yuji Nagata<sup>5</sup> Jiri Damborsky<sup>6</sup>

Department of Biochemistry and Molecular Biology, Monash University<sup>1</sup> Australian National University<sup>2</sup> Masaryk University<sup>3</sup> Palacky University<sup>4</sup> Tohoku University<sup>5</sup>

Haloalkane dehalogenases utilize water to transform haloalkanes into organic halides and alcohols. The industrial production of halocarbons and the persistence of the compounds in the environment has led to interest in the enzymes for bioremediation purposes.

We have determined the crystal structure of LinB, a 33-kDa haloalkane dehalogenase from *Sphingomonas paucimobilis* UT26, at 0.95 Angstrom resolution. LinB belong to the alpha/beta hydrolase family of enzymes and consists of two domains. The data have allowed us to directly observe the anisotropic motions of the catalytic residues. In particular, the side-chain of the catalytic nucleophile, Asp108, displays a high degree of disorder. It has been modeled in two conformations, one similar to that observed previously (conformation A) and one strained (conformation B) that approached the catalytic base (His272). The strain in conformation B was mainly in the C(alpha)-C(beta)-C(gamma) angle (126 degrees) that deviated by 13.4 degrees from the "ideal" bond angle of 112.6 degrees. On the basis of these observations, we propose a role for the charge state of the catalytic histidine in determining the geometry of the catalytic residues and that double-protonation of the catalytic base (His272) reduces the distance between the side-chain of this residue and that of the Asp108. Further, we were able to observe many alternative conformations of numerous side-chains and overlapping water networks.

**Antifungal activities of lactoferrin peptides: Crystal structural studies of complexes formed between fungal protease proteinase K and lactoferrin/designed peptides.**

R. Prem Kumar Amit Kumar Singh Nagendra Singh Sujata Sharma Asha Bhushan Punit Kaur T. P. Singh

Department of Biophysics,, All India Institute of Medical Sciences, New Delhi.

Proteins of the transferrin family fulfil a key role in controlling the levels of free iron in the body fluids of animals. Lactoferrin is a prominent member of the transferrin family. In addition to sequestering iron it has several other functions including presence of surface peptides with antibacterial and antifungal properties. Several complexes of proteinase K with proteolytic products of lactoferrin as well as with designed peptides were crystallized using hanging drop method. The lactoferrin peptides included GDEQGENK, VLLH, LLFND and KLKLLVVIRLK. Similarly a number of peptides containing sequences assumed to be having antifungal properties in lactoferrin were synthesized and their complexes with proteinase K were also crystallized. Crystal structures of these complexes were determined and positions of peptide atoms were refined. The structures have revealed that most of the peptides were located in the region between segments 100-105 and 131-136. The peptides were stabilized by several backbone hydrogen bonds and hydrophobic interactions with residues of ligand binding region. The prominent interactions included His 69, Gly 100, Gly 134 and Ser 224.

## Crystal structure of a pro-form of a bacterial leucyl aminopeptidase

Satoru Nirasawa<sup>1</sup> Masataka Horiuchi<sup>2</sup> Nobuo N Suzuki<sup>2</sup> Kiyohiro Takahashi<sup>2</sup> Fuyuhiko Inagaki<sup>2</sup> Kiyoshi Hayashi<sup>1</sup>

Enzyme Laboratory, National Food Research Institute<sup>1</sup> Department of Structural Biology, Graduate School of Pharmaceutical Sciences, Hokkaido University<sup>2</sup>

Aminopeptidases from *Aeromonas caviae* (apAC) and *Vibrio proteolyticus* (apVP) are translated as a prepro-enzyme consisting of several domains; a signal peptide, an N-terminal propeptide, a mature region and a C-terminal propeptide. The N-terminal propeptide acts as an intramolecular chaperone to assist the folding of enzymes and shows inhibitory activity toward their cognate mature enzymes. These aminopeptidases belong into clan MH. The peptidases in clan MH are cocatalytic zinc peptidases containing two atoms of zinc per molecule. Clan MH contains aminopeptidases, carboxypeptidases, dipeptidases and tripeptidases. The tertiary structures have been determined for aminopeptidase S, glutamate carboxypeptidase II and apVP, and each shows a six-stranded beta-sheet surrounded by helices. apVP is the type structure for clan MH. There are several members of the clan that are not known to be peptidases, for example the transferrin receptor and aminoacylase. Up to now, the structure of pro-enzyme consisting the N-terminal propeptide in the clan MH is unknown. In the present study, we determined a structure of pro-form of a chimeric aminopeptidase by replacing the N-terminal propeptide of apVP with that of apAC.

## X-ray phase-contrast imaging using an x-ray HARP camera

Keiichi Hirano<sup>\*</sup> Toshinomu Miyoshi<sup>\*</sup> Noriyuki Igarashi<sup>\*</sup> Soichi Wakatsuki<sup>\*</sup> Tohoru Takeda<sup>\*</sup> Jin Wu<sup>\*\*</sup> Thet-Thet Lwin<sup>\*\*</sup> Kenkichi Tanioka<sup>\*\*\*</sup> Norifumi Egami<sup>\*\*\*</sup> Misao Kubota<sup>\*\*\*</sup> Teruo Kawai<sup>\*\*\*</sup>

PF, KEK<sup>\*</sup> Department of Radiology, University of Tsukuba, Japan<sup>\*</sup> NHK, Japan<sup>\*\*</sup> NHK-ES, Japan<sup>\*\*\*</sup>

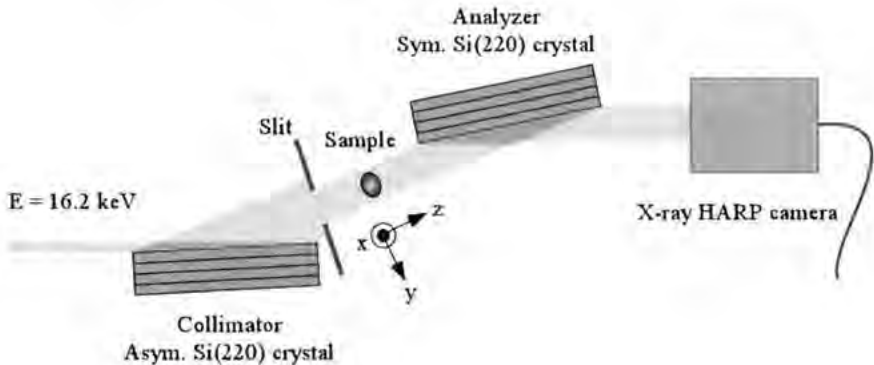
X-ray phase-contrast imaging is a very useful technique to observe inner structures of various objects [1, 2]. To date, area detectors such as x-ray films, imaging plates and x-ray CCD cameras have been widely used for the technique. However, for further improvement of the performance of overall imaging systems, an x-ray area detector with higher sensitivity and better spatial resolution is required. One of the most promising candidates, which can meet this requirement, is an x-ray HARP camera [3]. The x-ray HARP camera was applied, for the first time, to the x-ray phase-contrast imaging.

The experiment was performed at BL-14B of the Photon Factory. The experimental setup is shown below. Phase-contrast and absorption-contrast images of a rat liver were observed successfully. The sensitivity of the x-ray HARP camera was much higher than that of a fiber-coupled x-ray CCD camera. This result indicates that the x-ray HARP camera is indeed very useful for the x-ray phase-contrast imaging.

[1] A. Momose, T. Takeda, Y. Itai and K. Hirano: *Nature Med.*, **2** (1996) 473.

[2] K. Hirano : *J. Phys. D, Appl. Phys.*, **36** (2003) 1469.

[3] K. Tanioka and T. Hirai : *OYO BUTURI (Applied Physics)*, **71** (2002) 1376.



**Crystal structures of the complexes of secretory glycoproteins with designed peptides.**

A.S. Ethayathulla Devendra B. Srivastava Janesh Kumar Rishi K. Somvanshi Nagendra Singh  
Sujata Sharma Sharmistha Dey Asha Bhushan T. P. Singh

Department of Biophysics, All India Institute of Medical Sciences, New delhi.

Crystal structures of a new family of glycoproteins (SPX-40) that act normally as protective signalling factor and determine which cells are to survive the drastic tissue remodeling during involution, have been solved. This protein from Sheep (SPS-40), Porcine (SPP-40) and Goat (SPG-40) was isolated from dry secretions of mammary glands. Crystal structures of native as well as the complexes of SPX-40 with designed peptides Trp-Pro-Trp (WPW) and Trp-His-Trp (WHW) were determined. The structures revealed a topology with beta/alpha domain having the Triose-Phosphate Isomerase (TIM) barrel fold in the core and a small alpha + beta domain. These structures are similar to chitinases but lack chitin binding site due to structural differences and a loss of chitin hydrolyzing capability due to point mutations in the active site. Apparently, these proteins bind to cell surface receptors and protect the viable epithelial cells from extensive tissue remodeling during involution. These structures of complexes revealed that the interactions are predominantly hydrophobic interactions. The key protein residues involved in these interactions were W78, Q83, D186, W191, R192, P260, E269 and K270. The binding studies with fluorescence spectroscopy indicated a strong affinity between SPX-40 and the ligand. The real time kinetics measurement carried out using BIAcore-2000 showed a dissociation of  $10^{-7}$  M. The complexes with designed peptides have thrown a lot of light towards understanding their functions and suggested a good scope for the design of specific inhibitors of these proteins that might be eventually exploited as therapeutic agents against breast cancer.

## Crystal structure of human UDP-GalNAc: polypeptide $\alpha$ -N-acetylgalactosaminyltransferase 10 (pp-GalNAc-T10)

Tomoo Shiba<sup>1</sup> Tomomi Kubota<sup>1</sup> Shigemi Sugioka<sup>1</sup> Sanae Furukawa<sup>1</sup> Hiromichi Sawaki<sup>1</sup> Ryuichiro Kato<sup>1</sup> Soichi Wakatsuki<sup>1</sup> Hisashi Narimatsu<sup>1</sup>

Structural Biology Research Center, PF, IMSS, KEK, Present address: Graduate School of Arts and Sciences, The University of Tokyo<sup>1</sup> Glycogene Function Team of Research Center for Glycoscience (RCG), AIST, Japan<sup>1</sup> Structural Biology Research Center, PF, IMSS, KEK, Japan<sup>1</sup>

Biosynthesis of mucin-type O-glycan is initiated by the transfer of GalNAc which is catalyzed by UDP-GalNAc:polypeptide  $\alpha$ -N-acetylgalactosaminyltransferases (pp-GalNAc-Ts). To date, 15 human isozymes have been reported. Here we present crystal structures of the pp-GalNAc-T10 isozyme, which has specificity for glycosylated peptides, in complex with the hydrolyzed donor substrate UDP-GalNAc and in complex with GalNAc-serine (1). pp-GalNAc-T10 comprises two domains, catalytic and lectin domains (Fig), similarly to pp-GalNAc-T1 and pp-GalNAc-T2, which are reported by Fritz *et al* [2004 and 2006]. However, a distinct interdomain arrangement of pp-GalNAc-T10 results in a narrow cleft for acceptor substrates, compared with pp-GalNAc-T1 and pp-GalNAc-T2. The two domains are connected through a linker region, whose amino-acid sequences are not conserved among pp-GalNAc-Ts. GalNAc-Ser is bound to only the lectin  $\beta$  subdomain but not to the other two subdomains. The distance between the catalytic center and the carbohydrate-binding site on the lectin  $\beta$  subdomain influences the position of GalNAc glycosylation on GalNAc-glycosylated peptide substrates.

(1) T. Kubota *et al.* *J. Mol. Biol.*, **359**, 708-727 (2006)

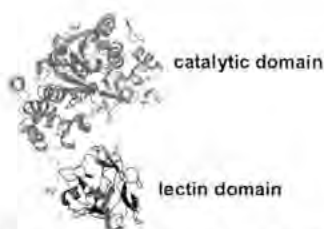


Fig. Crystal structure of ppGalNAc-T10

## Structural analysis on the human and mouse Galectin-9 N-terminal CRDs reveals flexible mechanism of carbohydrate recognition

Masamichi Nagae<sup>1</sup> Nozomu Nishi<sup>2</sup> Takeomi Murata<sup>3</sup> Taichi Usui<sup>4</sup> Takanori Nakamura<sup>5</sup> Soichi Wakatsuki<sup>1</sup> Ryuichi Kato<sup>1</sup>

Structural Biology Research Center, IMSS, KEK<sup>1</sup> Departments of Endocrinology, Faculty of Medicine, Kagawa University, Japan<sup>2</sup> Departments of Department of Applied Biological Chemistry, Faculty of Agriculture, Shizuoka University, Japan<sup>3</sup> Department of Applied Biological Chemistry, Faculty of Agriculture, Shizuoka University, Japan<sup>4</sup>

The galectins are a family of  $\beta$ -galactoside-binding animal lectins with a conserved carbohydrate recognition domain (CRD). They show high affinities for small  $\beta$ -galactosides and various binding specificities for complex glycoconjugates. The specific carbohydrate recognition is thought to be essential for their proper function. Galectin-9 has two tandem CRDs with a short linker peptide, and we report here the crystal structures of mouse and human galectin-9 N-terminal CRDs (NCRDs) in the presence of the *N*-acetyllactosamine dimer (LN2, Gal $\beta$ 1-4GlcNAc $\beta$ 1-3Gal $\beta$ 1-4GlcNAc). The structure of mouse galectin-9 NCRD forms the unique dimer, which is quite different from the canonical 2-fold symmetric dimer seen for galectin-1 and 2. We also observed that the mouse galectin-9 NCRD interacts with each other in solution as indicated by surface plasmon resonance measurements. On the other hand, human galectin-9 NCRD exists as monomer in crystals and the amino acid residues on the mouse galectin-9 NCRD dimer interface are not conserved. The recognition mechanisms of the LN2 molecule are quite different from each other. Dimeric mouse galectin-9 NCRD recognizes  $\beta$ -galactoside residue at the non-reducing end and cooperatively interacts with LN2 molecules. In the crystals of human galectin-9 NCRD in complex with LN2, there are two different types of  $\beta$ -galactoside recognition by the human galectin-9 NCRD: either the first or the third residue from the non-reducing end. A non-conserved asparagine residue in human galectin-9 NCRD allows two different types of carbohydrate recognition. We will discuss the structural difference in same proteins from the different species.

**Crystal structure of the Buffalo lactoperoxidase complex with thiocyanate at 2.75 Å resolution**

Ishfaq Ahmed Sheikh A. S. Ethayathulla Amit Kumar Singh Nagendra Singh Sujata Sharma T. P. Singh

Department of biophysics, All india institute of medical sciences, New Delhi -110029

The crystal structure of the complex of buffalo lactoperoxidase with thiocyanate has been determined at 2.75 Å resolution and refined to  $R_{\text{cryst}}$  and  $R_{\text{free}}$  factors of 0.182 and 0.216 respectively. The structure contains 4698 protein atoms, 43 heme atoms, 3 thiocyanate atoms, 4 carbonate atoms, 8 iodide ions, 1 calcium ion, 145 atoms from three glycan chains and 183 water molecules. The heme is covalently attached to the protein via two ester linkages between carboxyl groups of Asp<sup>94</sup> and Glu<sup>242</sup> and modified methyl groups on pyrrole rings of the heme group. In addition to these linkages, residues Ala<sup>100</sup>, Arg<sup>333</sup>, His<sup>337</sup> and Arg<sup>424</sup> interact through hydrogen bonds. The Ca<sup>2+</sup> ion is held in a coordination sphere with pentagonal pyramidal geometry. A single carbonate ion is held in a positively charge environment created by Asn<sup>81</sup>, Arg<sup>488</sup>, Arg<sup>490</sup> and NAG 1. It is a unique structure of lactoperoxidase with 8 iodide ions that are held at distal cavities. The secondary structure is largely alpha-helical with a very little beta-sheet. The structure determination has also confirmed the presence of a calcium-binding site and three sites of asparagine linked glycosylation (Asn<sup>189</sup>, Asn<sup>225</sup> and Asn<sup>317</sup>) as well as the identities of the proximal His<sup>336</sup> and distal His<sup>95</sup>. The structure determination has also revealed a number of halide-binding sites and their possible relevance to the catalytic mechanism of the enzyme. The complex formation with thiocyanate has been also analyzed in detail.

## High-Throughput and Automated Protein Crystallography at the Photon Factory

Masahiko Hiraki Ryuichi Kato Masanori Kobayashi Yusuke Yamada Naohiro Matsugaki Noriyuki Igarashi Yurii A Gaponov Soichi Wakatsuki

PF, KEK

For high-throughput protein crystallography, we are developing a fully automated X-ray structural analysis system that consists of several subsystems for protein crystallization, harvesting and freezing crystals, exchanging samples inside a hutch and data acquisition. Obtaining X-ray quality crystals might require setting up thousands of crystallization trials on different conditions for protein solutions and precipitants. To this end, we have developed a large-scale protein crystallization system (PXS) that allowed efficient crystallization trials of large protein complexes and structure-based drug design. It includes a dispensing system using disposable tips which are specifically designed for high dispensing accuracy, an observation system for acquiring images of drops according to a pre-programmed schedule and storing them to a file server, incubators and a plate-carrying robot. Users can access the file server from anywhere in the world through a Web browser for checking the status of their crystal growth. Protein crystals which have grown large enough for X-ray diffraction experiment are harvested using cryo-loops and plunged into liquid nitrogen. In order to pick up a frozen crystal from a Dewar and mount it onto a goniometer on an X-ray diffractometer automatically, we have installed two sample exchange robots based on the SAM (SSRL Automated Mounting) systems at our insertion device beam lines BL-5A and AR-NW12A at the Photon Factory. In order to reduce the time required for sample exchange further, a prototype of a double-tong system was developed. As a result of preliminary experiments, the sample exchange time was successfully reduced from 70 seconds to 10 seconds excluding the time required for pre-cooling and warming up the tongs.

**Preliminary X-ray crystallographic studies of GLUE domain of mammalian Eap45**

Satoshi Hirano<sup>1</sup> Nobuhiro Suzuki<sup>1</sup> Thomas Slagsvold<sup>2</sup> Masato Kawasaki<sup>1</sup> Daniel Trambaiolo<sup>1</sup> Ryuichi Kato<sup>1</sup> Harald Stenmark<sup>2</sup> Soichi Wakatsuki<sup>1</sup>

Structural Biology Research Center, PF, IMSS, KEK<sup>1</sup> Department of Biochemistry, Faculty Division of the Norwegian Radium Hospital, the University of Oslo<sup>2</sup>

Mammalian Eap45 is a component of ESCRT-II (endosomal sorting complex required for transport-II) involved in the multivesicular body (MVB) protein sorting pathway. It contains a novel ubiquitin-binding domain, designated GRAM-like ubiquitin-binding in Eap45 (GLUE) domain, as it shares similarities in its primary and predicted secondary structures with phosphoinositide-binding GRAM domains. In a recent study, it has been shown that Eap45 also binds phosphoinositides, hence, indicating the interrelationship between ubiquitin recognition and phosphoinositide binding. In order to investigate the interactions among Eap45, ubiquitin and phosphoinositides, and thereby to better understand the molecular basis for the functions of Eap45, we performed overexpression, purification, crystallization and preliminary X-ray diffraction experiments of mammalian Eap45-GLUE domain.

## **Recognition of Sugar Modules by C-Terminal Half (C-Lobe) of Lactoferrin: Crystal Structure of C-Lobe Complexes with Various Saccharides**

Rafia Mir Sujata Sharma Nagendra Singh Mau Sinha A. S. Ethayathulla R. Prem Kumar Punit Kaur Tej. P. Singh

Department of Biophysics, All India Institute of Medical Sciences, New Delhi-110029.

Lactoferrin is an iron-binding protein with a bilobed structure. Each lobe contains a high affinity binding site for a single  $\text{Fe}^{3+}$  ion and an associated  $\text{Co}_3^{2-}$  ion. In addition to it, lactoferrin is involved in various other roles. In order to identify new binding sites in lactoferrin, it is desirable to focus lobe-wise. Therefore, lactoferrin was hydrolyzed with proteinase K to generate N- and C- lobes. Lobes were purified and the purified C-lobe was used for determining the sugar binding sites on the C-lobe. It was co-crystallized with sugars, mannose, galactose, xylose, lactose, glucose, N-acetylglucosamine and sucrose, and their crystal structures were determined. A unique sugar binding site was identified to which different types of sugars bound repeatedly. Although the binding site is a shallow structure, it has preferred residues for interactions. The residues Glu 659, Tyr 660, Leu 661 and Glu 664. Atleast half a dozen hydrogen bonds are formed and an equally strong network of hydrophobic interactions has been observed. This appears to be an important site for carbohydrate recognition in the C-lobe of lactoferrin. Although its significance has not been fully understood it clearly appears to be a specific sugar binding site.

**The crystal structure of a conserved hypothetical protein, TTHA0132 from *Thermus thermophilus* HB8 with homology to the non-histone domain of macroH2A.**

Seiichiro Kishishita<sup>1</sup> Kazutaka Murayama<sup>2</sup> Takaho Terada<sup>1</sup> Mikako Shirouzu<sup>1</sup> Seiki Kuramitsu<sup>1</sup> Shigeyuki Yokoyama<sup>1</sup>

RIKEN GSC<sup>1</sup> Tohoku Univ.<sup>2</sup> RIKEN Harima<sup>3</sup>

We solved the crystal structure of a hypothetical protein, TTHA0132 from *Thermus thermophilus* HB8 at 1.77Å resolution. TTHA0132 indicates 35% homology against macro-domain on histone protein, macroH2A. The structure of TTHA0132 has a mixed alpha/beta fold that closely resembles the N-terminal DNA binding domain of the *Escherichia coli* leucine aminopeptidase, PepA. Karras *et al.* reported that the macro-domain contains ADP-ribose binding site [1]. In the crystal structure of TTHA0132, this binding site for ADP-ribose is highly conserved. These results suggest that the TTHA0132 plays an important role on ADP-ribosylation. We will discuss about the functions of TTHA0132 based on the structure.



**Reference**

- [1] Karras, G.I., Kustatscher, G., Buhecha, H.R., Allen, M.D., Pugieux, C., Sait, F., Bycroft, M. & Ladurner, A.G. *Embo J* 24, 1911-20 (2005).

## Structural analysis of putative transcriptional repressors from *Streptomyces coelicolor* A3(2) by the S-SAD method

Kazuya Kondo<sup>1</sup> Takeshi Hayashi<sup>2</sup> Nobuhisa Watanabe<sup>1</sup> Isao Tanaka<sup>1</sup>

<sup>1</sup>Graduate School of Science, Hokkaido University<sup>2</sup> Department of Food and Bioscience, Faculty of Food and Nutrition, Beppu University<sup>2</sup>

*Streptomyces coelicolor* A3(2) is a representative of the group of soil-dwelling, filamentous bacteria responsible for producing most natural antibiotic used in human and veterinary medicine. It is predicted that numerous regulatory genes are contained in the genome of *S. coelicolor* A3(2), and they are likely to adapt to a wide range of environmental condition. To reveal the regulatory mechanism of antibiotic and other useful secondary metabolite makes it possible to develop useful material production system by actinomycetes.

In the genome of *S. coelicolor* A3(2), it is estimated that 150 putative TetR family regulatory proteins are encoded. They control gene expression of their products that are involved in multidrug resistance, enzymes implicated in catabolic pathway, biosynthesis of antibiotics and so on. These proteins have two domains; a C-terminal regulatory domain and an N-terminal DNA-binding domain which contains highly conserved helix-turn-helix motif. Despite of a high degree of sequence similarity at the DNA-binding domain, structural determination of those proteins by molecular replacement has difficulty for low similarity at the regulatory domain. To elucidate the transcriptional mechanism, we attempt the S-SAD method, which means Single wavelength Anomalous Diffraction method using Sulfur atoms in the protein as anomalous scatterers, for analyzing crystal structure of transcription factors. Our targets are putative TetR family regulatory proteins; SCO0241, SCO0332, SCO7518, SCO7651 and SCO7815, and their  $\Delta F/F$  value at Cr/Cu K $\alpha$  radiation are expected as 1.653/0.806, 1.045/0.509, 1.086/0.529, 1.221/0.595 and 1.425/0.694 by those sulfur contents, respectively. In this conference, we'll discuss the results of in-house S-SAD method for structural determinations.

**Specific and non-specific interactions of water molecules between protein and DNA**Chin-Yu Chen<sup>1</sup> Tzu-Ping Ko<sup>2</sup> Chi-Rung Lee<sup>3</sup> Andrew H.-J. Wang<sup>1\*</sup><sup>1</sup>Institute of Chemistry, Academia Sinica<sup>2</sup> Institute of Biological Chemistry, Academia Sinica<sup>3</sup> Department of Chemical Engineering, Minghsin University of Science and Technology<sup>4</sup>

Recent surveys of high-resolution protein-DNA crystal structures have noted that solvent molecules are commonly present within the protein-DNA interfaces. Indeed, water-mediated interactions can be as common as direct H-bonds or salt links. Putting these results together has revealed that protein-DNA complexes are quite diverse in their use of water. In the non-sequence specific DNA binding proteins, interfacial water molecules may act as "modulators" for their binding to DNA of varying sequence without adding specificities. When sequence specific DNA binding proteins bound to non-cognate DNA, more waters remained at the interface of the complexes. These waters may behave as a kind of molecular glue allowing the protein to scan along the DNA for their specific binding sites. In different protein-DNA complexes, we also find that proteins switch their specificity, i.e., conversion of a nonspecific to a specific complex by replacing using water-mediated hydrogen bond interactions with direct hydrogen bond contacts. In many others, however, two to four water molecules remain at the interface and these play an important role in the specificity of recognition, in some cases facilitating a fluctuating network of hydrogen bonds between the sequence specific protein and DNA. Since DNA hydration patterns are sequence dependent, proteins recognize the DNA hydration structures rather than DNA sequence upon forming the complexes.

## Current Status of Public Beamlines for Protein Crystallography at SPring-8

Masahide KAWAMOTO<sup>\*</sup> Kazuya HASEGAWA<sup>\*</sup> Nobutaka SHIMIZU<sup>\*</sup> Hisanobu SAKAI<sup>\*</sup> Tetsuya SHIMIZU<sup>\*\*</sup> Kunio HIRATA<sup>\*\*</sup> Atsushi NISAWA<sup>\*\*</sup> Masaki YAMAMOTO<sup>\*\*\*</sup>

Research & Utilization Division, Japan Synchrotron Radiation Institute (JASRI)<sup>\*</sup> SPring-8/  
RIKEN<sup>\*\*</sup> SPring-8/JASRI, SPring-8/RIKEN<sup>\*\*\*</sup>

There are 9 beamlines for protein crystallography at SPring-8 as of May 2006. Two beamlines, BL38B1 (Structural Biology III) and BL41XU (Structural Biology I), out of them are dedicated for public uses.

The BL38B1 is designed based on a standard SPring-8 bending magnet beamline, consisting of a Si(111) double crystal monochromator and a 1m-long Rh-coated cylindrical bend mirror, and used for routine protein crystallography, including the "Mail-in data collection system". The installation of sample changer robotics, control and database system have already finished. Now we are doing final check of the entire system.

The BL41XU is an undulator beamline using the SPring-8 standard in-vacuum undulator as the light source. The undulator beam is monochromatized by rotated-inclined Si(111) double crystal monochromator, and focused by KB mirrors. Utilizing this high brilliant X-ray beam, we are focusing on a measurement in ultra-high resolution and a data collection from micro-crystals. The large area detectors and very short wavelength X-ray from undulator 3rd harmonics enables to collect diffraction spots over 0.5 Å resolution. We have succeeded to collect a dataset of Endopolygalacturonase I at 0.68 Å resolution ( $R\text{-free} = 10.8\%$ ). To collect efficient quality data from micro-crystals, it is necessary to use micro-beam to reduce the background noise. Presently, the size of 25 $\mu\text{m}$  beam with  $\sim 10^{11}$  photons/sec was achieved, and we could collect a dataset from lysozyme crystal sized  $\sim 20\mu\text{m}$  up to 1.9 Å resolution ( $R\text{-merge} = 6\%$ )

## **Crystal Structure Model-Assembly Program Using the Monte Carlo Method**

HIROYUKI MIURA

Department of Earth and Planetary Science, Hokkaido University

In order to study an unknown crystal structure by the Rietveld method, a correct structure model must be prepared in advance. This is usually very difficult when no information is available about the structure. A newly developed program, which automatically constructs a crystal structure model of the object-material, would simplify the process of solving the structure of the powdered material. This program requires XRD data, cell constants, a space group, a chemical formula, and a Z-number (the number of the formula in a unit cell). On the basis of atomic positions selected by the Monte Carlo method, this program calculates the R-factor of the model from theoretical and observed XRD data. Hundreds of models of a low R-factor are selected and stored. Then, they gradually converge to a true structure. Using this program and a personal computer, several unknown crystal structures could be solved, which demonstrates that this method is a powerful tool to solve the simple crystal structure of powder materials.

## Membrane Protein Crystallization under High Pressure

Hiroshi Y. Yoshikawa<sup>1</sup> Shinya Nakata<sup>1</sup> Ryota Murai<sup>1</sup> Tomoya Kitatani<sup>1</sup> Maki Syou<sup>1</sup> Hiroaki Adachi<sup>1</sup>  
 Tsuyoshi Inoue<sup>2</sup> Hiroyoshi Matsumura<sup>2</sup> Kazufumi Takano<sup>2</sup> Satoshi Murakami<sup>3</sup> Yusuke Mori<sup>3</sup>  
 Takatomo Sasaki<sup>3</sup>

<sup>1</sup> Graduate School of Engineering, and CREST JST, Osaka University; <sup>2</sup> Graduate School of Engineering, Osaka University, SOSHO Inc, and CREST JST, Japan; <sup>3</sup> The Institute of Scientific and Industrial Research, Osaka University, SOSHO Inc, and CREST JST, Japan

In protein crystallogenes, pressure is an attractive physical parameter because it can influence structure and/or association of macromolecules in solution. In principle, it affects only the volume of a system and the change in energy is better defined thermodynamically while temperature causes simultaneous changes in the volume and thermal energy of a system. Hence, preliminary pressure studies of model proteins like lysozyme [1] indicated peculiar pressure effects, for example, a reduction of unit cell volume, solubility change, and so on. From the viewpoint, membrane protein seems to be an interesting candidate for a pressure study because the crystals basically have much solvent region inside. Here, we have firstly crystallized membrane protein, AcrB [2], under high pressure. AcrB solubilized with dodecylmaltoside was crystallized using PEG 2000 as a precipitant at 25 °C in specially designed high-pressure equipment. At 50 MPa, we could obtain AcrB crystals with the largest size of 150 μm, which is acceptable size for X-ray diffraction measurement. From the statistical results, the pressure dependence of the crystallization was considered.

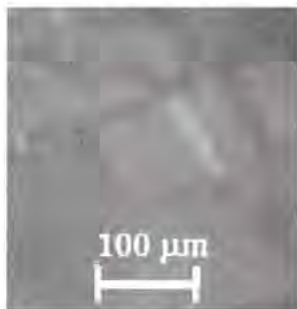
[1] A. Kadri et. al., *Acta Cryst.* **D61** (2005) 784.

[2] S. Murakami et. al., *Nature* **419** (2002) 587.

High pressure equipment



AcrB crystals grown at 50 MPa



**Structural insights into the Sec-tRNA(SeC) syntheses in archaea**Yuhei Arai<sup>o</sup> Hiroyuki Oshikane<sup>o</sup> Shuya Fukai<sup>o</sup> Dieter Soll<sup>o</sup> Ryuichiro Ishitani<sup>o</sup> Osamu Nureki<sup>o</sup>Department of Bioscience and Biotechnology, Tokyo Institute of Technology<sup>o</sup> Department of Molecular Biophysics and Biochemistry, Yale University, USA<sup>o</sup>

The 21st amino acid selenocysteine is present at the active site of selenoproteins. Selenoprotein synthesis requires translational recoding of the UGA termination codon to a selenocysteine insertion signal (SECIS). At the 3' UTR region on mRNA, there is a hairpin structure called SECIS element which is recognized by EF-Tu homologous EFSec and several related proteins. Thus SeC is incorporated into the translation reaction in ribosome. For SeC-tRNA(SeC) formation, two step reactions are required. First, tRNA(SeC) is acylated with O-phosphoserine (Sep) but not with selenocysteine directly by SepRS to form Sep-tRNA(SeC), which is then converted to SeC-tRNA(SeC) by SepSeCysS. Archaeal SepSeCysS was crystallized using the hanging-drop vapour-diffusion method. Multiwavelength anomalous dispersion (MAD) data set was collected using selenomethionyl-substituted crystals. The diffraction data set was collected at 2.5 Å resolution using synchrotron radiation and cryo-cooling. Crystals belong to the primitive monoclinic space group  $P2_1$ , with unit-cell parameters  $a = 75.7$ ,  $b = 108.1$ ,  $c = 110.4$  Å. There are four SepSeCysS molecules in the asymmetric unit. Now, we are trying to determine the structure of SepSeCysS by the multiwavelength anomalous dispersion method.

**Crystal structure of the archaeal transcription termination factor NusA**

Rie Shibata<sup>1</sup> Yoshitaka Bessho<sup>2</sup> Akeo Shinkai<sup>3</sup> Madoka Nishimoto<sup>4</sup> Emiko Fusatomi<sup>5</sup> Takaho Terada<sup>6</sup> Mikako Shirouzu<sup>7</sup> Shigeyuki Yokoyama<sup>8</sup>

Protein Research Group, RIKEN genomic science center<sup>1</sup> RIKEN Genomic Sciences Center, RIKEN SPring-8 Center Harima Institute<sup>2</sup> RIKEN SPring-8 Center Harima Institute<sup>3</sup> RIKEN Genomic Sciences Center, RIKEN SPring-8 Center Harima Institute, The University of Tokyo<sup>4</sup>

Many aspects of archaeal transcription are unknown, and especially, there is little evidence for termination mechanisms in archaea. Although the archaeal RNA polymerase (RNAP) more closely resembles the eukaryal RNAPs, bacterial transcription factor homologues are widely conserved in archaea. A homolog for bacterial transcription factor NusA is widely conserved in archaea. However, its function remained unknown since archaeal NusA consisted of only the two KH domains. In this study, we have found that *Aeropyrum pernix* NusA can strongly bind to a specific CU-rich sequence near a termination signal. This contrasts with its weak binding to the upstream portion of a hairpin region that reportedly interacts with bacterial NusA. Our crystal structure of *A. pernix* NusA suggests that its spatial arrangement is quite similar to that of the KH-domains of bacterial NusA. Remarkable differences between archaeal and bacterial NusA exist at the interface with RNAP. These evidences suggested that transcription termination in archaea is quite unique, as compared to all known bacterial and eukaryal termination systems, in terms of the use of the NusA transcription termination factor and a specific termination signal.

## Crystal Structure of a Bacteriophage-associated Hyaluronate Lyase

Parul Mishra<sup>1</sup>, V. Bhakuni<sup>1</sup>, R. Prem Kumar<sup>2</sup>, Nagendra Singh<sup>2</sup>, Sujata Sharma<sup>2</sup>, P. Kaur<sup>2</sup>, Tej P. Singh<sup>2</sup>

<sup>1</sup>Division of Molecular and Structural Biology, Central Drug Research Institute, Lucknow<sup>1</sup>  
<sup>2</sup>Department of Biophysics, All India Institute of Medical Sciences, New Delhi<sup>2</sup>

Hyaluronate lyases (HylP2) are a class of endoglycosaminidase enzymes with considerable complexity and heterogeneity. Their main function is to degrade hyaluronan, the main polysaccharide component of the host connective tissues into unsaturated disaccharide units as the final product. HylP2 was cloned, overexpressed, and purified. The recombinant HylP2 exists as a homotrimer of molecular mass about 110 kDa under physiological conditions. The enzyme shows sequential unfolding, with the N-terminal unfolding first followed by the simultaneous unfolding and dissociation of the stabilized trimeric C-terminal domain. The cloned purified protein was crystallized using hanging drop vapour diffusion method with sodium formate as precipitating agent. The crystals belong to space group H32 with cell dimensions of  $a = b = 59.6\text{\AA}$ ,  $c = 588.5\text{\AA}$ . The structure was determined and refined to an  $R_{\text{cryst}}$  factor of 22.3% ( $R_{\text{free}}$  factor of 23.6%). The final model contains 2518 protein atoms. The structure shows elongated molecule having a middle wider region made up of antiparallel  $\beta$ -strands, whereas the N and C-termini contain two and one  $\alpha$ -helices respectively. The active site is located in the middle part of the structure. There are three molecules of HylP2 intertwined together with a large number of intermolecular interactions between them to form a highly stable and biologically active homotrimer. The structure shows remarkable differences in the loop region A122 to S129, which lies near the active site residues, N135, D137 and Y149. This loop is probably involved in determining the substrate specificity of the enzyme.

## Structural studies on the SUF proteins involved in the biogenesis of iron-sulfur clusters

Norika Sumi<sup>1</sup>, Kei Wada<sup>1</sup>, Shintaro Kitaoka<sup>1</sup>, Kei Suzuki<sup>1</sup>, Yuko Hasegawa<sup>1</sup>, Yoshiko Minami<sup>2</sup>, Yasuhiro Takahashi<sup>1</sup>, Keiichi Fukuyama<sup>1</sup>

<sup>1</sup>Department of Biology, Graduate School of Science, Osaka University; <sup>2</sup>Department of Biochemistry, Faculty of Science, Okayama University of Science, Japan

Iron-sulfur (Fe-S) clusters are cofactors of Fe-S proteins that are required for a wide variety of biological processes, such as electron transfer, redox and non-redox catalysis, and the regulation of gene expression. The cellular assembly of the Fe-S clusters requires multicomponent systems, of which the SUF machinery, encoded in *E.coli* by the *sufABCDSE* operon, is conserved in the three domains of life. Among the SUF components involved, SufS (cysteine desulfurase) and SufE work in concert as a sulfur donor for the Fe-S clusters. The precise roles of the remaining components have yet to be elucidated, though SufC has a weak ATPase activity and forms a soluble complex with SufB and SufD.

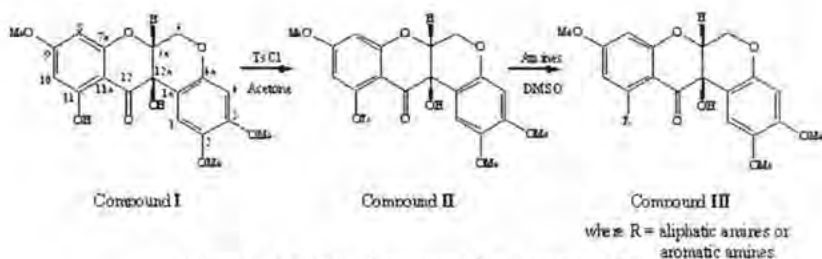
Here we report the crystal structures of the SufC monomer, the SufD dimer and the SufCD complex. SufC shows a structure similar to the ABC-ATPases. Interestingly, SufC has a unique salt-bridge that binds one catalytic residue (Glu171) to another domain, suggesting a regulatory mechanism of the ATPase activity. The SufD protein has three domains, the N-terminal helical domain, the core-domain comprising a right-handed parallel  $\beta$ -helix, and the C-terminal helical domain. The dimer interface of the SufD is held primarily by hydrogen bonds that form anti-parallel  $\beta$ -sheets. The crystal structure of the SufCD complex, consisting of two SufC monomers and a SufD dimer (SufC<sub>2</sub>D<sub>2</sub>), revealed the interaction between the Q-loop of SufC and the C-terminal helical domain of SufD. Of interest are the structural rearrangements of SufC including the cleavage of the key salt-bridge, which may occur upon association with SufD and allow interaction between the SufC monomers for ATP binding and hydrolysis. Possible interactions among SufB, C and D during the Fe-S cluster formation will be discussed.

## Crystal structures of 6-deoxyclitoriactal and its derivatives

Thapong Teerawatananond Nustha Kitpratuang Nattaya Ngamrojnavanich Wilaiwon Tirawanich Amorn Petsom Nongnuj Muangsin

Research Centre for Bioorganic Chemistry, Department of Chemistry, Faculty of Science, Chulalongkorn University

6-Deoxyclitoriactal is a substance extracted from the dried roots of *Stemona collinsae* Craib. It has been known to have a cytotoxic activity against various types of human carcinoma possibly due to its ability to intercalate with DNA as evidenced *in vitro* assay [1]. In order to enhance its activity, Compound I was derivatised to contain a functional group with more flexible and can be participated hydrogen bonding with DNA. The derivatives of 6-deoxyclitoriactal were prepared as shown in scheme 1. In this work, we studied the relationship between crystal structures, hydrogen bonding and cytotoxic activity of 6-deoxyclitoriactal and its derivatives based on spectroscopic and x-ray crystallographic techniques.



Scheme 1. Synthesis of compound II and compound III.

## Reference

- [1] Lin, L. J.; Ruangrungrri, N.; Cordell, G. A.; Shieh, H. L.; Min, Y.; Pezzuto, J. M., *Phytochemistry*, **31**, (1992), 4329-4331.

## Design of Specific Peptide Inhibitors of Phospholipase A<sub>2</sub>: Crystal Structures of two Complexes of Phospholipase A<sub>2</sub> with Two Pentapeptides

Rishi K. Somvanshi<sup>1</sup> Nagendra Singh<sup>1</sup> Sujata Sharma<sup>1</sup> Markus Perbandt<sup>2</sup> Christian Betzel<sup>2</sup> Sharmistha Dey<sup>1</sup> Tej P. Singh<sup>1</sup>

Biophysics, All India Institute of Medical Sciences<sup>1</sup> Institute of Medical Biochemistry and Molecular Biology, University of Hamburg, c/o DESY, 22603, Hamburg, Germany<sup>2</sup>

Phospholipase A<sub>2</sub> (PLA<sub>2</sub>) is an important target for the design of anti-inflammatory drugs. The structure of PLA<sub>2</sub> has shown that the substrate-binding channel contains inner hydrophobic face with Asp49 and His 48 at the end of the channel. In order to fit into such a substrate-binding channel, two new peptides Phe - Leu - Ser - Thr - Lys (FLSTK) and Phe - Leu - Ala - Tyr - Lys (FLAYK) were synthesized. The analysis of data obtained from the binding studies with Surface Plasmon Resonance gave dissociation constants (K<sub>d</sub>) of  $2.5 \times 10^{-8}$  M and  $1.4 \times 10^{-8}$  M respectively. PLA<sub>2</sub> was co-crystallized with both peptides. The X-ray intensity data were collected using synchrotron beamline to 1.2 Å and 1.7 Å respectively. The crystal structures were determined with molecular replacement method and refined to R factors of 19.2% and 17.5% respectively. The excellent qualities of electron densities were observed for the both peptides at the substrate-binding site. As per the design strategy in both complexes, the Lys residue formed ionic interactions with Asp 49. We also observed several solvent mediated hydrogen bonds and van der Waals interactions between PLA<sub>2</sub> and the peptides. The overall conformations of peptides were similar except at residues 3 and 4 because these residues were different in two peptides. The protein residues of the substrate-binding site in the two complexes have similar conformations as observed in the native PLA<sub>2</sub> structure. However, the side chains show considerable rotations about various bonds. Both peptides form tight complexes with PLA<sub>2</sub> and block the enzyme activity. These and other peptides with high binding affinities provide important leads for developing useful anti-inflammatory agents.

## The Crystallographic Study of Apple Latent Spherical Virus

Hisashi Naitow<sup>1</sup> Masamichi Isogai<sup>2</sup> Nobuyuki Yoshikawa<sup>2</sup> Shigeyuki Yokoyama<sup>1</sup>

<sup>1</sup>Advanced Protein Crystallography Research Group, RIKEN SPring-8 Center<sup>2</sup> Department of Agriculture, University of Iwate, Japan<sup>2</sup>

We did crystallization of apple latent spherical virus (ALSV) and X-ray diffraction data collection on a crystal of ALSV. In this time, we clarified the packing form of ALSV particle in the crystal lattice. ALSV particles were purified from *Chenopodium quinoa* infected by ALSV and crystallized by Hanging drop vapor diffusion method. We tried over 100 crystallization conditions and got good ALSV crystal. The X-ray diffraction data was collected under cryogenic conditions (100K) at SPring-8 BL45XU and BL44B2(RIKEN SPring-8 Center Hyogo, Japan). The data were processed using HKL2000 to show a unit cell of dimensions  $a = 335.1$ ,  $b = 313.8$ ,  $c = 350.3$ ,  $\alpha = 90.0$ ,  $\beta = 90.2$ ,  $\gamma = 90.0$  and space group  $P2_1$ . There are the diffraction spots over 3 angstrom resolution. The rotation function derived from the diffraction data show the icosahedral symmetry and an orientation of ALSV particle in crystal lattice.

## Biochemical and structural analyses of cooperative inhibition mechanism of 1,2- $\alpha$ -L-fucosidase (AfcA) by deoxyfuconojirimycin and lactose

Atsuko Tsuchiya<sup>1</sup> Masamichi Nagae<sup>2</sup> Soichi Wakatsuki<sup>3</sup> Ryuichi Kato<sup>2</sup> Takane Katayama<sup>3</sup> Kenji Yamamoto<sup>1</sup>

Graduate School of Biostudies, Kyoto University<sup>1</sup> Structural Biology Research Center, Photon Factory, Institute of Materials Structure Science, High Energy Accelerator Research Organization (KEK)<sup>2</sup> Research Institute for Bioresources and Biotechnology, Ishikawa Prefectural University<sup>3</sup>

Fucosidases have been used as a powerful tool to elucidate the function of  $\alpha$ -L-fucosyl residues. Recently, we had cloned a gene encoding  $\alpha$ -(1-2)-specific fucosidase (*afcA*), which comprises 1959 amino acids, from *Bifidobacterium bifidum*. We also showed that the middle of the polypeptide chain (Fuc domain) is responsible for the catalytic activity. We determined the crystal structure of Fuc domain of the apo form at 1.12 Å resolution and propose its catalytic mechanism.

To further investigate the biochemical aspects of Fuc domain, we searched for inhibitors of this enzyme and found that L-fucose or lactose weakly inhibits the fucosidase activity with a  $K_i$  value of mM range, and deoxyfuconojirimycin (DFJ) which is an analogue of  $\alpha$ -L-fucose competitively inhibits the activity with a  $K_i$  value of 42  $\mu$ M. We solved the crystal structure of the Fuc domain in complex with DFJ at 2.1 Å resolution. In the structure, DFJ bound to the putative catalytic pocket of the protein. Furthermore, we found that lactose synergistically inhibits the activity in the presence of DFJ. To elucidate the synergistic inhibition mechanism, we also determined the crystal structure of the Fuc domain in a ternary complex with DFJ and lactose. In this structure, the position of DFJ is identical to that of sole DFJ in the binary complex and the galactose moiety of lactose is deeply buried into the catalytic pocket, which prevents the release of DFJ from the protein. Based on these observations, we will discuss the inhibition mechanism of DFJ and the synergistic effect of lactose.

## Crystal structures of crotoembraneic acid and neocrotoembraneic acid

Wilaiwon Tirawanich<sup>1</sup> Thapong Teerawatananond<sup>2</sup> Narongsak Chaichit<sup>1\*</sup> Amorn Petsom<sup>2</sup>

<sup>1</sup>Department of Chemistry Faculty of Science, Chulalongkorn University<sup>2</sup> Department of Physics, Faculty of Science and Technology, Thammasat University, Bangkok, Thailand.

Two cembranoids, crotoembraneic acid, (1*E*,3*E*,7*E*,11*Z*)-1-isopropyl-4,8-dimethylcyclotetradeca-1,3,7,11-tetraene-12-carboxylic acid (**1**) and neocrotoembraneic acid, (1*E*,3*E*,7*E*,11*E*)-1-isopropyl-4,8-dimethylcyclotetradeca-1,3,7,11-tetraene-12-carboxylic acid (**2**), C<sub>20</sub>H<sub>30</sub>O<sub>2</sub>, were isolated from *Croton oblongifolius* Roxb. which had been used as Thai traditional medicine to treat human gastrointestinal track. In this work, we revealed their differences in *Z*- and *E*- molecular configurations by X-ray analysis. Cembranoids **1** and **2** were crystallized in space groups monoclinic *P2<sub>1</sub>/a* and triclinic *P(1)* with their unit cell parameters *a*=9.8513(5)Å, *b*=10.5630(10)Å, *c*=18.5873(11)Å, β=102.136(2)° and α=7.64120(10)Å, *b*=9.7269(2)Å, *c*=13.11200(10)Å, α=95.387(0)°, β=98.222(1)°, γ=98.899(1)°. Dihedral angles C10-C11-C12-C13 of **1** and **2** were -175.24(0.30)° and -2.08(0.30)°, respectively. Both stereoisomers formed a pair of inter-molecular hydrogen bonding between the hydroxyl and carbonyl groups. The crystal packing of **1** showed the O2H...O1 hydrogen bond distance of 2.626(3)Å, which was slightly shorter than a hydrogen bond of 2.6433(19)Å in molecular crystal **2**.

### Reference

- [1] Roengsumran S., Achayindee S., Petsom A., Pudhom K., Singtothong P., Surachetapan C., Vilaivan T., Two new cembranoids from *Croton oblongifolius*, *J. Nat. Prod.*, **61**, (1998), 652-654.

**Crystal structure of CbiL (CT0388), a methyltransferase involved in anaerobic biosynthesis of vitamin B<sub>12</sub>**Kei Wada<sup>1</sup> Jiro Harada<sup>2</sup> Hirozo Oh-oka<sup>1</sup> Hitoshi Tamiaki<sup>2</sup> Keiichi Fukuyama<sup>1</sup><sup>1</sup>Department of Biology, Osaka University<sup>2</sup> Department of Bioscience and Biotechnology, Ritsumeikan University

Vitamin B<sub>12</sub> (cobalamin) contains a cobalt-centered corrin ring (modified tetrapyrrole ring) that belongs to the same family of the metalloprosthetic groups as heme and chlorophyll. Vitamin B<sub>12</sub> biosynthesis represents one of the most complex metabolic pathways in nature, requiring approximately 30 enzymes to complete *de novo* synthesis. One of the unique features of Vitamin B<sub>12</sub> biosynthesis is the addition of eight methyl groups derived from *S*-adenosylmethionine to the tetrapyrrole framework during corrin construction. These methyl groups are added by the six separate methyltransferases. An *S*-adenosylmethionine-dependent methyltransferase CbiL catalyzes methylation at the C-20 position of the tetrapyrrole moiety. Interestingly, in subsequent step, both the methyl group and the C-20 carbon are lost during the ring contract process, extruded as acetaldehyde; the tetrapyrrole ring is converted to a corrin ring. Thus, the methylation of C-20 position is a key modification for the ring contract process, however, the methylation mechanism including the substrates recognition underlying the biosynthesis of vitamin B<sub>12</sub> is poorly understood.

Recombinant *Chlorobium tepidum* CbiL overproduced in *Escherichia coli* was purified, and crystallized by the hanging-drop vapor-diffusion method. A native data set was collected to 2.1 Å resolution using synchrotron radiation at SPring-8. The initial phase was obtained by the molecular replacement. Model building and structure refinement are currently in progress.

**Crystallographic Study of *Saccharomyces cerevisiae* Vac8p**Yoshiki Nagano<sup>1</sup>, Shuya Fukai<sup>2</sup>, Osamu Nureki<sup>1</sup>

Department of Biological Information, Graduate School of Bioscience and Biotechnology, Tokyo Institute of Technology<sup>1</sup>, Center for Biological Resources and Informatics, Tokyo Institute of Technology<sup>2</sup>

A single cell divides into mother and daughter cells during proliferation in a budding yeast, *Saccharomyces cerevisiae*. In this process, vacuole is fragmented and distributed in each cells. This vacuole inheritance process requires the MyosinV family protein, Myo2p. Myo2p and its adaptor proteins, Vac8p and Vac17p, form a complex and transport the vacuoles along cytoskeletal actin filaments. Vac8p contains an armadillo repeat motif and has been found to be necessary for the vacuolar inheritance, cytoplasm-to-vacuole protein targeting pathway, formation of the nucleus-vacuole junction, vacuole-vacuole fusion, and caffeine resistance. Armadillo repeat is a typical structural motif to mediate protein-protein interactions. For instance,  $\beta$ -catenin is essential for the Wnt signaling pathway and cadherin-based cell adhesion. A nuclear transport factor, Importin- $\alpha$ , recognizes its cognate nuclear localization signals to achieve selective nuclear import. Similarly, the armadillo repeats of Vac8p might be involved in the vacuole/cargo recognition. Here, we report the result from the preliminary crystallographic analysis of *S. cerevisiae* Vac8p. Vac8p was overproduced in *Escherichia coli* as a glutathione S-transferase (GST) fusion protein. The GST-tag was cleaved after purification by a glutathione column, and purified by anion-exchange, and size-exclusion columns. The purified Vac8p protein was crystallized using the vapor-diffusion method at 293 K. The Vac8p crystal diffracted X-ray up to 3.8 Å at BL41XU, SPring8. The crystal belongs to the space group *P2*, with unit-cell parameters,  $a = 300.6$  Å,  $b = 130.1$  Å,  $c = 300.9$  Å,  $\beta = 118.7$ . Refinement of the crystallization condition is in progress.

## Structural analysis of a DNA tetrahedron by electron cryomicroscopy

Takayuki Kato<sup>1</sup>, Russell Goodman<sup>2</sup>, Richard Berry<sup>2</sup>, Andrew Turberfield<sup>2</sup>, Keiichi Namba<sup>1</sup>

<sup>1</sup>Graduate School of Frontire Biosciences, Osaka university<sup>1</sup>, <sup>2</sup>Department of Physics, University of Oxford, United Kingdom<sup>2</sup>

The bottom-up approach to making nano-scale structures can mass-produce various nano-structures if self-assembly can be utilized and therefore is potentially more advantageous than the top-down approach. DNA is an ideal material for nanofabrication of rigid structures because it can be designed by base pairing of specific sequences and is relatively inexpensive and simple to execute.

We synthesized four single-stranded DNAs that are designed to form a stable tetrahedral structure. Stoichiometric mixtures of these four DNAs were heated to 95°C for 2 minutes and then cooled to 4°C over 30 seconds to let them form base pairs. The DNA tetrahedra thus produced were run on a 6% PAGE gel, and an appropriate band was cut out and eluted using the crush and soak method. Then purified tetrahedra were examined by electron cryomicroscopy (cryo-EM). Simple selection of particle images proved impossible because of the low contrast due to the small size of the objects (10nm). We therefore merged two images of the same area recorded at different defocus values by using a Wiener filter. This resulted in higher contrast, and single particle image analysis was successfully carried out to reconstitute the structure of the DNA tetrahedron at 20 Å resolution. The structure was close to what was designed, having an edge length of 7 nm that correlates well with the 20 bp length. We believe that this is the smallest structure revealed by cryo-EM and single particle image analysis, and this fast and simple method would be valuable in 3D nanofabrication.

## CCP4 : 6.0 and beyond

Charles C Ballard

CCP4/CSE, CCLRC

Earlier this year version 6.0 of the CCP4 suite for macromolecular crystallography was released. As well as updates of all the old favourites , such as *MOSFLM*, *SCALA* and *REFMAC5*, this release contained major new software for molecular graphics, *COOT* and *CCP4MG*, molecular replacement, *CHAINSAW* and *PHASER-MR*, and density modification, *PIRATE*. Plus, *BP3*, *SSM* and many other updates and improvements.

Early 2007 will see the release of 6.1 which will include the experimental phasing model building program *BUCCANEER*, an updated interface for *MOSFLM*, the automated molecular replacement pipeline *Mr BUMP*, validation tool *RAPPER*, and much more.

**Substrate recognition mechanism of L-lactate oxidase from *Aerococcus viridans* at 2.0Å resolution**

Yasufumi Umena<sup>1</sup> Kazuko Yorita<sup>2</sup> Takeshi Matsuoka<sup>3</sup> Akiko Kita<sup>4</sup> Kiyoshi Fukui<sup>5</sup> Tomitake Tsukihara<sup>6</sup> Yukio Morimoto<sup>7</sup>

Research Reactor Institute, Kyoto University, Japan<sup>1</sup> Institute for Enzyme Research, University of Tokushima, Japan<sup>2</sup> Fine Chemicals & Diagnostics Division, Asahi Kasei Pharma, Japan<sup>3</sup> Institute for Protein Research, Osaka University, Japan<sup>4</sup>

L-lactate oxidase (LOX) from *Aerococcus viridans* belongs to the  $\alpha$ -hydroxyacid oxidizing ( $\alpha$ -HAO) flavoprotein family. LOX catalyzes the oxidization of L-lactate to pyruvate by abstracting two hydrogen atoms. We determined the crystal structure of wild type LOX to 2Å resolution. This molecule forms the tetramer possessing a circular four-fold symmetry. Each monomer consists of a typical  $\alpha$ 8/ $\beta$ 8 TIM barrel structure and carries one FMN molecule as a cofactor bound at the carboxyl end of  $\beta$  strand barrel. The region around the N5 atom of FMN isoalloxazine ring on the *si*-side is accessible to the solvent in the catalytic site. Two arginine, Arg-181 and Arg-268, and one histidine, His-265, are conserved in the family and located above the *si*-side of FMN molecule in the active site. In this study, we carried out three mutants, R181M, R268M and H265Q, where the positively charged amino acid residues were replaced to non-charged ones, methionine and glutamine. These mutants showed dramatic decrease in the enzyme catalytic activity, and suggested that these residues, His-265, Arg-181 and Arg-268, are important for  $\alpha$ -HAO catalytic mechanism. In this report, we also determined the crystal structures of these mutants with 2 Å resolution. We suggested for the role of these residues in catalytic activity from the structures that both Arg-181 and Arg-268 may work for the binding of substrates and His-265 is the catalyst for abstracting a proton from  $\alpha$ -hydroxyacid. We also discuss the accessibility of the substrates to the active site by the location of water molecules and other structural feature.

## Construction of Comprehensive Protein-Analysis Database and its Applications

Ryogo Akasaka Machiko Hirafuji-Yamaguchi Akiko Urushibata Kazutaka Murayama Chie Takemoto-Hori Noboru Ohsawa Mutsuko Kukimoto-Niino Kanna Motoyama Mari Aoki Takaho Terada Mikako Shirouzu Shigeyuki Yokoyama

Genomic Sciences Center, RIKEN Yokohama Institute

The comprehensive protein-analysis database is essential for high-throughput protein analyses, because the number of those will become enormous, so that it will make difficult to reach necessary data. It is not only gathering data, but also it enables researchers to find out necessary data immediately and to extract easily statistics of protein crystallization conditions for instance.

We constructed the protein-analysis database for administrating or examination of many measured data for proteins. The results were recorded by researchers who examined each protein with analytical systems that are mass spectrometry (MALDI-TOF and Q-TOF), dynamic/static light scattering (DLS/SLS), electrophoresis, etc.

To investigate the protein crystallization conditions, we considered DLS and Native-PAGE data. These have been applied to evaluate protein samples in solution. In general, if the value of polydispersity of DLS measurement is very high, it is difficult to crystallize. In addition, contamination and/or aggregation, which are detected in electrophoresis as sub-bands, are also not suitable for crystallization. DLS and Native-Page analysis can judge sample condition whether sample has sufficient quality for crystallization. Analyzing these data, we examined the efficiency of crystallization. As a result, it is found that tight relationship between crystallization conditions and analytical values (the polydispersity of DLS and the presence of contamination/aggregations of samples).

As a new application of this crystallization database, our co-worker has already applied it for prediction of crystallization conditions, and reported in CSJ2005 (F. Konishi et al). We hope that the database can be used not only for a data platform but also for a new data mining tool.

## Parameters for specification of sharpness in powder diffraction peak shape

Takashi Ida

Ceramics Research Laboratory, Nagoya Institute of Technology

Powder diffraction peak profile is characterized by the intensity, position, line width, asymmetry and sharpness in peak shape. Those characteristics can be uniquely determined for finite-range peak profile functions by the moments of the function. The zeroth, first, second, third and fourth-order moments are respectively connected with the integrated intensity, mean position, standard deviation, asymmetry and kurtosis (sharpness in peak shape). However, it is well known that the moments higher than zeroth order cannot be defined for the Lorentzian function, while it is often observed that the experimental diffraction peak profiles have nearly Lorentzian-like characters. The higher order moments can neither be defined for the Laue function, which is the most elementary theoretical diffraction peak profile function.

In this study, the author has defined a kind of moments for the Fourier transform of the profile function (Fourier mean width and curvature width), and compared them with the integral breadth, full width at half maximum and Fourier initial slope for typical diffraction peak profile functions, Gaussian, Lorentzian, pseudo-Voigt, Voigt, Pearson VII, Laue and theoretical size broadening profile for log-normally distributed spherical crystallites (SLN profile). It is shown that the ratio of the Fourier mean width to integral breadth of a function can be treated as the indicator of the sharpness, and well represents the apparent characters of peak shape.

It is expected that application of this indicator of the sharpness will provide appropriate models or effective approximations for such a complicated theoretical peak profile functions as the SLN profile.

## Crystal Structure of Human Prostacyclin Synthase

Chia-Wang Chiang<sup>1</sup>, Hui-Chun Yeh<sup>2</sup>, Lee-Ho Wang<sup>2\*</sup>, and Nei-Li Chan<sup>1\*</sup>

<sup>1</sup>Institute of Biochemistry, College of Life Sciences, National Chung Hsing University, Taichung City 402, Taiwan. <sup>2</sup>Division of Hematology, Department of Internal Medicine, University of Texas Health Science Center at Houston, 6431 Fannin, Houston, TX 77030, USA.

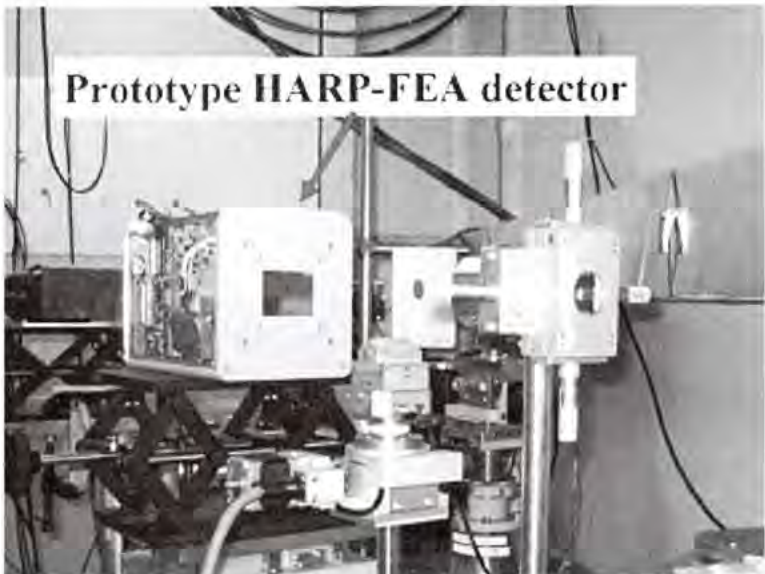
Prostacyclin synthase (PGIS) catalyzes an isomerization of prostaglandin H<sub>2</sub> to prostacyclin, a potent mediator of vasodilation and anti-platelet aggregation. Here we report the crystal structure of human PGIS at 2.15 Å resolution, which represents the first three-dimensional structure of a Class III cytochrome P450. While notable sequence divergence has been recognized between PGIS and other P450s, PGIS exhibits the typical triangular prism-shaped P450 fold with only moderate structural differences. The conserved acid-alcohol pair in the I helix of P450s is replaced by residues G286 and N287 in PGIS, but the distinctive disruption of I helix and the presence of a nearby water channel remain conserved. The side chain of N287 appears to be positioned to facilitate the peroxide bond cleavage, suggesting a functional conservation of this residue in activating oxygen. A combination of bent I helix and tilted B' helix creates a channel extending from the heme distal pocket, which seemingly allows binding of various ligands; however, residue W282, placed in this channel at a distance of 8.4 Å from the iron with its indole side chain lying parallel to the porphyrin plane, may serve as a threshold to exclude most ligands from binding. Although the primary sequence of the PGIS cysteine ligand loop diverges significantly from consensus, conserved tertiary structure and hydrogen bonding pattern are observed for this region. We also noticed that the propionate of heme ring-A forms a hydrogen bond to the apoprotein via a water bridge and that of ring-D lacks a defined structure, suggesting a somewhat plasticity of the heme lodging in PGIS.

## Development of a next-generation X-ray area detector : X-ray HARP- FEA detector

Toshinobu Miyoshi<sup>1</sup> Soichi Wakatsuki<sup>1</sup> Noriyuki Igarashi<sup>1</sup> Naohiro Matsugaki<sup>1</sup> Yusuke Yamada<sup>1</sup>  
Keiichi Hirano<sup>1</sup> Kazuyuki Hyodo<sup>1</sup> Masanori Kobayashi<sup>1</sup> Kenkichi Tanioka<sup>1</sup> Norifumi Egami<sup>2</sup> Misao  
Kubota<sup>2</sup> Teruo Kawai<sup>2</sup>

Photon Factory, IMSS/KEK<sup>1</sup> NHK science and technical research laboratories<sup>2</sup> NHK engineering  
service<sup>3</sup>

We are now developing the X-ray high-gain avalanche rushing amorphous photoconductor (HARP) detector in collaboration with NHK Engineering Service (NHK-ES), funded by the 'Development of Systems and Technology for Advanced Measurement and Analysis' program (FY2004-2009) of the Japan Science and Technology Agency (JST). The purpose of the program is to develop a new measurement system for biological macromolecules based on the HARP detector system coupled with a micro-focus beamline optimized for smaller size crystals. The detector consists mainly of amorphous selenium membrane and a matrix field emitter array (FEA). Characteristics of membrane avalanche effect and the single driven FEA show the following advantages over the currently available area detectors: (1) higher sensitivity, (2) higher spatial resolution, (3) a higher framing rate, and (4) other characteristics such as lower noise and radiation hardness. The maximum framing rate (120 frames/sec) matches the frequency of the next generation light source such as Energy Recovery Light source (ERL). The evaluation experiment of a prototype HARP-FEA detector has been performed with synchrotron light source in Photon Factory in KEK. In the presentation, the results will be shown.



## Crystal structure of *O*<sup>6</sup>-methylguanine-DNA methyltransferase

Masaru Tsunoda Nakamura T Kazuo

School of Pharmaceutical Sciences, Showa University

*O*<sup>6</sup>-methylguanine, a mutagenic, carcinogenic and toxic agent, causes base pair mismatch G:T. *O*<sup>6</sup>-methylguanine-DNA methyltransferase (MGMT) is a ubiquitous enzyme responsible for the repair of *O*<sup>6</sup>-methylguanine. The enzyme catalyzes the transfer of the methyl group from *O*<sup>6</sup>-methylguanine to the active site cysteine, preventing the incorrect base pairing. Here we report the crystal structures of MGMT from hyperthermophilic archaeon *Sulfolobus tokodaii* (*S*MGMT) to reveal the reaction mechanism of the methyl group transfer.

The crystal structure of *S*MGMT was determined by single-wavelength anomalous dispersion method at 2.0 Å resolution. In order to elucidate the reaction steps in detail, crystals of *S*MGMT were soaked in a solution of *O*<sup>6</sup>-methylguanine for four different time periods, and then they were used for X-ray diffraction experiments. The structures were determined by molecular replacement method using the apo-structure of *S*MGMT as a search model. Comparing the structures, we found that a hydrogen bond network (Glu-His-Water-Cys) in the middle of the enzyme increases the reactivity of the cysteine residue in the active site. After the reaction the network has been disrupted due to *S*-methylcysteine production. In the crystal structure of mutant C120S, another hydrogen bond network (Glu-His-Water-Ser) similar to that of the wild-type enzyme is observed in the active site, but the methyltransfer reaction does not occur. It is concluded that the hydrogen bond network is utilized for the activation of cysteine residue to facilitate the methyl group transfer.

**Crystal structure of a novel family 16 endo- $\beta$ -1,3-glucanase from *Nocardiosis* sp. F96**Takashi Kumasaka<sup>1</sup> Guntur Fibriansah<sup>2</sup> Sumiko Masuda<sup>1</sup> Satoshi Nakamura<sup>1</sup><sup>1</sup>Department of Life Science, Tokyo Institute of Technology<sup>2</sup> Department of Bioengineering, Tokyo Institute of Technology, Japan

BglF is an endo- $\beta$ -1,3-glucanase from alkaliphilic *Nocardiosis* sp. F96 which efficiently hydrolyzes insoluble  $\beta$ -1,3-glucans and shows the highest activity toward a  $\beta$ -1,3-1,4-glucan rather than  $\beta$ -1,3-glucans with optimum temperature of 70°C at pH 6.0. The crystal structure of BglF was determined at 1.3 Å resolution with SAD method of SeMet derivative. The structure shows a jellyroll  $\beta$ -sandwich consisting of seven and eight antiparallel strands whose structure is shared in the glycoside hydrolase (GH) family 16.

The comparison with other GH16 endo- $\beta$ -1,3-1,4-glucanase structures and the comparative modeling study with two substrate of  $\beta$ -1,3-1,4-glucan tetrasaccharide and laminarihexaose (consisting of  $\beta$ -1,3 linkages mainly, Figure) reveal the 16 residues contributing substrate recognition and suggest that Arg76, Trp118, Trp220 and the some additional loops narrowing the active site might play an important role in the recognition of its substrate. Several possible features including clustered prolines around the active site cleft, ion pairs and packing density that contribute to the thermostability of BglF are elucidated.



**Non-canonical SH3/Pro interface structure of the AMAP1 and cortactin binding**

Harumi Hosaka<sup>1</sup>, Shigeru Hashimoto<sup>2</sup>, Mayumi Hirose<sup>3</sup>, Ari Hashimoto<sup>4</sup>, Masaki Morishige<sup>5</sup>, Atsuko Yamada<sup>6</sup>, Ken-ichi Akagi<sup>7</sup>, Eiji Ogawa<sup>8</sup>, Chitose Oneyama<sup>9</sup>, Tsutomu Agatsuma<sup>10</sup>, Masato Okada<sup>11</sup>, Hidenori Kobayashi<sup>12</sup>, Hiromi Wada<sup>13</sup>, Hirofumi Nakano<sup>14</sup>, Takahisa Ikegami<sup>15</sup>, Atsushi Nakagawa<sup>16</sup>, Hisataka Sabe<sup>17</sup>

<sup>1</sup>Institute for Protein Research, Osaka University, Department of Molecular Biology, Osaka Bioscience Institute, Japan; <sup>2</sup>Department of Neurosurgery, School of Medicine, Oita University, Japan; <sup>3</sup>Laboratory of Structural Proteomics, Institute for Protein Research, Osaka University, Japan; <sup>4</sup>Department of Molecular Oncology, Osaka Bioscience Institute, Japan; <sup>5</sup>Kyowa Hakko BioFrontier Laboratories, Japan; <sup>6</sup>Research Institute for Microbial Diseases, Osaka University, Japan; <sup>7</sup>Department of Thoracic Surgery, Faculty of Medicine, Kyoto University, Japan

We have shown that AMAP1 forms ternary complex with cortactin via its proline-rich region, and the complex are detected in invadopodia of highly invasive cancer cells. Since inhibition of the complex formation by a small chemical compound, UCS15A, effectively suppresses the cancer cell invasion, the ternary complex is possible therapeutic target for cancer treatment. We determined the structures of AMAP1/cortactin complex in solution by NMR spectroscopy and in crystal by X-ray crystallography. The SH3 domains generally bind to peptides with a one-to-one stoichiometry. However, we found that a single molecule of proline-rich peptide binds to two molecules of the cortactin SH3 domain in the crystal, in which the two SH3 domains were related to each other by non-crystallographic 2-fold symmetry. Furthermore, a small chemical compound, UCS15A, affected the region containing six proline residues of AMAP1.

**Crystallographic analysis of SLT1D1 ES complex structure**

Takamasa Teramoto<sup>1</sup>, Kanako Inada<sup>1</sup>, Youichi Sakakibara<sup>2</sup>, Masahito Suiko<sup>2</sup>, Makoto Kimura<sup>1</sup>, Yoshimitsu Kakuta<sup>1</sup>

<sup>1</sup>Department of Bioscience and Biotechnology, Kyushu University, <sup>2</sup>Department of Biochemistry and Bioscience, Miyazaki University, Japan

The cytosolic sulfotransferase (SULT) transfer the sulfate group from 3'-phosphoadenosine 5'-phosphosulfate (PAPS) to a wide variety of endogenous and exogenous phenolic substrate, such as steroid hormones, thyroid hormones, drug, and xenobiotics. Mouse SULT1D1 is active toward small phenolic, and amine-containing molecules, but not active toward steroid or thyroid hormone. The mechanism is proposed to proceed via an  $S_N2$  nucleophilic attack of the OH group of phenol on the Sulfonate of PAPS through the direct in-line transition state. In this study, we have performed x-ray crystallographic structural analysis to reveal structural basis of a direct in-line sulfonic transfer mechanism of SULT1D1.

The crystals of SULT1D1 were obtained in presence of the substrate donor product 3'-phosphoadenosine 5'-phosphate (PAP). This obtained crystal was proceeded to soak in p-nitrophenyl sulfate solution to cause reverse reaction from PAP to PAPS. Finally the crystal containing PAPS was soaked in p-nitrophenol (PNP) for 30 seconds. The crystal structure of mouse SULT1D1 has been determined by molecular replacement using mouse SULT1E1 and has been refined to 1.7Å. In the result, we observed that PAPS interacts with PAPS binding motif which is conserved region in sulfotransferases and PNP binds at active site. Consequently, we observed ES complex structure of mSULT1D1.

## Crystallization and Structural Analysis of Archaeal Homolog of Ski-2 type RNA helicase from the Hyperthermophilic Archaeon *Pyrococcus horikoshii*

Takashi Nakashima<sup>1</sup>, Xiaodong Zhang<sup>2</sup>, Yoshimitsu Kakuta<sup>1</sup>, Makoto Kimura<sup>1</sup>

<sup>1</sup>Department of Bioscience and Biotechnology, Kyushu University<sup>1</sup>, Graduate School of Systems Life Sciences, Kyushu University, Japan<sup>2</sup>

The *SKI* (superkiller) genes were first identified from mutations that cause overexpression of a killer toxin encoded by the endogenous double-stranded RNA. Subsequent studies revealed that the products (Ski2p, Ski3p, and Ski8p) of SKI2, SKI3, and SKI8 genes, respectively, are necessary for the 3'- to -5' mRNA degradation and repression of translation of non-polyadenylated RNA in addition to their antiviral activities. Furthermore, it was found that Ski2p, Ski3p, and Ski8p form the Skicomplex and play an essential role in cytoplasmic mRNA turnover as cofactors for the exosome in yeast. However, the specific role of the Ski complex in 3' mRNA decay still remains elusive.

Ski2p is a putative RNA helicase with DEVH motif and conserved among eukaryote and archaea. We found that the gene PH1280 product (Ph1280p) from the hyperthermophilic archaeon *Pyrococcus horikoshii* shows sequence homology to the yeast Ski2p: the N-terminal domain of Ph1280p shares 36% identical amino acid with the putative catalytic DEVH helicase domain of the yeast Ski2p. In order to elucidate the molecular mechanism of the RNA helicase in the Ski complex, we overproduced Ph1280p in *Escherichia coli* cells and crystallized hanging drop vapor diffusion method.

The crystals diffract up to 3.6 Å resolution and belong to the space group C222, with unit cell parameters  $a = 283.3 \text{ \AA}$ ,  $b = 490.0 \text{ \AA}$ ,  $c = 76.2 \text{ \AA}$ . The crystal contains molecule in the asymmetric unit, with a solvent content of 54% and a  $V_m$  value of  $2.7 \text{ \AA}^3/\text{Da}$ . The MAD data collection was performed with two wavelengths near the absorption peak of selenium, and the model building of the Ph1280p is now in progress.

## **The structure and the inhibition of the activity of Human Monoamine Oxidase A**

Seyoung Son Yoshimura Masato Ma Jichun Tsukihara Tomitake

Laboratory of Protein Crystallography., Institute for Protein Research in Osaka University.

Monoamine oxidase(MAO) is a mitochondrial outer-membrane protein containing a FAD(flavin adenine dinucleotide). This enzyme catalyzes the oxidative deamination of several important monoamine neurotransmitters - in the central nervous system, such as serotonin (5-HT), norepinephrine (NE) and dopamine (DA). MAO plays a critical role in some psychiatric and neurological disorders, like depression and Parkinson's disease. Because MAO inhibition increases the level of neurotransmitters in the central nervous system, Searching for the effective inhibitors is one of the attractive means to treat neurodegenerative illnesses. MAO has two subtypes, MAOA and MAOB, which are similar in sequence with identities of approximately 70%. But each of them has unique substrate and inhibitor specificities. For example, MAOA oxidizes serotonin, but MAOB does not; MAOA is selectively inhibited by clorgyline and MAOB is highly inhibited by deprenyl. For developing the more effective and the newer inhibitors, it is important to understand the inhibitory and the catalytic mechanism with the three-dimensional structure. We determined the crystal structure of human MAOA protein at 3.0Å resolution using BL44XU beam-line at SPring-8. And also, we could confirm the structure of the single trans-membrane helix at C-terminal region. The inhibition and the catalytic mechanisms will be discussed.

## On A Method of Generating Space Groups and Calculating Structure Factors By Coset Decomposition

RYOKO OISHI<sup>1</sup> Masao Yonemura<sup>2</sup> Fumihito Shikanai<sup>3</sup> Shuki Torii<sup>4</sup> Toru Ishigaki<sup>5</sup> Takashi Kamiyama<sup>6</sup>

Visible Information Center, Inc.<sup>1</sup> Institute of Applied Beam Science, Graduate School of Science and Engineering, Ibaraki University<sup>2</sup> Institute of Materials Structure Science, High Energy Accelerator Research Organization (KEK)<sup>3</sup> Quantum Beam Science Directorate, Japan Atomic Energy Research Institute (JAERI)<sup>4,5,6</sup>

As a method of generating space group elements and calculating structure factors, a new algorithm using coset decomposition will be presented. This algorithm is a part of the Rietveld code developed for the versatile neutron diffractometer (IBARAKI Materials Design Diffractometer) in J-PARC(Japan Proton Accelerator Research Complex)that will be built by Ibaraki prefecture government to promote industrial applications for neutron beam.

When  $H$  is a subgroup of a space group  $G$ , the structure factor formula corresponding to  $G$  is decomposed into the term of the structure factor formula corresponding to  $H$  and the term expressed by coset representatives of  $G$  over  $H$ . In this reason, site symmetries, Wyckoff multiplicity, reflection multiplicity and extinction rules can be determined in the same process of generating space groups by coset decomposition. Since every space group and its subgroups have a normal subgroup of index 2 or 3, this algorithm can be executed by a recursive function that replaces its argument with one of the maximal normal subgroups of the previous group repeatedly.

For calculation of structure factors, our program contains tables on space groups as follows; Bravais lattice, all the maximal normal subgroups of 32 point groups, coset representatives for these subgroups, the translation vectors of the elements corresponding to the above coset representatives for the non-symmorphic space groups.

**Purification and crystallization of photosynthetic reaction-center and light-harvesting I complex from *Rhodospirillum rubrum***Takao Okabe<sup>\*</sup> Yuichi Kato<sup>\*</sup> Takashi Kumasaka<sup>\*</sup> Takayuki Odahara<sup>\*\*</sup>Department of Life Science, Tokyo Institute of Technology<sup>\*</sup> National Institute of Advanced Industrial Science and Technology (AIST), Japan<sup>\*\*</sup>

The photosynthetic reaction-center and light-harvesting I complex (RC-LH1) of purple non-sulfur bacteria is composed of a hetero-oligomeric RC complex and LH1 antenna subunits encompassing RC. Although the structure of RC-LH1 from *Rhodospseudomonas palustris* has been determined at 4.8 Å resolution (PDB: 1PYH), the intimate mechanism of photosynthetic reactions is not elucidated yet. To investigate its structural details, we are studying on the crystallization of RC-LH1 from *Rhodospirillum rubrum*.

The protein solution was prepared by the method described previously.<sup>1)</sup> *Rs. rubrum* was cultured in five days and its chromatophore was collected from the fraction by French press. RC-LH1 was solubilized by DDM and purified by molecular-sieve chromatography. Crystallization was performed on the initial conditions determined based on the solubility diagram as a function of precipitant and protein concentrations,<sup>1)</sup> and also using sparse-matrix screening kits. The large crystals of RC-LH1 were obtained from the solution containing PEG400, MgCl<sub>2</sub>, DM(Figure), but only diffracted X-rays to low resolution. Searching more suitable conditions is in progress.

Ref: 1) Odahara, T. *Biochim. Biophys. Acta* **1660**, 80 (2004).



## Crystal structure analyses of reconstituted water-soluble chlorophyll proteins from kale

Hiroshi Hara Hiroyuki Satoh Isao Oonishi Akira Uchida

Department of Biomolecular Science, Toho University

Water-soluble chlorophyll proteins (WSCP) have been considered as a chlorophyll (Chl) carrier in the Chl metabolic pathway because of its water-solubility, stress-inducibility and ability to protect Chl against photooxidation. WSCPs can be classified into two classes based on their photoconvertibility (Classes I and II). WSCPs having no photoconvertibility can be categorized further into two subtypes according to their Chl *a/b* ratio (Classes IIA and IIB). Class IIA WSCPs exhibit a Chl *a/b* ratio higher than the ratio in total leaf extract and Class IIB WSCPs possess lower ratio. In order to investigate whether Class II WSCPs discriminate between Chls *a* and *b*, we reconstituted kale-WSCP containing solely Chl *a* or *b*, and determined the crystal structures. A cDNA for kale-WSCP was used to express the apo-WSCP in *Escherichia coli*. A WSCP containing Chl *a* (WSCP-*a*) or Chl *b* (WSCP-*b*) was reconstituted *in vitro*. Crystals of WSCPs-*a* and -*b* were obtained from similar conditions by hanging-drop vapor-diffusion method. Native data sets of WSCPs-*a* and -*b* were collected with synchrotron radiation up to 1.9Å and 1.6Å, respectively at 100 K at the KEK-PF. The structures of WSCPs-*a* and -*b* were determined by the molecular replacement using a native kale-WSCP as a search model.

Current refined models of WSCP-*a* and -*b* have R-factors of 18.4 and 19.1 % and free R-factors of 24.5 and 23.6 %, respectively. The further refinements are in progress.

## **Crystallization and preliminary X-ray analysis of the bacterial membrane transporters**

Yoshiki Tanaka<sup>1</sup> Motoyuki Hattori<sup>2</sup> Shuya Fukai<sup>2</sup> Ryuichiro Ishitani<sup>2</sup> Osamu Nureki<sup>2</sup>

<sup>1</sup>Department of Bioscience, School of Bioscience and Biotechnology, Tokyo Institute of Technology<sup>2</sup> Department of Biological Information, Graduate School of Bioscience and Biotechnology, Tokyo Institute of Technology, Japan

Membrane transporters have critical physiological roles in all living organisms. To survive and function properly, cells exchange various transport substrates, such as amino acids, sugars and metal ions with their environment, which is performed by membrane transporters embedded in the cell membrane. Approximately 10 percent of bacterial genomes consist of membrane transporters. Although the structural information is essential for understanding the functional mechanism of membrane transporters, the number of their available high-resolution structure is limited, because membrane protein structure is very difficult to be determined. To determine the novel structure of membrane transporters, we have cloned the several membrane transporters from thermophilic bacteria. The membrane transporters were overexpressed in *E. coli*, purified, and tried to be crystallized. In the initial crystallization screening, a crystallization robot enabled us to perform high-throughput screening, despite the limited amount of purified transporter proteins. Until now, we have succeeded in crystallization of two full-length and one cytosolic domain of the membrane transporters. The native and selenomethionine-substituted crystals of the cytosolic domain diffracted to 2.1 and 2.2 angstrom resolution, respectively, using synchrotron radiation. The structure determination of the cytosolic domain by multi-wavelength anomalous dispersion method is now in progress. Moreover, we are developing its transport assay in the liposome- reconstituted system.

## Structure basis for recognition of the 3' -terminus of aminoacyl-tRNA by Leucyl/Phenylalanyl-tRNA protein transferase

Kyoko Suto` Yoshihiro Shimizu` Kozo Tomita`

Institute for Biological Resources and Functions, National Institute of Advanced Industrial Science and Technology (AIST)` Department of Medical Genome Sciences, Graduate School of Frontier Sciences, University of Tokyo, Japan`

The stability and degradation of proteins in living organisms plays a vital role in post-translational gene expression and is governed by the N1-end rule, where the N-terminal amino residue of a protein influences its metabolic stability. Proteins with N-terminal destabilizing amino acid residue are degraded by specific proteases. The aminoacyl-tRNA protein transferases are involved in this pathway in both eubacteria and eukarya.

Leucyl/Phenylalanyl-tRNA protein transferase (L/F-transferase) from eubacteria catalyzes the conjugation of Leu (and Phe) of Leu-tRNA<sup>Leu</sup> (and Phe-tRNA<sup>Phe</sup>) to the N-terminus of a protein starting with basic amino acid residues (Arg or Lys). The proteins with the destabilizing Leu (or Phe) at their N-termini are degraded by an action of the ClpAp proteasome complex. Therefore, the L/F-transferase is an essential factor for initiating protein degradation and for the quality control of cellular proteins in eubacteria.

Here, we present the crystal structures of *E. coli* L/F-transferase and its complex with an aminoacyl-tRNA analog, puromycin. The structure of C-terminal domain of L/F-transferase is GNAT superfamily fold and the puromycin is accommodated in a highly hydrophobic pocket of the enzyme. The shape of the puromycin binding pocket is suitable only for hydrophobic amino acid residues with an unbranched  $\beta$ -carbon. The base moiety of puromycin stacks with several hydrophobic amino acid residues, but is not specific to adenine. The presented structure and structure-based mutagenesis analysis of L/F-transferase explain its substrate specificity. We also present a model for tRNA binding to L/F-transferase.

Ref. A. Varshavsky, *Trends Biochem Sci.* **30**, 283-286, 2005.

## Crystal Structure of Bovine Lactoperoxidase at 2.3 Å resolution

Sujata Sharma<sup>1</sup> Amit Singh<sup>1</sup> Kouichirou Shin<sup>2</sup> Mitsunori Takase<sup>2</sup> Nagendra Singh<sup>1</sup> Tej Singh<sup>1</sup>

Department of Biophysics, All India Institute of Medical Sciences<sup>1</sup> Nutritional Science Laboratory, Morinaga Milk Industry Co. Ltd, Japan<sup>2</sup>

Lactoperoxidase is a heme containing enzyme that catalyzes the inactivation of a wide range of micro-organisms. It is a prominent member of a family of homologous mammalian peroxidases that includes thyroid peroxidase, eosinophil peroxidase and myeloperoxidase. This is the first crystal structure from the sub-family of lactoperoxidases. The protein was purified from bovine milk and crystallized using hanging drop method. The crystals belong to monoclinic space group P2<sub>1</sub>, with cell dimensions, a=54.5 Å, b=80.6 Å, c=77.6 Å, beta=102.6 with two molecules in the unit cell. The structure was refined to R<sub>cryst</sub> and R<sub>free</sub> factors of 0.173 and 0.218 respectively. The final structure contains 4697 protein atoms, 1 calcium ion bound firmly in the calcium-binding site, 1 heme prosthetic group, 2 nitrate ions, 1 carbonate ion, 1 molecule of hypothiocyanate and 318 water molecules. Bovine lactoperoxidase is a single polypeptide chain consisting of 583 amino acid residues with 4 potential N-glycosylation sites having N-X-S/T sequence motifs which are at N81, N189, N225 and N317. The electron densities of glycan chains have been observed at all the four sites. The heme group is covalently linked to the side chains of D94 and E244. It forms two strong ionic interaction with R334 and R426. The calcium ion is coordinated by the three backbone oxygen atoms of D96, T170 and F172, two carboxyl O<sup>δ1</sup> atoms of D96 and D174 and two O<sup>δ</sup> atoms of T170 and S176 resulting in the formation of a coordination sphere of the calcium ion with pentagonal bipyramidal geometry. The nitrate anion is hydrogen bonded to W32, L33, V328, R383 and T544 while carbonate anion interacts with N81, R82 and R490. Finally, hypothiocyanate is observed in contact with Q91, H95, and the heme Fe<sup>3+</sup> ion.

## Structural Studies of a New Class of Binding-Proteins Secreted during the Narrow period of Initial Involution

Tej P. Singh Devendra B. Srivastava Janesh Kumar Nagendra Singh Rishi K. Somvanshi Sujata Sharma Sharmistha Dey Asha Bhushan

Biophysics, All India Institute of Medical Sciences, New Delhi

During the early stage of involution in animals extensive restructuring of the tissue occurs, which includes the elimination of many secretory epithelial cells. However, the molecular processes during this period are very poorly understood. The protein profile of secretions during involution has been studied. It indicated a high concentration of new class 40 kDa glycoproteins. These proteins were designated as signaling proteins (SPX-40). They have been isolated from various animal species such as Human (SPH-40), Bovine (SPC-40), Buffalo (SPB-40), Goat (SPG-40), Sheep (SPS-40) and Camel (SPU-40). The crystal structures of SPX-40 from several species determined at high resolutions revealed that the protein folds into two domains, a large  $(\beta/\alpha)_8$  TIM barrel and a small  $(\alpha+\beta)$ . Its overall folding is similar to chitinases but it does not have chitinase activity due to mutations of active site residues. The sugar-binding groove is partly blocked. In order to understand its function, the crystal structures of several complexes with oligosaccharides of different lengths have been determined. Structures of these complexes show large scale conformational changes upon binding to sugars. The structures of SPX-40 also reveal a surface region consisting of three segments with significant disorders and a unique distribution of polar residues suggesting a potential of forming intermolecular interactions. In order to ascertain this aspect, its complexes were co-crystallized with designed peptides. Crystal structures of these complexes revealed that peptides bound to the protein at this site only. Finally, it seems that these proteins are evolved from the family of purely sugar-binding to protein-binding that could retain some sugar-binding capacity.

**Structure and function of new-type exfoliative toxin from *Staphylococcus hyicus*.**Katsuo Katayanagi<sup>1</sup> Kenji Yamamoto<sup>2</sup> Yasuyuki Fudaba<sup>1</sup> Takayuki Yamaguchi<sup>1</sup> Motoyuki Sugai<sup>1</sup><sup>1</sup>Graduate School of Science, Hiroshima University<sup>2</sup> Graduate School of Biomedical Science, Hiroshima University, Japan

Exfoliative toxin (ET) is an exotoxin derived from staphylococcal species, and it causes blisters in human and animal skin. This kind of skin syndrome (staphylococcal scalded skin syndrome: SSSS) is a generalized blistering skin disease that is primarily a disease of young children and neonates. In addition to ET from *staphylococcus aureus*, new type of ET from *staphylococcus hyicus*, which lives on the skin of the pigs, has been identified by gene analysis. They were classified to four isomers as ExhA, ExhB, ExhC and ExhD. In this study, we crystallized the four isomers to clarify the difference in the viewpoints of the structure and function relationships. The protein we used was expressed by *E. coli*.

Both of ExhA and ExhD were crystallized by hanging drop vapor diffusion method, whereas ExhB was crystallized by microbatch. The resolutions of ExhA, ExhB, and ExhD were 1.9 Å, 1.7 Å, and 2.1 Å, respectively, and space groups were P22<sub>2</sub>, P2<sub>1</sub>2<sub>1</sub>2<sub>1</sub>, and P2<sub>1</sub>2<sub>1</sub>2, respectively. Diffraction images were digitalized and merged using the programs HKL2000 and XdisplayF, and  $R_{sym}$  was estimated to be 0.073, 0.045, 0.075 for ExhA, B, and D. The number of molecules per asymmetric unit was calculated to be 2 for ExhA and B and 3 for ExhD. Although the ExhC crystal has grown to a large size, the resolution of this crystal was only 3.2 Å, and the lattice parameter was  $a = 130.78$  Å,  $b = 235.34$  Å,  $c = 265.96$  Å, and no good solution has been found yet.

Molecular replacement was applied using the coordinate set of ETs. Crystallographic refinement is now under way and the backbone structure was found to be quite similar as exfoliative toxins. But some different conformation of active site structure was found.

**X-ray crystallographic analysis of CooA homologue from Carboxydothemus hydrogenoformans**Hirofumi Komori<sup>1</sup> Sayaka Inagaki<sup>2</sup> Shiro Yoshioka<sup>2</sup> Shigetoshi Aono<sup>2</sup> Yoshiki Higuchi<sup>1</sup><sup>1</sup>Department of Life Science, University of Hyogo and RIKEN Harima Inst., <sup>2</sup>Okazaki Inst.for Integrative Biosci.

CooA, homodimeric heme-containing protein, is responsible for the transcriptional regulation in response to carbon monoxide (CO). Only CO-bound CooA can bind to the target DNA to be active as a transcription activator. CO replaces the N-terminus coordinated to the heme iron in the inactive form upon CO binding, which induces a conformational change to activate CooA. Although this ligand exchange is thought to be a trigger of the activation of CooA by CO, the detailed mechanism is unknown. Here, we have determined the crystal structure of the CooA from Carboxydothemus hydrogenoformans (Ch-CooA). Ch-CooA was overexpressed in *Escherichia coli*, purified and crystallized hanging-drop vapour-diffusion method. The crystal diffracted to a resolution of 2.3 Å resolution. They are monoclinic and belong to space group P2<sub>1</sub>, with unit-cell parameters  $a = 61.8$ ,  $b = 94.7$ ,  $c = 92.8$  and  $\beta = 104.8$ . The structure was solved by the single wavelength anomalous diffraction (SAD) method. We report the structural features of the Ch-CooA and the CO-sensing mechanism.



## Prototype Structures and Structure Algebra as an Aid to the Refinement of Problem Structures.

A. David Rae

Research School of Chemistry, The Australian National University

Many structures are problematic in that, although they are well organised in one or two dimensions, alternative relationships are possible between adjacent columns or layers. This allows the possibility of polytypes, stacking faults and twinning. A prototype structure is an ideally ordered structure from which a model of the observed intensities can be constructed and refined, assuming definable (or refinable) relationships ( $\mathbf{R}, \mathbf{t}$ ) between blocks of structure. Coherence between blocks in the evaluation of a structure factor only requires that the operator  $\mathbf{R}$  operating on a reciprocal lattice vector  $\mathbf{h}$  of the prototype, creates another such lattice vector  $\mathbf{h}' = \mathbf{R}\mathbf{h}$ . Structure factor algebra uses refinable population and twinning parameters to combine the structure factors of equivalent or pseudo equivalent reflections of the prototype structure. This may change the symmetry of the diffraction pattern from that of the ordered prototype structure.

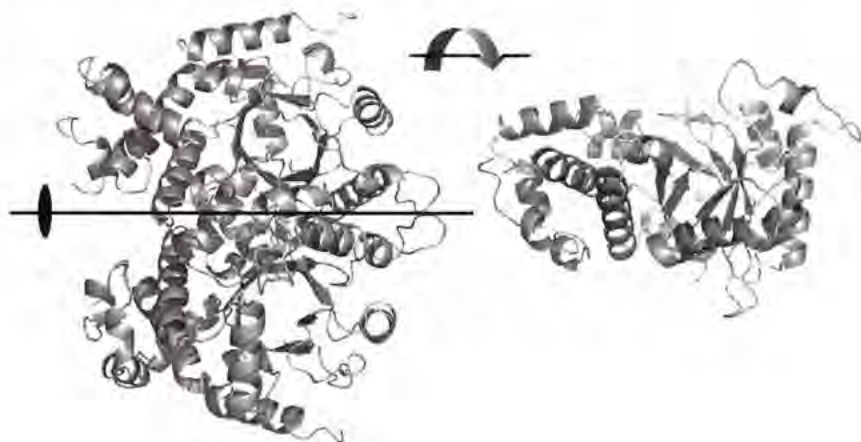
A common situation is when the prototype structure can be related to an idealised 1:1 disordered parent structure of higher symmetry. Alternative orderings may then be possible and symmetry operations destroyed upon ordering the parent structure can be used to identify possible polytypes and twin-disorder scenarios. Examples from recently studied structures using my program RAELS will illustrate the principles.

## The Crystal structure of orotidine 5'-monophosphate decarboxylase from the human malaria parasite *Plasmodium falciparum*

Keiji Tokuoka<sup>1</sup> Sudaratana R Krungkrai<sup>2</sup> Yukiko Kusakari<sup>3</sup> Tsuyoshi Inoue<sup>4</sup> Hiroaki Adachi<sup>5</sup>  
 Hiroyoshi Matsumura<sup>6</sup> Kazufumi Takano<sup>7</sup> Satoshi Murakami<sup>8</sup> Yusuke Mori<sup>9</sup> Yasushi Kai<sup>10</sup>  
 Krungkrai Jerapan<sup>11</sup> Toshihiro Hori<sup>12</sup>

<sup>1</sup>Department of Applied Chemistry, Graduate School of Engineering, Osaka University <sup>2</sup>Unit of Biochemistry, Department of Medical Science, Faculty of Science, Rangsit University, Thailand <sup>3</sup>Department of Applied Chemistry, Graduate School of Engineering, Osaka University, Japan <sup>4</sup>Department of Electrical Engineering, Osaka University, Japan <sup>5</sup>Department of Material and Life Science, Osaka University, Japan <sup>6</sup>Department of Cell Membrane Biology, Institute of Scientific and Industrial Research, Osaka University, Japan <sup>7</sup>Department of Biochemistry, Faculty of Medicine, Chulalongkorn University, Thailand <sup>8</sup>Department of Molecular Protozoology, Research Institute for Microbial Diseases, Osaka University, Japan

Orotidine 5'-monophosphate (OMP) decarboxylase catalyze the decarboxylation reaction to produce uridine 5'-monophosphate (UMP) in the final step of UMP synthesis. The crystal structure of recombinant malarian *Plasmodium falciparum* OMP decarboxylase has been determined in the apo form at 2.6 Å resolution. OMP decarboxylase is a dimer of two identical subunits. Each monomer consists of a triosephosphate isomerase barrel and contains an active site that is located across one end of the barrel and near the dimer interface. Comparing with OMP decarboxylase from *P. Vivax* in complex with substrate, we found the remarkable structural change of loop region (#264-277) that locates near the active site. *Plasmodium falciparum* is the causative agent of the most lethal and sever form of human malaria. Chemotherapy of malaria is available, but is complicated by both adverse effects and widespread resistance to most of the currently available anti-malaria drugs. The malaria parasite depends on *de novo* synthesis of pyrimidine nucleotides, whereas the human host has the ability to synthesize them by both *de novo* and salvage pathways. Anti-malaria drugs design by using the structure of OMP decarboxylase is in progress.



## Crystal structure and enzyme mechanism of esterase Est1 from an archaeon, *Sulfolobus shibatae*

Masami Kusunoki<sup>1</sup> Hideaki Unno<sup>2</sup> Yasuhiro Oshima<sup>2</sup> Tokuzo Nishino<sup>2</sup> Toru Nakayama<sup>2</sup>

<sup>1</sup>Institute for Protein Research, Osaka University <sup>2</sup>Graduate School of Engineering, Tohoku University, Japan

Carboxylesterases (esterases) catalyze the hydrolysis and ester transfer reaction of carboxyl esters, playing important roles in the metabolism, decomposition, and detoxification intra-cellular and extra-cellular processes. Most of the esterases belong to a large group of the proteins, a/b hydrolase super-family. Esterases are industrially important enzymes utilized in various fields. The thermal stability and optimal pH of these enzymes are important properties for such applications. Especially, esterases with their maximal activities at acidic pH are not reported yet and its availability is strongly requested. We started the biochemical and crystallographic study of esterase Est1 from *Sulfolobus shibatae*, a member of the hormone-sensitive lipase family of the a/b hydrolase super-family, in order to clarify the enzyme mechanisms of Est1 and to gain a structural basis for designing the mutant enzyme with the activity at acidic pH.

The recombinant enzyme of Est1 was overexpressed in *Escherichia coli* cells and was crystallized by the hanging drop vapor diffusion method. The native crystal belongs to the orthorhombic space group space I222 with cell dimensions a=58.40 b=71.94, and c=137.33 Å. The X-ray diffraction data to 1.5 Å resolution was collected at the beamline 44XU, SPring-8. The crystal structure was determined by the molecular replacement method with the CCP4 program Molrep and was refined with the program Refmac-5 with  $R_{work}$  and  $R_{free}$  values of 0.157 and 0.180, respectively.

The mutant enzymes His274Ala, His274Glu, and His274Asp were also prepared and their crystal structures were determined to gain insight into enzyme mechanisms. We are now examining these structures and will report the detail.

**Cation-pi interaction revealed by crystal structure of thermoalkalophilic lipase: relationship between enzymatic activity and alkali metal cation**

Hiroyoshi Matsumura<sup>1</sup> Takahiko Yamamoto<sup>1</sup> Leow Thean Chor<sup>2</sup> Abu Bakar Salleh<sup>2</sup> Tsuyoshi Inoue<sup>1</sup> Yasushi Kai<sup>1</sup> Raja Noor Zaliha Raja Abdul Rahman<sup>2</sup>

Department of Materials Chemistry, Osaka University<sup>1</sup> Enzyme and Microbial Research Technology, University Putra Malasia, Malaysia<sup>2</sup>

Cation-pi interactions are noncovalent binding forces that occur between cations and electron-rich orbitals of an aromatic ring. The interactions are increasingly recognized to play a dominant role in various molecular functions in chemistry and biology.

An extracellular lipase from *Geobacillus zalihaai* sp. strain T1 (T1 lipase) is a thermoalkalophilic enzyme that was isolated from Palm Oil Effluent (POE) in Malaysia. This enzyme is a secreted protein, which can catalyze the hydrolysis of long-chain triglycerides into fatty acids and glycerol at the interface between water and insoluble substrate at high temperature. Since POE contains high concentration of potassium ion, T1 lipase has the potential to catalyze the reaction under non-natural condition such as high concentration of potassium ion.

Herein, we have crystallized T1 lipase from *Geobacillus zalihaai* sp in presence of alkali metal cation (sodium and potassium ions), and have solved the crystal structure of T1 lipase at 1.5 Å resolution. The high resolution structure showed that an alkali metal cation was bound via cation-pi system in the vicinity of active site. Based on these observations, the enzymatic activity has been investigated under the buffer containing sodium and potassium ions. We will address the details of coordination structure of alkali metal cation and propose its enhanced mechanism.

**Variation of Measurability of Bijvoet ratios in MAD experiments**

Gayathri Dasara Raju<sup>1</sup> Zwart Peter<sup>2</sup> Velmurugan Devadasan<sup>1</sup>

<sup>1</sup>crystallography and biophysics, university of madras<sup>2</sup> Lawrence Berkely laboratory, USA<sup>2</sup>

The feasibility of SAD experiments can be assessed by the number of reflections with a significant Bijvoet difference and the substructure determination in any SAD experiment using modern direct methods program is directly related to the above number of reflections. The published work on the measurability of Bijvoet intensity ratio has a major drawback, namely, it lacks the incorporation of the effects of experimental errors. The strength of the anomalous signal can be judged by both the intensity and amplitude based anomalous signal to noise ratio and a quantity related to the average anomalous signal to noise ratio is the number or fraction of Bijvoet differences whose absolute value is larger than three times its standard deviation.

Recently, the relatively complicated integrations with the effects of errors on the expected Bijvoet ratio and measurability, which are not straightforward to solve by analytical means, have been bypassed by using a numerical approach. The numerical determination of the Bijvoet ratio and measurability in a SAD experiment involves the combination between the classical measurability and the anomalous signal to noise ratio criteria. The presentation will cover the estimation of the above in case of MAD data to assess the variation in measurability when one approaches the absorption edge of heavy atoms.

**X-ray scattering studies on structure of an enzyme protein in solution**

Kyeong Sik Jin Sangwoo Jin Moonhor Ree

Pohang University of Science &amp; Technology

To understand the conformational behavior of a protein, it is necessary to define not only the structure of its native state but also that of various denatured states. Recent studies have revealed the biological significance of denatured states in processes such as aggregation, chaperone binding, and transport across membrane. A variety of denatured states have also been identified, differing in their overall dimensions and the extent of residual secondary and tertiary structures. In particular, pepsin is a good model for the study of conformational behavior under various conditions because detailed information can be obtainable on the secondary structure, enzymatic properties, and zymogen activation. In the present study, we carried out solution X-ray scattering (SAXS) experiments on porcine pepsin, which is a gastric aspartic proteinase that plays an integral role in the digestive process of vertebrates, in order to obtain detailed information on the overall structure of porcine pepsin at the native state and its structural changes in solutions of various pH values. The solution SAXS data were analyzed in detail, providing important information on the structure and variations with pH conditions. From the SAXS profiles and determined parameters, structural models of the porcine pepsin were reconstructed, which was made inside the search volume of maximum diameter  $D_{max}$  calculated from the  $p(r)$  function. The reconstructed models were obtained without imposing any restrictions on the symmetry and anisometry of pepsin molecule. Under several pH conditions, the reconstructed models reveal various conformational states, when compare to the crystal structure. The structural differences between solution and crystal structure of pepsin can be account for the inherent conformations of the flexible subdomain under carefully controlled specific pH conditions.



# **Author Index**



Abe, Hiroshi	P22-007, P22-080	Aoyama, Tetsuya	P22-045 P22-025
Aburaya, Kazuaki	P21-135	Arai, Daisuke	OC23-103
Adachi, Eru	P23-234	Arai, kazuyosi	P21-030
Adachi, Hiroaki	P21-292, P22-327, P23-258	Arai, Masatoshi	OC21-102, OC23-001, P22-266, P22-275
Adachi, Shin-ichi	OC23-206		P22-293
Adachi, Wataru	OA22-002, P23-204	Araiso, Yuhei	P22-038
Adam, Martin	P21-208, P21-211	Araki, Hiromi	OC23-003
Adams, Timothy	OA23-103	Argyriou, Dimitri	P23-145
Agarwal, S.G.	P22-170	Arima, Takahisa	P21-193, P22-269
Agatsuma, Tsutomu	P22-313	Aroyo, Mois	OB23-102
Ago, Hideo	P22-272	Aruga, Kumiko	OB23-103
Ahmed, Ejaz	P21-141	Asaji, Tetsuo	P22-089
Ahuja, R.	P22-022	Asaka, Toru	P21-006, P22-016, P22-122, P23-035, P23-145
Aivazian, Karina	P23-094		P21-036
Aizawa, Kazuya	OC21-102, P22-266, P22-275	Ashida, Yasunari	P23-005
Akaboshi, Mayuko	P21-193	Asogawa, Sachiko	P22-180
Akagawa, Mitsugu	P21-220	Atkinson, Ian M.	P21-066, P21-075
Akagi, Ken-ichi	P22-313	Au-Yeung, Alex	P22-022
Akai, Naonori	OB21-104		OB22-104, OC21-103
Akasaka, Ryogo	P22-260, P22-307	Avasthi, D.	P22-037, P22-040
Akashi, Haruo	P23-130	Avdeev, Maxim	P21-250
Akatsuka, Takao	P23-097		P23-237
Akiba, Toshihiko	P23-195	Awaka, Junji	OB22-102, OC23-101, P21-138
Akimoto, Junji	P21-027, P22-037, P22-040		P23-073
Akitsu, Takashiro	P22-098	Baase, Walt	OA23-202
Akutsu, Masato	P21-229	Bachinger, Hans	OC23-002
Alexe, Marin	OC23-101, P21-138	Baik, Sunggi	P22-305 P22-113
Ali, Roushown	P23-067		P23-166
Amanokura, Natsuki	OB21-104	Baimark, Yodthong	OC22-002
Amemiya, Yoshiyuki	OC22-104, OC22-105, P22-010	Baker, Edward	OA23-001, P23-056
An, Pang Tsai	P23-050	Balcar, E.	P22-016
Anderson, Peter A.	OA22-105	Ballard, Charles	P21-208, P21-211
Ando, Masami	P23-097	Bamzai, Krishen	OA23-103
Ando, Yoshinori	P22-053	Barisic, Ivanka	P23-304
Anilkumar, G.N.	P23-017	Baron, Alfred Q.R.	P23-294
Aoki, Ken-ichi	P22-221	Bartlam, Mark	P21-259,
Aoki, Mari	P22-307		
Aono, Shigetoshi	P22-325	Belik, Alexei	
Aoyagi, Shinobu	OB23-104, OC22-202,	Benning, Matthew	
		Bentley, John	
		Berry, Richard	
		Bessho, Yoshitaka	
		Betzel, Christian	

	P21-298	Chen, Chien-Liang	P23-064
Bhadbhade, M.	P21-093	Chen, Chin-Yu	P21-289,
Bhakuni, V.	P21-295		P23-041
Bharat, Patel	P23-249	Chen, Chun-hsien	OC23-104
Bhushan, Asha	P21-274,	Chen, Chun-Jung	OB23-201
	P21-277,	Chen, Delphic	P21-084
	P21-280,	Chen, Hao-Hong	P21-063,
	P22-323		P22-065
Bilgrami, Sameeta	P23-231	Chen, I-Wen Peter	OC23-104
Bischoff, Nicole	P21-250	Chen, Jin-Ming	P23-079
Bishop, Roger	OB22-004	Chen, Ko Wa	P21-081
Biswas, Sampa	P22-188,	Chen, Liqing	P22-212
	P23-189	Chen, Minghuang	P22-212
Blanchard, Helen	P23-243	Chen, Sung-Yu	P23-064
Borah, S.M.	P22-074	Chen, Szu-Miao	OB22-106,
Bratoeff, Eugene	P22-239		P21-081
Brown, Peter	OA23-202	Chen, Xiao-Ming	P22-095
Buron-Le Cointe, Marylise	OC23-206	Cheng, Shequ-Wen	P22-116
Busabok, Chumphol	P23-171	Chiang, Chia-Wang	P22-309
Byram, Sue	P21-211	Chikaura, Yoshinori	P23-097
Cai, Yong	OC22-004	Chimnaronk, Sarin	OA23-101
Cailleau, Herve	OC23-206	Chin, Ko-Hsin	P22-309
Campbell, Stewart	OB22-201	Chiu, Elaine	OB23-001
Capillas, Cesar	OB23-102	Chiu, Hsien-Tai	P21-187
Caradoc-Davies, Tom	OA23-202	Chiu, Kenneth	P22-180
Carr, Leslie	OB22-002	Chiu, Mau-Sen	P22-062
Catanzariti, Ann-Maree	OA22-105	Chiu, Mou-Sen	P23-064
Cha, John	P21-072	Choi, Yong	OC23-003
Chacko, Jobichen	P23-243	Chollet, Matthieu	OC23-206
Chaichit, Narongsak	P22-301	Chopra, Deepak	P21-144,
Chainok, Kittipong	P21-165		P22-174
Chakrabarti, Chandana	P22-188,	Chor, Leow	P22-329
	P23-189	Choudhury, Debi	P22-188
Chakraborty, Santu	P21-150	Chowdhury, Krishna	P23-106
Chakraborty, Sibani	P23-189	Christen, David	OC23-001
Chan, Eric	P21-105	Christie, Michelle	OA23-201
Chan, Isa	OB22-004	Christopherson, Richard	P22-224
Chan, Nei-Li	P22-309	Chu, Chia-Hung	P23-064
Chandramani, R.	OC23-201	Chuang, Wei-Tsung	OB23-106
Chandrasekhar, Sosale	P21-153	Chuang, Woei-Jer	P21-190
Chang, Chia-Hao	P21-190	Chuang, Yu-Chun	P23-079
Chang, Shih-Lin	P22-062,	Coles, Simon	OB22-002
	P23-064	Collet, Eric	OC23-206
Chang, Wen-Ming	P21-114	Colman, Peter	OA23-204,
Chang, Yi-Wei	P21-187		P21-205,
Chang, Yu-Ning	P23-192		P22-191
Changsaluk, U.	P22-049	Cookson, David	P23-029
Channuan, Wasinee	P23-082	Cooper, Garth	OA23-202
Chatake, Toshiyuki	OA22-202	Coulibaly, Fasseli	OB23-001
Chatterjee, Partha	P23-026	Coulson, Barbara	P23-243
Chavas, Leonard	OA23-204,	Cowieson, Nathan	OB23-203
	P21-214	Craig, Donald	OB22-004
Chee, Clinton	P22-180	Crowe, Sonya	OC23-001

Czabotar, Peter	P22-191		P21-283,
Damborsky, Jiri	P23-276		P21-286,
Das, Amit	OB23-202		P22-254
Das, Partha	P23-142	Evangelista, Marco	P22-191
Dasara Raju, Gayathri	P23-330	Evans, Ivana	P23-070
Dasgupta, Jhimli	P21-268	Evans, John	P23-070
Dattagupta, Jiban	P21-268,	Fairlie, Walter	P21-205,
	P22-188,		P22-191
	P23-189	Fan, Haifu	OA22-103
De Souza, Alvaro	P23-048	Fang, De-Cai	P23-041
Deb, Apurba	P23-026	Ferrer, Jean-Luc	OB23-202
Desiraju, Gautam R.	OB22-001	Fibriansah, Guntur	P23-312
Devadasan, Velmurugan	P23-246,	Fitch, Andy	OC21-101
	P23-330	Forouhar, Farhad	OA23-003
Devendranath C., Reddy	P22-092	Forwood, Jade K.	OA22-105
Dey, Kalpama	P23-020	Frenkel, Maurice	OA23-103
Dey, Sharmistha	P21-280,	Frey, Jeremy	OB22-002
	P21-298,	Friese, Karen	P23-112
	P22-323	Fu, Ming-Dung	OC23-104
Dhakshnamoorthy, Balasundaresan	OA22-205,	Fucharoen, Suthat	OA22-203
	P23-186	Fudaba, Yasuyuki	P23-324
Diawara, Yacouba	P21-208	Fujihashi, Masahiro	P21-202
Dickson, James	OA23-202	Fujii, Hiroki	P22-134
Dodds, Peter N.	OA22-105	Fujii, Isao	P22-071
Domen, Kazunari	P21-096	Fujii, Kotaro	P21-036
Donald, Paul	OC23-001	Fujii, Yuji	P21-141,
Doyle, Declan	OA23-002		P22-137
Drinkwater, Nyssa	P21-196	Fujimoto, Kenjiro	P22-131
du Boulay, Douglas	P22-180	Fujita, Tarō	P23-151
Duangthongyou, Tanwawan	P23-121	Fujitsuka, Akira	P21-111
Duke, Monica	OB22-002	Fukai, Shuya	OA23-102,
Durst, Roger	P21-208		P21-238,
Dutt, R.	P22-022		P22-293,
Dyason, Jeffrey	OA23-204		P22-303,
Dyer, Collin	P21-250	Fukano, Michitaro	P23-320
Ebata, Kazuhiro	OC21-102,	Fukui, Kiyoshi	OB21-103
	P22-266,	Fukumori, Yoshihiro	P23-306
	P22-275	Fukumoto, Yuji	OA22-003
Ebihara, Akio	OA21-106	Fukushima, Akihito	OA21-101
Ebisusaki, Shutoku	P22-200	Fukuyama, Keiichi	OA21-102
Echigo, Takuya	P21-018		P22-251,
Egami, Norifumi	P23-279,		P22-296,
	P23-310	Fukuyama, Yoshimitsu	P23-302
Einaga, Yasuaki	P22-098		OB23-101,
Elkins, Jonathan	OA23-002		P22-161
Ellis, Jeffrey G.	OA22-105	Funahashi, Shiro	P22-043,
Enami, Nobuo	OA23-005		P23-044
Endo, Satoshi	P21-024	Funakubo, Hiroshi	OC23-105
Esaki, Nobuyoshi	P23-216,	Furukawa, Sanae	P22-281
	P23-228	Fusatomi, Emiko	P23-294
Ethayathulla, A.	P21-271,	Fusi, Paola	OA23-204
	P21-280,	Gaponov, Yury	OA21-104,
			P22-284,

Garboczi, D.	P22-257	Hanashima, Takayasu	P23-008
Garrett, Thomas	OA23-205	Hanesaka, M.	P22-057
Gee, Christine	OA23-203	Hansongnern, Kanidtha	P22-049
	OA23-201,	Hara, Hiroshi	P22-319
	P21-196	Hara, Takeshi	P22-164
Ghosh, Raka	P23-189	Harada, Jiro	P23-302
Ghosh, Soumen	P21-150,	Harada, Jun	OC23-203
	P21-156	Harakawa, Mayuko	OC23-203
Goessele, Ulrich	OC23-101,	Harata, Kazuaki	P23-195
	P21-138	Harjo, Stefans	OC21-102
Goldman, Alan	OC23-005	Harrowfield, Jack	P21-105
Gonnade, R.	P21-093	Harumoto, Takashi	P21-009
Goodman, Russell	P23-304	Hasebe, Sayoko	OB22-007
Goswami, Sanjeev	P22-170	Hasegawa, Kazuya	OA21-101,
Goto, Masaru	P23-216		P22-245,
Gotoh, Kazuma	P22-089		P23-255,
Gowda, K.V.Arjuna	P23-032		P23-261,
Gowda, Ramakrishna	P23-032		P22-290
Grenier, Stephane	OC23-005	Hasegawa, Tomokazu	OA21-103,
Grunewald, Gary	P21-196		OA22-104
Grupce, Orhideja	P21-087	Hasegawa, Yuko	P22-296
Grzechnik, Andrzej	P23-112	Hashimoto, Ari	P22-313
Gu, Jin-Zhong	OB21-105	Hashimoto, Eiko	P23-097
Gu, Yuanxin	OA22-103	Hashimoto, Hiroshi	P21-193,
Guerin, Laurent	OC23-206		P22-233,
Gulbis, Jacqueline	OA23-002,		P22-269
	P21-205	Hashimoto, Mitsuhiro	OC23-103
Guncar, Gregor	OA22-105	Hashimoto, Shigeru	P22-313
Gupta, Vivek K.	P22-170	Hashizume, Hiroo	P21-078
Guru Row, Tayur	P21-132,	Hassan, Imtaiyaz	P22-254,
	P21-153,		P23-231
	P23-142,	Hata, Yoshiaki	P22-134
	P23-160	Hatakeyama, Ryota	P22-122
Guruswamy, Shanmugam	P21-223	Hattori, Motoyuki	P23-320
Guss, J.	P22-224	Hayashi, Kiyoshi	P22-278
Gutmann, Matthias	P23-139	Hayashi, Makoto	P22-266,
Guttman, Sascha	OB23-001		P22-275
Haebel, Peter	OB23-001	Hayashi, Takeshi	P22-288
Hafezinejad, Nooshin	P23-175	Hayashi, Yoshihito	OC23-204
Haga, Mitsuru	P23-201	Hayashizaki, Yoshihide	P22-260,
Hagiwara, Yoshinori	P22-251		P23-234
Hagiya, Kenji	P22-149,	Hebert, Johan	OC23-206
	P23-154	Heo, Kyuyoung	OB23-105,
Hakamata, Wataru	OB23-203		OC22-101,
Hakoshima, Toshio	P22-227		P22-055
Hall, Syd	P23-181	Heras, Begona	P21-199
Haller, Kenneth	P21-099,	Hesse, Dietrich	OC23-101,
	P21-165		P21-138
Hamada, Kensaku	OA21-103	Hester, James	P21-123,
Han, Hee	OC23-101,		P23-029
	P21-138	Higashi, Tomohito	P21-238
Hanada, Kentaro	P21-247	Higashihara, Tomoya	OB23-105
Hanaoka, Takaaki	P23-148	Higashiura, Akifumi	P21-265

Higuchi, Yoshiki	P22-325, P23-225	Hosono, Hideo	P22-047
Hill, John	OC23-005	Hosoya, Hiroaki	P23-157
Hill, Jonathan	P21-012	Hosoya, Takaaki	P22-266, P22-275
Hilton, Douglas	OA23-203	Hossain, M.	OA22-002, P23-198
Hino, Kazuyuki	P21-117	Hosur, Madhusoodan	OB23-202
Hirafuji-Yamaguchi, Machiko	P22-307	Hou, Xiaomin	P22-212
Hiraki, Masahiko	OA21-104, P22-257, P22-284, P23-273	Howard, Christopher J.	K23-301, P23-070
Hirano, Keiichi	OC23-103, P23-273, P23-279, P23-310	Howard, Judith A. K.	OC22-201
Hirano, Satoshi	P23-285	Hoynes, Peter	OA23-103
Hirano, Shinya	P21-036	Hsiao, Chwan-Deng	OA23-003, P21-187, P21-190, P22-197
Hirao, Akira	OB23-105	Hsieh, Yin-Cheng	OB23-201
Hirata, Kazuto	P22-134	Hsu, Wen-Hwei	P23-192
Hirata, Kunio	P23-255, P22-290	Hu, Shu-Hong	OA23-201
Hirosaki, Naoto	P23-169	Huang, Cheng-Yang	P21-190
Hirose, Masaaki	OB23-004	Huang, David	P21-205, P22-191
Hirose, Mayumi	P22-313	Huang, Eugene	P22-143
Hirose, Raita	OA21-103, P22-245	Huang, Mingdong	P22-212
Hirota, Kazuma	P23-046	Huang, Tony	P22-143
Hirota, Tsuyoshi	P21-102	Huang, Yen-Chieh	OB23-201
Hirotsu, Ken	P23-216, P23-228	Hunter, Brett	P23-029
Hisaki, Ichiro	P21-129, P21-135, P21-147	Huo, Xia	OA23-001, P23-056
Hishida, Mafumi	OC22-103	Hursthouse, Michael	OB22-002
Ho, Wei-Lun	P22-083	Hussain, Altaf	P22-104, P23-020
Hodumi, Yasuaki	P21-009	Huyton, Trevor	OA23-203
Hofmann, Michael	OB22-201	Hyodo, Kazuyuki	P23-097, P23-310
Hokura, Akiko	P21-024	Ichihara, Shu	P23-097
Honda, Fuminori	OB22-202	Ichikawa, Misato	P23-130
Honda, Nobuo	P22-257	Ichiyonagi, Kohei	OC23-206
Hong, M.-H.	P23-064	Ida, Takashi	P23-308
Hongo, Chizuru	P22-194, P22-200, P23-201, P23-237	Ide, Yuya	OB21-103
Hoque, M.	P23-198	Ideo, Hiroko	OB23-203
Horii, Toshihiro	P22-327	Iga, Fumitoshi	P23-044
Horiuchi, Masataka	P22-278	Igarashi, Noriyuki	OA21-104, OA22-101, P22-257, P22-284, P23-273, P23-279, P23-310
Horiuchi, Hisanori	P21-238	Igarashi, Reiko	P22-242
Hosaka, Harumi	P22-313	Igari, Kumiko	P21-193
Hoshikawa, Akinori	OC21-102	Ihara, Hideshi	P23-258
Hoshino, Manabu	P21-162	Ihara, Kentaro	P21-214
Hoshino, Takayuki	P23-213		

Iida, Atsushi	P22-053		P23-177
Iino, Daisuke	P23-213	Ishizuka, Kazuo	P23-035,
Iishi, Kazuake	P23-179		P23-050
Ikeda-Saito, Masao	P22-215	Isobe, Kiyoshi	OC23-204
Ikeda, Naoshi	OC23-004	Isobe, Masaaki	P22-004
Ikeda, Susumu	P22-031	Isogai, Masamichi	P22-299
Ikeda, Takuji	P23-148	Ito, Kazuki	P22-007
Ikegami, Takahisa	P22-313	Ito, Kiyoshi	P22-218
Ikemizu, Shinji	P21-256	Ito, Koreaki	OA23-004
Imada, Katsumi	P23-270	Ito, Shigeru	P22-131
Imai, Kiyohiro	P23-264	Ito, Sohei	P21-220
Imai, Yasuhiko	OC23-103,	Ito, Yoshiyasu	OC23-102
	P22-158	Itou, Tetsuaki	P23-133
Imai, Yoshitane	OB22-007	Iturbe-Ormaetxe, Inaki	P21-199
Imai, Yuusuke	P22-080	Iversen, Bo	OB23-104
Imamura, Shigeyuki	P23-198	Iwai, Wakari	OA22-201
Imoda, Tomohiko	P21-102	Iwasaki, Hiroshi	P21-141
Imura, Hiroyuki	P23-169	Iwasaki, Kenji	A21-202
Inaba, katsuhiko	P21-030	Iwase, Kenji	P22-031
Inaba, Kenji	OA23-004	Iwata, So	K22-301
Inada, Kanako	P23-314	Izumi, Fujio	P21-232,
Inagaki, Fuyuhiko	P22-278		P23-067
Inagaki, Sayaka	P22-325	Izumi, Norikazu	P23-103
Inagaki, Yumi	P21-060	Izumi, Tetsuro	P21-214
Inaka, Koji	OB23-002,	Jabeen, Talat	P21-274
	P21-265,	Jadaprolu, Radha Krishna	P22-092
	P22-236,	Jain, Rishi	P21-274
	P22-248	Jaisankar, P.	P22-001
Inoue, Keisuke	P21-147	James, David	OA23-201
Inoue, Makoto	P22-260	Jamsai, Duangporn	OA22-203
Inoue, Michio	P21-241	Jayatilaka, Dylan	OC22-201
Inoue, Tsuyoshi	P21-292,	Jeng, U-Ser	OB23-106
	P22-327,	Jerapan, Krungkrai	P22-327
	P22-329,	Ji, Ran	OC23-101,
	P23-258		P21-138
Irie, Masahiro	P23-103	Jia, Min Ze	P23-252
Irifune, Tetsuo	P23-058	Jiang, Long	OB21-105
Ishibashi, Koichi	P21-030	Jin, Kyeong Sik	OB23-105,
Ishida, Hiroyuki	P22-089		OC22-101,
Ishida, Takayuki	P23-157		P22-055,
Ishigaki, Toru	OC21-102,		P22-331,
	P22-031,		P23-054
	P22-134,	Jin, Sangwoo	OB23-105,
	P22-317		OC22-101,
	P22-203		P22-331,
Ishiguro, Hiroshi	P22-209		P23-054
Ishii, Yudai	P21-078	Joo, Won-Chul	P23-054
Ishiji, Kotaro	OA22-201	Jovanovski, Gligor	P21-087,
Ishikawa, Takuya	OC23-004		P23-014
Ishikawa, Yoshihisa	OA23-102,	Juan, Ella	OA22-002,
Ishitani, Ryuichiro	P22-293,		OA22-004,
	P23-320		P22-206,
Ishizawa, Nobuo	P21-123,		P23-198,

Kadhirvel, Saraboji	P23-204	Katayanagi, Katsuo	P23-324
Kadowaki, Kazuo	P23-186	Kato, Kenichi	OB23-101,
Kagomiya, Isao	P22-134		OC22-202
	P21-060,	Kato, Ryuichi	OA22-001,
	P21-120		OA23-204,
Kai, Kentaro	P21-226		OB23-203,
Kai, Yasushi	P22-077,		OB23-204,
	P22-327,		P21-214,
	P22-329		P21-229,
Kaitner, Branko	P21-087		P21-241,
Kakimoto, Ken-ichi	P21-060,		P21-247,
	P21-120		P22-281,
			P22-284,
Kakiuchi, Toru	P23-133		P23-282,
Kakurai, Kazuhisa	OB22-204		P23-285,
Kakuta, Yoshimitsu	P22-315,		P23-300
	P23-314		P23-304
Kalyanam, N.	P21-042	Kato, Takayuki	P21-024
Kamada, Youichi	OB22-204,	Kato, Yasuhiro	P23-318
	OC23-004	Kato, Yuichi	P21-229
Kamariah, Neelakandan	P21-184	Katoh, Yohei	OC23-002
Kamikubo, Hironari	P21-214,	Katsumata, K.	P23-011
	P21-241	Katsuya, Yoshio	P22-272
Kamiya, Hiroyuki	P21-256	Katunuma, Nobuhiko	P23-163
Kamiya, Nobuo	OA22-002,	Kaung, P.	P22-113
	P21-226	Kaur, Balwinder	P21-259,
Kamiyama, Takashi	OC21-102,	Kaur, Punit	P21-277,
	P22-031,		P21-286,
	P22-134,		P21-295,
	P22-317		P22-254,
Kanagawa, Mayumi	OA21-106		P23-231
Kanazawa, Hiroshi	P22-269	Kawaguchi, Shigeta	P22-233
Kanehisa, Nobuko	P22-077	Kawaguchi, Tatsuya	P23-237
Kaneko, Koji	OB22-204	Kawai, Teruo	P23-279,
Kaneko, Masami	OB21-104		P23-310
Kaneko, Yoshio	P23-035,		P22-019
	P23-145	Kawaike, Yoichi	P22-290
Kanenari, Masakazu	P23-076	Kawamoto, Masahide	P23-052
Kanke, Yasushi	P23-112	Kawamura, Kazuo	P21-120
Kanng, P.	P22-092	Kawamura, Keizou	P21-202
Kanoda, Kazushi	P23-133	Kawarabayasi, Yutaka	OA22-001,
Kar, Manoranjan	P22-074	Kawasaki, Masato	P21-214,
Karita, Shuichi	P21-244		P21-229,
Karppinen, Maarit	P21-006		P21-241,
Kartini, Evvy	OC22-204		P23-285
Kasao, Takuro	OC21-102		P21-108,
Kashida, Shoji	P23-127,	Kawasaki, Takuro	P22-051,
	P23-136		P22-137
Kataoka, Kunimitsu	P21-027,		OC23-206
	P22-137	Kawata, Hiroshi	P23-148
Kataoka, Mikio	P21-214,	Kayamori, Syunsuke	P22-242
	P21-241	Kengaku, Yumiko	OC21-104,
Katayama, Takane	OB23-204,	Kennedy, Brendan	P21-003,
	P23-300		

Kennedy, Shane	P22-101,	Kita, Toru	P21-238
Khamrui, Susmita	P22-167	Kitade, Yukio	P22-221
Kiazadeh, Asal	OC22-204	Kitagawa, Susumu	K21-001,
Kigawa, Takanori	P21-268		OC23-205
Kihara, May	P21-159	Kitago, Yu	P21-244
Kijima, Naoto	P22-260	Kitano, Ken	P22-227
Kijima, Norihito	P23-270	Kitao, Akio	P23-270
	P23-169	Kitao, Tomoe	A21-202
	P21-027,	Kitaoka, Shintaro	P22-296
	P22-037,	Kitatani, Tomoya	P21-292,
	P22-040		P23-258
Kikkawa, A.	OC23-002	Kitaura, Ryo	OC23-205
Kikkou, Tatsuhiko	OA22-202	Kitayama, Nobuyuki	P22-161
Kikuchi, Keita	P23-204	Kitiphaisalnont, Panana	P22-128
Kim, Jehan	OB23-105,	Kito, Hijiri	P22-178
	OC22-101	Kitpratuang, Nustha	P23-297
Kim, Jin Kon	P23-054	Kiyonagi, Ryoji	P22-031
Kim, Jong-Woo	OC23-005	Klein, M.	OA23-205
Kim, Jungeun	OB23-101,	Klvana, Martin	P23-276
	P22-161	Knight, Kevin	P23-070
Kim, Kwang-Woo	OB23-105,	Ko, Tzu-Ping	P21-289
	OC22-101	Kobahashi, Tomoyuki	P22-236
Kim, Min Gyu	OC23-101,	Kobayashi, Hidenori	P22-313
	P21-138	Kobayashi, Isao	P22-010
Kim, Su Jae	P22-176	Kobayashi, Masanori	OA21-104,
Kimata, Mitsuyoshi	P21-018		P22-284,
Kimino, Taira	P22-071		P23-310
Kimoto, Koji	P21-006,	Kobayashi, Satoru	OC23-004
	P22-122,	Kobayashi, Takashi	P22-025
	P23-035,	Kobayashi, Tatsuo	OC23-205
	P23-145	Kobayashi, Tomoyuki	OB23-002,
Kimura, Fumiko	OC21-105		P21-265
Kimura, Hiroyuki	OB22-204,	Kobayashi, Yukiko	P21-202
	OC23-004	Kobe, Bostjan	OA22-105
Kimura, Kimihiro	P22-034,	Koch, Traugott	OB22-002
	P22-161	Koga, Hiroshi	OA22-001
Kimura, Makoto	P22-315,	Kohn, Kay	OB22-204,
	P23-314		OC23-004
Kimura, Sayaka	P22-176	Kojima, Yuko	P23-103
Kimura, Shigeru	OB23-101,	Kokila, M. K.	P23-017,
	P22-161		P23-023
Kimura, Tsunehisa	OC21-105	Komori, Hirofumi	P22-325
King, Tristan	P22-180	Kondo, Hiroshi	OA22-002,
Kinoshita, Isamu	P22-034		P23-198,
Kinoshita, Takayoshi	P22-203,		P23-204
	P23-219,	Kondo, Jiro	OA22-004
	P23-258	Kondo, Kazuya	P23-288
Kiran, Y.B.	P22-092	Kongaere, Palangpon	OA22-203
Kishimoto, Hiroyuki	OC22-105	Konno, Michiko	P22-263
Kishishita, Seiichiro	P22-287	Konosu, Hiroyuki	P21-217
Kita, Akiko	OA22-003,	Koritzanszky, Tibor	P23-048
	P22-230,	Kosada, Takashi	P22-242
	P23-306	Koshihara, Shin-ya	OC23-206

Koshima, Hideko	OB21-103	Kurihara, Kazuo	P22-266,
Kothri, Ashok	P22-022		P22-275
Kotru, Pushkar	P22-113	Kurihara, Masaaki	OB23-203
Kouyama, Tsutomu	OA23-005	Kurihara, Tatsuo	P23-228
Koyama, Atsushi	P23-273	Kurisu, Genji	P21-235
Krachodnok, Samroeng	P21-165	Kuroda, Kotaro	P21-060
Kraschnefski, Mark	P23-243	Kuroda, Reiko	OB22-007
Krishna, P.S.R.	P22-074	Kuroishi, Chizu	OA21-106
Krishnaiah, Musali	P23-091	Kuroiwa, Mika	P23-213
Krungkrai, Sudaratana	P22-327	Kuroiwa, Yoshihiro	OB23-101,
Ku, Chia-Jui	OC23-104		P22-161,
Kubota, Misao	P23-279,		P22-176
	P23-310	Kurokawa, Gentaro	P23-157
Kubota, Tomomi	P22-281	Kurokawa, Hirofumi	OB23-003
Kubota, Yoshiki	OC23-205	Kurokawa, Suguru	P23-228
Kudo, Norio	P21-247	Kurz, Mareike	P21-199
Kudoh, Yasuhiro	P23-058,	Kusaka, Katsuhiko	OB21-106,
	P23-100,		P22-266,
	P23-124		P22-275
Kukimoto-Niino, Mutsuko	P22-260,	Kusakabe, Kenichi	P21-021
	P22-307	Kusakabe, Yoshio	P22-221
Kulkarni, Geetha M.	P23-023	Kusakari, Yukiko	P22-327
Kulkarni, Guruprasad	P21-153	Kusano, Shuji	OC23-103
Kulkarni, M. V.	P23-023	Kusunoki, Masami	P22-242,
Kulprathipanja, Santi	P22-086		P23-328
Kulriya, Pawan	P22-022	Kutsuna, Shinsuke	P21-193
Kumagai, Keigo	P21-247	Kuwahara, Hideki	P22-122
Kumar, Amit	P22-022	Kvansakul, Marc	P21-205
Kumar, Janesh	P21-280,	Lai, Ying-Huang	OB23-106
	P22-323	Latham, Catherine	OA23-201
Kumar, Mahesh	P22-172	Lawrence, Michael	OA23-103
Kumar, Mukul	P22-053	Lee, Byeongdu	OC22-101,
Kumar, Penmetcha	OA22-205		P23-054
Kumar, Ravi	P22-113	Lee, Chi-Rung	P21-289,
Kumar, Vijay	P23-231		P23-041
Kumaradhas, Poomani	P21-042,	Lee, Erinna	P22-191
	P23-048	Lee, Gene-Hsiang	OB22-106,
Kumasaka, Takashi	P22-245,		P21-081,
	P23-312,		P22-083,
	P23-318		P22-110
Kunchithapadam, Swaminathan	P23-249	Lee, Jey Jau	P21-168
Kunii, Akira	P23-044	Lee, Mihwa	P22-224
Kuo, Anling	OA23-002	Lee, Woo Cheol	P23-252
Kuo, Jui-Chao	P21-084	Lee, Yen-Chung	P23-192
Kuramitsu, Seiki	OA21-106,	Leung, Andy	P21-072
	OA22-002,	Li, Hsou-min	OA23-003
	P21-226,	Li, Man-Rong	P21-063
	P22-287,	Li, Nan	P23-249
	P23-204	Licci, F.	P22-113
Kuribayashi, Takahiro	P23-058,	Liljas, Anders	OA22-005
	P23-100,	Lin, Hsiu-Mei	P22-116,
	P23-124		P23-118
Kurihara, Kazue	P21-021	Lin, Yi-Hung	OB23-201

Lin, Zhengjiong	OA22-103	Matsui, Yoshio	P21-006,
Ling, Chris	P21-090,		P22-122,
	P22-167,		P23-035,
	P23-094		P23-145
Liou, Yih-Cherng	P23-243	Matsuishi, Satoru	P22-047
Liu, Ming-Yih	OB23-201	Matsumoto, Osamu	OA22-202
Liu, Zhi-Min	OB22-005	Matsumoto, Shinya	P22-025
Long, C.	OA23-205	Matsumura, Hiroshi	P23-088
Loomes, Kerry	OA23-202	Matsumura, Hiroyoshi	P21-292,
Lou, Mei-zhen	OA23-203		P22-327,
Lou, Meizhen	OA23-103		P22-329,
Lovesey, S.W.	OC23-002		P23-258
Lovrecz, George	OA23-103	Matsuo, Ryuji	P21-030
Lu, T-H	P22-049	Matsuoka, Hideki	OC22-102
Lu, Tong-Bu	OB21-105	Matsuoka, Takeshi	P23-306
Lu, Wen-Guan	OB21-105	Matsuura, Kanna	P22-242
Luo, Cindy	OA23-203	Matsuura, Yoshiharu	P22-182
Lwin, Thet-Thet	P23-279	Matthews, Brian	P21-250,
Lyon, Elizabeth	OB22-002		P21-253
Ma, Jichun	P23-316	Mckenzie, Scott	P22-167
Machida, Yoshitaka	P23-267	McKern, Neil	OA23-103
Madamwar, Datta	P22-254	McKimm-Breschkin, Jennifer	OA23-204
Madras, Giridhar	P23-160	McLeish, Michael	P21-196
Maeda, Kazuhiko	P21-096	McMullen, Donald F.	P22-180
Maekawa, Sadamichi	OC22-003	Metcalf, Peter	OB23-001
Mahalakshmi, L.	P23-142	Metoki, Naoto	OB22-204
Mahale, Smita	OB23-202	Meunier, Fred	OA23-201
Mahapatra, Sudarshan	P23-160	Michaal, Otyepka	P23-276
Maher, Megan	P22-224	Michiue, Yuichi	P22-059
Makha, Mohamed	OB21-107	Mihara, Hisaaki	P23-228
Makita, Ryoko	P22-043	Miida, Rokuro	P21-126
Maksimenko, Anton	P23-097	Mikami, Bunzo	OB23-004
Mann, Maretta	OA23-204	Miki, Kunio	OA21-106,
Manoj, K	P21-093		OA22-003,
Martin, Jennifer	OA23-201,		P21-202,
	P21-196		P22-230
Martin, Jenny	P21-199	Mikouchi, Takashi	P22-149,
Mashima, Kazushi	P22-164		P23-154
Mashiyama, Shinichiro	P23-157	Milsted, Andrew	OB22-002
Masuda, Sumiko	P23-312	Minami, Yoshiko	P22-296
Masui, Ryoji	OA21-106,	Minamino, Tohru	P23-270
	OA22-002,	Mine, Tetsuro	P23-005
	P23-204	Mir, Rafia	P21-286
Masunaga, H.	P22-057	Mishima, Masaki	P21-256
Matsubara, Futoshi	P22-218	Mishra, Parul	P21-295
Matsubara, Mamoru	P22-203	Mishra, Yogendra	P22-022
Matsuda, Ryotaro	OC23-205	Misono, Tomoko	OA22-205
Matsugaki, Naohiro	OA22-101,	Mitchell, Geoffrey	P23-073,
	P22-257,		P23-082
	P22-284,	Mitchell, John	OC23-005
	P23-273,	Mitomi, Kenta	OA22-004
	P23-310,	Mitsuishi, Hajime	P23-052
	OA21-104	Mitsumi, Minoru	OC23-204,

	P22-034, P23-038	Morimoto, Yukio	P22-230, P23-306
Miura, Hiroyuki	P23-291	Morishige, Masaki	P22-313
Miyabayashi, Takayuki	P22-164	Morita, Yasuyo	P22-242
Miyahara, Ikuko	P21-226, P23-216, P23-228	Moritomo, Yutaka	OB23-101, P22-161
	P22-272	Moriyoshi, Chikako	P22-176
Miyano, Masashi	P22-206	Motohara, Moritoshi	OB23-002, P21-265, P22-236
Miyashita, Yuichiro	P21-129, P21-135, P21-147		P22-307
Miyata, Mikiji	OA22-104	Motoyama, Kanna	P22-086, P23-297
	P23-273, P23-279, P23-310	Muangsin, Nongnuj	P21-150, P21-156
Miyatake, Hideyuki	P21-102, P21-117		P21-015, P23-106
Miyoshi, Toshinobu	P23-148	Mukherjee, Alok	OC23-002
	P21-021	Mukherjee, Monika	OC22-201
Mizuguchi, Jin	P22-263		P21-292
	OA22-205	Murakami, Hironori	OA21-101, P22-245
Mizukami, Fujio	P23-237		OA23-004, OA23-104, P21-292, P22-327, P23-258
Mizukami, Masashi	P21-202	Murakami, Satoshi	P23-046
Mizukawa, Akiko	P23-267		P21-235
Mizuno, Hiroshi	OB23-004		P23-282
Mizuno, Kazunori	P22-209, P23-207, P23-210	Murakami, Youichi	P23-240
Mizushima, Akira	P22-134	Muraki, Norifumi	OB23-101, P22-161
Mizutani, Kenji	P23-017	Murata, Takeomi	P22-260, P22-287, P22-307, P23-240
Mizutani, Kimihiko	P22-174	Murayama-Kato, Miyuki	P22-092, P23-163
Mizutani, Ryuta	P23-073, P23-082	Murayama, Haruno	OB23-204, P23-282, P23-300
	P21-232, P23-124	Murayama, Kazutaka	P23-264
Mochiku, Takashi	P21-015		P21-006, P22-122, P23-035
Mohan, S.	OA23-204		P22-303
Mohand, S.	OB23-001	Musali, Krishnaiah	P22-122, P23-145
Molloy, Robert	P22-031, P22-134		P23-124
	P23-008, P23-085	Nagae, Masamichi	P23-252
Momma, Koichi	P22-182		P23-171
	P21-292, P22-327, P23-258	Nagai, Kiyoshi	P23-276
Mondal, Swastik	OC23-202	Nagai, Takuro	
Monti, Eugenio	OC21-102,		
Mori, Hajime	P22-266, P22-275	Nagano, Yoshiki	
Mori, Kazuhiro	P22-182	Nagao, Masahiro	
	P23-201		
Mori, Takeharu		Nagase, Toshiro	
		Nagata, Koji	
Mori, Yoshio		Nagata, Shinji	
Mori, Yusuke		Nagata, Yuji	
Moriguchi, Tadashi			
Morii, Yukio			
Moriishi, Kohji			
Morimoto, Tatsuya			

Naitow, Hisashi	P22-299	Naumov, Pance	P21-012,
Nakabeppu, Yusaku	P21-256		P21-087,
Nakagawa, Atsushi	OA23-004,		P22-013,
	P21-265,		P22-016,
	P22-248,		P23-014
	P22-313	Nayak, Susanta	P21-153
Nakagawa, Noriko	OA21-106,	Neelamegam, Sivakumar	P23-249
	P21-226	Nelson, Christie	OC23-005
	OA22-003	Ng, Seik Weng	P21-087
Nakagawa, Taro	OC23-204	Ngamrojnvanich, Nattaya	P23-297
Nakai, Hidetaka	P21-024	Ngiwsara, Lukana	OA22-203
Nakai, Izumi	OA22-002	Nguyen, Vi	OB22-004
Nakai, Tadashi	P22-010	Nicola, Nicos	OA23-203
Nakajima, Mitsutoshi	P22-218	Nielsch, Kornelius	OC23-101,
Nakajima, Yoshitaka	P23-005,		P21-138
Nakamoto, Yuki	P23-088	Niimura, Nobuo	OA22-201,
	P21-202,		P22-266,
	P23-213		P22-275
Nakamura, Akira	OA23-101	Nirasawa, Satoru	P22-278
	P22-242	Nirmala, K. A.	P21-042,
	P22-221,		P22-174
	P22-311	Nisawa, Atsushi	P22-245,
	P22-233		P22-290
Nakamura, Keishi	P22-178	Nishi, Nozomu	P23-282
Nakamura, Masaki	OC23-105	Nishibori, Eiji	OB23-104,
Nakamura, Masashi	P23-312		OC22-202,
Nakamura, Satoshi	OB21-106		P22-045
Nakamura, Setsuko	P23-103	Nishijima, Masahiro	P21-247
Nakamura, Shinichiro	P23-282	Nishimaki, Hirokazu	P23-157
Nakamura, Takanori	P21-256	Nishimoto, Madoka	P23-294
Nakamura, Teruya	P23-234	Nishino, Norikazu	P22-200
Nakamura, Yoshihiro	P21-009	Nishino, Tokuzo	P23-328
Nakamura, Yoshio	OA21-103	Nishiya, Yoshiaki	P23-222
Nakamura, Yuki	P22-221	Noda, Yukio	OB22-204,
Nakanishi, Masayuki	P22-313		OC23-004,
Nakano, Hirofumi	P23-234		P22-047
Nakano, Kazumi	P22-007	Nodumi, Yousuke	OC23-103
Nakao, Hironori	P22-218	Nogami, Takashi	P23-157
Nakashima, Kanako	P22-315	Nogi, Terukazu	A21-202
Nakashima, Takashi	P22-045	Noguchi, Keiichi	P22-194,
Nakashima, Takeshi	P23-210		P22-200,
Nakata, Ayako	P21-292		P23-076,
Nakata, Shinya	P23-179		P23-201,
Nakatsuka, Akihiko	OA22-001,		P23-237
Nakayama, Kazuhisa	P21-229	Noguchi, Yuji	P22-176
	P23-179	Nomoto, Daisuke	P23-011
Nakayama, Noriaki	P23-328	Nozawa, Shunsuke	OC23-206
Nakayama, Toru	P23-270,	Numoto, Nobutaka	OA22-003,
Namba, Keiichi	P23-304		P21-202
	P22-269	Nureki, Osamu	OA23-102,
Naoe, Youichi	P23-023		P21-238,
Narasimha Murthy, V. N.	P22-281		P22-293,
Narimatsu, Hisashi	P22-185		P22-303,
Natarajan, Sampath			

	P23-320	P22-200,
O'Neill, Scott	P21-199	P23-076,
Oakley, Aaron	P23-276	P23-201,
Ochi, Sadayuki	P22-272	P23-237
Oda, Masataka	P22-272	P23-228
Odahara, Takayuki	P23-318	OC23-102
Ogaki, Masao	P23-261	P22-313
Ogasahara, Kyoko	P22-248	OC23-003,
Ogata, Yoichiro	P23-046	P22-004
Ogawa, Eiji	P22-313	P22-218
Ogawa, Keiichiro	OC23-203	P22-043
Ogawa, Koza	P23-076	P22-319
Oh-oka, Hirozo	P23-302	OA22-204,
Ohashi, Haruo	P22-178	P21-217
Ohhara, Takashi	P22-266,	OB23-102
	P22-275	P22-051
Ohkubo, Koichi	P23-008	P22-293
Ohmiya, Hiromi	P22-152	P23-328
Ohnishi, Kuniharu	P22-230	P23-127,
Ohnishi, Yuki	OA22-201	P23-136
Ohno, Atsuko	OB23-104	P23-252
Ohno, Takeshi	P23-008	P23-157
Ohsato, Hitoshi	OB22-105,	OC23-204,
	P21-060,	P21-162,
	P21-120	P22-034,
Ohsawa, Kanju	P23-213	P22-161,
Ohsawa, Noboru	P22-307	P23-038
Ohsawa, Seiji	P23-085	OB21-106,
Ohshima, Ken-ichi	P21-027,	P22-266,
	P21-108,	P22-275
	P21-111,	P21-184
	P21-126,	Padmanabhan, Balasundaram
	P21-141,	Pal, Sarbani
	P22-007,	P21-150
	P22-051,	Palani, Kandavelu
	P22-137,	P21-184,
	P23-151	P22-001
Ohsumi, Kazumasa	P22-149,	Pan, Mei
	P23-154	Pandey, Dhananjai
	P22-317	P22-102,
Oishi, Ryoko	P23-318	OB22-103
Okabe, Takao	OA23-004	P21-072,
Okada, Kengo	P22-313	P21-075
Okada, Masato	P23-115	OB22-203
Okamoto, Kazuaki	P22-053	P23-264,
Okazaki, Naoto	OA21-101,	P23-267
Okazaki, Nobuo	P22-245	OC23-101,
	P22-203	P21-138
Okita, Kouki	P22-158	P23-002
Okitsu, Kouhei	P23-008,	P22-212
Okube, Maki	P23-085	OC23-104
	P23-179	P21-259
Okudera, Hiroki	P22-194,	P21-298
Okuyama, Kenji		OB23-102
		P23-330
		P22-301,
	Omi, Rie	
	Omote, Kazuhiko	
	Oneyama, Chitose	
	Onoda, Mitsuko	
	Onohara, Yuko	
	Onuki, Yoshichika	
	Oonishi, Isao	
	Ootaki, Masanori	
	Orobengoa, Danel	
	Osakabe, Takeshi	
	Oshikane, Hiroyuki	
	Oshima, Yasuhiro	
	Otaki, Yo	
	Otsuka, Jun	
	Ozawa, Kazuhiro	
	Ozawa, Yoshiki	
	Ozeki, Tomoji	
	Packianathan, Charles	
	Padmanabhan, Balasundaram	
	Pal, Sarbani	
	Palani, Kandavelu	
	Pan, Mei	
	Pandey, Dhananjai	
	Pang, Pokka	
	Park, Je-Geun	
	Park, Sam-Yong	
	Park, Yongjun	
	Park, Young-Ja	
	Peng, Qi	
	Peng, Shie-Ming	
	Perbandt, Marcus	
	Perbandt, Markus	
	Perez-Mato, Juan Manuel	
	Peter, Zwart	
	Petsom, Amorn	

Phat, Yong	P23-297	Sakai, Akihiro	P23-207
Phung, Son	P21-096	Sakai, Hisanobu	OA21-101,
Phurat, Chattrree	P21-111		P22-290
Pichierri, Fabio	P22-086	Sakai, Kei	P21-006
Ponnuraj, Karthe	P21-021	Sakai, Naoki	OA23-101
Ponnuswamy, M.N.	P21-223	Sakakibara, Youichi	P23-314
	P21-184,	Sakakura, Terutoshi	P22-047
	P22-001,	Sakamoto, Tatsuji	P23-258
	P22-185,	Sakata, Makoto	OB23-104,
	P23-183,		OC22-202,
	P23-186		P22-045
Porcar, Lionel	OC23-001	Sakata, Osami	OC23-105
Prashar, Vishal	OB23-202	Sakka, Kazuo	P21-244
Prem kumar, R.	P21-277,	Sakuma, Takashi	OC21-102
	P21-286,	Sakurai, Hidehiro	P21-235
	P21-259,	Sakurai, Jun	P22-272
	P21-295	Sakurai, Kenji	P21-012,
Puttaraja, P.	P23-017,		P22-013,
	P23-023		P22-016,
Qian, Wu	P21-196		P23-014
Quilici, Romain	P22-180	Sala, Kadsada	P21-099
Radhakrishna, Jadaprolu	P23-091	Salleh, Abu	P22-329
Rae, A. David	P21-087,	Samanchat, Chariwat	OA22-203
	P23-326	Sano, Satoshi	OB23-002,
Rahman, Raja	P22-329		P21-265,
Ramu, L.	OC23-201		P22-236
Rangsunvigit, Pramoch	P22-086	Saravanan, J.	P22-174,
Rao, Qunli	P22-068		P23-017
Rao, Zihe	K21-301,	Sasajima, Kumiko	P22-257
	OA23-001,	Sasaki, Katsuhiko	P21-060
	P23-056	Sasaki, S.	P22-057
Raston, Colin	OB21-107	Sasaki, Satoshi	OB23-104,
Ravi, S.	P22-074		P23-008,
Ray, Dipa	P23-109		P23-085
Raynuthala, RaviKumar	P23-163	Sasaki, Takatomo	P21-292
Ree, Moonhor	OB23-105,	Sasaki, Takayoshi	OC23-003
	OC22-101,	Sasaki, Yasuyuki	P23-213
	P22-055,	Sasaki, Yoichi	P23-038
	P22-331,	Sasaki, Yoshiki	P22-080
	P23-054	Sasayama, Yuichi	OA22-003
Row, Tayur	P21-144	Sateesh, M. K.	P23-023
Roy, Subrata	P22-104	Sato, Akira	P22-178
Ruscher, Claus	P23-020	Sato, Hironori	P22-140
Ryan, Philip	OC23-005	Sato, K.	OC22-104
Sabe, Hisataka	P22-313	Sato, Kazuyuki	P21-117
Saijo-Hamano, Yumiko	P23-270	Sato, Mamoru	P21-193,
Saines, Paul	P21-003		P22-233,
Saito, Kazuya	P22-155		P22-269
Saito, Koh	P21-039	Sato, Masaru	OB23-002,
Saito, Masatoshi	P21-033		P21-265,
Saitoh, Hideki	P22-155		P22-236
Saitoh, Hiroyuki	P22-007	Sato, Tokushi	OC23-206
Saitoh, Koh	P23-050	Sato, Tomohiro	OB22-007

Sato, Yoshiteru	OA22-004, P22-206		P21-165 P23-064
Sato, Yusuke	P21-238	Shen, Yu-Chi	OB22-106,
Satoh, Hiroyuki	P22-319	Sheu, Chou-Fu	P21-081
Satoh, Mie	P22-025		OB23-106,
Satoh, Tadashi	OA22-101, OB23-203	Sheu, Hwo-Shuenn	P22-083 P22-107
Saul, A.	OA23-205	Shi, Yao-Cheng	P22-248
Sawa, Hiroshi	OC23-004, OC23-206, P23-133	Shiba, Kohei	OA22-001, P21-235, P22-281
Sawaki, Hiromichi	P22-281	Shiba, Tomoo	P23-294
Saxena, Ajay	OA23-205	Shibata, Rie	P22-233
Scagnoli, V.	OC23-002	Shichijo, Naoki	OB23-106
Schierbeek, Bram	P21-208	Shih, Wei-Ju	P23-171
Schirra, Horst	OA22-105	Shikama, Tatsuo	P22-031,
Schmid, Siegbert	P23-166	Shikanai, Fumihito	P22-317
Schulze-Briese, Clemens	OB23-001		P21-060
Scott, Abby	OC22-204	Shimada, Takeshi	P23-255,
Scott, Stacy	P23-243	Shimizu, Nobutaka	P23-261, P22-290
Scudder, Marcia	OB22-004		P23-008
Seki, Yuusuke	P23-127, P23-136	Shimizu, Norio	OA22-004,
Sekiguchi, Takeshi	OA22-002, P22-206, P23-198, P23-204	Shimizu, Satoru	P22-206, P23-198 P22-290
Sekine, Akiko	OB23-103	Shimizu, Tetsuya	P21-193, P22-233,
Sen, Udayaditya	P21-268	Shimizu, Toshiyuki	P22-269
Sengupta, Siba	P23-026, P23-109		P22-321
Sengupta, Suparna	P23-109	Shimizu, Yoshihiro	P22-242
Seo, Daisuke	P21-235	Shimizu, Yukiko	P23-130
Serre, Laurence	OB23-202	Shimose, Sachie	P23-237
Seto, Hideki	OC22-103	Shimura, Masaki	OA22-001
Seto, Makoto	OC22-001	Shin, Hye-Won	P23-322
Seto, Takatoshi	P23-169	Shin, Kouichirou	OB22-102, OC23-101,
Sharma, Neeraj	P21-090	Shin, Namsoo	P21-138 P23-294
Sharma, Sujata	P21-259, P21-262, P21-271, P21-274, P21-277, P21-280, P21-283, P21-286, P21-295, P21-298, P22-323, P23-322	Shinkai, Akeo	OC22-104, OC22-105, P22-010
Shashidhar, M.	P21-093	Shinohara, Yuya	P21-256 P21-238
Sheikh, Ishfaq	P21-283		OC22-203
Shek, Fanny	P21-069,	Shirakawa, Masahiro	OA21-106, P22-260, P22-287, P22-307, P23-240, P23-294
		Shirakawa, Ryutarou	P21-126
		Shirotani, Ichimin	P23-023
		Shirouzu, Mikako	
		Shishido, Toetsu	
		Shivaprakash, N. C.	

Shizuya, Mitsuyuki	P22-004	Somvanshi, Rishi	P21-280,
Shomura, Yasuhito	P23-225		P21-298,
Shyu, Shin-Guang	P22-116		P22-323
Sigamani, Sundaresan	P21-184	Son, Seyoung	P23-316
Singh, Akhilesh	OB22-102,	Song, Pei Chee	P23-243
	OB22-103	Soni, Badrish	P22-254
Singh, Amit	P21-271,	Soriano, Maunel	P22-239
	P21-277,	Souno, Katsuya	OB23-103
	P21-283,	Spackman, Mark	OC22-201
	P23-322	Spadaccini, Nick	P23-181
Singh, Fouran	P22-022	Srinivasan, P.C.	P22-001
Singh, K.	OA23-205	Srivastava, Devendra	P21-280,
Singh, Nagendra	P21-259,		P22-323
	P21-262,	Staub, U.	OC23-002
	P21-271,	Stenmark, Harald	P23-285
	P21-274,	Stephen, A.David	P21-042
	P21-277,	Stetsko, Yu	P22-062
	P21-280,	Stower, A.	OA23-205
	P21-283,	Streltsov, Victor	OA23-103
	P21-286,	Su, Cheng-Yong	OB22-005
	P21-295,	Su, Dan	OA23-001,
	P21-298,		P23-056
	P22-323,	Su, H.	OA23-205
	P23-322	Subash, Gopinath	OA22-205
Singh, Satendra	OB22-103	Subramanian Manimekalai, Malathy Sony	P23-183
Singh, Tej	P21-259,	Suda, Katsumi	P22-152
	P21-262,	Sueda, Yuichiro	P23-058
	P21-271,	Sugai, Motoyuki	P23-324
	P21-274,	Sugawara, Yoko	OA22-204,
	P21-277,		OC23-202,
	P21-280,		P21-217
	P21-283,	Sugioka, Shigemi	P22-281
	P21-286,	Sugishima, Masakazu	A21-201,
	P21-295,		P22-251
	P21-298,	Sugita, Hiroaki	P23-088
	P22-254,	Sugiyama, Hiromu	OA22-004
	P22-323,	Sugiyama, Hiroshi	P23-097
	P23-231,	Sugiyama, Kazumasa	P21-033,
	P23-322		P22-140
Sinha, Mau	P21-262,	Sugiyama, Shigeru	OB23-002,
	P21-286		P21-265,
Siripaisarnpipat, Sutatip	P22-128,		P22-236,
	P23-121		P22-248
Siripitayananon, Jintana	P23-073,		P22-107
	P23-082	Sui, Chun-Xia	P23-314
Siu, Alvin	P21-072	Suiko, Masahito	P23-103
Sivaraman, Jayaraman	P23-243	Sukata, Shinichiro	P22-031
Skelton, Brian	P21-105	Sulistyanintyas, Dyah	P22-296
Slagsvold, Thomas	P23-285	Sumi, Norika	P23-100
Smith, Christopher	OB21-107	Sumioka, Keiko	P22-155
Sobolev, Alex	OB21-107	Sumita, Masato	OA23-001,
Sogabe, Yuri	P23-258	Sun, Fei	P23-056
Soll, Dieter	P22-293		

Sun, Yuh-Ju	OA23-003, P21-187, P21-190	Takahashi, Takahashi	P22-236 P23-151
Sundaresan, Etti	P21-223	Takahashi, Tetsuo	P22-209
Sung, Herman	P21-066, P21-069, P21-072, P21-075, P21-165	Takahashi, Toshio	OC23-103
Suo, Yin	P21-126	Takahashi, Yasuhiko	P21-027, P22-037, P22-040, P22-051
Suresh C., Reddy	P23-091	Takahashi, Yasuhiro	P22-251, P22-296, P23-115
Suryanarayana Rao, Vijayanthimala	P23-246	Takahasi, Yukio	P22-071
Suto, Kyoko	P22-321	Takakura, Yasuaki	P23-213
Suttisawat, Yindee	P22-086	Takamizawa, Tadashi	P22-010
Suwa, Hiroyuki	P22-045	Takamori, Kenji	P22-131
Suwa, Tsuyoshi	P21-123	Takano, Kazufumi	P21-292, P22-327, P23-258
Suzuki, Atsuo	OA21-102	Takano, Yoshiki	OC21-102, P22-266, P22-275
Suzuki, Kaoru	OA22-002, P22-206, P23-198, P23-204	Takase, Mitsunori	P23-322
Suzuki, Kei	P22-296	Takashima, Hiroshi	P22-077
Suzuki, Kenzi	P22-230	Takata, M.	P22-057
Suzuki, Mamoru	OA23-004, P21-265	Takata, Masaki	OB23-101, OC22-202, OC23-205, P22-057, P22-161
Suzuki, Nobuhiro	P23-285	Takayama-Muromachi, Eiji	P22-004
Suzuki, Nobuo	P22-278	Takeda, Tohoru	P23-279
Suzuki, Shotaro	P21-060	Takemaru, Yasutaka	P21-033
Svasti, Jisnuson	OA22-203	Takemoto-Hori, Chie	P22-307
Swain, Diptikanta	P21-132	Takenaka, Akio	OA22-002, OA22-004, P22-206, P23-198, P23-204
Syou, Maki	P21-292	Takusagawa, Hideaki	OA22-204, P21-217
Tachikawa, Osamu	P22-149	Tamaru, Yutaka	P22-233
Tada, Toshiji	P22-203, P23-219, P23-258	Tame, Jeremy	P23-264, P23-267
Tadjarodi, Azadeh	P21-159, P23-175	Tamiaki, Hitoshi	P23-302
Taguchi, Takeyoshi	P22-028	Tamura, Noriko	P23-222
Takada, Kazunori	OC23-003	Tamura, Tomohiro	P23-222
Takada, Tsuyoshi	P21-096	Tanabe, Aiko	OB23-004
Takagi, Junichi	A21-202	Tanabe, Yasuhiro	P22-152
Takagi, Tetsuo	P22-260	Tanaka, Akiko	P22-260
Takahashi, Hiroo	P21-102, P21-117	Tanaka, Hiroaki	OB23-002, P21-265, P22-236
Takahashi, Kiyohiro	P22-278	Tanaka, Ichiro	OA22-201,
Takahashi, Kunimitsu	P23-151		
Takahashi, Masaya	P22-272		
Takahashi, Miwako	P21-141, P22-137, P23-139		
Takahashi, Sachiko	OB23-002, P21-265,		

Tanaka, Isao	P22-266, P22-275 OA23-101, P21-244, P23-288	Thiruvencatam, Vijay Thomson, Robin Tirawanich, Wilaiwon	P21-144 OA23-204 P22-301, P23-297 P23-032
Tanaka, Kiyooki	OC22-203, P22-043, P22-047, P23-044	Tiruvencatam, Vijay Toda, Fumio	OB22-003, P21-036 P23-171 P21-129, P21-135, P21-147
Tanaka, Koichi	OB23-103	Toh, Kentaro	OC22-003
Tanaka, Masahiko	P21-012, P22-004, P22-019, P23-011, P23-124	Tohnai, Norimitsu	P22-327 P23-035, P23-145
Tanaka, Michiyoshi	OC22-205	Tohyama, Takami	P21-256
Tanaka, Nobuo	P23-050	Tokuoka, Keiji	P23-035, P23-145
Tanaka, Nobutada	P22-221	Tokura, Yoshinori	OC23-206
Tanaka, Tetsuo	OB23-002, P21-265, P22-236 P23-201	Toma, Sachiko Tomioka, Yasuhide	P23-261 OA23-102, P22-321 P22-031
Tanaka, Toshiki	OC23-002	Tomita, Ayana	OC21-102
Tanaka, Y.	OB23-101, P22-161	Tomita, Kouichi	OC23-002
Tanaka, Yoshihito	P23-320	Tomita, Kozo	P21-214 P22-317
Tanaka, Yoshiki	P23-041	Tomiyasu, Keisuke	OB23-101, OC23-204, P21-162, P22-034, P22-161, P23-038
Tang, Ting-Hua	P23-279, P23-310	Tomota, Yo	P23-085
Tanioka, Kenkichi	P23-252	Tonnerre, J.M.	P21-036
Tanokura, Masaru	P22-057	Torii, Seiji	P23-285
Tashiro, K.	P23-177	Torii, Shuki	P22-022
Tateishi, Kenji	P22-043	Toriumi, Koshiro	P21-190
Tatewaki, Hiroshi	OC23-206		OC23-104
Tazaki, Ryoko	P22-301, P23-297	Toyoda, Takeshi	P22-025
Teerawatananond, Thapong	OA22-105 P21-120	Toyota, Shinji	OB23-204, P23-300
Teh, Trazel	OA21-106, P22-260, P22-287, P22-307, P23-240, P23-294	Trambaiolo, Daniel	P23-171
Terada, Mio	P21-024	Tsai, Kuang-Lei	OC22-205, P23-046, P23-052
Terada, Takaho	P23-314	Tseng, Wei-Hsiang	P22-272
Terada, Yasuko	P21-096	Tseng, Wei-Hsiang	P23-038
Teramoto, Takamasa	P23-052	Tsuchida, Daisuke	P22-119
Teramura, Kentaro	P22-227	Tsuchiya, Atsuko	P21-202
Terauchi, Masami	OA23-204	Tsuchiya, Bun	P22-077
Terawaki, Shin-ichi	P23-163	Tsuda, Kenji	P22-182, P23-306,
Tettamanti, Guido	P22-170		
Than, Zao Oo	P22-092	Tsuge, Hideaki	
Thappa, R.K.		Tsuge, Kiyoshi	
Thetmar, Win		Tsuji, Takayuki	
		Tsujimura, Masaya	
		Tsukahara, Keiichi	
		Tsukahara, Tomitake	

Tsukushi, Itaru	P23-316		OA22-001,
Tsunoda, Masaru	P22-031		OA22-101,
Tsutsui, Kenji	P22-311		OA23-204,
Turberfeld, Andrew	OC22-003		OB23-203,
Turner, Mike	P23-304		OB23-204,
Turner, Peter	OC22-201		P21-214,
Tyndall, Joel	P22-180		P21-229,
Tzou, Der-Lii	P21-196		P21-241,
Uchida, Akira	P22-116		P21-247,
Uchida, Kingo	P22-319		P22-057,
Uchida, Koji	P23-103		P22-257,
Uchikubo-Kamo, Tomomi	P21-220		P22-281,
Uehara, Shinji	P22-260		P22-284,
Ueji, Yoshinori	P21-129		P23-273,
Uekusa, Hidehiro	P22-158		P23-279,
	OB21-104,		P23-282,
	OB23-103,		P23-285,
	P21-036,		P23-300,
	P21-162		P23-310
Ueno, Go	OA21-101,	Wakimoto, Shuichi	OB22-204
	P22-245	Wan, Gavin	P21-066
Ueno, Satoru	OC22-104,	Wang, Andrew H.-J.	P21-289
	P22-010	Wang, Aojin	OA23-001,
Umehara, Takashi	P23-234		P23-056
Umena, Yasufumi	P23-306	Wang, Ching-I A.	OA22-105
Unno, Hideaki	P22-182,	Wang, Han-Hong	P21-084
	P23-328	Wang, Hsin-Ta	P22-110
Unno, Masaki	P22-215	Wang, Lee-Ho	P22-309
Unzai, Satoru	P22-233,	Wang, Li	P23-061
	P23-264,	Wang, Shih-Chi	OB22-106
	P23-267	Wang, Sue-Lein	OB21-101,
Upton, Mary	OC23-005		P21-114
Urushibata, Akiko	P22-307	Wang, Wen-Ching	P23-192
Usui, Taichi	P23-282	Wang, Yu	OB22-106,
Van Delft, Mark	P21-205		P21-081,
van der Laan, G.	OC23-002		P21-168,
Van Nguyen, Tri	P23-173		P22-083,
vasu, vasu	P22-174		P22-125,
Vedavati G., Puranik	P23-091		P23-079
Venerando, Bruno	OA23-204	Ward, Colin	OA23-103
Vijayan, Kalyani	P22-172	Watanabe, Masashi	P22-047,
Vijayan, Mamannamana	OA21-105		P22-137
von Itzstein, Marc	OA23-204	Watanabe, Nobuhisa	OA22-102,
Wada, Hiromi	P22-313		OA22-103,
Wada, Kei	P22-296,		P21-244,
	P23-302		P23-288
Wada, Satoshi	P22-161	Watanabe, Satoru	P22-260
Wada, Tatsuo	P22-025	Watanabe, Takayuki	OC23-105
Wakabayashi, Yusuke	OC23-004,	Watanabe, Yoshihiko	P22-230
	OC23-005,	Westbrook, John	P23-181
	P23-133	White, Allan	P21-105
Wakatsuki, Soichi	A21-203,	Whitten, Andrew	OC22-201
	OA21-104,	Wilce, Matthew	P23-276

Williams, Ian	OB21-102, P21-066, P21-069, P21-072, P21-075, P21-165	Yamamoto, Takahiko Yamamoto, Tamotsu Yamamura, Shigefumi	P23-261, P22-290 P22-329 P23-198 OA22-204, OC23-202, P21-217
Win, Zaw	OC22-203		P22-155
Wondratschek, Hans	OB23-102	Yamamura, Yasuhisa	OB23-002,
Wong, Wan-Yee	P21-069	Yamanaka, Mari	P21-265, P22-236
Wong, Wing-Tak	OB22-006		P23-088, P23-005
Wu, Chih-Chien	P21-187		OA21-102
Wu, Hsin-Mao	P23-192	Yamanaka, Takamitsu	OA21-103, OA22-104
Wu, Jin	P23-279		OA23-004
Wu, Lai-Chin	P22-125	Yamane, Takashi	OB23-203
Wu, Mingmei	P21-066	Yamano, Akihito	P21-238
Wu, Po-Wei	P23-064		P22-242
Wu, Sung-Hsun	OC23-104	Yamashita, Eiki	P22-182
Wu, Xueji	P23-243	Yamashita, Katsuko	P21-006
Wuernisha, Tuerxun	P22-031, P22-134	Yamashita, Masami	P23-216
Wyatt, Mathew	P22-180, P23-181	Yamashita, Reiko	P22-122
Xiong, Ding-Bang	P21-063, P22-065	Yamashita, Tetsuo	OB21-106
Xu, Jianxing	OA23-001, P23-056	Yamauchi, Hisao	P21-006, P22-122
Xu, Yue	P22-218	Yamauchi, Takae	P23-127, P23-136
Xue, Hong	P21-069	Yamauchi, Yutaka	P22-212
Yadav, Savita	P22-254, P23-231	Yamawaki, Takuto	P23-054
Yagi, Daichi	OA22-201	Yamazaki, Atsushi	P21-063, P22-065
Yajima, Shunsuke	P23-213		OA22-103
Yamabe, Shinichi	P22-077	Yanadori, Yuu	OA23-101
Yamada, Atsuko	P22-313	Yang, Feng	P22-068
Yamada, Norifumi L.	OC22-103	Yang, Seung-Yun	OB22-101, P21-096, P22-019, P22-119, P23-067
Yamada, Yusuke	OA21-104, OA22-101, P22-257, P22-284, P23-273, P23-310	Yang, Xin-Xin	P22-152
Yamagata, Tsuneaki	P22-164	Yao, Deqiang	OB23-101, P22-161, P23-038
Yamagata, Youhei	OB23-003	Yao, Min	P21-039
Yamagata, Yuriko	P21-256	Yao, Xin	P23-157
Yamaguchi, Asako	P23-219, P23-258	Yashima, Masatomo	A21-202
Yamaguchi, Takayuki	P23-324		P22-134
Yamamoto, Kenji	OB23-204, P23-300, P23-324	Yasuda, Eiichi	P23-222
Yamamoto, Masaki	OA21-101, P22-245, P23-255,	Yasuda, Yosifumi	P22-309
		Yasui, Masanori	P23-118
		Yasui, Norihisa	P21-072
		Yasuoka, Hiroshi	
		Yasutake, Yoshiaki	
		Yeh, Hui-Chun	
		Yeh, Shi-Fang	
		Yen, Yu-fong	

Yethiraj, Mohana	OC23-001		P23-056
Yi-Hung, Liu	OB22-106	Zhang, Jian-guo	OA23-203
Yoda, Yoshitaka	OC23-103, P22-158	Zhang, Weizhu	P23-145
Yokoo, Tetsuya	OC23-001	Zhang, Xiao-Wei	OC23-103, P22-158
Yokoyama, Shigeyuki	OA21-106, P22-260, P22-287, P22-299, P22-307, P23-234, P23-240, P23-294	Zhang, Xiaodong	P22-315
Yokoyama, Tomomi	OC23-204	Zhao, Jing-Tai	P21-063, P22-065
Yoneda, Shigetaka	OC23-202	Zheng, Chaode	OA22-103
Yonemura, Masao	OC21-102, P22-031, P22-317	Zheng, Hong	OC23-005
Yonezawa, Takae	OC23-204	Zhou, Qingdi	OC21-104, P22-101, P22-167
Yoon, Jinhwan	OB23-105, OC22-101, P22-055, P23-054	Zhu, Bei-Bei	P22-107
Yoon, Songhak	OB22-102, OC23-101, P21-138	Zhuang, Mingzhu	OC22-105
Yorita, Kazuko	P23-306	Zolensky, Michael	P22-149, P23-154
Yoshiasa, Akira	P23-179		
Yoshida, Shingo	P22-161, P23-038		
Yoshikawa, Hiroshi	P21-292		
Yoshikawa, K.	OC22-103		
Yoshikawa, Naokazu	P22-077		
Yoshikawa, Nobuyuki	P22-299		
Yoshimori, Tamotsu	P21-241		
Yoshimoto, Tadashi	P22-218		
Yoshimura, Keiko	OA23-005		
Yoshimura, Masato	P23-316		
Yoshimura, Tohru	P23-216		
Yoshino, Masashi	OC21-105		
Yoshioka, Shiro	P22-325		
Yousef, Mohammad	P21-250, P21-253		
Yu, Jian-Yuan	OC23-104		
Yu, Shu-Cheng	P22-143		
Yu, Xing	P23-243		
Yu, Xiuzhen	P22-146, P23-035, P23-145		
Yuasa, Tetsuya	P23-097		
Yufit, Dima.	OC22-201		
Zaharko, Oksana	OB22-102		
Zhai, Yujia	OA23-001,		

P 22-315 P. horikoshii Ski 2 type  
PH 1280 p RNA helicase

---

Check for Ski 3

Ski 7 homologs

2

# タンパク質結晶化ロボットの 決定版です。

- 同時分注のマルチディスペンサー(96または384)。
- 非接触分注のナノディスペンサー(1または8チャンネル)。
- 3段ステージ上の9つのプレートポジション。

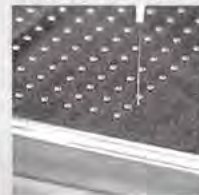
これらを一台に搭載し、同時に複数の結晶化作業も楽々ごします。  
新規プレート設定やプログラム作成、メンテナンスも簡単になりました。

## 96、384の同時分注に 交換型マルチディスペンサー



ヘッドは手作業で簡単に交換が出来ます。  
シリンジ容量は100ul、290ul、580ul、1mlの4種類。テフロンコートステンレスニードルとフレキシブルニードルがあり、様々な用途に容易に対応可能です。

## サンプルの微量分注に 非接触型ナノディスペンサー



ナノディスペンサーの、96wellへのタンパク質溶液の分注スピードは30秒以内。最小分注量50nLまでスケールダウンが可能です。オプションで8チャンネルもご用意できます。

## 分注プログラムの作成は簡単！ 制御ソフトウェア



アイコンをドラッグ&ドロップするだけで、フレキシブルなプロトコールが簡単に作成できます。溶液の粘性に合わせた分注スピードの設定も行なえます。

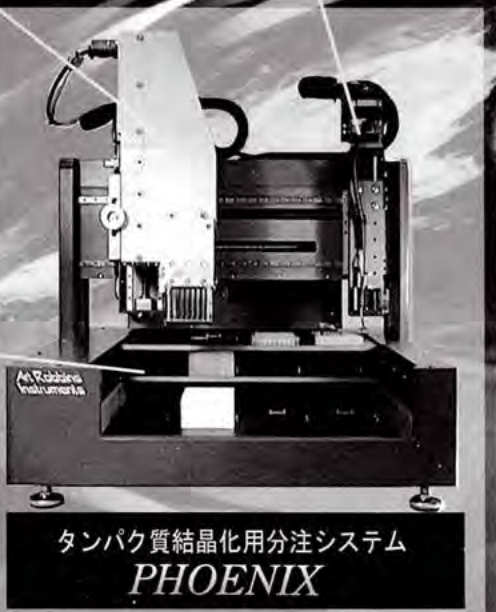
## マルチステージ構造がポイント！

9つのプレートポジションを分注・洗浄用に自由に設定できるので幅広い用途に使えます。ステージが常に水平に保たれるので、微量分注時にも分注ミスがありません。

## 2年保証



Art Robbins Instruments社の経験と実績あるシリンジテクノロジーと、完成された駆動システムにより、本体の2年保証を実現しました。



タンパク質結晶化用分注システム  
**PHOENIX**

お問い合わせ、御用命は

Towards the Healthy Future.



株式会社 ラボ

□[本 社]  
〒001-0027 札幌市北区北27条西6丁目2-12  
Phone: 011-758-4515 Fax: 011-758-4729 e-mail: head@labo.co.jp

□[東京営業所]  
〒113-0033 東京都文京区本郷3-42-5 本郷7F  
Phone: 03-3818-8786 Fax: 03-3818-9794 e-mail: so@labo.co.jp

URL : <http://www.labo.co.jp>

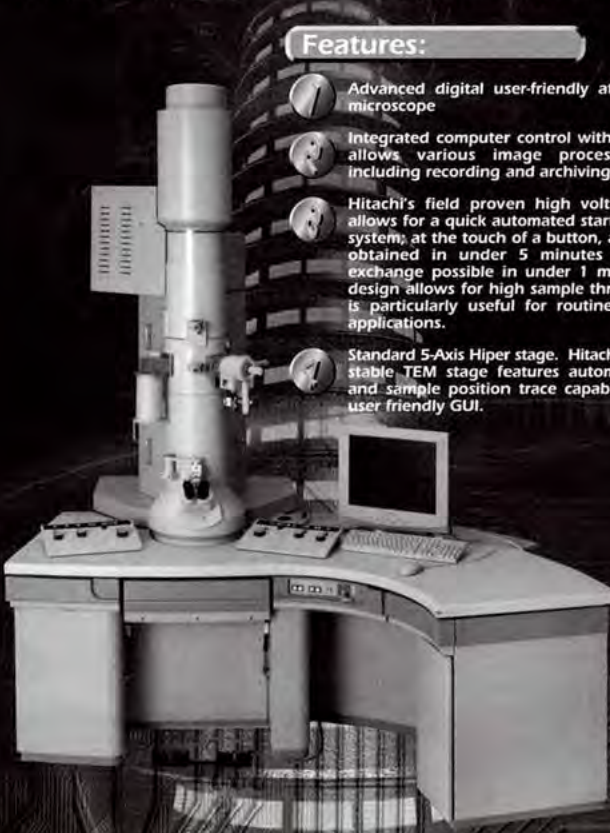
# H-9500

## Transmission Electron Microscope

### High-throughput high-resolution electron microscopy.

The H-9000 300kV TEM has been meeting the rigorous demands of the scientific community for more than a decade by offering extraordinary stability and field proven performance and reliability. The new H-9500 300kV TEM follows these standards of excellence. This new, state of the art TEM, utilizes modern computer control and digital cameras to enhance user-friendliness. The H-9500 is an indispensable tool for a broad range of applications, from semiconductors to materials science, allowing atomic resolution microscopy of a variety of materials.

#### Features:

- 
- 1. Advanced digital user-friendly atomic resolution microscope
  - 2. Integrated computer control with digital cameras allows various image processing functions including recording and archiving.
  - 3. Hitachi's field proven high voltage technology allows for a quick automated startup of the entire system, at the touch of a button, a 300kV beam is obtained in under 5 minutes with specimen exchange possible in under 1 minute. This new design allows for high sample throughput, which is particularly useful for routine semiconductor applications.
  - 4. Standard 5-Axis Hiper stage. Hitachi's exceptionally stable TEM stage features automatic navigation and sample position trace capabilities utilizing a user friendly GUI.

 Hitachi High-Technologies Corporation

Tokyo, Japan

<http://www.hitachi-hitec.com>

24-14 Nishi-Shimbashi 1-chome, Minato-ku, Tokyo, 105-8717, Japan